Doctoral Dissertation
Doctoral Program in Civil and Environmental Engineering (32nd cycle)

Optimisation of geothermal resources in urban areas

Matteo Baralis
* * * * * *

Supervisor
Prof. Marco Barla

Doctoral Examination Committee:
Prof. Alessio Ferrari, Referee, Università degli Studi di Palermo
Mag. Gregor Götzl, Referee, Geologische Bundesanstalt
Dr. Jannis Epting , Universität Basel
Prof. Donatella Sterpi, Politecnico di Milano
Dr. Francesco Tinti, Università di Bologna

Politecnico di Torino
July 15, 2020

I hereby declare that, the contents and organisation of this dissertation constitute my own original work and does not compromise in any way the rights of third parties, including those relating to the security of personal data. Part of the work described in this dissertation has been previously published by the candidate. The pertaining references are listed in the *Candidate publication list* at the end of this dissertation.

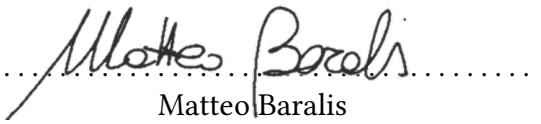

Matteo Baralis
Turin, July 15, 2020

A Giovanni, Imelda, Maria Agnese e Renato,
capostipiti di una stupenda famiglia
che vegliano da lassù o da quaggiù.

Acknowledgements

My first thanks goes to my supervisor, Professor Marco Barla, for being the first to make me consider enrolling in the Ph.D., the most challenging times I have ever experienced. He gave me guidance and constant stimulus to improve and to work at my best on a theme that I appreciated a little more each day.
I would like to thank Prof. Alessio Ferrari, Mag. Gregor Gotzl to have accepted to revise my thesis and for their useful comments towards improvement of the Dissertation as well as all the other members of the Ph.D. jury, Dr. Jannis Epting, Prof. Donatella Sterpi and Dr. Francesco Tinti for their time and interest in this work.
Thanks also to Prof. Luca Giordano and Prof. Claudio Scavia that followed and validated the study being part of the internal commission.
I'm thankful for the numerous chances of collaboration and help that contributed to this research. In particular I would like to acknowledge Prof. Sethi and Dr. Casasso for the precious suggestions and clarification about the geothermal potential assessment method that constitutes one of the most relevant bases for this work.
I would also like to thank the Città Metropolitana di Torino (Metropolitan authority) and the Città di Torino (Municipality) for the data provided for geothermal potential assessment in Torino central districts.
Furthermore I kindly acknowledge the financial support of Regione Piemonte (INFRA-P funding) and the Energy Center Interdipartimental Lab of Politecnico di Torino for supporting the realisation of the experimental site of the energy wall system.
My sincere acknowledgement goes to the COST Action TU1405 *European network for shallow geothermal energy applications in buildings and infrastructures* and its members for supporting Short Term Scientific Mission in Warsaw and Basel.
My sincere acknowledgement to the Polish Geological Institute and the University of Basel that kindly welcomed me and fruitfully helped in the development of this work.
Dziekuje to Grzegorz, Mateusz and Witold for the great time I had in Warsaw as my first international experience. Danke schn̈ to Horst and Jannis who warmly welcomed me, making my staying in Switzerland pleasant. Thanks for being not only temporary colleagues but new Swiss friends.
During these years I had the chance to cross paths with a lot of people who enriched my person. Thanks Alice for being inspirational to me, for your warmth and friendship but also for the mountain trips (especially the few with sunny weather!). Francesco, thanks

for the many times you supported me giving advices and listening to my doubts. Many thanks to Fabio for being always willing to share personal experience and encouraging to dream big.
I want to thank the people of the PoliTo group who I can truly call the DISEG family, even if some of them took other ways. Alessandra, constant reference in any personal and technical debate: we don't simply shared a room but also the joys and anxieties of the PhD student life. Giovanni, sincere and loyal friend, thank for sharing ideas, feelings and fears while always finding the silver lining in situations and people. Fabrizio for the happiness in each other's company that only close friends share when meeting even after long times. I have to thank Erica for the many laughs, jokes and for being a point of reference and a good friend at the same time. I am grateful I did not stop after our first meet when you made me realize I wouldn't have never been handsome.I want to say thank to the people that supported me during the most exciting and difficult times of this experience, stimulating me to hold on and giving me the best times to relax and recharge my energies. Special thanks to Danilo for being generous and humble friend, the person that who made me discover the passion for climbing. You taught me not only a way of keeping in touch with nature but also the real sense of trust putting our lives in each other's hands. Thank to Alessia and Carlotta, irreplaceable and sensitive friends, and to Francesco for your inspiring resourcefulness and the thousands laughs, also concerning our resourcefulness. I want to thank Matteo for our trainings and evening jogs, healthy distractions in these years, especially in last times. Thank for being always there in any joyful moment as in any tough time.
Last but not least, my most sincere gratitude to my parents, Enrico and Gabriella, and to Ilaria for being the ones who always believed in me even when I did not. It is impossible to express the many reasons why and how I am grateful. You are my blessing.

Summary

Shallow geothermal energy has been experiencing a rapid growth due to the energy policies promoted by national and international agencies. Climate change challenges are indeed pushing to renewable, distributed and low-impact energy sources in the heating and cooling sector. This sector accounts for half of the primary energy consumption. The Shallow Geothermal Energy (SGE) systems are a promising solution due to the pervasive availability. Conversely, high initial drilling and investigation costs prevent a wider application. Uncertainty about the exchangeable heat represents another obstacle especially in densely inhabited areas where interactions with subsurface uses are common and complicate the quantification of the geothermal potential.
The aim of this Thesis is to contribute to the optimisation in the use of shallow geothermal resources in urban areas. Tools and technologies are developed able to identify and use the portions of the subsurface that allow for the maximum impact of SGE on the energy supply mix is performed.
Following the introduction about the technologies that enable the heat exchange with the soil, the research examines the available methods to qualitatively or quantitatively assess the geothermal potential. This allows to evidence how in urban areas the need arises for a sound evaluation that tackles the advection and dispersion contributes in the heat transfer. A specific adaptation was developed in this Thesis for a semi-analytical formula used for the quantification of the geothermal potential from Borehole Heat Exchangers (BHE) including these contributions. This allows to fully consider the hydrodynamic regime in areas where an aquifer is present.
This formula is hence included in the *rOGER* four step procedure that is proposed for the optimisation in the use of SGE. This process is based on the integrated use of Geographic Information System (GIS) and of numerical analyses. This combination leads to the definition of multiple key metrics useful for spatial planning.
Since land scarcity issues affect urban areas, horizontal exchangers are usually not employed and the first meters below the surface are underexploited. In this perspective, a novel energy wall system that can be externally applied to earth-contact surfaces of new or renewed buildings is proposed. The first prototype of the system was designed and installed in Turin as part of this study and equipped with a wide monitoring network. Thermal performance tests allowed to quantify the heat exchange rate during winter heating operation in the range of 15-24 W/m^2 while virtually not affecting the

thermal status of the subsoil except for the very narrow surroundings of the system. This suggests that potential superposition of this system with deeper SGE can be obtained.
Subsequently the method was applied to the specific settings of a central portion of Turin metropolitan area. The *rOGER* procedure was applied by building a Geographic Information System and setting up a detailed numerical model. Several sources were employed to populate the GIS. A trend in shallow geothermal energy use was defined and a scenario was built. A three-dimensional Finite Element thermo-hydraulic model was built to reproduce and predict the thermal and hydraulic regime. The built heritage influence was accounted by proper handling of the related information. Results were then post processed and allowed to evidence the high potential of the area and the preferential location for new installations.The results suggest that the potential can be more than doubled with respect to hydrostatic conditions when considering advective contribution with the formula proposed in this Thesis.
Local peaks values of the geothermal potential of up to 0.5 MWh/y per square meter were obtained. Superposition of BHE and energy wall potential suggest that up to 57% of the built heritage may fulfil its energy needs relying on SGE. The general validity of the method proposed in this Thesis was demonstrated by its application to the study area.

Contents

Chapter 1

Introduction

1.1 Problem statement

Climate change represent a dramatic challenge for the entire world society today and in the next decades. The urgent need of implementation of the mitigation and adaptation strategies pushes social and economic paradigm shifts as never before in the human history. Technological and technical advances are promoted as partial response to these issues also in the heating and cooling sector. This sector represents a relevant share of the world energy consumption. Research and development towards sustainable buildings conditioning has been progressively oriented to distributed energy sources, as the solar energy, that provide a systemic response to the distributed nature of the demand. In this perspective, shallow geothermal energy fits to the arising energy paradigms. Indeed shallow geothermal, in contrast to deep geothermal, does not need a particular geological context to be effective. Several shallow and very shallow geothermal technologies may allow for the diffused and distributed satisfaction of the thermal loads in most rural and urban areas. In particular the shallow geothermal energy may play a relevant role in achieving the Sustainable Development Goals (SDG) 7 and 11 (*Affordable and green energy* and *Sustainable cities and communities*) stated by the United Nations for 2030 agenda. Strict interconnections can be found with other SDGs too.
The capacity of shallow geothermal systems to respond to the climate change challenges while being competitive on the renewable energy sources market was widely demonstrated in the last decades by impressive growth in the number of installations worldwide (Lund and Boyd, 2016; Raymond et al., 2015).
However deep understanding of the geothermal reservoir dynamics is still incomplete, especially in cases where significant density of installations is present. In these conditions indeed the available quantity of energy, namely the geothermal potential, can result to be considerably altered. Such conditions are verified more and more frequently in urban and metropolitan areas that are already subject to the urban and subsurface heat island effect. On the one hand this knowledge gap hampers a clear and robust assessment of the geothermal potential. This prevents public opinion engagement and

interest in stakeholders that have to cope with high initial investments and relevant results uncertainties. On the other hand, rational and balanced use of the geothermal resources cannot be achieved because of the knowledge gap. The lack of a scientific sound base in these resource management issues is increasingly leading to unfairness of the market that is still frequently governed on the basis of a *first come, first served* rule. This is being more and more reflected by interferences among existing and new installations in densely urbanised areas. On the contrary, some portions of the *reservoir* may be inadequately used, with under- or overexploitation.
The present Thesis hence deals with the management of the shallow geothermal resources, specifically addressing the issue of potential assessment in urban areas and its use optimisation. The main purpose of this work is hence of producing useful tools for the definition of the geothermal potential at the district and city scale and for the spatio-temporal optimisation in the use of this underground resource. This objective is pursued by the study of two particular systems: the borehole heat exchangers and a novel energy wall system. Firstly, the site suitability for the installation of a geothermal system will be qualitatively and quantitatively assessed. Secondly the Thesis purpose is relevant in order to allow city planners and policy makers to unlock larger parts of the geothermal potential to make our cities sustainable.

1.2 Aim and objectives

The scope of this Thesis is to contribute in bridging the gap between theoretical geothermal potential and the technically exploitable one. This gap indeed still prevents adoption of city and district scale solutions in geothermal potential use. The development path passes through spatio-temporal optimisation in the resource uses. On the one hand a robust assessment of the site geothermal potential allows for better design of single installation. Better planning of city and district scale solution for governing the rapid underground use increment would result as well. On the other hand the interest was also devoted to the development and testing of a novel system exploiting the very shallow depths through structural elements.
The approach involved theoretical processes development as well as numerical and experimental investigations. Development from a theoretical point of view allowed to base the geothermal potential assessment procedure on two main pillars. These are the georeferred databases and the numerical models. In particular a numerical approach was adopted both for the site scale and the city/district scale by means of proper Finite Element numerical models. On the one hand this allowed to include heat transport mechanisms that are usually neglected in the site specific geothermal potential assessment. On the other hand, numerical modelling allowed to preliminarily apply the theoretically developed methodology to real conditions. Finally experimental investigations allowed to define the efficiency and the impact of a technological solution to optimise the use of very shallow depths.

The following main tasks were undertaken:

- a detailed bibliographic study to identify the state of the art on the technological solutions for shallow geothermal systems and the main methods developed to deal with the potential assessment at the city and district scales;
- the development of a workflow to delineate through integration of georeferred databases and numerical modelling the accurate mapping of real thermal state and of shallow geothermal potential; this allows to optimise the planned use of the resources and achieve higher impacts on the energy balance at the district and city level;
- the extension to the hydrodinamics settings of the field of validity of a semi-analytical formulation for borehole heat exchanger geothermal potential calculation in order to account for realistic site settings;
- the design of a novel energy wall, of its first prototype (together with the experimental apparatus) in the city of Turin and the conduction of an experimental campaign to assess the thermal efficiency and the impact of this technology on the thermal state and on the geothermal potential of deeper devices;
- the assessment of shallow geothermal potential through implementation of the developed procedure on a limited centrally located sector of the Turin metropolitan area in order to define possible optimisation in the future deployment of further installations.

1.3 Plan of the Thesis

The present Thesis is organized in seven chapters and three appendices. Following this chapter that aims at providing a general overview of the relevant issues that were addressed in this work and how they were faced, the next two chapters provide a selected bibliographic study. Chapter 2 focuses on the fundamentals that underlie the shallow geothermal resources but also on the technological aspects. The management, legal and social issues that are related to the rational mining of the heat resource are examined as well with special reference to the urban areas challenges. With the aim of outlining the main aspects related to the assessment of the energy that can be exchanged with the subsurface, Chapter 3 moves from a precise definition of the focus of this study, namely the *technical geothermal potential*, to the critical review of the main methods for potential assessment adopted so far. Advantages and disadvantages in the perspective of the city scale applications and their optimisation in densely populated areas will be analysed in detail.
The second part of the Thesis is instead devoted to the theoretical definition of proper

workflow for the optimisation of the geothermal resources in urban areas. The definition of a procedure that allows to assess the shallow geothermal resources impact at the city scale is here presented and analysed in depth with special reference to the two main elements on which the workflow is based. On the one hand the use of Geographical Information Systems that is the best choice when dealing with spatially variable data. On the other hand the integrated use of numerical models able to catch the real thermal and hydraulic conditions of an area and to predict thermal state in future scenarios. In this chapter main attention is devoted to fully take advantage of these powerful tools. To this end, a detailed parametric study was carried out by means of numerical modelling. This allowed to expand the field of validity to the hydrodynamic conditions of a semi-analytical formula for the definition of borehole heat exchangers technical potential.
In Chapter 5 a novel energy wall system is introduced to the aim of optimising the use of very shallow geothermal systems in urban settings where land scarcity usually prevents such installations. The concept and the novelties related to this particular technology are analysed in general and with reference to a prototype realization in Turin. The settings and the extensive monitoring systems of the experimental site is here analysed together with the interpretation of the experimental campaign, carried out mainly in winter heating conditions. Due to the extensive monitoring network included in the experimental site, a large amount of data was collected. In line with the ongoing transition towards policies of open access to research data (European Commission, 2019), data were listed in Appendix A where each test is described separately.
Chapter 6 collects the inputs from the previous two chapters and applies them to the specific context of the selected study area of Turin central districts. The details and limits in dataset availability and quality are highlighted with reference to the interoperability with the Finite Element numerical code. Results of the modelling phase are then post-processed according to the theoretically developed workflow and aggregated with thermal performances from an hypothetical city-wide application of the above mentioned energy wall system. The chapter hence closes suggesting important implications about the optimisation in future geothermal resource use and about the impact on the energy balance.
Finally, Chapter 7 collects conclusions and recommendations for future research and development.
Data from a dedicated measurement campaign on the hydraulic and thermal values of Turin shallow aquifer are included in Appendix B. Similarly numerical analyses developed for Turin central districts in the framework of the present research are shown in Appendix C in terms of temperatures both on specific points and over the entire area and in terms of geothermal potential.

Chapter 2

Technical aspects about shallow geothermal energy utilization

2.1 Introduction

Renewable energy sources have gained fundamental importance for the modern society during the last decades. Climate change mitigation is strictly related to the development of sustainable energy resources. Transportation, industry and building sectors cover the greatest shares of energy consumption and in turn of greenhouse gases (GHG) emissions. In this framework shallow geothermal energy (SGE) can play a primary role due to its pervasive availability and stability with respect to atmospheric conditions and low environmental impact. These characteristics make the SGE, also known as "low enthalpy geothermal energy", especially suitable for the usage in building heating and cooling.
The aim of this chapter is to describe the usage of shallow geothermal resources in the urban context. After a brief overview on the shallow geothermal energy technologies, heat transfer mechanism are illustrated. Then specific aspects related to the resource management, planning and legal framework are described to introduce the idea of geothermal potential that is the object of the following chapters. In this chapter the expression *geothermal potential* will be used as a synonym of *exchangeable heat*. A proper definition of geothermal potential will be given in Chapter 3.

2.2 Low enthalpy geothermal systems for heating and cooling of buildings

Geothermal energy has been known since ancient times and it has been used mainly for bathing purposes. However geothermal space heating, which is one of the common uses nowadays, was already utilized in ancient Roman times too. These applications are

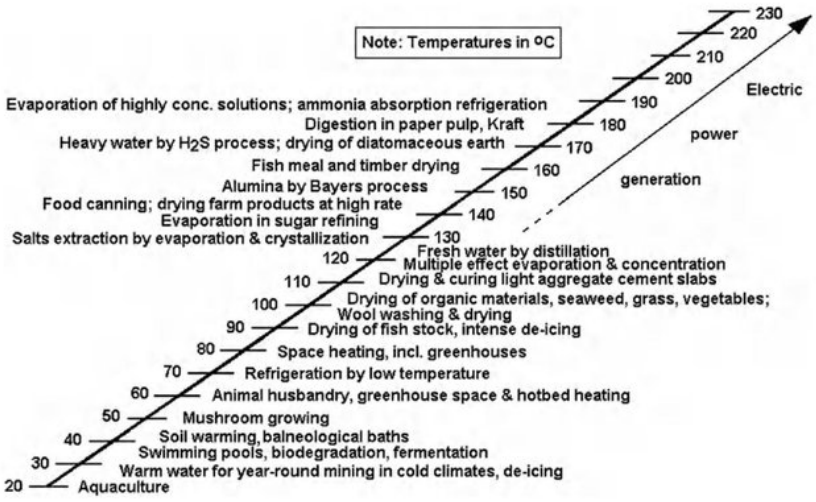

Figure 2.1: Lindal diagram explaining relationship between uses and temperatures (Le-van, 2015).

included among the so-called direct uses which are distinguished from the indirect uses that include power generation. The possible uses of a geothermal system are strictly related to the temperature of the geothermal fluid. This relationship is generally described by the Lindal diagram represented in Figure 2.1.
Recent assessments about direct uses of geothermal energy worldwide highlight a prevailing use for space heating and cooling through Ground Source Heat Pumps with more than 50 GWt of capacity installed in 2015 (Lund and Boyd, 2016). Comparison with previous surveys highlights a strong increase of more than 50% in five years time in the number of units installed.
There is a strong variety in the characteristics of heat extracted from the ground, mainly in terms of temperatures, operational depth and specific energy. To this respect several classification were suggested in the past. They were based on enthalpy, exergy, temperature or depth. This work refers to the distinction of geothermal systems in terms of operational depth. It is generally accepted to name shallow geothermal resources the sources that can be exploited up to a maximum depth of 400 m.
Apart from the depth, the main difference between shallow and deep geothermal resources is the origin of the exploitable heat. Deep resources are characterized by high temperatures due to the heat flux from the inner strata of the Earth. This heat comes from the original formation of the planet and the decay of radioactive elements. By contrast, (very) shallow geothermal systems show low temperatures and are mainly driven by solar irradiance. As a consequence of the above-mentioned mechanism the temperature is constant below 5-10 m depth, not being affected by daily or seasonal air temperature variation (see Figure 2.2).
The penetration of temperature variation in the ground can be indeed described by a

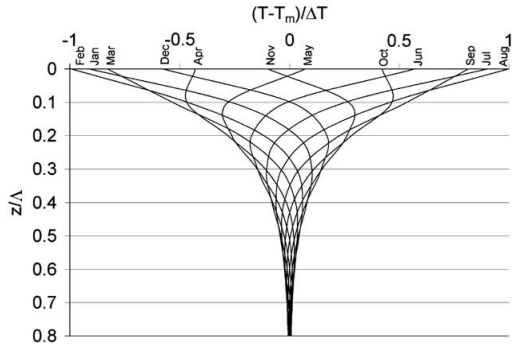

Figure 2.2: Temperature profile versus depth evolution throughout a year (Taylor and Stefan, 2009).

sinusoidal function that is exponentially smoothed while increasing depth (Baehr and Stephan, 1998):

$$T(z,t) = T_m + \Delta T \cdot \exp\left(-\frac{2\pi z}{\Lambda}\right) \cos\left[2\pi\left(\frac{t}{t_0} - \frac{z}{\Lambda}\right)\right] \tag{2.1}$$

with ground temperature T at depth z and time t that is function of the mean yearly air temperature T_m, its variation (ΔT) over time t_0 (one year, expressed as 365 days) and soil thermal diffusivity α through the wavelength of temperature fluctuation $\Lambda = 2\sqrt{\pi \alpha t_0}$. It should be noted in Equation 2.1 the presence of the exponential dampening factor and a phase retardation, both dependant on the depth, due to the thermal capacity of the ground. Hence at about 10-15 m depth the soil temperature is usually equal to the mean annual surface air temperature. This level can be indicated as *homoeothermic depth* (Barbero et al., 2016). Below this depth the temperature increases with a geothermal gradient which usually varies between 1°C to 3°C every 100 m because of the endogenous heat flux.

As a result of the typical temperatures pertaining deep geothermal systems, the ground is treated as a heat source. On the contrary in shallow geothermal systems the subsoil is seen as an exchange and storage medium because of the high thermal capacity.

The most common use of shallow geothermal energy is for heating and/or cooling buildings or infrastructures. Low temperature heating systems require operational temperatures of 35°C to 45°C. Anyway, shallow geothermal systems are characterized by lower temperatures, usually between 5°C and 15°C. Because of their low enthalpy, such systems are not suitable for heating purposes directly. Hence, they are generally coupled with heat pumps which increase the temperature level from the circuit on the ground side to the circuit on the user side. Consequently, the circuit where heat is transferred is duplicated (see Figure 2.3).

On the one hand, the so called *primary circuit* exchanges heat (and, in some cases, mass) with the subsurface. On the other hand the *secondary circuit* exchanges heat with the building. The secondary circuit of the building, because of the low temperature of the

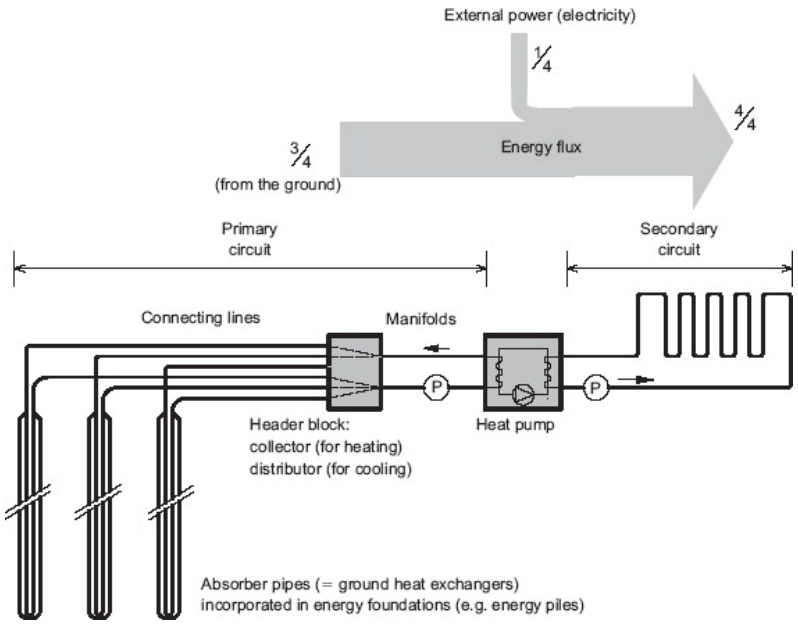

Figure 2.3: Scheme of a geothermal energy plant. A coefficient of performance of 4 is assumed(Brandl, 2006).

heat source, is a fluid-based network which works at low to medium operational temperature (e.g. radiant heating).
As regards the primary circuit a distinction between Closed Loop schemes (CL) and Open Loop schemes (OL) can be done. The main difference is that in latter case there is an exchange of heat and mass by the primary circuit with the subsurface, while in the former case just heat is exchanged. Both closed and open loop are generally indicated as Geothermal Heat Pump systems (GHP) and include a large variety of sources and deployment as shown in Figure 2.4. Closed loop schemes are either indicated as Ground Source Heat Pump (GSHP) systems (Alcaraz et al., 2016; Bayer et al., 2014; Casasso and Sethi, 2014; Erol and François, 2018; Zhu et al., 2010) or Ground Coupled Heat Pump (GCHP) systems (Baek et al., 2017; Carotenuto et al., 2016; García-Gil et al., 2015a; Kalogirou et al., 2015; Luo et al., 2018; Tinti et al., 2016).
On the contrary Open Loop systems can differ depending on the water body they use:

- Groundwater Heat Pumps (GWHPs) or open loop schemes with direct use of water from the subsoil;
- Surface Water Heat Pumps (SWHPs) using surface water bodies as open loop schemes or closed loop ones.

As a rule, Open Loop Systems request lower amounts of electric power to deliver the same heat load. They are characterized by high efficiency levels. The efficiency of a heat pump is synthetically conveyed by the *Coefficient of Performance* (COP) which is

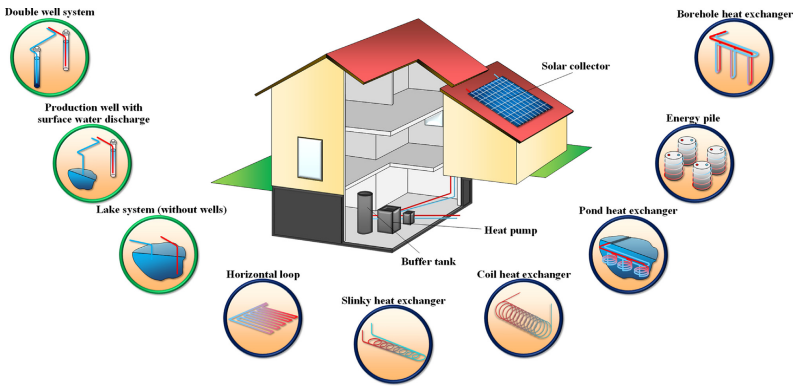

Figure 2.4: Geothermal Heat pump systems overview (Somogyi et al., 2017).

the ratio of energy delivered to the secondary circuit over the energy exchanged within the primary circuit:

$$COP = \frac{energy\ output\ from\ heat\ pump\,[kW]}{energy\ input\ from\ source\,[kW]} \tag{2.2}$$

A geothermal installation needs electricity not just for running the heat pump. Usually there is also electricity consumption due to the circulation pumps that move the heat carrier fluid in the primary circuit. In order to account for all these consumption the Seasonal Performance Factor is defined:

$$SPF = \frac{exploitable\ energy\ output\,[kWh]}{energy\ input\ of\ the\ plant\,[kWh]} \tag{2.3}$$

GWHP and GSHP have their own typical COP and SPF because of a different configuration of the systems. COP and SPF upper limit is represented by the efficiency of the Carnot cycle which is the ideal thermodynamic cycle operated by an heat pump:

$$COP_{th} = \frac{T_H}{T_H - T_C} \tag{2.4}$$

where T_H and T_C are the temperatures of the hot and the cold sides respectively under the circumstances of heating operation mode. It is thus clear that the efficiency of a heat pump is also related to the difference of the temperature level between the user and the source.
The standard components of these systems are described in the following paragraphs.

2.2.1 Groundwater heat pumps

The typical configuration of a GWHP system is made up of (at least) a couple of wells which draw and re-inject water from and to an aquifer. In between the energy of the water is extracted by a heat transfer system, namely the Heat Pump (Figure 2.5).

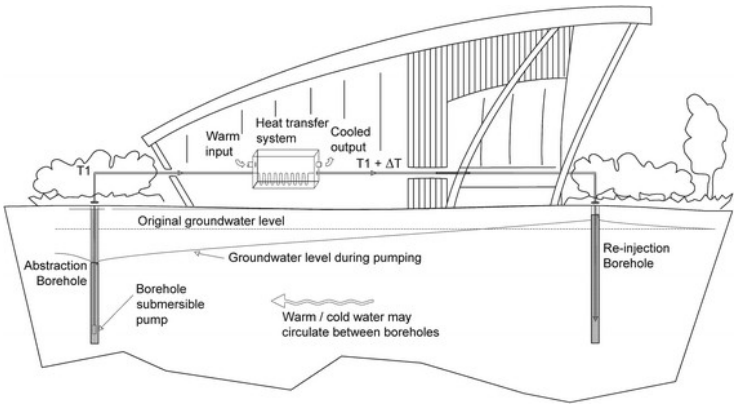

(a)

(b)

Figure 2.5: (a) Scheme of a groundwater heat pump system with a single abstraction borehole well and a single re-injection borehole well (Arola et al., 2014); (b) an injection well head as part of a groundwater heat pump system in Politecnico di Torino.

GWHP systems take advantage of a direct heat transfer from the flowing water to the heat pump and then to the secondary circuit. Thus, these systems have better performance compared to closed loop ones with the same temperature gap. On the contrary, the installation of an open loop scheme requires particular conditions. First of all, the presence of a relatively shallow aquifer with sufficient hydraulic conductivity in order to make possible the water withdrawal at the desired rate. Values of 10^{-5} to 0.1 m/s are referred to be adapt for installation (Arola et al., 2014). Hence only layers characterized by relatively high percentage of coarse grains as gravel and sand deposits are suitable for groundwater heat pump systems (see Table 2.1). It should be mentioned that most of the large urban areas lye on easily accessible aquifers as water supply has always played a relevant role in human activity. By the way aquifer layers are not always sufficiently productive to fulfil GWHP system needs in a sustainable manner. Further detail on legal restraints and sustainability will be given in Section 3.4. Beyond the conductivity, also good groundwater quality is a binding requirement. To this respect chemical properties have to be suitable for the installation of a geothermal energy plant: iron (Fe), Manganese (Mn) but also carbon dioxide and chloride may cause corrosion and clogging to the system (further detail in Section 3.4).
These factors may represent a strong limitation to the installation of GWHP systems, especially in urban and industrialized areas where shallow aquifers are often affected by significant pollution due to the actual and past industrial processes. Moreover, regulations often prohibit installations in areas and aquifers used for drinking water abstraction.
Even in the context of these hampering factor, open loop schemes are commonly used in several countries and urban areas (Barla et al., 2018; Böttcher et al., 2019; Epting et al., 2017a; Herbert et al., 2013).

Table 2.1: Typical hydraulic conductivity values for different geological materials.

Material	Hydraulic conductivity (ms^{-1})
Gravel	$10^{-2} - 1$
Coarse sand	$10^{-6} - 10^{-2}$
Medium sand	$10^{-6} - 5 \cdot 10^{-4}$
Fine sand	$2 \cdot 10^{-7} - 10^{-4}$
Silt, clayey sand	$10^{-9} - 10^{-5}$
Silt	$10^{-8} - 10^{-6}$
Clay	$10^{-11} - 10^{-6}$
Unweathered clay	$10^{-12} - 10^{-9}$
Sandstone	$10^{-10} - 5 \cdot 10^{-6}$

In the favourable conditions of meeting quality requirements and permeability needs, the heat potential Q_{OL} $[J]$ that can be exchanged in the period of time between the start of operation t_s^* and the time t^* is:

$$Q_{OL} = \int_{t_s^*}^{t^*} \dot{m}_w c_w \left(T_{out} - T_{in}\right) dt \tag{2.5}$$

where $\dot{m}_w$ is the pumping rate $[kg/s]$, c_w the specific thermal capacity of water $[J/kg\ K]$, T_{out} and T_{in} the outlet and inlet temperature $[K]$ from the heat pump respectively.

2.2.2 Ground source heat pump systems

Closed loop systems are the most common type of geothermal utilization system due to their ability to be installed almost in every site (Link et al., 2015; Raymond et al., 2015; Sanner, 2016). Hence a lot of studies addressed the issue of determining the achievable exchanged heat with the ground of these installations and the influencing factors (Erol and François, 2018; Hein et al., 2016a,b; Hu, 2017; Javadi et al., 2019; Li et al., 2018; Man et al., 2010; Rivera et al., 2015; Tang and Nowamooz, 2019).
GSHP systems use a circuit of pipes embedded in the ground (often within a concrete grouting) which represent the heat exchanger with the source. Hence there is a reduced risk of environmental damage during the operation compared to open loop systems where mass is passed through the plant. In addition to this, there are no particular technical restriction which prevent the installation of GSHP. Anyway the global efficiency of a GSHP is generally lower than a GWHP because of the multiple heat transfers required.
The heat exchanger pipes can present a variety of shapes. Depending on the way the pipe network is deployed, different closed loop systems can be distinguished: horizontal collectors, geothermal baskets, pond/lake collectors and borehole heat exchangers

(a) (b) (c)

Figure 2.6: Examples of closed loop systems: (a)horizontal collector (source: http://www.we-buildahome.ca), (b)geothermal basket (source: http://www.sunenergybalkan.com) and (c) borehole heat exchanger (source: http://www.grz.ethz.ch) as examples of closed loop systems.

(see Figure 2.6). Within the pipes, usually made up of crossed-linked polyethylene (PeXa), a heat carrier fluid is circulated. The heat carrier fluid is usually water or a mixture of water and antifreeze fluid (glycol).
Among closed loop systems, boreholes heat exchangers (BHE) are particularly known and used. They usually consist of a vertical borehole equipped with single (1U) or double U-shaped (2U) plastic pipes. Also coaxial pipe with annular (CXA) or centred (CXC) inlet borehole heat exchanger exist but are less common.
Especially in the case of borehole heat exchangers the initial investment cost represents an hampering factor. Indeed the need of drilling for the specific purpose of conditioning is in many cases relevant. This is also true, even if with lower incidence, for horizontal or near-surface installations. This latter type of installation needs large areas to be deployed and it is not usually possible in the case of urban areas. Furthermore these installations are less efficient from an energetic point of view. This is mainly related to the very low depth reached that cause influence of the seasonal air temperature variation, according to Equation 2.1.
In GSHP systems, the ground exchanges heat with the heat carrier fluid across the walls of the pipes. Then the fluid is pumped to the heat pump that raises (or lowers in the summer season) the temperature level of the heat so that it can be used by the user that is directly linked with the secondary circuit.
It was previously mentioned that because of the indirect contact of the heat source with the heat pumps, GSHP systems usually present lower COP values compared to Open Loop systems. The performance of an heat pump is influenced by several factors. Among them, temperature difference between the source and the user is of primary importance. It is then advisable to apply GSHP to heating systems with low/medium temperature (in the range of 35 to 45 °C). It is furthermore advisable to maintain the heat carrier fluid temperature in the primary circuit above the 0 - 5 °C level in order to avoid freezing (Anstett et al., 2005).

(a) (b) (c)

Figure 2.7: Examples of energy geostructures: (a) piles (Delerablee et al., 2017) , (b) energy wall (Amis et al., 2011) and (c) energy tunnels (Barla and Insana, 2018).

2.2.3 Energy geostructures

An interesting application of Ground Source Heat Pumps is related to the so-called *energy geostructures* (Adam and Markiewicz, 2009; Barla and Perino, 2015; Brandl, 2006; Laloui and Di Donna, 2013). These are realized by embedding the primary circuit of a CL system in structural elements in contact with the ground. The main advantage of this technology is related to the initial costs. Opposite to the case of borehole heat exchangers, here the drilling (or excavation) costs should be in any case faced for the stability of the structure (or infrastructure) under design. Thus the elements in contact with the ground accomplish both a structural and an energetic function at low extra costs compared to traditional geostructures. As in traditional Ground Source Heat Pumps Systems, the pipes network is connected through an heat pump to the conditioning system of the building or infrastructure and a heat carrier fluid is circulated in the pipe network, usually in turbulent regime (Brandl, 2006).
In general, all kind of geotechnical structure in contact with the ground can be thermally activated. The vast majority of energy geostructures present at this time is represented by energy piles (see Figure 2.7). These structures are partly similar to borehole heat exchangers even if they have larger diameters and shorter lengths. In more recent times also other kinds of structures have been activated: walls and tunnels. The latter structures gained attention in recent years with respect to both the shallow urban tunnels (Barla and Perino, 2015) and the deep mountain tunnels (Tinti et al., 2017b). Nonetheless operational examples are still limited to small sections or experimental fields (Barla et al., 2017, 2019; Buhmann et al., 2016; Franzius and Pralle, 2011). Some examples are documented in literature about energy walls serving big commercial buildings (Adam and Markiewicz, 2009; Brandl, 2016) rather than residential buildings (Sterpi et al., 2018b).
GSHP systems are designed in order to satisfy the heat and/or cooling loads of the users. Thus the dimension of the installation are an output of the design. On the contrary, energy geostructures geometry and dimensions are determined on the basis of

the structural design of the element. On the one hand, the need arises to precisely determine the exchangeable heat rate. On the other hand, the thermal design of the heat exchanger becomes fundamental. Proper thermal design can indeed optimize the quantity of exchangeable energy within given dimension of the structure. Although several studies addressed the thermal performance assessment of energy geostructures, proper handling of transient boundary conditions is still complex especially as regards indoor temperature for tunnels and energy walls (Sterpi et al., 2017). It is thus fundamental to understand the driving parameters, the physics of the heat exchange and the mechanisms that govern the usage of shallow geothermal energy. It was demonstrated that in energy walls most influential parameters are related to geometrical deployment (panel width and pipe spacing), thermal properties (thermal conductivity) and operative conditions as fluid velocity (Di Donna et al., 2016).
In an energy geostructure system three circuits are involved. The first circuit concerns the heat exchange between the soil and the reinforced concrete structure; the second circuit implicates the heat exchange between the geostructure and the heat pump through the heat carrier fluid circulated within the pipes; finally the third circuit delivers the thermal load to the user involving the heat exchange between the heat pump and the heating/cooling plant of the building.
Operational limits of a classical GSHP system are valid also for energy geostructures. It is important to avoid freezing in the ground during heat extraction: in that case soil thermal properties may vary considerably and thermo-mechanical effect may induce larger strains and stresses on the structural element.

2.3 Heat transfer

Shallow geothermal energy systems base their functioning on the principles of thermodynamics. It was mentioned in the previous paragraphs that heat exchange occurs in several points to provide the heating/cooling load required by building occupants.
In heating operation mode, the heat is *moved* from the ground (or directly from groundwater in the case of open loop system) to the circulating fluid and then to the heat pump. On the contrary, in the cooling season the heat pumps disposes heat to the heat carrier fluid and then to the soil.
Even if all the heat transfer physical mechanisms are involved in this process, usually conductive and advective contributions are the most relevant and allow to neglect the rest of the contributions.

2.3.1 Physical mechanisms

Soils are porous media made up of different phases: solid and fluid. Fluid phase can be in turn constituted by either air or water or both of them, depending on the saturation. Most of the conceptual models consider the material as an equivalent continuous

medium composed by the weighted average of the corresponding phases. An assumption that is often made in common applications is the thermal equilibrium of the phases at any time. This assumption makes it possible to use effective thermal properties of the porous medium.
Heat transport in porous media involves conduction, convection, dispersion, radiation and latent heat of evaporation. Nonetheless, some of these mechanisms are neglected since their contribution is order of magnitude lower than others in common operative conditions. Radiation accounts for 1% only of the total energy in usual conditions. Similarly, latent heat flux $\bar{q}_{lat}$ $\left[W/m^2\right]$is described by:

$$\bar{q}_{lat} = L_0 \cdot \rho \cdot \bar{v} \tag{2.6}$$

where L_0 $[J/kg]$ represents the latent heat of phase transformation at the temperature T_0, ρ $\left[kg/m^3\right]$ is the density of the material and $\bar{v}$ $[m/s]$ is the velocity vector.
Latent heat is involved whenever there is a phase transformation. This is usually not the case in geothermal applications. It is in fact advisable during operation to avoid soil and heat carrier fluid freezing, as it would results in damages to the installation. Latent heat should instead be taken into account in unsaturated soils since the condensation and evaporation alter dramatically the thermal conductivity that depends on saturation (Dong et al., 2015). From all the above, heat fluxes related to phase change will be neglected in this work unless otherwise stated.
Thus only advection and conduction are considered in common applications. The former mechanism dominates in the case of absence of groundwater flux and in unsaturated conditions. The heat transferred through conduction $\bar{q}_{cond}$ is described by the *Fourier's equation* that in three dimensions and anisotropic materials can be written as:

$$\bar{q}_{cond} = -\left[\lambda\right] \cdot \nabla T \tag{2.7}$$

where $[\lambda]$ is the thermal conductivity tensor and ∇T is the temperature gradient. This heat transport contribution is always present as it does not imply motion and the driving force is a temperature difference.
On the contrary, advection transfers heat through the movement of mass. It is thus directly linked to the velocity:

$$\bar{q}_{conv} = c \cdot \rho \cdot \bar{v} \cdot \left(T - T_{ref}\right) \tag{2.8}$$

where T_{ref} is a reference temperature and c is the specific heat capacity $[J/KgK]$. Advective heat transport is involved whenever a groundwater flux is present at the site of the installation. In closed loop installations advection also dominates the heat exchange from the material in contact with the ground to the heat carrier fluid that circulates within the pipes. The convective heat flux is indeed proportional to the velocity of the fluid. In closed loop installations, turbulent regime of fluid within the pipes induces a decrease in thermal resistance at the pipe wall and thus allows larger heat exchange and

higher efficiency of the system. However the turbulent regime requires higher energy rates for the circulation pump. Thus, usually the system is run either in turbulent flux or transient regime (Reynold's number in the order of $2.5 \cdot 10^3$).
Whenever there is convective heat transport in the ground, the constituents parts (diffusion and advection) play a significant role, leading to thermal dispersion. The total heat transfer $\bar{q}$ can thus be defined as:

$$\bar{q} = \bar{q}_{lat} + \bar{q}_{cond} + \bar{q}_{conv} \tag{2.9}$$

These energy transportation mechanisms are then involved in the equation of energy conservation law valid for the elementary volume dV:

$$\frac{\partial (\rho \cdot c \cdot T)}{\partial t} + \nabla \cdot \bar{q} = Q \tag{2.10}$$

where the first term represents the time derivative of the thermal energy content, the second term accounts for the heat transfer and Q is any heat source or sink. It should be noted that in most cases specific heat capacity can be considered independent from time with obvious simplification of Equation 2.10.
Advection and convection result in an increase of the thermal exchange. On site measurements are not usually able to distinguish the conductive part in the heat transfer mechanism. Hence advection and dispersion are sometimes included for practical reasons in a global conductive term resulting in an increase of the thermal conductivity of the material. Thus the equivalent conductive term is usually referred as *effective thermal conductivity* and can be calculated as: $\lambda_{ij} = \lambda_{ij}^{cond} + \lambda_{ij}^{disp}$.
Thermal conductivity is defined as a second order tensor. In purely conductive and isotropic media it can be reduced to a scalar quantity. On the contrary in non-isotropic media and whenever non conductive terms are involved, the thermal conductivity tensor components can be calculated as:

$$\lambda_{ij} = \left[n\lambda_f + (1-n)\,\lambda_s \right] \delta_{ij} + \rho_f c_f \left[\alpha_T \,|\bar{v}|\, \delta_{ij} + \left(\alpha_L - \alpha_T\right) \frac{v_i v_j}{|\bar{v}|} \right] \tag{2.11}$$

where subscripts f and s refer to the fluid and the solid phase respectively; n is the porosity; v_i is the fluid velocity component in the i-th direction, $\bar{v}$ the modulus of the velocity vector; δ_{ij} is the Kronecker delta and α_T and α_L are the transverse and longitudinal thermal dispersivities respectively.

2.3.2 Thermo-hydraulic coupling

The heat exchange in a porous medium is a complex phenomenon. In very few cases the thermodynamics can be considered as a stand-alone problem. In porous and multiphase media, temperature variations result in changes in the mechanical, hydraulic and chemical fields. These *physics* in turn may influence the temperature and hence

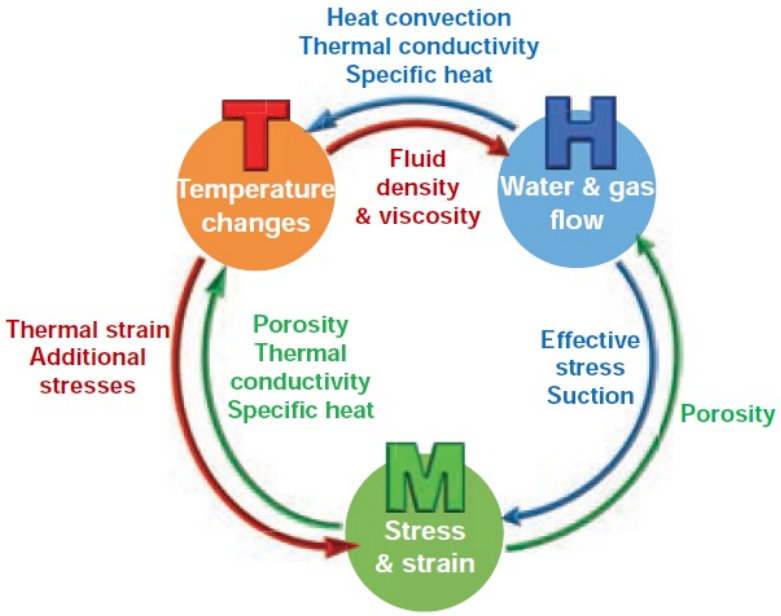

Figure 2.8: Scheme of thermal, hydraulic and mechanical coupling in shallow geothermal energy applications.

the thermal status. This mutual relationship defines the coupled problems. In fact, intensive properties (e.g. fluid density, porosity, dynamic viscosity, specific heat, thermal conductivity, etc.) of the multiphase material vary with state parameters like temperature, hydraulic head and chemical concentration.
The operative temperature range of a shallow geothermal installation is usually kept sufficiently narrow in order to avoid chemical and biological effects on the surrounding soil. These are undesirable effects especially in open loop systems that can be otherwise affected by clogging and corrosion due to mineral precipitation (Arola et al., 2014; Brandl, 2006; García-Gil et al., 2016). For the sake of simplicity, chemo-related aspect of shallow geothermal energy will be neglected in the following.
Thermal alterations lead to changes in soil strength parameters and, in the case of energy geostructures, to additional stresses and induced strains. The thermo-hydro-mechanical coupling is well described in Figure 2.8. Except for energy geostructures and the small volume at the wall interface of a GSHP system, mechanical aspects are usually neglected. In fact these are extremely reduced even at short distance from the installation.
The present work focuses on the coupled phenomena from the thermal and hydraulic point of view which are relevant at the scale of geothermal potential assessment and for *thermal design* purposes. Nonetheless, thermo-mechanical coupling and the structural effects of thermal variation will be analysed with reference to energy walls in Chapter 5. The stronger link between thermal and hydraulic fields is represented by the hydrodispersive components of heat transfer. The velocity of fluid phase appears in

Equation 2.11 indeed. This is in turn determined by the hydraulic head field h through the *Darcy's law*:

$$\bar{v} = [K] \cdot \nabla h \tag{2.12}$$

where $[K]$ is the soil hydraulic conductivity second order tensor. Also the fluid density, can be regarded as a function of the temperature T and pressure p:

$$\rho_f = \rho_f(p, T) \approx \rho_{f,ref} \left[1 + \tilde{\gamma} \cdot \left(p - p_{ref}\right) - \tilde{\beta} \cdot \left(T - T_{ref}\right)\right] \tag{2.13}$$

where the dependency on the chemical species concentration is neglected. It should be noted that fluid density variation implies a proportional change in the specific heat capacity value ρc. In Equation 2.13, $\tilde{\gamma}$ denotes the fluid compressibility, $\tilde{\beta}$ is the fluid thermal expansion coefficient and the subscript *ref* indicate reference conditions. Anyway $\tilde{\gamma}$ and $\tilde{\beta}$ cannot be considered constant in most of the practical cases (Diersch, 2009). Also dynamic viscosity dependency on the temperature has to be accounted in geothermal applications: $\mu_f = \mu_f(T)$. This dependency is usually modelled in terms of empirical relationships (Huber et al., 2009).
Thus, whenever the advection becomes relevant, e.g. in the presence of groundwater flow at the site of installation, thermo-hydraulic coupling has to be accounted and the hydraulic field must be solved in order to properly assess the exchangeable heat with the geothermal system.

2.4 Geothermal resources management

The physics of the thermo-hydraulic problem is relatively complex. However, the physical and technical aspects are not sufficient to determine the exchangeable heat over a territory. Conflicting interests and mutual dependency with other social, environmental, economical and technical factors should be considered to properly handle this assessment issue. Some of these aspects are particularly relevant in urban areas where population density is higher. In this perspective management is strictly related to the identification of main strategies in the shallow geothermal energy field. In particular a proper management should comprise the identification of policies, objectives, strategies and measures that are iteratively calibrated and adapted to the territorial context of application (García-Gil et al., 2020). Especially in this context the legislation should balance opposite interests for the sake of long term community well-being but also efficiently prevent environmental damages, long term depleting of the resource.

2.4.1 Legislation aspects in Italy and in Europe

Italy, being part of the European Union, regulates the shallow geothermal energy by transposition of European Directives. Anyway, this transposition is not complete and

the legislative scheme is complicated by concurrent legislative competences. Thus regional authorities legislated with partly different requirements with respect to neighbouring territories. Moreover, some administrative bodies still lack of local legislation concerning geothermal energy. The superposition of national and regional laws and regulations lead to an heterogeneous and fragmented legislative framework at the national scale (Tsagarakis et al., 2018). This is even more noticeable when dealing with different nations within Europe.
Italian classification of geothermal energy is based on *enthalpy* and thus on the resource temperature. It should be noted that there is not a perfect agreement about the limit temperature among low, medium and high enthalpy classes and different authors suggested slightly different threshold temperatures (Lee, 2001). Italian national law (Legislative Decree 11st February 2010, n. 22, 2010) is in line with the classification of Muffler and Cataldi (1978): geothermal fluid temperature lower than 90°C identifies low enthalpy geothermal resources. *Small local utilisations* are identified as those satisfying two requirements:

- Capacity lower than 2 MWt;
- Maximum depth reached lower than 400 m.

Moreover vertical borehole heat exchangers are classified as small local utilizations too. According to the principle of article 13 of the European Directive 2009/28/EC (European Parliament; European Council, 2009), these installations can benefit from simplified authorization procedures.
Regulation and administrative process is in charge of Regional or other delegate authorities for these simplified procedures. Some regions, mainly distributed in the southern Italy, still lack of proper regulations. Amongst others, Lombardia has one of the most comprehensive approaches identifying closed loop systems shallower than 150 m subject to simplified procedures and to compulsory registration to a regional inventory. In Piemonte region, that comprises the area that will be used as the case study in Chapter 6, a similar approach was suggested. Nonetheless, the regional inventory still not has been established. Thus information on the number and location of closed loop schemes is missing at the date of writing (Barla et al., 2018).
As previously mentioned shallow geothermal systems require in most cases drilling work. In the case of Open Loop systems, water wells have to be drilled too. Hence, in the absence of regulations particularly focused on GSHP or GWHP, these installation are subjected to the restrictions that are typical for the construction works of their components. Indeed, both groundwater withdrawal and reinjection have to be authorized in the case of open loop schemes. Furthermore these two interactions with groundwater follow separate bureaucratic paths.
Common requirement about GWHP systems is the injection of abstracted groundwater back to the same aquifer. This is intended to avoid groundwater level depletion. Furthermore groundwater is usually taken from shallower aquifers that are not used as

Country	Protection of groundwater as a resource for drinking water	Leakage of hazardous materials	Changes in groundwater ecology	Hydraulic contacts between different aquifer systems	Accumulation of temperature changes	Interaction with other shallow geothermal systems
Croatia	✓					
Cyprus						
France	✓	✓	✓	✓		
Greece	✓	✓				
Italy	✓	✓		✓	✓	
Latvia	✓					
Lithuania	✓					
Poland	✓	✓		✓		
Portugal	✓	✓	✓			
Serbia	✓	✓	✓			✓
Slovenia	✓	✓	✓			
Spain	✓	✓	✓			
Sweden	✓	✓	✓	✓	✓	✓
Turkey	✓	✓				

Figure 2.9: Criteria considered in 14 European countries in authorisation process for shallow geothermal installation (Tsagarakis et al., 2018).

drinking water supplies. Drilling must be performed carefully and must ensure sealing in order to avoid contact and mixing of water from different aquifers. Regarding closed loop schemes, an harmless heat carrier fluid should be preferred. This is a mandatory requirement in several areas (e.g. Lombardia, Piemonte and Provincia Autonoma of Bolzano). The fluid has also to be biodegradable in order to avoid environmental damages in case of leakage from the pipe circuit. This kind of requirements is quite common also in other european countries (see Figure 2.9). Neither closed loop installation can be drilled within *water protection areas*, comprising the surroundings of drinking water supply wells and their recharge areas (e.g. map of the Piemonte region in Figure 2.10).
These spatial constraints need to be considered whenever assessing the exchangeable energy with the ground (see Chapter 3). What is more, the Civil code regulates minimum distances of some buried structures and wells. Also BHE are encompassed in these restrictions, depicted in Figure 2.11. These spatial constraints have different values even moving from Italy to rather similar countries, like Greece (Tsagarakis et al., 2018). By the way homogeneity in legislation is far from being achieved at the European level. Indeed in some countries, like Austria, Germany or Switzerland, it is required that the temperature changes are limited within a certain range at a given distance from the installation. On the contrary, in Finland, even though it has a strong background in water protection, such a limitation is not imposed. From all the above, the need arises of common approach to the SGE at different legislation levels. Standardization should involve the local authorities starting from the national and international laws (e.g. European Union). This can adequately sustain and foster the use of shallow geothermal energy. Also planning tools as maps (e.g. traffic-light maps) can help to overcome the uncertainty experienced both by authority bureaus and stakeholders. Uncertainty and bureaucracy represents indeed one of the hampering factors to the market of SGE.

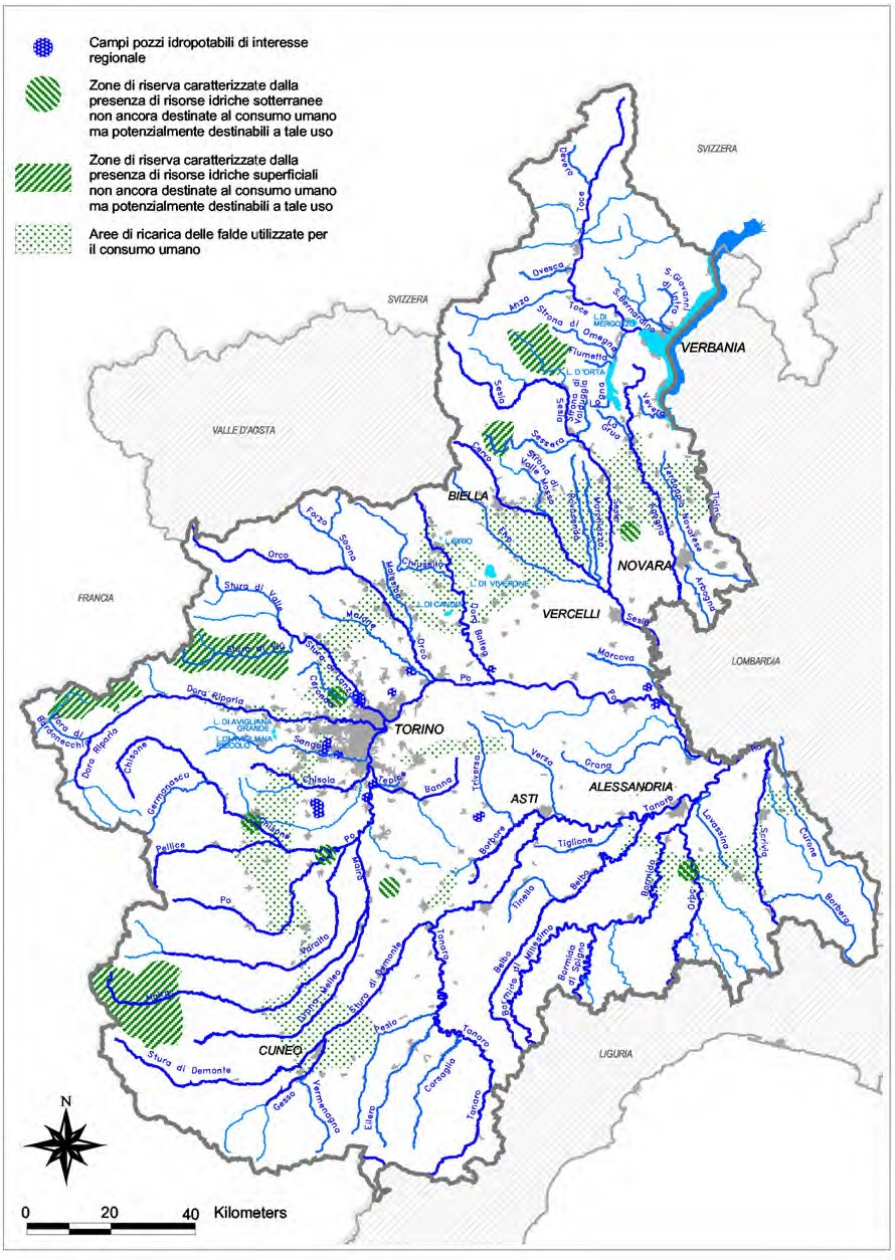

Figure 2.10: Protection areas for drinking water supply in Piemonte Piemonte regional authority (2007).

2.4.2 Interaction at the district and city scale

Shallow geothermal systems exchange heat with the ground during operation. Even if the heat transfer has been deeply studied, the impact of multiple geothermal installations on the subsurface in the long term is still not fully understood.

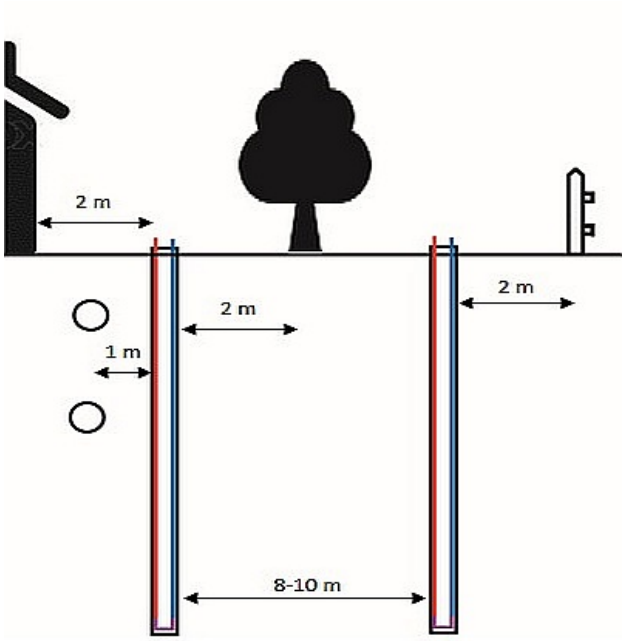

Figure 2.11: Spatial restraints for OL wells and BHE installation. Limits are valid in the Piemonte region from the combination of Director of the environment and territory protection of Piemonte region (21/04/2016) and Civil Code of Italy, Art 889 (1942).

In shallow geothermal energy applications the ground is regarded as an energy sink or an energy source, depending on the season. In the case of combined cycle, the ground can be also used as a seasonal heat buffer, namely a storage medium. The heat exchange induces thermal alterations in the surrounding ground. It is conventionally accepted to name *thermally affected zone (TAZ)* the area that experience a temperature variation higher than a threshold value. This value is usually assumed as 1 K (Barla et al., 2018; Lo Russo et al., 2014; Piga et al., 2017; Somogyi et al., 2015).
Thermal alteration spreading is extremely relevant as system efficiency depends also on the site temperature. In urban areas where significant density of installations is possible, an installation can cause an interference on another installation. Also other heat sources (see Section 4.2.3) can induce thermal interference on shallow geothermal energy systems.
The temperature at the extraction well is the most significant parameter in open loop systems. This parameter can be altered either by an external source or by the other well of the installation itself (the system is actually an hydraulic dipole). In the latter case a distinction between thermal feedback (if the injection temperature is fixed) or thermal recycling (if the temperature difference is fixed) was suggested by Milnes and Perrochet (2013). Proper knowledge of the site and consequent design is crucial to avoid these internal interference phenomena; in simple cases, analytical solutions are available to

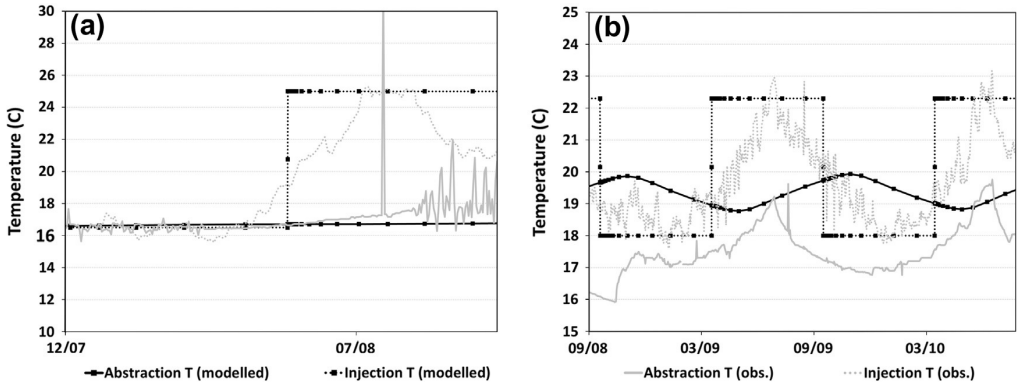

Figure 2.12: Thermal interference effects on an open loop extraction well temperature in the case of (a) thermal feedback, where injected hot water is captured again by abstraction well, or (b) external interference where temperature of abstracted water is influenced by other sources and cannot be related to the injected temperature (Herbert et al., 2013).

calculate the time and magnitude of thermal breakthrough of a well doublet:

$$t_{f,th} = -\frac{d_w \cdot \rho \cdot c}{v_w \cdot \rho_w \cdot c_w} \cdot \left[1 + \frac{4\zeta}{\sqrt{-1-4\zeta}} \arctan\left(-1-4\zeta\right)^{-0.5}\right] \tag{2.14}$$

where d_w is the distance between wells, ρc refers to the aquifer thermal capacity, the $\rho_w c_w$ refers to the water thermal capacity and ζ is $\dot{m_w} \cdot \left(2\pi v_w BL\right)^{-1}$, with B that is the aquifer thickness. Thermal recycling takes place only in the case also hydraulic recycling happens. Moreover the first phenomenon is retarded of a factor R_{th}:

$$R_{th} = \frac{\rho c}{n_e \cdot \rho_w c_w} \tag{2.15}$$

where n_e is the effective porosity that accounts the fraction of the pore system (V_e) that is interconnected and permits fluid flow within the reservoir volume V_r (Bear, 1988):

$$n_e = \frac{V_e}{V_r} \tag{2.16}$$

In most cases the maximum temperature for reinjected water of an open loop system is imposed for environmental protection reasons. Thus thermal feedback results to affect the exchangeable energy that is directly dependent on the extracted water temperature (see Equation 2.5). Thermal interference can involve also external causes, either for open loop schemes or closed loop ones (see Figure 2.12).To this regard, it is important to notice that in the case of several installations in the same area, the same reservoir is used. Being its capacity a finite quantity, interferences may arise. These interactions can be either disadvantageous or beneficial, depending on the physical quantity altered and on the cycle of each installation. Interaction were detected in some urban areas

like London (Fry, 2009; Herbert et al., 2013) and Turin (Barla et al., 2015, 2018).
While intra-installation interference can be due to a combination of poor design of the installation and land scarcity, inter-installation interference happens whenever the TAZ of an installation interest the site of a second installation (as in Figure 2.12b). It is thus clear that the higher the density of installations, the higher the risk of interference. Urban areas usually present land scarcity issues (Ryżyński and Bogusz, 2016) and thus are affected by elevated interference risks.
In the case of bi- or tridimensional energy installation (e.g. energy geostructures or, to some extent, dense borehole heat exchanger fields), also hydrological interference like dam effect may happen. In this case, groundwater level and groundwater flow direction and velocity result to be altered and affect the heat transfer, mainly in the advective components.
It is worth to notice that soil-atmosfere interaction may play an even more relevant role in urban areas due to the Urban Heat Island effect. Surface sealing and increased temperature are reflected in raised ground and aquifer temperatures (Epting and Huggenberger, 2013). Anthropogenic heat sources, including transportation tunnels, sewage and district heating network, deep basements, can be relevant indeed (Benz et al., 2015; Epting et al., 2017b).
These factors complicate the handling of a rational geothermal resource management. Indeed the deep understanding of heat and hydraulic regime is of primary importance to avoid reservoir overexploitation as well as conflicting uses (García-Gil et al., 2020). Interactions are typically far from being steady state and these heat fluxes are strictly related to spatial distributions (e.g. placement of district heating pipes, building and district layouts, etc.). This latter aspect makes reasonable the use of proper tools to handle the spatial variability. The main and most reliable tool to handle spatial planning issues nowadays is represented by *Geographic Information Systems* that are described in the following paragraph.

2.4.3 Planning tools: Geographic Information Systems and maps

Urban areas are experiencing high development and are increasingly attracting people: 55% of world population was living in urbanized areas in 2018 (United Nations, 2018). In this perspective the rational planning of urbanisation and its relation to the territory is becoming more and more compelling and complex. Complexity arises due to the multiple aspects that influence and constrain the urbanization and reshaping process of cities. In this respect, urban planning is a typical example of *wicked problem*.
One of the several issues that compose this problem is also the energy planning of cities, both from the point of view of the distribution grid and of the energy production. To this respect the technology development is pushing to renewable and distributed energy sources (e.g. solar, shallow geothermal, micro-aeolian, etc.) and standard users will be replaced by an high number of *prosumers* (customers that become small producers). Since these energy sources are dependant on a series of site-specific factors, the

Figure 2.13: Historical map of a portion of the city of Turin in 1866 (Source: Archivio di Stato di Torino).

energy planning and management is getting more and more connected to the spatial planning.
In order to handle this complexity, spatial planning take advantage from the representation of quantities and entities on scaled reproduction, namely *maps*. These maps may include different kind of information depending on the scope they are developed. Especially in the urban context the complexity of several different kind of data can be better interpreted with the aid of thematic maps.
Maps originate from the acquisition of data of the territory obtained through measurements and surveys. These data are then transposed and replaced by a representation on the maps.
Natural evolution of hand made traditional cartography (on paper, see Figure 2.13) was automatic cartography where the use of technology was limited to the drawing phase on the sheet of paper. After that, technology development enabled to digitize the information thus leading to digital maps. The digitalisation of the information, being georeferenced to a particular coordinate systems, lead to important benefits with respect to traditional cartography. Datasets present an accuracy dependant on the acquisition technique and not on the support (representation scale of the paper). Secondly, entity location can be coupled with several non-spatial information realizing a connection of geometry to data. Digital information storage and handling is thus based on computers but an information system (a database) needs also tools, softwares and people to be properly named Geographic Information System (GIS). Geographic information system enable collection, management, storage, processing, analysis and distribution of data that are spatially located. This latter feature distinguish a *normal* database from a GIS. Thus GIS comprises, beyond the representation of objects (*entities* being points, lines or polygons or *raster* dataset) and their location, also other information like attributes, descriptors (*metadata*) and relationship among objects. A GIS is a special relational database.

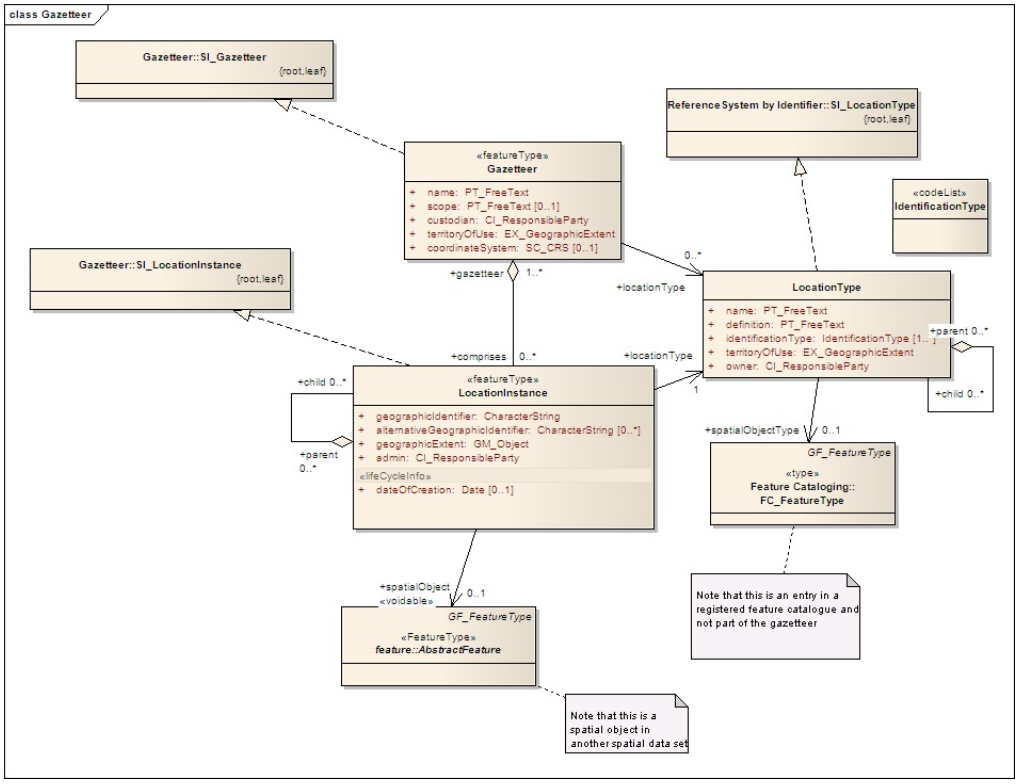

Figure 2.14: Formal representation of an Entity-Relation model according to INSPIRE Specification where classes of information are grouped and the link and their cardinality is clearly visible (INSPIRE Thematic working group Geographical Names, 2014).

GIS are nowadays used for a variety of applications from fleet management, to emergency response dispatch, to urban planning, etc. Depending on the aim of the GIS, the architecture of the system should be planned accordingly. Indeed GIS include an ideal representation of real world objects. Some simplification to the reality has to be performed in order to achieve a structure that is manageable by informatics systems. Hence a modelling process proceeds from an *external model* that selects the objects to be represented and the operations that can be done on them to a *conceptual model*. Conceptual model translates in terms of standardised and formal language the features highlighted in the external model. Typical example of this kind of standardisation is the entity-relationship (ER) model (as shown in Figure 2.14) where it is possible to clearly visualize the links between objects and the *cardinality* of such connections. The GIS is thus realized through further standardization in the logical model and finally *translated* in the internal model that is directly used by the computer.
Thus GIS is a powerful tool that can help to handle not only geo-referred geometries but also a multitude of related information. Furthermore the GIS softwares include a set tools able to perform operation on data and elaborate them. This aspect is of particular interest in scenario definition (elaboration of present or future or even *virtual*

properties). Also the ability of performing complex map algebra is of extreme importance to elaborate and assess quantities that are known from the integration of datasets of different nature. A perfect example of such a quantity is represented by the geothermal potential that is the focus of this work and will be in depth discussed in the next chapter.

2.5 Summary

Shallow geothermal energy systems have experienced high evolution in last decades differentiating the kind of installations (e.g. GSHP, GWHP and energy geostructures) and their shape. Thermal design of these systems is based on thermodynamics concepts. Whereas heat transfer mechanisms are well known (e.g. conduction, convection, radiation), non-linearity and coupling of thermal and hydraulic problem at the district and city scale triggers the need to use numerical methods. Indeed the increasing efficiency of Shallow Geothermal Energy systems fosters its use and creates the precondition for urban centres to show significant system density. Whereas the thermal design of SGE system focuses on stand-alone installation, in such a scenario interaction among facilities cannot be neglected. Management and planning of subsurface resource usage represents thus a wicked problem that involves several and conflicting aspects. Legislation should then appropriately evolve from present situation to carefully counterbalance environmental, social and economic interests. Implementation of proper tools (e.g. Geographic Information Systems) in a similar context can lead to resource usage optimisation and to a fair market for the underground resource. Basic requirement to achieve this goals is assessment of the amount of available energy, namely the *geothermal potential*, in the territory. Methods and techniques that allow to evaluate these quantities are in depth analysed in the following chapter.

Chapter 3

Geothermal potential assessment methods

3.1 Introduction

Shallow Geothermal Energy (SGE) systems can be installed virtually everywhere. Limitation to their deployment is usually introduced to prevent conflicting uses of the subsurface (as for water resources protection) or because of particular geological formations. This is the case of karst rocks that can originate relevant ground displacement at the surface and thus generate damages to the built environment. These limitations hence define areas where exchangeable heat at the site is null. Apart from these areas, the quantification of exchangeable energy is more complex. The more energy is available the more the complexity lies in its determination. However the exchangeable heat available, namely the geothermal potential, is strictly linked to the competitiveness of the energy resource which is the first indicator to arise stakeholders interest.
This chapter aims at defining in detail the geothermal potential and the state of the art in its determination. By the end of the chapter it will be clear that geothermal potential definition is not unique and that it is possible to name *potential* different quantities. Once clarified the definition that is adopted in this work, comparison of methods for geothermal potential assessment will be presented. They will be showed referring to the two main families: qualitative and quantitative methods. Attention will be focused on closed loop systems and especially on Borehole Heat Exchangers unless otherwise stated.

3.2 Definition of geothermal potential

Up to this point, the term geothermal potential has been used in the general meaning of exchangeable heat. Anyway a clear definition of this quantity is arguable. In previous literature even the measure unit is not unique (Bayer et al., 2019). It has been addressed

as energy, specific energy per area or volume or even power (energy over time).
In the context of geothermal resources, the potential has the physical meaning of energy that is available in a defined domain over a defined time period. According to Rybach (2015) this quantity can be named *theoretical potential* or *heat in place*. It represents an enormous quantity that however cannot be fully exploited, neither in the perspective of technological evolution.
Its determination can be simply derived by the definition of the heat capacity of a reservoir of given volume V_r:

$$E_{th} = \left[n \cdot \rho_w c_w + (1-n)\,\rho_s c_s\right] V_r \left(T_0 - T_1\right) \tag{3.1}$$

where $\rho_s c_s$ represents the volumetric heat capacity of the solid phase of the soil. It is thus clear that theoretical potential is based on the assumption of being able to bring the full volume of a reservoir from the natural (mean) temperature T_0 to the one pertaining the extraction/injection system T_1, neglecting the spatial distribution of heat and especially the fact that the reservoir is not a physically enclosed system. Lateral fluxes resulting from un-stationary boundary conditions (e.g. air temperature, hydrologic regime, etc.) thus would suggest to postulate the previous definition of the heat in place as a balance equation including recharge and storage terms in time dependent derivative form.
In this perspective, also the quantification of heat that is instead brought by lateral fluxes can be assumed as theoretical potential. In the case of a reservoir that is hosted in aquifer levels, the main heat flux is represented by the recharge and the discharge operated by groundwater entering and exiting the reservoir domain. Epting et al. (2018), based on the results of numerical 3D thermal and hydraulic models, evaluated the available heat in place beneath the city of Basel (Switzerland):

$$E_{th} = q_D \cdot \rho_w c_w \cdot \Delta T \cdot t \tag{3.2}$$

In this case proper numerical models allow the spatial determination of the ambient temperature T_0 and the hydralic fluxes q_D $\left[m^3/s\right]$ interesting the reservoir during the time period t.
The complexity of potential determination dramatically increases as a result of heat injection and extraction and other anthropogenic effects, such as the *subsurface urban heat island* (SUHI) that has been experienced in a lot of cities (Barla et al., 2018; Herbert et al., 2013; Liu et al., 2011; Lokoshchenko and Korneva, 2015; Menberg et al., 2013). All these aspects lead to an extremely complex transient thermal regime where also the ground thermal properties are heterogeneous and affected by large uncertainties.
On the contrary, some studies that better focused on the anthropogenic heat fluxes demonstrated that SUHI heat can fulfil cities energy requirements (Ferguson and Woodbury, 2007; Zhu et al., 2010).
Due to the aim of this work, the focus will be put on the part of energy that actually can be used by mean of available technology (mainly borehole heat exchangers). It is thus

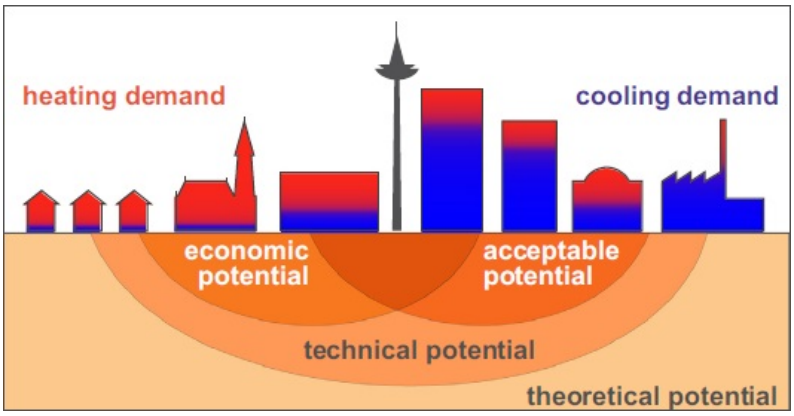

Figure 3.1: Geothermal potential definitions referred to the urban context (Bayer et al., 2019).

clear that this power is just a fraction of the total amount of the thermal content that is stored within the subsurface. Because of unavoidable administrative and technical limitations a fraction of the theoretical potential cannot be seen as an available resource. The remaining part can be named *technical potential*. Technical potential hence refers to the energy that can be used given a specific technology.
However, the technically reachable heat is unlikely to be used as it is economically not convenient. As mentioned before, economical convenience is also determined by comparison with other accessible energy sources. The part of geothermal energy that leads to overall costs that are lower than the other sources available define the *economical potential*. This part of the theoretical potential is hence the part that can be directly exploited at current market conditions.
It was previously mentioned that excessive usage of subsoil for thermal purposes can lead to conflicting uses but also to depletion of the resource. Thus, in order to avoid these drawbacks it might be reasonable or compulsory by regulation, to exploit just a part of the economic potential. It should be noticed that in case of excessive use of the resource, the economic potential usually decreases over time because of the additional costs related to heat pump electricity consumptions. On the contrary, the evaluation of the economic potential can be positively affected in the case that also externalities costs are taken into account. In both cases this potential can be named *acceptable potential* (Bayer et al., 2019). A schematization of the different kinds of potential above mentioned can be seen in Figure 3.1.
In this work, the main focus is devoted to the technical potential. Thus the term *geothermal potential* will refer to this quantity unless otherwise specified.
Beside these definitions, potential is often used as an indicator for assessment of site suitability to host a geothermal installation. Indeed the geothermal potential basically depends on the site specific characteristics once that the technical properties of a *benchmark* installation have been defined. This quantity can thus define the best areas where to invest in geothermal energy, in a comparative perspective with other energy sources.

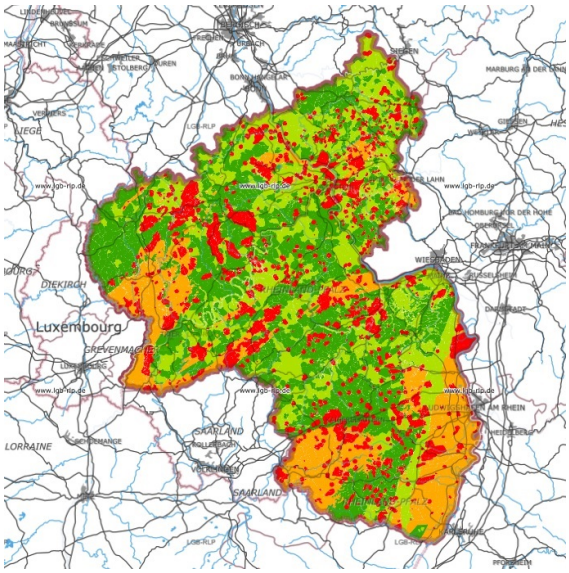

Figure 3.2: An example of qualitative geothermal map based on legal requirements and hydrogeological conditions in the region of Rheinland-pfalz. Red areas delineate regions where borehole heat exchangers cannot be installed except for exceptional cases (Source: LGB-RLP.de).

On the other hand, being dependent on the site properties, geothermal potential is usually highly uncertain in its quantification. This is the main reason for lot of assessment methods being limited to just qualitative evaluation. These latter methods represent mainly a dissemination tool to foster the public engagement on this kind of green energy.
In the following section some qualitative methods will be examined with regards to both open loop systems and closed loop ones.

3.3 Qualitative assessment methods

Geothermal potential depends on a variety of factors that are highly uncertain and hard to be determined by measurement. Moreover, even in the case of relatively small areas to be investigated, quantification of the underground properties involves significant costs. Due to these difficulties, just comparative evaluations are sometimes conducted. Therefore the result of mapping can be the indication of the most suitable technology to exploit shallow geothermal energy as described for example in Hamada et al. (2002) where a Geospatial Decision Support System was developed. It is furthermore envisaged to proceed for a qualitative mapping as a first step before the quantification of the geothermal potential.
In the category of qualitative maps the ”traffic light maps” are included (an example is shown in Figure 3.2). These highlight the best locations for shallow geothermal energy utilization. These maps are usually based on the ranking of the properties of bedrock

or subsurface layers up to a certain depth (about 100-200 m). This kind of map also indicates areas where shallow geothermal energy cannot be used because of legislative or technical restrictions (e.g water protection areas, buffer areas around structures, etc, as explained in Chapter 2).
As previously mentioned, geothermal potential is affected by several factors. While maps regarding a single influential factor have just minor sensitivity to the operators choices, whenever multiple factors are considered the subjectiveness influence rises. In this perspective, the development of decision support tools has been accurately treated with the use of techniques as Multi Criteria Decision Analysis (MCDA). In such evaluations, even when starting parameters are to some extent quantitative, they have to be reduced to a common *measurable* unit. An example of such a structured approach combining the Analytical Hierarchy Process to MCDA for the assessment of local suitability to shallow geothermal energy systems can be found in Tinti et al. (2018). By adoption of this kind of approach indexes that are mapped and then combined together to derive comparative and qualitative evaluation of geothermal potential that can be technically exploited, usually in the form of traffic light maps.
This kind of maps cannot directly be used for the feasibility study of a geothermal installation but is most often used by city planners to highlight the presence of favourable or unfavourable conditions. Furthermore the traffic light symbolism is easily comprehensible for laypersons, representing a good dissemination and promotional tool.

3.3.1 Open loop systems

Open loop systems rely on the availability of an adequate amount of groundwater to withdraw from the subsurface. In general this requirement can be translated into practice with minimum hydraulic conductivity in the subsurface that has to be higher than 10^{-5} m/s (Sanner et al., 2001).
Concerning the groundwater resource, the theoretical potential can be assumed as the heat content of the water within a reservoir. In the case of groundwater fluxes, Equation 3.2 can be used. It is thus obvious that the basic criteria for usage of open loop systems lies in the water quantity available and in its temperature.
By the way, also technical factors should be taken into account to assess the possibility to use such a resource. Among them, the water quality plays a major role. In fact, being the wells and the heat pump directly in contact with groundwater, technical risks of bad water quality include corrosion, incrustation and clogging affecting the system components. Crucial importance is thus given especially to the acidity of soil and presence of heavy metals, as highlighted in several regulation like the Japan Refrigeration and Air Conditioning Industry Association standard (see Figure 3.3). In order to estimate viability of a site for GWHP installation the Langelier index I_l is commonly used in practice (Milenić et al., 2010) where the acidity of groundwater is evaluated through its content of calcium, hydro carbonate and the dry residue.

	Item	Cooling water			Cold water		Hot water				Tendency	
		Circulating water system		transient system			Lower Hot water system		Higher Hot water system			
		Circulating water	Makeup water	transient water	Circulating water [Up to 20℃]	Makeup water	Circulating water [20～60℃]	Makeup water	Circulating water [60～90℃]	Makeup water	Corrosion	Scale genesis
Standard Value	pH (25.0℃)	6.5～8.2	6.0～8.0	6.8～8.0	6.8～8.0	6.8～8.0	7.0～8.0	7.0～8.0	7.0～8.0	7.0～8.0	○	○
	electric conductivity (mS/m)	up to 80	up to 30	up to 40	up to 40	up to 30	up to 30	up to 30	up to 30	up to 30	○	○
	chloride ion (mg/ℓ)	up to 200	up to 50	up to 50	up to 50	up to 50	up to 50	up to 50	up to 30	up to 30	○	
	sulfate ion (mg/ℓ)	up to 200	up to 50	up to 50	up to 50	up to 50	up to 50	up to 50	up to 30	up to 30	○	
	M alkali level (mg/ℓ)	up to 100	up to 50	up to 50	up to 50	up to 50	up to 50	up to 50	up to 50	up to 50		○
	total hardness (mg/ℓ)	up to 200	up to 70	up to 70	up to 70	up to 70	up to 70	up to 70	up to 70	up to 70		○
	calcium hardness (mg/ℓ)	up to 150	up to 50	up to 50	up to 50	up to 50	up to 50	up to 50	up to 50	up to 50		○
	ionized silica (mg/ℓ)	up to 50	up to 30	up to 30	up to 30	up to 30	up to 30	up to 30	up to 30	up to 30		○
Reference	iron (mg/ℓ)	up to 1.0	up to 0.3	up to 1.0	up to 1.0	up to 0.3	up to 1.0	up to 0.3	up to 1.0	up to 0.3	○	○
	copper (mg/ℓ)	up to 0.3	up to 1.0	up to 1.0	up to 1.0	up to 1.0	up to 1.0	up to 0.1	up to 1.0	up to 0.1	○	
	sulfide ion (mg/ℓ)	Not to be detected	Not to be detected	Not to be detected	Not to be detected	Not to be detected	Not to be detected	Not to be detected	Not to be detected	Not to be detected	○	
	ammonium ion (mg/ℓ)	up to 1.0	up to 0.1	up to 1.0	up to 1.0	up to 0.1	up to 0.3	up to 0.1	up to 0.1	up to 0.1	○	
	residual chlorine (mg/ℓ)	up to 0.3	up to 0.3	up to 0.3	up to 0.3	up to 0.3	up to 0.25	up to 0.3	up to 0.1	up to 0.3	○	
	free carbon dioxide (mg/ℓ)	up to 4.0	up to 4.0	up to 4.0	up to 4.0	up to 4.0	up to 0.4	up to 4.0	up to 0.4	up to 4.0	○	
	stability index	6.0～7.0	–	–	–	–	–	–	–	–	○	○

(1) The item appellation and its difinition and the unit belong to JIS K 0101.
(2) The "○" marks in the chart show the factor relevant to corrosion or scale genesis.
(3) When high temperature (over 40℃) ; generally, using corrosive steel, materials which have no protective coating against water, anticorrosive measure shall be done such as adding corrosion prevention material, degasser and etc.
(4) Under the Cooling water system with hermetically-closed cooling tower; the closed-circuit circulating water and its Makeup water are based on Hot water standard, spreading water and its Makeup water are based on circulating Cooling water system.
(5) Supplied / replenished water needs to be tap water or industrial water or groundwater.
Deionized water, regeneration treated water and softening treated water are excluded.
(6) Upper 15 items are shown as a typical factor for corrosion and/or scale genesis.

Figure 3.3: Water quality standard for cooling water, cold water, hot water and makeup water according to Japan Refrigeration and Air Conditioning Industry Association.

The water quality hence plays a role similar to regulation restrictions in the definition of areas with null geothermal potential.
Both aspects were included in the evaluation of groundwater thermal potential for 23 wards in Tokio (Japan) operated by Nam and Ooka (2011) where the macro-potential of the area was derived from large-scale geology to evaluate the groundwater flow mean velocities for each ward. Aiming at the avoidance of water level depletion, it was assumed that no new wells can be constructed in the metropolitan area as imposed by legislative framework. Assuming a constant temperature difference, it was found that 318 TJ of energy can be mined from the subsurface. On the contrary, it was also found that among the existing wells only a minor part of them met the quality requirements needed for direct use, as shown in Figure 3.4. On the one hand, this study highlights the importance of both the site conditions (which include the geology as well as the groundwater chemistry) and regulative aspects. On the other hand, the assessment method still refers mainly to a sort of theoretical potential that would be misleading at the city or district planning level and it also misses the requirement of getting an evaluation at a sufficiently small scale for spatial planning purposes.
Similarly, also other qualitative assessment of groundwater heating potential have been performed worldwide. This is the case of the study carried out by Arola et al. (2014) that accounts for the potential of using the surface water and quaternary aquifers based on productivity and groundwater fluxes. The Finnish groundwater areas where identified comprising nearly 6000 areas where the land use and the recharge value were

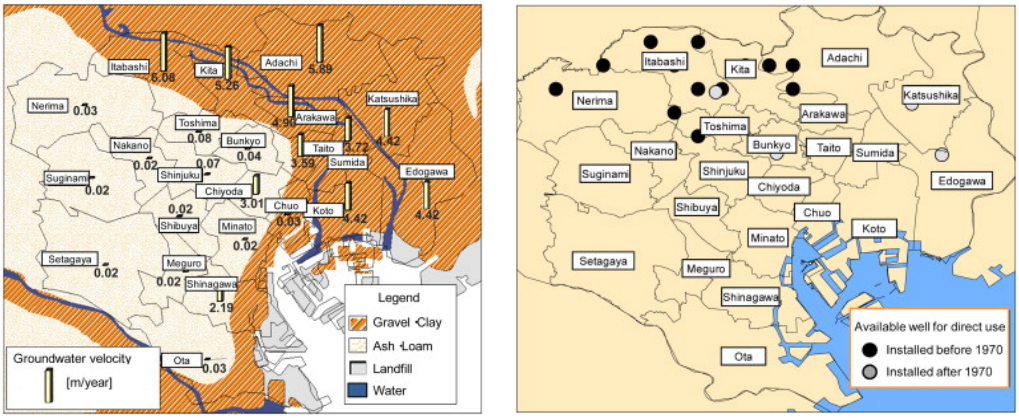

(a) (b)

Figure 3.4: Example of assessment about (a) hydrogeological conditions and (b) water wells that meet the water quality requirements for heat exchange in Tokio (Nam and Ooka, 2011).

assigned cross-referencing national spatial databases on the aquifer areas, city/town planning schemes and data from operating water wells. By performing this superposition of data, the usability of the potential, if any, was estimated through scaling of the recharge available in the area where installation of GWHP system was possible. Similarly aquifer zones where no drilling can be realized were excluded from the evaluation of the geothermal potential. This evaluation substantially based on Equation 3.2 is partly affected by the low natural groundwater temperatures, possibly leading to overestimation of the available temperature drop. Nonetheless over 60 MW of energy can be delivered to users from Finnish aquifers. This is an high quantity of energy but also the variability is extremely high depending on the aquifer body, ranging from 10 kW to nearly 2 MW for each aquifer zone.
Determination of deliverable energy is thus based on a constant temperature drop of 3 °C and fixed heat pump COP of 3.5. Even if the method is rough, this study is valuable in pointing out the existence of a relevant geothermal potential even in hard climatic conditions and in the comparison with the expected energy need of target buildings. Energy needs were indeed evaluated on the basis of climatic zones through specific building energy balance simulations. Different classes of building differentiated by age and method of construction were chosen to show qualitatively that also in cold climate conditions the geothermal potential can be valuably used and mapped with reference to the usage possibility. On the contrary, the quantitative evaluation is quite uncertain and does not really take into account the groundwater natural temperature that can be a technical hampering factor. Moreover the georeferenced aquifers include wideness information just as an attribute and are thus included in the database as map points (see Figure 3.5).

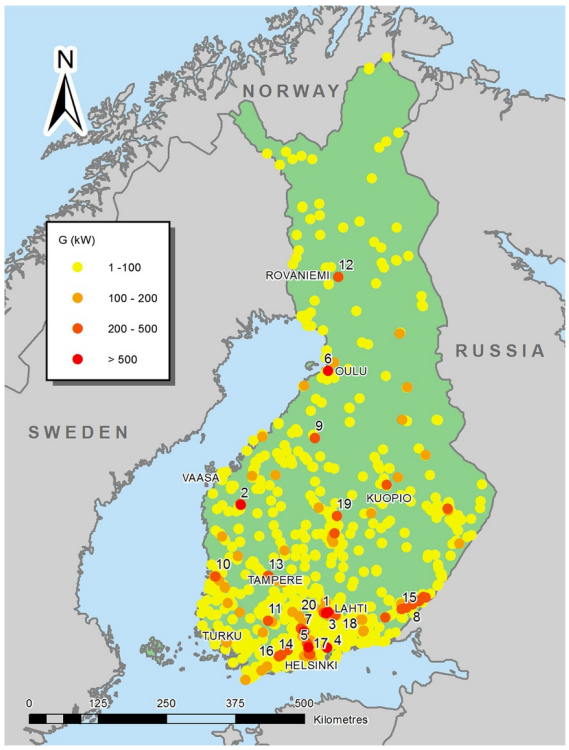

Figure 3.5: Example of geothermal theoretical potential assessment for aquifers in Finland (Arola et al., 2014).

3.3.2 Socio-economic models

The benefit of shallow geothermal energy is also defined by comparing its profitability to other energy sources. Profitability can be defined by computing the overall costs per unit of energy by different sources. A comprehensive evaluation should indeed include not only technical aspects but also social, environmental and economical ones too. These latter aspects involve the assessment of the so-called *externalities* as environmental costs of greenhouse gases (GHG) emission, and subsidies or taxes imposed by energy policies.
These issues were at least partly included in the study of Gemelli et al. (2011) that analysed a portion of the Marche region, Italy. A really simplified geological model, together with the rough evaluation of surface air and ground temperature through regression of the meteorological data, was the base to assess the lenght of BHE that fulfil the typical heat load of a domestic dwelling (e.g. 5 kW). On the one hand the data used in the specific application to the Marche region lacks in precision but on the other hand the methodology to evaluate the technical potential is valuable to be used even with refined input data and has the advantage of scalability. By the way, it neglects heat transfer mechanisms apart from conduction. On the social and economic side, the main driving cost is related to the probe length, estimated as explained above. Comparison

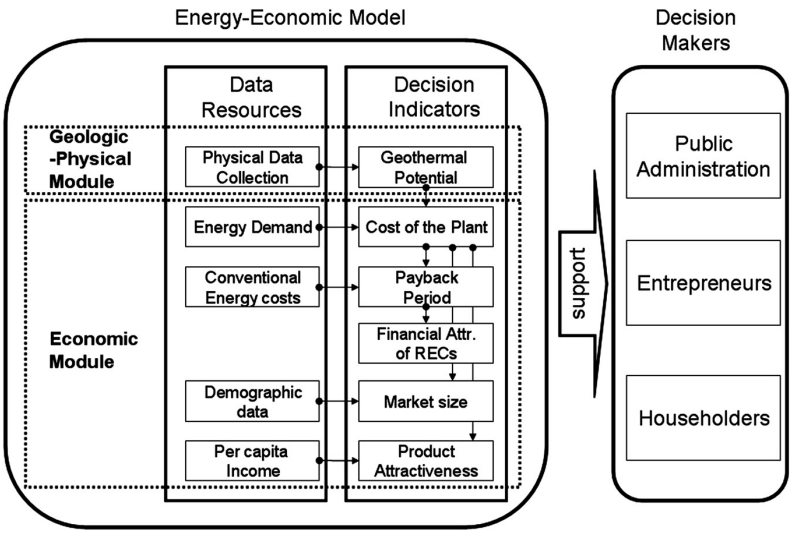

Figure 3.6: Example of a scheme for decision support tools based on the social and economic aspect of shallow geothermal energy market (Gemelli et al., 2011).

of this cost divided by the energy consumption over a reference time with the savings in fuel consumption defines the payback period. This quantity briefly describes the time needed to return the initial investment and hence is a key economical indicator for stakeholders.

European Union introduced the *Renewable Energy Certificates* (REC) that are a policy tool introduced to give economical value to GHG emissions savings for virtuous communities. Thus the more emissions saved, the more the economical benefit. Indeed the ratio between the cost of installation and the GHG emissions saved is a key indicator of the attractiveness of the REC. This value is particularly important for policy makers to assist the transition to renewable energy sources and strategically push the diffusion of a certain energy source in the territories where the maximum impact is envisaged.

In the private stakeholder point of view, market size and product attractiveness are the key factors to determine the investment. These indicators can be evaluated as the cost of installation of BHE to fulfil the heat loads produced by all the population on a territory and by the proportion of cost related to the GDP per capita.

The above mentioned social and economic aspects can be included in a platform to create a decision support tool as depicted in Figure 3.6. By the way, these economical aspects are all affected by the computed depth required by BHE to provide a certain power. This represents a strict assumption that can be plausible in case of residential districts that are pretty homogeneous in the building features. That is not usually the case at the municipality scale where the building heritage is various in age and designated use. Furthermore, due to the way the potential is evaluated, the subsurface has to be assumed vertically homogeneous (eventually and average value) and the specific heat extraction value is a priori defined irrespective of the BHE length.

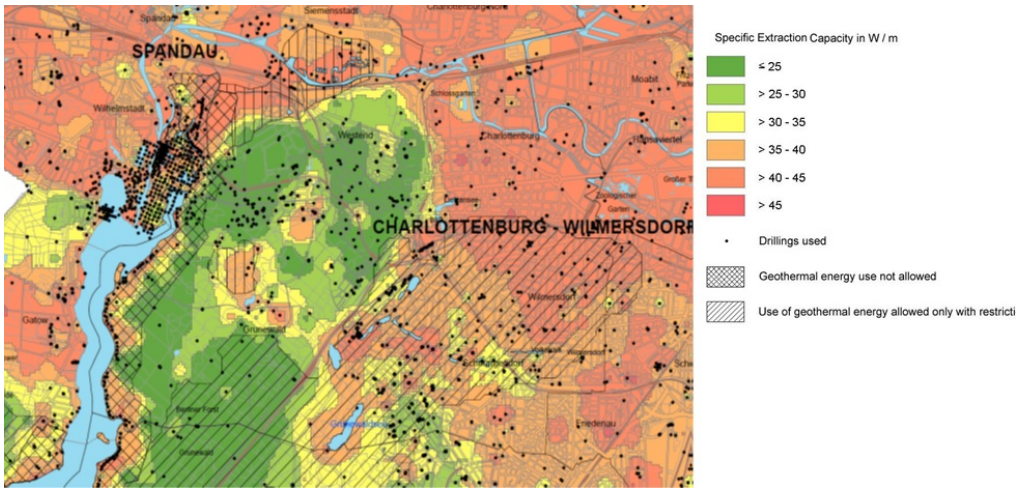

Figure 3.7: An example of quantitative geothermal potential map. The map refers to the City of Berlin, Germany (HGC Hydro-Geo-Consult GmbH).

3.4 Quantitative assessment and urban planning

Qualitative geothermal potential maps have a relatively important role in the dissemination and promotion of this fairly unknown source of energy. Because of the easy logic of traffic light maps and the relative easiness of the evaluation they are also valuable decision aid tools.
However qualitative maps are mostly descriptive, just subdividing the territory on the basis of rough cathegories (usually the thermal conductivity of rocks). Indeed purely comparative evaluation are not sufficient to pre-design single geothermal installations. On the contrary quantitative assessment methods allow to identify, even if under certain simplified conditions, the exchangeable energy on a certain territory. These methods are hence needed in the case of energy planning to build plausible scenarios of the impact of shallow geothermal in the energy mix of a district, a whole city or a region.
Quantitative maps can depict the values of thermal parameters of the subsurface up to the proper depth (depending on the kind of installation) or can directly provide an estimation of the thermal power exchangeable at each site as in the example shown in Figure 3.7.

3.4.1 Open Loop systems

In the case of open loop systems some conditions have to be met at the site as it has been shown in previous paragraphs. Water quality needs to be sufficiently good to avoid damages to the installation and an aquifer with sufficient capacity of extraction has to be present. Actually the evaluation of geothermal potential is focused on this latter aspect. In most cases the potential is indeed assumed as the heat content that causes a fixed increment/decrement in the temperature of the maximum extractable flow rate.

This flow rate is thus determined purely on the basis of the hydraulic problem.
The problem is usually reduced to the calculation of the drawdown produced by water extraction (Casasso and Sethi, 2017; García-Gil et al., 2015a; Muñoz et al., 2015). In its simplest form, the drawdawn at distance r, $s(r)$, is limited to a percentage of the saturated depth of the aquifer and the solution is the well known Thiem's analytical solution for steady state pumping test:

$$s(r) = \frac{Q_p}{2\pi\tau} \cdot \ln\left(R \cdot r^{-1}\right) \tag{3.3}$$

where R is the radius of influence of the well and τ the transmissivity of the aquifer. Thus from Equation 3.3 the maximum pumping rate Q_p can be calculated and then converted to a mass rate to be used in Equation 2.5, with a constant temperature drop.
However steady state conditions are rare, especially in aquifers beneath urban areas. Multiple groundwater users may indeed affect the water level and groundwater dynamics that have to be determined through more sophisticated solutions. In addition to this, also the thermal recycling and thermal feedback occurrence has to be avoided or at least, in worst cases, managed.
A more comprehensive approach to technical geothermal potential assessment regarding open loop systems was proposed by Böttcher et al. (2019) and was illustratively applied to the city of Munich, Germany (see Figure 3.8). The definition of the maximum pumping rate for each doublet is obtained through semi-analytical formulas considering three main limiting factors. These limits ensure that the drawdown at the extraction well, the level rise at the injection one and the hydraulic recycling are limited below sustainable threshold. As a consequence the maximum pump rate of a single well doublet is calculated as:

$$Q_p = \min\left(0.195kb; \frac{\pi}{1.96} v_d b d_w; \Delta z k b^{0.789} e^{29.9|\nabla h|}\right) \tag{3.4}$$

where k is the hydraulic conductivity, b the saturated thickness, v_d the Darcy velocity, d_w the distance of the wells, $|\nabla h|$ the hydraulic gradient and Δz the maximum allowable rise. Each of the terms accounts for a different hampering factor and the numerical coefficients were derived from a wide parameter numerical analysis.
While this approach organically addresses the technical and legislative limits to groundwater thermal use and represents a valuable example of semi-analytical approach to the potential assessment, the formulation is affected by steady state assumption. Although the evaluation can be carried out adopting variable temperature drops depending on the site temperature, the most critical factor issue is represented by the breakthrough that in this study is conservatively assumed to take place simultaneously to hydraulic recycling. This means that the thermal delay is neglected, according to the steady state assumption of the method and thus optimisation can be pursued on the spatial scale only.

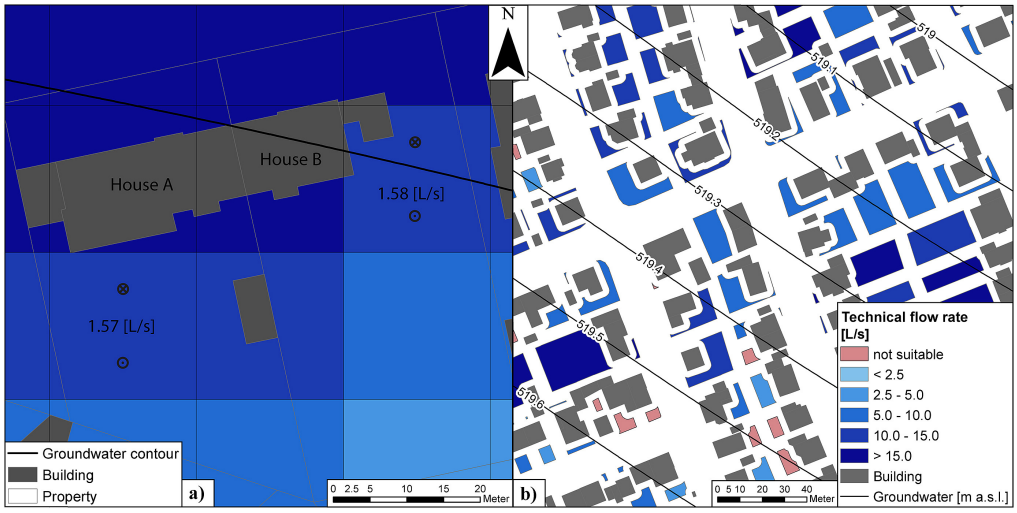

Figure 3.8: Illustrative application from Böttcher et al. (2019) for the city of Munich (Germany) of open loop potential assessment through (a) maximum pump rate definition. (b) Example of cadastral plot matching to the pump rate assessment.

3.4.2 Empirical methods

Due to the complexity and the number of parameters involved, several methods have been developed with different strategies to quantify the sustainable heat exchange for Borehole Heat Exchangers. In most cases the developed methods have been based on assumptions that are often derived from the specific territory where these methods were conceived. On the contrary, another strategy is to derive the values of heat exchange through experience and hence in an empirical way. To build these model it is necessary to collect a representative number of applications with specific features in known boundary conditions.
Among these methods the most known is represented by the German standards (VDI, 2010) that is also at the base of a lot of feasibility studies for small plants in scientific literature (e.g. Muñoz et al. (2015); Ondreka et al. (2007); Schiel et al. (2016)). These standards are widely recognized as engineering standards not only in Germany thanks to the relatively long history and the high profile of the author's panel (Reuss et al., 2006). VDI4640 are also widely adopted due to the easy use of specific heat extraction rates (expressed in W/m) that have been derived for a number of lithologies. These values are based on predetermined operating time over the year (2400 h/y and 1800 h/y respectively) and take into account heating mode only. Despite their easy use, the assessment of geothermal potential neglects different climatic conditions (and hence a different operating time) and the uncertainty is relatively high due to the categorization of lithology only. Ground temperature is indeed neglected even if it is a key parameter in potential assessment. Moreover this kind of method is unable to deal with interference and cumulative effects due to long term temporal scale.

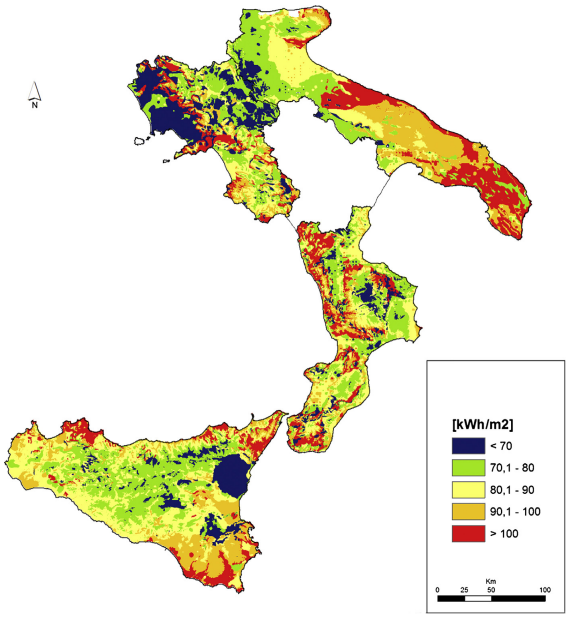

Figure 3.9: Example of empirical geothermal potential assessment in southern Italian regions from Galgaro et al. (2015)

Based on these standards, Ondreka et al. (2007) assessed the potential of two study areas in south-western Germany. The specific heat extraction values from VDI (2010) were averaged depending on the thickness of the single layers that were reconstructed within an hydrogeological model. As in many other cases the modelling was also carried out by mean of a GIS software.
An empirical approach was also developed by Galgaro et al. (2015) where the technical potential was computed on the basis of a quite large number of numerical simulations. Thus the total BHE length to satisfy the energy needs of standard buildings in predefined climatic conditions was determined. By means of regression, an explicit formula linking the specific geothermal potential per unit area q_{BHE} $[W/m^2]$ with the thermal conductivity and the average temperature within the BHE depth was obtained:

$$q_{BHE} = A \exp\left[-B \cdot \left(a \cdot \lambda_g + b \cdot T_{\bar{g}} + c\right)\right] \tag{3.5}$$

where A, B, a, b, c are the numerical coefficient obtained through regression and λ and $T_{\bar{g}}$ are the thermal conductivity and the mean ground temperature, respectively.
The relationship adopted is really flexible and has the advantage of taking into account both the operating modes, heating and cooling. On the contrary, the numerical coefficient included in Equation 3.5 are specifically derived for the VIGOR project (Galgaro et al., 2012) area in southern Italy where the assessment was carried out (see Figure 3.9). Hence the coefficient should need calibration for each specific area of study, differently from the VDI (2010) derived potentials.
A numerical regression was adopted on the basis of a specific dataset also by Signorelli

(2004) to link BHE length (strictly speaking a compensation length to BHE dimensioning) with ground surface temperature and in turn to altitude and surface air temperature. The same kind of relationship was adapted for the case of Marche region (Italy) as part of the study (Gemelli et al., 2011), explained previously.
Recent studies implementing artificial intelligence should be also included in the category of empirical methods. The application of artificial neural networks to the evaluation of geothermal potential or of thermal properties in an area is in fact linked to the training of the neural network with a dataset of input and output values. Such a kind of approach was used to build the thermal conductivity map of the territory of Cyprus (Kalogirou et al., 2015) where a limited number of boreholes with known lithology, rainfall, and temperature vs depth were used to assess the average thermal conductivity of the first 100 meters subsoil.
It should be noted that the method is widely exportable in its architecture to other contexts. Conversely it is impossible to extract from an Artificial Intelligence algorithm the relationship that links input parameters to the output. Furthermore the relationship that governs the blackbox is dependant on the training dataset and is thus specific to the area of study. Hence the need arises to know in a certain number of locations within the study area not only all the input parameters, as in any other method, but also the geothermal potential.

3.4.3 Methods based on geometrical optimisation

Studies focused on the district and city scale usually are conceived to assess the maximum share of energy that can be included in the energy supply mix. Thus the two main components in this kind of approaches are the quantification of the single installation potential and the geometrical deployment of the installations. Area availability is indeed one of the most influential limiting factor in densely populated areas.
A few studies have been carried out in recent years to this respect. Zhang et al. (2015) demonstrated that in the City of Westminster, U.K., up to 80% of building heritage can meet the heating loads. Surprisingly, even if the theoretical potential is extremely higher than the energy needs of the city, when both the heating and cooling loads are considered only 14% of buildings (in the worst case scenario) can entirely rely on BHEs. This discrepancy effectively shows the importance on land availability in urban areas. In this perspective it is a really valuable information the percentage of energy that can be delivered by the BHEs. The algorithm applied in GIS environment indeed allows to calculate the length of BHE required by each building for heating (L_h) or cooling (L_h)

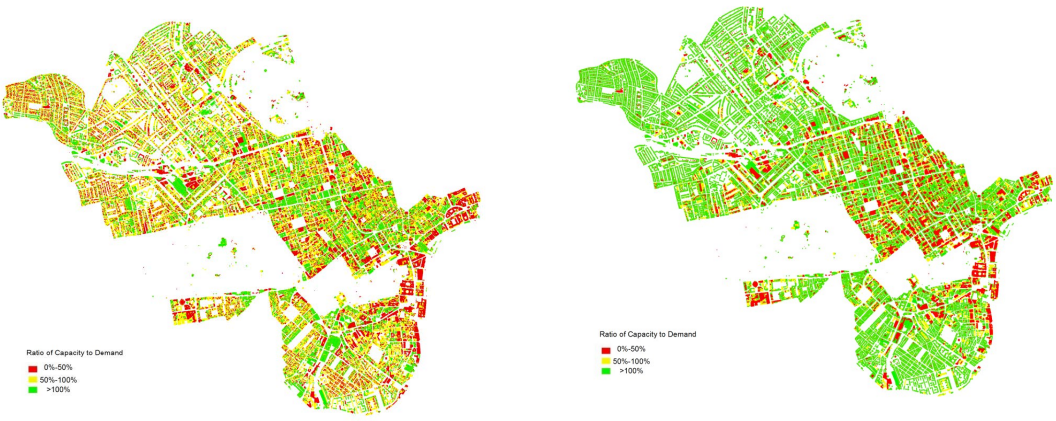

Figure 3.10: Example of the assessment of the ratio of heating and cooling load to geothermal potential in the City of Westminster, U.K. (Zhang et al., 2015).

as indicated by ASHRAE standards (Kavanaugh and Rafferty, 1997):

$$L_h = \frac{q_a R_{ga} + \left(q_{lh} - \bar{W}_h\right)\left(R_b + PLF_m R_{gm} + R_{gd} F_{sc}\right)}{T_0 - 0.5 \cdot \left(T_{wi} + T_{wo}\right) - T_p} \cdot 10^{-3} \tag{3.6}$$

$$L_c = \frac{q_a R_{ga} + \left(q_{lc} - \bar{W}_c\right)\left(R_b + PLF_m R_{gm} + R_{gd} F_{sc}\right)}{T_0 - 0.5 \cdot \left(T_{wi} + T_{wo}\right) - T_p} \cdot 10^{-3}. \tag{3.7}$$

where F_{sc} is the short-circuit heat loss factor, PLF_m is the part-load factor during design month, q_a is the net annual average heat transfer to the ground, q_{lh} and q_{lc} is the building design heating and cooling block load respectively, R_{ga}, R_{gd} and R_{gm} are the effective thermal resistance of the ground in annual, daily and monthly pulse, R_b is the thermal resistance of borehole, T_0 is the undisturbed ground temperature, T_p is the temperature penalty for interference of adjacent boreholes, T_{in} and T_{out} are the heat carrier fluid temperature at the inlet and outlet respectively, while $\bar{W}_h$ and $\bar{W}_c$ are the power input at design heating and cooling load respectively.
In order to calculate the required probe length, the heating and cooling loads of the building, thermal conductivity and diffusivity of the subsurface and the ground temperature are needed. Then it was determined if the available area was sufficient for the installation of as many 150 m-long BHE as needed. In the case the fulfilment of energy demand was not possible, the number of deployable BHE was anyway determined with respect to the footprint of the buildings and to a buffer area around the building while respecting mutual distances (as shown in Figure 3.10). The partial shortage of input data about subsurface temperature prevents the application from being realistic. On the contrary the approach is extremely useful in demonstrating the close connection with surface usage and area availability in urban areas. Main limitation is anyway related to the restriction to purely conductive heat transfer.

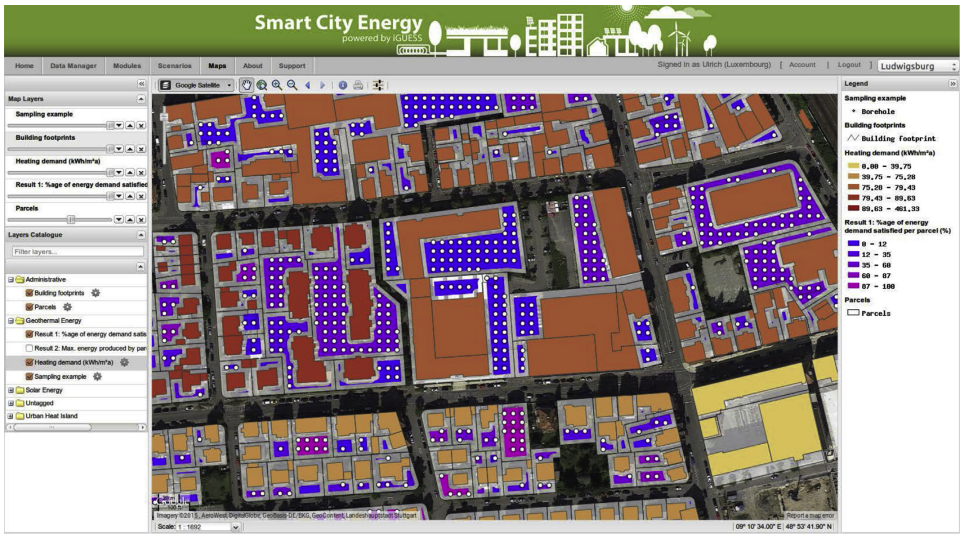

Figure 3.11: Example of spatial optimisation in BHE deployment within parcels for a district in Ludwigsburg, Germany (Schiel et al., 2016).

In line with these conclusions, Schiel et al. (2016) demonstrated the influence of the urban pattern on the capability of shallow geothermal energy to fulfil energy needs at the district and city scale. Based on the consumption of buildings (categorized by *settlement type*) and specific heat extraction rates from VDI (2010), the GIS tool developed optimises the number of BHE fitting within each parcel of the study area. It should be noted that the optimisation in BHE deployment was performed by recursive random sampling of the parcel areas (adjusted by removing building footprint and a buffer of 3 meters). Then the worst case scenario for each parcel was assumed as the representative situation (see Figure 3.11). Thus all the BHE that can fit the parcel based on the geometrical deployment optimization were considered with their entire allowable drilling depth. This assumption locally determines surplus or deficit in energy even in neighbouring parcels. This is indeed reasonable on the basis of actual regulations. On the other hand it is unlikely that all the BHE determined by the procedure would be really drilled in parcels where surplus energy is envisaged. Furthermore the presence of neighbouring surplus and deficit parcels actually do not lead to a real optimization in usage of geothermal resources at the district/city scale. This assumption also affect the assessment of carbon dioxide savings performed. By the way it was demonstrated that over 40% of the parcel can completely rely on geothermal energy and that these buildings are almost exclusively included in residential settlements. That means that potential city scale benefit from shallow geothermal is also directly linked with the urban pattern : less dense urban patterns are indeed more appropriate for using shallow geothermal energy to fulfil the energy needs.

Similarly, also Miglani et al. (2018), applied an optimisation algorithm for BHE deployment as part of the definition of district scale geothermal potential. This optimal deployment is at first merely based on cadastral geometry: common limits as buffer around plot borders and buildings and minimum spacing among neighbouring boreholes are applied. Particularly detailed heating demand profiles are derived by thermal simulation of the buildings with known characteristics. Once determined the total BHE length with a simplified version of Equation 3.7, the allowed drilling depth for each point representing a BHE is compared. Based on the simulation of multiple BHE operation, via spatial and temporal superposition by means of the so-called *g-function* (Eskilson and Claesson, 1988), the technical potential is determined as the part of the heating demand that is met by BHEs without excessive cooling of the heat carrier fluid.
Even though the study also demonstrates that the interference among BHEs has to be accounted in order not to overestimate the geothermal potential, convection is neglected in the formulation of Finite Line Source (Carslaw and Jaeger, 1959) which is at the base of the method. Indeed the superposition principle would neither be applicable in case of groundwater fluxes due to non linearity. By the way the inclusion of interference is a valuable element in assessment of geothermal potential that almost neglected by previous work. The approach developed is really demanding from the input data point of view (especially as regards the building demand side) and computationally demanding as requires the heating load profiles on hourly base and the calculation of the transient temperature history for each of the BHE. This latter aspect likely represents one of the main barriers to the application of this approach at large scales.
In the perspective of potential assessment on large scale is indeed preferable to apply map algebra-based algorithms on GIS. These algorithms may be purely analytical or semi-analytical but rigorously expressed as closed formula.

3.4.4 Methods based on analytical formulation

Analytical formulation linking geothermal potential with installation features and site-dependent parameters (e.g. soil thermal properties and climatic data) can be easily used in map algebra operations in a GIS environment. This aspect is particularly important for mapping purposes, especially in the case of a large number of cells in the study area. This is the case if the objective of the study is a large scale mapping or either at the small scale but with high resolution. This latter situation is likely needed in most urban areas, where the variability in the thermal and hydraulic regime is extremely pronounced as a result of various usages of surface and subsurface.
Analytical formulation based on Infinite Line Source model (Carslaw and Jaeger, 1959) was used by García-Gil et al. (2015a):

$$T(r,t) = \frac{q_l}{4\pi\lambda}\left[\ln\left(\frac{4\alpha t}{r^2}\right) - \gamma\right] \tag{3.8}$$

where $T(r,t)$, the temperature at distance r from borehole at time t, is dependant on the heating rate per unit length q_l, the thermal conductivity λ and diffusivity α while γ is the

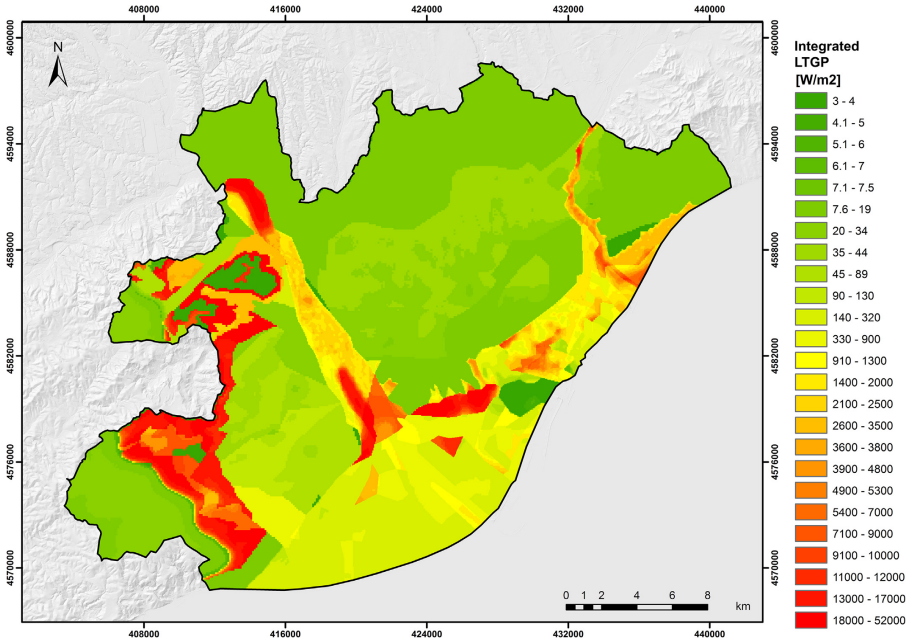

Figure 3.12: Example of analytical geothermal potential assessment in the metropolitan area of Barcelona, Spain (García-Gil et al., 2015a).

Euler's constant. This equation does not take into account the advective contributions. Hence in the saturated depth, the conduction-advection analytical solution for heat transfer is as follows:

$$\Delta T(x,y) = \frac{q_l}{2\pi\lambda} \cdot \exp\left(\frac{v_d \rho_w c_w x}{2\alpha\rho c}\right) K_0\left(\frac{v_d \rho_w c_w \sqrt{x^2+y^2}}{2\alpha\rho c}\right) \tag{3.9}$$

where the temperature difference at relative x,y coordinates depends on the thermal properties of the subsoil, the heat exchange rate but also on the groundwater flow velocity through the modified Bessel function of second kind order zero (K_0). Hence the geothermal potential at a specific point can be assumed as the sum of the potential of single hydrogeological layers along the vertical direction:

$$Q_{BHE} = \sum_{i=0}^{n} \frac{th_i \cdot q_{li}}{A_{plume,i}} \tag{3.10}$$

where the plume area A is defined as the area that experience a temperature variation higher than a certain value (usually 1°C according to the Thermally Affected Zone definition) and th_i is the thickness of the i-th layer. Thus this quantity can be mapped over the study area once maps of the thermal properties and the threshold parameters are fixed (see Figure 3.12).
The fundamental contribution of fluid flux related heat transport mechanism is also

included in the geothermal potential assessment approach developed by Alcaraz et al. (2016). The shallow geothermal potential is indeed defined on the basis of the Moving Infinite Line Source model analytical solution:

$$q_{BHE}\,[W/m] = \frac{\Delta T(r) \cdot 4 \cdot \sqrt{\lambda_l \cdot \lambda_t}}{\exp\left(\frac{v_D \rho_w c_w x}{2\lambda_l}\right)} \cdot \\ \cdot \frac{1}{\int_0^{\phi'} \phi^{-1} \exp\left(-\phi - \phi^{-1} \cdot \left(x^2 \lambda_l^{-1} + y^2 \lambda_t^{-1}\right) v_D^2 \rho_w^2 c_w^2 \cdot \lambda_l^{-1}/16\right) d\phi} \tag{3.11}$$

where

$$\phi' = \frac{v_D^2 \rho_w^2 c_w^2 t}{4 \rho c \lambda_l}$$

and the l and t pedices represent the properties in the longitudinal and transverse direction to the groundwater fluxes while t is the time from the BHE operation start. This latter value can be assumed as the length of the longest operative season. In previous Equation 3.11 the potential is thus dependent on the allowable temperature increment at distance $r = \left(x^2 + y^2\right)^{0.5}$ and on time. Thus, once defined the allowable temperature change in the subsoil (hence at the BHE wall distance) or at the property boundary, it is possible to define the geothermal potential depending on the dimensions of the property plot. The maximum length included along the groundwater flow direction hence represent a fundamental input data together with the thermal properties of the subsurface.

Main advantages of this approach is the coherence with real groundwater flow field, through adaptation of the shape of the thermal plume with the main axis in the flow direction (see Figure 3.13). By the way, due to the assumption of Moving Infinite Line Source the entire approach is focused on 2D while also vertical heterogeneity, at least in temperature and velocity field, is common. An explicit formulation makes however the solution a valuable tool for a fair administration of the shallow geothermal subsurface. On the contrary, the tool is specifically designed for the management of existing users and for evaluation of possible interferences due to ongoing authorization processes rather than to evaluate the potential at the district and city scale. It is indeed necessary an arbitrary operator intervention to define the position and the desired usage of each installation. This makes the tool developed less suitable for the definition of potential and of the energy policy at urban area level. Furthermore the whole approach is bidimensional, deriving from an homogeneous infinite space assumption and the heat exchange rate is necessarily constant during all the period. This means that no long-term optimisation can be pursued neither the migration of the thermal plumes after the end of yearly operation can be taken into account.

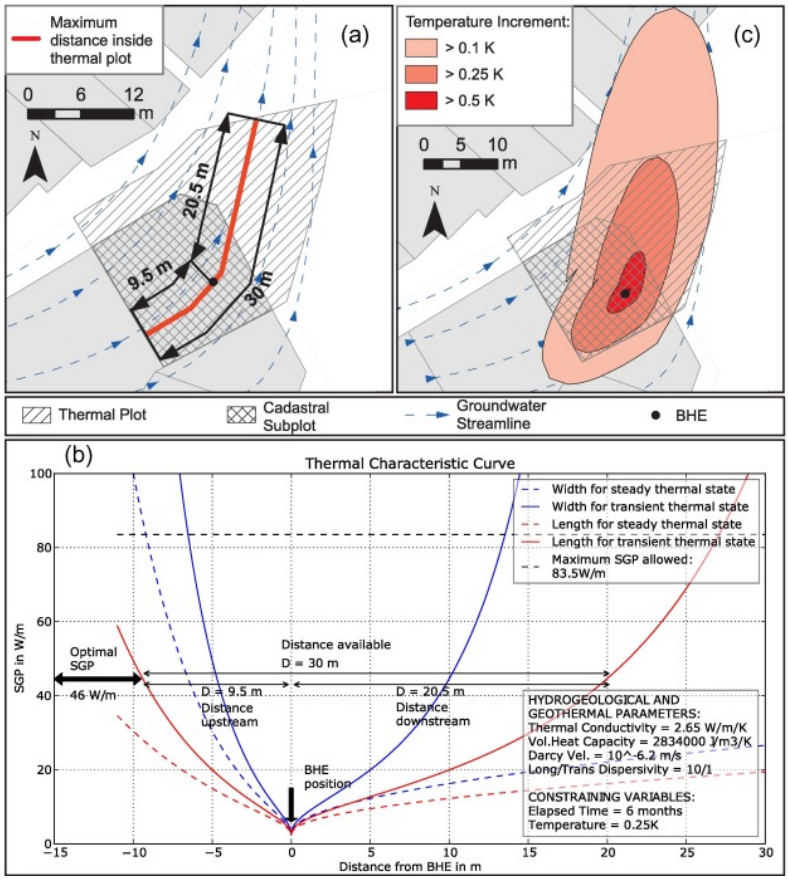

Figure 3.13: Example of BHE deployment optimisation of the deployment in a cadastral plot, based on the Moving Infinite Line Source analytical solution (Alcaraz et al., 2016).

3.4.5 Semi-analitical methods

Steady-state conditions are rare in real settings. Transient boundary conditions are indeed typically represented by discontinuities and changes in heat extraction rates at various time scales: from monthly to sub-hourly scale the variation in heat loads of building is significant. The analytical solutions usually are not able to handle such a situation.

This issue was overcome in the semi-analytical approach G.POT. proposed by Casasso and Sethi (2016). It resulted in a numerically calibrated explicit formula for technical geothermal potential quantification of a Borehole Heat Exchanger. In this case the failure is associated when the temperature of the heat carrier fluid exceeds the technically suitable range. Neglecting the advective contributions, the superposition principle is valid within the Infinite Line Source model (Carslaw and Jaeger, 1959) and thus the

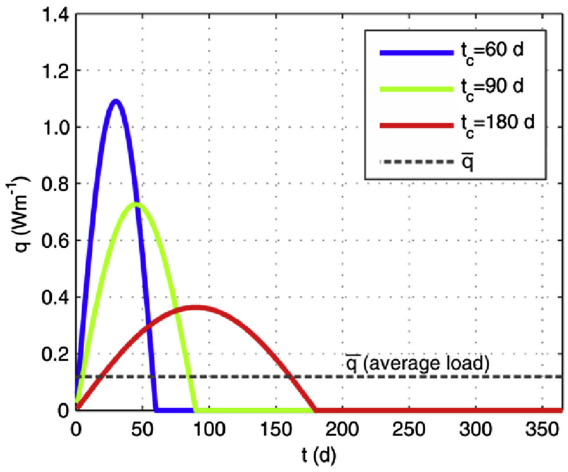

Figure 3.14: Emi-sinusoidal thermal load functions used to derive the semi-analytical formula G.POT. (Casasso and Sethi, 2016).

varying thermal load $q(t)$ can be approximated by piece-wise constant function leading to a thermal alteration ΔT_g at the time t given by:

$$\Delta T_g(t) = (4\pi\lambda)^{-1} \cdot \sum_{i=1}^{N-1} \left[\left(q_{i+1} - q_i\right) \cdot Ei\left(\frac{r_b^2}{4\alpha t_i}\right) \right] \tag{3.12}$$

where r_b is the borehole radius and Ei is the exponential integral. The temperature at the BHE wall is in turn linked to the temperature of the heat carrier fluid. As a first approximation, the BHE itself can be considered as a thermal resistance R_b once the thermal inertia effect is exhausted:

$$\Delta T_{BHE} = q(t) \cdot R_b \tag{3.13}$$

Thus the extreme working conditions for a BHE were assumed as the time when the heat carrier fluid temperature reaches the safety limit T_{lim}. Under the assumption of contemporary maximisation of the temperature drop respect to the background temperature T_0, the extreme condition that defines the geothermal potential can be expressed in the form:

$$\left(T_0 - T_{lim}\right) = q_{max} \cdot R_b + q_{max} \cdot \frac{\psi}{4\pi\lambda} \tag{3.14}$$

where ψ is a non dimensional function and q_{max} is the maximum thermal load. The form of this function was indeed obtained by fitting a large number of numerical simulations under the assumption of cyclic thermal load with an emi-sinusoidal shape. The thermal load functions consist of an operation period followed by a recovery period that cumulates a time span of 1 year. Various peak thermal load and operative time were selected. In order to make all the thermal load function comparable, it was chosen to keep constant the mean thermal load per unit length (see Figure 3.14).

The fitting of a large number of numerical simulations decouple the parameters obtained from site-specific parameters. Hence, even if the relationship is empirical, the method can be still considered valid independently from the region where it is applied. The empirical relationship is then dependant on three non dimensional parameters that are in turn linked to the load cycle time t_c, to the lifetime of the installation t_s, to the year duration t_y (or period between the start of two operative seasons), to the thermal properties of the soil α and the geometrical properties of the BHE r_b:

$$\psi = -0.619 \cdot \frac{t_c}{t_y} \cdot \ln\left(\frac{r_b^2}{4\alpha t_s}\right) + \left(0.532\frac{t_c}{t_y} - 0.962\right) \cdot \ln\left(\frac{r_b^2}{4\alpha t_c}\right) - 0.455\frac{t_c}{t_y} - 1.619 \quad (3.15)$$

Hence the technical geothermal potential of a Borehole Heat exchanger with length L is expressed in the explicit formula:

$$Q_{BHE}[W] = \frac{8 \cdot \left(T_0 - T_{lim}\right) \cdot \lambda \cdot L \cdot \frac{t_c}{t_y}}{\psi + 4\pi\lambda \cdot R_b} \quad (3.16)$$

Based on this formulation, the geothermal potential is thus a function of:

- the borehole characteristics (geometry: L, r_b and thermal properties: R_b that can be expressed as a function of the thermal conductivity of the borehole grout and the pipes number within the borehole);
- the thermal properties of the ground (conductivity and thermal capacity);
- the way the BHE is conducted (length of the operating season and service life).

Equation 3.16 is easily implementable either on GIS or on spreadsheet representing the distribution of the site-dependent variables. This makes the method, as the purely analytical ones, particularly suitable for geothermal potential mapping as shown in Figure 3.15. The method was indeed successfully tested and adopted in several European areas (Casasso et al., 2018, 2017; Casasso and Sethi, 2017). However, the approach relies on the Infinite Line Source model and is thus limited to homogeneous subsurface and takes into account conduction heat transfer mechanism only. This can lead to excessively conservative evaluations of the geothermal potential in areas where a significant groundwater flux is present. This is the case of most urban areas that are usually located where water (both from rivers and from the subsurface) is easily accessible.
In the next chapter (see Section 4.4) these issues are better in depth analysed and subsequently overcome with a slight modification in the formula reported in Equation 3.16.

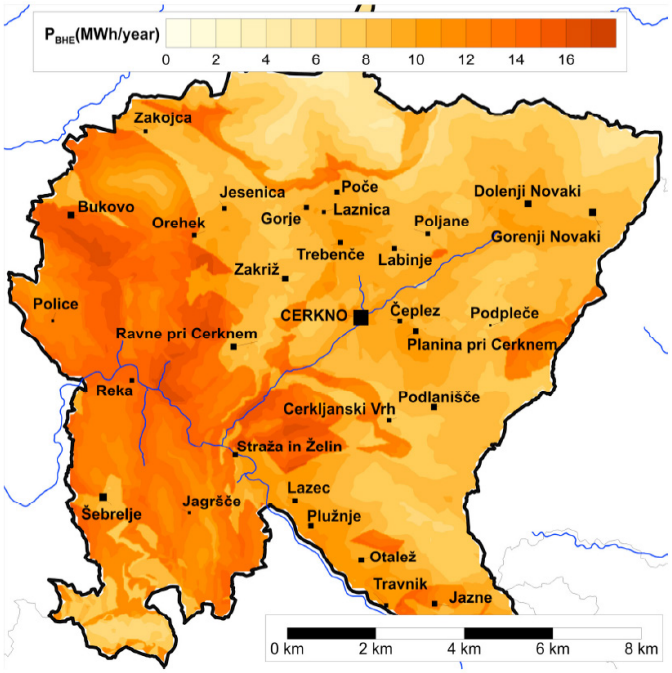

Figure 3.15: Example of BHE geothermal potential calculation with the G.POT. method in the area of Cerkno, Slovenia (Casasso et al., 2017).

3.5 Summary

Renewable energy resources are nowadays extremely competitive from the financial point of view. This is also due to subsidies and energy policies that are pushing the energy transition. This however also means that there is extreme competition among green energy sources from the economic point of view. Shallow geothermal energy presents several advantages respect to other renewable sources, as stability over weather conditions and decentralized production. By the way high installation cost related to drilling make the oversizing of the installation unprofitable from the economical point of view.

Thus it is evident that much effort has to be put in quantification of exchangeable heat or *geothermal potential*. However definition of the heat that can actually be exploited, namely the *technical geothermal potential*, is complex due to the high number of influencing factors that are affected by high uncertainty. Because of this several approaches have been proposed in scientific and technical literature. Some of them focus on the promotion of shallow geothermal, highlighting in qualitative manner the best places and technologies to adopt depending on the site. Other methods are instead intended to give a pre-dimensioning information for installers and stakeholders. Most of the approaches in this latter class focus on borehole heat exchangers, being the most common technology adopted. These methods aim at managing the installations deployment

rather than at defining the overall potential over a territory. In the first class geometrical deployment of installation is of central importance, while in the second class an explicit formula is the main resulting tool. This formula can derive from analytical theory rather than from empirical correlation or calibration.
To the aim of this work, the assessment of the potential over an urban area with possible large extension is the main focus. In the following the adaptation of a semi-analytical formula will be explained in the broader context of a method to deal the specific issues of the urban areas in the quantification of the technical geothermal potential.

Chapter 4

A new procedure for the optimisation of geothermal resources in urban areas: the rOGER method

4.1 Introduction

Urban areas are attracting more and more population in recent decades and are going to represent the 68% of the world population by 2050 (United Nations, 2019). As a result, land scarcity issue is becoming increasingly crucial in urbanized areas. Moreover because of this rapid growth the need arises for sustainable energy supply. Shallow geothermal can represent a valuable sustainable source of energy and its growth will definitely need a rational planning to avoid overexploitation or conflicting uses of the subsurface.
Thus the need arises for sound methods for assessment and management of the shallow geothermal resources that are able to deal with the peculiar issues of the urban context. The assessment of shallow geothermal potential cannot disregard the real thermal conditions in the territory. This thermal conditions are usually highly heterogeneous and time-varying. Optimisation in the usage of shallow geothermal hence moves from the management of a tridimensional resource domain in transient conditions. Optimisation also needs to take into account all the heat transport mechanisms, as convection and dispersion. In the case these issues are not properly addressed, a not negligible part of the technical geothermal potential would remain unexploited. Also interference among users will become more and more common and environmental protection might be undermined.
In this chapter a novel method named *rOGER* (acronym for *Optimising GEothermal Resources in urban areas*) for geothermal potential assessment will be presented. This approach aims to address the specific issues related to the urban context through the integrated use of a refined semi-analytical method and numerical modelling for real

Figure 4.1: Conceptual scheme of rOGER method for geothermal potential assessment.

thermal condition assessment. The method is basically conceived as a four step procedure that is based on the use of georeferred database. Requirements of the database and its tools but also the characteristics of the dataset needed are the focus of the first part of the chapter. The second part of the chapter will be devoted to the modelling of the real thermal conditions with specific reference to numerical modelling. Subsequently in a third section the assessment of the site-specific shallow geothermal potential will be addressed thanks to the extension of a semi-analytical formula to the hydrodynamic field. Finally a fourth section will explain the process to extend results from site scale to the city and district scales. By reaching the city scale, the method is intended to provide valuable tools for city planners and energy managers to drive and optimize the usage of shallow geothermal potential beneath urban areas.

4.2 Georeferred database

The main aim of the procedure described in this chapter is to provide a refined assessment of geothermal potential in urban areas at the discrict and city scale. Hence the expected output is the localisation of this potential. The best option to deal with spatially variable inputs and outputs is a georeferred database that is the base of a Geographical Information System. The GIS represent the backbone of the method rOGER. The conceptual scheme of the method is shown in Figure 4.1.
It is clear the different phases are developed within a GIS platform except for phase 2 which requires the usage of numerical modelling tools.
The GIS requirements and the dataset included in the database are in depth analysed in following paragraphs.

4.2.1 Requirements of the GIS

The design of a georeferred database is based on the aim that is pursued. This is thus strictly connected to the operations that have to be implemented and datasets that is necessary to handle. All these aspects were at first included in the *external model*.
This geodatabase aims to quantitatively assess the technical geothermal potential of Borehole Heat Exchangers taking into account real (or realistic) thermal and hydraulic conditions. The reference scale to reach the accuracy that is proper to a planning tool is the metric to decametric scale. Hence the factor 1:5000 should not be exceeded over the entire urban area. With this resolution the area extension covered can reach the order of magnitude of about 10000 km^2 . Although returns will be in 2D, the database has to manage elevation data in order to handle heterogeneities in vertical direction. Vertical resolution has to be smaller than the decametric scale up to the maximum depth pertaining the BHE (about 150 m below the surface). A common grid should be adopted for the field data, namely *raster* datasets, in order to allow the adoption of map algebra. Thus resampling and rasterization geoprocessing has to be supported in the GIS. This indeed is a common basic feature of GIS softwares.
The database needs interface capability to the numerical modelling codes that are used in stage 2 of the rOGER method (see Figure 4.1) both for data export and import. This depends on the specific software package that is used for modelling. However, most of the codes allow for data exchange in the form of shapefile (.shp) and/or Drawing Interchange Format (.dxf). This capability is included in the general data processing and spatial analysis capabilities that are required by this geodatabase. Among these latter capabilities there are the update of data, the interpolation and extrapolation of spatial data and the map algebra.
Other capabilities proper of the geospatial database are (Alcaraz et al., 2016):

- Storage and data management including transformation of single or multiple attributes and editing of the characteristics of the entities;
- Conceptual modelling and spatial data processing and analysis related to hydrogeological conditions and situation.

The dataset that are included in the database are classified as:

1. geology;
2. hydraulic and thermal properties related to the different subsoil classes;
3. surface water bodies (e.g. lakes and rivers) and monitoring network;
4. groundwater bodies and relative monitoring network ;
5. building heritage or land use;

6. deep underground structures (e.g. Deep basement, underground car parkings, etc.);
7. underground linear infrastructures (e.g. urban road and rail tunnels, metro lines, district heating network, etc.);
8. thermal and non thermal users of the aquifer (e.g. Water wells for industrial purposes, geothermal open loop systems);
9. thermal tridimensional field;
10. geothermal potential.

In Figure 4.2 the simplified conceptual model of the database is shown. It should be noted that links represent not only the matching fields but also the main data resulting from processing of the related table. This is the case of the hydraulic gradient field that is linked with the velocity field of the n-th layer by combination with the hydraulic conductivity. It should also be noted that under the class *Stratigraphy* several data are grouped which are usually in the form of raster data. The number of geological layers depends on the specific area comprised by the study. Links shown on layer *N* represent similar links on all the layers comprised in the stratigraphy.
For the sake of simplicity the above mentioned dataset will be grouped and presented in the following paragraphs depending on the nature of the related information: hydrogeology, entities producing thermal and hydraulic impact, built environment and hydro-thermal regime.

4.2.2 Hydrogeology

The geothermal potential is strongly affected by subsurface properties and groundwater flow at the site, as extensively discussed in Chapters 2 and 3. Hence the data included in the hydrogeology class are extremely relevant and this class is in turn the most populated.
The class comprises the data defining the medium of the area where the geothermal potential has to be assessed. The main dataset is represented by the stratigraphy. Stratigraphy is represented by the sequence of layers that can be assumed homogeneous from hydraulic and thermal point of view. The geological model is derived by interpolation and interpretation of borehole drillings in (and around) the study area. The geological model is hence described as a series of layers that partially or entirely cover the area under exam from the surface (know from Digital Terrain Models) up to a certain depth that depends on the aim of the model and on the available borehole drillings.

Figure 4.2: Simplified conceptual model of the spatial database.

The stratigraphic sequence can be described as a set of raster dataset identifying the contact surface (hence the related value represents the absolute height) between two adjacent strata. It should be noted that in the case that such a representation of the stratigraphy is available, a common grid for the set of rasters is needed. Indeed the result of the geoprocessing activities related to geology has to be a point shape file with equally spaced points for each cell that include the top of each layer (the first one is bounded by the topographic surface) and the relative identification. This identification code then relates to the *geological layer* table that reports for each of the units included in the domain the hydraulic and thermal parameters. These parameters will be then used in the numerical modelling phase to assess the thermal and hydraulic regime of the study area as will be discussed in Section 4.3. The parameters can be derived from laboratory testing or even from literature, especially as regards the thermal properties that are difficult to determine (also because of the expensive tests needed) and rarely known from direct investigation. These parameters are: *horizontal and vertical hydraulic conductivity, effective porosity, thermal conductivity, specific thermal capacity.* It should be noted that hydraulic conductivity values have been distinguished in a vertical and an horizontal one. This results from the adoption of an orthotropic material model where principal direction are aligned to horizontal and vertical ones. This assumption is commonly valid for most deposits (e.g. Alluvial deposits where deposition process reduces vertical hydraulic fluxes). If this is not the case, the geological layer should include three conductivities values along principal direction together with the information about the orientation of the principal axes.
On the basis of the parameters listed above, it is clear that the geological sequence usually matches the subdivision useful for geothermal potential assessment. Anyway, it may not be always the case like in aquiclude layers with extremely heterogeneous compaction characteristics.
In this class of features also the hydraulic and hydrological ones are included. They are basically constituted by groundwater bodies and surface water body. Surface water bodies indeed strongly affect the hydraulic regime of the shallow aquifer. This aquifer is commonly used for non drinking usage, included heating and cooling.
Thus the *surface water body* feature includes not only some identification data but also some important information to be used in the numerical modelling phase (see Section 4.3). These include, beyond the location, the evolution over time of the hydraulic head and the temperature. In the case the surface water body is a river, these temporal sequences need to be differentiated over different sections and the identification of pertinent monitoring network points (if any) are included. Among data characterising the surface water body, the fluid transfer coefficient depends on the river or lake bed and the related clogging layer. It should be noted that, strictly speaking, the inflow and outflow transfer coefficient may be different. This is true especially in case of river-aquifer interaction when the bottom of the river bed presents a clogging layer much thicker (o with extremely lower hydraulic conductivity) rather than the sides and the river tends to feed or to receive water from the aquifer.

As regards the *groundwater* layer, it is characterized basically by the piezometric field. This in turn defines the hydraulic gradient field both in terms of module and direction. The piezometric field is usually represented in a GIS as a raster surface or through contour lines. The passage from these two representation is straightforward with common geoprocessing tools. In the end the groundwater is represented by a shape file of equally spaced points (on the basis of the raster grid). A crucial parameter that has to be included is the thermal dispersivity of the aquifer. Thermal dispersivity is actually an extremely difficult parameter to determine. It is indeed related to the scale of the problem. Its determination is usually derived from literature, from tracer tests (Epting et al., 2013) or by calibration. In next sections the role of calibration through numerical modelling will be discussed.
Both groundwater and surface water body feature are linked with the *environmental monitoring* class. This feature class includes the network monitoring the groundwater. This is basically made up of piezometers. The information included in this feature class contain the detail of piezometric levels and temperature records when available. These informations, in the form of time-value pairs, namely time histories, need to be linked to this feature class. This connection can be in the form of a unique identified appended to the point features of the class. In the case the piezometer is equipped with continuous monitoring sensor, it is also crucial to know the depth at which it is located where the sensor is installed. Indeed in the urban context, vertical temperature profile may present significant discontinuities and heterogeneities. This is due to the increased probability of thermal interference that are actually located at precise depth (e.g. discharging wells with altered temperatures). Depth is also useful to identify multiple sensors along the same piezometer in the case of multi-level measurement. Multilevel sensors are indeed used in monitoring networks to highlight vertical heterogeneities and highlight any thermal stratification in the aquifer in large monitoring networks (Köhler et al., 2015). In the case of multiple aquifers in the study domain (e.g. a shallow unconfined aquifer and a deeper aquifer confined by an impermeable layer) also the information about the groundwater body that is measured by the sensor is important.
It is worth to know that in Italy piezometers are also installed as part of the authorisation requirements for the installation of open loop systems for environmental protection reasons. Hence these piezometers are a precious source of information for conceptual model verification and for the monitoring of the thermal affection produced by these entities. The entities producing thermal impact on the aquifer are the focus of next paragraphs.

4.2.3 Entities producing thermal and hydraulic impact

The urban context is characterized by the intensive usage of the surface and subsurface resources. Due to urbanization, several anthropogenic heat fluxes exert an influence on the subsurface beneath modern cities (Benz et al., 2015; Menberg et al., 2013; Zhu et al., 2010). It is indeed widely accepted that several anthropogenic factors determine the so

called *subsurface heat island effect* (SUHI) (Ferguson and Woodbury, 2007) as previously cited in Section 2.4.2.
In this category the thermal and non thermal uses of the aquifer(s) are included. These uses include the existing borehole heat exchangers that can be included in a point shape file. In order to properly model the thermal impact of the heat exchanger, its maximum depth has to be known together with the thermal load profile. Alternatively the temperature at the external wall can be taken into account too. The temporal profile representing the use of the single BHE, as already explained for the case of environmental monitoring layer, is a list of *time - value* pairs that can be stored in an external file. In this case the attribute in GIS contains the reference to the proper time history.
Among the other *active users* of the aquifer, water wells are to be included in the *aquifer use* layer that is made up of the entities that exchange mass with the aquifer. Hence wells for water abstraction are included as well as discharging wells from industrial processes or open loop shallow geothermal systems. Crucial information related to groundwater use is, beyond the pump rate profile (conventionally a negative quantity is regarded as injection while positive values represent water abstraction), the range of depths at which the well is screened. From these data it is possible to identify the aquifer that is interested by the mass exchange. In most cases it is the shallower one due to water protection reasons.
In the case of water discharge within an aquifer, also the temperature of discharged water has to be defined. The temperature and the pump rate complete profiles can be stored in external tables/spreadsheet files and hence in the GIS the unique identifier is included.
It was previously mentioned that monitoring piezometers are usually installed as requirement for authorisation in open loop shallow geothermal systems in Italy. In the case a monitoring network exist for the sake of observation of the thermal plume, the identifiers of these points of the *environmental monitoring* layer are included.
Thermal impacts on the subsurface are also operated by *passive users*. These users are entities that are exchanging heat fluxes with the subsurface because of their underground location. Among them there are linear infrastructures (e.g. urban tunnels, district heating network, sewer pipe network, etc.) and large underground structures (e.g. car parks and building basements). From the topological point of view they differ because of the dimensions involved: infrastructure are characterized by their axis and cross section while underground structures are geometrically defined by the footprint area and the depth.
Linear infrastructures include urban tunnels as metro lines, railway or road tunnels but also distributed systems as sewage and district heating. Their main dimension is the longitudinal extension. Because of this, section information are provided (with the height and width defining the size) together with the axis that actually represents the entity position (included the elevation). Since they are in contact with the ground, internal temperature profile has to be identified analogously to the thermal users with time histories. Differently from BHE and aquifer users, in this case the thermal transfer

coefficient ϕ_{th} has to be evaluated and related to each of the entities. This coefficient is related to the thermal conductivity and the thickness of the medium separating the internal environment from the ground. This can be calculated analytically:

$$\phi_{th} = \left(\sum \frac{th_i}{\lambda_{s,i}} \right) \tag{4.1}$$

where $\lambda_{s,i}$ is the thermal conductivity of the i-th layer while th_i is its thickness. Similarly underground structures fields include the reference to a profile of the internal air temperatures and heat transfer coefficient. They can be usually linked with a cadastral code that identifies univocally the structure. Also the knowledge of structure typology is of a certain importance. Indeed it is possible to relate the use of the underground space to the thermal profile in the case that monitored data are missing (e.g. analytical formulation for unheated underground space temperature reported by Tinti et al. (2017)) Underground structures are, for example, large underground parks that are increasingly being constructed in urban areas (Ryżyński and Bogusz, 2016) or basement level of buildings. In this latter case, it is usually possible to assume that the indoor temperature is kept substantially constant throughout the year. A crucial attribute is the depth reached by the structure. In the case of a building basement, it might be unknown. Hence depending on the number of storeys above the ground level it is possible to assess in a simplified manner the necessary underground storeys (e.g. cellar and private parking). In this study it was assumed an average height of the underground levels of about 3 m, slightly lower than for the levels above the ground (3.125 meters from Dorfner (2011)).
High density of buildings in urban area result in an unmanageable number of entities within a numerical model of the subsurface. This will be evident in the application of the method to Turin urban area (see Chapter 6). It is thus clear the need to generalize and aggregate neighbouring basements depending on the depth reached. Buildings are actually the focus of the next paragraph.

4.2.4 Built environment

Urban areas are characterized by the high density of constructions and population. Furthermore, in the perspective of this work, the built environment constitutes one of the key aspects representing the demand side of the energy planning.
Hence the heating and cooling loads represent the minimum set of information about structures, beyond their footprint. Indeed thermal loads are not always given by the cadastre or the local authorities. In the case thermal loads are not known, information about the height H or the number of storeys n_{fl} can be used for a first approximation calculation. In the case number of storey is not directly known, it is necessary to use the height of the building and apply known relationships as, starting from Schiel et al. (2016):

$$n_{fl} = 0.32 \cdot \left(H - H_{roof} \right) \tag{4.2}$$

where H_{roof} is a correction due to the height of the roof space that should not be taken into account when considering thermal loads.
The number of storeys is thus connected to the number of housing units that compose the building. These in turns are linked with the service space as cellars and car parking. Hence the height can be turned indirectly linked to the number of underground storeys and hence to the basement depth as previously explained (see Section 4.2.3).
The number of storeys define, together with the footprint area the useful factors to calculate the floor area to be conditioned. This value is of particular importance in the common case that the energy consumption of the building is not monitored or otherwise not known. By knowing the building typology it is indeed possible to calculate the thermal loads for each building. *Building class* hence collect the data subdivided by building typology. This is useful as several studies focused on the definition of typical building typology (Corrado et al., 2012) classified on the basis of their use destination, age of construction and dimensions (being the surface to volume ratio rather important when dealing with the thermal balance of a building). For every building typology, also based on Energy Certification (in Italy it is compulsory to certify the energy performance of each dwelling that is hired or sold), the yearly thermal load per unit area is thus known. This value is then simply multiplied by the total area to be served.
Once defined the heating and cooling demand of the building, it can also be related to the geothermal potential of the area beneath and around the building (as explained in Section 4.5). Thus the satisfaction ratio for energy supply both for the heating and cooling season can be easily calculated, leading to the definition of energy deficit or surplus (see an example in Figure 3.10).

4.2.5 Hydro-Thermal regime

The thermal and hydraulic regime theme basically collects the results from the numerical modelling phase. Thus this category of data includes a series of site-dependent quantities that might be mapped in order to represent the thermal state of the aquifer. For each of the layers identified in the *stratigraphy* class, the couple of values of groundwater velocity and of temperature are defined. Hence within this feature class a vertical profile of temperature and groundwater velocity can be obtained over all the area at equally spaced points. This information can then be post-processed (as explained in Section 4.4.2) to calculate the proper attribute value of *heating potential* and *cooling potential*. These values represent the first and main result of the method. It should be noted that without the knowledge of the groundwater velocity field, conduction is the unique mechanism that can be taken into account.
It should be noted that due to the time-dependent boundary conditions (e.g. Air temperature, river levels, hydraulic head, discontinuous aquifer exploitation, etc.) the thermal and hydraulic regime is typically transient. This is especially important for the thermal regime, as the temperature can significantly vary during the season as a consequence of the thermal users of the aquifer.

The maximum and minimum temperature during the cooling and the heating season respectively will be taken as conservative assumption of the operative conditions that define the geothermal potential. These "thermal pictures" of the domain are in line with the post-processing procedure that is carefully analysed in Section 4.4.2. From the above, the *hydro-thermal regime* theme includes multiple thermal pictures at different time moments. In general, the significant thermal pictures are at the beginning and end of the heating and cooling seasons respectively, in order to define the dynamics and movement of thermal plumes. In addition to these four conditions the extreme temperature variation within the operative seasons have to be defined to calculate the geothermal potential of each cell.
Once the heating and cooling geothermal potentials are defined, the satisfaction ratio of the heating and cooling demand of the buildings (this attribute is associated with the built environment theme) can be quantified through the GIS tools. The overall potential of the area can indeed be calculated by simple summation of the site-specific potentials by the proper dimension of the cell. This latter aspect will be specifically addressed in Section 4.5.

4.3 Real thermal condition assessment

Several approaches for geothermal potential assessment have been proposed in recent years as it has been showed in Chapter 3. The main novelty in the method presented in this work lies in the integration of classical approaches with the numerical modelling tools. One of the main downsides when dealing with geothermal potential assessment in urban areas is the improper handling of highly heterogeneous and time variable thermal conditions at the site.
The aim of this second step within the procedure described in Figure 4.1 is to provide a reliable temperature field. Indeed the comprehension of thermal regime is of the outmost importance when dealing with the shallow geothermal energy management (García-Gil et al., 2020). The derived temperature field can be then subsequently processed through the GIS tools to calculate the geothermal potential.
Only numerical models are able to properly capture the thermal regime (and the hydraulic one) within a domain where multiple external and internal transient boundary conditions are involved. Beyond the planimetric position, due to anthropogenic heat fluxes and to the topographic boundary, the vertical dimension is of the outmost importance. Hence the need arises for tridimensional models. From a topological point of view groundwater bodies should be entirely included within the models independently from the urbanisation boundaries. This is because the single groundwater body is defined as a volume of groundwater for which hydraulic, thermal and chemical boundary conditions can be defined. Models can include single or multiple groundwater bodies that can be connected or isolated.
Most of the largest cities were established where large water resources are available.

Hence most of them are placed along rivers and above an aquifer zone that can supply clean water. Unless it is otherwise stated, it will be assumed that an aquifer is present within the domain where the geothermal potential has to be assessed. The discussion results to be obviously simplified in the case that no aquifer levels are present in the area. In such a case the groundwater velocity field becomes negligible and one may take into account the conduction heat transfer mechanism only.
It was demonstrated (García-Gil et al., 2015a) that neglecting the groundwater flow whenever it is present and the relative advective contribution to heat transfer is extremely conservative and leads to significant error. In the perspective of optimisation in shallow geothermal energy resource, the advection and dispersion hence represent an essential issue. It is clear that the need arises to adopt also in the numerical solution the coupled mathematical formulation of hydraulic and thermal physics.
A series of factors as level variations of surface water bodies, discontinuous use of abstraction wells, rainfall infiltration, etc. induce non-stationary hydraulic conditions. Also thermal regime does not reach steady state conditions as a result of seasonal air temperature variations, urban tunnel thermal fluxes and time-dependent uses of the aquifer (e.g. heating and cooling season of GWHP systems). Thus the numerical models adopted in this phase must be able to handle transient conditions.
The software package that is used for the numerical modelling phase needs interface capability in order to import the datasets of the previously explained classes (*hydrogeology, entities producing thermal and hydraulic impact* and *built environment*). Also export of the hydraulic and thermal field has to be performed to the georeferred database in proper format.
Once the area of interest is defined, the model domain has to reach at least the maximum BHE drilling depth. In the case BHE are already present within the study area, it should be verified that a minimum vertical tolerance is maintained in order to properly account for vertical diffusion effect at the bottom of the heat exchanger. It should be noted that usually horizontal thermal diffusion is prominent, especially when a groundwater flow is present.
Heterogeneities in the model domain are described by the stratigraphy dataset from GIS. Hence the numerical model domain has to be subdivided in homogeneous parts before assigning the proper hydraulic and thermal parameters (obtained by the attributes in the database).
Several elements have to be taken into account in the model domain discretization. Surface water bodies, underground structures and infrastructures have to be fully included in the 3D geometry. This allows to define the interface area where heat and fluid exchange take place. On these surfaces proper transfer coefficients have to be applied in combination with the proper boundary condition (see Section 4.3.1). Water wells (including the Open Loop systems) and BHE have to be taken into account during the mesh generation process as well. Due to the relative dimensions of the cross section with regards to the extension of the model, their geometry has to be simplified. Hence they have to be modelled as linear vertical (or transverse) elements. Due to the highly

transient conditions that they induce in the subsurface during operation, a denser mesh is requested around these point.

4.3.1 Initial and boundary conditions

Urban areas present intensive use of resources like energy and land surface. As a response to the land scarcity, cities are developing in height both above and below the terrain level (Brandl, 2016; Mielby et al., 2017; Parriaux et al., 2004). The increasing use of the subsurface resources induces permanent temperature level increase, namely the *Subsurface Urban Heat Island* (SUHI) (Rivera, 2016). Also wider variations in hydraulic and thermal regime respect to rural areas are identified below cities.
Anthropogenic heat fluxes hence gain much importance and have to be modelled properly for the sake of optimisation of geothermal resources in urban areas. These heat fluxes may indeed be regarded either as thermal pollution or as an additional resource (Banks, 2009; Rivera et al., 2017; Zhu et al., 2010).
From all the above, a *potential natural state* can be distinguished from the *present thermal state* (Epting and Huggenberger, 2013). In the following the boundary conditions will be listed and analysed starting from the natural boundary conditions. In fact the latter scenario is built adding the anthropogenic boundary conditions to the potential natural state.
Assuming that model boundaries match groundwater bodies borders, the delineation of boundary conditions is quite easy. Regarding hydraulics on the lateral boundaries three conditions may occur:

- known hydraulic head: it usually happens when groundwater monitored data are available thanks to the presence of piezometers in proximity to the GWB border;
- surface water body: rivers and lakes may feed or drain the shallow aquifer depending on the relative hydraulic head difference (these situations can coexist at different locations or can alternate depending on the level variations);
- impermeable outcrops, low-permeability layers or flow barriers : this situation occurs when bedrock layers emerge (usually associated with topographic discontinuities as hills) or when the hydraulic gradient field is known to be parallel to the boundary. In this case the mass exchange can be neglected through the lateral boundary.

In the first situation the hydraulic head is directly imposed to the solution, delineating a Dirichlet's boundary condition. In the second situation, hydraulic heat is imposed through a transfer coefficient that defines the *opposition* to groundwater level variation due to clogging layers. This is a typical example of Cauchy's boundary condition. In the third case a condition of null water flux is imposed as Neumann's boundary condition. Neumann's boundary condition indeed imposes a flux entering or leaving the model

domain. Anyway it is rare to know the water quantity leaving the large surfaces that bound a city scale model. In the case rivers run within the domain (e.g. in the case multiple GWB are included in the model), a Cauchy's boundary condition has to be imposed at proper location.
Upper and lower surfaces may account for rainfall infiltration or mass exchange with underlying aquifers. In the latter case, null values are common as the depth within the model domain is usually sufficient to reach bedrock or very over-consolidated layers with low permeability. As regards the upper surface, it should be mentioned that only a minor part of the rainfall infiltrates. The share of infiltrated water is even smaller in urban areas where sealed areas are extremely relevant. In the case of absence of data, infiltration rates can be obtained simply scaling data from rain gauges by a reduction factor (e.g 1/3 for unsealed surfaces and 1/30 for sealed ones (Epting and Huggenberger, 2013)).
From the thermal point of view conditions to be imposed at the outer boundaries of the model are:

- known temperature (Dirichlet's boundary condition): along the surfaces where flow enters the model temperature has to be imposed. This is usually the case of data from environmental monitoring (e.g. piezometers, river water quality station) or from weather stations (surface air temperature);
- heat flow (Neumann's boundary condition): this is the case of geothermal heat flow.

At the upper boundary air temperature can be imposed. Enhancement regarding upper thermal boundary condition can profit from recently developed tools that reduce computational effort, limiting the model to saturated zones only (e.g. SoilTemp tool (Kupfersberger et al., 2017)). Lower boundary thermal condition can be either modelled as geothermal flux (it can be known from regional studies, e.g. Geothopica Project (Consiglio Nazionale delle Ricerche, 2014)) or as fixed temperature in the case deep boreholes temperature measurements are made available.
All the boundary conditions described so far take into account natural processes that can take place also in rural areas without any anthropic settlements. In urban areas, beyond the natural processes, anthropic presence induce several effects that can be modelled with the entities described in Section 4.2.3.
Active users of the subsurface aquifer(both thermal and non thermal ones) can be treated as mass (and eventually heat) sources or sinks. Depending on the top and bottom depths at which the wells are screened, the proper number of nodes has to be set as an internal boundary producing or draining the fluid or heat budget. Due to the discontinuous nature of aquifer uses, also time discretization on the boundary condition plays a role. It was demonstrated (Lo Russo et al., 2014) that at least monthly average values of discharge pumping rate and water temperature are needed to reliably replicate the thermal alteration (TAZ) development. In the case a time history is available with far better detail, for the sake of limiting the computational effort, it can be advisable to aggregate the

data through algorithms (Bernier et al., 2004; Bonsor et al., 2015; Marcotte and Pasquier, 2008) or even simply averaging on hourly or daily basis. As regards thermal uses of the aquifer, thermal Dirichlet's boundary condition, namely imposed temperature, has to be applied only to the nodes of injection wells.
Borehole heat exchangers instead exchange with the ground only heat and not mass. Hence heat transfer boundary condition can be imposed in the case the mean fluid temperature and the borehole thermal resistance is known. Alternatively, also simplified numerical mono-dimensional formulations can be employed (Al-Khoury et al., 2010; Eskilson and Claesson, 1988).
Passive users exchange heat fluxes with the ground because of their position. Hydraulic influence is indeed purely caused by impermeability and not by mass exchange. Hence no fluid flux boundary condition has to be established at the corresponding locations. Otherwise, in the case the entity geometry is fully reproduced, hydraulic influence can be simulated by simply applying extremely low values pertaining the hydraulic conductivity. From the thermal point of view, these passive entities imply the use of heat transfer boundary conditions (Cauchy's BC) that impose a thermal resistance through the heat transfer coefficients between the domain and the temperature of the internal boundary.

4.3.2 Uncertainties on parameter estimation

The present work focuses on the assessment of geothermal potential at the city scale. Because of the purpose of this work, attention is focused on large urban areas. Extension of typical study area (GWB scale) and dependence of geothermal potential on several properties of geomaterials result in uncertainties. Hydraulic and thermal regime are indeed derived from numerical models that are based on input properties as hydraulic conductivity, thermal capacity, thermal dispersivities, etc. Heterogeneities in the geological layers and the need for simplification in the mesh generation process further lower the precision of the results.
The basis to limit the uncertainties is the precision of input data (external boundary conditions and material properties). As regards external boundary conditions, the values have to be known from monitored data or from verified hydrogeological conceptual models. In case data are not available at the location of the external boundaries, interpolation and extrapolation techniques have to be used. This is especially true in the case of hydraulic heads. Whenever river levels or piezometric heights are known in proximity to the boundaries, the values can be shifted by adding a correction term depending on the riverbed/bottom of the aquifer. Similarly whenever temperature of recharge water is not known, it can be assumed from monodimensional thermal calculations up to the depth of the piezometric surface. It should be noted that in the case the aquifer lies below the omoeothermic depth, a constant temperature value can be assumed in the case no thermal uses are made upstream to the model boundary.
As regards material properties influential factors are many. Thermal conductivity is

the most influential for borehole heat exchangers (Casasso and Sethi, 2014; Han and Yu, 2016). Hydraulic conductivity is of primary importance not only for open loop schemes (Lo Russo et al., 2014) but also for closed loop schemes in order to account advective contributions. Thermal dispersivity is of extreme importance when dealing with groundwater fluxes. Nevertheless the determination of its value is subject to large uncertainties and can be related to the scale of the problem (Sethi and Di Molfetta, 2007). Reported values in literature range from 0,1 m to 20 m (Casasso and Sethi, 2015; Epting et al., 2013; Molina-Giraldo et al., 2011; Sethi and Di Molfetta, 2007) and are mainly derived from numerical evaluations rather than from dye tracer tests. Typical ratio between longitudinal and transverse thermal dispersivity is 1/10.
Material properties values should be then preferentially chosen on the basis of site and laboratory tests. On vast areas it is however extremely expensive to carry out proper test because of the number of lithologies included in the subsurface volume under examination. Hence in order to enhance accuracy of the model results, numerical calibration can be performed whenever a sufficient amount of monitoring data are available at multiple locations.

4.4 Site-specific geothermal potential

Most of the methods to assess shallow geothermal energy potential require a background temperature as input parameter (see Chapter 3). To this regard, the highly detailed results from a thermo-hydraulic numerical simulation can be interpreted as a technical enhancement in the definition of the potential.
Besides the temperature field, numerical modelling results in an highly detailed description of the hydraulic regime. In order to take advantage of these results, a method that accounts for heat transport mechanisms related to groundwater fluxes has to be adopted. As previously mentioned, only few methods are capable to deal with advective contributions. Hence an enhancement of the method developed by Casasso and Sethi (2016) is proposed in the following in order to account for groundwater flux effects on heat transfer.

4.4.1 Influence of advection and dispersion on borehole heat exchanger potential

The G.POT. method (Casasso and Sethi, 2016) among the approaches discussed in Chapter 3, has the advantage of a strong analytical and theoretical background that makes its explicit formulation not limited to specific geological or geographical context.
The method is however based on Infinite Line Source model (Carslaw and Jaeger, 1959). This results in the limitation of the field of validity to homogeneous semi-infinite space and to purely conductive media.
For the sake of simplicity the expression of the geothermal potential Q_{BHE} is reported

in extended version:

$$Q_{BHE}[W] = \frac{8 \cdot \left(T_0 - T_{lim}\right) \cdot \lambda \cdot L \cdot \frac{t_c}{t_y}}{-0.619 \cdot \frac{t_c}{t_y} \cdot \ln\left(\frac{r_b^2}{4\alpha t_s}\right) + \left(0.532\frac{t_c}{t_y} - 0.962\right) \cdot \ln\left(\frac{r_b^2}{4\alpha t_c}\right) - 0.455\frac{t_c}{t_y} - 1.619 + 4\pi\lambda \cdot R_b} \tag{4.3}$$

where T_0 is the background temperature, T_{lim} is the heat carrier fluid limit temperature, λ and α the ground thermal conductivity and diffusivity respectively, L the borehole length, t_c the length of the operative season, t_s the borehole lifetime, t_y the year duration (or cyclicity of the operative season), r_b the borehole radius and R_b the borehole thermal resistance.
From the above, the driving parameters involved are: the threshold and starting temperature values, the thermal resistance, the radius and the length of borehole, the thermal conductivity and diffusivity of the soil, the fraction of time over the year of operation and the time-span t_s on which the geothermal potential has to be assessed.
Once the borehole heat exchanger is defined through its dimensions, materials and operative use, the dependency on remaining factors can be rewritten in the following form:

$$Q_{BHE} = \frac{C_1 \cdot \lambda \left(T_0 - T_{lim}\right)}{C_2 - C_3 \cdot \ln\left(C_4/t_s\right)} \tag{4.4}$$

where

$$C_1\ [W/K] = 8 \cdot \lambda L \cdot \frac{t_c}{t_y}$$

$$C_2 = \left(0.532\frac{t_c}{t_y} - 0.962\right) \cdot \ln\left(\frac{r_b^2}{4\alpha t_c}\right) - 0.455\frac{t_c}{t_y} - 1.619 + 4\pi\lambda \cdot R_b$$

$$C_3 = -0.619 \cdot \frac{t_c}{t_y}$$

$$C_4 = \frac{r_b^2}{4\alpha}$$

For the purpose of simplicity, the dependency in Equation 4.4 of C_3 and C_4 values from soil thermal conductivity is not made explicit. These two quantities indeed depend on soil thermal diffusivity α. This is in turn defined as the ratio of thermal conductivity over thermal capacity of the material.
The thermal conductivity is in general calculated through Equation 2.11. In the absence of any groundwater flow (or null thermal dispersivities) and under the assumption of

isotropic behaviour all the components of the second order tensor:

$$[\lambda] = \begin{bmatrix} \lambda_{ii} & \lambda_{ij} & \lambda_{ik} \\ \lambda_{ji} & \lambda_{jj} & \lambda_{jk} \\ \lambda_{ki} & \lambda_{kj} & \lambda_{kk} \end{bmatrix} \tag{4.5}$$

assume the same value. Thus the tensor degenerates in a scalar quantity and can be rewritten as: $\lambda = \lambda \cdot \mathbf{I}$. Although thermal behaviour is known to be anistropic in geomaterials (van Rooyen and Winterkorn, 1957), a simplified approach is often adopted due to lack of determination of the directional behaviour of materials especially when dealing with the territorial scale. Furthermore in the case that the groundwater velocity vector is not null, the components values vary and the tensor describes the heat transport in the three dimensions.
On the contrary the geothermal potential is defined as a scalar quantity. However Equations 3.16 and 4.4 are not intended for use with a matrix of thermal conductivities. In order to deal with hydrodynamic conditions, the need arises to define a proper scalar quantity to replace the hydrostatic value of thermal conductivity. This scalar quantity needs to average the thermal behaviour of the ground volume interested by heat exchange. The spherical part of the tensor of the thermal conductivities was selected to this end:

$$\Lambda_1 = \frac{tr\,[\lambda]}{3} = \left[(1-n)\,\lambda_s + n\lambda_f\right] + \frac{\rho_f c_f v_D \left(\alpha_L + 2\alpha_T\right)}{3} \tag{4.6}$$

In order to verify this assumption, a set of numerical analysis were performed. The analyses were devoted to the assessment of the long term geothermal potential of a Borehole Heat Exchanger.
For the sake of consistency with the G.POT. method (Casasso and Sethi, 2016), a numerical model was set up reproducing the thermal behaviour of a single Borehole Heat Exchanger subjected to a cyclic thermal load. The thermal load profile presents an emi-sinusoidal shape over the operating time followed by a recovery time lasting the rest of the year. The magnitude of the peak load is determined, according to the original work, from the yearly average thermal load Q_{BHE}. The entire service life of the installation was assumed to be 50 years as in standard civil engineering projects.
Numerical coupled TH simulations were performed using the Finite Element Method and the code FEFLOW was employed in this study.
Model domain was carefully chosen to avoid the influence of boundary conditions restraints on the heat budget of the borehole heat exchanger. Therefore the BHE was placed in the centre of a square area of 100 m side length. For the purpose of investigating plausible settings in real conditions, the BHE length was chosen equal to 100 m. Hence the model was extended up to 150 meters depth in order to ensure sufficient distance with external boundary (see Figure 4.3). The domain was made up of 177861 prismatic elements (triangular base). Tridimensional mesh was obtained through extrusion of 2D domain discretization with the *Triangle* algorithm (Shewchuk, 1996).

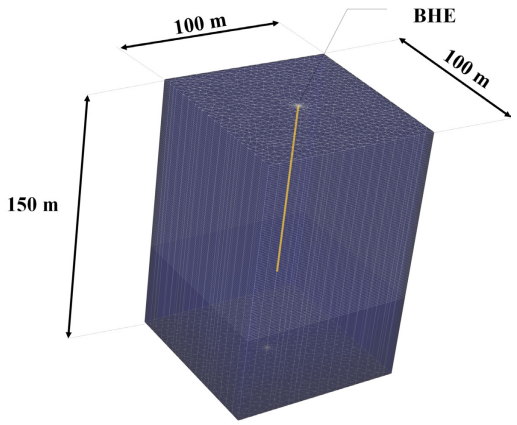

Figure 4.3: Numerical model geometry adopted for calibration of semi-analytical method: at the centre the Borehole Heat Exchanger (yellow line) along with the discretization in 101 layers and 177861 elements.

Mesh density was increased near in the central zone around the Borehole Heat Exchanger. In the vertical direction, domain was subdivided in layers of 1 meter thickness while an additional layer was placed at the bottom of the BHE to reach the maximum model depth. Because of the extreme dimensions ratio (few centimetres in width compared to 100 meter length), the Borehole Heat Exchanger was simulated through a mono-dimensional finite element representation. This *condensed* element follows the analytical formulation by Eskilson and Claesson (1988) that is implemented in the Finite Element code FEFLOW that was utilized in this work (Diersch, 2009).
Boundary and initial conditions were varied in order to analyse the long term geothermal potential of the BHE in a wide range of conditions. Analysis were focused on saturated conditions. Hence hydraulic heads in the model were kept above the top surface of the model. Hydraulic head boundary conditions were imposed at the lateral boundaries in order to reproduce a proper hydraulic gradient. This in turn determines, depending on the hydraulic conductivity, the desired groundwater flux velocity. The groundwater velocities investigated range from hydrostatic conditions to 1 meter per day.
At model bottom no hydraulic or thermal fluxes were expected due to the far position with respect to the Borehole Heat Exchanger. A large horizontal to vertical hydraulic conductivity ratio was adopted to properly limit vertical fluxes. In order to be consistent with the analytical model assumption, temperature was kept constant and equal to the initial one at the upper boundary surface.
Hydraulic and thermal parameters that were kept constant independently from the simulation are listed in Table 4.1. Parameters dependent from the particular condition to be reproduced are reported in the following.

Table 4.1: Parameters adopted in numerical validation of geothermal potential formula.

Parameter	Value
Porosity [−]	0.3
Vertical to horizontal hydraulic conductivity [−]	0.1
Thermal volumetric capacity $[Jm^{-3}K^{-1}]$	$3.01 \cdot 10^6$
Fluid thermal conductivity $[Wm^{-1}K^{-1}]$	0.65
Grouting thermal volumetric capacity $[Jm^{-3}K^{-1}]$	$2 \cdot 10^6$
Borehole radius $[m]$	0.065
Number of pipes [−]	4
Borehole length $[m]$	100
Heating season length $[d]$	120
Simulation time $[y]$	50

Due to the specific boundary condition adopted by the software, the setup of the borehole heat exchanger model needs the definition of a pump rate value in addition to the thermal load profile. Since the original method did not take into account the internal dynamics of the borehole heat exchanger, this value was determined through calibration of the numerical model. Thus a series of simulations were run adopting conditions included in the field of validity of Equation 3.16. The pump rate is linked to the instantaneous heat exchange by the energy balance equation:

$$Q_{BHE} = \dot{m} \cdot c_f \cdot (T_{out} - T_{in}) \tag{4.7}$$

where $\dot{m}$ denotes the heat carrier fluid mass rate, c_f the specific thermal capacity of the fluid, T_{in} the temperature at the inlet side and T_{out} the temperature at the outlet. Calibration was carried out by adopting a comparison criterium focused on the term $(T_0 - T_{lim})$ of Equation 4.4. The exact pump rate was thus obtained by trial and error, reducing or amplifying the value whenever the simulated temperature drop was excessively low or high, respectively. Indeed the temperature drop identifies the technical limit that defines the potential:

$$\left(T_0 - T_{lim}\right)_{FEM} = \frac{C_1 \cdot \lambda \cdot Q_{BHE}}{C_2 - C_3 \cdot \ln\left(C_4/t_s\right)} \tag{4.8}$$

The limit temperature resulting from the numerical analysis was chosen equal to the minimum value assumed by the heat carrier fluid mean temperature (see Figure 4.4):

$$T_{lim} = \min\left[\left(T_{in} + T_{out}\right)/2\right]$$

Calibration hence consisted of minimisation of the difference of second term of Equation 4.8 with respect to numerical simulation. It should be noted that once the mean

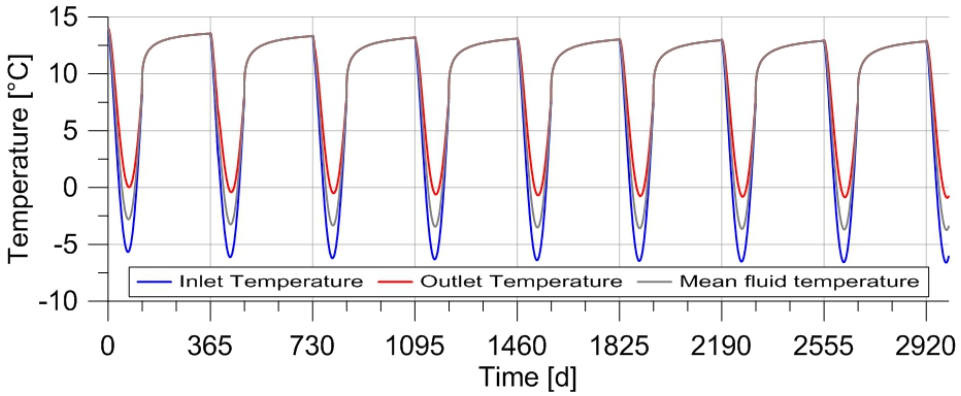

Figure 4.4: Simulated temperature evolution of the inner fluid of BHE. Model *C2* is taken as example. In grey the mean temperature. The local minima are assumed as the values of T_{lim} for the specific cycle.

Table 4.2: Model parameters for BHE pump rate numerical calibration.

Model [−]	Pump rate $[m^3/d]$	K_h $[m/s]$	i [−]	V_D $[m/s]$	α_L $[m]$	Pe [−]	$T_0 - T_{lim}$ $[°C]$
C1	15.80	10^{-3}	0	0	5	0	16.0
C2	27.95	10^{-3}	0	0	5	0	16.0
C3	15.80	10^{-5}	10^{-3}	10^{-8}	10	0.09	16.0
C4	27.95	10^{-5}	10^{-3}	10^{-8}	10	0.09	17.5
C5	27.95	10^{-3}	0	0	10	0	14.0
C6	27.95	10^{-3}	0	0	10	0	18.0

thermal load is fixed the only independent variable left in Equation 4.8 is the simulation time. Hence it is possible to define for an arbitrary simulation time the difference between limit temperature and initial value. This allowed to better compare numerical results with analytical prediction, substantially multiplying the number of compared values by a factor of 50. Figure 4.5 shows the results of six simulations. The pertaining parameters are listed in Table 4.2. The scatter plot represents the maximum temperature drop predicted by analytical formulation versus the numerical results. Thus an ideal consistency of the numerical model to the analytical prediction would lead to alignment along the bisector of the scatter plot. On the contrary, points located below this line denote underestimation of the revised analytical formulation, while points located above the bisector represent an overestimation.
Simulations *C1* and *C2* were obtained in hydrostratic conditions with different pump rate values. The fist attempt value was equal to 15.8 m^3/d correspondant to a heat carrier fluid velocity of 0.15 ms^{-1}. On the contrary model *C2* depicts the optimised result with a flow rate of 27.95 m^3/d. Simulations *C5* and *C6* were obtained by adoption of a

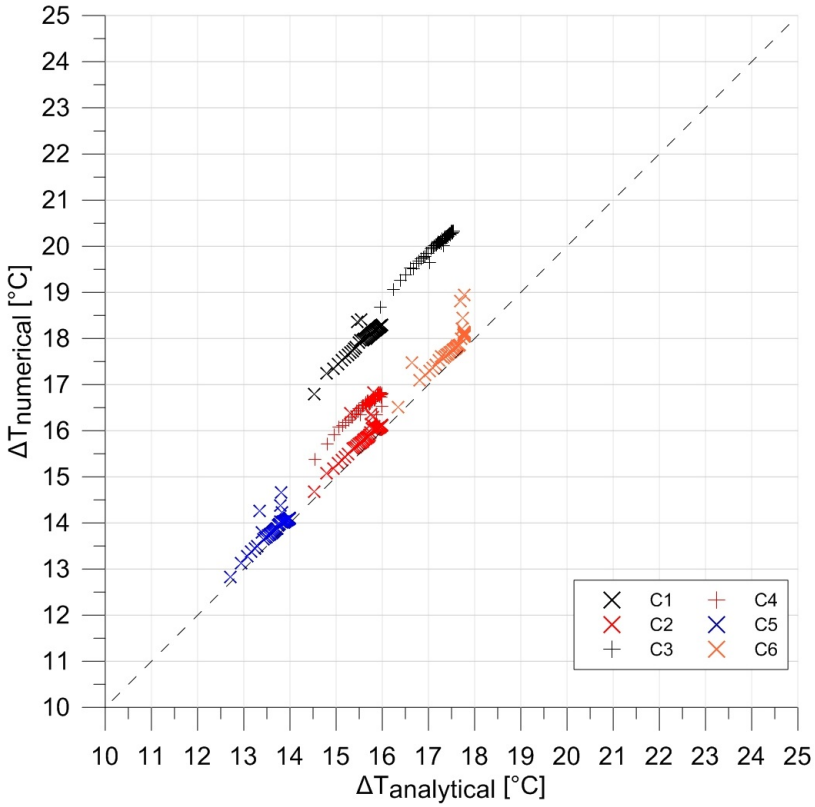

Figure 4.5: Calibration of the numerical model on the pump flow rate. Model parameters are listed in Tables 4.1 and 4.2.

different background temperature condition of ± 2 °C with respect to simulation *C2*.
It is clear that depending on the pump rate, the limit temperature changes. This is due to the inverse proportionality of the temperature drop with the pump rate (see Equation 4.7).
The bisector in Figure 4.5 delineates the perfect coincidence of numerical results with analytical prediction. Hence, the closer the points to the line, the best is the calibration of the numerical model. Among results of simulation *C1* and *C2* there is a remarkable bias of about 2.2 °C. Results of model *C2* are appreciably closer to the theoretical line and barely match it. An average difference of results to prediction of only 0.2 °C was obtained.
Results of models *C5* and *C6* that are obtained with the same pump rate of simulation *C2* show a distance with the theoretical line virtually equal to results from model *C2*. Hence the pump rate of 27.95 m^3/d was considered as the best esteem available and adopted in the following simulation to verify the assumptions on hydrodynamic conditions.
Comparison of simulation *C1* and *C2* with results from model *C3* and *C4* respectively,

Table 4.3: Model parameters for BHE long term potential numerical calibration in hydrodynamic conditions.

Model [−]	Pump rate $[m^3/d]$	K_h $[m/s]$	i [−]	V_D $[m/d]$	α_L $[m]$	Pe [−]	$T_0 - T_{lim}$ $[°C]$
D1	27.95	10^{-5}	$1.16\ 10^{-4}$	10^{-4}	5	0.0052	20.0
D2	27.95	10^{-5}	$1.16\ 10^{-4}$	10^{-4}	10	0.010394	18.0
D3	27.95	10^{-5}	$1.16\ 10^{-4}$	10^{-4}	10	0.010394	30.3
D4	27.95	10^{-3}	$1.16\ 10^{-4}$	10^{-2}	5	0.52	16.0
D5	27.95	$5\ 10^{-3}$	$1.16\ 10^{-4}$	$5\ 10^{-2}$	10	5.2	16.0
D6	27.95	10^{-3}	$1.16\ 10^{-3}$	10^{-1}	5	5.2	6.4
D7	27.95	10^{-2}	$1.16\ 10^{-4}$	10^{-1}	10	10.39	16.0
D8	27.95	10^{-3}	$1.16\ 10^{-3}$	10^{-1}	15	15.59	16.0
D9	27.95	$2\ 10^{-2}$	$1.16\ 10^{-4}$	$2\ 10^{-1}$	10	20.79	16.0
D10	27.95	$3\ 10^{-2}$	$1.16\ 10^{-4}$	$3\ 10^{-1}$	10	31.18	16.0
D11	27.95	$4\ 10^{-2}$	$1.16\ 10^{-4}$	$4\ 10^{-1}$	10	41.57	16.0
D12	27.95	10^{-3}	$1.16\ 10^{-2}$	1	5	51.97	4.3

delineates a marked increase in the deviation from theoretical bisector line. These results would suggest that the beneficial effect of the advection and dispersion on the Borehole Heat Exchanger potential is overestimated by adoption of Λ_1 in Equation 4.4. A number of simulations were then run to verify the assumptions explained previously about adaptation of Equation 3.16 to hydrodinamic conditions. Twelve further simulations were run in homogeneous thermal conditions with non null groundwater flow velocity. Parameters of these numerical simulations are listed in Table 4.3 while the scatter plot in Figure 4.6 shows simulation results. Also results from simulation *C4* that were obtained for hydrodynamic conditions are reported as well. The reference background temperature of 14°C was kept constant except for model *D1*. In this case a background temperature of 12°C was assumed. Limit temperature at the end of simulation was instead not kept constant for all the simulations. This allowed to investigate a wide range of temperature drops $T_0 - T_{lim}$ from 4.3 °C up to 30 °C.
Models *D2* and *D3* differ in the allowable temperature drop only, while all the other parameters were equal. Comparison of their results show that the driving parameter is actually the allowable temperature drop that was taken as the focus for verification.
Numerical results show without exception higher temperature drops than expected by analytical formulation. The analytical underestimation of temperature drop may indeed drive the installation in real conditions to excessively low temperatures. This can imply in extreme conditions freezing of the heat carrier fluid. This may damage or block the operation of the installation. Thus the application of the term Λ_1 needs a correction factor in order to reliably assess the technical geothermal potential of the

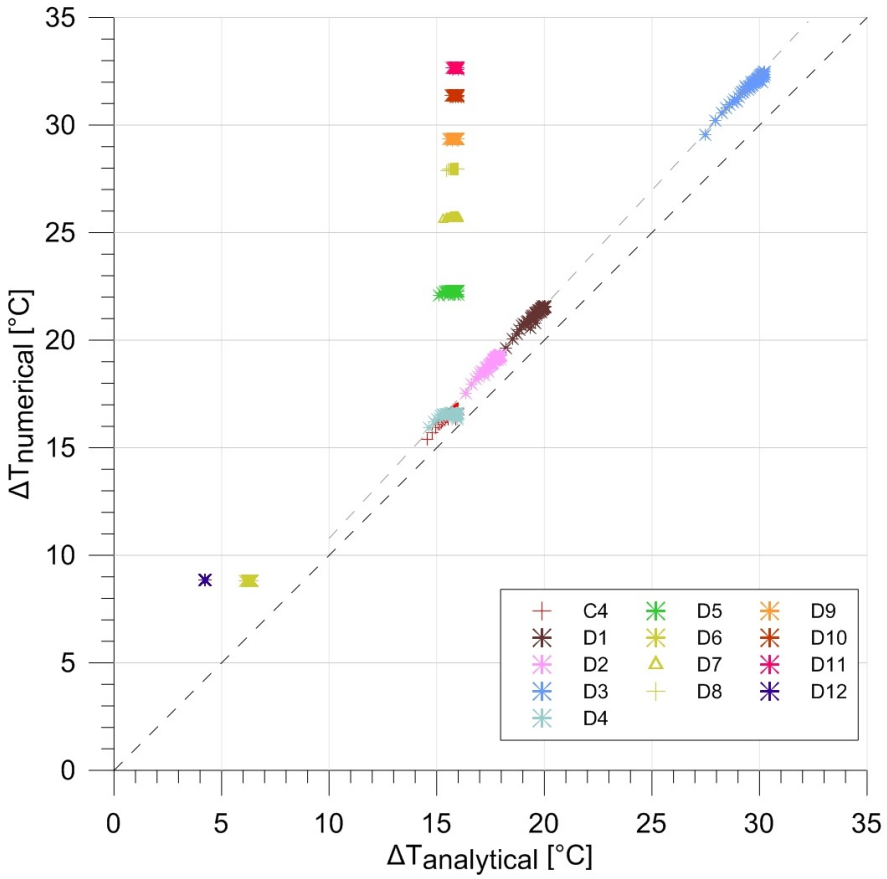

Figure 4.6: Verification of analytical predictions in hydrodynamic conditions through numerical models. Model parameters are listed in Tables 4.1 and 4.3.

Borehole Heat Exchanger. Comparison of results under different boundary conditions show a dependency of such a correction factor from hydraulic field.
It should be noted that model with lower groundwater flow velocity show a marked proportionality among analytical and numerical results (see results from models *D1, D2, D3*). This results in a substantial alignment along an inclined line on the scatter plot. From an analytical point of view this line represents an almost constant ratio of numerical temperature drops over the analytically determined ones. Almost perfect alignment would suggest dependency on the groundwater flow related parameters, even if results from model *D1* show a slighly larger distance with this virtual line. On the contrary, models with higher flow velocities result in an horizontal alignment on the scatter plot. This is due to the slight evolution of temperatures predicted analytically with respect to a numerical solution that does not show any trend. This may suggest that the numerical models are able to catch the complete recharge during the rest period of the subsoil interested by heat exchange with better detail than the analytical solution. Indeed at extremely high flow velocities, the x-axis range results significantly reduced. It

is evident from results of model *D12* that nearly collapse on a single point. As a result, the ratio of numerical over analytical temperature drops is to some extent dependent on the simulation time too.
The thermal dispersivity is a crucial factor in the assessment of non conductive components. It should be mentioned that its practical measurement still represents a challenge as it is dependent on the scale of the problem. With regards to thermal dispersivity influence, simulation *D6* and simulation *D8* were obtained with the same limit temperature at the end of the life of service. All the parameters were kept equal in these two models except for the thermal dispersivities that are increased by 3 times in the latter case. Numerical results significantly differ among the two models depicting higher temperature drops in the case the thermal dispersivity is higher. This is also confirmed by the significant difference of these two simulations with results of simulation *D7* with same groundwater velocity. The thermal dispersivity is indeed a middle value between the one assumed for models *D6* and *D8*. As a result, numerical predictions are included between the ones obtained by the two above mentioned models. Hence, the correction factor that has to be applied to Equation 4.4 cannot be simply related to the groundwater velocity. A reasonable relationship can instead be established with parameters that weights the advective and dispersive contribution versus the conductive ones. From the definition of Λ_1 in Equation 4.6 the first term represents the conductive mechanism while the latter one includes hydro-dispersive components. The ratio of the latter term over the first one hence describes their relative weights in the determination of Λ_1. Such a parameter is dimensionless and is commonly know in fluid dynamics as *Peclet number*:

$$Pe = \frac{\rho_f c_f v_D \left(\alpha_L + 2\alpha_T\right)}{3\left[n\lambda_f + (1-n)\,\lambda_s\right]} \tag{4.9}$$

In this study the extension to hydrodynamic conditions of the formula 3.16 is analysed. Then the hydrostatic conditions have to be included too. In hydrostatic regime the Peclet number is null as a consequence of the null Darcy velocity. Furthermore a linear relationship among the correction factor C_{gw} and the logarithm of the Peclet Number seems to be established in case of groundwater flow presence (see Figure 4.7). A relationship in the form of the following equation can be thus researched and numerically interpolated:

$$C_{gw}(Pe) = 1 + a \cdot \ln(Pe + 1) \tag{4.10}$$

The addition of the unit to the Peclet number allows the argument of the logarithm to be semi-defined positive. Indeed in case of hydrostatic conditions the second term assumes a null value and thus the correction factor assumes the unitary value. This is reasonable because in hydrostatic conditions Λ_1 equals the static thermal conductivity and no correction is hence needed. Quantitative assessment of the numerically fitted parameter a will be in detail discussed in the next, after the addition of further numerical results.
Range of application of original formulation of the method here analysed is limited to

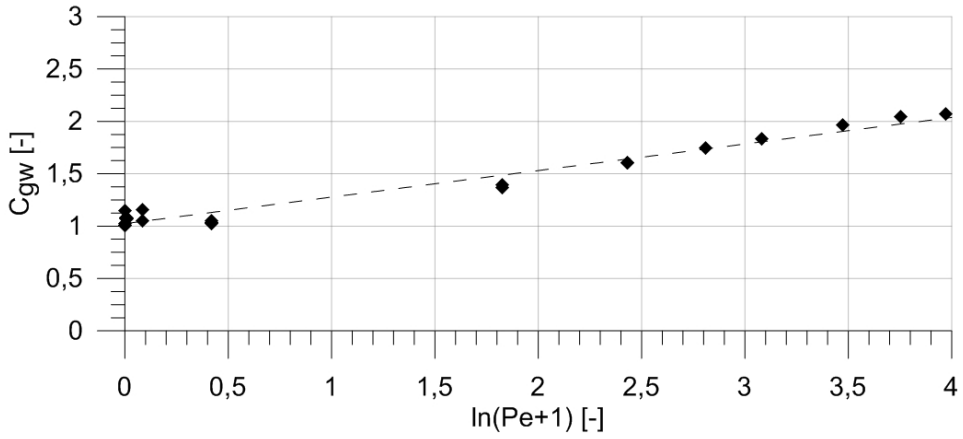

Figure 4.7: Ratio of the numerical results over the analytical prediction about the temperature drop. The quantity is plotted against the Peclet number for simulations reported in Table 4.2 and 4.3 with pump rate of 27.95 m^3/d.

homogenous temperature only due to the ILS assumptions. Anthropogenic interferences that are likely to take place in cities, result in discontinuities in the temperature vertical profile. Hence in such conditions, or whenever there are vertical heterogeneities, a depth weighted average value was chosen as representative for the entire borehole length. As an example it is possible to consider the background temperature T_0 at the site as:

$$T_0^* = \frac{\sum \left(T_{0i} \cdot th_i\right)}{L} \tag{4.11}$$

The same kind of relation is valid for the remaining position-dependent parameters. Several simulations indeed were conceived to test the use of a depth-weighted average value for the background temperature. Hence temperature differences were to be kept among different layers for the entire simulation time. This was possible by imposing as initial and external lateral boundary conditions an appropriate temperature value. Furthermore the vertical head flux was limited at the interface between layers at different temperatures. Hence a large ratio of vertical to hydraulic conductivity of 1/10 was chosen to recreate horizontal fluid flux. Nonetheless this anisotropy ratio can be representative of layers originated by sedimentation. Furthermore no heat flux was imposed as internal boundary condition at the interface between strata at different initial temperature (except for the vertical line of the BHE crossing the horizontal interface). This allowed to maintain this thermal difference during all the simulation time. By doing this, consistency of the assumption with the analytical solution was evaluated. It should be mentioned that simulations in heterogeneous thermal conditions were conceived in hydrodynamic conditions only, since the recharging water temperature is essential to keep the different thermal background thermal level. This is indeed representative of

Table 4.4: Model parameters for BHE long term potential numerical calibration in thermally heterogeneous conditions. In the temperature profile column numbers in brackets represent the range of depth to which the altered temperature is applied, base temperature is indicated after the semicolon.

Model [−]	K_h [m/s]	i [−]	V_D [m/d]	α_L [m]	Pe [−]	T_0^* [$^\circ C$]	Temperature profile
T1	10^{-5}	$1.16\ 10^{-4}$	10^{-4}	5	0.005	11	14°C (0-25); 10°C
T2	10^{-5}	$1.16\ 10^{-4}$	10^{-4}	5	0.005	12	14°C (0-50); 10°C
T3	10^{-5}	$1.16\ 10^{-4}$	10^{-4}	5	0.005	13	14°C (0-50); 12°C
T4	10^{-5}	$1.16\ 10^{-4}$	10^{-4}	5	0.005	15	14°C (0-50); 16°C
T5	10^{-4}	$1.16\ 10^{-3}$	10^{-2}	5	0.52	12	14°C (0-50); 10°C

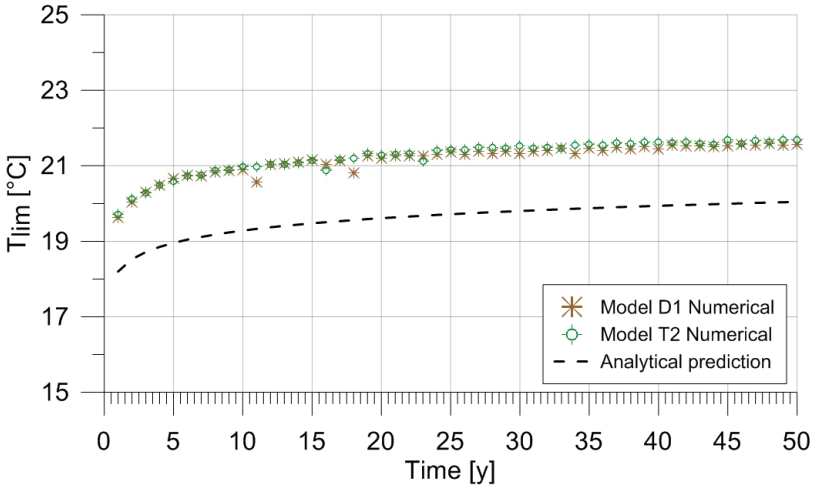

Figure 4.8: Numerical result comparison of heterogeneous model to equivalent homogeneous one.

possible real situations of interference due to heat sources/sinks in the upstream direction generating a thermal plume that involves the site of interest. Parameters adopted in the simulations with heterogeneous thermal conditions are listed in Table 4.4.
Model *T2* was obtained with the same parameters of model *D1* but with different thermal boundary conditions. Indeed both of them showed an average background temperature of 12°C and an allowable temperature drop of 20.0°C. However, model *D1* had homogeneous initial temperature field while model *T2* presented a discontinuity at the middle of the BHE. Figure 4.8 compares the results of these two models showing a virtually identical thermal behaviour of the borehole heat exchanger fluid in the two conditions. This extremely good agreement confirms the assumption of equivalence expressed by Equation 4.11. Results of the simulations listed in Table 4.4 are represented in scatter plot of Figure 4.9 together with the results of simulations *C4, D1* and *D3* that

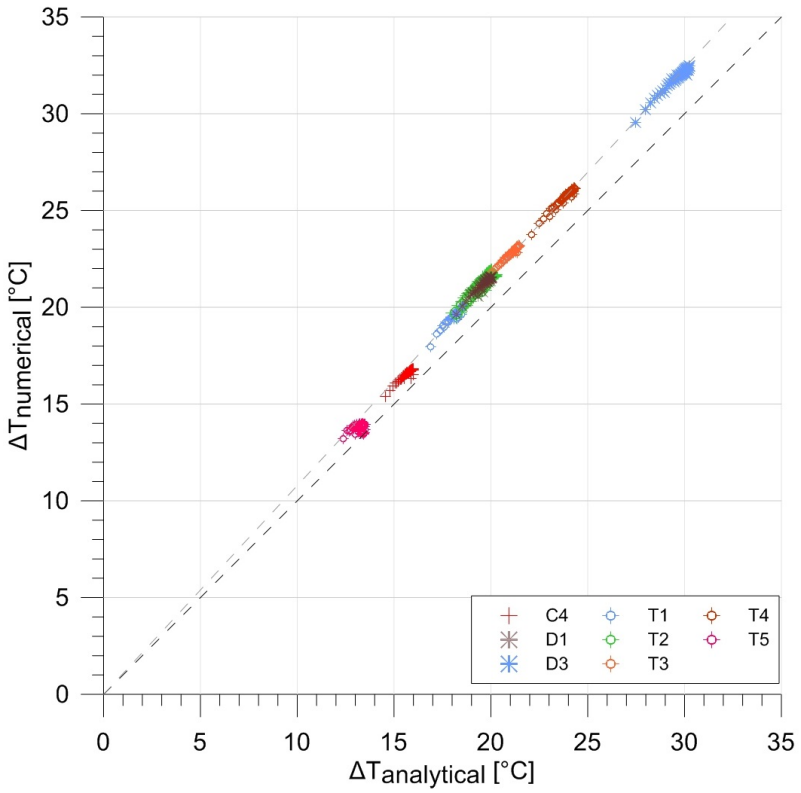

Figure 4.9: Verification of analytical predictions in thermally heterogeneous conditions through numerical models. Model parameters are listed in Tables 4.4 and 4.1.

have a virtually equal groundwater velocity.
Models *T1* to *T4* were set up with same hydraulic and thermal parameters. They only differed by the thermal background temperature. This was changed on various depth and temperature levels. These results are in line with the ones from hydrodynamic conditions, defining again a virtually perfect alignment on the scatter plot.
It should be noted that the data from heterogeneous conditions are situated on the same alignment of results from simulation *D3* with equal Peclet number. The mutual position of the dataset confirms that heterogeneous background temperature can be treated as an equivalent homogeneous situation. In fact evolution of temperatures in numerical models is barely defined by the mean temperature drop with respect to undisturbed conditions while the value from 4.11 correspond in analytical solution to this behaviour. It was previously mentioned that numerical model can better predict the complete thermal recovery of the subsoil. This results in higher differences of numerical results with respect to analytical predictions, especially when dealing with smaller number of cycles. Then the numerical interpolation of Equation 4.10 is expected to return different values of parameter a depending on the time. It should be however noted that this dependency is actually related to the ratio of the number cycles occurred over the total

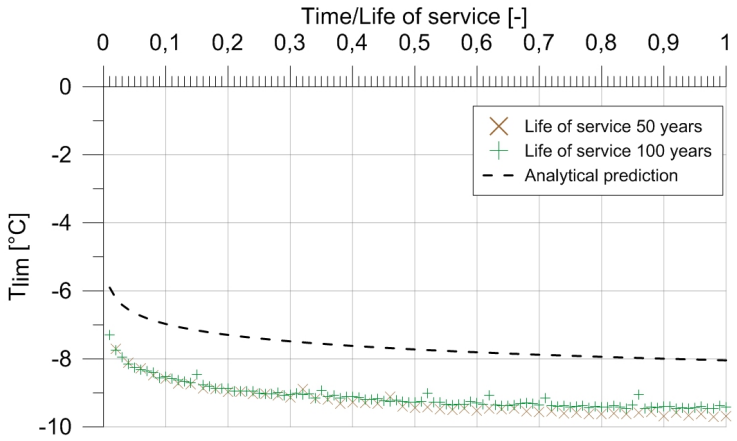

Figure 4.10: Numerical result comparison for different life of service duration. Model D1 is taken as reference case.

number of cycles in the life of service. Indeed temporal evolution of seasonal maximum temperature drop is virtually identical taking into account the same limit temperature at the end of a period of 50 or 100 years (see Figure 4.10). Thus the evolution of the temperature drop evolution with the number of cycle can be reported in non dimensional terms, gaining generality of results. Figure 4.11 indeed shows the resulting numerical interpolation for the parameter a at different time stages where the number of cycles of each of the graphs are normalised to the service life of the installation.
Interpolated values for parameter a tend to slightly evolve as the number of cycles rises. It should be also mentioned that the correlation factor is more than satisfactory above the 95% even if it marginally decreases for longer simulation times. Since the value is relatively stable with time and the aim of BHE fluid temperature limitation is to avoid risks for the installation during the whole life of service, the value that is adopted in the following is the one pertaining to $t = t_s$. This indeed is the most critical time in the entire life of service.
From all the above, the technical geothermal potential of a Borehole Heat Exchanger can be evaluated taking into account the advective and dispersive contributes by adopting the formula:

$$Q_{BHE}[W] = \frac{8 \cdot \left(T_0^* - T_{lim}\right) \cdot \Lambda_1 \cdot \left[C_{gw}\,(Pe)\right]^{-1} \cdot L \cdot \frac{t_c}{t_y}}{-0.619 \cdot \frac{t_c}{t_y} \cdot \ln\left(\frac{r_b^2}{4\alpha^* t_s}\right) + \left(0.532\frac{t_c}{t_y} - 0.962\right) \cdot \ln\left(\frac{r_b^2}{4\alpha^* t_c}\right) - 0.455\frac{t_c}{t_y} - 1.619 + 4\pi\Lambda_1 \cdot R_b} \tag{4.12}$$

where α^* and $C_{gw}(Pe)$ stand for the thermal hydrodispersive diffusivity of the soil and the hydrodynamic correction factor respectively:

$$\alpha^* = \frac{\Lambda_1}{(1-n)\,\rho_s c_s + n\rho_f c_f} \tag{4.13}$$

$$C_{gw}(Pe) = 0.262 \cdot \ln(Pe + 1) + 1 \tag{4.14}$$

The Peclet number is derived from Equation 4.9 and the spherical part of the tensor of thermal diffusivity Λ_1 is computed as:

$$\Lambda_1 = \left[(1-n)\,\lambda_s + n\lambda_f\right] + \frac{\rho_f c_f v_D \left(\alpha_L + 2\alpha_T\right)}{3}$$

The applicability of the above mentioned formulation to hydrodynamic and heterogeneous context is of high theoretical and practical importance in geothermal potential assessment. Nonetheless, the inclusion of thermal dispersivity values can represent a possible source of error. Its determination is indeed a major challenge in real applications. On the contrary, dispersivity values are used in practice to assess the thermal impact of single installations or the evolution of thermal plumes from various kind of sources. This implies that this issue is commonly handled for purposes related to the design of the installation and hence does not represent an additional source of error on the planning. Furthermore numerical calibration of dispersivity values can be performed in case monitored data are available. In worst cases a quantification of related uncertainty can be carried out through numerical analysis.
In conclusion, by the adoption of Equation 4.12 it is possible to fully take advantage of numerical modelling tools to assess the technical geothermal potential whenever a groundwater flow is present and existing users of the reservoir induce thermal alterations. These conditions are extremely relevant in urban areas. This will be particularly demonstrated in the case of Turin central districts (Italy) where significant thermal alterations are present due to geothermal utilization (Barla et al., 2018). Application of the Equations 4.12 and 3.16 will be compared in Chapter 6 in relation to this context.

4.4.2 Post-processing of temperature fields

Assessment of local geothermal potential can benefit from the knowledge of the thermal and hydraulic regime of the study area. On the one hand advective and dispersive components of the heat transport mechanisms can be included in the potential evaluation through Equation 4.12 presented in the previous paragraph. On the other hand numerical models provide a detailed description of thermal and hydraulic regime of the area that has to be evaluated. Hence results from numerical models have to be returned in a suitable form for application of semi-analytical formulation. This is computed through proper implementation in the GIS platform described in Section 4.2. To this aim both

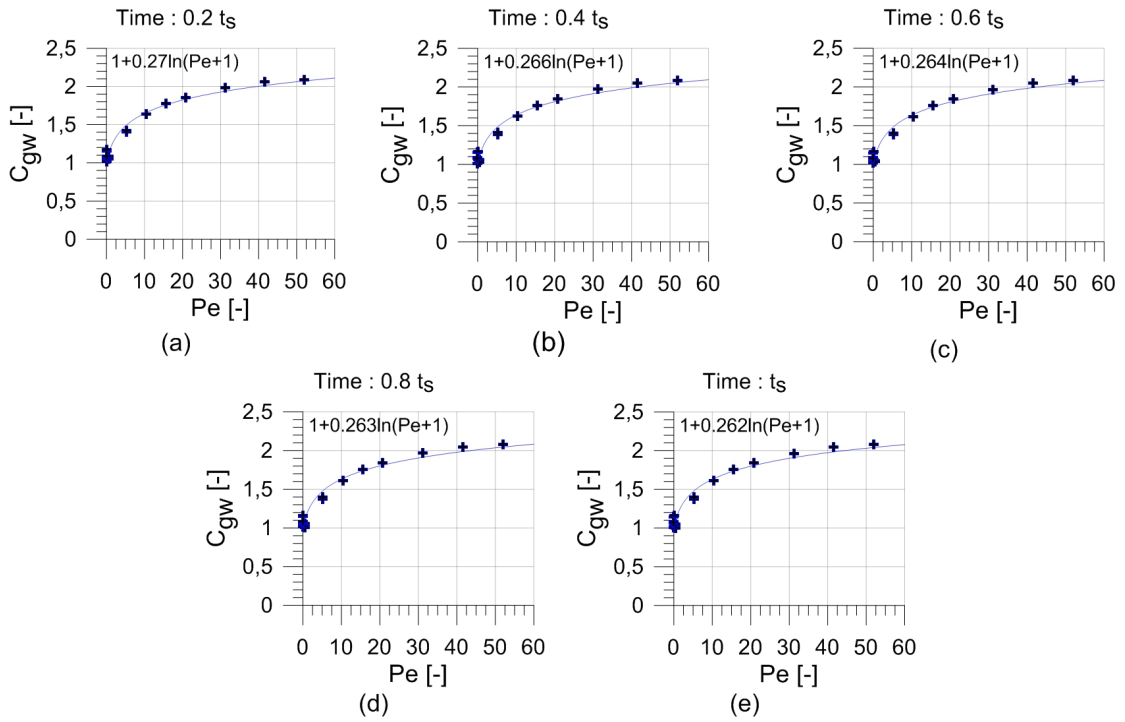

Figure 4.11: Numerical interpolation of hydrodispersive correction factor at several time stages: (a) 20% of simulation time, (b) 40% of simulation time, (c) 60 % of simulation time, (d) 80% of simulation time and (e) at the end of simulation time.

temporal and spatial variability issues have to be addressed.
As regards spatial variability, numerical models represent a spatial discretization of the subsurface volume beneath the studied area. Not only primary variables are of interest and have to be exported in the form of vector or raster dataset. Indeed the location of the result is of extreme importance, both in term of planimetric and altimetric position. Hence the first dataset that has to be known is the elevation of the nodes. Layered models result in multiple Digital Elevation Models (DEM), namely one for each of the layers of the model. Maps of thermal status and groundwater flow can be then produced at different depths from the surface directly from the model results. DEMs furthermore allow to define the depth pertaining to the parameters involved in Equation 4.12 and create the common frame for interpolation of dataset on a raster grid. Indeed GIS requires a constant grid step to handle raster dataset in map algebra and during geo-processing operations. Due to the not constant spatial distribution of mesh nodes, the need arises to resample the data by interpolation. By doing so, definition of the correspondent potential value can be performed on each cell. Export of the hydraulic thermal parameters (e.g. the hydrostatic thermal conductivity and the thermal dispersivities) has to be performed as well. It is also obvious that temperature and Darcy's velocity has to be exported to the GIS from each node of the model mesh.

By importing all the above mentioned data, it is possible to refer the parameters involved to in the geothermal potential assessment to a range of depths that are included in two raster datasets. Through map algebra capabilities which are typical of GIS tools, it is possible to calculate the depth-weighted average values of thermal dispersivity, capacity, conducitivity, diffusivity, the average Peclet number (and the pertaining correction factor C_{gw}) and the background temperature. The resulting raster dataset represent also an intermediate output. These can be useful for qualitative geothermal potential assessment. This is the case of average thermal conductivity values as it was mentioned in Chapter 3.

Spatial discretization is a crucial factor. Indeed the method here presented does not take into account the possible interference occurring between neighbouring *virtual* BHE. It is thus required that the spatial discretization avoids the risk of interaction. To this end, cell size of 7 meters was selected, based also on literature values mentioned in Chapter 3 (Galgaro et al., 2015; Miglani et al., 2018; Signorelli, 2004).

As regards the temporal variability, hydraulic and thermal regime are typically transient phenomena. However the method explained in previous paragraph does not deal with transient boundary conditions, except for the heat load profile of the borehole heat exchanger. Hence a static and conservative evaluation of the hydraulic and thermal field have to be used in the geothermal potential assessment. The definition of these fields should be carefully evaluated on the basis of the single case study, depending on local sources of variation (boundary conditions). However some general consideration may be done.

As regards hydraulic regime, larger ranges of variation are expected in proximity to surface water bodies. This is the case of rivers that are typically affected by rainfall and snow melting periods. Typical non stationary boundary conditions in urban areas are represented by users of the aquifers. However, both rivers and aquifer users usually show seasonal trends due to climate conditions. In particular flood periods with related higher hydraulic levels in the rivers are seasonally defined while aquifer users show daily or sub-daily variability with cyclic characteristics. This is the case of industrial processes but also of existing open geothermal installations. These latter are generally used on a seasonal base. Hence hydraulic variations are assumed to be relatively limited and then a mean value of the groundwater flow velocity averaged on the operative season can be assumed for potential definition.

As regards thermal variability instead this can be relevant since the thermal boundary conditions can significantly change. Indeed thermal fluxes from the surface, from infiltrating water, from buildings and from geothermal installations can significantly vary. In addition to this, the possible presence of groundwater flow induces migration of thermal plumes that thus can interest a certain site just partially during the operative season. Moreover in the assumption that the temperature limit is given by the typology of installation, the background temperature is directly proportional to the geothermal potential, according to Equation 4.12. It is thus of extreme importance to provide a conservative evaluation of this parameter. For the sake of caution, the extreme temperature

value registered at each node during the operative season is selected for geothermal potential assessment purposes. This corresponds to the maximum temperature during the cooling season and to the minimum one during the heating season. Once the temperature value is defined for each of the nodes within the numerical model, it can be processed as previously explained through the use of GIS technology.
Thus the definition of the operative season to investigate should be performed a priori to the potential calculation. It thus results in the appropriate background temperature value selection. A priori choices typically interest parameters as BHE geometry and operation. Indeed these should be kept constant over the entire study area to allow comparative evaluation of the more efficient areas where to install geothermal plants. In the case that drilling is restricted in certain parts of the area, due to technical or legislative limitations, the spatial variability of the allowed borehole depth can be included in a further raster dataset. This in turn can be processed with map algebra to determine the local technical geothermal potential.

4.5 District and city scale geothermal potential

Shallow geothermal energy potential is a locally defined scalar quantity. In the previous section the quantification of the potential was carefully addressed and the advancement in the determination through a semi-analytical approach has been proposed and in depth analysed. The local quantification of geothermal potential is of great importance for practitioners and stakeholder that are interested in the choice of the heating or cooling system for new or existing buildings. Thermal maps and geothermal potential maps answer to the need of quick and easy to use tools for single and comparative evaluation of different areas.
Especially from the city planners and energy policy makers point of view, this is not sufficient to properly define the impact that geothermal energy can have. In order to overcome this barrier quantification of energy potential of larger areas have to be carried out. In the following the way the information of local scale geothermal potential can be aggregated to the above mentioned aim is described.

4.5.1 Assessment of the potential impact at the district and city scale

Shallow geothermal energy can be exploited by different kind of installation. It was previously explained how the shallow geothermal potential can be assessed from numerical results by means of semi-analytical formulas.
In order to assess the role at the city scale that the shallow geothermal energy can play, several results can be given. Temperature maps can be at first reconstructed by interpolation of the results from numerical modelling at several depths. Directly

based on these maps, information can be provided on the best areas where the temperatures are favourable for utilization. This in turn depends on the thermal operation desired. Indeed high temperatures (related to subsurface urban heat island effect, hot tunnels, sewage or district heating network leakage, building basement,etc.) are most favourable for heat extraction during the winter season. On the contrary low temperatures are favourable for cooling mode where ground is used as an heat sink. Thermal heterogeneities in the vertical direction would also allow to better plan the use of the geothermal energy. Indeed utilization at different depths can be pursued with different technologies. In the next chapter, a novel prototype of energy wall will be described and experimentation will show that the thermal impact at relatively short distance can be negligible. In this perspective alteration of the geothermal potential of deeper structures (e.g. Borehole Heat Exchangers, energy piles or energy tunnels) is extremely limited. This results in an optimisation in the contemporary use of shallow geothermal potential with very shallow one.
Tridimensional temperature mapping can thus help the planning of further extensive installations. Indeed commercial building usually require relevant cooling loads as well as hospitals and factories dealing with industrial thermal processes. These uses may be optimised in their location where expected temperatures are favourable because of natural thermal state or due to waste heat from other uses.
In the perspective of environmental protection, high temperature may induce chemical and microbial alterations (see Chapter 2). In the same way low temperatures may induce chemical alterations and in worst cases soil freezing. This would affect significantly the soil mechanical behaviour. Most of the regulations on shallow geothermal hence include limitations on the maximum induced thermal affection rather than on the range of temperature induced. This is particularly true, at least in the specific Italian context, for open loop systems. On the one hand the *first come, first served* rule results from this kind of limitations. On the other hand the aquifer status can be preserved. From all the above, a further simple elaboration of thermal maps can be provided depicting the still available temperature shift T_{res} in the studied area to reach the maximum allowed temperature in the subsurface:

$$T_{res} = \left| T_{lim} - T_0 \right| \tag{4.15}$$

It should be noted that positive values would define areas where still some potential has not been exploited, while negative values would highlight areas where overexploitation already exists. By means of these thermal map, local authorities may foresee correction in the authorization limits or proper countermeasures in order to preserve the aquifer. Relative residual geothermal potential can result directly available from thermal maps under the assumptions that legislative limits are valid within the studied area. To this end, the Integrated Relaxation Factor IRF (Epting et al., 2017a; García-Gil et al., 2015b) can be adopted and mapped:

$$IRF = \frac{T_\Delta - T_0}{T_{lim} - T_0} \tag{4.16}$$

where the definition of a threshold temperature pertains to public authorities (usually kept among 25 to 30°C in European temperate climate areas) while the temperature drop T_Δ can be defined on the basis of numerical results of aquifer uses. Mapping of the two values resulting from Equations 4.15 and 4.16 need the knowledge of the thermal status and the definition of legislative limits, where available.
Local geothermal potential, as calculated by the procedure explained so far, might be indicated in non exploitable areas too (e.g. drinking water protection areas). Thus in these areas the geothermal potential has to be imposed to the null value because of the existing legal limits. This work focuses on borehole heat exchangers, that may be drilled up to a considerable depth. In order to quantitatively compare the areas where higher residual geothermal potential exist, installation characteristics are usually kept constant over the entire domain of interest. Nonetheless this might not be the case if drilling depth restrictions exist. Wherever the limits are more restrictive than the desired length, the geothermal potential evaluation has to consider the maximum allowed depth only and hence neglects the remaining vertical profile. Under these conditions, the geothermal potential can still be evaluated by Equation 4.12 considering a variable depth value. This information can be resumed in a grid based dataset that is thus included in map algebra computation.
In order to quantitatively define the energy potential of the entire domain or of a part of it, summation of the single values on each cell of the grid has to be performed. Extreme relevance lies in the choice of the dimension of the raster grid cell, as already mentioned in Section 4.4.2. Indeed up to this point, the grid dimensions only had effect on the precision of the assessment. No resolution loss is obtained unless the grid is coarser than the numerical mesh as interpolation is an intrinsic feature of the Finite Element Method. By contrast, the definition of the dimensions of the cell at the base of raster dataset strongly affects summation of local geothermal potential values. Indeed the method adopted in this work cannot deal with mutual interference of the virtual BHEs whose potential is evaluated. Hence no *penalisation* can be applied to excessively fine resolution. This results in the requirement of minimum spacing among these virtual BHEs that implicitly avoid interferences on neighbouring cells. These assumptions are indeed one of the main focuses of some geothermal potential assessment methods described previously in Section 3.4.3. A 7 m by 7 m grid was selected balancing the avoidance of mutual interference with the need of sufficient geometrical accuracy in an urban area subject to land scarcity issues. In areas where the groundwater flux is considerably high, the avoidance of interference should be further investigated and the cell dimensions should be enlarged where appropriate.
In conclusion summation of the cell values leads to an assessment of the maximum technical geothermal potential. This is actually a largely overestimated value. In fact the installation of BHE is usually not possible in case within already existing buildings due to the need of sufficient room to host equipment both for the construction and the operation of a BHE field. The focus on the single building, which is at an intermediate scale between the local and the district or distict scale, is the focus of the next paragraph.

Figure 4.12: Allocation of geothermal potential to the appropriate energy user. Squares depicted highlight the cell margins. Highlighted yellow cells have their centroid within the external perimeter of the building are considered as a first approximation scenario.

4.5.2 Local energy surplus/deficit ratio

Beyond the availability of energy resources, the value of the energy unit depends on the local energy need. The use of low enthalpy geothermal energy as part of new fourth generation of district heating network is still a challenging perspective. At the time of the writing, proximity of the user to the geothermal installation is still a binding constraint. Also property of the energy that can be mined is strictly related to spatial mutual interaction of the energy user and of the energy producer. Hence the definition of the share of energy need that can be fulfilled by shallow geothermal is an important result from geothermal potential assessment. To this end the suitable area for borehole heat exchanger has to be linked to the single entity that may profit of this energy, namely the target of geothermal energy.
The definition of the energy available for the single target unit can be performed analogously to the geothermal potential assessment at the city scale. In particular summation of the value of the pertaining cells has to be addressed. In this scenario the selection of the available area is of extreme impact on the quantification of energy availability. Multiple scenarios can be made depending on this choice. To a first approximation cells can be considered to contribute to the satisfaction of the building energy needs in the case their centroid is included within the external footprint perimeter of the construction (see Figure 4.12). This approach allows to univocally relate a cell to one potential energy user only. Indeed the inclusion of cells whose centroid is included in a buffer area around the building footprint may result in multiple counting of the same cell with different users. The adopted approach instead appears to be more robust while using automatic geo-processing algorithms in order to avoid this kind of overestimation. Nonetheless, it should be mentioned that coincidence among the calculated geothermal potential and the city scale potential is not achieved. Indeed open and green areas as streets and urban parks are not taken into account in this evaluation.

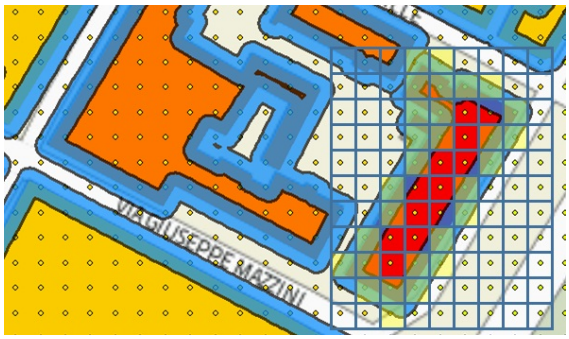

Figure 4.13: Allocation of geothermal potential to the existing building users. Squares highlight the cell margins with pertinent centroids. Blue area delineates the area considered for BHE installtion. Cells highlighted are assumed to contribute to the energy supply of the building.

A second approach can partially overcome this downside. According to Zhang et al. (2015), a buffer area around the building perimeter can be considered suitable for installation. The overestimation effect due to areas that are inaccessible to drilling equipment is extremely limited as locations beneath the building can be reached at very shallow depth by directional drilling. In this study a maximum buffer distance of 3.5 m was considered around the perimeter of built units (see Figure 4.13), thus including also public areas like streets and gardens. Also internal courts perimeter have been considered as suitable installation area even if in some cases they might present difficult access to drilling machinery. Thus a zone of nearly 7 m width is defined at building borders, according to the cells dimensions where the geothermal potential is defined. As previously mentioned, extreme attention has to be paid in order not to consider the potential of cells multiple times with respect with distinct neighbouring housing units. In the case the buffer areas of adjacent buildings partially or completely overlap it is thus necessary to locally reduce the zone width by taking into account the proximity of the buildings involved. This area manipulation can be operated in GIS by geoprocessing operations as the creation of Thiessen polygons based on the building perimeter. Based on the above, the first approach might better account the available energy potential on a cadastral plot and is better representative of possible utilization in the case of demolition and rebuilding. The latter approach instead might lead to limited overestimation related to minimum distances to pipelines, trees or property borders (see Section 2.4.1). On the contrary it might better represent the achievable energy utilization of existing buildings and thus the potential impact on the energy balance.
Once the definition of the exchangeable energy has been performed, this can be related through the GIS tools to the building or structure entity as an attribute. These amount of energy has to be subsequently related to the energy need of the built environment entity in order to define an easy-to-use indicator of the relative importance of shallow geothermal. On the one hand the energy need has to be determined by monitoring, energy balance model application of by classification (see Section 4.2.4). On the other

hand the energy that is exchanged with the subsurface has to be manipulated to assess the deliverable energy to the user. Heat pumps are in fact adopted to shift the temperature range of the fluid at suitable values for the secondary circuit. A reasonable constant value of 4-4.5 can be selected for coefficient of performance in heating mode while an Energy Efficiency Ratio of 4.0 can be suitable for cooling operating modes according to Santilano et al. (2016) and the actual technological level. Thus the energy need of a structure for heating or cooling can be related to the geothermal deliverable energy through a *satisfaction ratio* SR that can be calculated as:

$$SR = \frac{\sum_1^N Q_i \cdot \frac{COP}{COP-1}}{Q_b} \tag{4.17}$$

where the Q_i is the single cell geothermal potential of the cells whose centroid is included in the building footprint while Q_b is the seasonal thermal load of the building. The cooling load satisfaction ratio can be accordingly derived by substitution of the COP with the Energy Efficiency Ratio (EER).

4.6 Summary

Urban areas need enormous amount of energy as a result of the intense density of population and facilities. A significant share of the energy consumption is devoted to the heating and cooling need of buildings. Hence in order to implement green energy policies, this sector has to be driven to cleaner and more environmentally friendly energy sources. In this perspective shallow geothermal energy is promising due to its distributed production attitude. On the contrary relevant density of anthropogenic heat sources including the rising number of geothermal installation may induce severe effects on subsoil thermal state, depleting the reservoirs and leading to conflicting uses. In order to govern on a rational and scientific basis the development of such technologies in urban areas, the novel method *rOGER* has been explained in detail to assess the geothermal potential. The pertaining strength and weakness points have been highlighted. The method moves from the collection of all the relevant data on hydrogeology, thermal fluxes, land area uses and hydro-thermal regime in a properly designed geographical database architecture. It proposes the integration of analytical and easy-to-use analytical formulation with the potentialities of numerical modelling tools. In order to unlock the full potentiality of the thermo-hydro numerical models that are being increasingly implemented worldwide, an extension of a semi-analytical method for geothermal potential assessment has been achieved by numerical parametric analyses and the calibration and interpolation. By doing this, advective and dispersive heat transport mechanisms can be included in geothermal potential assessment. The processes to treat numerical results to the aim of using this extended analytical formula were described. Mappable qualitative and quantitative results have been explained together with their possible uses.

In the next chapter a novel kind of energy wall will be presented with pertaining prototype realisation and experimental investigation. It will be demonstrated also by means of the experimental results that negligible thermal variations are induced at short distances from the structures. Furthermore the relatively low depths of installation result in the absence of significant alteration of the potential from deeper installations.
In Chapter 6 the theoretical method here described will be used in the specific context of Turin (Italy). It will be thus demonstrated at the city scale that the thermal affection induced by shallow energy walls do not undermine BHE, according to formulation presented in previous paragraphs. Hence the two main elements of this work will depict the contribution to move a step further to the optimisation in the use of shallow geothermal energy.

Chapter 5

GeothermSkin: a very shallow energy wall

5.1 Introduction

Traditional shallow geothermal systems require excavation or drilling which represents an high initial cost. These investments may limit the usage of this renewable energy source. This issue is partially overcome in energy geostructures and very shallow geothermal systems like horizontal closed loop collectors. Indeed energy geostructures incorporate the initial costs in the structural requirements, while very shallow geothermal systems significantly reduce the excavation and the related expenses. However both these solutions show some disadvantages related to their applicability in urban areas, especially in already well developed ones. Indeed developed urban areas are characterized, especially in central districts, by scarcity of free land and by a high share of already existing buildings.
In this chapter a novel solution in the field of very shallow geothermal energy systems is presented. This system aims at combining the advantages of the solutions mentioned above. The concept of such system, that leaded to patent filing, is explained with reference to both new and existing buildings. Its first realization at the prototype scale in the city of Turin is the focus of the following paragraphs. Particular attention will be devoted to the most important components of the system. The design and deployment of the wide monitoring system that serves the experimental site will be analysed as well. Results from experiments will be showed in the last part of the chapter.

5.2 The concept

Climate change and greenhouse gases emissions are among the main concerns of contemporary society. Because of the rising public attention to these topics, international

authorities are pushed to deal with actions in both direction of climate change adaptation and climate change mitigation. European Union is actively involved in climate change mitigation policies. These policies mainly regard regulation on transportation, industry and building sector. Intervention in the building sector is extremely relevant, especially in the heating and cooling needs as half of the primary energy needs in the European Union are devoted to this end (European Commission, 2016). Hence, directives and regulations have been promulgated in last decades at international, national and local levels to give substance to the energy strategy.
Directive 2002/91/CE (European Parliament and European Council, 2002) is the main reference in the building sector as regards the energy efficiency. This directive is better known as *EPBD* (Energy Performance of Buildings Directive). Its latest version was promulgated in 2010 where updates of the regulative framework were included in Directive 2010/31/UE (European Parliament and European Council, 2010). Indeed policies are forcing the construction sector to higher efficiency standards as regards the primary energy supply. These standards apply to both the new constructions and the existing building stock. In particular these directives and their national transposition impose the requirement for hot water production of a minimum share of 50% from renewable energy. Fulfilment is required to all newly built constructions and to buildings undergoing relevant renovation too (Italian ministry of Economic Development, 25/06/2015).
Low enthalpy geothermal systems have been used since centuries for space heating. Their application offer sustainable energy provision using the subsoil as heat source or heat sink or energy storage reservoir depending on the operative mode. Anyway traditional shallow geothermal system as well as photovoltaic or solar thermal energy panels, may require significant amount of free surface for installation.
Thus requirements set by the legislation can be a particularly strict for buildings in dense urban areas where available surfaces are limited. This limitation may indeed result in insufficient production from solar energy installation or from traditional geothermal systems. In this perspective, thermal activation of earth-contact area of the buildings can help to satisfy these requirements without drilling or excavation costs related to BHEs installation. In past years a few examples of energy walls embedding pipes circuit in the steel reinforcement cage have been documented also with regards to common residential buildings (Sterpi et al., 2017).
A link of almost direct proportionality between the number of storeys above the ground level and the depth reached by the building underground parts exists. Hence buildings with limited number of storeys (8-10 floors) do not present foundations at depths greater than the *homoeothermic depth* (Bucci et al., 2017). This means that the underground parts of such buildings are in contact with ground volumes at slightly less favourable temperatures than the ones pertaining vertical shallow geothermal systems. Furthermore the internal air temperature was demonstrated to be relavant (Sterpi et al., 2017), usually inducing reduction in thermal performances both in heating and in cooling seasons. On the one hand, the efficiency expected by a system installed at these depths is relatively low. On the other hand, the costs related to installation of very shallow

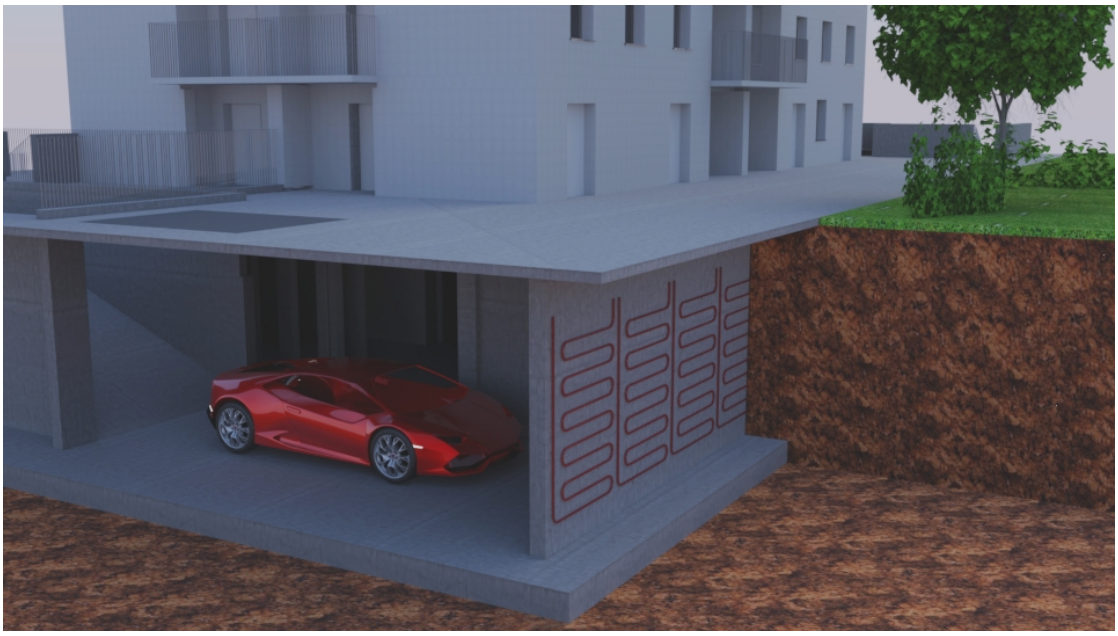

Figure 5.1: Render of the *GeothermSkin* energy system applied to a residential building basement.

geothermal systems are also low, especially in the case of new construction. Hence the cost-benefit balance is still of great interest.
In this perspective a novel energy system, called *GeothermSkin*, was conceived to minimize installation-related costs. Because of the innovations introduced, the system is undergoing patent filing process in Italy. This system is intended to be installed during building construction or refurbishment. This means to extend the energy geostructure concepts to the existing building stock. The basic idea of this system is to provide a full or at least a partial fulfilment of the renewable energy requirements of a building. The system allows to transform the earth-contact area of a building into an heat exchanger for heating and cooling of the building itself. The system covers as a skin the primary or secondary structural elements which are in contact with the ground as shown in Figure 5.1.
The installation of the system is done once structural works are completed. In the case of new construction the system can be deployed just after the removal of formworks and before the backfilling of the ground. On the contrary, in the case of existing construction, excavation to clear the exterior wall surface is needed. Hence the GeothermSkin system can be put in place and then buried by the excavation backfilling.
Although industrial optimization is an open issue at the date of the writing, the geothermal exchanger need an appropriate support system. This needs to ensure the fixing to the wall and the stability of the exchanger during the installation phase and backfilling. In the simplest cases the supporting system can be represented by clamps that are fixed to the external wall while more sophisticated systems may be coupled to pre-fabrication

of semi-rigid circuits and can thus solve to double function of support and circuit shape keeping. In order to maximise the heat exchange with the ground, no protection or armouring is applied to the exchanger pipes. This however implies that backfilling has to be carried out with higher attention to reduce the risks of damaging the circuits.
The solution here presented has the advantage of negligible horizontal area occupancy. As mentioned above, this aspect is of particular interest in urban areas. Indeed the system gets bounded to the reinforcement of the earth-contact structural element or to the outer surface before the backfilling phase of the construction. The system can be adopted, even if at higher costs, during building renovation. The system is made up of modular panels presenting a maximum width of 2,50 m. A proper support system provides the bounding to the vertical element. The support and fixing system can also be represented by common anchoring systems used for radiant panel-based heating systems. These modules compose a network of polymeric pipes (crosslinked polyethylene PE-Xa or high density polyethylene PE-D) that constitutes the hydraulic circuit. Pipes are especially designed and suitable as part of heat exchanger system, with proper resistance to high temperatures, high pressures and corrosion. The dimensions of the panel allow the modules to be assembled directly on site without the need of special transportation.
Pipes are placed in a convenient manner. Taking inspiration from recommendations for energy geostructures (Delerablee et al., 2017), a minimum spacing of 30 cm from the digging bottom and 10 cm from the wall edges is preferable. Furthermore pipes show an internal diameter of 20 to 30 mm with 2 to 4 mm thickness. The heat carrier fluid that is circulated within the pipes is a mixture of water and glycol that allows to operate safely the system in a range of temperatures down to -20°C (freezing point of -30°C). By doing this, the limiting factor is thus soil freezing.
Figure 5.2 summarizes the main components of the *GeothermSkin* system. Indeed the entire earth-retention energy system (element *1* in Figure 5.2) is placed on the outer surface of the underground wall (indicated as *10*). The single modules can present different shapes differentiated by the preferential direction in pipes deployment. Indeed they can be preferentially placed horizontally (circuits indicated as *20* and *30* in Figure 5.2) rather than vertically (referred to circuit numbered with *40*). Single modules can work independently, namely in parallel. Modules shape is however conceived to make possible the connection in series of a variable number of elements. In the first case the connection to the collector pipes can be brought to the inner side of the building by appropriate holes. In the case of installation on a new building, careful realization may allow to appropriately design sealing (e.g. bituminous foil deployment and geo-textile to avoid fine particle inflowing together with rubber elements rather than isolating foams) and avoid water inflow (ascendant deployment of the aperture). Application in existing buildings should be accurately realized in order to prevent durability issues. In this latter case, the drilling may intercept rebars. In such cases the ends of steel bars end should be appropriately passivated (e.g. by means of epoxy resin). Then holes can be sealed similarly to the new building installations. The pipes are conveyed in manifolds

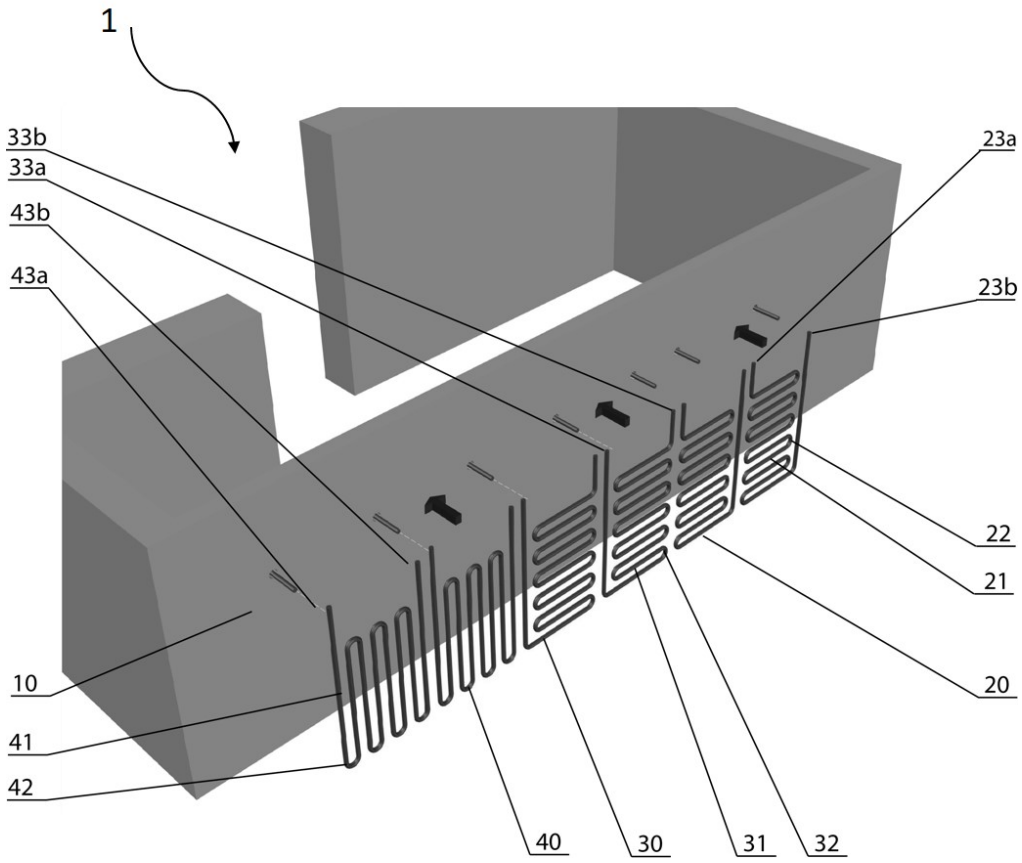

Figure 5.2: Main components of the novel energy wall system *GeoThermSkin*. Single modules may present different shapes depending on main pipes deployment direction. In modules 20 and 30 pipes are mainly deployed in horizontal direction while module 40 presents mainly vertical pipes.

that are in turn connected to the heating/cooling distribution system by means of an heat pump. In the latter configuration instead direct connection between the exit end of a circuit and the entrance end of the neighbouring one is established directly on the exterior wall surface. Connection at the inner side can be done so that inspection and intervention in case of damage can still be possible after ground refilling. The deployment of manifolds is conceived to facilitate inspection. The modularity of the system and its ability to be inspected make possible the detection failure of single modules and exclusion of damaged pipes from the network. This allows to keep the functionality of the overall system even if local damages happen to the heat exchangers. This risk is more pronounced during burial of the wall and subsequent ground settlement while it is believed that settlements during the life of service can be completely accommodated by the pipes. Also durability issues of the circuit, unless extremely aggressive environment from the chemical point of view is present at the site, should be avoided by

appropriate selection of material, with an highly resistive oxygen barrier. These properties are also common for materials adopted in radiant system or classic geostructures as they are designed to cope with highly alkaline environment.
As mentioned before, the system usually lies, as horizontal heat exchangers and *classic* energy walls, within the depths where surface air thermal influence is relevant. Nonetheless the investment costs are limited and are believed to lead to profitable costs-benefit ratios. The initial cost is extremely dependent on the application as the major part of investment is represented by excavation works. These have to be computed as related to GeothermSkin system only in the case of application to existing construction. Otherwise initial costs are presented by materials and labour cost beyond the thermal plant (Heat Pump, heating/cooling apparatus, etc. that are commonly related to every kind of HP system). These costs may be quantified, also considering the thermal performances predicted (see Section 5.4), in a range of 650 - 1050 €/kW. This is a slightly lower value with respect to traditional BHE systems (750 - 1500 €/kW) and slightly higher than horizontal collectors (600 - 900 €/kW) that however require high area occupancy.

5.3 Experimental site design

The first realization of the novel shallow energy wall system was designed for experimental purposes. This realization indeed is intended to provide insight into the system energy performances and into the thermal impact that is exerted on the surrounding ground. Thus the realization here presented allowed to boost the Technology Readiness Level (TRL) to level 3-4. The design that was carried out includes a set up that is still at the smallest practical scale at midpoint from a real full-scale application to the laboratory level. Components that are available on the market, especially regarding the distribution system, were employed. However, they are not sized in order to fulfil the energy needs of the hosting building neither of a typological one.
Pipes deployment was chosen in order to test a set of different conditions and configurations in the same location, providing sufficient heat supply for a small size commercial heat pump.
Design was started in 2017 with reference to the experimental facility of the Energy Center Laboratory in Turin (Italy) whose location is shown in Figure 5.3. The building was recently built and hosts private and academic research offices and laboratories. An auditorium is also present at the ground level of the building for a total gross floor area of about 7000 m^2. The building was conceived as a smart energy building with high efficiency standards to control and monitor energy consumption. An extremely large number of smart sensors monitor indoor environment and energy consumption on all the 4 elevated storeys and on the basement level, including the 2000 m^2 undeground car park.
Design of this experimental facility handled the main limitation of budget availability and of constructional feasibility. Indeed construction works had to be limited in terms

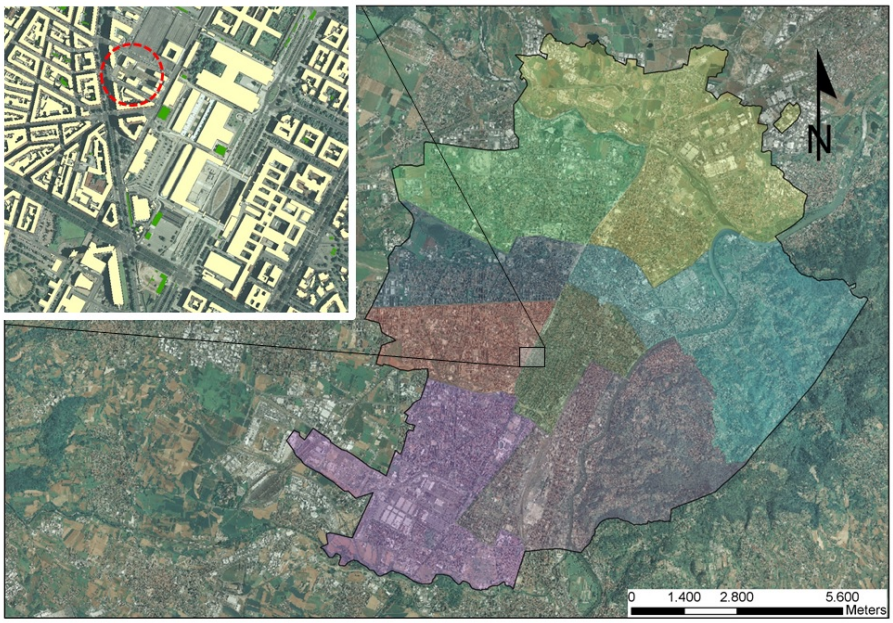

Figure 5.3: Map of the city of Turin (Italy). The experimental site location is highlighted with a red circle within the magnifier.

of time and occupied area as the building spaces are constantly used for work and to host events and neither temporary decrement in serviceability level was possible. Constraints included interference with other experimental facilities under construction at the same time of the energy wall system. Avoidance of serviceability limitations to the building resulted in constraint on location and extension of the excavation works. Construction took place in 2019, from May to July and will be described in the following in relation to the components of the prototype installation.
Due to the experimental nature of the prototype installation, a wide monitoring system was designed and put in place during its construction. Hence construction phases were partially modified respect to a real settings due to the need of sensors deployment within the subsurface.

5.3.1 Pipes layout

Due to the experimental and demonstrative nature of the installation here presented, the pipes network was designed to provide a sufficient energy supply from the ground to the thermal machinery, namely the heat pump. This thermal load is not directly linked to building energy demand. On the other side the minimum space had to be interested by the construction works in order to not interfere with the continuous functionality of the building that hosts offices and frequent events in the auditorium.
The ground heat exchanger position was thus limited to a portion of the earth-retaining

Table 5.1: Heat exchanger circuits experimental setup details.

Circuit	Pipes direction	Pipe length [m]	Entrance end	Exit end
1	Horizontal	26.6	H2	H1
2	Horizontal	27.0	H3	H2
3	Vertical	29.3	H4	H3

exterior wall of the building, on the south-eastern facade. Indeed the selected area allowed to maintain the yard area completely included in the garden within the cadastral plot of the building. The equipped portion was carefully selected as it is on the most distant corner of the facade from the underground car park that exceeds the elevation footprint of the building. By installing the heat exchanger in that position, any thermal influence exerted on the ground volume interacting with the geothermal system is extremely reduced.
A set of three different modules of the energy wall system was installed on the exterior surface of the 80 cm thick reinforced concrete earth-retaining wall fencing the technical cavaedium. Due to the experimental end of the installation, the three modules present both the preferred pipes configurations (see Table 5.1).
Indeed two modules show preferentially horizontal deployment direction while the third one on the right side of the wall shows a prevailing vertical direction of the hydraulic circuit (see Figure 5.4). By doing this, it is possible to comparatively test at identical working conditions both the configurations. A properly designed manifold connection hence allows to select the modules to be tested with parallel rather than sequential connection. Further details will be given in Section 5.3.2. Hydraulic circuit was driven to the inner side of the wall by means of four small diameter holes (as it is shown in Figure 5.4 and indicated with letter *H*) located about 50 cm below ground surface (b.g.s.). The holes were drilled with a 130 mm diameter coring equipment simoultaneously to the pipes deployment. This operation can be obviously avoided in case of installation in new buildings. In this latter case it is indeed possible to prepare adequate perforated patterns before casting concrete. It should be noted that another larger core drilling was realized in the middle circuit in order to bring the sensors cables of the monitoring system to the acquisition unit. Further detail will be included in Section 5.3.3. The depth where to locate the core drillings was chosen so that no interference would take place with pre-existing tubes on the inner side of the wall. The entrance and the final end of each of the circuits represent the shallower point of the modules. Indeed in order to reduce the thermal influence of the air temperature at the ground level, the heat exchanger coil covers the wall from about 150 cm b.g.s. up to the maximum depth of the basement level. Hence maximum depth reached is approximately 4.60 m b.g.s., just above the footing of the wall. Each of the circuits hence presents the exchanger coil extending on an area of 210 cm width per 300 cm height. This results on an effective exchanging area of 6.3 m^2 per each module while neglecting the relatively

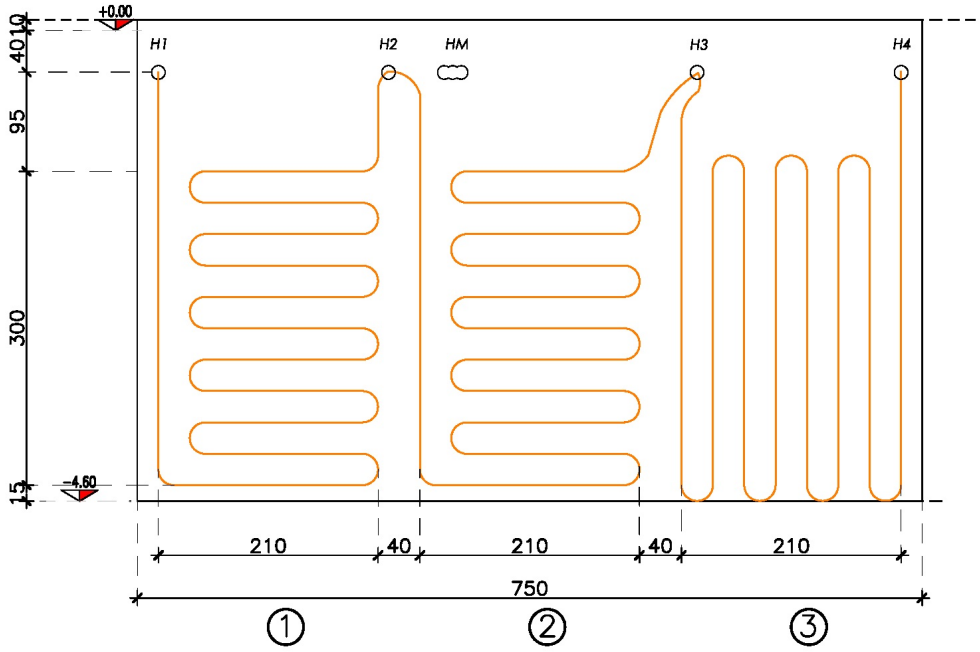

Figure 5.4: Deployment of the pipes network in the experimental site with the identification of the modules and of the drilled holes *H1 - H2 - H3 - H4* for manifold connection and *HM* for monitoring sensors wires. Dimensions are indicated in centimetres.

small shallower parts reaching the ends.
In order to expose the external surface of the wall, excavation works had to be performed. As mentioned above, these operations would not be needed in the case of new construction. In this case excavation to the foundation level would already be performed before casting the wall. In the experimental site, due to the small extension of available area for yard area and for temporary storage of the excavated material, excavation faces were built vertical. Because of the shape of the excavation and the depth reached, the shaft was secured by means of relevant iron trench shores (Figure 5.5). Non-cohesive nature of the ground excavated requested particular caution. The construction operations required additional time due to difficulties in handling the metallic elements up to the desired depth. Indeed the interlocking nature of the piles and the panels leaded to the clamping of one of the elements on the existing wall side. These aspect should be thus accounted in terms of additional installation costs in the case of application of this energy wall system to existing buildings.
Once the excavation was completed, the pipes network was fixed to the exterior surface of the wall and the three circuits were manually put in place. Operational time to put in place a single circuit, including the placing of the supporting system, can be evaluated in about 5 men-hours considering from experience gained at the experimental site. The simultaneous presence of two workmen is requested to perform this operation. The

(a) (b)

Figure 5.5: Excavation works with trench shoring for the installation of the GeoThermSkin prototype at the Energy Center building in Turin. (a) early stage of excavation and (b) bottom of the excavation, equalized before pipes installation.

placing of the circuit was however relatively simple due to low weight per meter of the polymeric material selected for pipes.
Specifically designed pipes for radiant systems were employed to ensure sufficiently high resistance to pressures and temperatures with high thermal conductivity. Circuits were hence realized with crosslinked polyethylene (Pe-Xa) tubes commercially known as *Rautherm S* pipes by *Rehau*. Selected diameter was 20 mm with 2 mm wall thickness. Supporting elements are represented by a series of simple metal clamps with approximately 75 cm spacing as it is shown in Figure 5.6. The presence of the metallic trench shoring shield partially complicated the installation of the pipes and the related supporting system. These geometrical interferences resulted in the shift of the drilled hole *H4* to the right of about 30 cm, as it is visible in Figure 5.4. On the contrary, the ability of the system to adapt to these discrepancies respect to the design give evidence to the flexibility of the solution proposed.
Once the pipes were fixed to the exterior wall surface, excavation was gradually backfilled with extreme caution to not damage the pipes. Further details of these phases will be given in Section 5.3.3, as monitoring system deployment determined these phases. In particular backfilling included also thin sand layers limited to the very narrow surroundings of the wall. This caution was employed to reduce shear forces on the pipes network during soil compaction process. Indeed partial compaction was immediately induced as the backfilling process was done by means of artificial compaction with small size steamroller. However a residual compaction phase interested the moved ground

Figure 5.6: Circuit 1 pipe deployment before backfilling. Supporting clamps are clearly visible at almost regular distances.

volume also after works completion after first rainfalls. This compaction however interested only the shallower parts of the excavation. This is testified by settlement measurements on a plane at 2.00 m depth.

5.3.2 Distribution system

Ground heat exchangers inject or extract heat to/from the ground, transferring it by means of the heat carrier fluid to an heat pump. Hydraulic circuit brings the fluid to the heat exchangers and viceversa by a series of connection valves that are in turn attached to the main flow and return pipes of the heat pump. In particular the hydraulic circuit has been equipped with a manifold that allow to test different configurations of the heat exchangers (see Figure 5.7). Indeed the series of valves mounted on the manifolds allow to singularly exclude from circulation one or more of the modules. The manifold furthermore allows to link the modules in parallel rather than sequentially.
The heat pump is located in a technical room at the basement level on the north-east

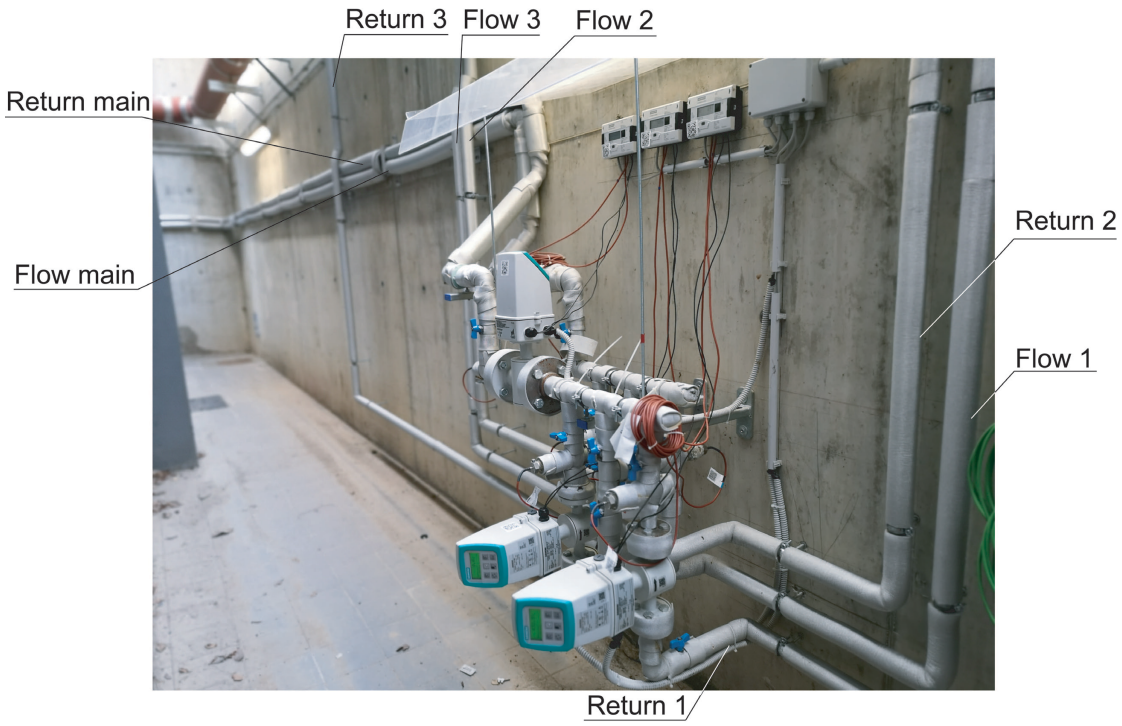

Figure 5.7: Manifold connecting the pipes from/to the heat pumps with the heat exchanger modules.

side of the building. This room was formerly hosting the air handling unit of the common areas of the building together with the HVAC components, thus facilitating the possible connection to the building system. Because of the distance between the heat pump and the heat exchanger, proper collector/distributor pipes had to be put in place with a massive thermal insulation barrier. Indeed pipes connecting the manifold to the heat pump cover a particularly long distance of about 65 m as it is shown on Figure 5.8. Since the flow in these main flow and return pipes has to be able to feed multiple heat exchanger circuit simultaneously, they show a larger nominal diameter of 32 mm (DN32) respect to the heat exchanger. These main collectors are constituted of high density polyethylene PE100 with nominal resistance to pressure of 16 bar at 20°C (PN16). The line was robustly fixed to the cavaedium wall by a series of almost equally spaced clamps. Insulation is realized by a 20 mm thick closed cell elastomeric coating with nominal thermal conductivity of 0.034 W/mK at 0°C. Hydraulic sealing among pipes pieces is ensured by electrofusion fittings. A proper test was performed against leakage before connection to the manifold system. Indeed the system was pressurised up to 2 bar and pressure decrease over time was measured by means of an appropriate pressure gauge (see Figure 5.9).
As mentioned above, the heat pump is located in the technical room on the north-east side of the building. A thermal machinery was installed whose size is commercially

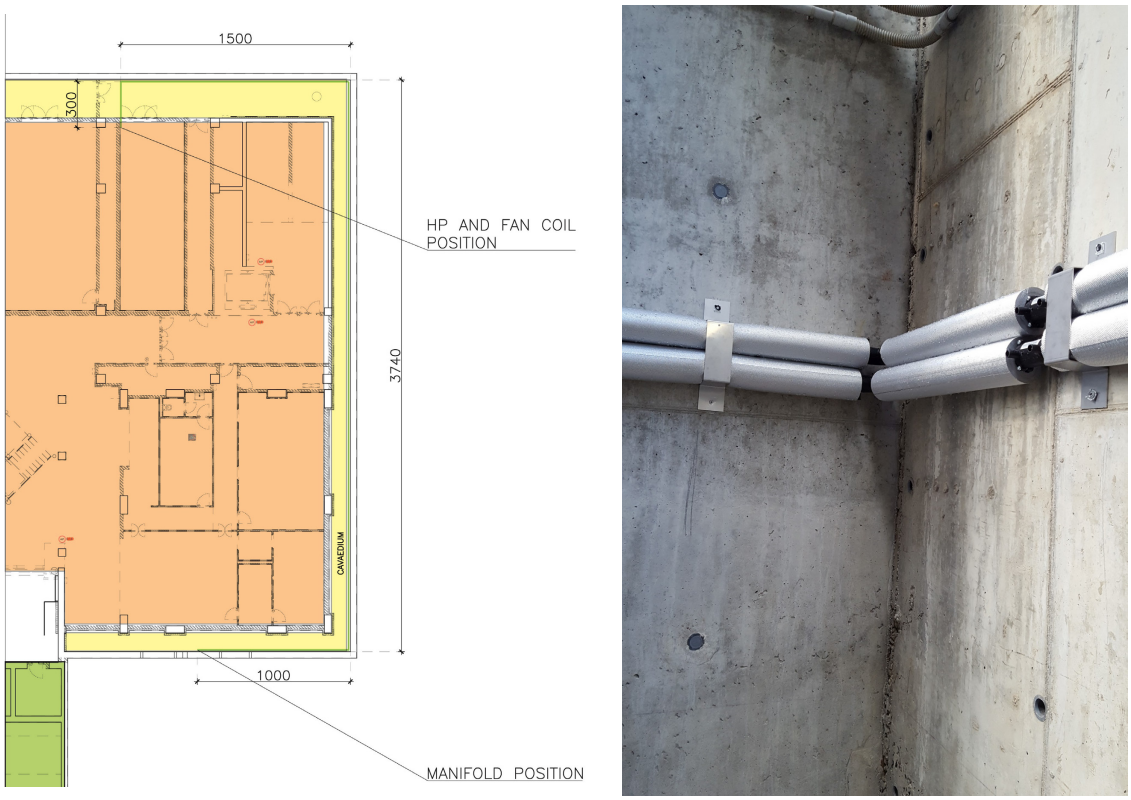

(a) (b)

Figure 5.8: Main flow and return pipes from/to the heat pump. (a) Sketch of the eastern part of the basement level of the building with distance between the heat exchangers and the technical room. The orange background highlights the indoor space, yellow the cavaedium while car park is shadowed in green colour; (b) Detail of a right-angle turn of the plastic insulated pipes.

available for small housing units. It is worth to mention that, due to the interdisciplinary nature of the research center, the heat pump can be substituted with other analogous products to carry out efficiency experiments on machineries from other producers and develop them. Nominal heat power of currently installed system is of 3.15 kWt with a declared COP of 4.72. Thus electric supply is about 0.67 kWe including consumption from the two circulation pumps which are embedded in the heat pump. Each of the circulation pumps is conceived to serve separately the user side rather than the ground side. They are set to work at variable flow velocity depending on the head losses. While on the ground side nominal flow rate is 0.65 m^3/h, a significantly lower flow rate (0.29 m^3/h) is setted up at the user side. Flow rate is also directly measured at the heat exchanger side where some energy meters were installed in proximity to the manifold in the cavaedium. Further details will be given in Section 5.3.3. The model *NIBE Fighter 1155-6* heat pump that was installed is a reversible thermal machine. This means that it can operate in both heating and cooling mode. In this latter case cooling

Figure 5.9: Leakage test on main flow and return pipes to the heat pump.

load can be provided both by active cooling, meaning that internal compressor is activated, and by free cooling. Free cooling mode is automatically run by the heat pump logic unit depending on the thermal load on the user side. Passive cooling is possible thanks to the electrically driven switching of the three-way valves mounted at the flow and return ends of the primary and secondary circuit.
The heat pumps internally performs a thermodynamic cycle on R407C type refrigerant fluid (working volume 1.16 kg) which is composed by HFC components (mixture of 23% R32, 25% R125 and 52% R134A) that allows to provide water at high temperatures up to 65°C at the hot side of the cycle. In the case the need arises to cover extra thermal load in heating mode, the heat pump is equipped with electrical thermal resistances of up to 7 kW. In order to exclude external sources of energy during the experimental campaign, these additional thermal resistance were disabled at any time. Compressor start is governed by the measurement of the heat load requested by the user. This is derived by temperature measurement on the flow and return ends of the secondary circuit.
In particular the user (secondary) circuit is composed of a fan coil to dissipate the refrigerant/heating energy and a buffer accumulator tank (Figure 5.10). Secondary circuit pipes are 22 mm diameter galvanized steel pipes thermally insulated. Thermal insulation is identical to the primary circuit. Pipes were deployed so that they can be also connected to the building heating/cooling system or to other experimental facilities that will to be hosted in the research centre (e.g. a test living lab).
As previously mentioned, the user is reproduced by means of a fan coil that can dissipate the heat produced by the heat pump during winter season. On the contrary, during the summer season the fan coil heat up the temperature of the heat carrier fluid. The internal fan coil heat exchanger can be feeded with heat carrier fluid at temperatures

Table 5.2: Thermal and physical properties of the heat carrier fluid mixture used in the experimental facility at different temperature levels.

		Temperature [°C]				
		-5	0	20	40	60
Concentration	[%]			25		
Freezing point	[°C]			-10		
Density	$[kgm^{-3}]$	1032,7	1031,2	1023,4	1013,8	1002,3
Specific heat	$[kJkg^{-1}K^{-1}]$	3,86	3,87	3,92	3,97	4,01
Thermal conductivity	$[Wm^{-1}K^{-1}]$	0,437	0,443	0,467	0,488	0,502

in the range of 5°C to 85°C. Electrical ventilation engine allows to produce a flow rate of 340 m^3/h.
Once the heat carrier fluid passes through the fan coil it is discharged in the 100 litres capacity puffer shown in Figure 5.11 before returning to the heat pump.
The puffer allows to smooth the operation of the heat pump and limit the number of compressor starts, thus extending the life of service of the thermal machine. Indeed thermal energy can be stored in the puffer and the temperature in the vessel (BT25 sensor in Figure 5.10) is used by the heat pump logic to calculate the thermal load, as mentioned above. The puffer is appropriately insulated by polyurethane foam allowing to store fluid whose temperature ranges from -10°C to 90°C. Since the primary and secondary circuits can be directly connected in a single loop during free-cooling operative phases, the heat carrier fluid has identical characteristics. In particular the heat carrier fluid is composed by a mixture of water and 25% propylene glycol whose thermal and physical properties are reported in Table 5.2. The temperature levels at the different points of the cycle are registered by the computer embedded in the heat pump. Given that the heat pump is provided with an Ethernet and an USB port, the data that are collected regarding the parameters of the cycle can be uploaded in the internet or to an external device at desired intervals. The functioning of the heat pump is remotely accessible through the internet even if the control has to be operated directly on site.
Continuous recording capability will be used in the following sections to derive the thermal energy provided by the heat exchangers during tests. A better detail of the monitored parameter is also reported in the following in relation to the complex and extensive monitoring system that was installed together with the system.

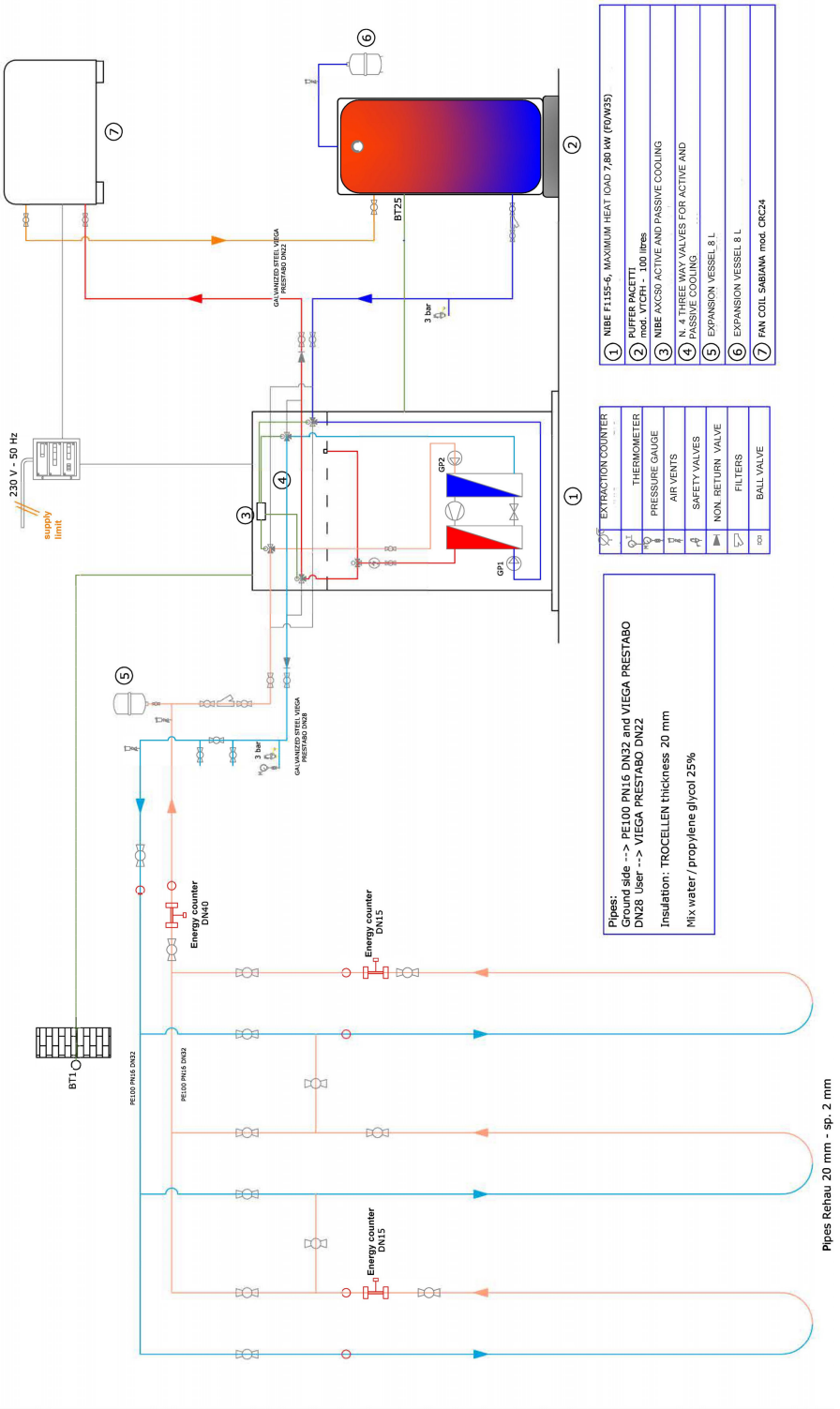

Figure 5.10: Scheme of the geothermal heat pump system.

(a) (b)

Figure 5.11: Main components of the system in the technical room. (a) The fan coil and the 100 l insulated puffer with the related expansion vessel; (b) the heat pump installed.

5.3.3 Monitoring system

Due to the experimental nature of the project and the need to characterize the heat exchange in partially saturated porous media, an extensive monitoring system was designed to analyze thermo-mechanical induced effects on the wall and thermal alteration, water content and pore pressures in the ground volume facing the GeothermSkin prototype.
In natural conditions wall external surface is virtually at the same temperature as the surrounding ground. This temperature generally slightly differs from the one pertaining the underground in free field conditions. Indeed the air presence at the inner wall surface partly influence the thermal status of the closest ground portions. This alteration is even more pronounced in the case an heat exchanger is present within the structure or at its extrados. This latter case represents the situation of the here presented energy system. Indeed the presence of the heat exchanger induces a thermal alteration exactly beyond the external surface of the equipped wall. The heat carrier fluid is circulated in the pipes and during heating season arrives from the heat pump at the heat exchanger with low temperatures. On the contrary, high temperature levels are entering the circuit during the cooling season. This is especially true at the entrance end of the circuit while along the path the temperature drop/increase respect to the wall temperature decreases as a result of the heat exchange with the ground. In solid mechanics temperature changes and heterogeneities induce deformations unless

(a) (b)

Figure 5.12: Strain gauges installation at the experimental facility (a)fixing dowels positioning prior to installation and (b) after the installation.

some constrain exist. In this case, additional stresses and strains arise. These effects are generally proportional to the temperature variation. Although the main interest of this work focuses on the thermal and hydraulic coupled physics (see Section 2.3.2) the thermo-mechanical aspects were also considered. A proper monitoring system was designed to measure the stress and strain variations. Because of the interest in the different physics associated to the wall thermal activation, several sensors were placed. It is possible to divide the description of the monitoring apparatus in:

- Sensors for structural effects monitoring;
- Sensors for ground impact assessment;
- Sensors for system performance evaluation;
- Data management hardware and software.

Monitoring of structural effects

The experimental facility was equipped with a set of sensors to monitor stresses and strains related to the thermal activation on the wall surface. Hence a preliminary and qualitative description of collected mechanical behaviour data will be given as well.
Sensors were carefully placed externally to the wall to detect the mechanically measurable variables directly on the plane of the heat exchanger coil. Strains are hence measured by a series of 5 gauges that were firmly fixed to the wall. Two dowels glued by chemical anchoring agent in specifically drilled holes (see Figure 5.12) were used to this end. Sensors were carefully placed at different locations and with different axis alignment. Details about location and alignment of each sensor is depicted in Figure 5.13 and listed in Table 5.3.

Table 5.3: Location of stress and strain sensors on the wall surface. The axis column indicates the direction of measure (V = vertical, N = normal, H = horizontal, H* = due to excavation backfilling, accidental hit induced a 15° counter-clockwise rotation of the plate).

Loop	Instrument	Depth [cm]	Axis	Code
1	Strain gauge	170	H	Be1
1	Pressure cell	200	N	Cp2
1	Strain gauge	260	V	Be4
1	Strain gauge	350	H	Be7
1	Pressure cell	410	V	Cp3
2	Strain gauge	170	V	Be2
2	Strain gauge	260	H	Be5
2	Strain gauge	350	V	Be8
2	Pressure cell	410	H	Cp4
3	Strain gauge	170	H	Be3
3	Pressure cell	170	V	Cp1
3	Strain gauge	260	V	Be6
3	Pressure cell	350	H*	Cp5
3	Strain gauge	350	H	Be9

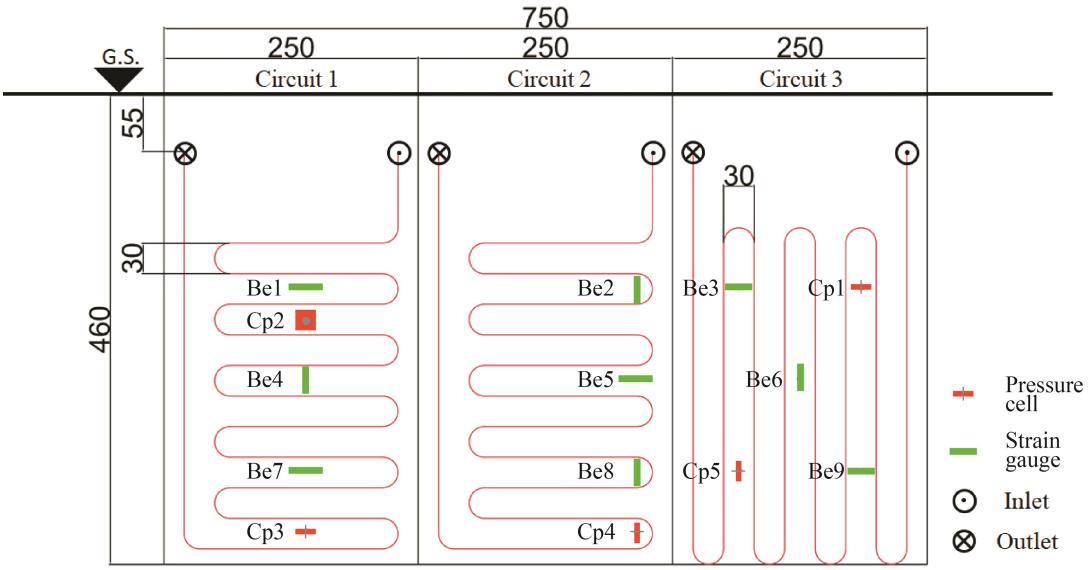

Figure 5.13: Heat exchangers prototype layout and sensors for monitoring of stresses and strains on the wall surface.

In order to characterize the stress field acting at the wall surface in different directions, 4 pressure cells sensors were put in place in addition to the previously mentioned strain gauges. Both the typologies of sensors allow a precise and accurate measurement

Table 5.4: Specifications of structural and temperature sensors deployed.

	Strain gauge	Pressure Cell	PT-100
Range minimum	-1500 $\mu\epsilon$	0 MPa	-40°C
Range maximum	+1500 $\mu\epsilon$	6 MPa	+60°C
Resolution	1 $\mu\epsilon$	0,1 MPa	0,01°C
Accuracy	0,2 % FS	0,3 % FS	0,1 °C
Working conditions	-10/+50°C	-20/+60°C	-40/+60°C

thanks to the calibration that was carried out prior to installation, depending also on the length of the cable to the acquisition unit. Sensors features are listed in Table 5.4. Cells measures are based on the pressure that is exerted by the de-aerated oil contained within the plate. Pressure is then converted through a transducer in an electrical signal conveyed to the acquisition unit and data-logger. Thus, the instrument detects the pressure acting on the direction normal to the measure plate. Placement and accurate positioning of the sensor was performed according to the scheme of Figure 5.13 so that contact was established on both faces of the plate. Indeed loss of contact may result in inaccurate measures as the contrast to the internal oil pressure would not be ensured. In particular sensor *Cp2* allows to measure the normal direction to the wall that cannot be investigated by means of the strain gauges. Indeed strain gauge cannot be oriented normal to the wall as there was no possible support for the dowels. For the sake of providing perfect contact between sensor *Cp2* and the wall surface, some concrete was cast behind the plate filling the 5.5 cm thick void space (see Figure 5.14). The other pressure cells were instead checked during backfilling and granular material was manually compacted on both sides of the plate to ensure full contact between ground and sensor. It should be noted that since the wall was already existing, the sensors had to be placed externally to the structure. This is particularly true in the case of the pressure cells that were fixed to the wall with the same system of clamps adopted for the pipes. This results in the small shift of the mean measurement axis of 5-10 cm out of the plane of the wall. This small shift is virtually equal to the shift of the average plane where pipes are installed, few centimetres externally from the surface.
Sensor cables were conveyed to the internal cavaedium where the acquisition and transmission unit is placed through the drilled hole *HM* shown in Figure 5.4. Due to the expected settlements after backfilling of the ground surrounding the prototype, particular attention was devoted to the cables deployment to avoid them from ripping out and consequent inability of acquisition. Indeed cable overrun was kept in along all their length, especially on turns and near to the vertical branches.

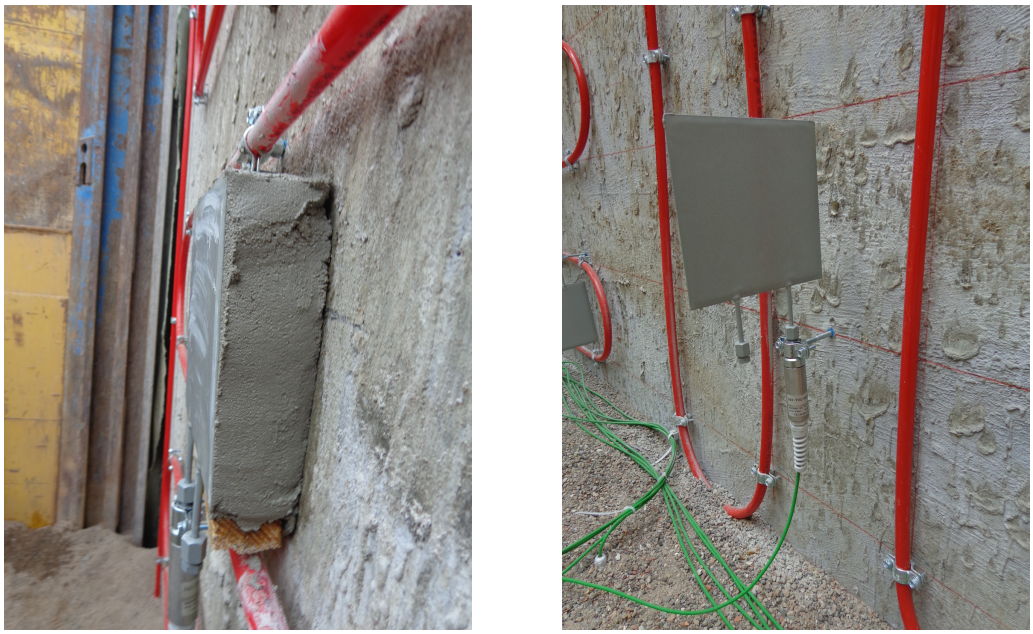

(a) (b)

Figure 5.14: Installation of the pressure cells of the monitoring system on the wall surface: (a) Cp2 with backfilling to guarantee perfect contact and (b) Cp4 positioning.

Monitoring of impacts on the surrounding ground

The same caution was adopted for the sensors devoted to the temperature and hygrometric monitoring of the ground. As regards temperature measurement, a large number of PT-100 (see Figure 5.15a) were positioned on four planes at different depths that were materialised during backfilling operations. The thermoresistances are specifically designed for ground monitoring and allow for an accurate measurement of the thermal status (specifications of PT-100 are listed in Table 5.4). They are indeed equipped with a metallic protection that avoids damages by the possible aggressive environment of the subsoil. This caution protects also the measuring parts from damages during backfilling operations. Indeed impacts with larger particles or boulders that are included in the heterogeneous ground at the site might potentially severely damage the sensors or their cables.
Ground monitoring system installation hence required to execute backfilling in stages, realizing the planes that are shown in Figure 5.15b. On each of the materialized planes the ground was roughly compacted and equalized. By doing these operations depth to the surface was kept virtually equal on all the plane and design was respected. Temperature sensors were organized in each of the planes in strings composed of 4 or 8 sensors, depending on the depth and on the specific alignment. In particular a smaller maximum distance between measurement point and the wall corresponds to deeper planes. In fact it is expected that here thermal gradients are smaller respect to the ones

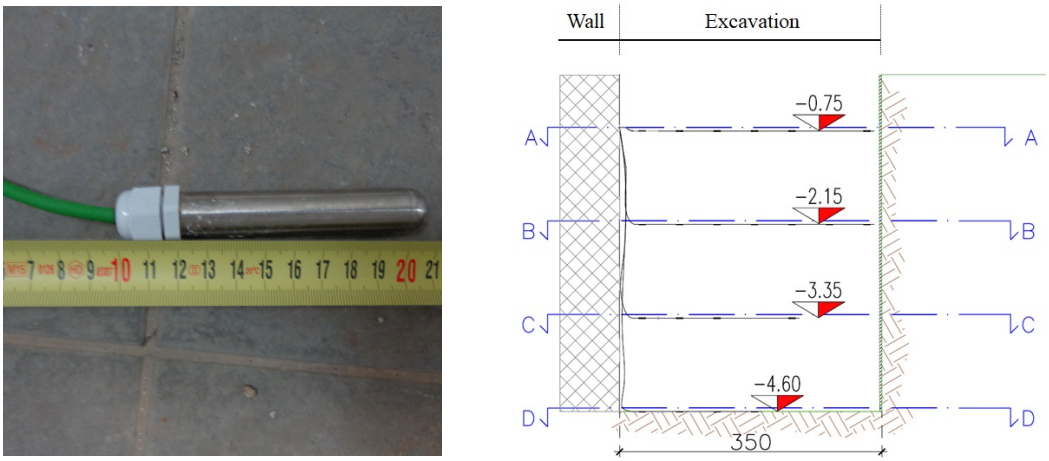

(a) (b)

Figure 5.15: Temperature monitoring network. (a)Sensors specifically designed for ground monitoring and (b) depth location of the sensors along planes.

at the ground surface. The location of the sensors on the different planes is reported in Figure 5.16 and Figure 5.17. Sensors were carefully deployed at desired locations by digging small holes with the help of trowels. This allowed to maintain perfect contact between the body of the sensor and the ground. Furthermore precise digging resulted in smaller differences respect to the rest of the plane in terms of compaction that would have resulted from inserting sensors in larger digs before compaction. For the sake of protection of the upper part of the sensor a thin sand layer was placed over sensor caps. Indeed the connection between the sensor and the cable is the most fragile part of the sensor and might have been otherwise damaged by hurts with pebbles during the backfilling that was realized with excavator. Due to the heterogeneous nature of the geomaterial, at few locations presence of pebbles prevented from the exact placement of the sensors. In these cases little shifts were accorded. Hence the position of the sensors was accurately measured just after installation. Only negligible shifts in the order of magnitude of 5 cm were observed with respect to the designed location. For the sake of simplicity positions reported in Figures 5.16 and 5.17 are referred as the designed ones. It should be noted that alignment on subsequent planes is designed to be alternated. This results in a 3 dimensional network of monitored points that are deployed on stagger rows to optimize the tridimensional reconstruction of the ground thermal state.

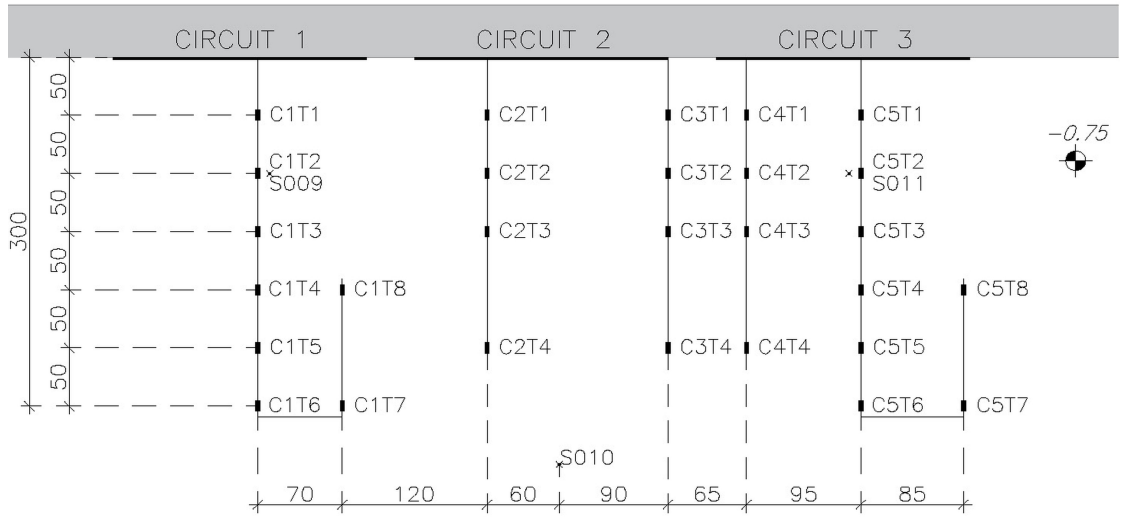

(a)

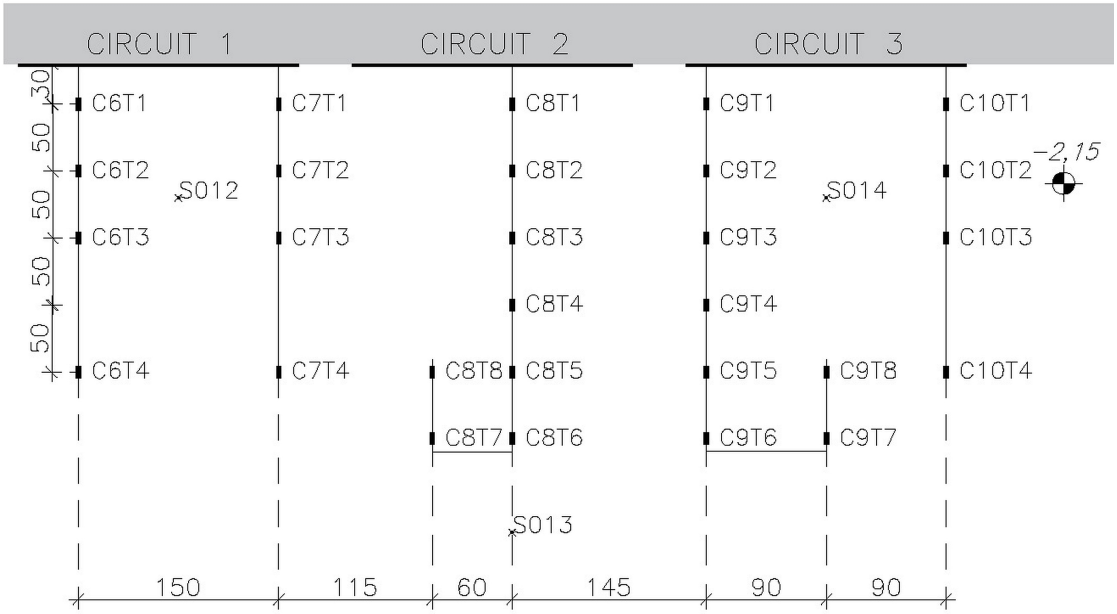

(b)

Figure 5.16: Temperature sensor location on (a) Plane A and (b) on Plane B along with their codification. Also some hygrometer sensors nominated as S0xx are depicted.

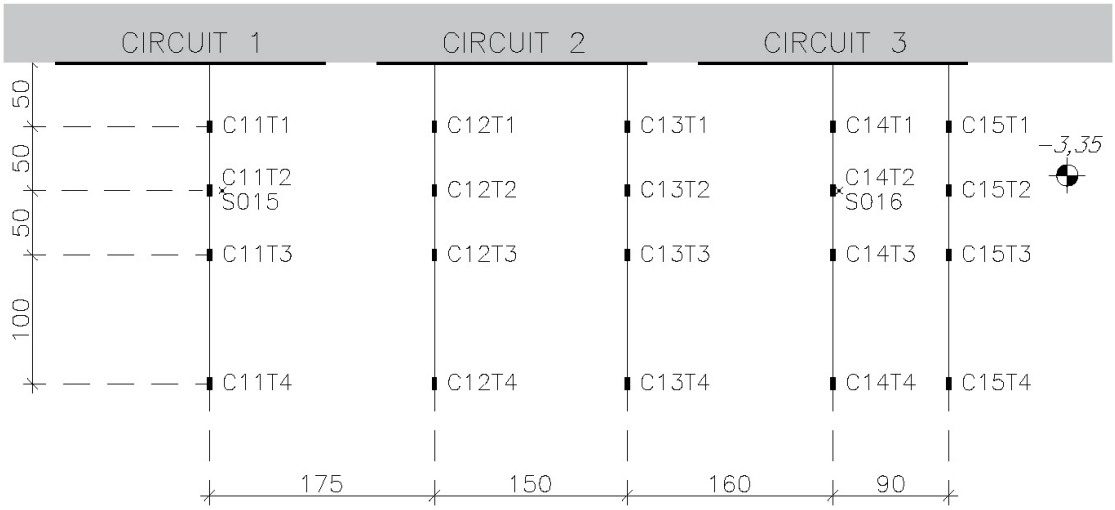

(a)

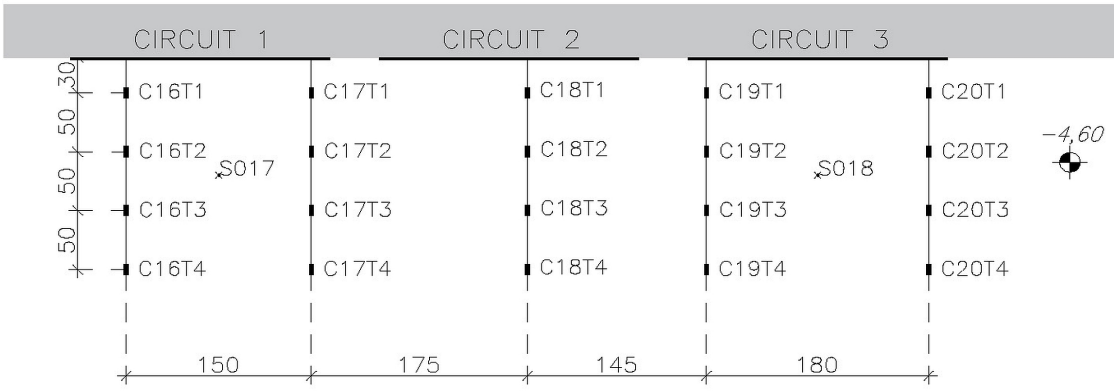

(b)

Figure 5.17: Temperature sensor location on (a) Plane C and (b) on Plane D along with their codification. Also some hygrometer sensors nominated as S0xx are depicted.

Beyond the thermal monitoring apparatus, in Figures 5.16 and 5.17, the hygrometer sensors are indicated with the label *S* together with progressive numbering indicator. A total of 18 hygrometers are included in the monitoring system up to the maximum depth (4.60 m b.g.s.) reached by the wall. Hygrometers measure the volumetric content

Table 5.5: Specifications of sensors about saturation in the ground and system performances.

	Hygrometer	Tensiometer	Energy meter
Range minimum	0 %	100 kPa	0,5 m^3/h; -15°C
Range maximum	80 %	-0,009 kPa	3 m^3/h;+50°C
Resolution	10^4	0,1 kPa	10 W
Accuracy	0,03%	10% + 2 kPa	20 W
Workin conditions	-20/+60°C	-40/+60°C	-

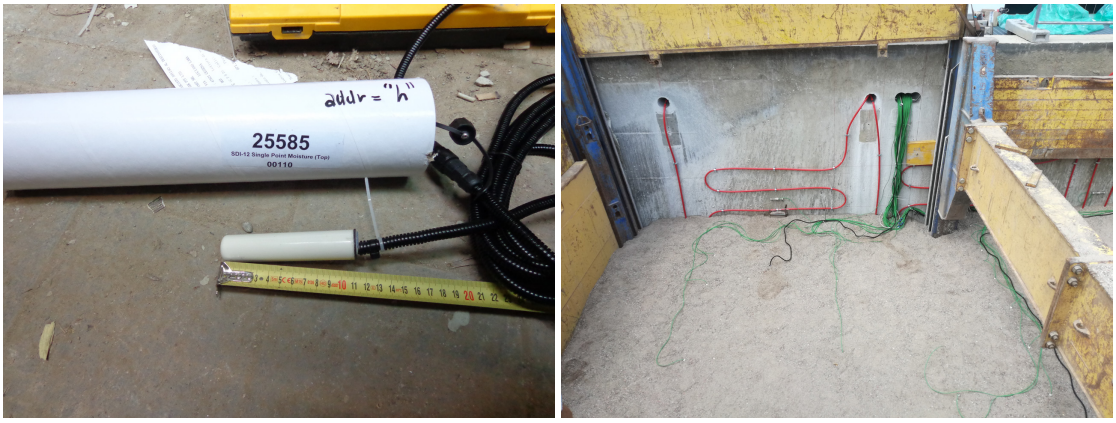

(a) (b)

Figure 5.18: Volumetric water content sensor installed at the experimental facility in Turin (a) before installation and (b) once installed before burial on plane B where the green cables are connected to the temperature sensors while the thicker black ones are the hygrometer sensors cables.

of water as a percentage of the total volume investigated by the probe. Measure precision is 0.03% volume and also temperature measurement is embedded in the 10-cm long sensor (see Figure 5.18) with 2°C accuracy as specified in Table 5.5. Since the shallower plane was at -0.75 m b.g.s. and the infiltration due to rainfalls (or garden watering) starts from the ground surface with significant gradients in the very shallower layers, a total number or 8 sensors were installed above *plane A*. In order to protect the cables these sensors were installed before final ground backfilling. They were indeed placed within resistant plastic tubes, commonly used in the construction sector as provisonal gutter, which have been removed only after the ground levelling. Accurate positioning was ensured by fixing the cables with steel wire that was as well removed only after the tubes were filled with finer ground parts (mainly sands) as shown in Figure 5.19. The vertical alignment of these sensors respected the alignment on the deeper planes that can be desumed from Figures 5.16 and 5.17. In order to characterize the non-saturated soil behaviour induced also by thermal alteration, 3 tensiometers were

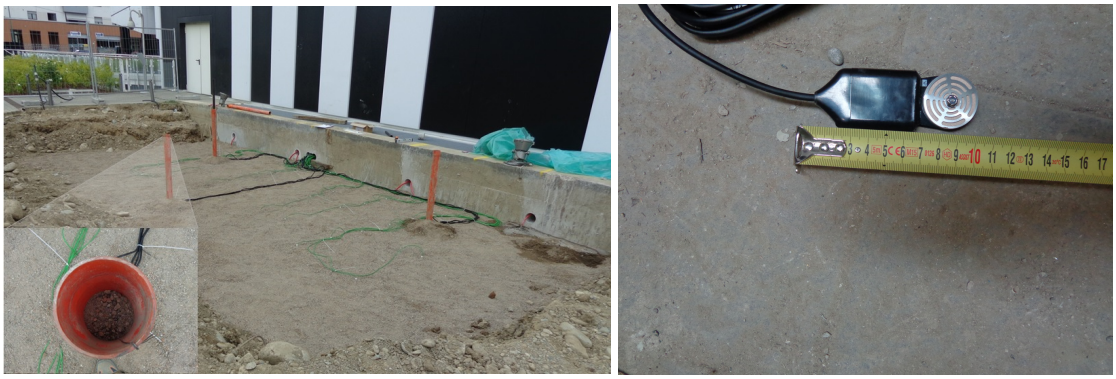

(a) (b)

Figure 5.19: (a)Installation of hydraulics sensors above the plane at very shallow depths within plastic pipes filled with sand before ground backfilling. Sensors included 8 hygrometers and (b) 3 tensiometers.

installed at very shallow depth. Deployment was carried out as described for shallower volumetric water content sensors. The *TEROS 21* sensors allow to evaluate the negative water pressure in partially saturated soils by measuring dielectric permittivity of the sensor solid matrix. The solid matrix is constituted by a porous ceramic medium which was accurately saturated by 15 hour water immersion before installation within the soil. Once installed, the ceramic matrix desaturates up to the level of the surrounding soil. Once the equilibrium is established the water potential in the ceramic medium balances with one of the surrounding soil, thus allowing the evaluation of the suction potential of the subsurface.
The combination of the measurement about suction water potential and water content with hygrometers allows to experimentally reconstruct the soil moisture characteristic curve of the geomaterial.

System performance monitoring

Beyond the structural and the environmental impacts of the thermal activation, heat exchangers functioning is monitored too. Indeed on the collector manifold three different energy meters were installed. Each of these meters is made up of two separate pieces: on the one hand the flow rate of the heat carrier fluid is monitored with a ultrasonic flow meter on the return pipe with high accuracy (see Table 5.5). On the other hand the exchanged energy is measured coupling the flow rate measurement with the double temperature measurement at two distinct points by PT-500 thermoresistances. These points are associated with the inlet and outlet ends of the circuits. Their deployment is reported in Figure 5.10. One energy meter was installed to measure the data from circuit 1 and 3 respectively. This allows to compare the thermal performances of the two

distinct pipes deployment of the GeothermSkin system. A third energy meter was installed on the main flow and return pipe so that the global energy flow from the ground heat exchangers can be measured. At the date of writing it is planned to equip these flow meters with a remote connection. On the contrary at present, just manual readings from the above mentioned sensors is possible. It is especially used to evaluate the flow rate on the main circuit and how it is distributed when multiple circuits are working in parallel. Temperature measurement on the heat carrier fluid is on the contrary continuously sampled at the heat pump location, thanks to the recording function of the thermal machine. While circulation is active, continuous measurement is obtained. Data collected regard the circulation pump speed of both the primary and secondary circuit, the inlet and outlet temperatures of both the circuits, the temperature of the buffer tank on the secondary circuit and the cavaedium air temperature.
In order to delineate heat pump efficiency and the unit energy cost of the system, it is planned to acquire further parameters as the power consumption of the heat pump through a dedicated electricity meter and the flow rate on the secondary circuit through the installation of an additional energy meter.

Data management software and hardware

All the cables pertaining to sensors of structural effect and to sensors of effect on the environment were driven to specifically drilled hole *HM* in the wall shown in Figure 5.13. All drillings were then filled with expanding polyurethane foam to avoid infiltration in the wall structure and finer soil parts to be dragged with infiltrating water. Cables were carefully positioned in the cavaedium with an excess length to avoid straps during ground settlements. The acquisition unit was installed in the cavaedium. Power supply for the acquisition unit is directly provided by the electrical system of the building. Nonetheless a backup battery was installed in order to ensure continuous operations and avoid data losses. Acquisition unit is also equipped with a GSRM module to upload all the collected data on the internet cloud so that they can be remotely consulted and downloaded.
All the data, except for the system performance, are available from a specifically designed online interface that allows browsing in desired time frames both in tabular and graphical form. In this latter case aggregation of data from different sensors is possible in order to compare data and trends, also by averaging them on a hourly rather than daily basis. The data can also be directly downloaded in exchangeable formats for the desired time periods.
On the contrary the data collected from the heat pump can be displayed from the producer web site. However accurate data from continuous monitoring (acquisition frequency can be adapted by the user) need to be collected through hardware USB interface that results in log files covering 24h period each.

5.4 Experimental campaign

The installation of the system was completed in July 2019. However circuit saturation and acceptance testing was carried out until September 2019. It was thus immediately started an experimental campaign in cooling mode. Two tests were carried out until the outdoor air temperatures were sufficiently high during low-intensive cooling periods. Conversely a wider number of settings was tested in heating mode during winter season 2019/2020.

5.4.1 Site characterization

As mentioned above, the experimental site is located in the City of Turin (Italy) near the Porta Susa station and the courthouse. The city of Turin lies on the end section of the great alluvium of the Dora Riparia river. The study area is thus characterized by typical geological setting of an alluvial plain. The upper 50 m of subsoil in Turin form a geological unit characterized by the presence of a sand and gravel deposit, ranging from medium to highly dense, with lenses of cemented soil that however are mainly present below 10 m depth (Barla and Barla, 2005, 2012; Barla and Camusso, 2013). The shallower unconfined aquifer is hosted in this unit and is underlaid by finer silty-clayey deposits with low hydraulic conductivities.
The shallower aquifer thickness ranges from 20 up to 50 m in the metropolitan area. The depth to the water table in the Turin metropolitan area ranges from 35 meters in the north western part of the territory to few meters in the eastern part near the Po river (Bove et al., 2005). Indeed this watercourse, dividing the alluvial plain from an hilly area with different geological characteristics, acts as the main drainage for the shallower aquifer of the plain that thus presents the main flow direction along the axis WNW-ESE. Further details on the geological settings of the Turin alluvial plain will be given in Chapter 6. Nonetheless, in this paragraph attention will be devoted to the specific characteristic at the experimental site, mainly limited to the depth interested by heat exchange.
Although geotechnical investigations were not carried out prior to the construction of the experimental facility, different geotechnical units were identified from Standard Penetration Tests conducted in an adjacent area (Lavezzo and Monti, 2012). On the basis of in situ tests the following units were identified:

- GU0: Anthropogenic deposits;
- GU1: Gravels in sandy/silty matrix;
- GU2: Sands and gravels.

The water table is expected to be present slightly above 20 m depth. Thus groundwater flow does not interest the ground volume involved in the heat exchange with the energy wall.

Figure 5.20: Core drilling from borehole at the Energy Center location.

Table 5.6: Main geotechnical parameters of Geotechnical Unit 1 (Lavezzo and Monti, 2012).

Property	Symbol	Units	Value
Unit weight	γ	$[kN/m^3]$	17
Relative Density	D_r	[%]	33
Peak friction angle	ϕ_p	°	26
Const. vol. friction angle	ϕ_{cv}	°	24
Cohesion	c'	$[kPa]$	0
Undrained resistance	C_u	$[kPa]$	25
Poisson's ratio	ν	[−]	0,3
Young modulus	E	$[MPa]$	2,3
Edometric modulus	M	$[MPa]$	3,9

Due to the very shallow depths interested by the excavation, a relevant layer of anthropogenic deposits and topsoil is present at the site. Overlaid by 30 cm topsoil, there is a layer made by gravels with pebbles in a sandy and locally silty matrix that can be related to the realization of the building or even prior construction testified by brick fragments (Aiassa and Antolini, 2019; Lavezzo and Monti, 2012). This deposit shows thickness of up to 3 meters and is under-lied by the fluvioglacial unit represented by the sandy-gravelly deposits. This latter deposit presents oxidation evidences and alteration on the first meters up to the depth of interest of the experimental facility, namely 5 meters. The main geotechnical parameters of GU1 are listed in Table 5.6. From the seismic profile derived from in situ tests (Lavezzo and Monti, 2012), it is expected that higher cementation degree and compaction is present starting from 10 m depth. Figure 5.20 shows the core of a borehole that was executed at about 10 m from the building facade. It should be noted that during the excavation works for prototype installation even meter-sized boulders and concrete elements have been found (see Figure 5.21)

Figure 5.21: Material excavated during construction works of the prototype energy wall system.

5.4.2 Experimental tests carried out

The ground heat exchangers installation, together with the thermo-hygro-mechanical monitoring system, was completed in July 2019. The hydraulic circuit was completely saturated with the water-glycol mixture in August 2019 and thus the experimental campaign started in September 2019. Two tests were run in cooling mode until external air temperatures were sufficiently high.
By the end of October 2019 until February 2020 a set of 6 different tests were carried out in heating mode. Although the experimental tests program is far from being completed, especially regarding the cooling performances, at the date of writing partial results are already available. These results in particular regard the thermal performances of the installation, the ground thermal affection and the mechanical actions on the wall.
A synthesis of the tests driven can be found in Table 5.7. The tests cover a variety of possible configuration from the heat exchanger geometry point of view. In fact variation to the linking between different circuits (3 tests carried out with sequential linking and 4 test with parallel link) and the circuits employed was performed. Indeed the thermal performances during the tests conducted with circuits 1 and 2 with the ones regarding circuits 2 and 3 allow to comparatively define the more efficient solution from the thermal point of view. Furthermore, the experimental programme investigated the dependency of the ground heat exchange rates on the temperatures to be delivered to the user. Nonetheless, in order to fully characterize the system functioning further combination of activated circuit will be explored in the next future, including single circuit activations also in the winter season or contemporaneous activation of circuit 1 and 3. This latter configuration will enable to test the relevance of thermal interference among neighbouring modules. Although the heat carrier fluid circulation is continuous, the thermal cycle operates discontinuously. To this regard, optimisation of overall system performances (including electricity consumption) would require careful parametrization of target temperature through the *climatic curve*. However tests were carried out with the intention of analysing the potential ground exchange. This implied testing in less than ideal conditions for the heat pump. Some of the experiments

Table 5.7: List of tests carried out. In the 'link' column the letter *S* stands for sequential link while the letter *P* indicates an in parallel connection. Tests are identified with the first letter indication the operative mode (H='heating' and C='cooling') and the following numbers indicate the activated heat exchangers according to numeration in Figure 5.13.

Test code	Link	Starting Time	Ending Time	Duration [h]	Target Temp. [°C]
C_2-3_20190916_20190919	S	16/09/2019 10:30	19/09/2019 10:36	72,1	5
C_3_20190923_20190925	-	23/09/2019 10:50	25/09/2019 11:00	48,2	5
H_1-2-3_20191024_20191119	S	24/10/2019 11:20	20/11/2019 14:20	651,0	45
H_1-2_20191128_20191202	S	28/11/2019 12:25	02/12/2019 16:00	99,6	45
H_2-3_20191207_20191210	S	07/12/2019 10:00	10/12/2019 09:25	71,4	45
H_1+2_20191220_20200113	P	20/12/2019 19:30	13/01/2020 10:53	567,4	45
H_1+2_20200124_20200128	P	24/01/2020 17:27	28/01/2020 09:20	87,9	55
H_1+2_20200131_20200203	P	31/01/2020 17:56	03/02/2020 09:26	63,5	35

with discontinuous regime would indeed be undesired by end user in domestic application. Discontinuous thermal cycle is testified by the temperature of the fluid delivered to the fan coil user. Indeed the temperature oscillates around the calculated supply temperature that is imposed by the heat pump logic. This logic relates cavaedium air temperature and the supply one by means of a curve that can be adjusted manually on the heat pump. Furthermore the thermal cycle starts when the difference between the calculated target temperature T_{target} and the real one exceeds an imposed value:

$$DegreeMinute = \sum \left(T_{real} - T_{target}\right) \cdot t \tag{5.1}$$

where T_{real} is the outlet temperature at the user side (namely BT3 in Figure 5.22), while t is the time. In the test here analysed the threshold value was set to the maximum allowed of -30 DM in order to shorten the inactive part of the heat pump cycle. Indeed the time interval between two subsequent compressor starts was virtually stable along the whole duration of the test and equal to 220 minutes. The cycle are composed of a first par of 70 minutes when the compressor is activated and rise up the temperature at the user side (including the buffer vessel) followed by 150 minutes inactivity when the temperature slowly decreases.

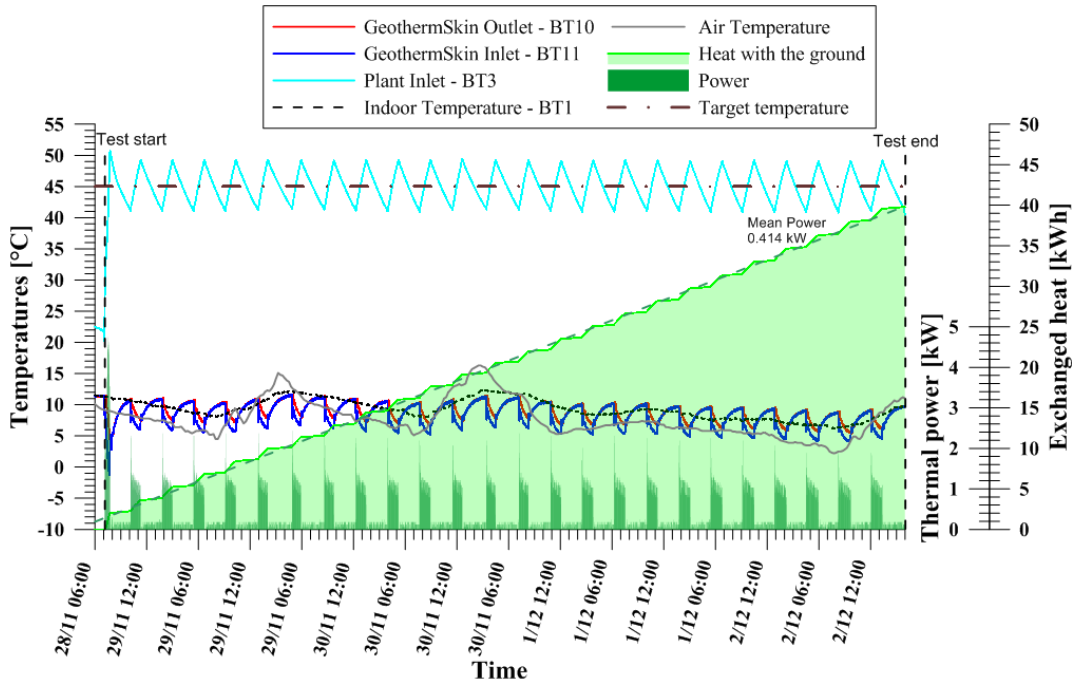

Figure 5.22: Thermal performance interpretation of experimental test *H_1-2_20191128_20191202* with sequential link of circuit 1 and 2 in heating mode.

It should be mentioned that experiments were carried out to ensure the shortest inactivity time, while optimal system compressor operations would present longer cycles, possibly with variable compressor frequency governed by an inverter to reduce the number of ignitions.

5.4.3 Energy wall thermal performances

Parameters monitored during every test allowed to determine the thermal performance of the system in terms of instantaneous and mean exchanged thermal power, temperature range of the inlet and outlet of the system. It should be noted that these temperatures were detected as outlet and inlet of the heat pump, thus neglecting the heat losses interesting the main collector/distributor pipes in the cavaedium. The influence is however limited due to the small temperature gradient between the heat carrier fluid and the cavaedium ambient temperature. Furthermore the pipes have been completely and heavily insulated, as described in previous paragraphs.
An example of the interpretation of test thermal performance is shown in Figure 5.22 referred to test *H_1-2_20191128_20191202*. The test lasted approximately 4 days while external air temperatures ranged from 5 to 15 °C. Since the undisturbed ground temperature was about 12°C at 0.75 m depth up to 18.5°C at 4.60 m, the temperature of the heat carrier fluid was frequently higher than the air temperature. It is thus obvious that

Table 5.8: Values adopted for calculation of heat exchange rate in experiment *H_1-2_20191126_20191202*.

Quantity		Value
Propylene Glycol to water mixture	[%]	25
Flow rate	$[ls^{-1}]$	0.15
Unit weight	$[kgm^{-3}]$	1023.44
Specific heat capacity	$[KJkg^{-1}{}^{\circ}C^{-1}]$	3.917

in these time frames the ground source heat pump can be more efficient than air source heat pumps. This can be related to the higher thermal inertia of the ground compared to the external air. Indeed the ground shows relatively higher temperatures even if it is bounded both from the upper surface and from the wall surface by cold temperatures. It should be noted that air temperature in the cavaedium behaves almost accordingly to the external air variations due to the direct connection of the ceiling to the open air. Daily variations are however extremely damped respect to surface air and seem to be reflected with good agreement to the mean temperature level of the heat carrier fluid. Heat exchange is calculated on the basis of the temperature difference at the inlet and outlet ends of the ground loop, according to equation:

$$\dot{q} = Q \cdot \rho_f \cdot c_f \cdot \left(T_{in} - T_{out}\right) \tag{5.2}$$

where Q is the flow rate, registered by the flow meter mounted on the main collector pipe, ρ_f is the unit weight of the fluid, c_f is its specific heat capacity, T_{in} and T_{out} are the inlet and the outlet heat pump temperatures on the ground loop respectively. Parameters adopted for the interpretation are listed in Table 5.8.
These values are referred to the mixture of the propylene glycol to water mixture at the specified proportions in volume and considering the mean temperature of the fluid of 10°C. Indeed the dependency of the unit weight and the specific heat capacity (see Section 2.3) was neglected due to the limited temperature ranges experienced. As regards system performance, instantaneous heat exchange rate peak value was recorded during the initial heating ramp and was equal to 4.74 kW, corresponding to a temperature difference of 7.8°C. Apart from this starting ramp, maximum temperature change was of 3.9°C corresponding to an heat exchange rate of 2.37 kW. During the compressor activation phase the power generated is about 1-1.5 kW (as clearly shown in Figure 5.22). It is however of wider interest to define the mean thermal power that can be exchanged by the system. This can be evaluated as the ratio of the total amount of heat provided by the system over the test time:

$$\bar{q_{th}} = \frac{\int_{t_{start}}^{t_{stop}} \dot{q} dt}{t_{stop} - t_{start}} = \frac{\sum \dot{q} \cdot \Delta t}{t_{stop} - t_{start}} \tag{5.3}$$

Table 5.9: Thermal performances of the energy wall from experimental results interpretation.

Test code	Flow rate	Peak		Average	
		Power	Temp. change	Power	Ex-change rate
	$[l/h]$	$[kW]$	$[°C]$	$[kW]$	$[W/m^2]$
C_2-3_20190916_20190919	575	5,71	8,9	0,603	26,21
C_3_20190923_20190925	575	4,05	6,3	0,536	46,61
H_1-2-3_20191024_20191119	670	3,80	5,1	0,615	17,83
H_1-2_20191128_20191202	546	2,37	3,9	0,414	18,00
H_2-3_20191207_20191210	530	1,94	3,3	0,411	17,87
H_1+2_20191220_20200113	910	2,13	2,1	0,492	21,39
H_1+2_20200124_20200128	910	2,33	2,3	0,548	23,83
H_1+2_20200131_20200203	923	2,56	2,5	0,333	14,47

where t_{start} and t_{stop} are the start and ending times of the test respectively and $\dot{q}$ is calculated according to Equation 5.2. This means that power can also be interpreted as the slope of the interpolating line of the cumulated exchanged energy depicted in Figure 5.22. In the test that is here analysed, mean thermal power reaches the considerable value of 414 W. Table 5.9 reports the heat exchanges for the tests carried out. Detailed information and graphs regarding the tests carried out are extensively reported in Appendix A.

Comparison of heat exchange rates in the several tests carried out suggests that a considerably higher heat exchange would to be obtained in summer cooling operations rather than during the winter heating ones.

Results are virtually identical in terms of mean heat rates in the case circuits with different pipe main direction are employed. This finding might be associated with the similar distance of circuit ends and with the limited influence of thermal short-circuits along the pipes (Sterpi et al., 2014, 2017b). This is particularly evident comparing results from test *H_1-2_20191128_20191202* and test *H_2-3_20191206_20191210*. In addition to this, the sequential connection of different modules seems to be slightly less efficient from the thermal point of view when compared to parallel connection. This mechanism is confirmed by the maximum temperature differences obtained. In particular sequential connection allows higher thermal drop (up to 5,1°C) rather than parallel connection (2,1 - 2,3°C). However, the values pertaining the tests driven with parallel linking proportionally show higher values respect to the ones obtained with sequential links. This means that the temperature change is more marked in the first part of the circuit where the gradient is higher. This is in turn reflected, accordingly to the Fourier law, in the heat flux.

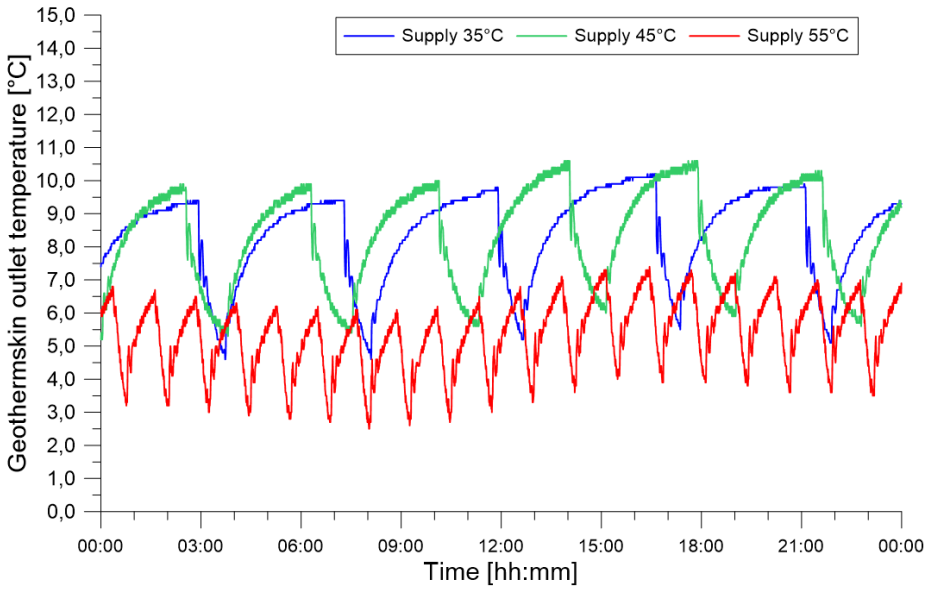

Figure 5.23: Comparison of thermal levels in heating tests depending on the supply temperature.

Mean thermal power values were then normalized by the wall area interested by each circuit. In particular, the shallower portion of the wall that was not equipped with the heat exchanger was computed too. The inclusion of this area leads to conservative evaluation of the heat exchange rate. Results show a thermal efficiency of about 15-25 W per unit area in heating mode. These values are almost in line with previous literature referred to classical energy wall (Bourne-Webb et al., 2016; Brandl, 2006; Di Donna et al., 2017) or slightly above for cases with similar climate and boundary conditions (Sterpi et al., 2020).
It should be noted that no measurement of the heat flux towards the inner facade of the wall was carried out. This heat flux is believed to be relatively small as the thick concrete wall has a not negligible thermal resistance due to its thickness. Furthermore the hydraulic circuit is not directly connected to the external facade as the support system ensures a minimum distance (about 5 cm) and soil is interposed between the circuit and the wall.
Temperature ranges of the brine in the heat exchanger are almost stable, independently from the temperature to be delivered to the user. Indeed tests carried out with circuit 1 and 2 with parallel connection in heating mode highlight only slight differences in the thermal range. This difference is more pronounced in the case of the highest supply temperature (see Figure 5.23) even widely damped respect to the differences at the user side.
On the contrary the duration of each cycle seems to be considerably affected by the target temperature. The higher the temperature to reach at the fan coil, the shorter is the interval between two subsequent compressor activations. In addition to this, the

slope of the cooling portion of each cycle, namely the one when the compressor is active, results to be steeper as the supply temperature increases. Such a cyclic behaviour can play a role in the efficiency of the heat pump, with negative impact on electricity consumption. Furthermore, the gap between the source temperature and the one pertaining the user terminals is crucially linked to the efficiency of the heat pump with an inverse proportionality. The more frequent activation of the compressor also leads to augmented wear and shortening of the service life of the components.

5.4.4 Environmental impact on the surrounding ground

Geothermal installations use the subsurface as an heat source/sink depending on the operative mode. Injection or extraction of thermal energy thus can negatively impact on the temperatures at the site, depleting the resource either in the short or the long term. Source affection can be concisely represented by the heat plume generated. Thus the characterization of such a plume in its magnitude, extension and position is of crucial relevance in order to define possible alteration to the geothermal potential.

Thermal impact of GeothermSkin system

For the sake of precise characterization of the thermal plume generated by the energy wall system, an extensive network of PT-100 sensors were installed in the experimental site. The definition of the sensors deployment is reported in previous paragraphs (see Section 5.3.3).
An extensive series of data resulting from the experimental campaign is reported in Appendix A. For the sake of brevity, some typical and representative results only are shown in this paragraph.
As expected, the ground temperature is more stable than the outdoor air temperature. Indeed daily fluctuations can be identified at shallower depths and at the nearest location to the wall. On the contrary, the temperature trend is almost constant at bigger distances from the cold boundaries (upper surface and wall facade) and reflects the seasonal thermal fluctuation, as shown in Figure 5.24. During the experimental campaign in heating mode, the mean thermal level resulted to be hotter at higher depths. This is evident by comparing the records of paired sensors on string 2 and string 12 that are located at same planimetric position but different depths (0.75 m b.g.s. and 3.35 m b.g.s. respectively).
As the temperature of the brine along the pipes is not far from the one pertaining the surface air and the air within the cavaedium, the thermal activation of the system seems to have small impact on the ground temperature even at small distances from the wall. Indeed the thermal activation seems to induce on temperature only a slight decrease. Since the forcing action is weak, the alteration is not highlighted by a step shaped drop. On the contrary, a small influence can be inferred by the wider distance between the

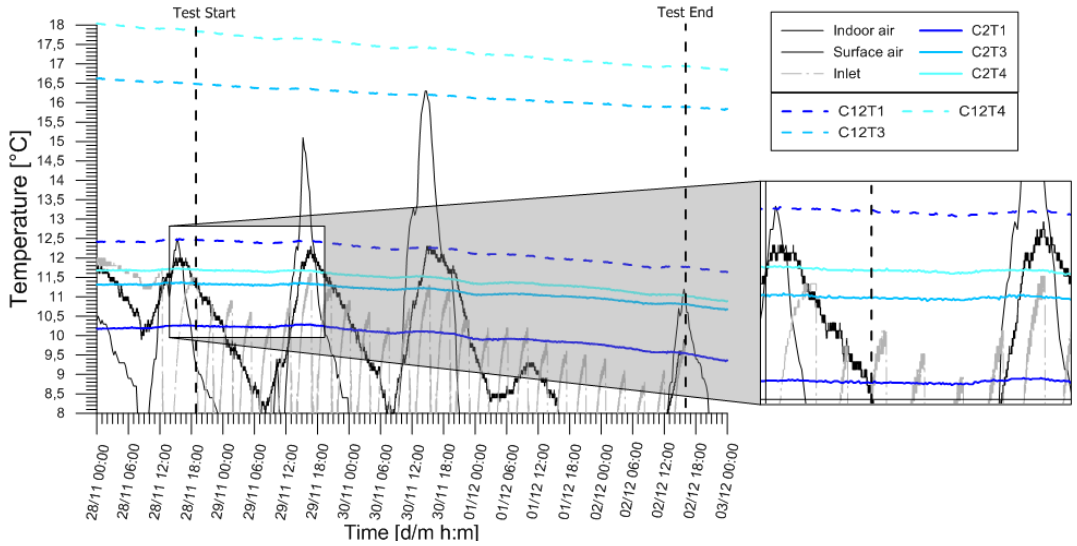

Figure 5.24: Thermal records along string 2 (plane A) and string 12 (plane C) during experiment H_1-2_20191128_20191202.

curves *T1* and *T3* at the end of the test rather than at the start at both the planes investigated.
On the contrary, during the cooling tests, alteration on ground thermal status seems to be far more relevant due to the higher gap between subsurface and carrier fluid temperatures. Figure 5.25 shows temperature records along the sensor strings placed in front of the center of circuit 2 that was activated during test *C_2-3_20190916_20190919* at two different depths. Rise in thermal values can be clearly identified on sensors placed at 30 cm and 80 cm distance from the wall. A particularly high increase of 5°C was registered at 30 cm distance from the wall and 2.15 m depth along with a rather immediate response to the thermal activation of the system. Retardation can be thus appreciated on sensors that are located at larger distances from the wall. Indeed at 80 cm distance the temperature rise took place after about 24 hours from test start while at 130 cm distance the slight temperature variation starts only 48 hours after thermal activation. At higher depths system operation influence appears to be reduced. Indeed the sensor C18T2 at 80 cm from the wall shows a small rise respect to the sensors placed at bigger distances. Experimental results thus seem to suggest that virtually no influence on the ground temperature is exerted by the system as far as it is used in heating mode during the winter season. Although the system running in cooling mode leads to a thermal plume, the thermal affection exponentially decreases depending on the distance from the system. As a result the thermal status of the ground is virtually equal to the undisturbed conditions starting from very few meters from the system„ especially at higher depths. This is of great theoretical and practical importance. Indeed the usage of this system even at large scales would not interfere with the geothermal potential of deeper installations as Borehole Heat Exchangers, open loop systems or energy tunnels.

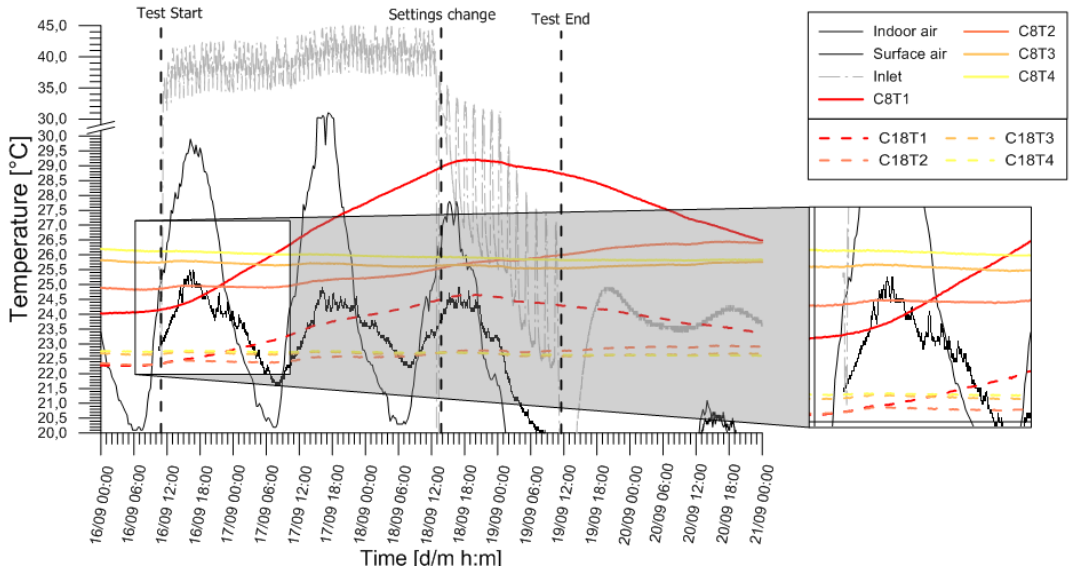

Figure 5.25: Thermal records along string 8 (plane B) and string 18 (plane D) during experiment C_2-3_20190916_20190919.

Impact on the ground partial saturation

Due to the low influence also from the thermal point of view, no significant alteration seems to be exerted by the thermal activation on the hygrometric equilibrium of the ground near the wall. Indeed results shown in Figure 5.26 seem to be virtually unaffected by any external influence. Indeed the absence of significant water infiltration due to rainfall leads to a limited volumetric water content, slightly decreasing in time. It should be noticed that water content is decreasing with depth and at the base of the wall is below 3% while on instrumented plane *A* it about 10-11%. The weak trend of drying is in line with the little rise in water tension registered by the tensiometers, especially sensor *T1* that shows a difference at the end of the test of about 25 kPa with respect to the start of the test. Nonetheless it seems that the changes on settings of the heat pump, testified by a significant decrease of the inlet temperature, had no influence on the drying trend shown.
In general, temperature rise is expected to induce a reduction of the volumetric water content adjacent to the wall with a migration of the moisture in the form of vapour towards colder regions. This in turn results in local gradients as the migrated vapour condensate in these regions. As a result, cyclic movement of water vapour can be expected (Lekshmi and Arnepalli, 2017). Being the heat transfer in partially saturated soil dependant on the water content, the above mentioned changes affect the heat exchange. As a consequence the thermal conductivity results to be critically dependent on the moisture content.
Among others, Wang et al. (2016) developed a model predicting dramatic increase of such values for small water content variation in the field of low degree of saturation

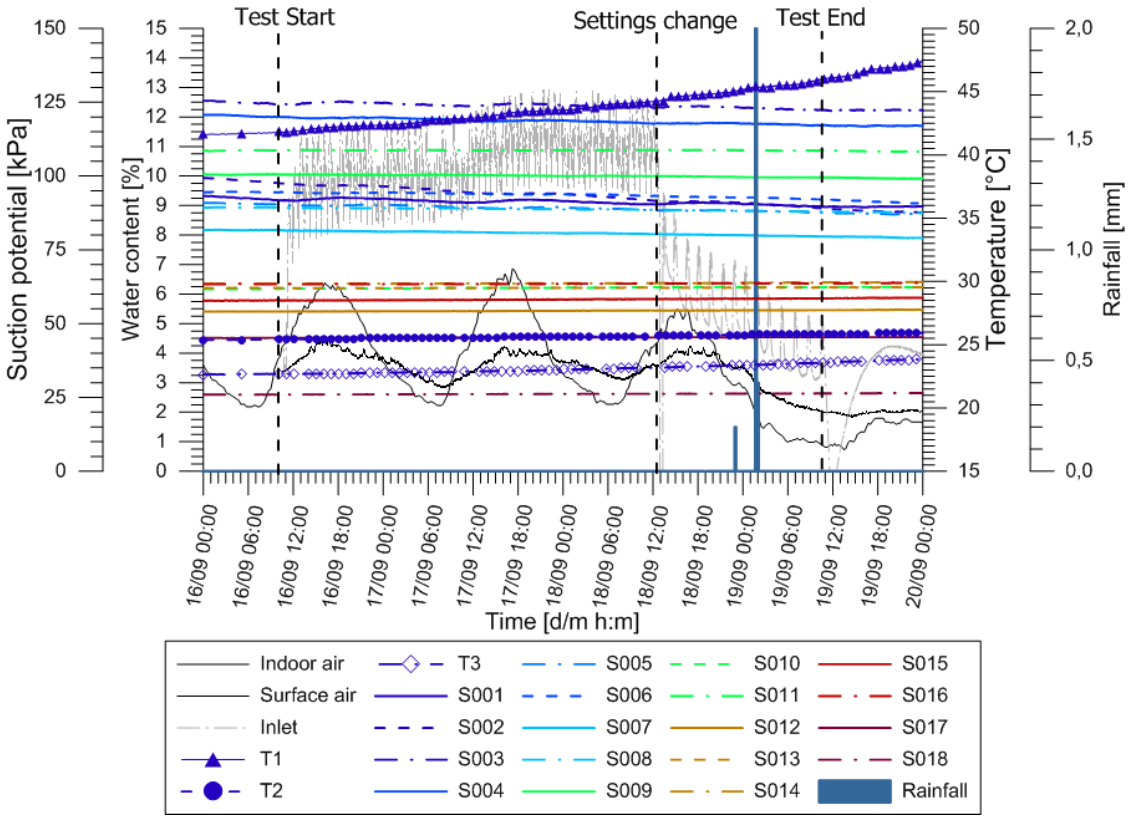

Figure 5.26: Volumetric water content and suction potential records from test C_2-3_20190916_20190919.

(0-5%), even if such influence has lower impact for the range of temperatures of interest. Although further investigation is needed in the analysis of the experimental site presented, it should be noted that the mean water content is above the mentioned range and that temperature changes registered at the sensor location are limited. As mentioned in Section 5.3.3, both the tensiometers and the hygrometers are equipped with temperature sensor.
Even if the daily thermal excursion are relevant at extremely low depths, namely above the instrumented plane *A*, all the sensors from *S001* to *S008* show negligible response from the water content point of view. This is in line with the absence of response to wall thermal activation, as the thermal plume is extremely limited even at the distance of 100 cm corresponding to the location of the nearest hygrometers.

5.4.5 Structural effects on the supporting wall

Beyond the environmental aspects, the structural impact of system operation on the supporting wall structure seems to be extremely low. Indeed data collected by strain gauges and pressure cells installed reveal a low variation resulting from the thermal

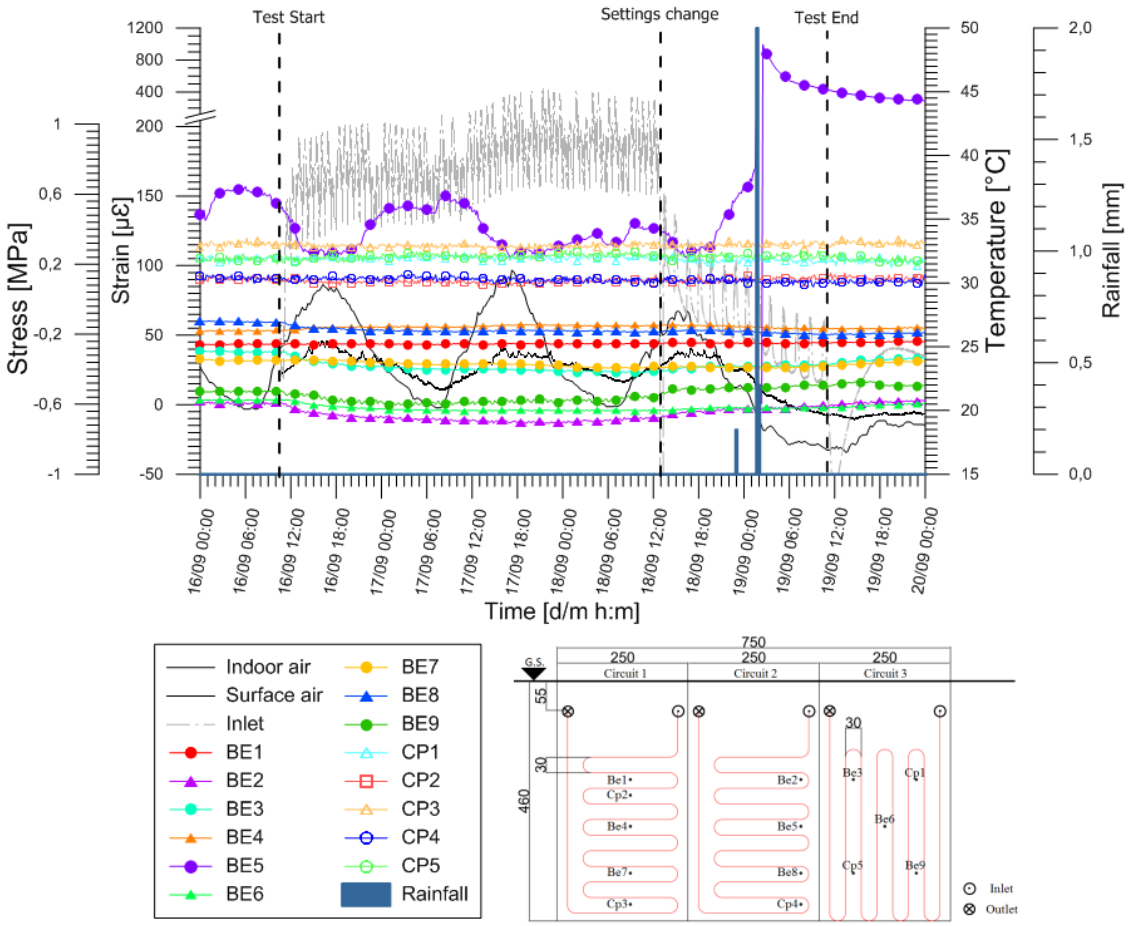

Figure 5.27: Strain gauges and pressure cells records from test C_2-3_20190916_20190919.

activation (see Figure 5.27). In particular, apart from BE5 that seems to be crucially affected by rainfall and presents high variations even without thermal activation, remaining strain gauges are almost stable during all the test duration. A barely detectable contraction of up to 20 $\mu\epsilon$ was observed during the test. The major part of the deformation took place rapidly after the test start, while a residual decrease in the values was observed in the following hours. Data collected highlight a substantial return to the conditions prior to the test start as the temperature of the heat carrier fluid decreases when the heat pump settings were changed. In contrast to this evidences, pressure cells did not recoded any relevant changes during system activation.
The low variations registered during the test are confirmed by the rest of the experimental campaign. Figure 5.28 shows the stress and strain variations registered for each of test carried out. It should be noted that the data refer to the sensors that were directly interested by the activation, namely the points that were included in the activated circuits. Furthermore measures from sensor BE5 (that shows, as already mentioned, a critical affection of measurement by rainfalls) were filtered in order to better study the

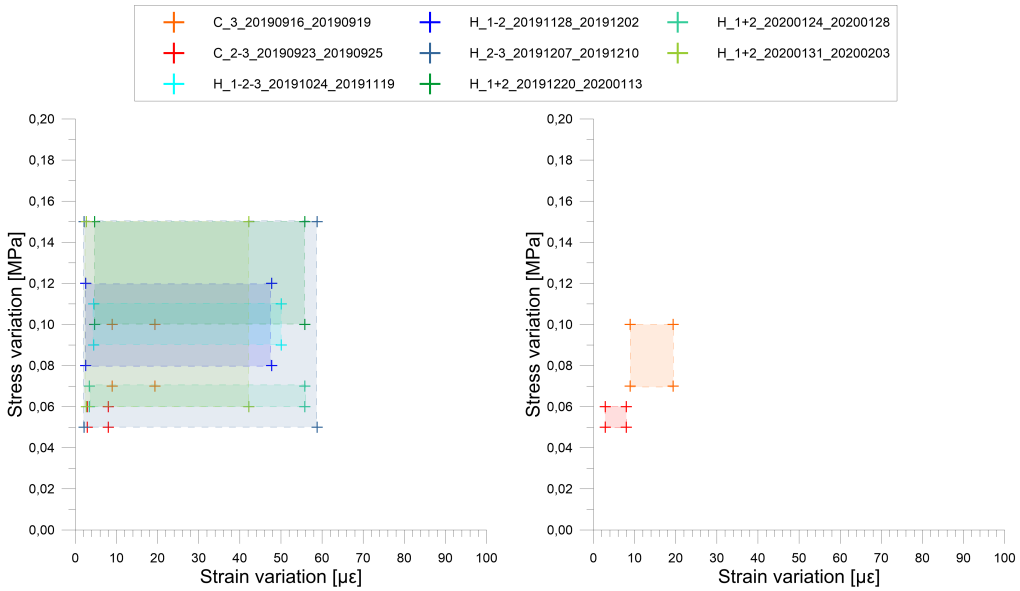

Figure 5.28: Stresses and strain variations induced by GeothermSkin thermal activation during the heating and cooling experimental campaign.

effects of thermal activation. It should be noted that, although the thermal influence of the circuit in cooling operation is signigicantly higher than in heating mode, structural effects seem to be limited and in line with the ones experienced during the heating tests. From the tests carried out, it is clear that the impact in term of deformation in extremely limited (from almost null to a maximum of about 60 $\mu\epsilon$).
Also stresses variations are extremely limited (from 50 to 150 kPa on an average load of about 200-450 kPa), confirming that the impact that is exerted on the wall because of the thermal activation is limited. This evidence seems to suggest that from the technical point of view, structural design of such structures might be carried out without taking in consideration the application of the GeothermSkin system.
From all the above, collected data suggest that no relevant impacts are exerted by the system both from the wall structural point of view and on the surrounding ground.

5.5 Summary

Among the main challenges of modern cities, a crucial role is played by spatial planning and by energy supply strategies. Indeed sustainability of our urban areas is closely related to the use of energy from renewable resources. To meet the demands, these resources need to be distributed and easily accessible. The peculiar aspect of densely inhabited areas is that the *energy density*, namely the amount of energy per equipped unit area, needs to be high because of the land scarcity issues.
In this perspective, the use of the subsoil is extremely promising, especially considering

that the resource can be mined at different and distinct depths. Indeed optimisation in the use of geothermal resources may be pursued on a tridimensional scale.
In this respect the use of very shallow geothermal system, namely horizontal ground heat exchangers, is extremely relevant. Indeed they exploit portions of the subsurface with limited relevance on typical vertical systems like borehole heat exchangers, geothermal piles or open loop wells. On the contrary, these systems require a wide area extension which is in contrast with land scarcity issues mentioned above.
In this chapter the concept and the realization of a very shallow geothermal system that exploits the earth-contact area of the buildings was presented. The system, called *GeothermSkin*, allows to employ the geothermal energy avoiding the high initial costs related to excavation and drilling needed in classic geothermal systems. This system is conceived as an external application of modular heat exchangers. These modules can be applied on the underground walls of buildings and interest extremely limited depths, thus having the potential to not interfere with deeper systems.
The realization of a prototype system made up of three modules of various configuration reaching 4.6 m depth, allowed to test the thermal performance of the system. The impact on the structure and the surrounding ground in terms of stresses, strains, temperatures and water content was studied as well. The extensive monitoring system installed allowed to collect numerous data during the experimental campaign which is still running at the time of writing. Although some interesting conclusion can already be done, experimental campaign investigated mainly the heating mode behaviour of the system. Hence further experiments will specifically address the cooling mode behaviour for the sake of complete characterization. Moreover deep comprehension of heat transport in partially saturated ground will derive from numerical modelling and from the back analysis of the future as well as already performed tests.
A total of 8 tests were driven, out of which 6 in heating operative mode. As regards the heating operations, it resulted that the system can continuously produce up to 24 W per equipped unit area, in good agreement with expectation from similar systems known in literature. This heat exchange rate is equivalent to the considerable mean thermal power of 0.25 kW per module according to its 11.5 m^2 extension. Sequential rather than parallel module linking was showed to weakly influence the thermal performances. A concentration of heat exchange in the first part of the heat exchanger resulted in slightly higher potential for the latter kind of module linking. On the contrary the temperature at which the heat is delivered to the user is demonstrated to affect thermal performance and the intermittent heat pump starts. Although higher exchange rate can be obtained by rise of supply temperature, the more frequent activation may induce premature wear of the heat pump.
On the basis of thermal performances, the system is expected to provide a valuable contribution to the fulfilment of clean energy production from new and refurbished buildings. Furthermore the system may be used in combination with other renewable energy sources (as the solar thermal panels) to make the housing completely self-sustaining. This results may be better achieved by supplying the electricity used by the system

from renewable energy (e.g. photovoltaic panels, micro-wind power generators, etc.).
The extensive monitoring plan allowed to identify the extremely low thermal plume genesis both in term of magnitude and extension. Indeed thermal alteration resulted to be extremely reduced even in the cooling season when the gradient between carrier fluid and ground is much wider than in heating season. Also strains on the equipped walls surface were found to be limited below 20 $\mu\epsilon$. It was moreover detected virtually no affection on hygrometer values and on stresses at wall-ground contact.
The preliminary experimental results suggest that this very shallow geothermal system allow to obtain a satisfying amount of energy virtually not affecting the geothermal potential of deeper systems. Although real full-scale applications should better confirm this evidence, the thermal status of the ground except for the very few meters from the system seems not to be noticeably altered.
In this perspective the system may be adopted as a supplementary energy supplier beyond deeper installations as Borehole Heat Exchangers, open loop wells, energy piles and tunnels, virtually with a parallel exploitation. This kind of energy system may indeed play a role in the optimisation of the geothermal resources use, allowing to efficiently mine the heat at very shallow depths even in densely inhabited areas.

Chapter 6

Application of the rOGER methodology to the study area

6.1 Introduction

Urban areas attract the major part of human activities all around the world. In Italy they concentrate the major part of national population covering only 17% of the country extension (CENSIS, 2008). As a result of the related high transportation and housing demand, urban areas are also the most prone to environmental pollution. In particular the poor air quality is increasingly being regarded as a major question being responsible each year for over 400 thousands premature deaths in Europe (European Environment Agency, 2019). This issue is particularly serious in northern Italian cities lying on the Po valley due to the particular territory conformation hampering the dispersion of pollutants.
Main local response to this problem has been represented by vehicular traffic restrictions so far. Nonetheless, more than half of the primary energy supply in Europe is related to building sector. Hence main attention should be devoted to the heating and cooling of the buildings and structures. In this perspective, geothermal energy may play a key role. Its rational use should be implemented to maximise its impact on the energy supply mix. Indeed shallow geothermal is a distributed and efficient energy source, especially in areas with thick aquifers like the Po valley.
In previous chapters the rOGER method and a novel energy wall system have been presented as pieces of an energy strategy to optimise the utilization of shallow and very shallow geothermal energy. In this chapter it will be given substance to the methodology theoretically described in Chapter 4 by its application to a study area in Turin, Italy. Once the study area is defined, the different sections will focus on the four main steps of the procedure, namely *Database management, Real thermal condition assessment, Potential assessment* and *Impact on energy balance.*

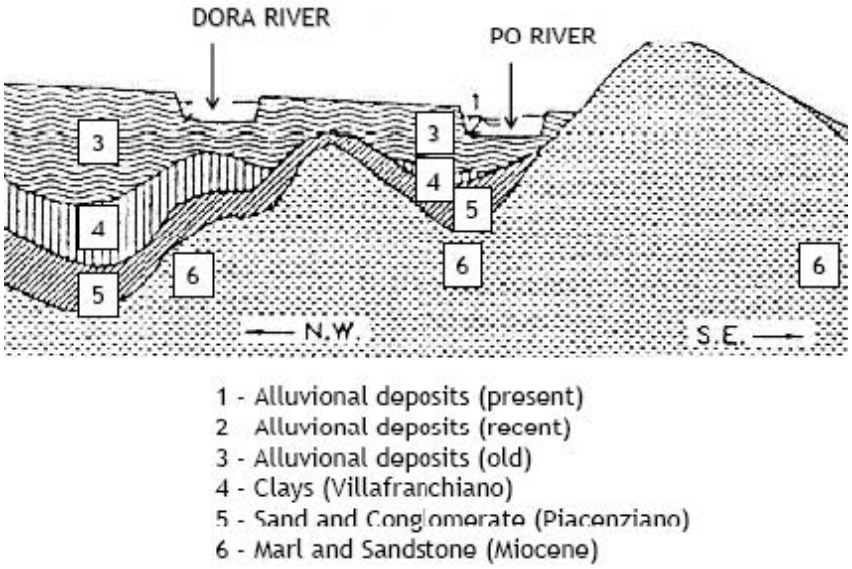

Figure 6.1: Geological section of the subsurface of Turin (Bottino and Civita, 1986).

6.2 Description of the site

For the sake of demonstrating the applicability of the *rOGER* method described in Chapter 4, the central districts of the City of Turin have been selected. The city has been experiencing extreme interest in shallow geothermal energy (Barla et al., 2015; Lo Russo and Civita, 2009; Lo Russo et al., 2011). Thanks to the presence of a very productive shallow aquifer, an exponential growth in the number of open loop systems was documented (Barla et al., 2018).
The Turin metropolitan area lies on the narrow portion of the western Po plain, northwestern Italy, and extends over 130 km^2. The central districts of the city are located on a level area enclosed by the rivers Stura di Lanzo, Sangone and Po. This latter surface water body acts as the main discharge axis and separates the plain sector from an hilly area made up of Pleistocene marls and sandstones representing the low reliefs of Monferrato.
The geological setting of the plain area is rather well known thanks to numerous boreholes drilling and to the experience gained with multiple deep foundations and urban tunnel projects (Barla and Barla, 2005, 2012). The major part of the city is located on the lowest portion of the Dora Riparia river alluvium fan. Altitude of the urban area is comprised between 270 m a.s.l. and 220 m a.s.l. (Bottino and Civita, 1986). Important heterogeneity has been documented as a result of the geological origin of the shallowest strata in the area. Figure 6.1 shows the stratigraphic sequence that is made up of:

- Coarse fluvio-glacial and fluvial deposits mainly constituted by pebbles, gravel and sand in a sandy-silty matrix; this horizon represent the upper 25-50 m of Turin subsoil. Horizon thickness decreases moving from southern to northern

part of the urban area. Its heterogeneity is accentuate due to highly variable degree of cementation. Cemented portions are distributed randomly and originate lenses with the characteristics of conglomerate rock (also known with the term *Puddinga*).

- *Villafranchiano* formation: a succession of lacustrine and fluvial-lacustrine deposits represented by clays and silts locally including gravel lenses whose origin is the Upper Pliocene - Lower Pleistocene.
- Ancient terrigenous succession of marine clayey and fossiliferous sand deposits originated in the Eocene - Middle Pliocene.

Cementation in the fluvial-glacial deposits is mainly related to calcareous deposition processes due to water mixing from different origins. However cementation was also observed above the water table and can be related to rainfall water seepage. Its random distribution originates a vertical and horizontal variability of the characteristics of the soil. This refers also to the hydraulic conductivity and the soil thermal properties. Due to the discontinuous pattern of cementation within the subsoil (Camusso, 2008) a precise mapping of cemented areas cannot be carried out. Nonetheless, the frequency of cementated layers can be inferred by analysis of borehole continuous samplings. By doing this cementation classes can be identified and their spatial distribution is reported in Figure 6.2. Cementation was documented to be predominantly distributed along horizontal lenses with decimetric to metric thickness.
The shallower geotechnical unit hosts a very productive aquifer whose thickness ranges from 15 to 30 m and is under lied by the thick *Villafranchiano* clayey aquiclude. Main direction of groundwater flow is from North-West to South-East where the Po river is located and acts as drainage for the plain area.
The geothermal and industrial use of water is of extreme importance in the metropolitan area of Turin due to the easy access (maximum depth to the water table approximately 20-25 m). In the last decades, due to the reduction in water abstraction for industrial purposes, the water table was found to basically rise over time (Barla and Vai, 1999). Nonetheless there are evidences suggesting that the equilibrium has already been reached.
In the next paragraphs, the geological and hydrogeological settings will be used to properly handle site information within the geodatabase used in the *rOGER* procedure. Settings will also be used to derive the parameters adopted in the geothermal potential definition.

6.3 Creation and management of the georeferred database

Careful definition of the geothermal potential at the metric to decametric scale has to be carried out to achieve the optimal management of shallow geothermal resources.

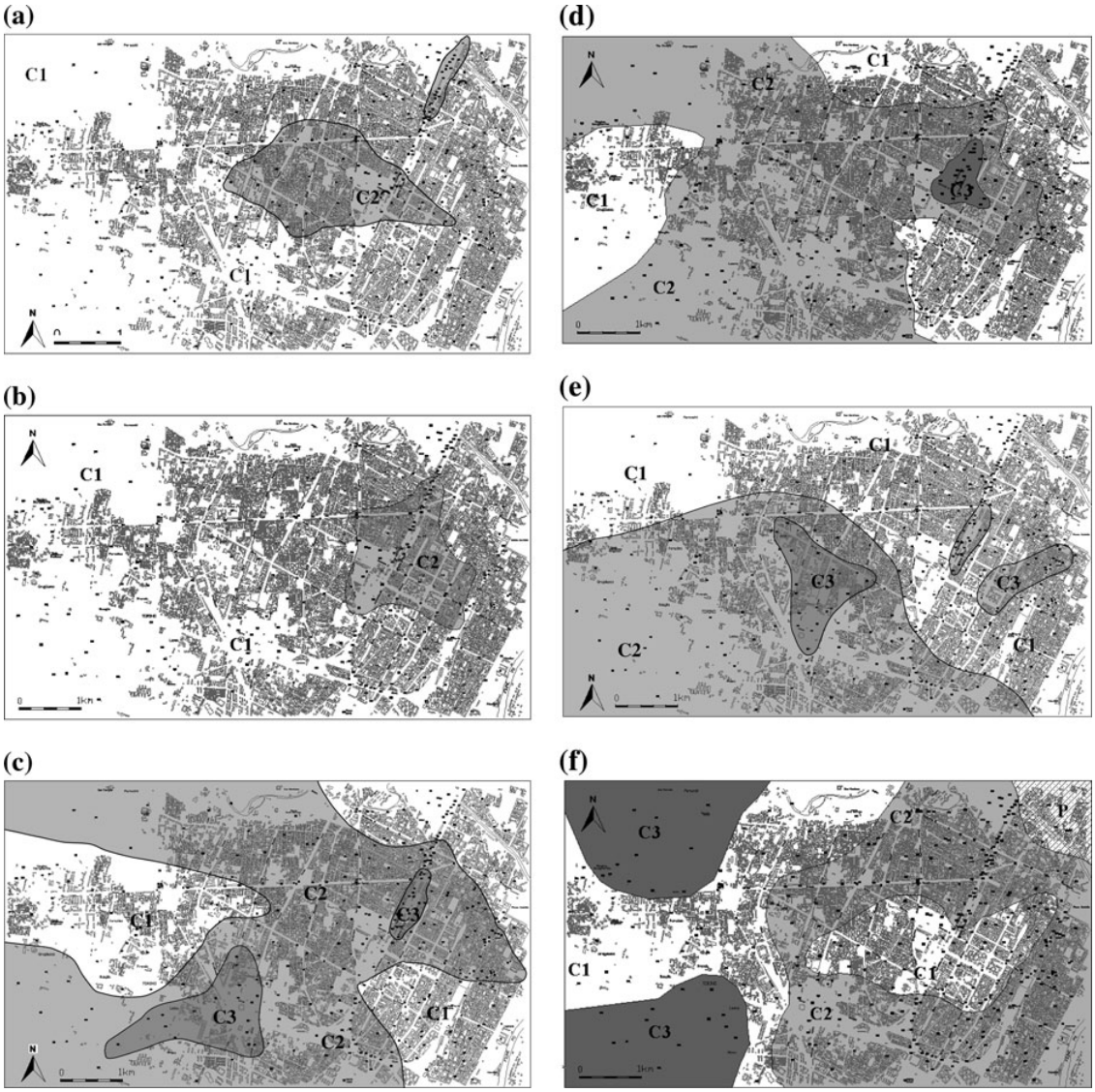

Figure 6.2: Degree of cementation distribution within the fluvio glacial deposits in the Turin subsoil at a depth of (a) 5 m from the ground level; (b) 10 m; (c) 15 m; (d) 20 m; (e) 25 m; (f) 30 m. From the study of de Rienzo and Oreste (2011).

The GIS is the most suitable tool to handle this operation as geothermal potential is dependent on site conditions. In Chapter 4 main attention was devoted to the *structure* of the GIS. In this section the application of this structure is described with reference to the metropolitan area of Turin. The specific dataset available in the metropolitan area of Turin are described. Geoprocessing procedures adopted to obtain the proper attributes are detailed as well. Due to the robust and various geoprocessing options the commercial GIS package ArcGIS 10.6 was employed in this study to handle the several dataset involved for modelling.

6.3.1 Definition of the domain of interest

The definition of the domain to be studied has to be carried out as the first step of the *rOGER* procedure. This process is iterative as the studied domain has to fulfil requirements that are related to numerical analyses.
The area of interest can be preliminarly defined on the basis of administrative boundaries (e.g. municipal boundaries, district boundaries, etc.). In the case of the here presented case study, the municipal boundaries were considered at first. Due to the preliminary and illustrative nature of the application, particular interest was devoted to the central districts where there is a significant density of geothermal open loop systems (Barla et al., 2018).
The definition of the domain of interest however has to cope with the needs of numerical modelling. The domain was sufficiently enlarged to allow proper boundary conditions without definition that did not excessively force the thermal and hydraulic solution in the area of interest. In this perspective an hydraulic conceptual model has to be defined in order to delineate the boundaries of a Ground Water Body (GWB).
The study area is included in the *Pianura Torinese Sud* GWB (literally Southern Turin plain) identified by the Environmental Protection Regional Agency of Piemonte (Vanzetti, 2015). The GWB covers over 278 km^2. Hence areas external to the City of Turin are comprised. To the sake of computational effort limitation, a portion of the GWB was delineated. The piezometric monitoring network (ARPA Piemonte, 2015) and the mean piezometric surface of the area (Civita and Pizzo, 2001) were considered to perform this operation. An area of about 25.7 km^2 was thus delimited as shown in Figure 6.3.
The boundaries were chosen according to an isopiezometric line to the Po riverbed on the west and east borders respectively. On the contrary the north and the south boundaries were chosen perpendicular to the expected groundwater flux near to the location of some piezometers.
According to the rOGER requirements, proper elevation limits need to be defined. In this study the depth of 100 meters below the ground surface was selected as representative for BHE installation. In general, at least an additional 20% depth should be studied should be modelled. In this particular case, however, the Villafranchiano formation and the aquiclude were roughly modelled as an homogeneous layer. Hence the hydraulic and temperature distribution at the bottom of the domain were constrained even in the case the domain was further extended. The isolated domain thus allowed to optimise the computational effort. Furthermore a finer representation of the main object of the study, namely the shallow aquifer unit was possible under the same computational effort.

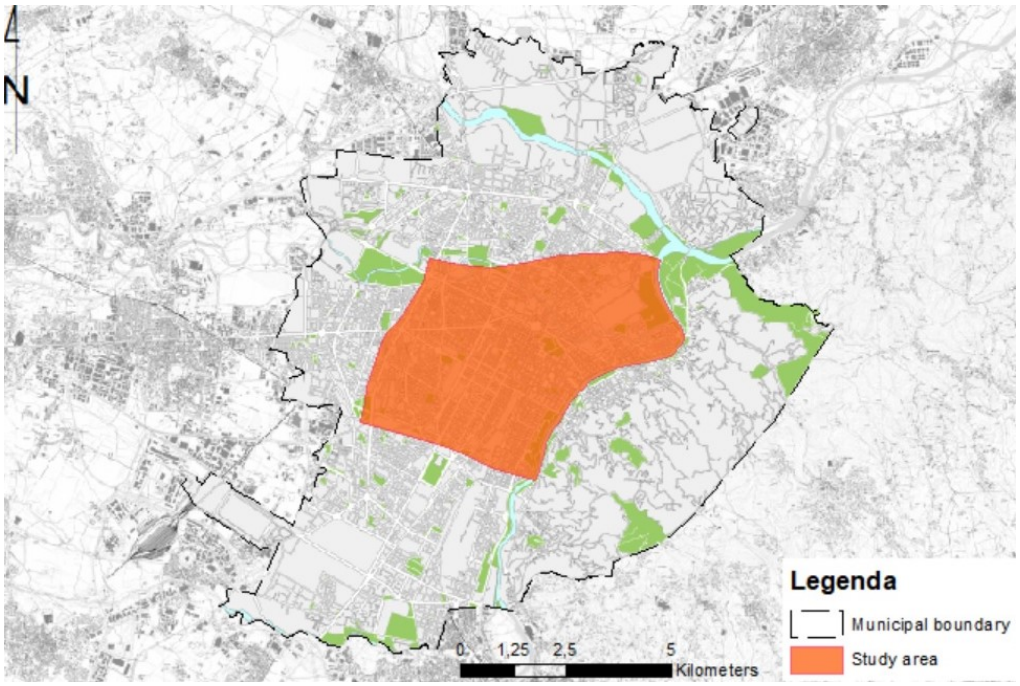

Figure 6.3: Selected area for geothermal potential assessment within the City of Turin (administrative boundaries of the municipality are shown with dashed line).

6.3.2 Hydrogeological conceptual model

The study area is comprised in the final section of the Dora Riparia alluvium fan. The stratigraphy is characterised by a first geological unit mainly composed by heterogeneous gravels with local and randomly distributed cemented layers and hosts an unconfined aquifer. For the sake of complete geometrical definition of this shallow aquifer unit, the Digital Terrain Model (DTM) of the area and the bottom of the geological unit were included in the database.

For the sake of obtaining the digital terrain model of the area, data from the *Base Dati Territoriale di Riferimento degli Enti* (BDTRE), namely the Territorial reference dataset for public administration of Piemonte Region (version 2018) were considered. The spot elevation points referred to the street level and included within a buffer of 250 m from the domain were selected to this end. The raster Digital Elevation Model of the urban area was not employed as it was originated from remote sensing namely reconstructing a Digital Surface Model. Due to the lack of filtering of the buildings and constructions presence, this DEM was far from being perfect. Based on the relatively smooth topography of the area, the above mentioned points were used to generate a raster with 20 m resolution. It should be noted that this raster was in turn converted to point feature dataset (one point for each cell centroid) to allow interoperability with the numerical modelling software.

A raster dataset was obtained for the bottom of the aquifer unit. The contour lines

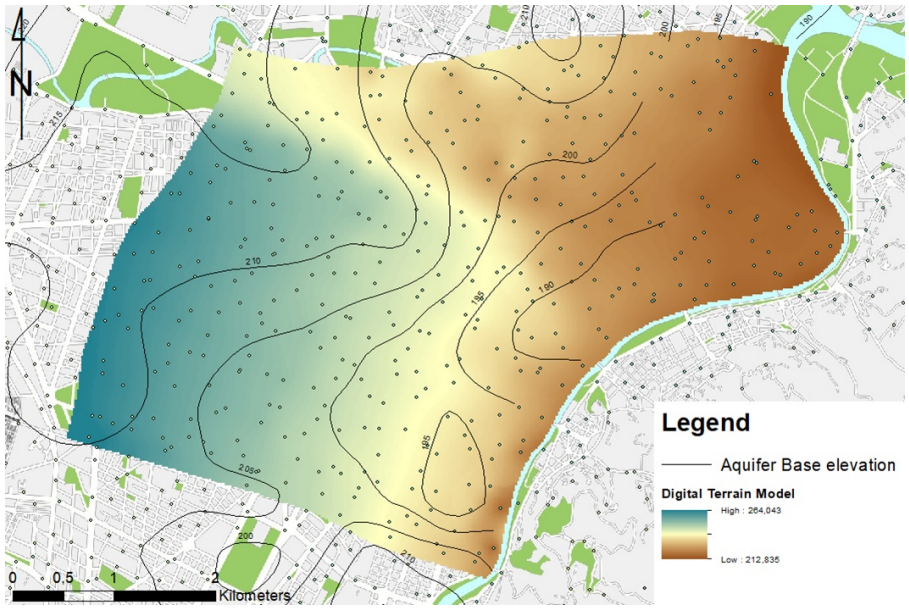

Figure 6.4: Digital Terrain Model (Color ramp) and Shallow aquifer base (contour lines) in the domain of interest. The original spot elevation points are also depicted.

of the *Geoportale Piemonte* were employed from the official cartography (Environment bureau of the Piemonte region, 21/04/2016). The raster was then converted to a point-feature shapefile dataset as it was done with the DTM. Both the DTM and the base of the shallow aquifer are shown in Figure 6.4.
The heterogeneous characteristics of the shallowest geological unit have been widely discussed in previous sections. The random distribution of cementation degree cannot be described in a deterministic way both from the epistemical point of view (cemented levels are known just by borehole data and from underground open face excavations, e.g. the railway link urban tunnel) and from the computational effort one. The intrinsic heterogeneity at the micro- and meso-scale has to be handled with an equivalent homogeneous approach. This heterogeneity was properly taken into account at the district macro scale by the definition of zones where the cementation degree statistically occurs between 0-25%, 25-50% and 50-75% (de Rienzo and Oreste, 2011). The maps shown in Figure 6.2 were at first georeferred and later digitized as distinct polygon features in an appropriate shape file. Unfortunately these maps do not cover the entire domain area. The definition of remaining areas was hence guessed on the basis of adjacent areas and based on the depth of the aquifer base. While an organic processing of borehole drilling following the criteria of de Rienzo and Oreste (2011) on the whole study area would allow a better definition of the areas, this was beyond the scope of application of *rOGER* procedure in this study. The use of these polygons and the data extrapolation will be further described in the section devoted to the description of numerical set up. The data mentioned up to this point are constituted the stratigraphy information in the *rOGER*

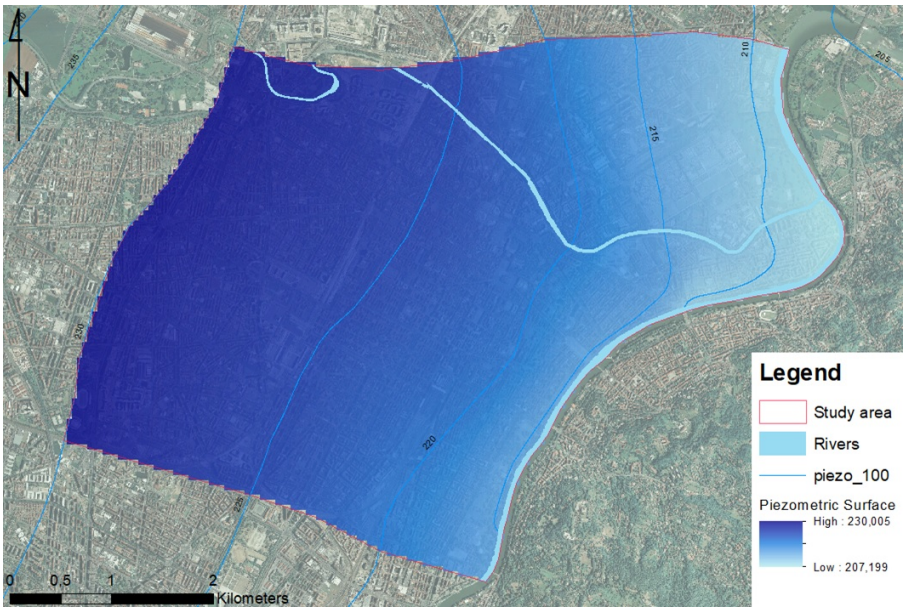

Figure 6.5: Mean piezometric height and surface water bodies in the study area.

method as conceived in Section 4.2.2.
In addition to stratigraphy, surface water bodies comprised in the study area were included as a dedicated polygon feature shape file. Accurately clip to the domain area extension was performed (see Figure 6.5). The dataset is populated by the riverbeds of the Dora Riparia and Po rivers. Connection of the latter with the groundwater has been previously described. On the contrary, infiltration and exfiltration from the Dora Riparia is known to be extremely limited because of the extensive artificial embankments. Indeed impermeable cover characterise almost the whole Dora riverbed within the urbanized area. Further evidence of the negligible connection is given by hydraulic numerical model calibration that will be discussed in following sections. Nonetheless, the fluvial area of the Dora Riparia was included to have further evidence from of the exchange rate from numerical calibration.
Due to the peculiar conditions of Turin subsurface the main focus was put on the shallow aquifer that is particularly productive. The mean piezometric surface from Civita and Pizzo (2001) was obtained as a raster dataset (shown in Figure 6.5) from the available contour lines. In order to provide a consistent hydraulic initial condition for the numerical modelling phase of the *rOGER* procedure. On the contrary, the dynamics of the water table is afterwards derived from numerical models as a result from thermo-hydro simulations.
A crucial role is played by the environmental monitoring network in the application of the *rOGER* method to the study area. On the one hand it allows to calibrate numerical analyses and to verify numerical results accuracy. On the other hand the data from

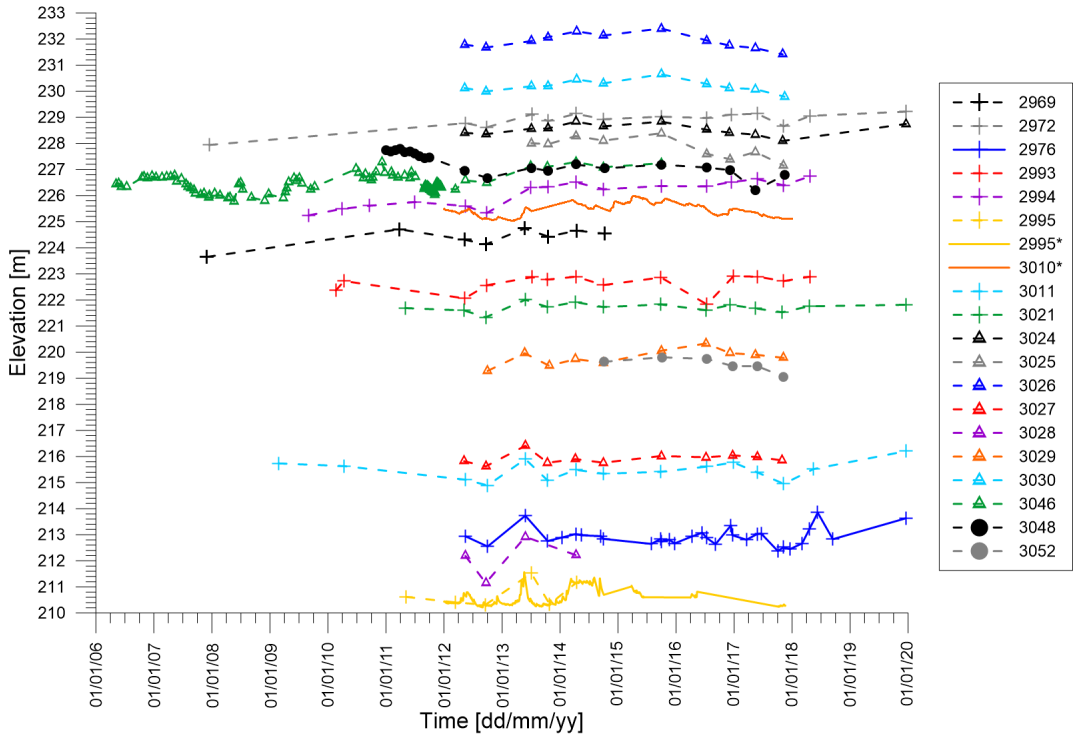

Figure 6.6: Groundwater elevation at piezometric monitoring network points within the study domain.

the monitoring network are essential for the definition of boundary and initial conditions. The 19 piezometers included in the studied area were extracted from the publicly available point-feature shape file of the metropolitan authority monitoring network. All the measurement points of the network are represented by open tube piezometers that in most cases are periodically (twice a year) surveyed. The primary key of these features allows the unambiguous identification used to associate historical data about water table depth with the location. Indeed, external spreadsheets were used to collect and organize the measured data that cover a time scale from 2003 to 2019 (see Figure 6.6).

It should be mentioned that the time period covered by the data from local authorities is to some extent heterogeneous. In most cases the measurement frequency is equal to about six months and does not allow for dynamic variation understanding. In only two points, piezometers *2995* and *3010*, measures were taken continuously. Furthermore most part of the piezometers reference elevation is known with low precision and has thus consequences on the accuracy of the water table elevation measusement. Indeed this latter quantity is usually measured as depth from the surface. Because of this, a specific measurement campaign was conducted in December 2019. A bunch of points were measured in the study area and in its proximity. The scopes of the measurement were the better quantification of the elevation and of the temperature of groundwater

Figure 6.7: Surface water bodies environmental monitoring.

near the borders of the domain of interest. Beyond the depth of the water table, the absolute height of about half of the above mentioned points was measured by means of a GNSS antenna. Nearest base Real Time Kinematic (RTK) correction was used to precisely determine the elevation of the point. In order to better filter the error of geoid offset correction, the elevation of neighbouring altimetric reference points (when available within a distance of less than 200 m) was measured as well.
The temperature of the air within the piezometer tube and of the water at different depths was monitored. A water level meter equipped with a thermocouple (0.1°C precision, 0.1% accuracy) was employed to this end. Groundwater temperature was investigated at different levels down to each piezometer bottom. Denser interval of measure was adopted in proximity to the water table to properly capture possible thermal stratification. The data collected in the measurement campaign are reported in Appendix B.
Also the surface water bodies crossing the study area are monitored as well. The municipality of Turin is provided with a network of water gauges along the main rivers (see Figure 6.7). The measures pertaining to these points are shown in Figure 6.8. In addition to the water gauges managed by municipality, one more location managed by the regional authority was taken into account in this study. At this latter location the temperature and other quality-related parameters are measured. These are hence used in the hydrothermal modelling phase of the *rOGER* procedure. Analogous measurement is carried out at the lowest section of the Dora river directly upstream to the confluence with the Po river. Both the river temperatures are shown in Figure 6.8 together with

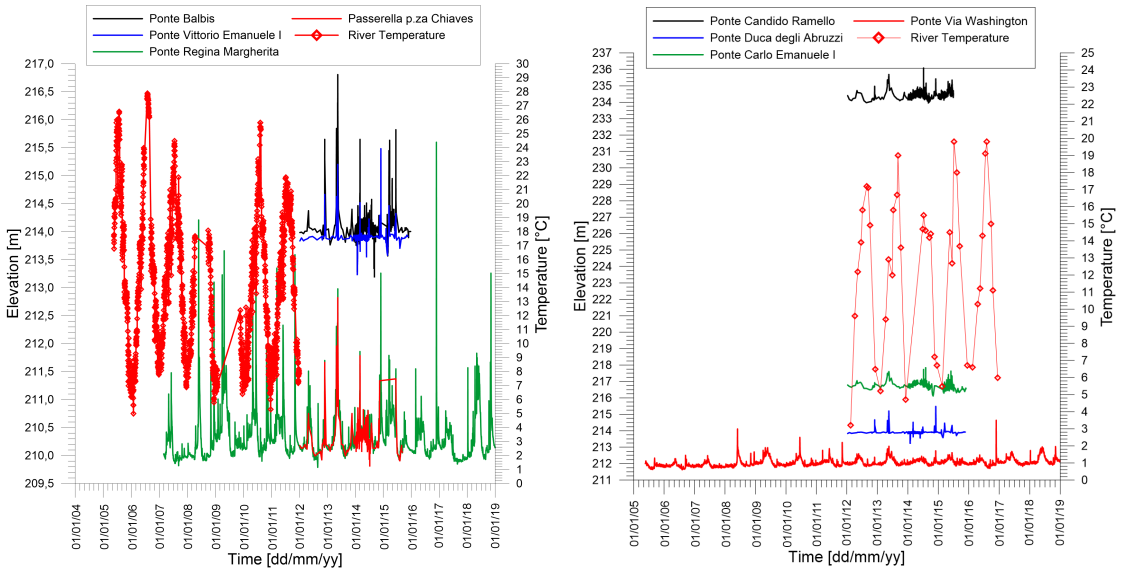

(a) (b)

Figure 6.8: Measures from water gauges along the Po and the Dora Riparia rivers.

the water level absolute elevations.
Other piezometers are usually installed to track hydraulic and thermal affection related to geothermal open loop system. In the metropolitan area of Turin the realization of such environmental monitoring is requested without exception by local public authority as part of the authorisation requirements. For the sake of simplicity such data are treated in the following section that is devoted to open loop systems and to the other entities hydraulically and/or thermally affecting the subsurface.

6.3.3 Entities producing thermal and hydraulic impact

In Chapter 4 entities which are able to affect hydraulically and/or thermally the subsurface have been divided into active and passive users. The latter class comprises the anthropic structures whose main aim is different from the exploitation of subsurface resources. On the contrary the first class of entities aim at the use of the heat from either the groundwater or the ground. The water wells and the Borehole heat exchanger have been indicated as the most important typologies among active uses.
Unfortunately in the City of Turin it does not exist any repository about closed loop installations. Nevertheless the impact of such installation can be reasonably considered negligible in the study area. Indeed the presence of a shallow and productive aquifer likely drove the geothermal resources market. Furthermore the built heritage covers the most part of the metropolitan area and legislation hampers drilling in public areas. This results in a predominance of open loop solutions in the study area. A dedicated

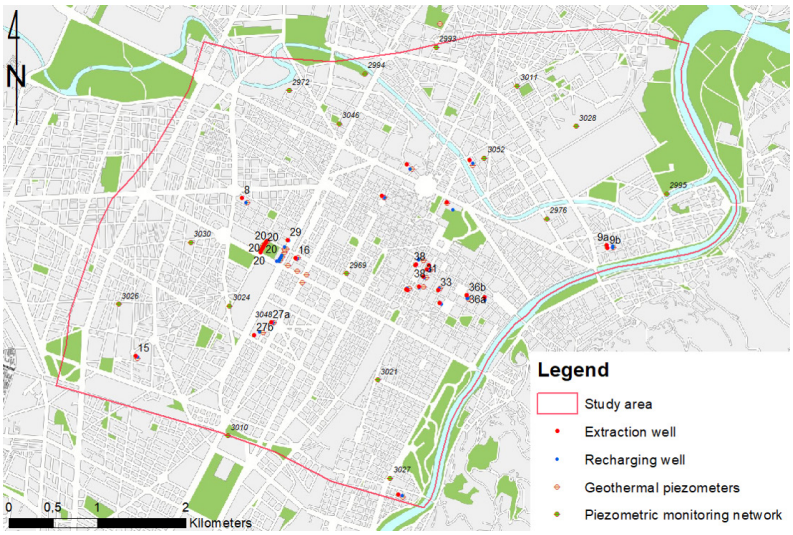

Figure 6.9: Location of geothermal wells and relative monitoring points in the study area. Features not labelled refer to installation that are still not active. The piezometers of the metropolitan monitoring network are shown as well.

survey into public archives and specialized companies may allow for partial identification of BHE, this aim was beyond the scope of this study as the BHE thermal affection involves small areas. To this end the establishment of BHE regional inventory would give an extremely relevant contribution. Although it has been set by law, it is still not running at the date of writing.
Open loop systems are rather common in the urban area of Turin, according to Barla et al. (2018). In this study a total of 12 open loop system installations were included as are known to be active at the date of writing. Although the number of systems authorised is slightly higher, they are located mainly near the downstream boundary of the domain or have just been recently authorised or activated. In these latter cases no data are available in relation to groundwater use. This made impossible to reliably model their impact. Nonetheless the main installations in the study area have been accurately modelled in terms of location and screened depths (see Figure 6.9). A total of 25 extraction wells and 24 injection well were characterised in terms of flow rates during operations until 2018. It should be noted that due to the different authorisation prescriptions data from monitoring systems are heterogeneous. Indeed extracted and injected groundwater volumes as well as their temperatures should be collected by the local authorities. However the frequency and detail of measurement has been progressively changed and improved in recent years. In a minor part of cases, the data are available only on annual rather than monthly basis. In few cases the indirect access to data and the failure to report by some of the installation owners resulted in partial loss of data. On the contrary, the data quality was more than satisfying in various cases as it is shown in Figure 6.10 by extremely small interval between two subsequent measures.

Due to environmental reasons, the water volumes extracted from the subsurface were injected back into the subsurface through injection wells without exception. At these locations it is crucial to know the temperature of injected water to accurately assess the subsurface thermal affection. Data about injected water temperatures were carefully collected and are shown in Figure 6.10. Considerations about data heterogeneity and exhaustiveness are analogous to what was previously discussed for water volumes data. In a few cases also the extracted water temperature was monitored. In these cases these information were later used for numerical calibration and verification.
The most part of the geothermal installations is equipped with at least a piezometer located downstream respect to the injection wells, due to requirements set by local authorities. At these locations the water table depth and the aquifer punctual temperature is in most cases measured.
All the above mentioned data were accurately collected and treated populating the environmental monitoring theme described in the *rOGER* method. On some occasions flow rates, groundwater depth and temperatures were available only in non-editable version. Thus the data were grabbed from the archived tables and graphs. In this latter case the values suffer from an higher uncertainty degree. Nonetheless the time-value pairs are considered exact at least in the order of magnitude. Each of these time hystories was then accurately copied and analysed in separate spreadsheet identified with the same unique identifiers shown in Figure 6.9. This option was selected for ease of use and updating. However the time-value pairs could also have been stored together with the unique identifier information in internal tables of the geographic database to be joined with the adequate point-feature dataset.
Among non thermal users of the aquifer, the domestic and industrial water wells were not considered. Due to the illustrative aim of the application of the rOGER method to the study area an extensive survey about non thermal groundwater uses from shallow aquifer was beyond the scope of this study. Nonetheless the effect of water exchanges is partly compensated by obtaining the correspondence of the mean water table elevation with measured values that are affected by such uses. A satisfactory replica of the water table elevation can be considered acceptable at the scale of the study.
All the above mentioned aspects were related to active uses of the aquifer. However in the *rOGER* procedure also passive aquifer users have to be considered. Two main underground infrastructures were considered in the domain area: the railway link urban tunnel and the metro line 1. A second metro line is at preliminary design stage at the date of writing and can represent an interesting opportunity for large scale application of energy geostructures (Barla et al., 2019b).
Railway track was derived from the open data repository BDTRE by querying the dataset with the tunnel section typology (see Figure 6.11). A total tunnel length of 6.3 km resulted to be included within the domain. The tunnel was constructed by cut and cover technique and presents a single or multiple box-shape structure. Diaphragm walls are driven at higher depths respect to the rail level. For the sake of simplicity a constant transverse cross section was considered along the whole tunnel length.

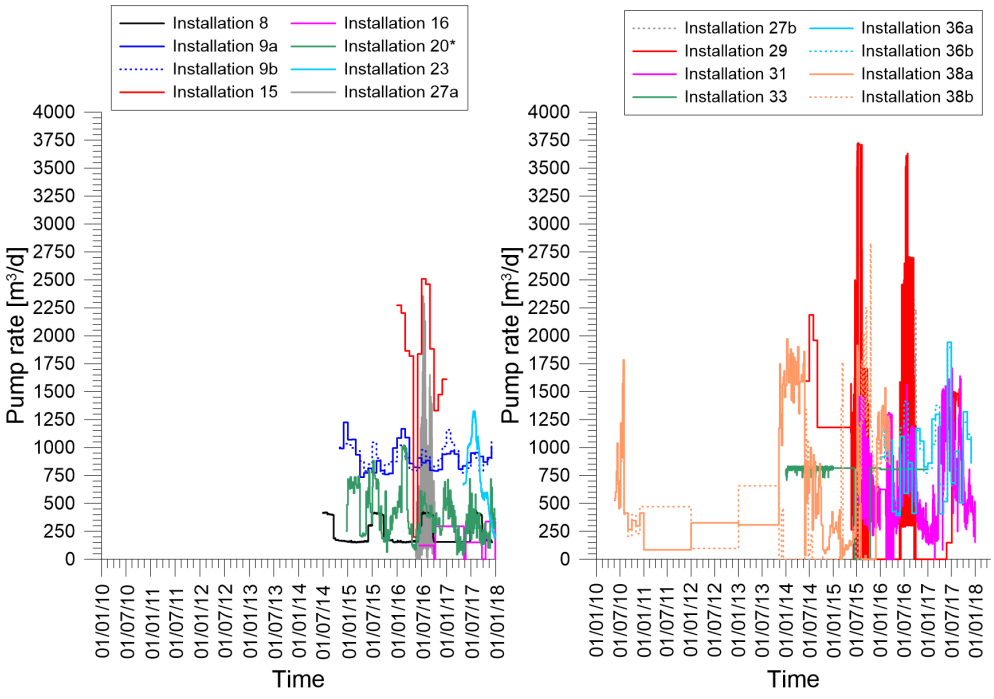

(a)

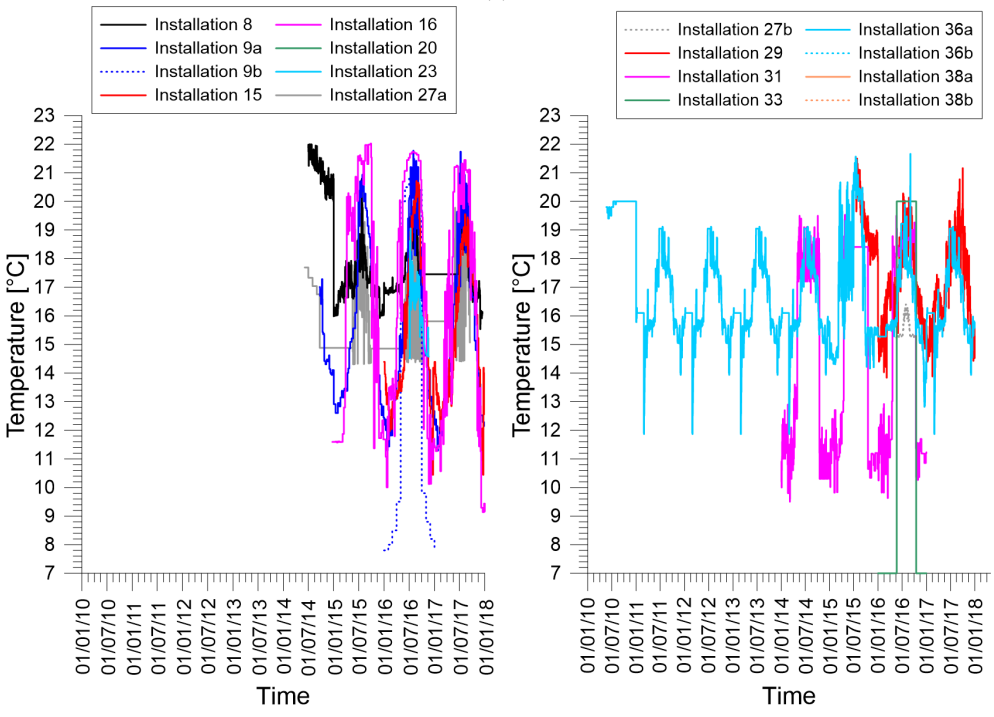

(b)

Figure 6.10: (a) Flow rates monitored at geothermal installation in study area. (b) Temperature of injected water into the subsurface as monitored during installations operation. Please note that volumes of Installation 20 have been divided by a factor of ten for the convenience of the reader.

The transverse cross section was simplified to a rectangular shape down to the maximum depth of the diaphragm walls. Indeed groundwater flow is expected to be negligible in the inner portion of soil surrounded by wall due to the perpendicularity of the track respect to the groundwater direction. The depth reached by diaphragm wall was assumed equal to 20 m, according to Barla et al. (2013b). A constant width of 25 meters was considered in order to account for the presence of multiple parallel tracks and of the Porta Susa station.
With respect to metro line 1 tunnel, the axis runs almost parallel to E-W direction starting from the West border of the domain up to the Porta Susa and the Porta Nuova districts. From Porta Nuova it deviates in ENE-WSW direction, mainly perpendicular to the groudwater flow, up to the southern border of the domain (see Figure 6.11). It was possible to accurately recreate the axis tridimensional location and its depth variations from the as built project documents. Indeed the metro tunnel cover varies significantly along the track. In particular it passes under the railway tunnel near Porta Susa station. For the sake of simplicity the 12 stations included within the domain were neglected and the tunnel transverse cross section was kept constant along the track. The real 6.88 m diameter was taken into account (Barla et al., 2019). This high geometrical detail will be then used in partial remeshing of the numerical model and will be further described in the following section.
Since accurate information about underground utilities (e.g. sewage network and district heating pipelines) was not available, pipelines were not included in the model. Although in other cities (Benz et al., 2015) it was demonstrated that they can deliver significant heat fluxes to the subsoil, district heating serves just a limited section of the area under investigation, mainly at the outer portions of the model. Thus, underestimation of possible heat losses from the network is expected to be limited.
In the *rOGER* procedure buildings basements and car parks are included in the underground structures theme. The exact footprint of public underground car parks was obtained directly from the Turin municipality transportation department in the form of project documents. The plans of each structure were carefully georeferred within the geographic database and the footprint was subsequently recreated in the form of polygon features. A consistency check on the floor area was also carried out in order to substantially preserve the overall contact ground contact area. The depth of each entity was precisely obtained from project documents except for two cases (the *Bodoni* and *Stati Uniti* car parks). In these cases the depth reached was assumed from the number of levels and considering an height of 3 m for each level. 25 structures were found within the study area. It should be noted that private car parks were not considered in this study due to lack of precise data. However the most part of private car parks are comprised within the footprint of the building they serve. Hence most of them are included when considering the basement level of the buildings.
As regards buildings underground levels, no precise information is available for Turin

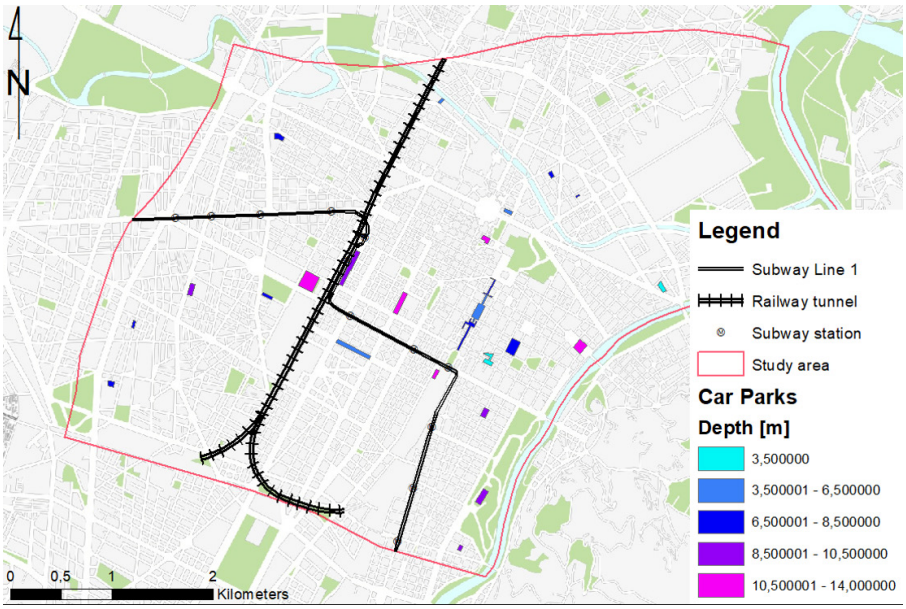

Figure 6.11: Aquifer passive users: Infrastructures and main public underground car parks in the study domain.

municipality. Hence the depth and geometry was derived from the aboveground structure information. For the sake of simplicity, the way these data were treated is described in the following section pertaining to the built environment theme of the *rOGER* database.

6.3.4 Built environment

Urban areas settings are tremendously influenced by the built heritage both above and below the ground surface. Chapter 4 focused mainly on the quantification of the heating/cooling demand related to this class of features. In the application of the *rOGER* method to the study area in Turin, the built environment is however used for the definition of the anthropic interventions in the subsurface.
In some countries (e.g. Basel Canton in Switzerland) information on the underground buildings level can be derived from insurance policies. Unfortunately this is not the case in the urban area of Turin. No direct information is thus available about the maximum depth of buildings basements or the number of underground storeys. Thus the characteristics of the above-ground structures were used to infer the below-ground features. Furthermore the high number of small and articulated geometries of buildings cannot be handled with a reasonable computational effort in the numerical modelling phase of the *rOGER* procedure. In particular the meshing operation would result both in bad elements shape and an unworkable number of elements. To this end the datasets about the volumetric units, the single buildings and their aggregation by common construction

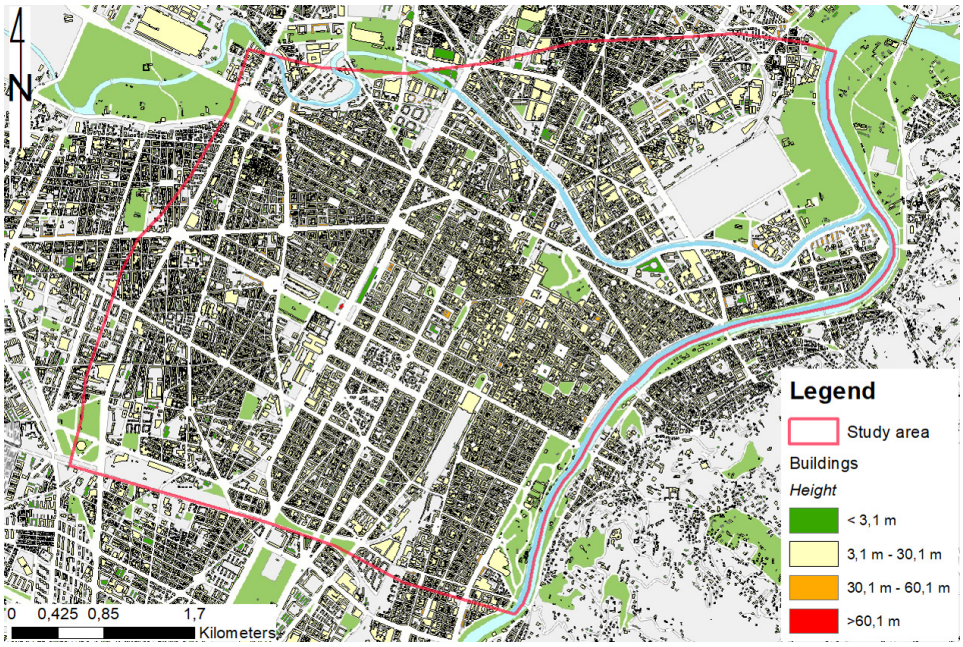

Figure 6.12: Polygon feature dataset regarding the built environment considered for the study area.

features (e.g. age, use and contiguity) were derived from the BDTRE database (Regione Piemonte and CSI Piemonte, 2016). Among the over 71000 polygon features within the municipality territory (Figure 6.12), 23153 were found within the domain of interest. At first the intended use was spatially joined to each volumetric unit through geoprocessing. By doing this, the height of each volumetric unit was associated with the intended use before the calculation of its volume. These volumes were then associated with the appropriate building aggregate. This operation allowed to reduce the polygons number by about a factor of 4 (6111 entities) and to calculate the global volume of each entity. Subsequently only the entities showing an area larger than 100 m^2 and an height larger than 3.1 m (a total of 4980 elements) were associated with the adequate block. Each block height was desumed from the median of the value of the buildings aggregates. Block area has been defined by subtraction from the municipality territory of the green areas (e.g. parks and gardens), built surface and their relative appurtenant areas. The geoprocessing operations however lead to some minor inconsistencies. The ratio of the built area over the total block area was calculated for each entity and adopted to identify low density areas that can be neglected in terms of heat demand.
Once the inconsistencies were solved, a total of 1681 entities were identified within the domain of interest. These entities were classified based on their height and on the inferred number of floors, according to Equation 4.2. Based on this classification, the number of underground levels was assumed as follows:

- 1 underground level if the block elevation storeys are less than 10 (tallness lower

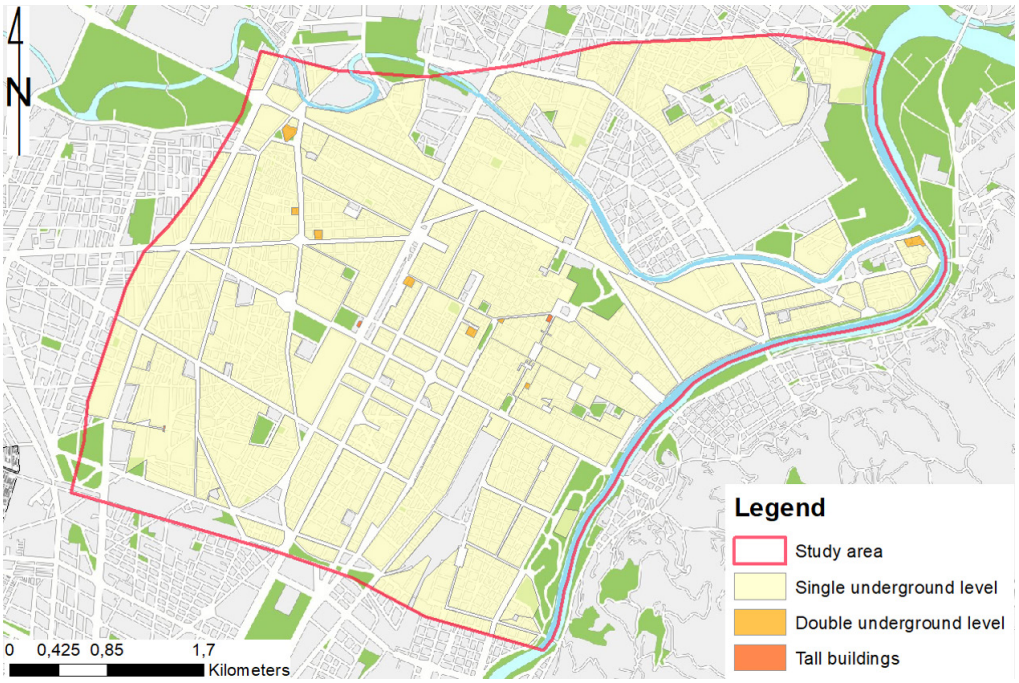

Figure 6.13: Geometries adopted for underground level recreation within the study area.

than 30 m);

- 2 underground levels if the block elevation storeys are comprised between 10 and 20 (tallness lower than 60 m);
- in depth analysis of relevant and particularly tall buildings (three within the study area taller than 60 m).

Since the number of entities to be included in the numerical model was still too large to handle, the entities with same classification were aggregated by neglecting separating distances shorter than 10 m (e.g. low traffic roads). Eventually small correction were made manually in order to rectify edges and reduce the number of vertices. Although these operation are to some extent affected by operator's sensitivity, complete automation cannot be pursued due to intrinsic accuracy of remote sensing input data and to alignment defects of the urban fabric. As a result of the geoprocessing operation a total of 153 entities recreating single basement level areas were identified, while 10 entities with a double basement level were detected. The above mentioned geometries (Figure 6.13) were hence used as part of the geometrical input for the numerical models described in the following section.

6.4 The numerical model of the study area

The assessment of real thermal conditions, namely the second step of the *rOGER* method is addressed in this section. The definition of the geothermal potential both at the site and at the territorial scale, is strictly linked with the thermal and hydraulic regime of the subsurface. The definition of the real thermal condition assessment is hence a crucial improvement in the quantification and localisation of the geothermal potential. According to the procedure proposed in Chapter 4, this action is pursued by means of proper numerical analyses. In the case of the application of the *rOGER* procedure to the central portion of Turin, a detailed numerical analysis was set up to the end of thermal and hydraulic regime assessment. These aspects were already studied in the area by Barla et al. (2018). In this study numerical set up is enhanced with higher level of detail to properly handle thermo-hydrogeological settings of the area. The numerical model is based on the informations hosted in the specifically designed geographic database described in previous section. In the following paragraphs the numerical setup and the results from numerical analyses are in depth analysed.
In the next section, results from numerical model will be used in the geothermal potential assessment phase of the *rOGER* method by means of the dedicated GIS and of the novel formula developed (Equation 4.12).

6.4.1 Model setup

The main interest regarding the shallow geothermal resources in Turin is represented by the unconfined aquifer where significant groundwater velocities have been reported (Barla et al., 2016). Further relevance of the aquifer is obtained in potential assessment in the basis of the modified G.POT. formula (Equation 4.12) that emphasises the advective contribution in the heat transport.
The commercial FEM code FEFLOW (Diersch, 2009) was adopted to cope with coupled TH transient conditions in three dimensions. Thanks to the interoperability features between the georeferred database and the numerical code, the values of the variables in the model are precisely georeferred.
At first the model domain was defined on the basis of the area of interest defined in Section 6.3.1. The proper geometries of underground structures and infrastructures were included in the model by incorporation of the appropriate polygon feature shape file. By doing this, the mesh generator was forced to comply with these geometrical constraints. The polygons representing the fluvial areas, the underground structures (namely the public parkings) and the buildings basement (see Section 6.3.4) were carefully adapted to *supermesh* constraints, solving the deficiencies related to polygons overlapping and inscription. In order to adequately refine the mesh density close to the urban tunnels, the pertaining line features were included in the model in addition to the 146 area subdivisions (see Figure 6.14). Finally the location of water wells was incorporated together with the relative piezometers. Piezometric monitoring network points were comprised

Figure 6.14: Mesh generation framework elements for the numerical model of the study area.

in the model as well.
The *Triangle* (Shewchuk, 1996) mesh generator was adopted to partition the model domain in 181283 element. The mesh density was gradually increased around the underground infrastructures and the point features. As regard the point features, mesh refinement around water wells was operated to properly capture the local behaviour and prevent numerical instability.
The *supermesh* polygons were used to assign a slightly different density of the elements within the fluvial areas and the deeper underground structures (parkings and high rise buildings). The bidimensional geometry was converted to a tridimensional domain, according to the definition of the volume of interest in Section 6.3.1. The upper surface of the model was obtained by application of the elevation from the Digital Terrain Model (see Section 6.3.2). Inverse Distance Weighted method (IDW) was adopted for node elevation interpolation. By doing this, basement levels of buildings are included within the model domain. The model bottom was defined with a fixed depth of 100 m from the model top surface. The domain volume above the aquitard was subdivided in eight layers. Those layers were intended to present an homogeneous thickness of 5 meters to allow for proper incorporation of cementation zones depicted in Figure 6.2. By the way, some elevation conflicts with the base of the aquifer were detected in some portions of the model. In those cases a minimum thickness of 0.5 m was enforced by moving the nodes of the aquifer volume. By doing this, the bottom elevation of the aquifer was easily identified by the analysis of the layer thickness. In these cases the appropriate thermal and hydraulic properties pertaining to the aquitard material can be assigned. Due to the highly uncertain location of the boundaries of cementation degree zones, the geometrical definition of such zones was neglected during the domain partitioning.

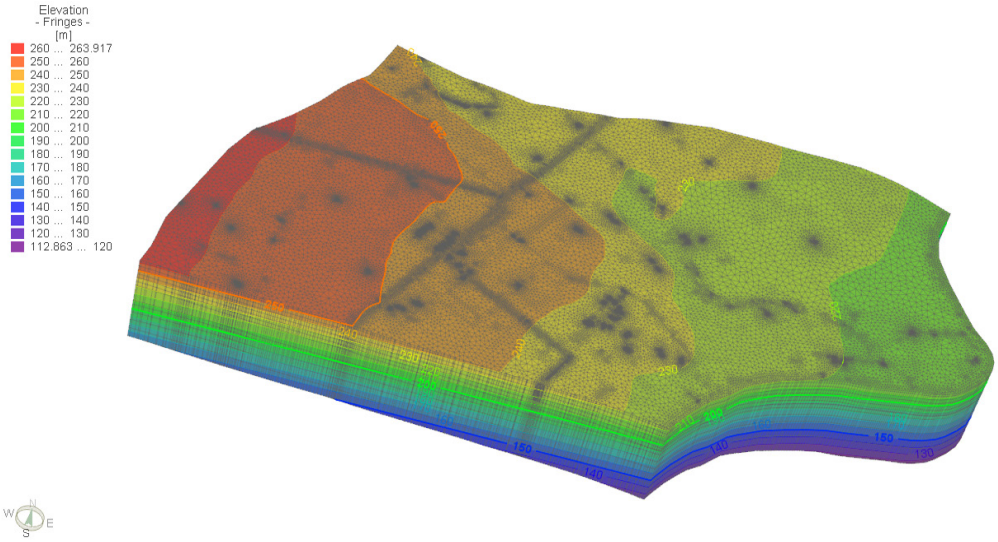

Figure 6.15: 3D numerical TH model of Turin central districts. The color ramp represents the nodes absolute elevation.

The volume below the base of the shallow aquifer was approximated as an homogeneous material. By the way, to the sake of numerical stability and proper handling of the interface, a proper vertical partitioning was selected. Layer thickness was carefully reduced in proximity to the aquifer interface. As a result, a total of 2356679 elements was obtained to model the $2.6 \cdot 10^9$ m^3 domain volume (see Figure 6.15).
Once the structured three-dimension domain partitioning was obtained, a partial mesh un-structuring was performed in order to accurately reproduce the highly variable depth of the Metro line 1. By doing this, it was possible to reconstruct the circular tunnel tridimensional geometry with affordable computational effort. The cylinder representing the underground infrastructure was modelled within the GoCAD software suite (Paradigm Ltd., George Town) and then appropriately meshed with three noded faces. The resulting geometry was later imported into the FEM model and used as input geometry for the TetGen mesh generator (Si, 2015). The partial remeshing operation resulted in a total of about 200000 additional elements, most of them represented by tetrahedra (8.3% of the global domain elements). The resulting mesh can be seen in Figure 6.16.
A pseudo-saturation approach was chosen instead of Richard's equation for non saturated flow (Diersch, 2009) in order to reduce the computational effort. In particular a residual water depth of 0.1 m per layer was assumed in the phreatic approach, namely fixed mesh settings, as the water table was expected to interest different layers. The eight shallower layers, above the aquitard, were assumed to be possibly interested by water table crossing during the simulation.
The analyses cover a time period that starts from 2013 to the end of 2025. Three time intervals can be identified in the numerical analysis:

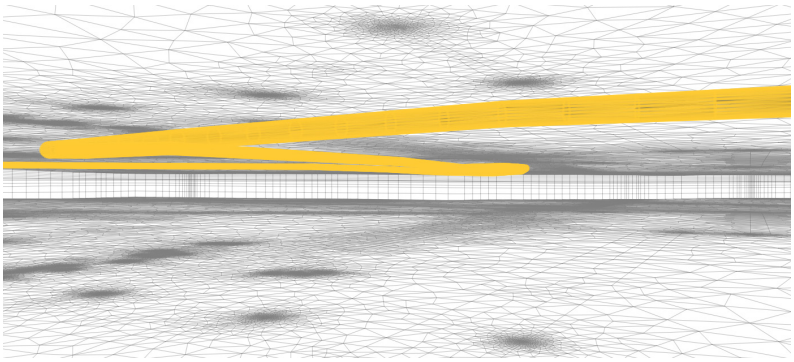

Figure 6.16: Metro alignment geometry inclusion through TetGen partial mesh unstructuring.

- 2013 - 2015: Calibration phase. Monitoring data within this period allowed the hydraulic calibration of the numerical model.
- 2015 - 2018: Verification phase. Monitoring data within this time frame can be compared with numerical results beyond calibration.
- 2018 - 2025: Prediction phase. No measured data are available and the model is used to examine possible thermal evolution under the assumption that the actual utilization is hold constant in the next years.

In the calibration phase it was possible to analyse the hydraulic regime in the absence of active geothermal wells. This allows for comparison with monitored data and then for investigation of the hydraulic and thermal impact of geothermal installation operation. The Algebraic Multigrid SAMG solver (Thum, 2009) was adopted with an automatic second order approximation control scheme (Forward Adams-Bashforth / Backward Trapezoid rule time integration scheme) on the time-step variation.
The zones identified by de Rienzo and Oreste (2011) were at first adopted to handle the ground heterogeneity. According to the nomenclature of the identified zones, three different set of hydraulic and thermal parameter were chosen. Values in line with previous work carried out in the metropolitan area of Turin (Barla et al., 2019b) were adopted and are listed in Table 6.1. Underground anthropic structures (namely tunnels, car parks and building basements) and aquitards layers were considered with isotropic characteristics from the hydraulic point of view.
On the contrary, the shallow aquifer and the unsaturated zone materials were considered orthotropic, according to the origin of the deposit. Indeed the deposition process induces vertical hydraulic conductivities 10 to 20 times smaller than the horizontal values. This is also testified by the predominantly horizontal groundwater direction in alluvial soils. In this study a reduction factor of 20 was selected in line with previous studies (Barla et al., 2013b, 2019b). Parameter values proper of the concrete were defined up to the pertaining depth of each anthropic entity. Slight variations respect to the expected depth values resulted from the node predetermined position. The nearest

Table 6.1: Turin subsoil material properties adopted for TH numerical analysis. Thermal properties are referred to the solid phase only.

	Zones			Aquitard	Concrete
	C1	C2	C3		
Hydraulic conductivity $[10^{-3} m/s]$	1,93	1,1	0,42	10^{-5}	10^{-13}
Anisotropy ratio	0.05	0.05	0.05	1	1
Porosity [%]	17,5	15	12,5	5	0
Thermal conductivity $[W/mK]$	2,7	3	3,3	1,7	1,5
Specific thermal capacity $[MJ/m^3K]$	1,8	1,7	1,7	2,3	2,19

node was selected to approximate reached depth of deep buildings and parks. Buildings with a single basement level were modelled with a depth of 2.5 m while 7.5 m depth was assigned to the buildings with two underground levels. Finally the railway underground tunnel was assumed to extend from 2.5 m depth to 25 m (thus including also the diaphragm below the rail level) while the elements within the metro line were appropriately defined thanks to the re-meshing operation.
Although no direct measurement was available for the selection of the thermal dispersivity values, a ratio of 1/10 of the longitudinal to transverse value was selected according to previous literature. The value of $\alpha_L = 3.1\ m$ was chosen for the entire area. This value was obtained from local scale models (the site lies at short distance from the domain area near the south-western corner of the model area). The same values were already adopted in analysis at different locations in the metropolitan area for geostructures thermal design purposes (Barla and Insana, 2018). Nonetheless, further investigation rather than numerical calibration might enhance confidence on the quantification of this relevant parameter that exerts a crucial impact on the geothermal potential definition. By doing this heterogeneous values may be adopted over the domain area thus considering natural water bodies variability.
Initial conditions were chosen both from the hydraulic and the thermal point of view. The water table resulting from Civita and Pizzo (2001) was adopted while an homogeneous temperature value of 14.2°C was assumed according to the monitored temperatures at the extraction wells of installations 8 and 20.
Accurate modelling of thermal sources/sinks (e.g. passive users of the aquifer, surface water bodies, etc.) requires the definition of appropriate transmissivity values. Values adopted in this study were chosen from literature and are reported in Table 6.2. The same coefficient was considered for incoming and outcoming heat fluxes since the isolating layer thickness is unique in both the directions. The value selected for buildings and car parks is referred to the minimum requirement imposed by law in climatic zone *E* (Italian ministry of Economic Development, 26/06/2015) where Turin is located. Although the structures considered were constructed before this compelling requirement,

Table 6.2: Thermal transfer parameters. Temperatures of urban tunnels and rivers are defined as range of the data hystory that are explained in the section devoted to boundary conditions.

	Transfer rate $[W/m^2K]$	Temperature [°C]
Buildings	0,3	15
Car parks	0,3	15
Urban tunnels	1,3	7,5 - 29,3
Rivers	0.015	5,0 - 26,6

this value is also in line with Epting et al. (2013). Due to similar settings characteristics the heat transfer values pertaining surface water bodies was obtained from Epting and Huggenberger (2013). On the contrary, the transfer coefficient pertaining to the urban tunnels was derived from real thickness of the tunnel segmental lining. It was calculated from the series of $\phi_{air} = 1.77\ W/m^2K$ Barla et al. (2019b) and of the 30 cm thick concrete layer (thermal conductivity: $\lambda_c = 2{,}19\ W/mK$):

$$\phi_{tunnel} = \left[\phi_{air} + \frac{t}{\lambda_c}\right]^{-1} = \left[1{,}77\frac{W}{m^2K} + \frac{0{,}3\ m}{2{,}19\ W m^{-1}K^{-1}}\right]^{-1} = 1{,}3\ \frac{W}{m^2K} \tag{6.1}$$

The temperature values and ranges listed in Table 6.2 will be in depth described in Section 6.4.2.

6.4.2 Boundary and internal condition definition

One of the main advantages of the database management in the *rOGER* method is the possibility to import and export data from or to the numerical model. This capability is particularly useful for handling of boundary conditions along the external model boundaries where *measured values* are available in few points only.
The geo-referred data histories were automatically interpolated along the pertaining borders of the numerical model using the line features dataset. This operation was repeated both on the upstream boundaries (hydraulic head constraint) and on the river ones. In all cases the measured time dependant parameters were assigned to all the nodes included within a distance of 50 m from the *measured* point. No temporal interpolation was carried out. In fact the river length included in the study area can be considered sufficiently short to neglect the delay related to the wave propagation. The delay of water table variations along the other borders are intrinsically included in the measured time histories.
A second aspect has to be mentioned regarding the future scenario definition as the temporal extension of monitored data had to be performed. The cyclic repetition of the last measured annual time history was imposed in all the cases. The yearly basis seems a reasonable approximation to embrace the most part of the variations on the variables

analysed. This is also clear from the analysis of the measured values (see Figures 6.6, 6.8 and 6.10).
Dirichlet's transient hydraulic boundary conditions were imposed at the north, west and south border of the model. Although the main inflow boundary is the west border, as a precautionary measure the flow was not inhibited at the north and south borders. Lateral inflows related to natural slight direction variability of the groundwater flow are allowed by fixing the piezometric level. The data histories were exactly imposed at the nearest location to the points of the metropolitan piezometric network. The values were linearly interpolated in all the other locations along the borders. Since the boundaries were not located at the exact position of piezometers, a proper adaptation to the recorded values was applied. A vertical shift was imposed on the basis of the elevation of the base of the shallow aquifer. Based on the assumption of negligible saturated thickness variation, the values were corrected by the difference between the aquifer base elevation at the exact piezometer location and at the correspondent point on the border. Three piezometers (identified as *3045*, *3026* and *3030*) were identified on the west boundary. No extrapolation was adopted as the boundary is aligned to the piezometric contour line. Two more points were considered at the north and south boundary respectively. As these latter borders are parallel to the groundwater mean flow, also extrapolation was allowed. Boundary conditions were adequately applied to the model nodes along these borders on all the aquifer thickness.
A properly defined Neumann's boundary condition was imposed at the east border, on the basis of the water gauges data measured along the river. The east boundary was subdivided in two zones for the interpolation according to the presence of the Michelotti dam. Interpolation from the south-east corner to the dam (upper portion) was made through the data measured near both the location (*Ponte Balbis* and *Ponte Vittorio Emanuele I* in Figure 6.8). Extrapolation of the two remaining water gauges values was performed on the remaining part. Consistency with the hydraulic jump of the dam was positively checked after extrapolation. The resulting mean river level at the end section, corresponding to the model north-east corner, is at about 206 m a.s.l.. Neumann's boundary conditions were extended to all nodes within the riverbed on the three uppermost layers. A summarising sketch of the hydraulic boundary conditions is shown in Figure 6.17. Regarding the top surface of the model, infiltration due to rainfall was neglected due to the relatively low amount expected to reach the aquifer. This aspect is also in line with the very low water content variations that were measured in the experimental site presented in Chapter 5, even at shallow depths, during autumn wet season. On the basis of annual precipitation and of a reduction of 1/25 due to surface sealing, maximum inflow was theoretically calculated to be less than 2 mm/d. Data from the Regional Authority further confirm that the metropolitan area does not represent an *aquifer recharge area*. This assumption may be slightly conservative in the perspective of heat transport, especially for the green areas. Nonetheless green areas represent about 11% of the modelled surface while built areas account for 69% of the model while sealed surfaces represent the remaining part.

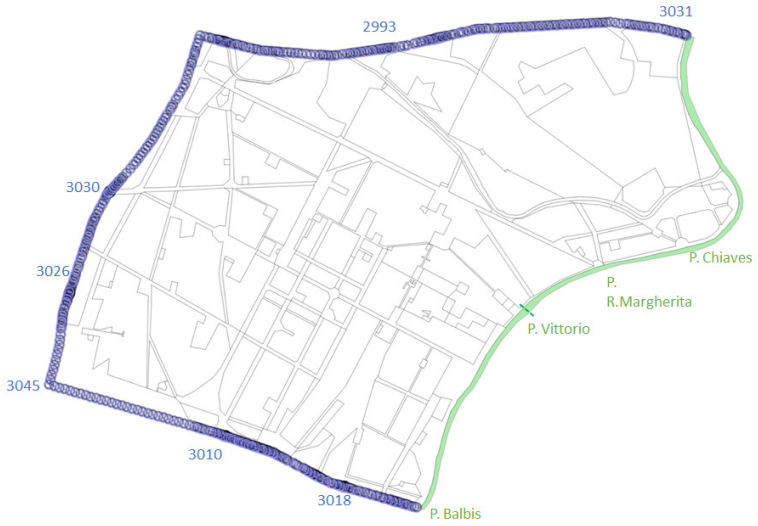

Figure 6.17: External hydraulic boundary conditions. The labels indicate the point used for interpolation. The division among interpolation zones on the Po river is depicted by the dashed green line.

Up to this point, external boundary conditions have been treated. On the contrary, anthropic entities were identified and included in the model as internal boundary conditions at proper location within the model domain. The volumes represented by the built environment were modelled adopting concrete material properties (see Table 6.1). Due to low hydraulic conductivity values, these volumes are virtually impermeable.
Other internal boundary conditions represent the existing geothermal installations. The simulation of the geothermal water wells was obtained with a sink/source internal boundary condition at proper mesh nodes. The appropriate boundary condition was thus assigned to the nodes included in the screen interval of each well. Negligible approximation in their absolute elevation and length resulted from the a priori distribution of the mesh nodes. The data from active installation were processed to the sake of accurate simulation at affordable computational effort. At first, the data histories of pump rates were resampled on a daily basis. Based on previous study, this level of detail is expected to be sufficient (Bonsor et al., 2015; Lo Russo et al., 2014). Although the daily average pump rates are typically *constant step* data, high gradients resulting from sudden boundary condition changes may result in inaccurate results in the numerical models with an unreasonable compression of the time step length. Thus a small linear transition (one hour duration) between two subsequent measures was inserted in the time histories to the sake of avoidance of numerical instabilities. The time series were later extended to the prediction phase of the numerical analysis when measures were not available. The time histories referred to the last monitored year (in most cases it was year 2016 or 2017) were selected to be replicated until the simulation time end. By doing this the scenario that was investigated takes into account a stable utilization

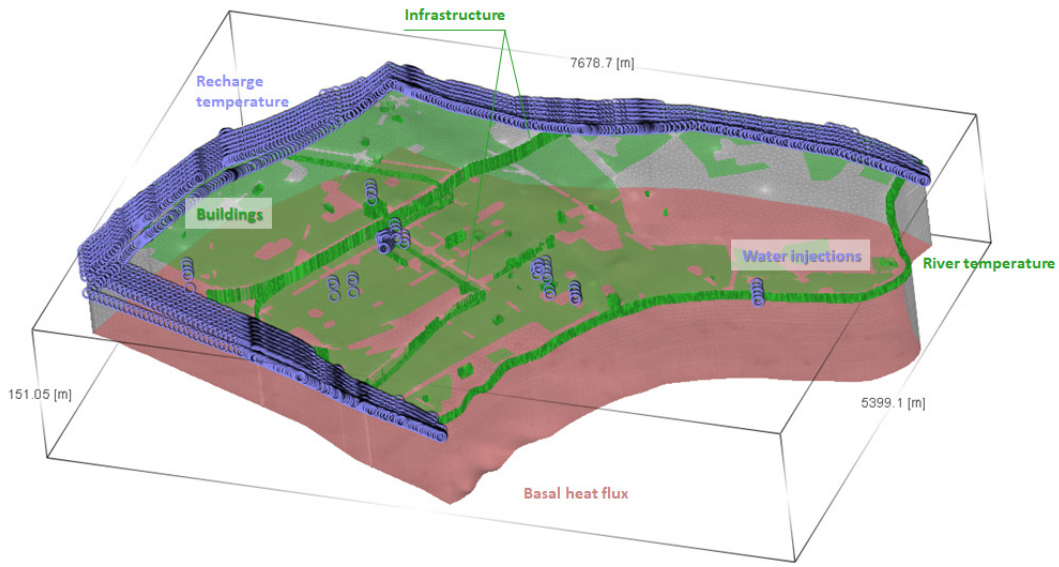

Figure 6.18: Thermal boundary conditions. The labels indicate the typology of the thermal boundary conditions. Colours of the labels are associated with the relative boundary conditions.

of the shallow geothermal resources in the area. Although this might be unrealistic, such an assumption gives the basis for better understanding of sustainability of the actual utilization level. Total pump rates per installation were eventually divided by the number of nodes of the injection and extraction well respectively. Temperature at the injection well nodes was assigned neglecting possible thermal stratification. The treatment of measured temperature data was, beyond this aspect, identical to the process employed for pump rates calculation.
In few cases some data were missing, due to lack in the reports or to sensor failures. In these cases, gaps were covered up by processing the time histories to avoid thermal impact underestimation. The corresponding period of the following monitored year was repeated to cover up the missing data.
A constant heat flux was assigned at the bottom surface of the domain (see Figure 6.18). The basal heat flux value of $0.06 W/m^2$ was selected from mapped data at national level (Consiglio Nazionale delle Ricerche, 2014). This value was assumed to be homogeneous over the domain. Furthermore the temperature of the recharge water on the north, west and south borders of the saturated zone was assigned with a constant temperature of 14.2°C. This value was assumed in line with the initial thermal condition and assuming that no thermal alteration is exerted outside of the domain. Although this assumption may result inaccurate at the north and south border, the limited groundwater flow exchange reduces the impact this assumption. On the contrary, constant and undisturbed groundwater temperatures can be assumed at the west boundary as a result of the relatively high unsaturated thickness.
The remaining heat fluxes within the domain have been modelled through Neumann's

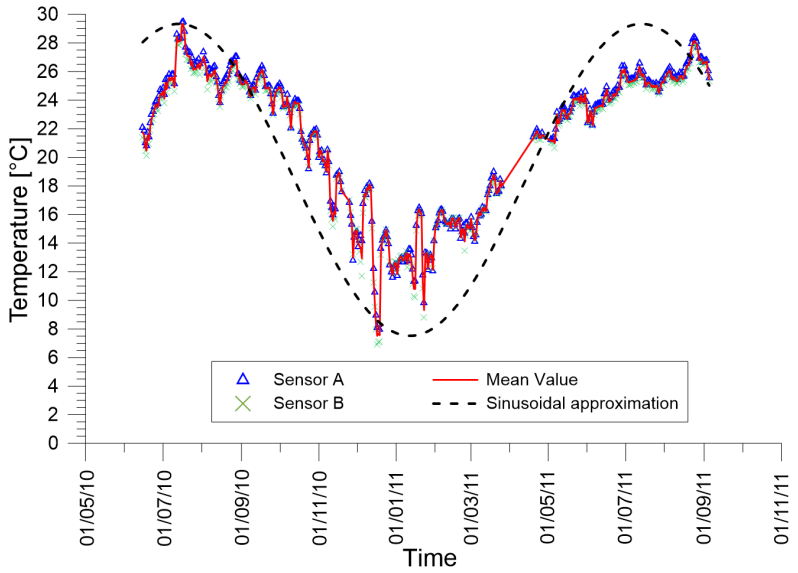

Figure 6.19: Temperatures monitored in Turin metro line 1 and model approximation.

boundary conditions. The heat transfer coefficients have been already explained in Section 6.3.3 and listed in Table 6.2. As regards the coupled temperatures profiles, the two urban tunnels were considered by including an approximation of the measured temperature. These records are referred to the metro tunnel during 2010-2011 (see Figure 6.19). A sinusoidal approximation was selected on the basis of the range and the average temperature values observed on the annual time frame:

$$T_{tunnel} = \bar{T} + \frac{T_{max} - T_{min}}{2} \cdot \sin\left(\frac{2\pi}{365} \cdot t\right) = 18.42 - 10.91 \cdot \sin\left(\frac{2\pi}{365} \cdot t\right) \tag{6.2}$$

where the time t has to be inserted in days.
A constant temperature of 15°C was supposed throughout the year in buildings basement and underground car parks that were fully included in the model as volume entities. Although temperature variation may exist in these structures (Tinti et al., 2017), especially in environments with high air volume exchanges with the surface, an important damping on thermal variation can be supposed (Sterpi et al., 2017). Furthermore this value is in line with previous literature in similar climatic conditions (Epting et al., 2013).
No heat flux was considered on the remaining upper boundary of the model since no measurement was available to calibrate the heat transfer coefficient. The heat fluxes to the aquifer are limited by the high depth of the water table over the entire area, virtually below the *homoeothermic* surface.
Finally heat exchanges with the surface water bodies were considered. The measured water temperature values at the Murazzi water quality station were adopted to this end in the model. The time history was repeated cyclically over the entire period analysed.

6.4.3 Numerical results

The actual thermal and hydraulic regimes of the central districts of the urban area of Turin were determined by numerical modelling. Results from the numerical analyses allow the accurate prediction of the parameters used in the geothermal potential assessment phase of the *rOGER* method. The analyses investigated not only the past period when some monitored data were available, but also a projection in future times. Past periods included both a calibration and a verification phase. In the first phase, measured data are employed for the calibration of the hydraulic parameters adopted in the model. On the contrary the second phase allows the verification of the model results accuracy. These phases referred to the past times that constitute the *hystory matching* part of the numerical analyses.
With regards to the future prediction, a scenario was built to examine thermal evolution under the assumption that the actual utilization level is hold in the next years. To this end the monitored aquifer uses were extended by cyclic reproduction of the usage profiles. The last annual cycle available (in most cases corresponding to year 2016 or 2017) was employed for scenario construction. Although consistency of the results with monitored values can be to some extent incomplete due to the uncertainty on the input data and on the measured values, the numerical model is intended to be representative of the hydraulic and thermal regime at a rather large scale. The analysis presented allows a satisfactory investigation of these aspects. The numerical results enhance the opportunity to study the thermal evolution with respect to the previous knowledge gathered in the study area. Enhancement of the results accuracy may be obtained by refining the input quality in a long and iterative process that is commonly accepted as the development path for subsurface resources management (Bonsor et al., 2015). The application of the *rOGER* method in this perspective can stimulate the interest on the almost unexplored potential of the subsurface resources in the metropolitan area of Turin.

Calibration phase

The hydraulic parameters reported in Table 6.1 were selected as initial parameter values for the hydraulic model calibration. The infiltration and exfiltration coefficient pertaining to the surface water bodies were calibrated as well. The PEST (Doherty and Hunt, 2010) utilities were adopted through the interface and interoperability capabilities provided by FEPEST. Hydraulic conductivities and the fluid transfer coefficients were numerically calibrated.
Fluid transfer coefficients were kept constant within the riverbeds in the calibration process to reduce the computational effort. This is in line with rather homogeneous characteristics of riverbeds in their urban portion. It resulted that the Dora Riparia had almost no connection to the groundwater, as already mentioned in Section 6.3.2. Thus the transfer coefficient was approximated to the null value. On the contrary the Po river runs in a natural bed, and calibrated coefficent resulted to be equal to 650 d^{-1}. As

the river acts as a drainage only the in-transfer coefficient results to be effective.
Conversely, an approach based on pilot points was preferred for hydraulic conductivities calibration to better handle the uncertain demarcation of cementation zones and the intrinsic heterogeneity of the alluvial deposit. The horizontal hydraulic conductivities were imposed to be identical in both direction and the anisotropy ratio was kept constant. This allowed to increase density of the pilot points grid with reasonable computational effort. The pilot points were equally distributed among the saturated and unsaturated zones of the model. The PEST optimisation allowed to reduce the *objective function* to about the 15% of the initial deviation from the measured levels in the piezometers of the metropolitan network. For the convenience of the reader the comparison of the resulting hydraulic heads with the measured data histories is analysed in the verification phase paragraph as this phase concludes the history matching part of the numerical analyses.
The time period analysed for calibration was chosen from 2013 to 2015. By doing this, the flow regime was investigated both in undisturbed condition and in conditions affected by the activation of some geothermal installation. Respect to the zone-based approach a smoother variation of the hydraulic conductivities resulted in the ranges from $1.05 \cdot 10^{-2}$ m/s to $9 \cdot 10^{-4}$ m/s. These values are in line with data from pumping tests carried out in a central portion of the modelled area (Barla et al., 2013b) that indicate an hydraulic conductivity of $3.7-4.5 \cdot 10^{-3}$ m/s. Further confirmation derives from the collected design data from open loop geothermal installations (Barla et al., 2018) ranging from $2 \cdot 10^{-4}$ m/s to $5.9 \cdot 10^{-3}$ m/s. The calibrated values of the hydraulic conductivity were later adopted in the verification and prediction intervals of numerical analyses.

Verification phase

Based on the general experience on the study area (Barla et al., 2018; Bottino and Civita, 1986), the model seems to correctly capture the main groundwater flow direction from the west to the east. Steeper hydraulic gradients at north-east edge are obtained. The depth of the water table shows high variability with higher values in the southern part of the model. A good agreement with the expected values from the Regione Piemonte data is reached (as shown in Figure 6.20). Although some local discrepancies about the water table depth still exist at some points (especially at south-east border and in the extreme north portion of the model), history matching in the central part of the model shows a satisfactory agreement. Furthermore an almost constant bias with numerical results is usually obtained at the points that present major discrepancies. This might be related to inaccuracy of the altimetric reference of such measuring points. As shown in Figure 6.21, the biggest differences seem to be related to model underestimations of the water table elevation. In these cases the advective and dispersive contributions are limited to smaller depths and the geothermal potential assessment will result slightly conservative. The numerical results do not show clear raising or descending trends in

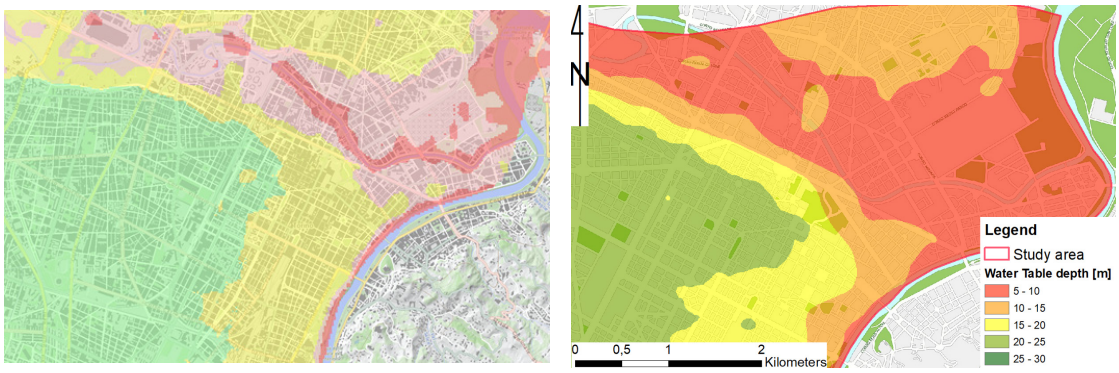

(a) (b)

Figure 6.20: Water table depth in the model area.(a) Values interpolated from the Geoportale of the Piemonte regional authority and (b) values obtained by numerical analysis.

line with measured data. Hydraulic head variability is low to extremely low in most cases and limited to the decimetric ranges. On the contrary wider ranges are obtained for points *2976, 2995* and 3028. These points are located near the Po river at the east border of the domain. The entire area at the confluence of the Dora Riparia and the Po rivers seems to be highly influenced by the base level of this latter surface water body. This evidence together with the rapid variations of the water table suggest that a quick response to the river level variations is exerted on this portion of the domain. This might be related to the relatively high hydraulic conductivities.
Comparison of the piezometric levels in proximity to the geothermal installation results in similar considerations. A good correlation between the monitored values and the numerical results can be found (see Figure 6.22). The differences respect to prediction are limited to the centimetric or decimetric scale except for two installations that are located at close proximity to one another. Although some major differences arose at the piezometers placed downstream to the installations *23* and *31*, numerical results predict a lower elevation with a conservative impact on the geothermal potential assessment phase.
On the contrary, numerical results close to the Po river (downstream boundary) show an extremely good match with expected values at the monitored points downstream to geothermal wells. Analogously, good correspondence can be established both in term of mean level and of variation trends at the location of the most upstream installations (e.g. installation *8* and *20*).
A significant comparison can be done with respect to the thermal field on the geothermal installation monitoring systems. Indeed no temperature measurement was available on the metropolitan monitoring network points. Only measurement from the campaign of December 2019 that was carried out within the framework of this study were available. Nonetheless data from the monitoring points situated downstream to the geothermal installations allow to locally test the consistency of numerical results to real

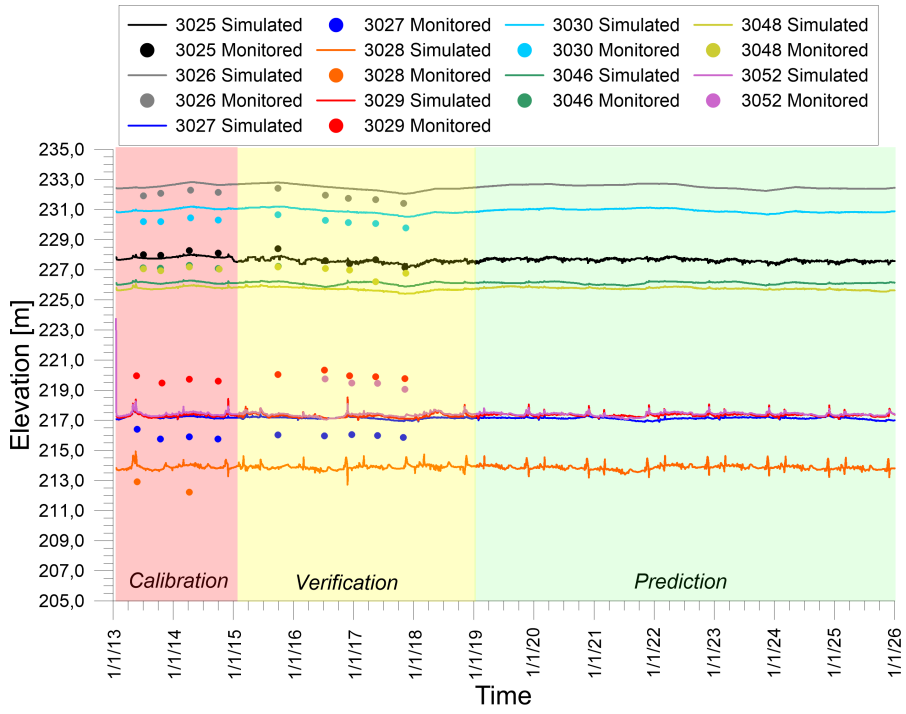

(a)

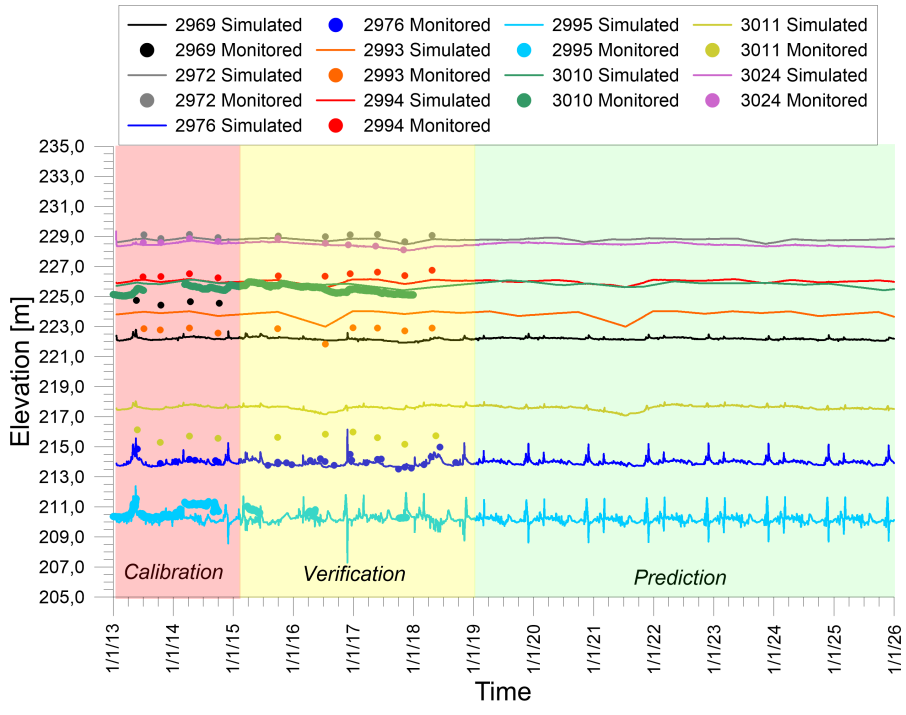

(b)

Figure 6.21: Water table at piezometric monitoring network points.

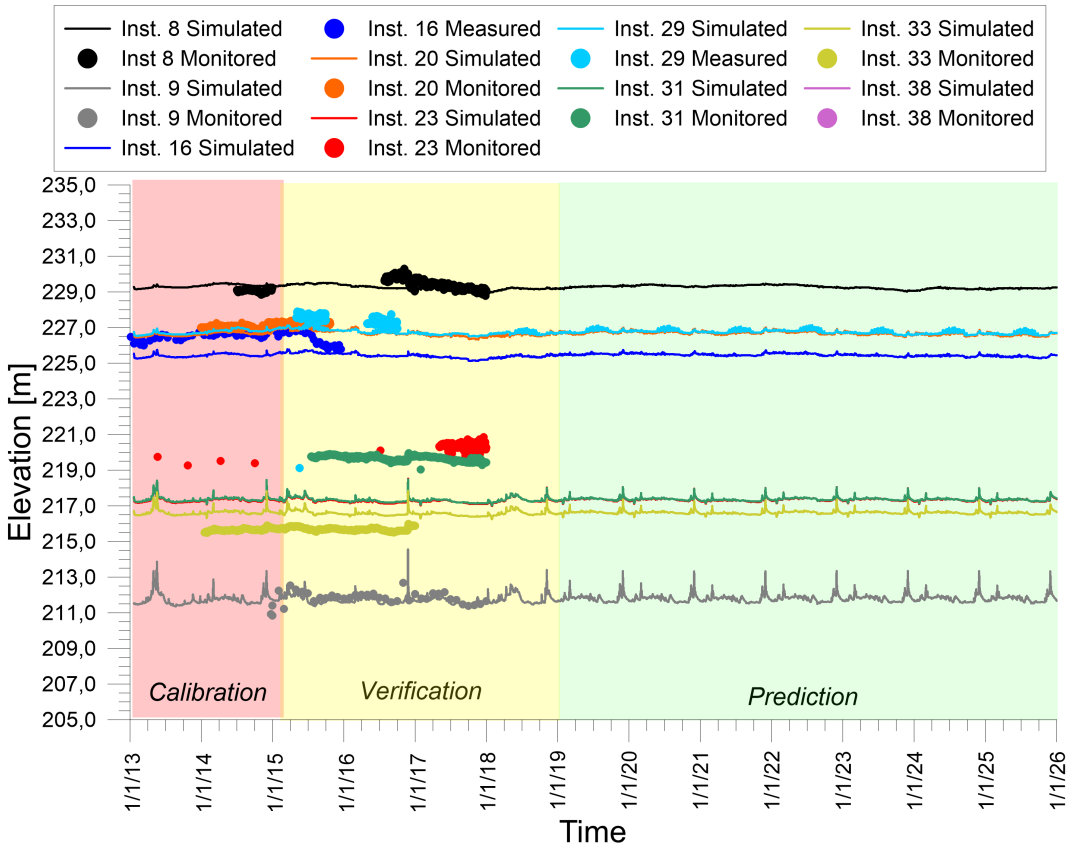

Figure 6.22: Water table at geothermal installations piezometers.

thermal regime. A good coherence of the numerical results with the measured values was obtained in most cases. Verification of the thermal results can be obtained through comparison with measured data (see Figure 6.23 and Appendix C). Correspondence is virtually perfect in the east portion where the groundwater discharges in the Po river. Such an evidence is highlighted by time histories of installation *9* in Figure 6.23. Similar conclusion can be drawn with the geothermal plant nearest to the west upstream border (installation *8*). In this latter case a marked discrepancy can be identified during year 2014. This difference can be however explained by the reported fall of the probe at the bottom of the piezometer. The measured value thus refers to a relatively deeper location and testifies a thermal stratification. These measures gave further robustness to the choice of the initial thermal conditions with similar values. Initial temperature agreement is also the main aspect highlighted by the point *Installation 20_C* in Figure 6.23 whose temperature is constant and not affected by any geothermal plant.
Conversely in the case of Installation *16* a thermal alteration would result from numerical analyses that appears to be smoothed and delayed with respect to expectation. This behaviour cannot be however identified at close upstream and parallel monitoring points (*20_F* and *20_M* respectively). Possible source of error might be the inaccurate

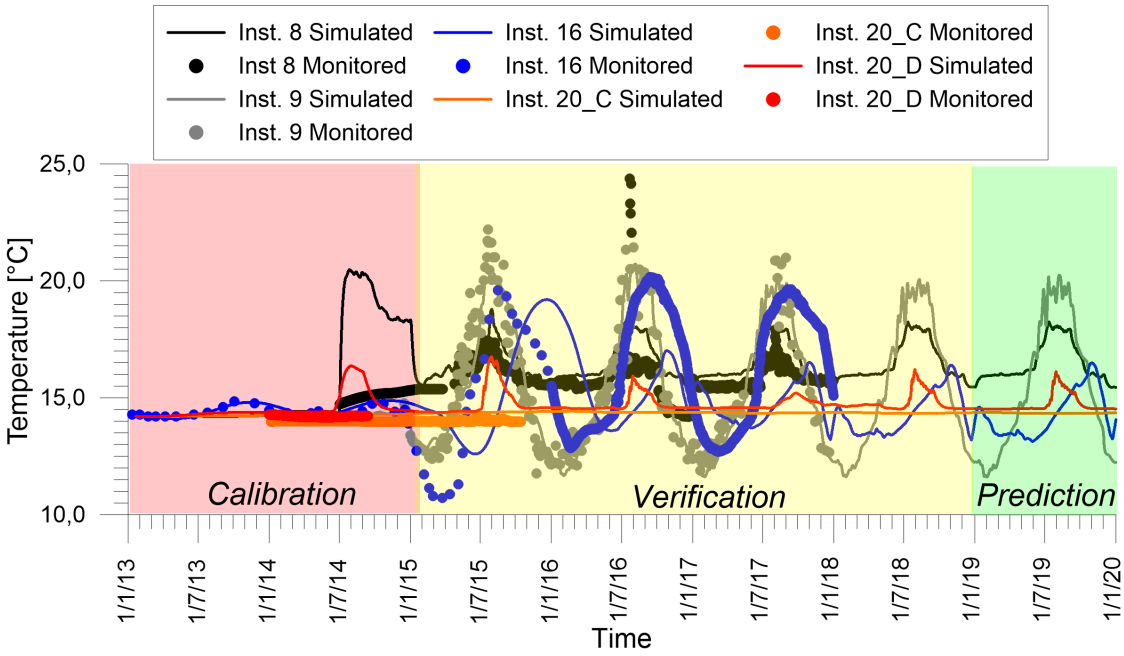

Figure 6.23: Temperatures at geothermal installations piezometers. The numerical trends obtained for year 2018 are identically duplicated with cyclic behaviour until the end of the simulation.

geometrical representation of the railway tunnel, the positioning of the monitoring point rather than the pump rates of the close injection well. The presence of geometrical discontinuities in the railway tunnel, due to the station proximity may impact on the transmission of the thermal plume from installation *20*. This local defect was accepted within this study. Although deeper knowledge of the specific site might allow for more accurate tuning, this was beyond the scope of this study. With regards to the historical city centre, a good agreement is ubiquitously found. Further data and comparison with the measured values can be found in Appendix C.

Prediction phase

The prediction phase of the analyses allowed the investigation of a future scenario under the assumption of a constant utilization level in the future years. In the context of the *rOGER* procedure application main attention will be devoted to results in the winter season. This is due to the subsequent comparison of geothermal potential with energy demand. This comparison will be better analysed in the following section but was possible only with reference to the heating season.
A direct consequence of the scenario investigated is the cyclic behaviour of the thermal regime starting from year 2018-2019. In fact the scenario was based on the hypothesis

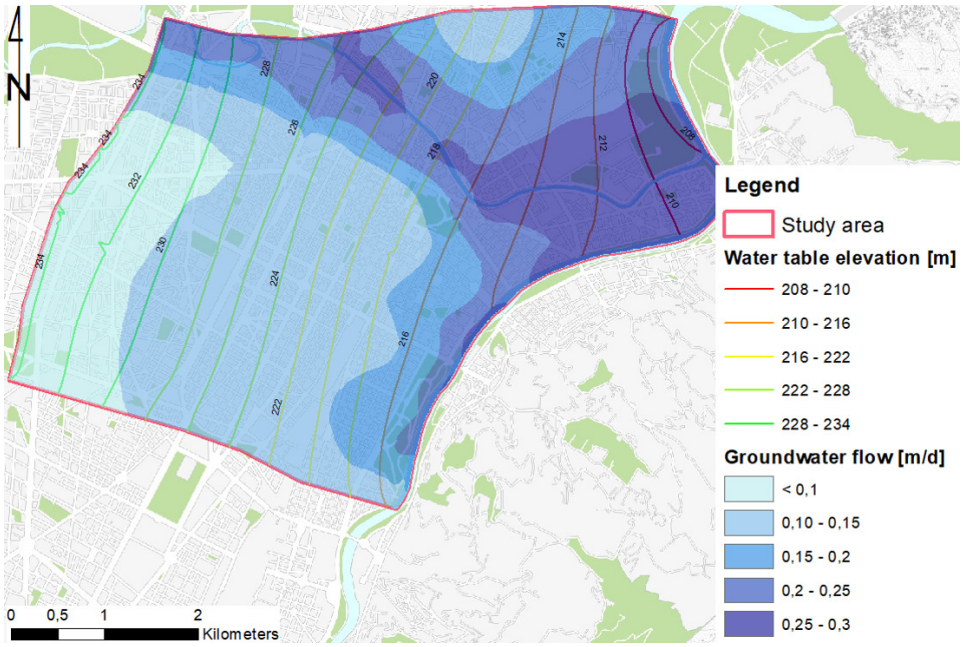

Figure 6.24: Water table and groundwater velocities resulting from the numerical analysis in heating season referred to the prediction phase of the analysis.

of keeping the geothermal utilization constant for the next future. Nonetheless investigation of a sufficiently extended future time, allows the analysis of the sustainability of the actual exploitation in the long term. Also the *thermal memory* of the aquifer can be related to the groundwater velocity.
Groundwater velocity is a crucial aspect in the definition of the geothermal potential according to the modified version of the G.POT. formula (Equation 4.12). The depth-weighted mean water velocity shows a good correlation with water table depth. The shallower the water table, the higher impact that the saturated aquifer thickness exerts on the above mentioned velocity. Since aquitard depth are considered in the averaging process of the velocity and barely represent null contributes, relatively low velocity values are obtained (see Figure 6.24). At the depths pertaining to the saturated thickness of the aquifer, flow velocities of up to 1.5 m/d are experienced. These values are in line with previous investigations carried out in the area (Barla et al., 2018).
A thermal map of the study area within the saturated zone was obtained to better study the extension, persistence and migration of thermal plumes. The groundwater flow drives the thermal plumes to the east towards the Po river. An important persistence of the plumes results from numerical analyses as it is clearly shown in Figure 6.25. Such thermal maps were derived also for intermediate times and during other seasons and are reported in Appendix C. For the sake of exemplification, winter 2017 and summer 2025 were reported. Urban tunnels exert a clear impact on the aquifer temperature since they are partially immersed in the saturated zone. The relatively high impact seems to

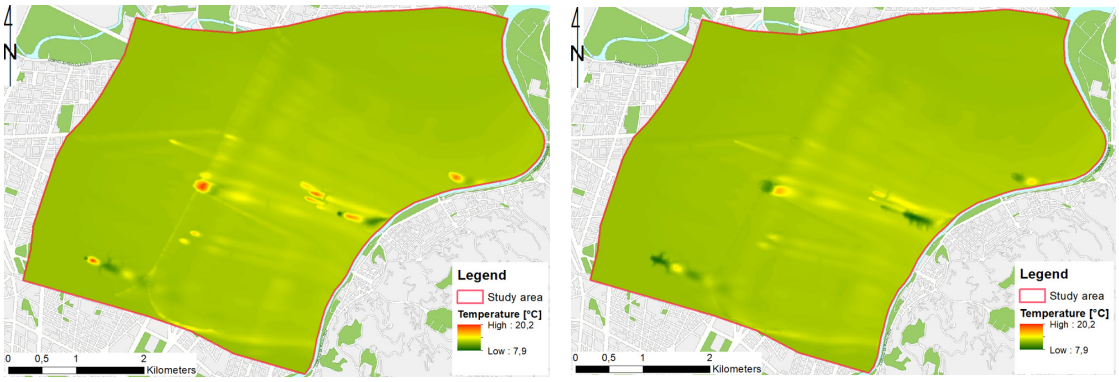

(a) (b)

Figure 6.25: Temperatures expected in the model area (a) at the beginning of the winter heating season and (b) at the end of the heating season.

be related to the high thermal differences observed during the summer season. Indeed the highest temperature in the tunnels reaches 29 °C with a difference respect to the undisturbed temperatures of up to 15°C. On the contrary, the minimum tunnel temperature determines a smoother gradient of 7°C only.
Since the railway tunnel partly exceeds the domain at the north boundary, within the central portion of the model an higher degree of confidence is obtained, while at the north and south-east portions of the domain boundary effects may be not negligible.
Geothermal open loop systems seem to exert a similar influence. The flow rates and the temperature of the injected water during the summer exerts a far stronger action on the aquifer rather than during the winter season. Although the persistence of the thermal alterations is pronounced, their magnitude is significantly reduced with the distance from the installation. The link with the distance seems to be related to the mean groundwater flow that makes the plumes migrate downstream. Hence an indirect relation with time can be reasonably inferred. This aspect will be further clarified in the next section where the depth weighted average site temperature is obtained through numerical results post-processing.

6.5 Geothermal potential in the area and city scale implications

The numerical results described in the previous section allow the definition of representative hydraulic and thermal regime of the study area. These results are employed in geothermal potential assessment phase of the *rOGER* procedure.
In this application of the *rOGER* procedure, winter heating season was taken into account due to the lack of characterisation of the cooling demand of the buildings. The

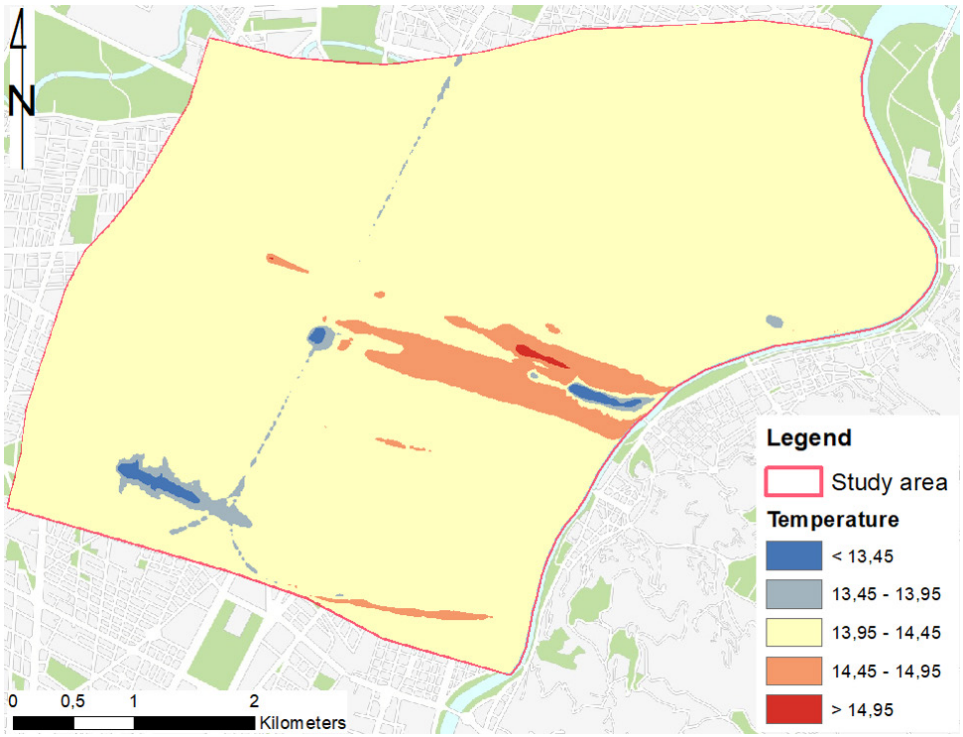

Figure 6.26: Background temperature T_0^* for heating season in the study area.

heating season was selected to illustrate the potential assessment due to the clear definition of the operative season. On the contrary, no restriction binds the season neither the duration of the cooling operations (based on the climate data the cooling season can be supposed from June to mid August).
The geothermal potential can be defined both from a qualitative and quantitative point of view from the obtained results. The definition of thermal status represents the first outcome of numerical analyses. Thermal maps have been showed in the previous section and in Appendix C. The suitability of the site for a geothermal installation should be however evaluated on the basis of the extreme conditions that are expected during the whole operative season. The background temperature T_0^* in Equation 4.12 identifies these conditions. The resulting map in Figure 6.26 is substantially the envelope of the cold thermal plumes during the heating season (from mid October to mid April, as legally prescribed for climatic zone *E*).
The background temperature at the site widely ranges from 11.5 °C to 15.9 °C. The wider variation respect to the undisturbed conditions is registered towards lower temperatures (minimum of 2.68°C respect to the expected temperature). Conversely, higher temperatures (maximum deviation from the expected thermal status was 1.67 °C) are verified on wider portions of the domain. This testifies that the current shallow geothermal utilization in the study area is unbalanced and biased towards the cooling loads. This confirms and broadens the conclusions from the study of Barla et al. (2018).

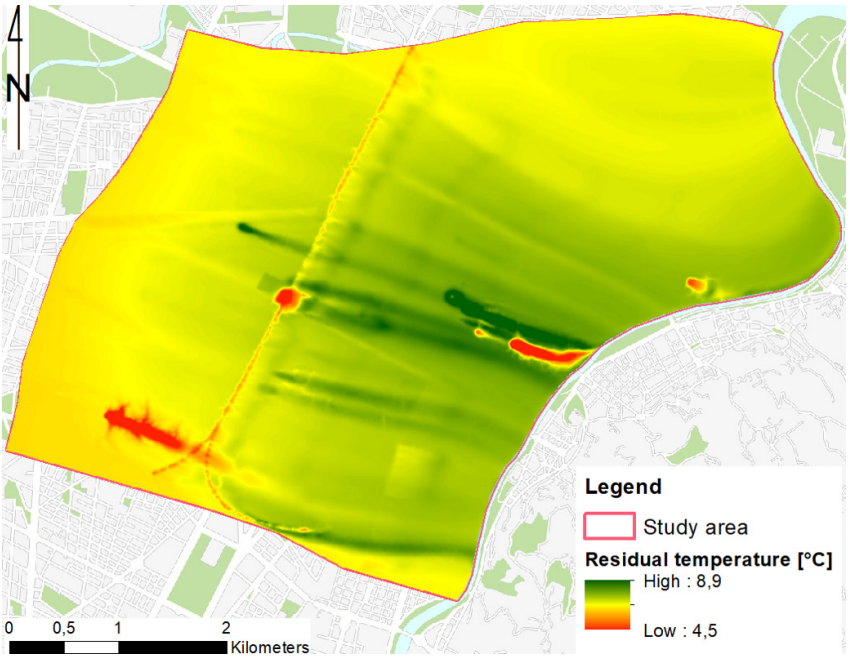

Figure 6.27: Predicted residual temperature map in heating season in the study area.

During the cooling season, differences with the undisturbed site temperature are more pronounced. This determines less favourable conditions for cooling purposes on a wider area than in undisturbed conditions. Positive differences of up to 2.5 °C are verified in the long term in the study domain, as shown in the relative thermal maps reported in Appendix C. A relatively wide area corresponding to the historical city centre is subject to a progressive heating. Comparison of the thermal situation simulated in the early stages of the simulation (year 2016/2017) with future previsions supports this conclusion. However this rise in the temperature is limited in magnitude and extension. Indeed the areas with thermal alteration larger than 1.25°C are extremely confined.
Once the *thermal picture* was obtained, definition of the residual temperature drop was performed. A maximum deviation from the thermal natural state of about 7°C was assumed and hence the threshold temperature limit adopted was equal to 7°C. As a result of the slightly elevated temperatures in the study area, the allowable temperature drop is comprised between 4.6°C and 8.8°C (see Figure 6.27). This latter value is slightly higher than in natural state conditions. The allowable temperature drop is sufficiently high to allow for further utilization even in the most unfavourable locations. The Integrated Relaxation Factor was calculated over the domain of interest and the relative map is reported in Appendix C. Slightly negative values are obtained within the study area according to the thermal picture previously described. In these areas the installation of geothermal plant for heating purposes would benefit from the hot thermal pollution. In this perspective geothermal heating installations might be interpreted as remedial strategy to restore the thermal status of the aquifer. This kind of map can further push

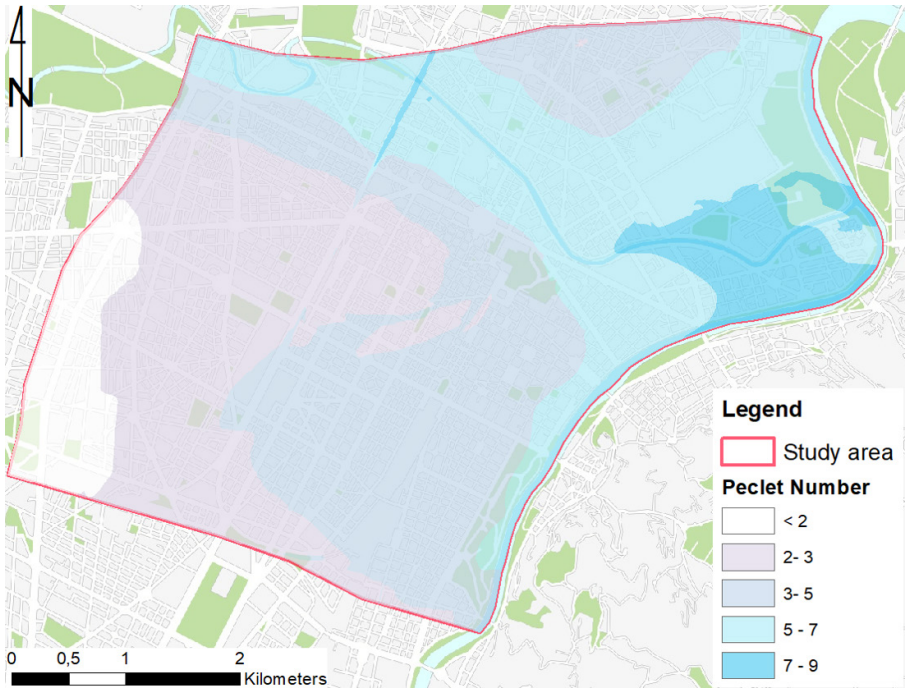

Figure 6.28: Average Peclet number calculated for the study area.

the spatio-temporal optimisation in the geothermal resources uses by identifying the appropriate intervention areas. The areas that would benefit from the thermal interference are located at a certain distance from existing active or passive users and not directly downstream to them. Thermal maps and the relative processing may play a significant role in planning the optimal location of installations depending on the energy needs of buildings.
The hydrodynamic aspect is a relevant parameter in the quantification of the site specific geothermal potential in the *rOGER* method, following Equation 4.12. The depth-weighted average Darcy velocity has been already shown in Figure 6.24 and analysed in the previous section. The hydro-dispersive and advective components of the heat transport were directly derived from the groundwater flow. The *Peclet number*, was thus evaluated on the basis of the Darcy velocity shown in Figure 6.28 (an average value over the operative season was selected). As clearly expected, an evident correlation is established between Peclet Number and the mean Darcy velocity. The *Pe* values range significantly from 1.6 to 10.4, clearly highlighting the extreme significance of the advective contribution respect to the conductive contribution. These differences will be then smoothed in the definition of the geothermal potential thanks to the contribution of the correction factor C_{gw} (Equation 4.14) that is proportional to the Peclet number.
It should be mentioned that the uncertainty related to the longitudinal thermal dispersivity value exerts a linear influence on the Peclet number determination. This is in turn reflected through a logarithmic trend on the dynamic geothermal potential value.

As a result the obtained geothermal potential shows, within the range of interest for practical applications, an high sensitivity to rather small variations of the Peclet number.
The site specific geothermal potential variability is about 40% and the influence of the most pronounced thermal alterations can be inferred from the results shown in Figure 6.29. Particularly high geothermal potential values of up to 26 MWh/y are obtained in the study area. This value is due not only to the high groundwater fluxes but also to the waste heat that rises the background site temperature. The temperature increase is beneficial to the regards of the heating season, while it would be unfavourable for cooling season.
Comparison with classic G.POT. formulation in hydrostatic conditions (the relative map is shown in Appendix C) shows relevant differences. The values of the geothermal potential result to be doubled respect to the hydrostatic conditions in most cases. The range varies from the original 7.7-10.7 MWh/y to 15.0-26.3 MWh/y by considering the advective and dispersive components of the heat transport.
The ratio between the potential in hydrodynamic conditions and the value in hydrostatic one ranges from 1.8 to 2.9, which is in line with the analytical prediction corresponding to the Peclet number values of Figure 6.28. The distribution of the values results to be completely altered in the two situations. In the case of the *static* evaluation the geothermal potential in the northern portion of the domain is slightly penalised by lower thermal conductivity. In this zone the base of the aquifer is relatively shallower and hence the low conductive aquitard layer gains relevance. On the contrary in the north/north eastern area the geothermal potential is expected to be high due to the relatively high groundwater flow velocities. This implies that at the urban planning scale, the most promising area where to develop shallow geothermal is the portion at the confluence of the Dora Riparia and the Po rivers where a single BHE is expected to provide up to 2.97 kW of thermal energy.
The study area is extremely valuable for geothermal installations since the high values are ubiquitously present within the domain of interest. The evaluations carried out considering the conduction rather than advection and dispersion mechanisms, return extremely high potential of 4800 GWh/y and 11400 GWh/y respectively when considering the entire domain.
Thermal loads should be defined to assess the impact at the local rather than at the city scale of shallow geothermal energy. The volume of each building entity was taken into account to this end. A reference building was considered in order to define a specific heating load per unit volume. In this study, according to the main features of the built heritage in Turin, an apartment block located in the Climatic Zone *E* (where Turin is placed) was selected from the *TABULA* database (Corrado et al., 2012). A relatively recent building was selected, since the development of the city took mainly place in the second half of the 20th century. Hence the building typology *IT.MidClim.AB.05.Gen* was selected to the end of this study. Although the installation of a geothermal system or of the GeothermSkin system on existing building would be accompanied by a more

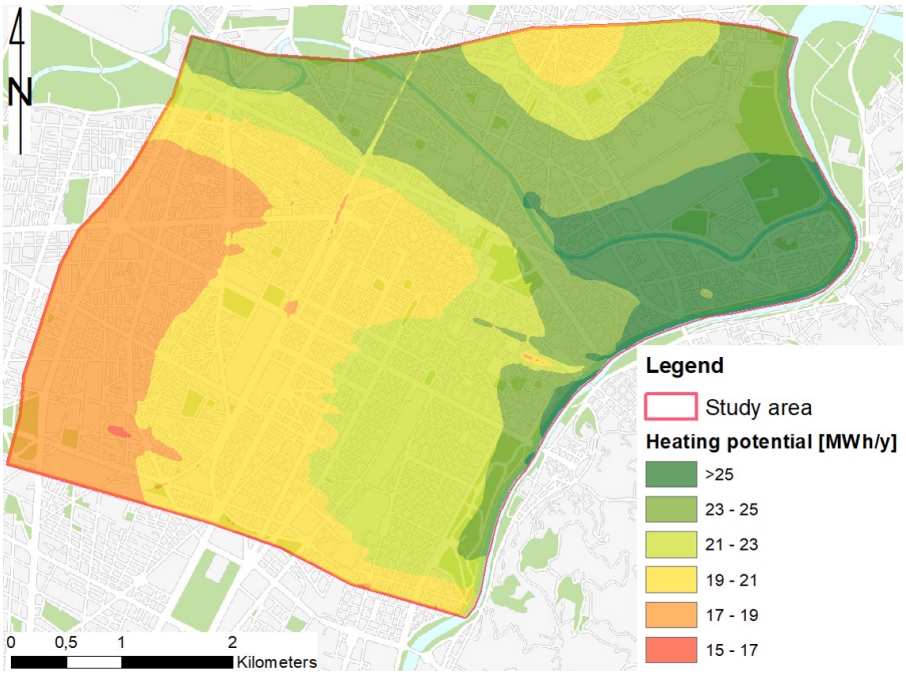

Figure 6.29: Site specific shallow geothermal potential in the study area accounting for groundwater fluxes and borehole heat exchangers of 100 m length.

comprehensive refurbishment, the conservative assumption of actual state energy consumption was adopted. The thermal load of 99.2 kWh/m^2y was selected accordingly. The reference volume and surface of the building typology were later considered in order to refer the specific thermal load to the unit volume. Finally the heating thermal load of each building was calculated with the specific factor of 30.16 kWh/m^3y. It was assumed that the volume to be heated for each building corresponds to the 90% of the entity total volume since small portions of the buildings are not completely heated during the winter season.

Previous chapter demonstrated the interest in the very shallow depths in the perspective of spatio-temporal optimisation in the use of shallow geothermal energy. The promising efficiency of a novel energy wall system and its attitude to be associated with new or refurbished buildings renovation enhance the advantage of system related to the strictly local thermal affection. The potential impact on the energy supply at the local and city scale was evaluated on the basis of the surface that can be equipped. Although this projection is substantially theoretical, the picture can provide a further evidence of the enormous potential that is stored beneath cities. This approach can be exported to other districts and cities of new urbanisation due to the general validity of the method proposed.

The potential heat supply that can be provided by the extensive application of the GeothermSkin system was calculated on the basis of the earth-contact area that can be equipped. The depth of the underground levels of buildings was assumed equal to

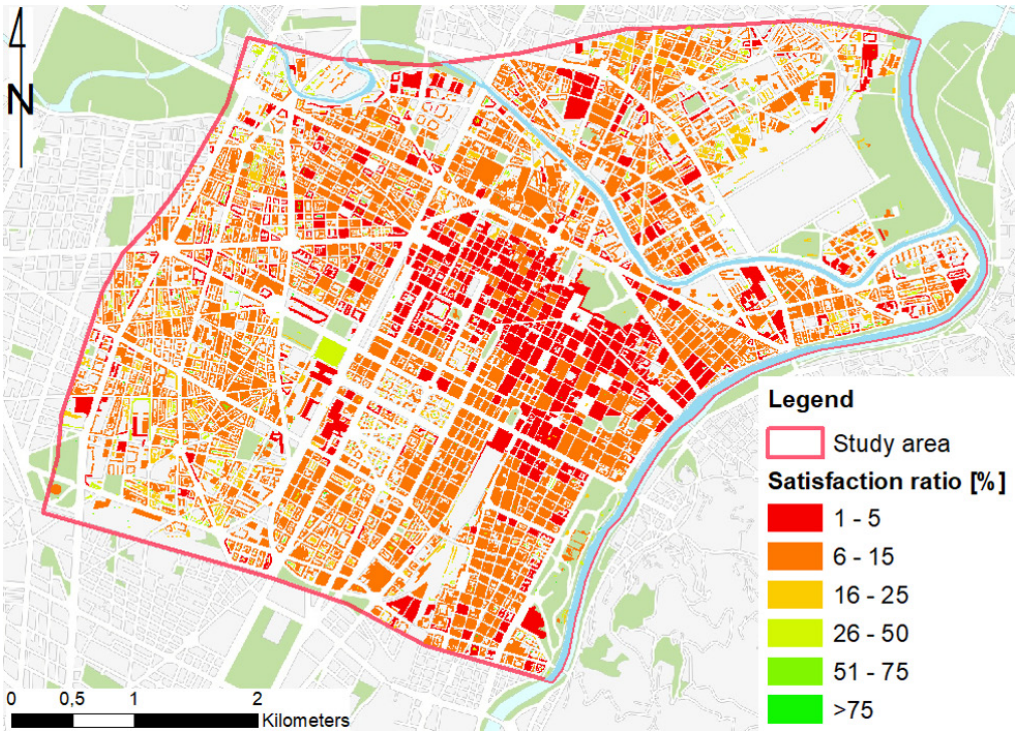

Figure 6.30: Projection of the heat demand satisfaction ratio from Geothermskin system in the study area of Turin.

3 m per floor. Consequently the number of the underground floors was derived according to the classification reported in Section 6.3.4. The system was assumed to cover the entire perimeter of the structure. The thermal power per unit area of 18.9 W/m^2 was adopted according to the heating experimental campaign results (the tests with target user temperature of 45°C were selected to the sake of homogeneity).
The energy that can be supplied to the user during the season was carefully calculated under the assumption of 2400 full operation hours (VDI, 2010) and a constant COP of 4 (Baralis et al., 2018). In Figure 6.30 the heating thermal load satisfaction ratio referred to the Geothermskin system is reported. Results suggest that the system would be able to provide in most cases only partial response to the energy needs of the buildings. Such contributions may play a significant role in the achievement of the minimum share of renewable energy sources for the new constructions. In a majority of cases the system may provide a contribution of up to the 50% of this share (a relevant part of the housing units show a satisfaction ratio near to the 25% of the total energy need). Some patterns can be highlighted in terms of spatial distribution of the satisfaction ratio values. Indeed the historical city centre was generally found with very limited values due to the compactness of the buildings (low perimeter to volume ratio). On the contrary higher satisfaction ratios were obtained when moving to the external parts. This might be mainly due to the shape ratio but also to the higher number of volumetric units

with multiple underground levels. Furthermore some low buildings, prominently for commercial or industrial uses, show a relatively high perimeter to volume ratio. The common presence of multi-level underground car parks in large commercial structures can potentially provide an extremely large area to equip for heat exchange.
Potential satisfaction from Borehole Heat Exchanger field installation has been investigated as well taking into account both the scenarios depicted in Chapter 4. The energy that can be provided by BHEs installed within the external perimeter of each building was calculated for the first scenario. The energy that can be provided to the user was calculated under the assumption of 95% efficiency. This conservative efficiency value was assumed to completely exclude any overestimation related to superposition of contributes from BHEs and GeothermSkin system. For the sake of consistency a COP of 4 was assumed to calculate the deliverable energy. Assessment of the satisfaction ratio was carried out for conductive contribution only (with the *classic* G.POT. formula) rather than for advective and dispersive contribution too. In this latter case the adapted version of the formula proposed (Equation 4.12) was employed. The results obtained are mapped in Figure 6.31.The definition of the most productive scenario is of clear interest even if the approximation in energy needs assessment ant the optimistic application of SGE in existing buildings affected the accuracy of the assessment. This scenario suggests that geothermal energy may effectively play a significant role even without maximising the utilization of the resources.Another scenario analysed, according to Chapter 4, the potential satisfaction ratio in the case that BHE can be installed only in a limited band around the perimeter of each building. For the sake of consistency, also in this case the assessment was carried out for conductive contribution only and for the hydrodynamic contributions too with the enhanced formula proposed in this work (see Figure 6.32). It is evident from comparison of the two scenarios analysed that in the latter case lower satisfaction ratio are obtained as a result of the lower extension of the area where BHE can be drilled. As mentioned in Chapter 4, the latter one may be more representative of drilling with the actual building heritage, without considering demolishing and rebuilding. This is obviously true in the major part of the studied area as central districts include historical buildings that are subjected to architectural-historical heritage constraints. This might not always be the case at the outer portions of the study area. It should also be mentioned that public areas and the entirety of the private courts are not included as this second scenario account the building surrounding only.
Further scenario may analyse the installation of BHE fields in public areas and in the surroundings of the buildings, namely within the pertinent cadastral plot. These areas account for the 65% of the total geothermal potential within the domain.

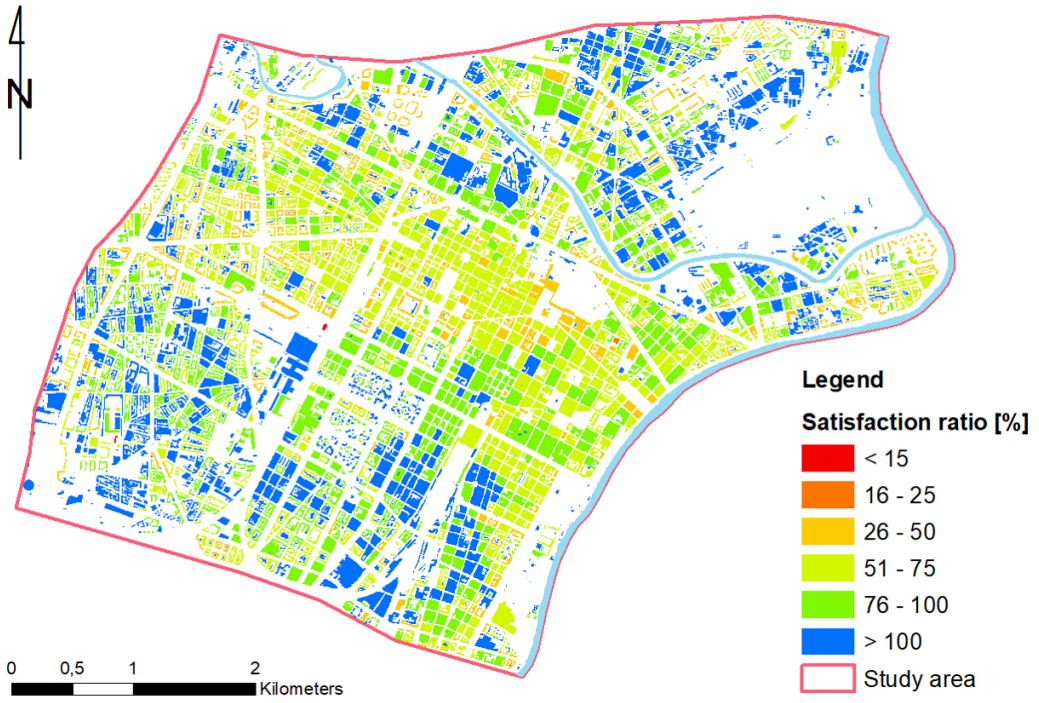

(a)

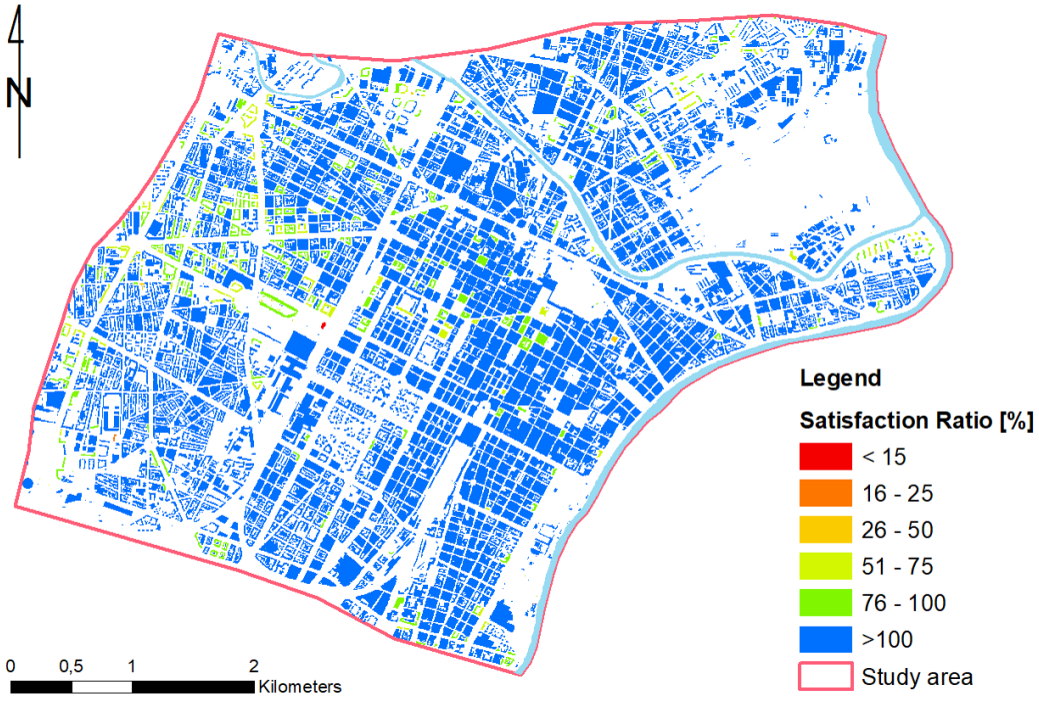

(b)

Figure 6.31: Satisfaction ratio of the buildings energy needs from geothermal energy accounting for BHE installed within the footprint of the built area. (a) Classic G.POT. formulation (conduction only) and (b) adaptation of the G.POT. formula proposed in this work (advective and dispersive components) are considered.

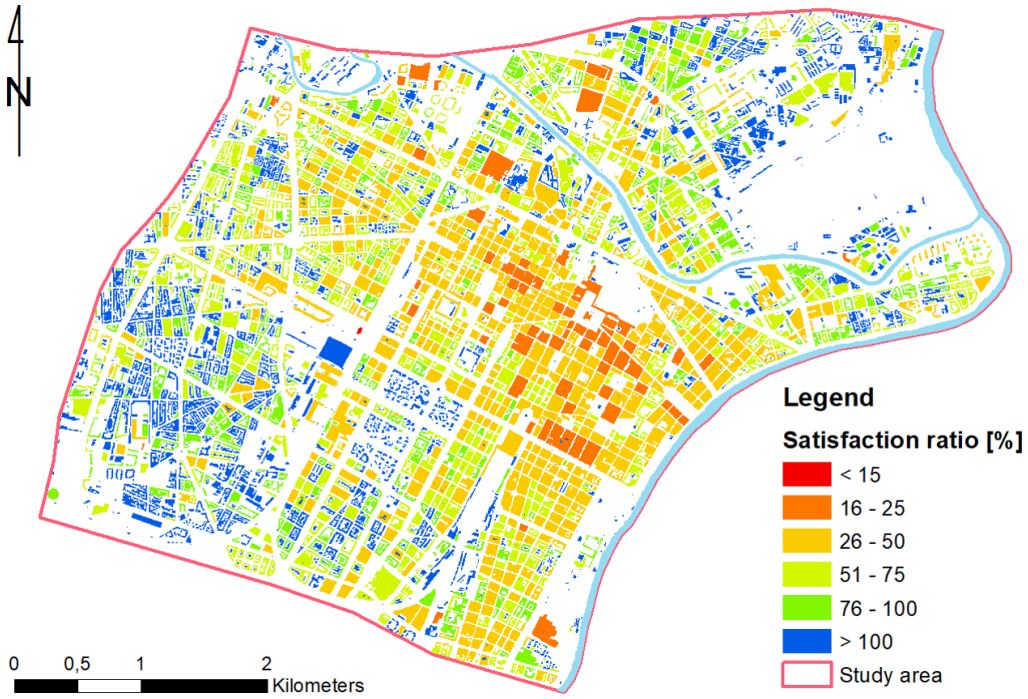

(a)

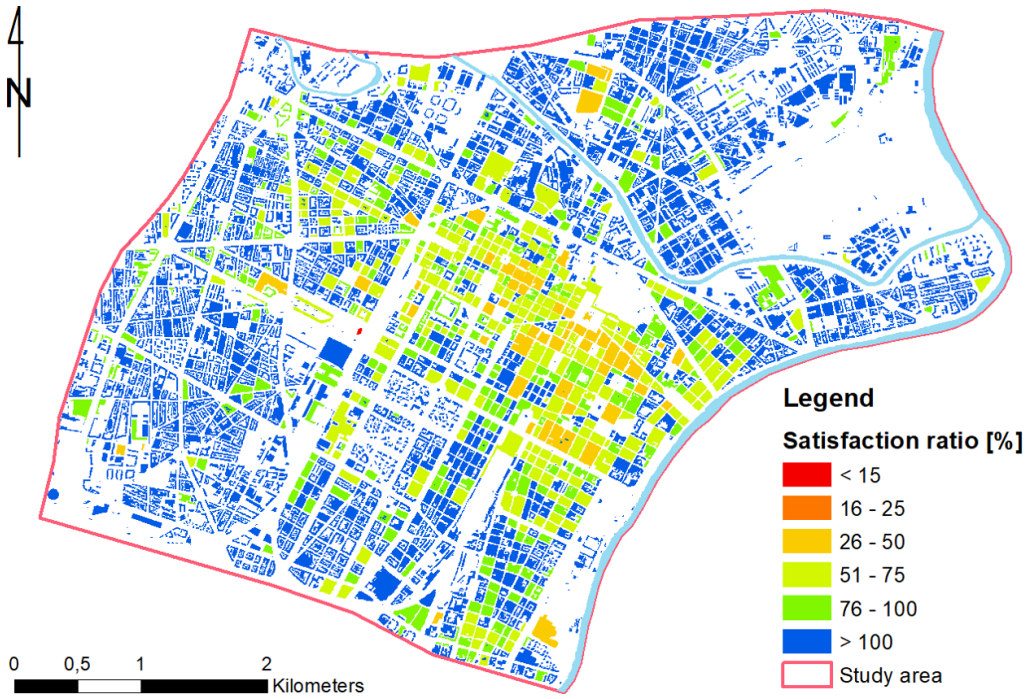

(b)

Figure 6.32: Satisfaction ratio of the buildings energy needs from geothermal energy calculated by (a) classic G.POT. formula (heat conduction only) and (b) the corrected formula proposed in th this work (advective and dispersive components). A band of 7 m around built perimeter was considered as BHE drilling area.

Predicted energy surplus distribution clearly highlight the higher potential obtained by accounting the advective and dispersive contribution. In the purely conductive scenario, the city centre generally shows lower ratios and only a few cases virtually can produce an energy surplus. On the contrary energy surplus is more frequent when moving towards the periphery. The scenario that takes into account the groundwater fluxes thanks to the proposed adaptation of the G.POT. formula on the contrary shows lower values of the SR in the west and north sectors. This can be related to diverse destination use and age of construction in these sectors. From the second scenario, it can be seen that about 62% of the built area (representing about 57% of the volume to be heated) can rely on geothermal energy for full satisfaction of the thermal heating load. Among the remaining 38% , a share of 87.4% can satisfy requirements for energy supply from renewable sources (that are imposed to new constructions and refurbished buildings by regulation). Energy needs are largely not met virtually only in the case of the tallest buildings in the metropolitan area.
In the perspective of optimisation in the use of shallow geothermal resources, these highly-demanding structures can be supported by neighbouring buildings that present an energy surplus. This would lead to smart communities and smart thermal grids. In this perspective, the refined assessment of the geothermal potential would be useful in order to optimise the number of installations and the grids extension. From a purely conductive conservative evaluation the thermal grids would be forced to cover significant distances that may prevent stakeholders interest.
Finally a better and less conservative (but still safe) assessment of the potential may lead to the optimisation of the dimensions and number of the exchangers even at the single installation scale.

6.6 Summary

The Po valley is one of the areas that most suffer from air pollution in Europe because of the peculiar geographical settings and the intense urbanisation. The metropolitan area of Turin lies in the western part of this area and represents the second city in northern Italy and the fourth in the country. The city energy demand is enormous and a relevant part of it is related to the heating and cooling loads of buildings.
In this perspective, geothermal energy has already been addressed as a valuable resource because of favourable groundwater flow settings. Several open loop systems have been installed in last decade (Barla et al., 2018). This generated some concerns on possible overexploitation of the resource.
In this chapter the application of the *rOGER* method to a central portion of the City of Turin is presented. The efficiency and the capability of the method is demonstrated with reference to the study area. As a result of the application it was possible to evaluate the geothermal potential of the domain of interest, the optimisation in resource

usage and its possible impact on the energy balance were evaluated. In particular the methodology developed in the previous chapters was here applied to the specific context of Turin. By applying the methodology the major limits, drawbacks but also the advantages of the procedure were highlighted. Although the input data were to some extent affected by uncertainties, the application of the procedure allowed to build a representative model of the thermal and hydraulic regime. The applicability of the process to data that are to some extent incomplete testifies an intrinsic flexibility of the assessment procedure. Indeed when inputs are scarce or poor in quality, several scenarios can be analysed thanks to the flexibility given by numerical analyses. Although enhancement in the input data quality was beyond the scope of this study, both the geographic database and the numerical models can be used in the iterative refinement of the assessment whenever new data are made available.
In the specific context of the study area, the data availability and the construction of a conceptual hydrogeological model was exposed with reference to an area of about 25.7 km^2 up to 100 m depth. Special attention was devoted to the shallow aquifer where anthropogenic heat fluxes are present. Furthermore time-dependent boundary conditions characterize the thermal and hydraulic regime of the studied volume. The numerical modelling phase, together with the collection of monitoring data allowed to infer the substantial consistency of the simulated behaviour with real settings. The general suitability of the models in the predictive analysis of the thermal and hydraulic regime was used to investigate the long term potential. The scenario accounting for the future persistence of the actual level of underground utilization was analysed.
The heterogeneity in the temperature field allowed to identify some quali-quantitative key indicators related to actual utilization level. It was found on a quantitative basis that the subsurface use is partly unbalanced towards aquifer heating. Indeed temperatures results to be locally elevated or, in narrower areas, decreased. Residual admissible temperature drop and the Integrated Relaxation Factor confirm this conclusion. The optimal location for future installation can be hence deduced. The promotion of discordant thermal injection at precise location can be pursued as a remedial strategy for thermal imbalance.
The hydraulic and thermal regime of the studied domain was then employed for borehole heat exchanger potential assessment by including also the advective and dispersive components of the heat transport. This was possible trough the application of the enhanced version of the G.POT. formula developed in this study. It was found that the enormous heating load of up to 11400 GWh/y can be provided by the subsoil in the area, with particularly high values of about 25 MWh/y concentrated in the north and east part of the studied domain.
Profitable energy from energy wall system described in previous chapter was derived by geospatial analysis of the built heritage. The heating loads of buildings were as well approximatively calculated by means of the geographic information system that underlies the entire geothermal potential assessment process. The analysis of energy demand

and geothermal supply allowed to highlight that energy wall systems may provide a significant contribution to reach minimum requirements with respect to the supply from renewable sources. Results show that the energy needs of the most part of buildings may be completely satisfied when GeothermSkin is adopted in combination with borehole heat exchangers. Especially in the case that advective and dispersive contribution can be taken into account by means of the proposed formula, local energy surplus can be used to optimise the number of installation and to generate local and smart thermal grids.
In conclusion, the flexibility and the ability of the method in defining the geothermal potential and some elements for the optimal use of the resources were demonstrated by the application of the *rOGER* method to a wide urban area.

Chapter 7

Concluding remarks

Shallow geothermal energy is a renewable, pervasively distributed and stable source of energy. The affirmation of the technologies based on shallow geothermal energy for heating and cooling buildings is gaining attention in urban areas. Main issues related to such technologies are related to the lack of reliable tools to preliminary evaluate the profitable energy at the single installation scale. The need arises for a sound rational resource management able to avoid overexploitation, environmental damages and market unfairness. Geothermal potential assessment needs then to address both these issues. This may allow for the optimisation in the spatio-temporal use of the resource and to eventually get the most from the subsurface while limiting adverse environmental effects.

In urban areas anthropogenic heat fluxes and subsurface structures have the potentiality to significantly alter the potential natural state. In order to improve the use of shallow geothermal resources in this context, it was decided to study a geothermal potential assessment procedure that allows for the accounting of real thermal state elaborated by means of numerical analyses. Indeed numerical modelling can reconstruct the highly heterogeneous thermal regime of entire cities or districts and allow for prediction in the long term under different scenarios too.

Optimisation in the use of shallow geothermal resources passes through the spatio-temporal enhancement of installation deployment and a rational and sound planning. Nonetheless the use of very shallow geothermal resources is difficult in urban areas due to land scarcity issues. Hence a novel vertical very shallow system dedicated to anthropic structures was developed in this study to employ this usually overlooked subsurface portion.

Such theoretical concepts were then applied to a study area in Turin to provide a preliminary evidence of the capabilities of the tools developed.

With the intent to summarise the work of the present Thesis, the following paragraphs revisit the main tasks accomplished and describe the aspects that should be further investigated in future studies.

7.1 Shallow geothermal energy use and borehole heat exchangers technical potential

A detailed bibliographic study was carried out to describe the principles and technologies currently adopted for shallow geothermal energy use and management. Technological aspects together with the physics principles and the legal bounding aspects allowed for a clear and unambiguous definition of the meaning of *technical geothermal potential*. Its optimal use and planning at the city scale represents the main focus of the Thesis.
A series of methods previously proposed in scientific literature were revisited and categorised on the basis of the qualitative rather then quantitative nature of the outcomes. As the specific installation typology binds the definition of the technical geothermal potential, the distinction among assessment methods was carried out accordingly. Particular attention was devoted to Borehole Heat Exchangers due to their prominence in the closed loop shallow geothermal systems market.
The attention was hence moved to the semi-analytical G.POT. method (Casasso and Sethi, 2016) due to its soundness in potential assessment and easiness of implementation on geographic information systems. Although the accounting of heat transport components related to hydrodynamic regime was demonstrated to be extremely relevant (García-Gil et al., 2015a), the G.POT. method is derived for purely conductive scenarios which are usually not representative of real cities settings. In fact cities are usually located where ground and surface water resources are widely available.
A parametric numerical study was thus carried out to the sake of extending the field of validity of the above mentioned formulation to hydrodynamic conditions. Multiple corrections were adopted to re-conduce the vectorial fields to the scalar value of the geothermal potential. In particular the first invariant of the thermal conductivities second order tensor was adopted. The pertinent corrections were calibrated on the basis of the relative importance of the conductive component against the advective and dispersive ones, namely the Peclet number.
Vertically heterogeneous settings, representative of urban settings where interferences among installations may occur, were carefully studied as well. Results confirm that a good value of the vertically heterogeneous site characteristics can be obtained by depth-weighted averaging the pertinent values along the whole depth of the borehole.
It should be noted that the entire formulation is based on the theory of the Infinite Line Source. This means that the vertical extension of the geothermal installation has to be extremely larger than the horizontal one. This hampers the applicability to short boreholes and to energy piles. Further research in the field may address these issues by moving from the Finite Line Source model rather than by analysing adaptation of the potential formula. In this latter case the ratio of planar to depth dimensions ratio can be regarded as one of the parameters to accurately analyse.

7.2 The rOGER method for the assessment and the optimisation of geothermal potential use

Shallow geothermal potential depends on site specific characteristics and hence may present relevant spatial variability. The highly variable and complex interaction in the subsoil at the district and city scale of active and passive users, structures and infrastructures requires flexible and powerful tools to investigate the thermal and hydraulic regime and to predict future scenarios. Geographic Information Systems are extremely suitable in potential assessment procedure as widely demonstrated in previous studies. Numerical modelling approach was futhermore selected to accurately analyse the transient hydraulic and thermal behaviour.
The attention was then focused on a procedure that helps decision makers and stakeholders to optimise the use of shallow geothermal resources. The *rOGER* method was thus conceived in four main steps. It is based on the combined use of Geographic Information Systems and detailed numerical tridimensional models able to account for coupled simulation of hydrodynamics and heat transport.
At first the main elements characterizing the GIS and pertaining dataset were exposed and classified in four main categories: *hydrogeology, entities producing thermal and hydraulic impact, built environment* and *hydro-thermal regime*. Mutual relationship and nature of such dataset was analysed with the intent of highlighting the useful elements that are then exchanged with the numerical model codes.
Secondly the numerical analyses are adopted to obtain a fine reproduction of the thermal and hydraulic regime of the studied domain before being post processed again within the GIS platform.
Treatment of the numerical results constitutes the third passage of the rOGER procedure. This step is devoted to the local geothermal potential assessment through manipulation and post-processing of the data in the *hydro-thermal regime* category. To this end the enhanced formulation for BHE potential assessment in hydrodynamic conditions is adopted to fully get advantage of the numerical modelling capabilities.
The final step of the procedure assesses at the scale of the district or of the city the best locations and strategies for spatio-temporal optimisation in the use of shallow geothermal resources by aggregating site-scale geothermal potential and geo-processing these data with the energy demand. In this perspective, the addition of very shallow geothermal systems can be adopted to unlock, at low market prices, the potential of the first meters below ground without exploitation of large horizontal areas. To the end of best locating new installations, a bunch of indicators may be used like the *residual temperature shift, Integrated Relaxation Factor, Satisfaction ratio* and the same *geothermal potential*.
It should be noted that the geothermal potential is calculated over a regular grid of points. Each of these points virtually represent a possible borehole installation. The potential mapping is carried out under the assumption that no interference takes place

among these virtual boreholes and thus the calculation grid needs to ensure this requirement. In this study the minimum distance of 7 m was chosen on the basis of commonly accepted values. This distance might be further optimised in most cases based on thermal loads and site conditions (especially groundwater flow).
The choice of the grid resolution has a dramatic impact on the above mentioned indicators. Further research in the field may consider the adaptation of the calculation grid to the site settings. Full optimisation of the geothermal resource use should further move towards the use of distinct depths in the perspective of balancing the thermal fluxes to the subsoil and hence preserving the resources and the environment.

7.3 A novel energy wall system for very shallow potential use

Urban areas suffer from land scarcity issues. This constitutes an hampering factor in the adoption of horizontal collectors, geothermal baskets and very shallow geothermal systems in general. Hence the potential at very shallow depths is rarely used.
On the contrary the use of energy geostructures is appealing even if limited to new constructions. A novel energy system was conceived to be applied at the external side of ground-contact surfaces of buildings that include underground levels used as cellars or car park. The external deployment allows for easy installation and application also in existing buildings that undergo advanced refurbishment. Both new and newly refurbished constructions indeed need to cover half of the energy needs from renewable sources due to bounding legal requirements.
In this perspective the novel energy wall system was developed and the first system prototype was installed in an experimental site. The experimental campaign approximately quantified the thermal efficiency in winter heating mode in the range of $15 - 24\ W/m^2$. The monitored temperature values in the ground suggest that thermal effects on the subsoil are negligible at the very short distance of 2-3 m from the equipped surface. Hence the potential of such an application can be virtually overlapped to the potential of deeper systems without undermining them.
Starting from this evidence, some projections were performed with reference to a study area in the central portion of Turin and its built heritage.

7.4 The application of the rOGER method to the central districts of Turin metropolitan area

The rOGER procedure developed in this Thesis was applied to the real settings of the central districts of Turin, Italy. The potential from the novel *GeothermSkin* energy wall system was calculated at the city scale too.

In particular the definition of an hydrogeological conceptual model and the identification of the key aspects of the subsurface allowed to identify a study area of about 25.7 km^2 as domain of interest. A depth of 100 m typical for borehole systems was investigated. A satisfactory detail was achieved as regards the shallower depths up to the base of the shallow aquifer. On the contrary, the deeper multilevel aquifer detail can be enhanced by interpretation and representation of the levels interested by groundwater fluxes. This aspects were however beyond the scope of this study that focused on the extremely productive shallow aquifer.
The creation and management of a georeferred database resulted in the collection of a wide variety of data from environmental monitoring network pertaining to groundwater, aquifer thermal users and surface water bodies. Although the data collected are to some extent incomplete the application of the procedure allowed the set up of numerical analyses able to capture the hydraulic and thermal regime of the area. Representativeness was obtained through numerical calibration and verified against measured data.
Handling of the data about built environment was carefully carried out with the intent of generalising the pertaining geometrical representation. Indeed the 71000 polygon features were strongly reduced to about 150. Such number of entities can be then handled in the numerical mesh generation process.
A finite element numerical model was accurately set up by superimposing the variety of data from the georeferred database. Analysis carried out allowed the prediction of a future scenario. A stable utilization level in the future was assumed to build the scenario in order to define the actual trend of shallow geothermal energy use.
History matching of numerical analysis resulted to be satisfactory in the major part of the points where real measures were compared. Furthermore the regime of the water table well corresponds to expectations from previous studies (Civita and Pizzo, 2001). Also comparison of temperatures downstream to open loop systems is in most cases more than satisfactory. In some cases almost perfect matching was achieved. The good general agreement of thermal data seems to suggest that the numerical model is able to appropriately capture the thermal and hydraulic regime of the area.
Resulting temperature and hydraulic dynamic distributions were then post processed within the GIS database to obtain indicators of actual level of utilization of geothermal resources. Elements for optimisation of new plant location were derived taking into account the heating season in the long term. Obtained Integrated Relaxation Factor values were limited to 0.4 while being slightly negative in some portions of the area due to the unbalanced cooling load. Evidence of this unbalance comes also from the comparison of thermal maps elaborated for past and future years. To this regard, this work contributes to highlight best locations for new installations. A system of subsidies could be envisaged to stimulate appropriate location of new installation considering them as a remedial measure to the current unbalanced situation.
Geothermal potential calculation was performed thanks to the enhanced version of the G.POT. formula developed in this Thesis. High values of up to 26 MWh/y were obtained. Comparison of the distributions in hydrostatic and hydrodynamic conditions

delineates the relevance of the high groundwater flow in the determination of the potential within the area.
It results that the best location within the study area for new geothermal installation is at the confluence of the Dora Riparia and the Po river, where a single BHE can provide up to 2.97 kW.
It should be noted that also the choice of the thermal dispersivity value has a relevant impact on the final results. Although a reasonable value for the area was employed, the related uncertainty that reflects into potential assessment might should be further limited by in situ testing rather than numerical calibration.
The preliminary definition of the impact of shallow geothermal on the energy balance at the city scale was carried out by accounting the energy needs of built volumes. To this regard, a realistic assessment of the energy demand was beyond the aim of the study but can enhance the accuracy of the calculation of this indicator. The potential from the energy wall system developed within the framework of this Thesis was evaluated based on building footprint and height. It resulted that in most cases the system may provide up to half of the required energy supply from renewable sources for new and refurbished buildings.
The impact of *traditional* BHEs installation was evaluated on the basis of the site specific geothermal potential mentioned before. The assumption of intensive drilling below existing buildings underlies this evaluation in a first approximation scenario. Although this is pretty unrealistic, the potential in the non-built area (e.g. appurtenant areas, green and public spaces) accounts for about two thirds of the overall potential and could be alternatively used. Further scenario analysis considered a band zone around building perimeters and resulted in more conservative evaluations from the quantitative point of view. Results suggest that by considering the enhanced version of the G.POT. formula, developed in this Thesis, buildings that may completely fulfil their heating demand by geothermal energy represent about 57% of the total volume. In addition to this also a large percentage of the remaining buildings can satisfy the requirements for supply from renewable energy sources.
Use of the local energy surplus can be envisaged to optimise the number of verticals to be drilled as well as the supplying to neighbouring units. To this regard this latter potential evaluation would suggest that the dimensions of such thermal grids may result sufficiently small to limit heat losses and investments related to energy transportation.
The application of the *rOGER* procedure to a wide area demonstrated the ability of the method to define elements for the optimisation of shallow geothermal energy potential use. The general validity of the elements composing the procedure, including the enhanced version of the G.POT. method developed in this Thesis, confirm the wide applicability of the method to all urban areas.

Appendices

Appendix A

Results from experimental campaign of the energy wall system prototype in Torino

The novel energy wall system prototype installed in Torino has been tested in several conditions. The main information of the experimental campaign are included in Chapter 5. In the following pages the extensive amount of data collected during those tests are reported in graphical form. Each paragraph is devoted to a single test whose main data are summarised in a proper table. Hence the interpretation of the test in terms of thermal performance is reported before introducing the data from the thermal sensors placed within the ground volume interested by heat exchange.

A.1 Test C_2-3_20190916_20190919

Table A.1: Main features of the test.

Test start time	16/9/19 10.30
Test end time	19/9/19 10.36
Duration [h]	72.1
Operative mode	Cooling
Active circuit(s)	2; 3
Circuit link	Sequential
Target temperature user [°C]	5
Flow rate at the ground side [l/h]	575

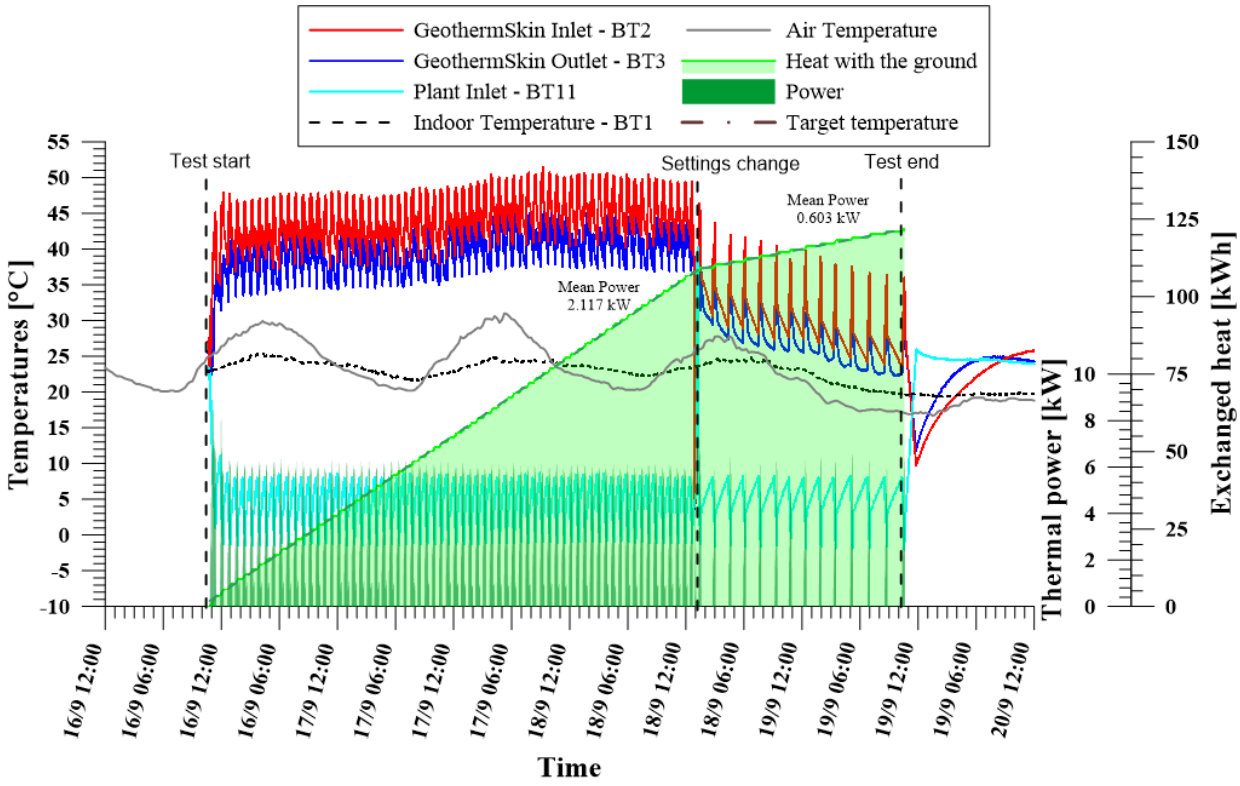

Figure A.1: Thermal performance interpretation of experimental test *C_2-3_20190916_20190919* with sequential link of circuit 2 and 3 in cooling mode.

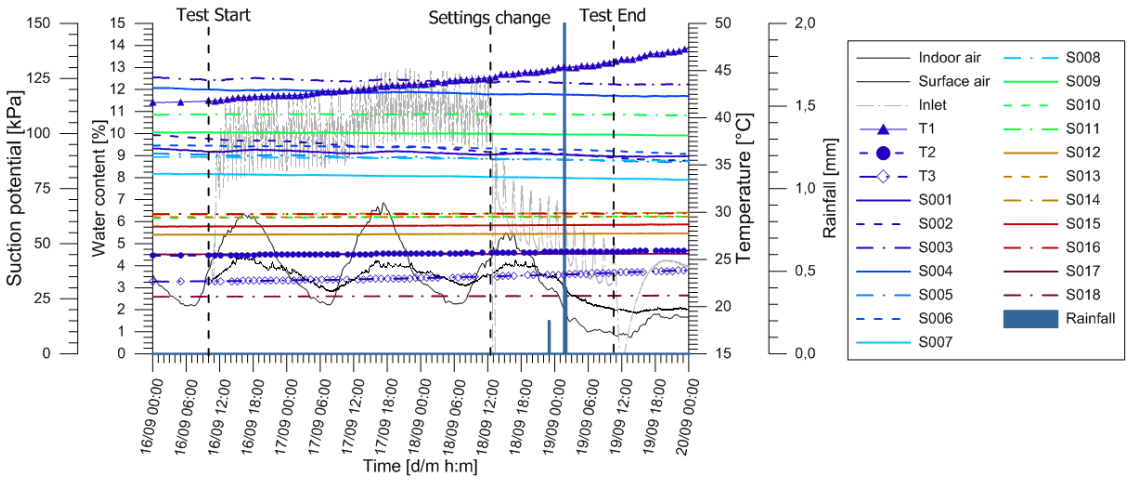

Figure A.2: Tensiometer and hygrometers records of experimental test C_2-3_20190916_20190919 together with monitored rainfall from Politecnico weather station.

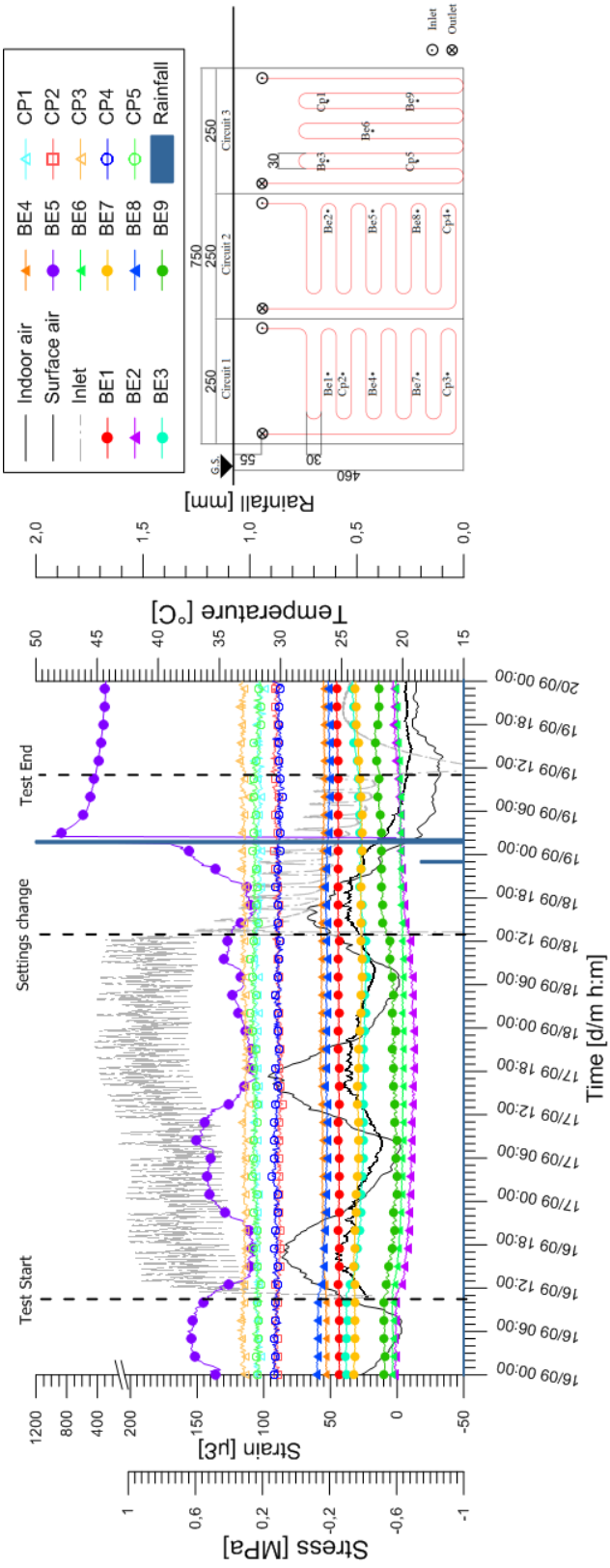

Figure A.3: Stresses and strains monitored at the wall external facade during experimental test C_2-3_20190916_20190919.

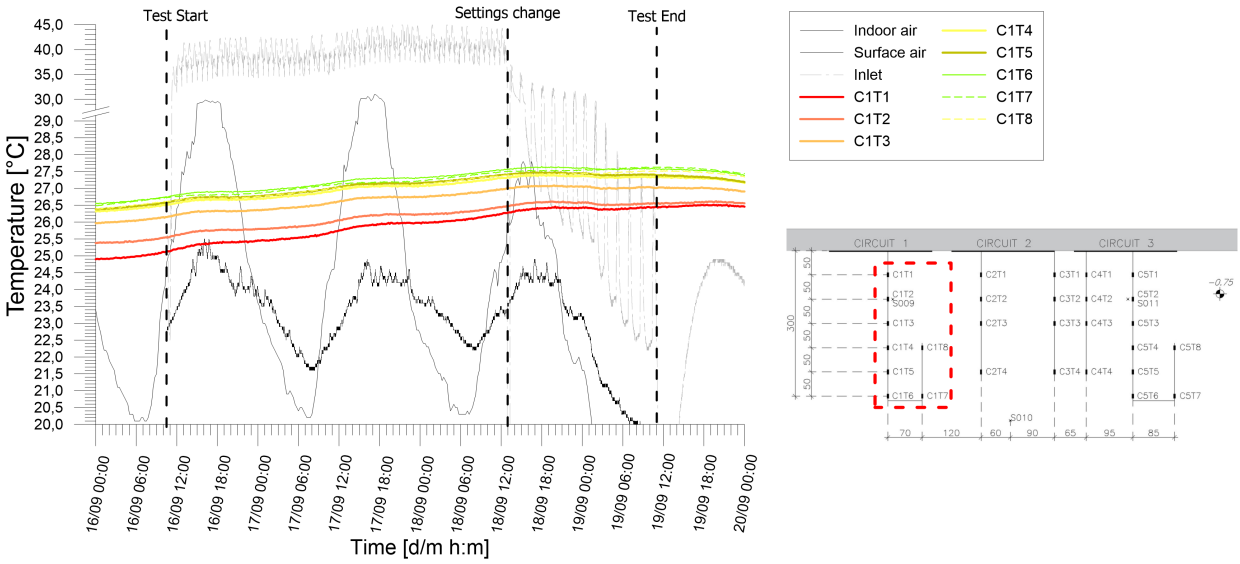

Figure A.4: Temperatures records from chain 1 of experimental test C_2-3_20190916_20190919.

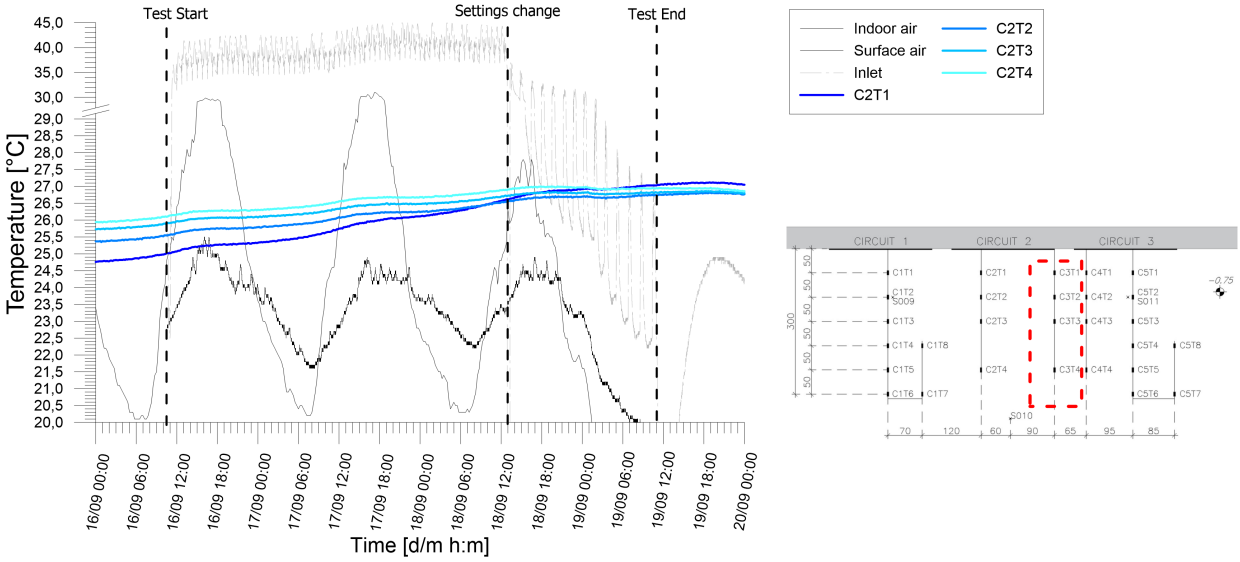

Figure A.5: Temperatures records from chain 2 of experimental test C_2-3_20190916_20190919.

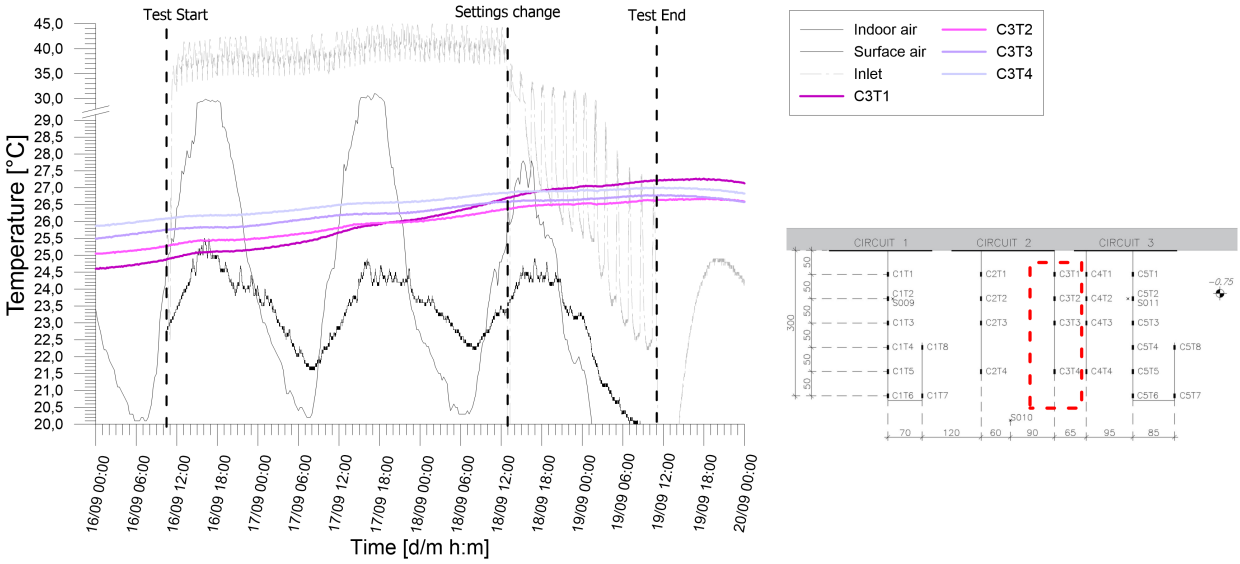

Figure A.6: Temperatures records from chain 3 of experimental test C_2-3_20190916_20190919.

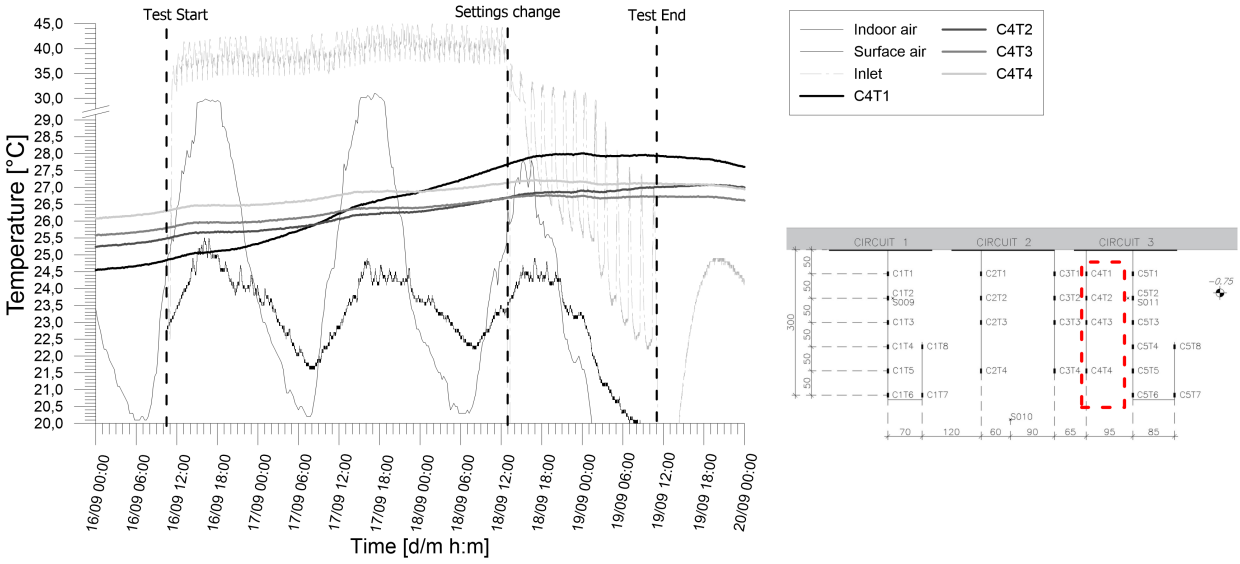

Figure A.7: Temperatures records from chain 4 of experimental test C_2-3_20190916_20190919.

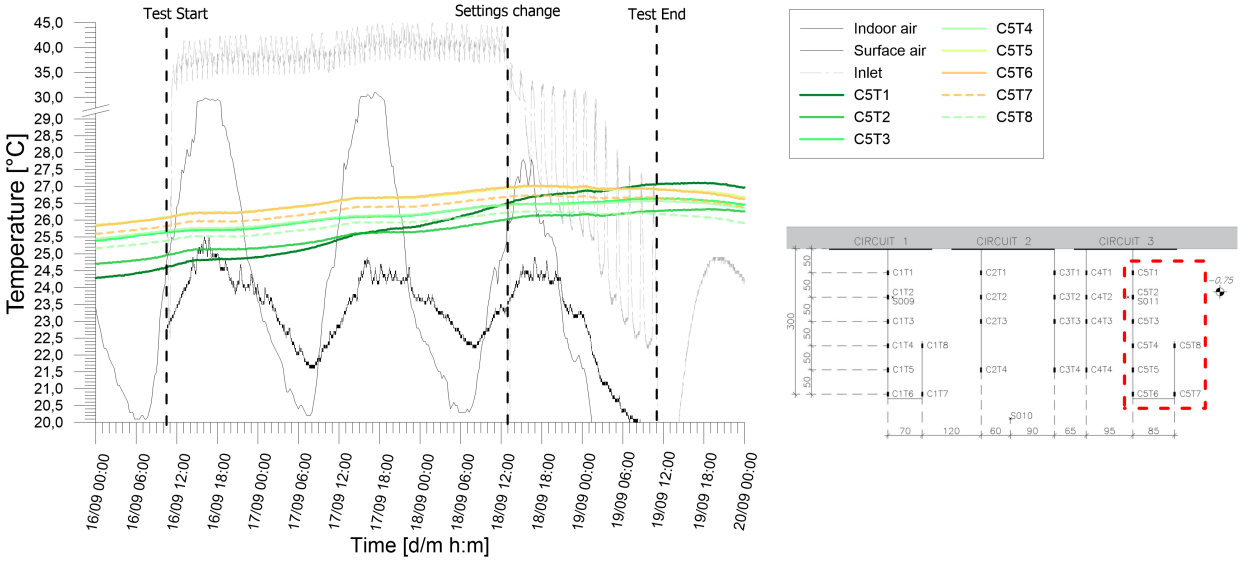

Figure A.8: Temperatures records from chain 5 of experimental test C_2-3_20190916_20190919.

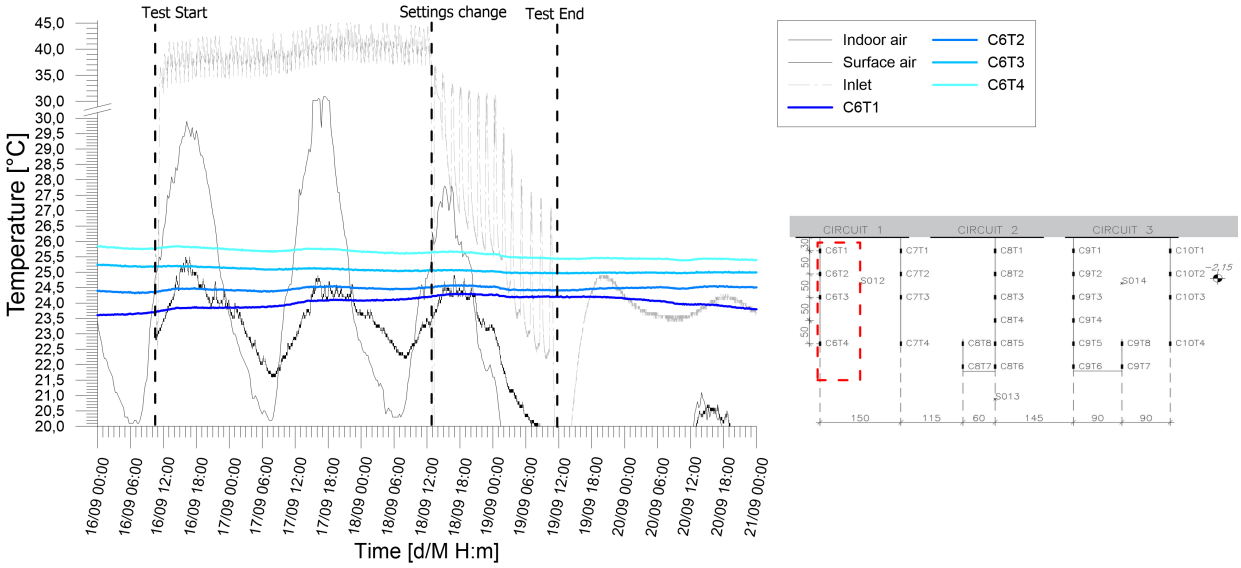

Figure A.9: Temperatures records from chain 6 of experimental test C_2-3_20190916_20190919.

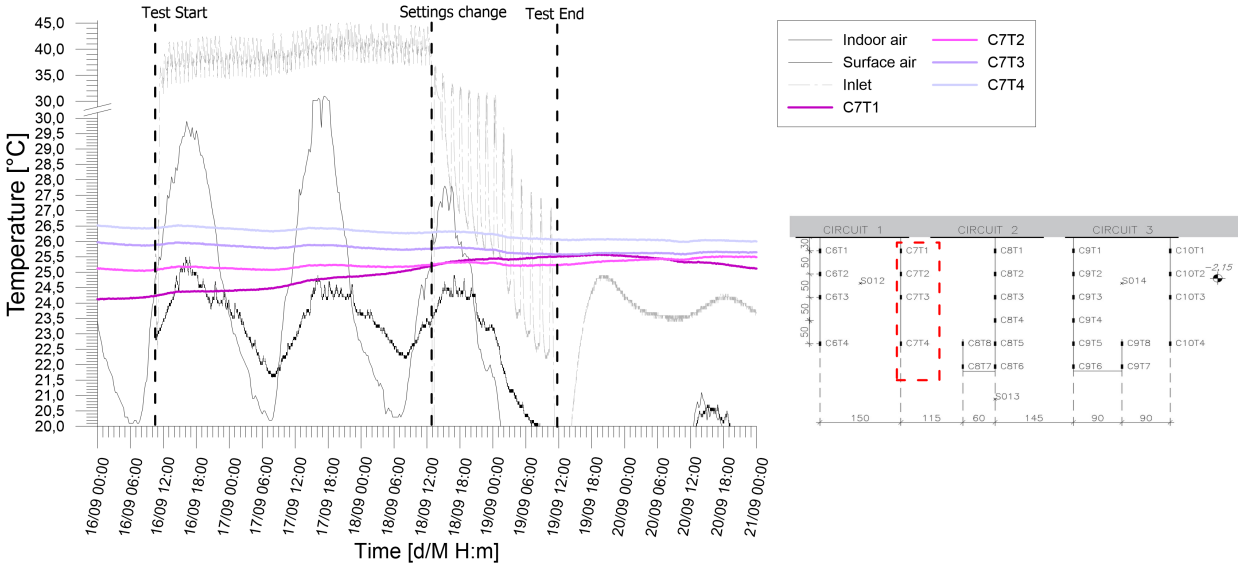

Figure A.10: Temperatures records from chain 7 of experimental test C_2-3_20190916_20190919.

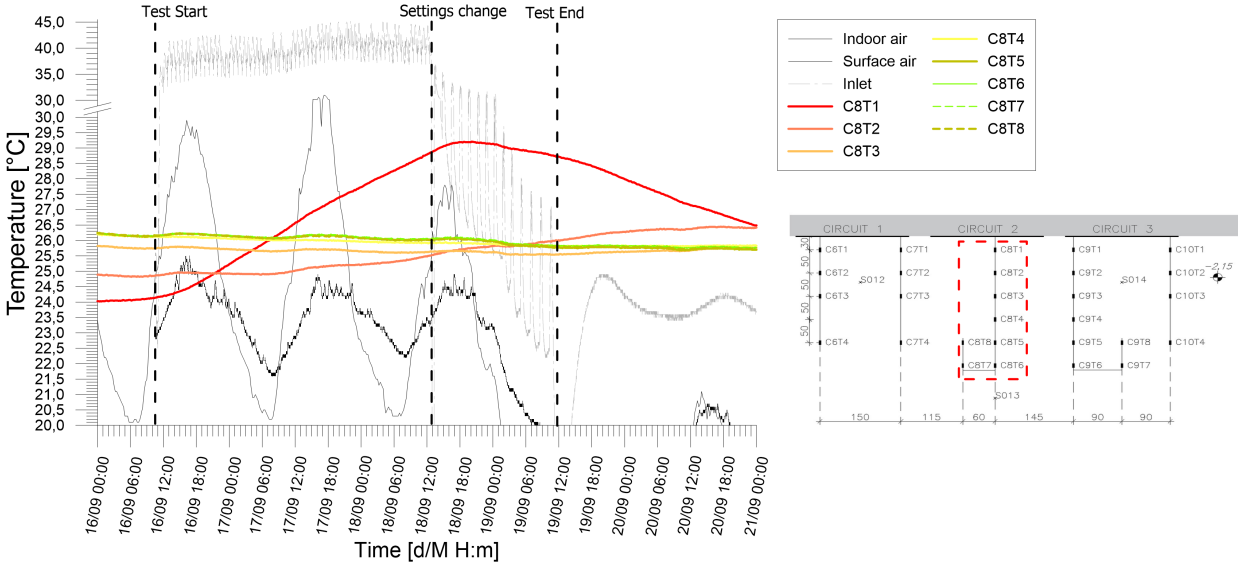

Figure A.11: Temperatures records from chain 8 of experimental test C_2-3_20190916_20190919.

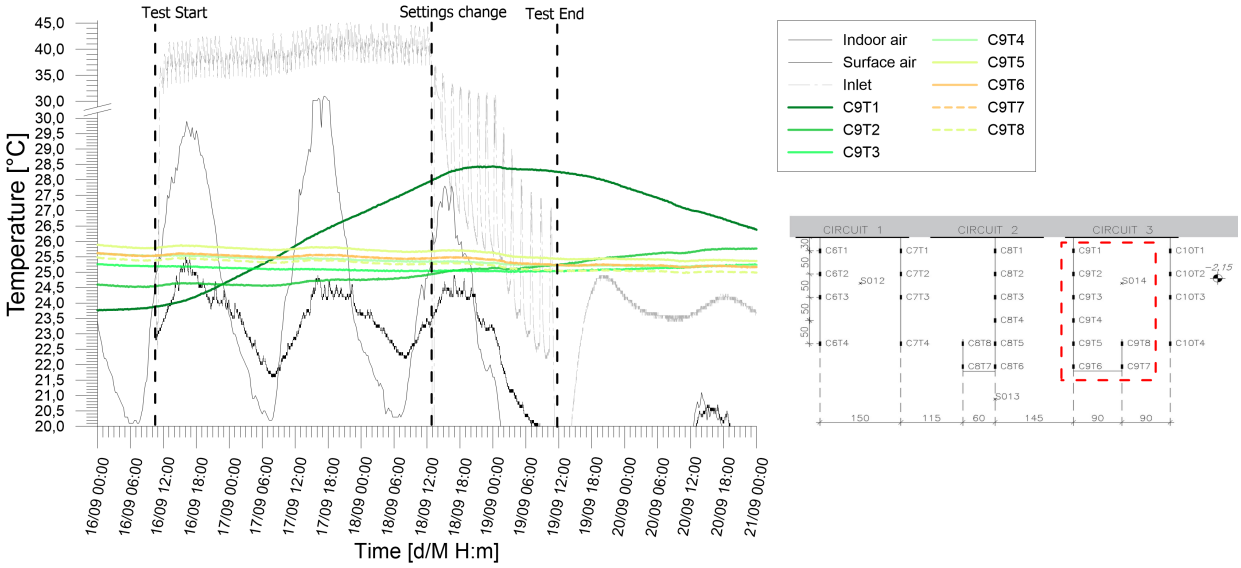

Figure A.12: Temperatures records from chain 9 of experimental test C_2-3_20190916_20190919.

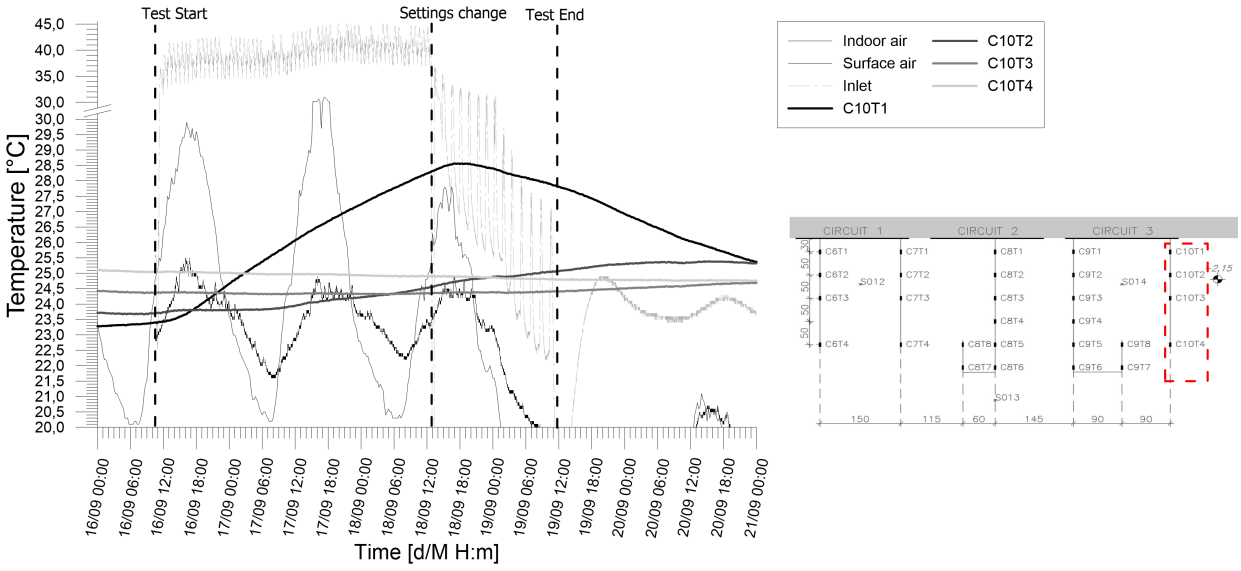

Figure A.13: Temperatures records from chain 10 of experimental test C_2-3_20190916_20190919.

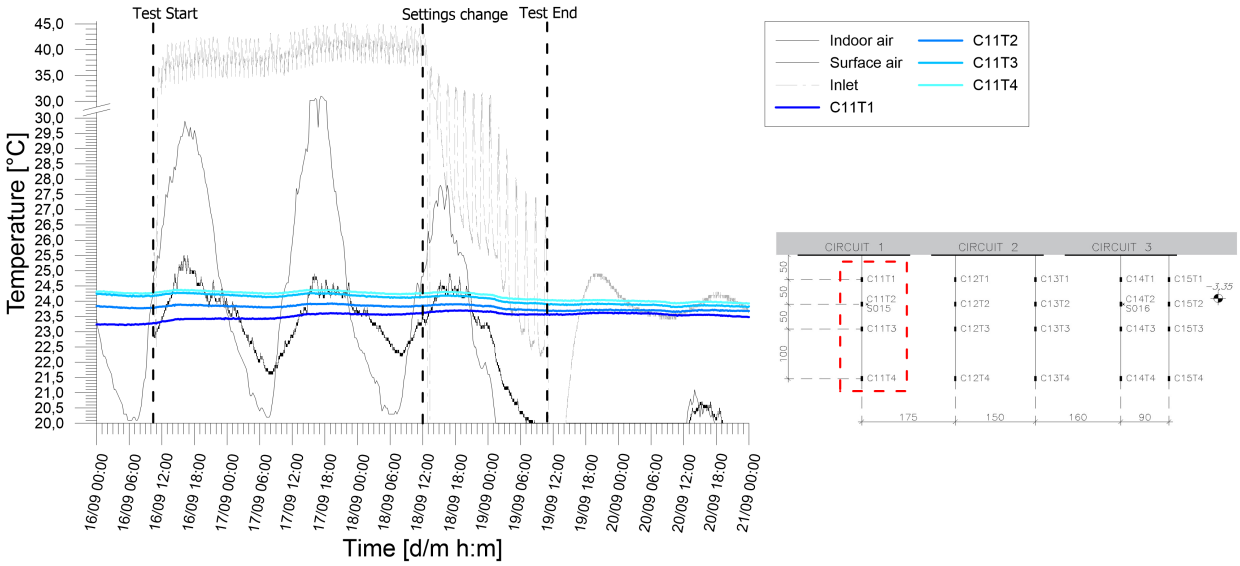

Figure A.14: Temperatures records from chain 11 of experimental test C_2-3_20190916_20190919.

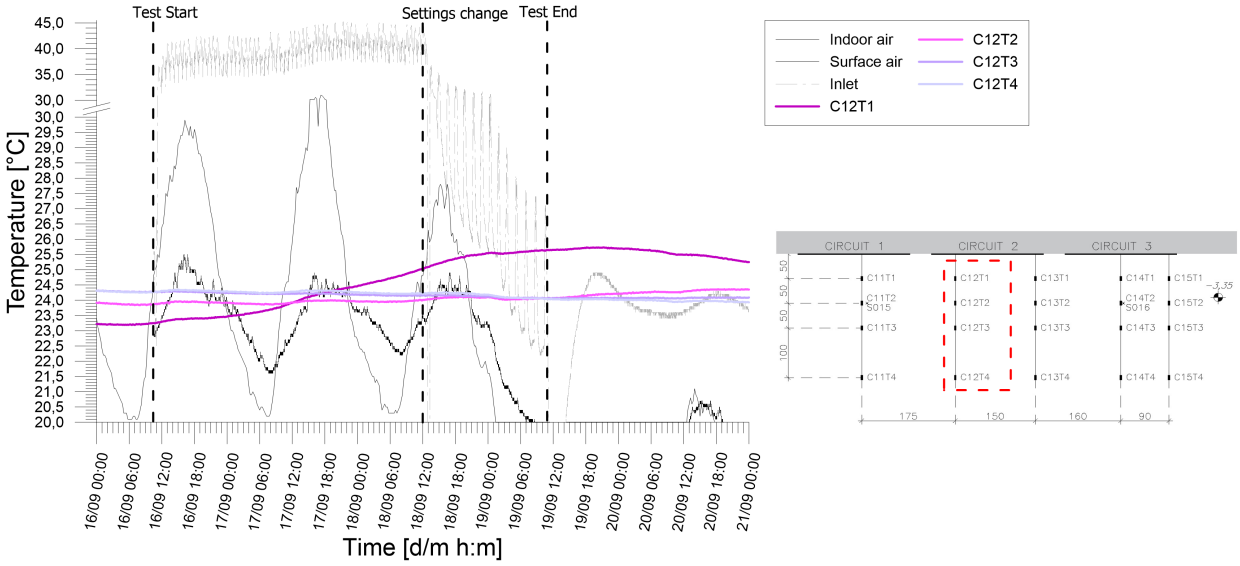

Figure A.15: Temperatures records from chain 12 of experimental test C_2-3_20190916_20190919.

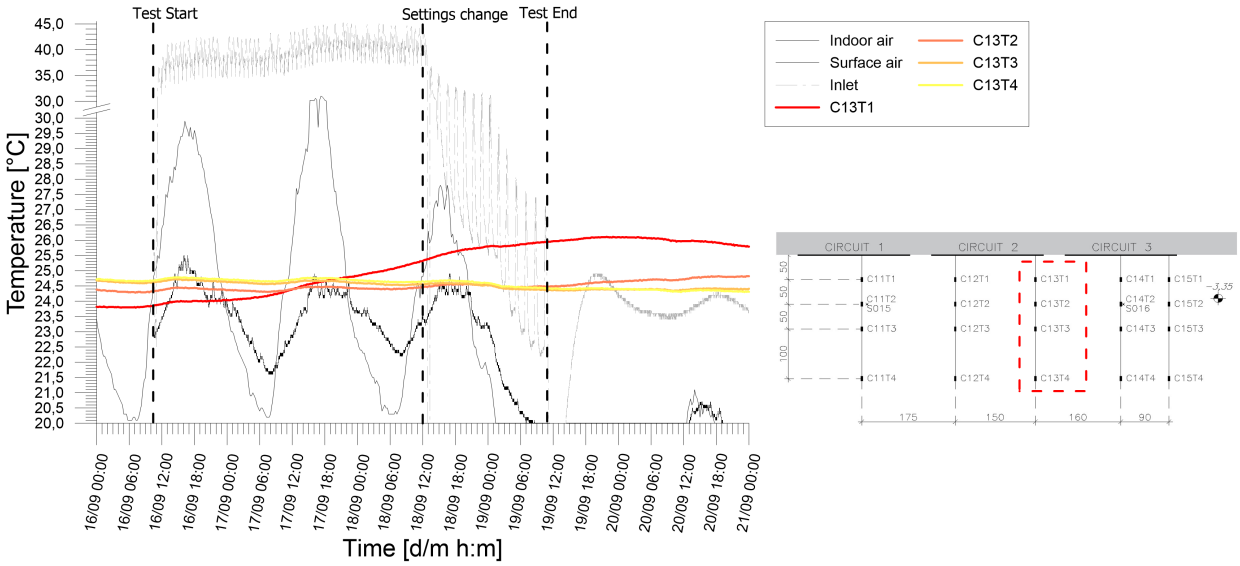

Figure A.16: Temperatures records from chain 13 of experimental test C_2-3_20190916_20190919.

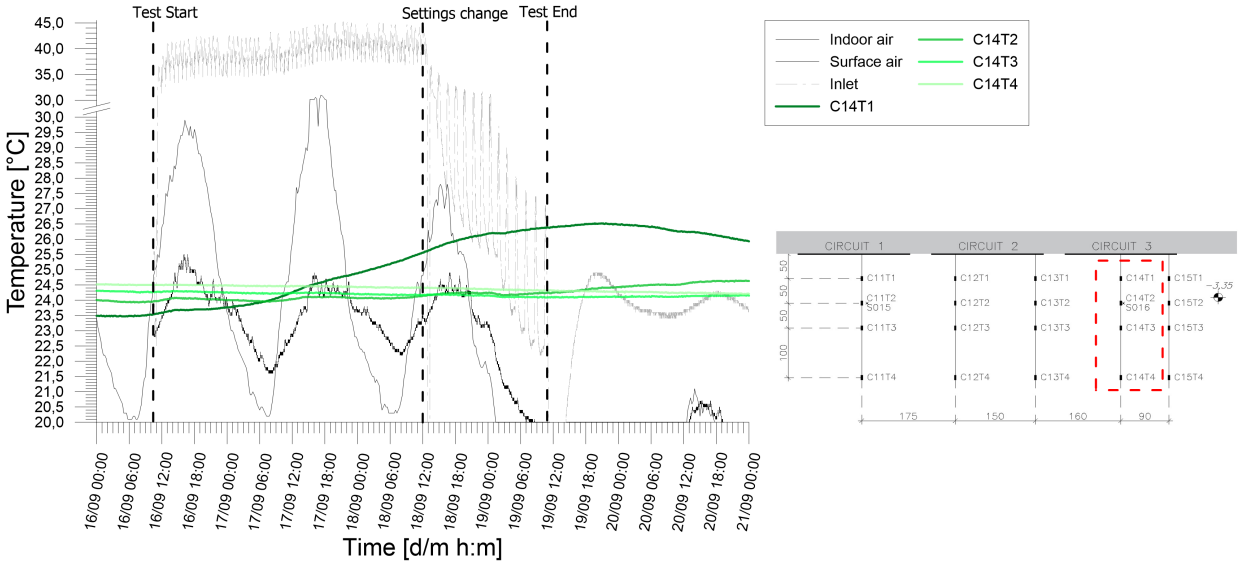

Figure A.17: Temperatures records from chain 14 of experimental test C_2-3_20190916_20190919.

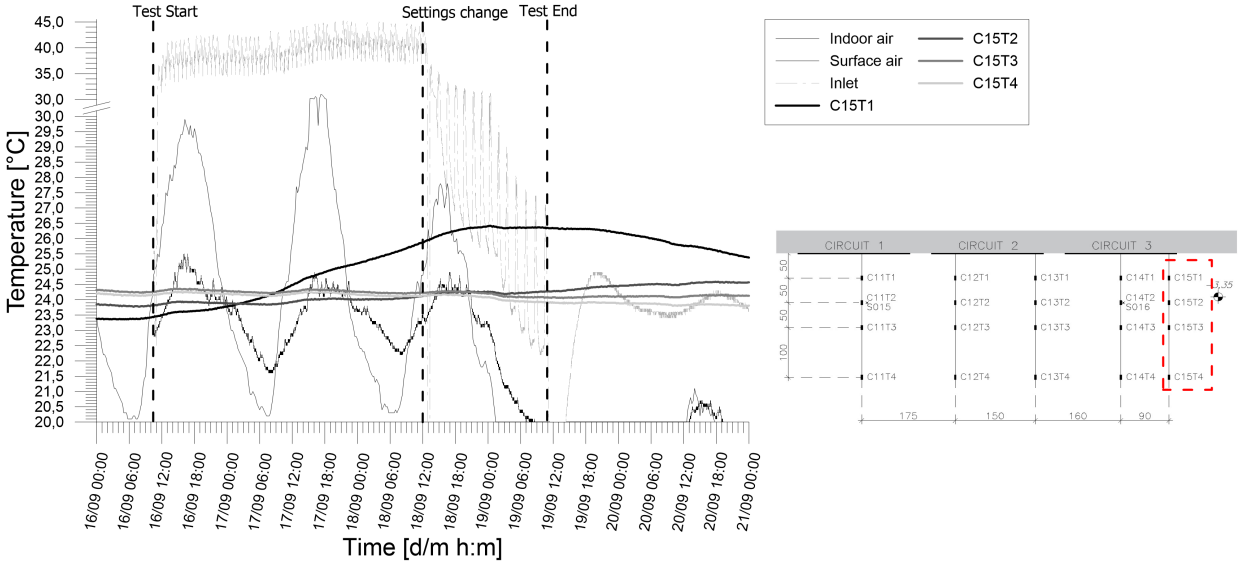

Figure A.18: Temperatures records from chain 15 of experimental test C_2-3_20190916_20190919.

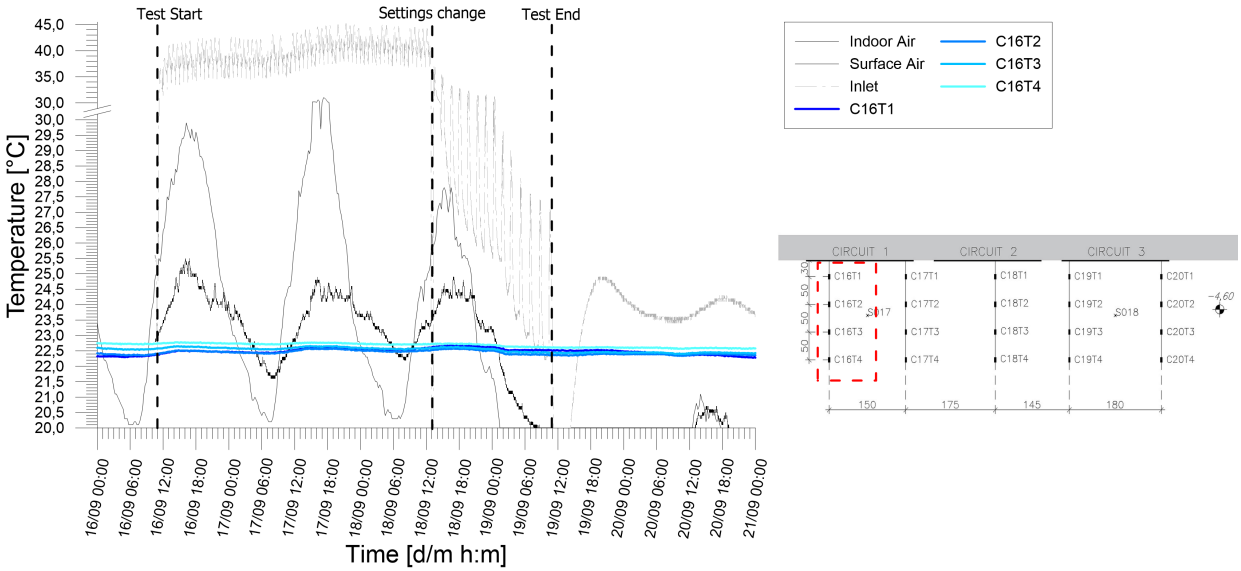

Figure A.19: Temperatures records from chain 16 of experimental test C_2-3_20190916_20190919.

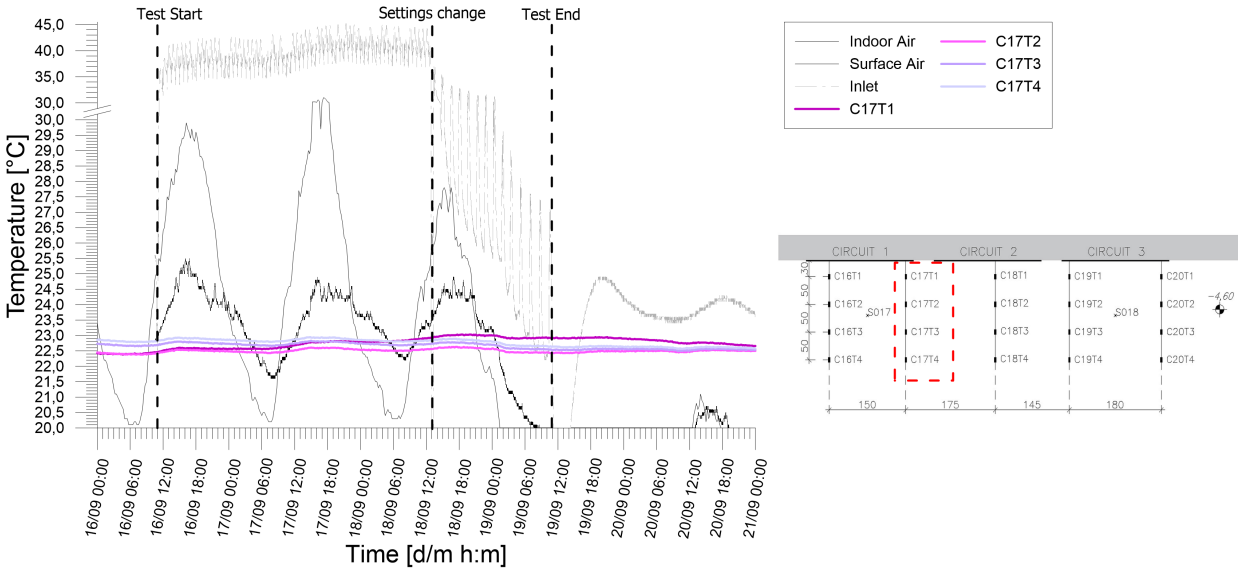

Figure A.20: Temperatures records from chain 17 of experimental test C_2-3_20190916_20190919.

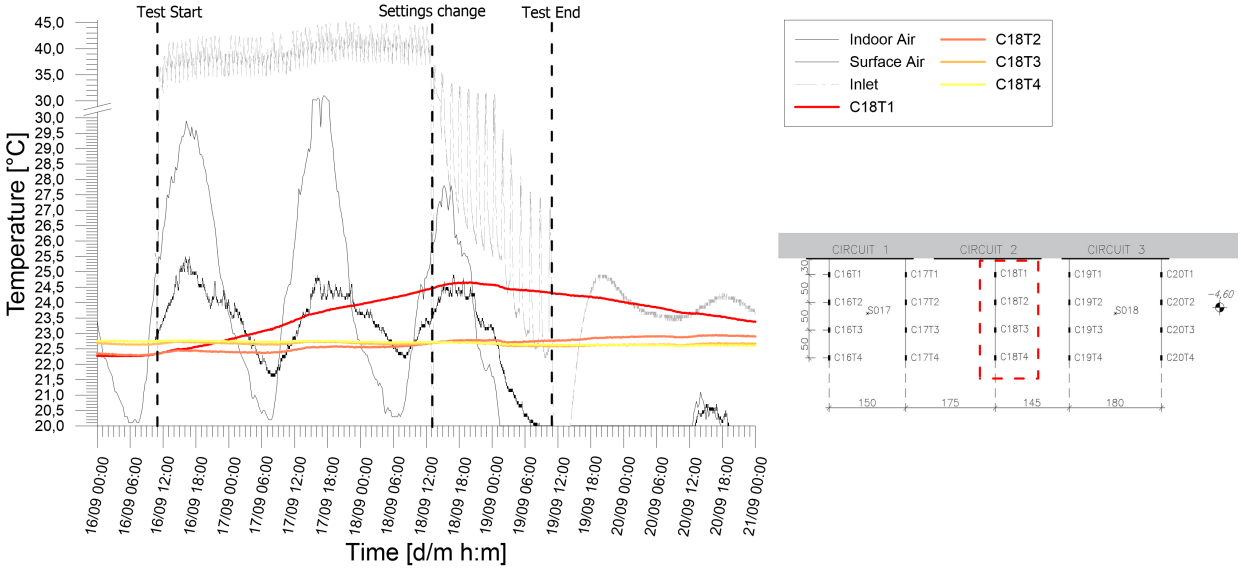

Figure A.21: Temperatures records from chain 18 of experimental test C_2-3_20190916_20190919.

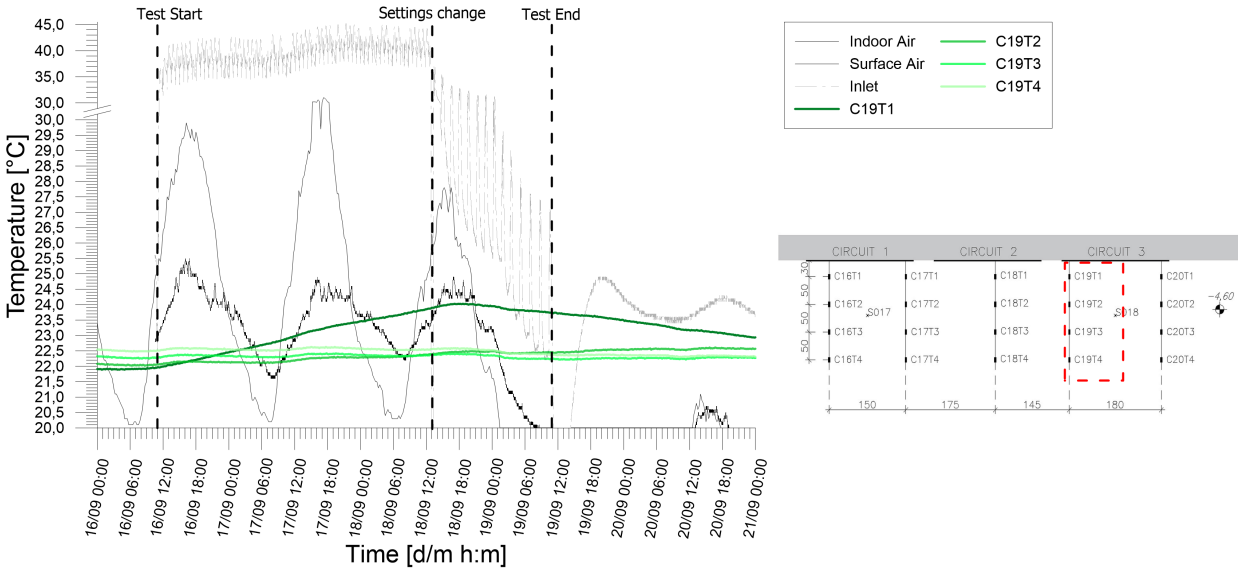

Figure A.22: Temperatures records from chain 19 of experimental test C_2-3_20190916_20190919.

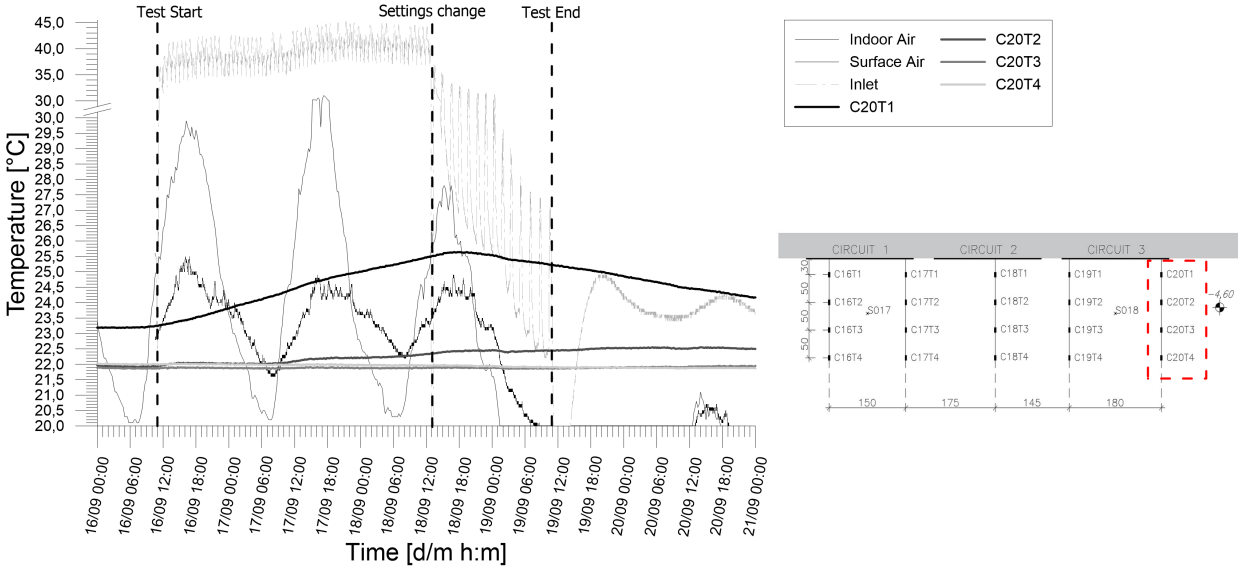

Figure A.23: Temperatures records from chain 20 of experimental test C_2-3_20190916_20190919.

A.2 Test C_3_20190923_20190925

Table A.2: Main features of the test.

Test start time	23/9/19 10.52
Test end time	25/9/19 11.00
Duration [h]	48.2
Operative mode	Cooling
Active circuit(s)	3
Circuit link	-
Target temperature user [°C]	5
Flow rate at the ground side [l/h]	575

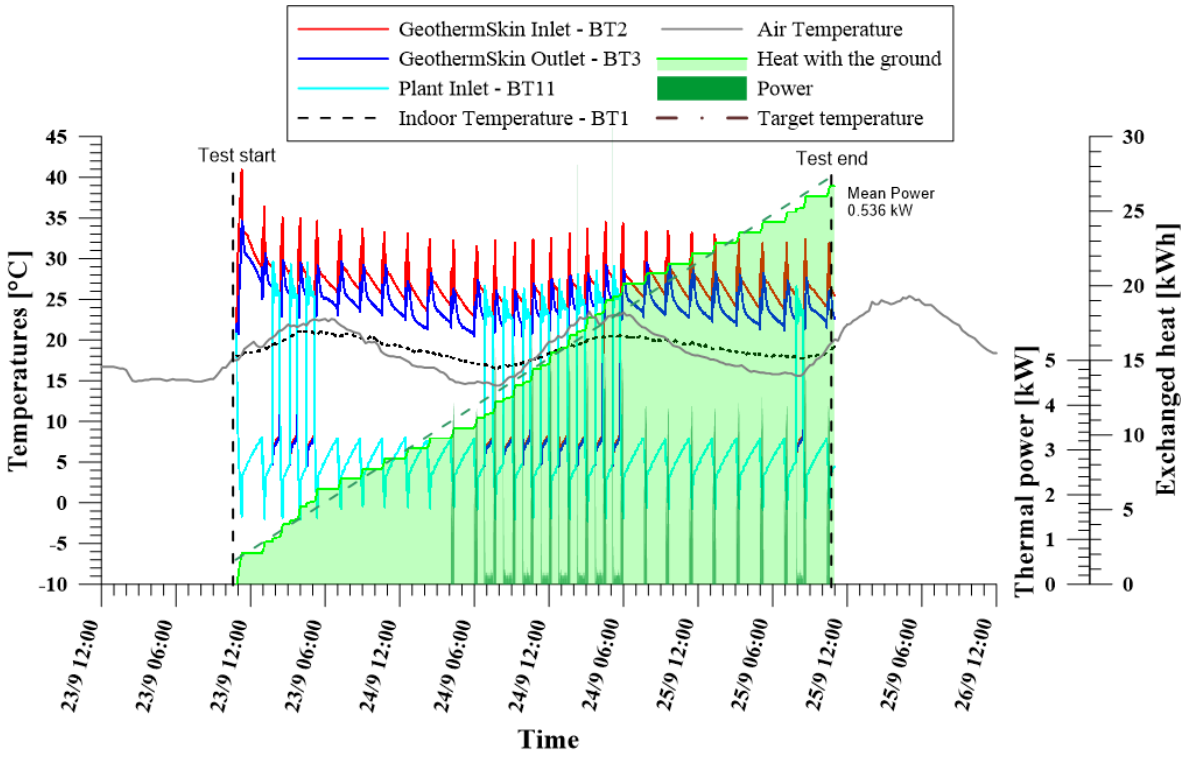

Figure A.24: Thermal performance interpretation of experimental test *C_3_20190923_20190925* with circuit 3 in cooling mode.

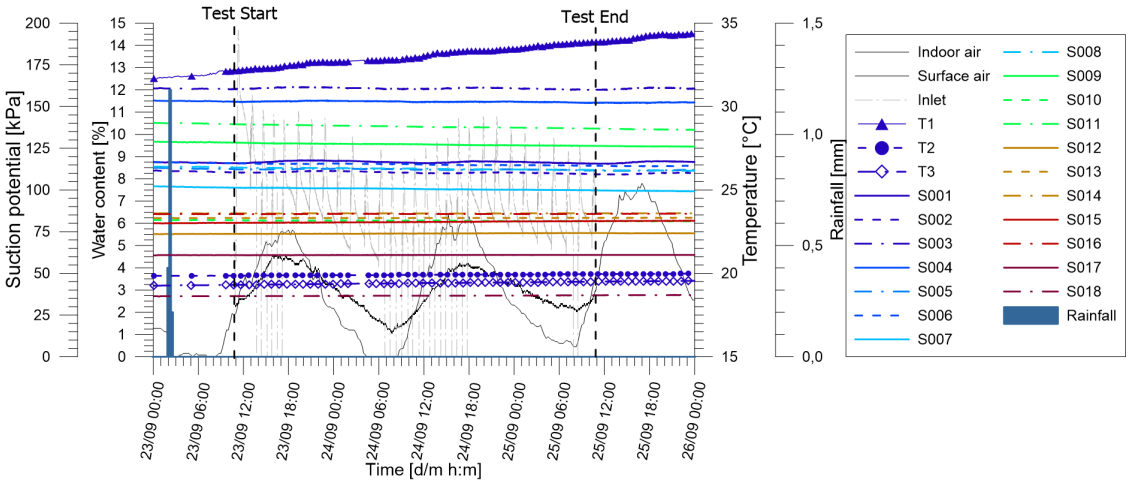

Figure A.25: Tensiometer and hygrometers records of experimental test C_3_20190923_20190925 together with monitored rainfall from Politecnico weather station.

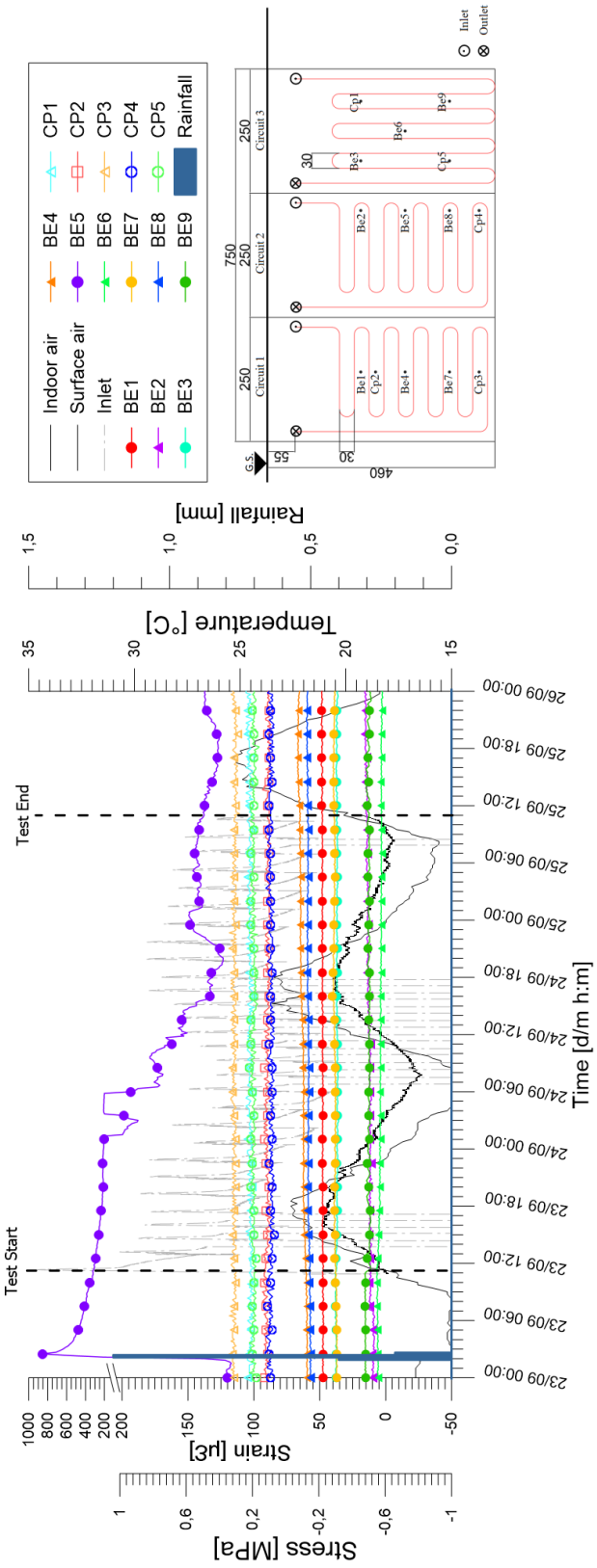

Figure A.26: Stresses and strains monitored at the wall external facade during experimental test C_3_20190923_20190925.

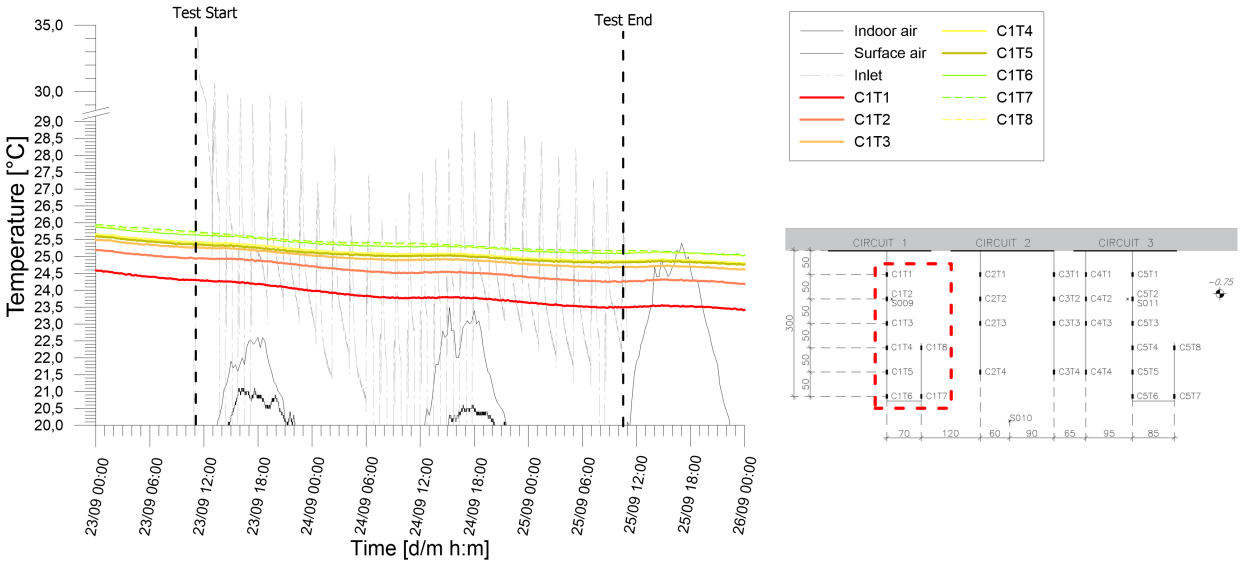

Figure A.27: Temperatures records from chain 1 of experimental test C_3_20190923_20190925.

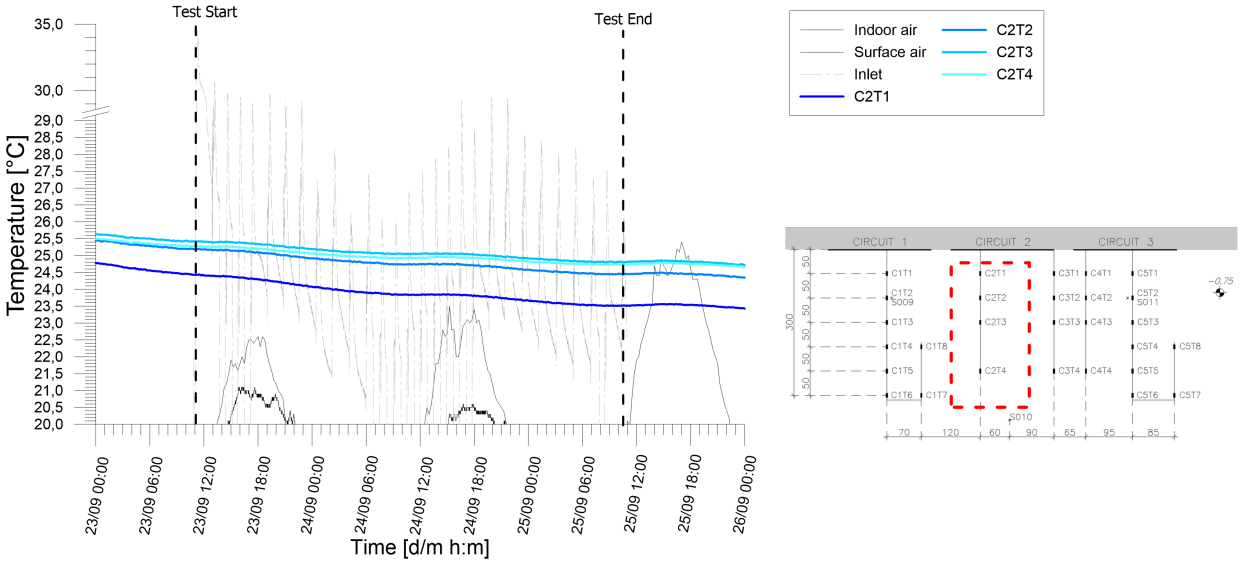

Figure A.28: Temperatures records from chain 2 of experimental test C_3_20190923_20190925.

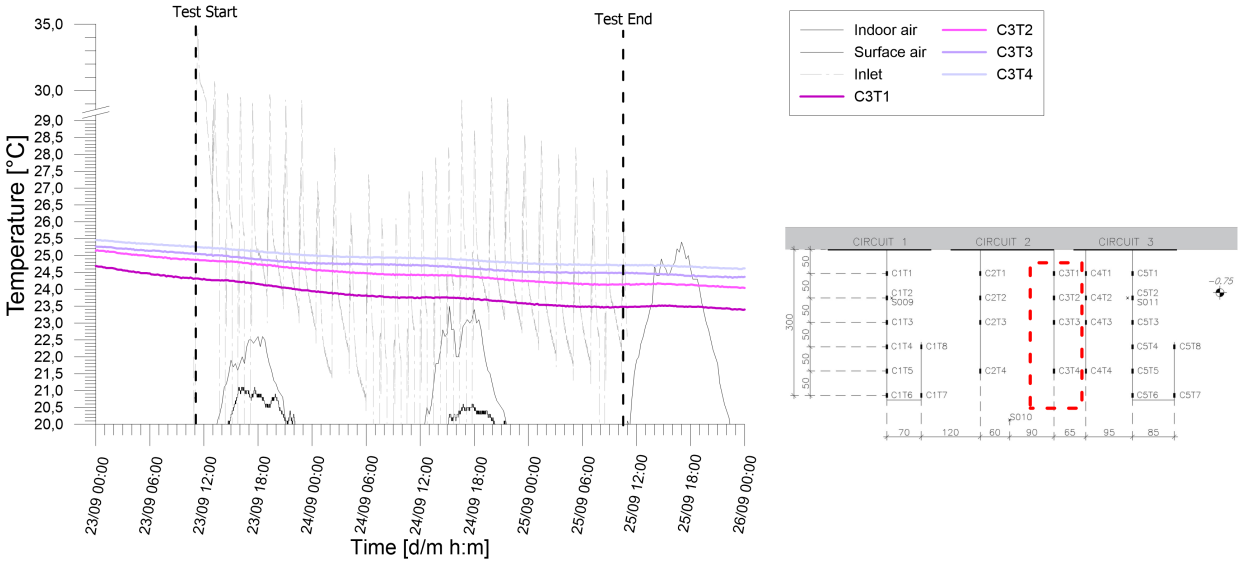

Figure A.29: Temperatures records from chain 3 of experimental test C_3_20190923_20190925.

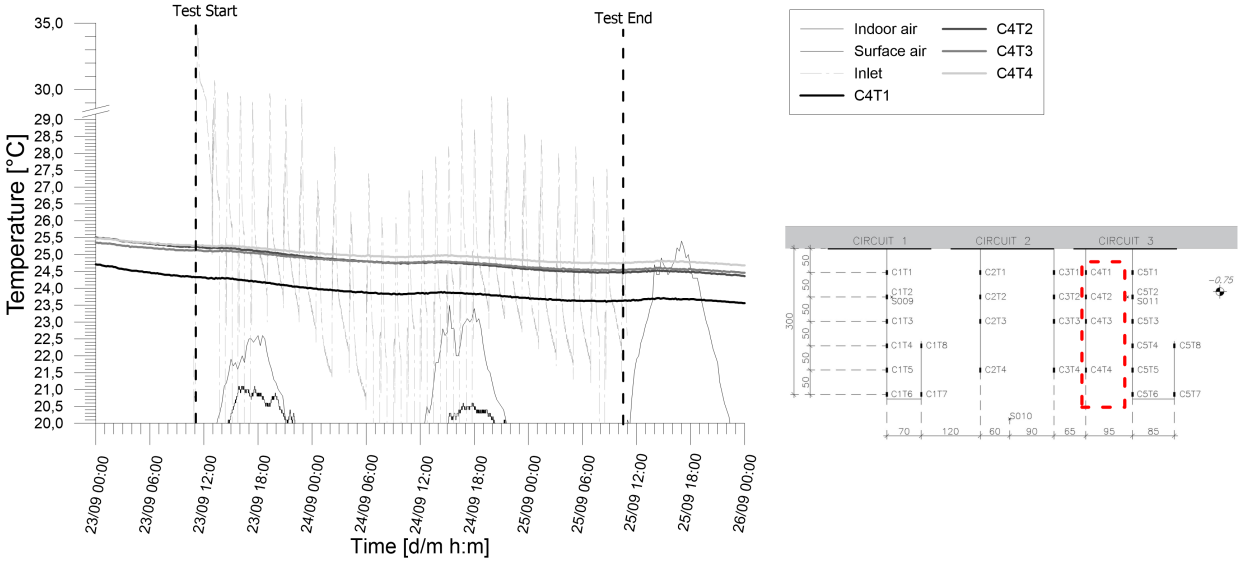

Figure A.30: Temperatures records from chain 4 of experimental test C_3_20190923_20190925.

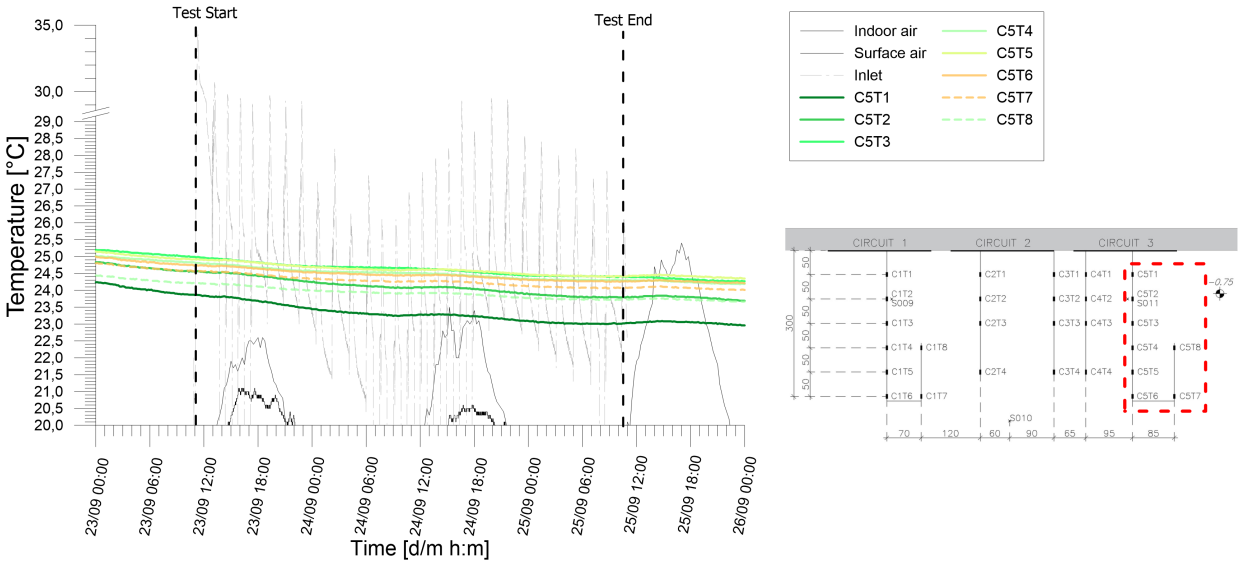

Figure A.31: Temperatures records from chain 5 of experimental test C_3_20190923_20190925.

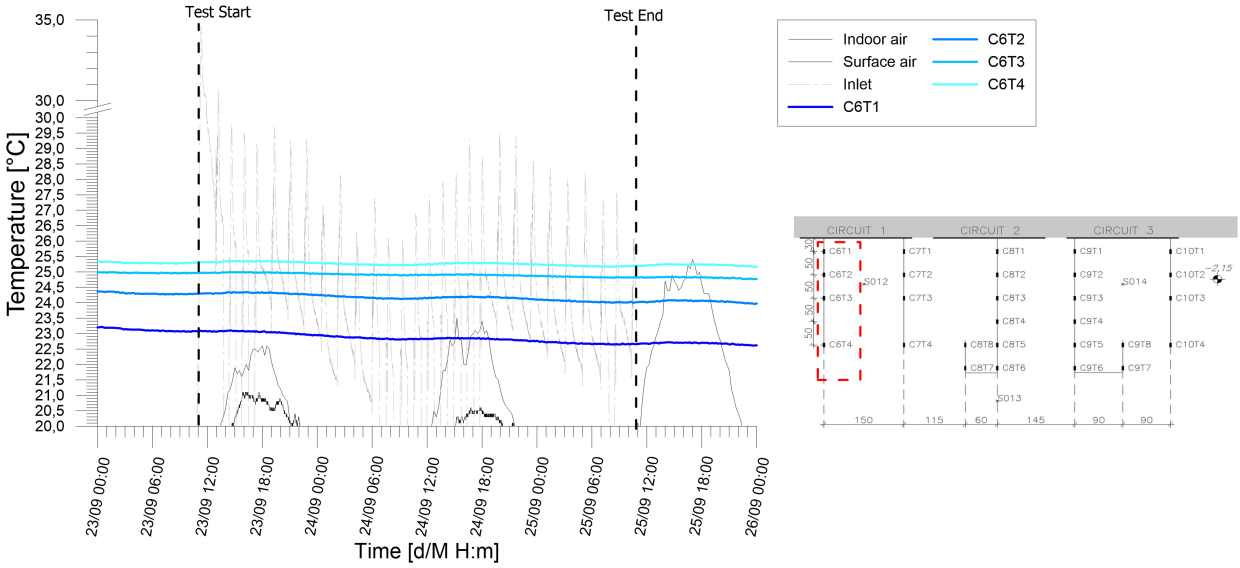

Figure A.32: Temperatures records from chain 6 of experimental test C_3_20190923_20190925.

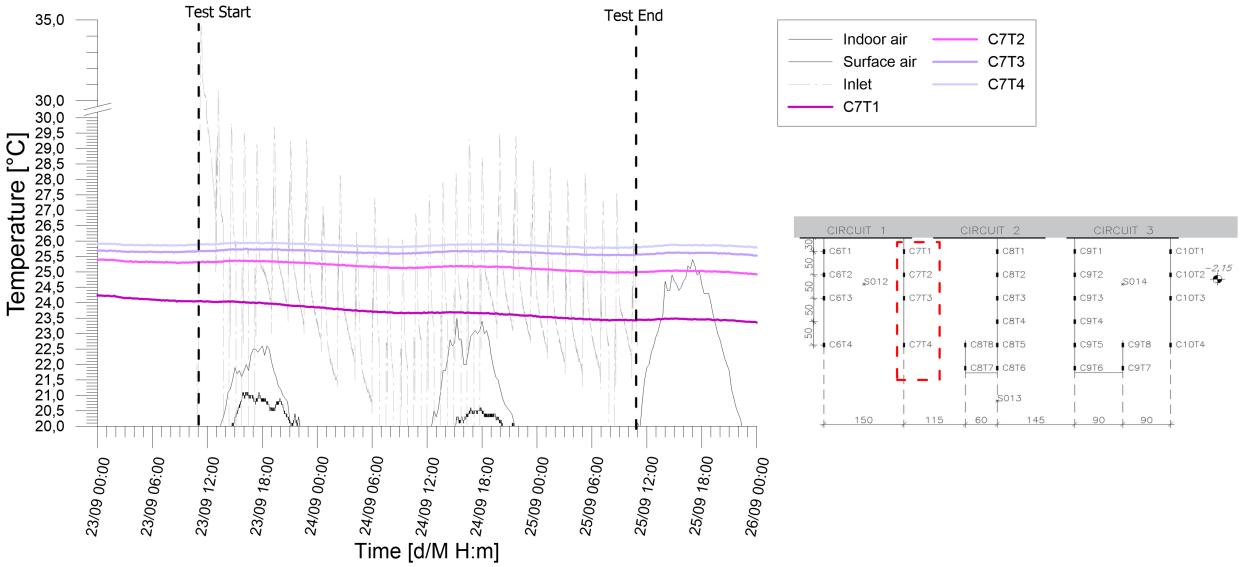

Figure A.33: Temperatures records from chain 7 of experimental test C_3_20190923_20190925.

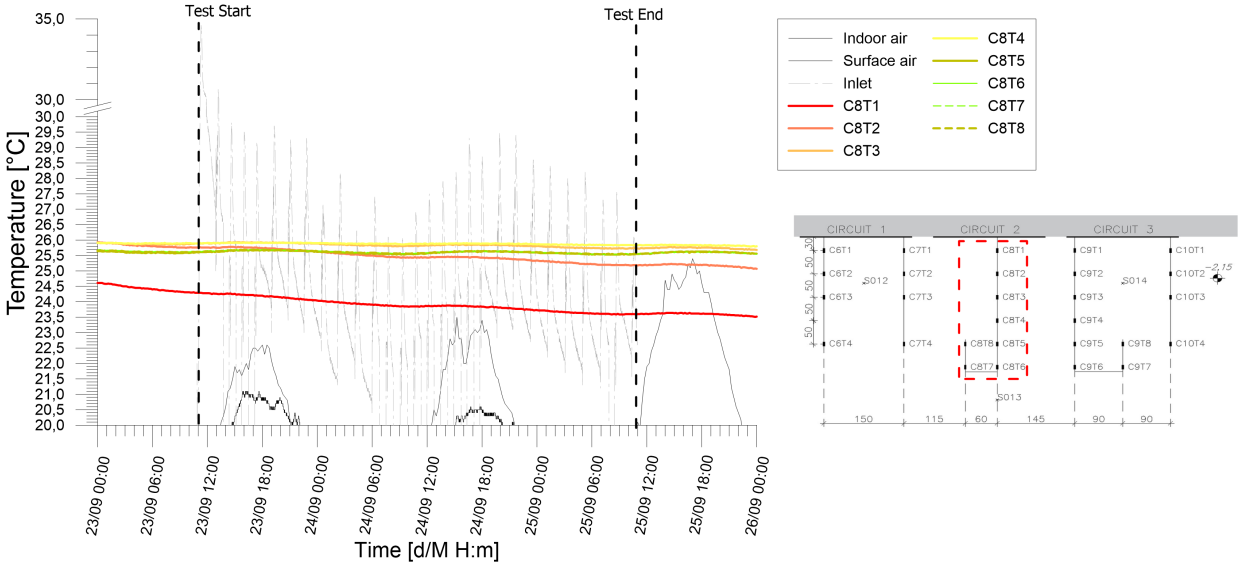

Figure A.34: Temperatures records from chain 8 of experimental test C_3_20190923_20190925.

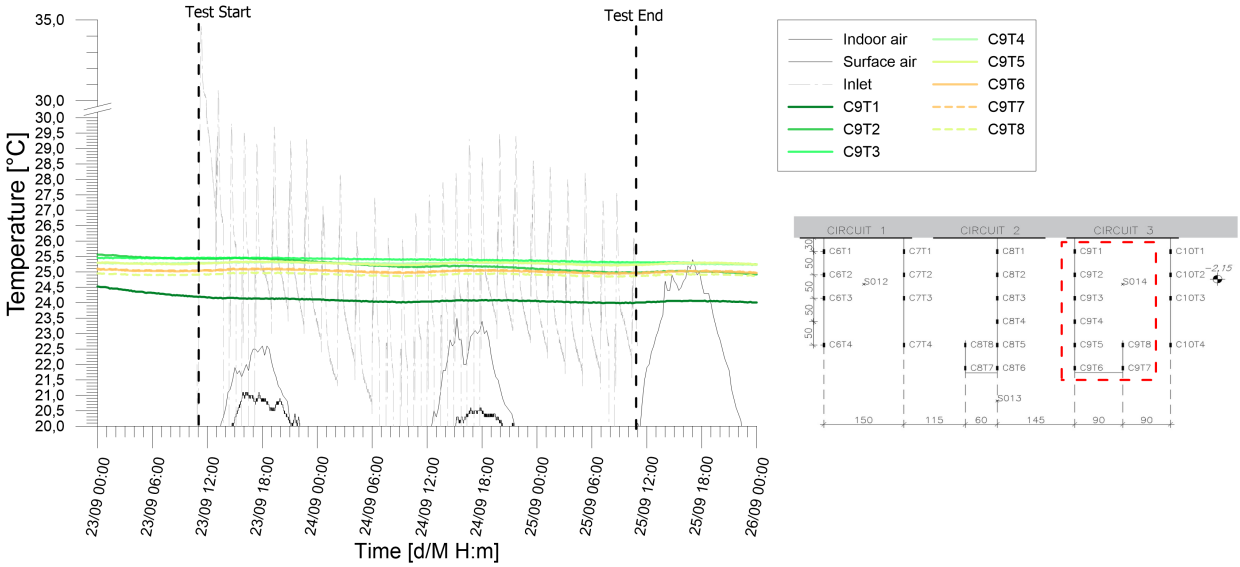

Figure A.35: Temperatures records from chain 9 of experimental test C_3_20190923_20190925.

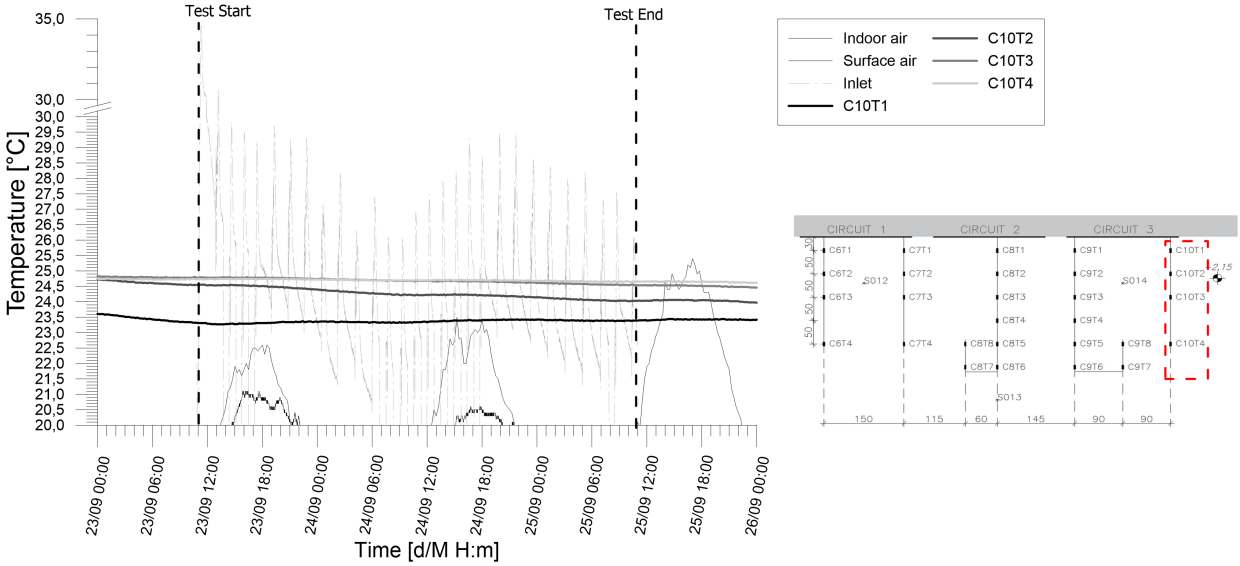

Figure A.36: Temperatures records from chain 10 of experimental test C_3_20190923_20190925.

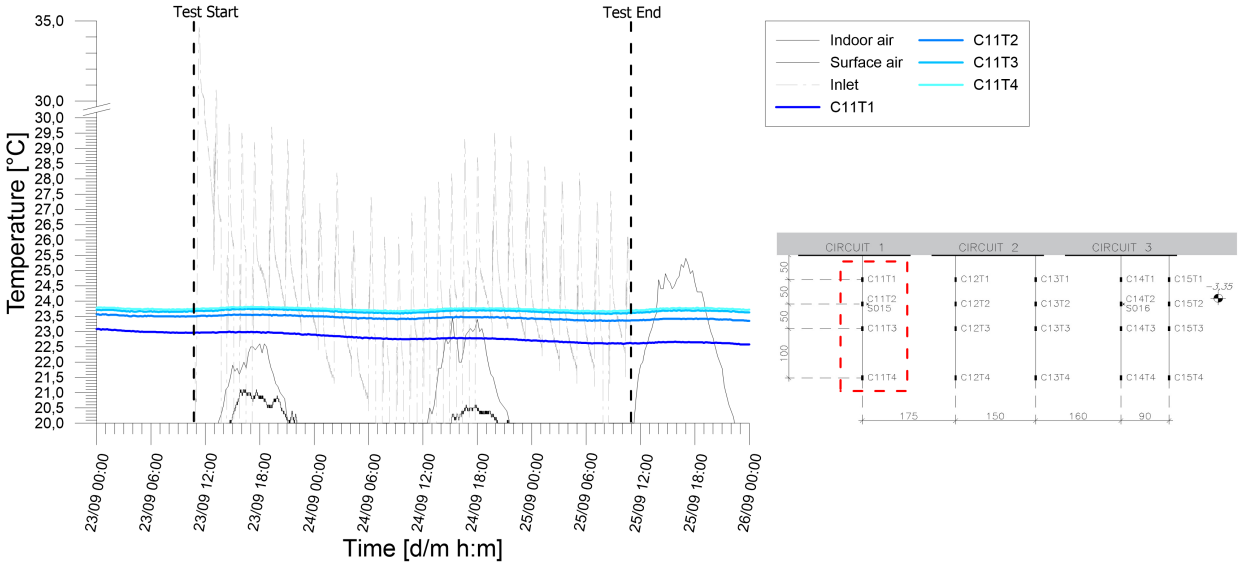

Figure A.37: Temperatures records from chain 11 of experimental test C_3_20190923_20190925.

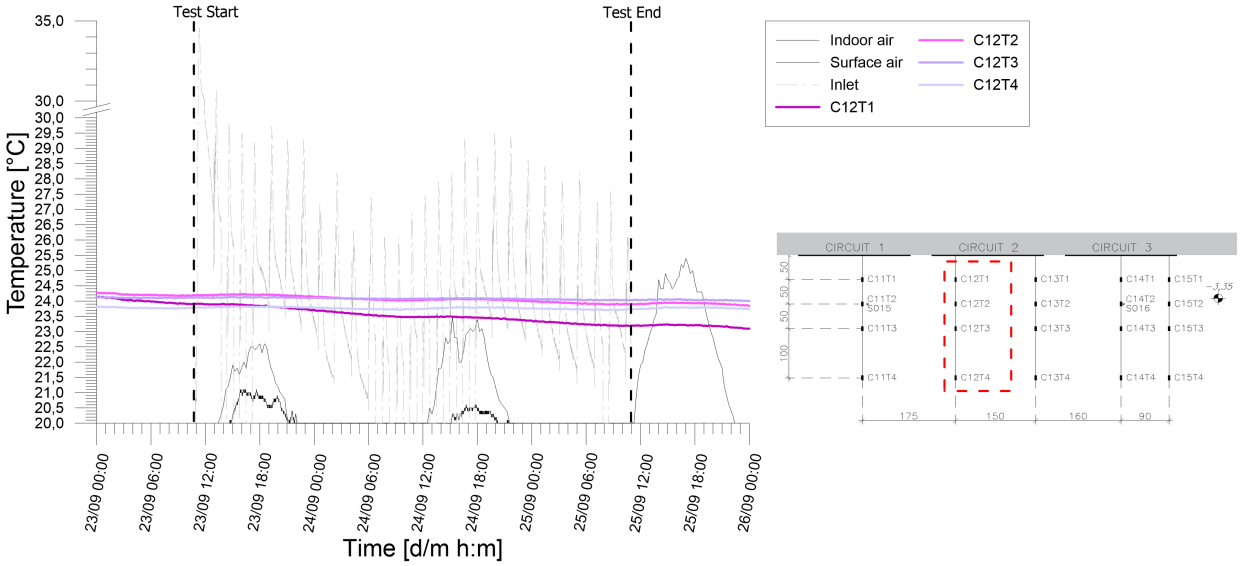

Figure A.38: Temperatures records from chain 12 of experimental test C_3_20190923_20190925.

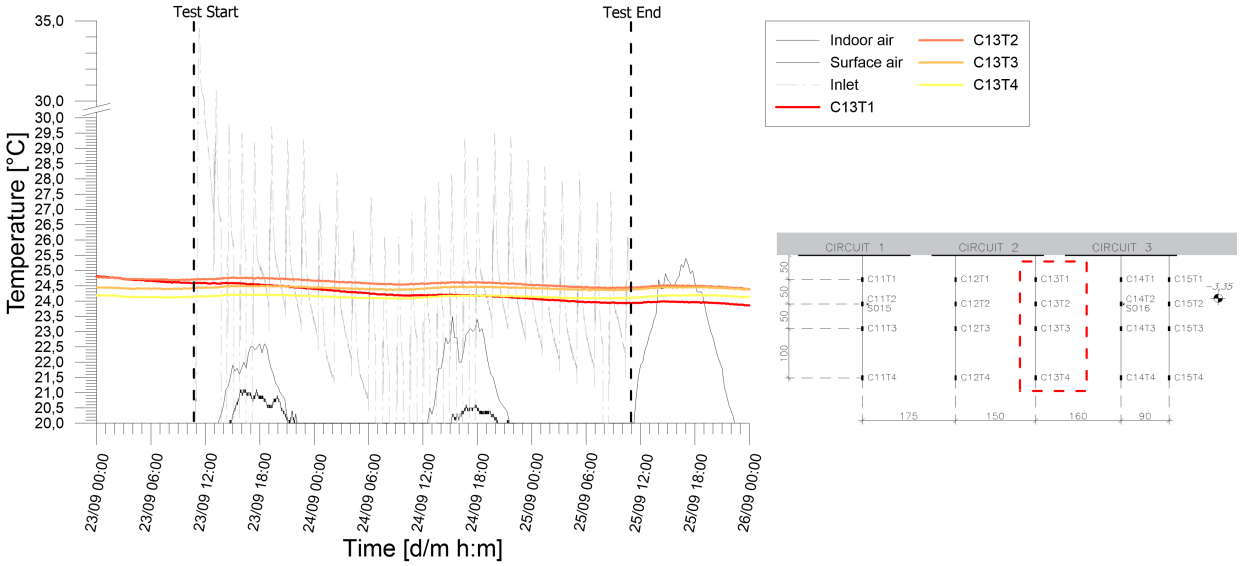

Figure A.39: Temperatures records from chain 13 of experimental test C_3_20190923_20190925.

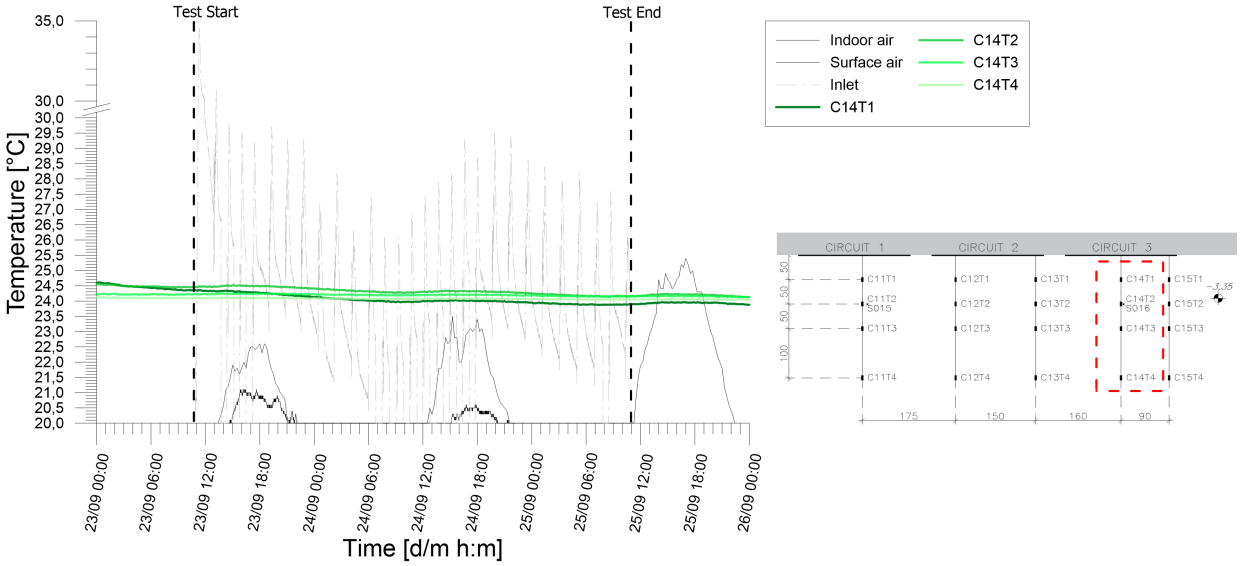

Figure A.40: Temperatures records from chain 14 of experimental test C_3_20190923_20190925.

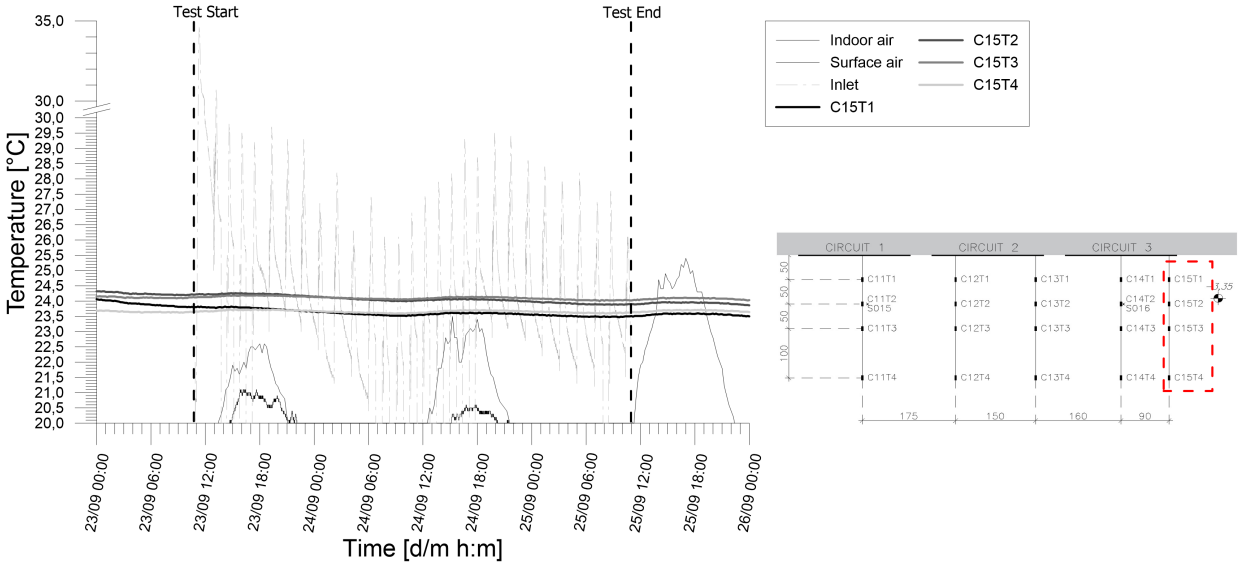

Figure A.41: Temperatures records from chain 15 of experimental test C_3_20190923_20190925.

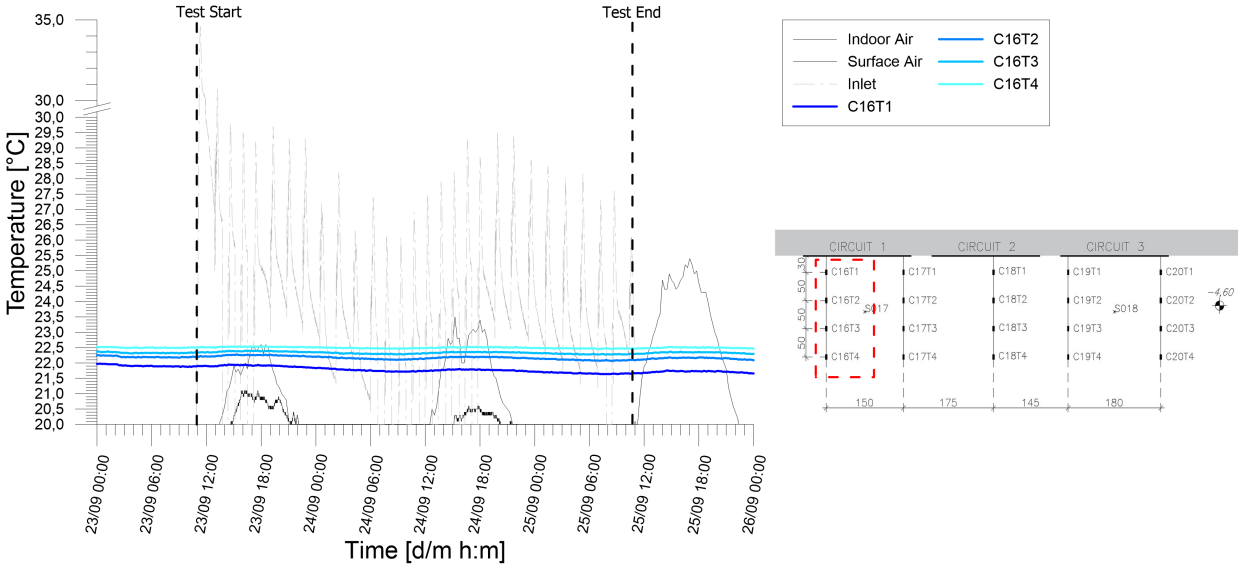

Figure A.42: Temperatures records from chain 16 of experimental test C_3_20190923_20190925.

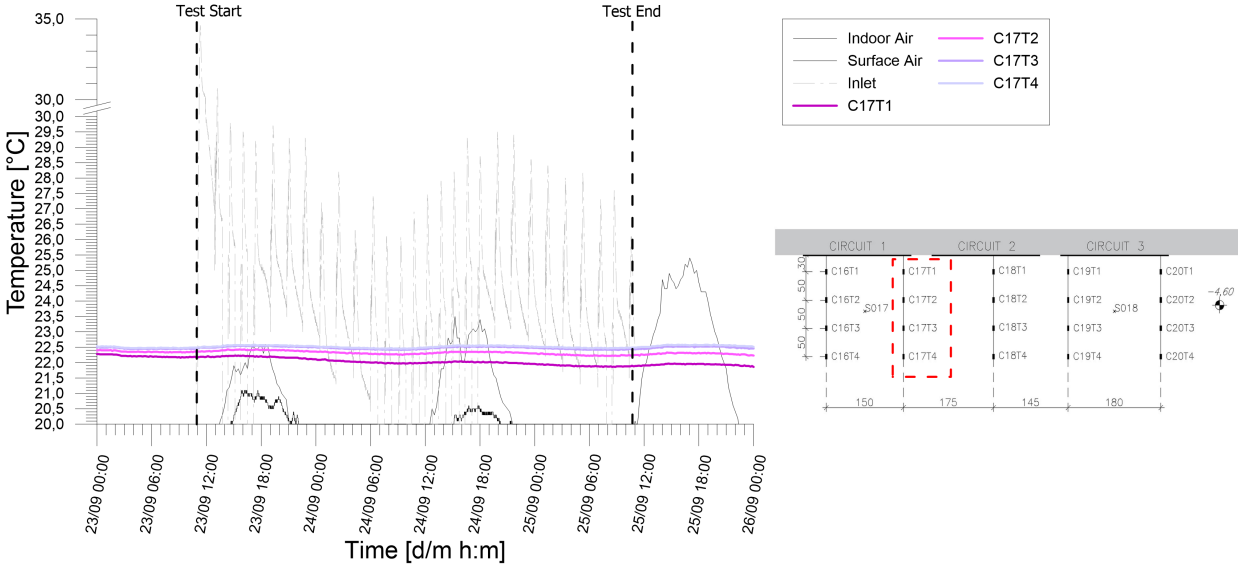

Figure A.43: Temperatures records from chain 17 of experimental test C_3_20190923_20190925.

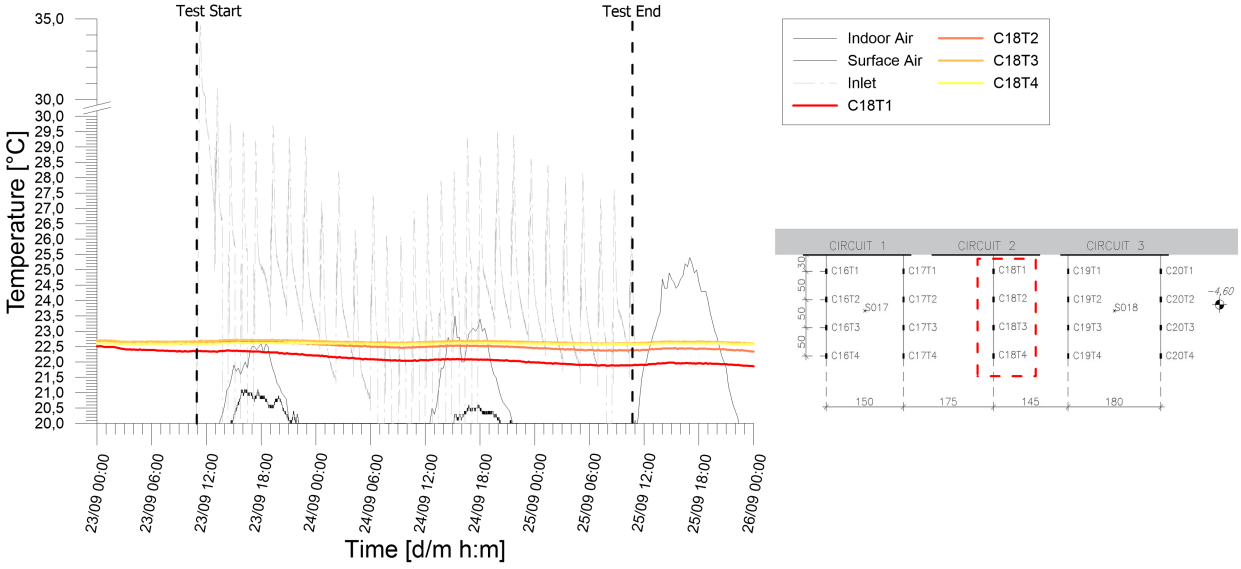

Figure A.44: Temperatures records from chain 18 of experimental test C_3_20190923_20190925.

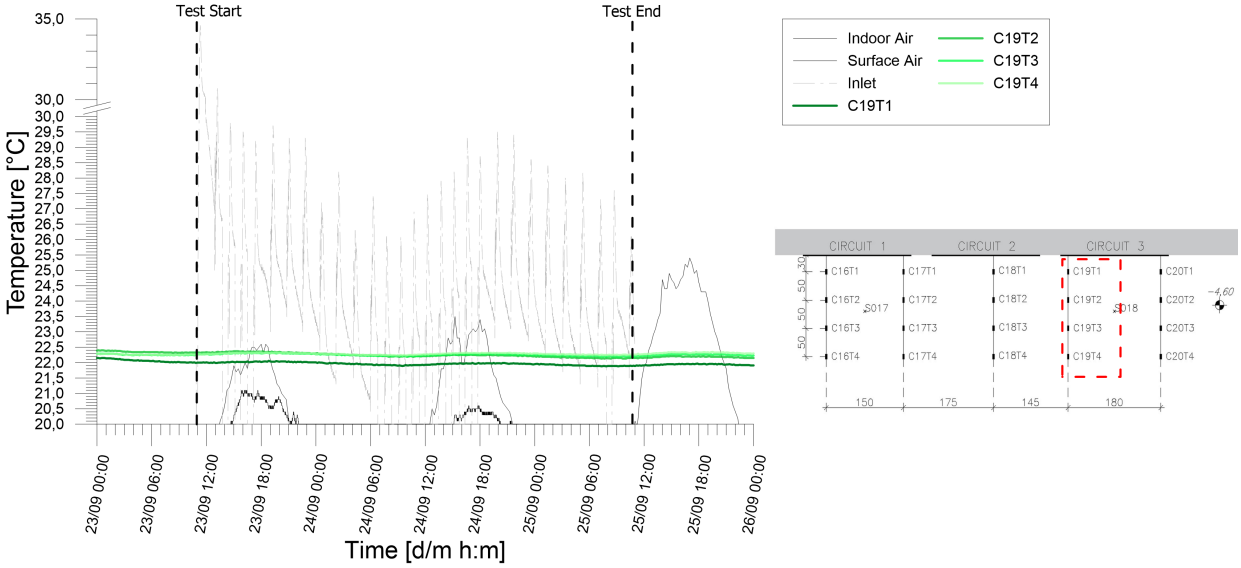

Figure A.45: Temperatures records from chain 19 of experimental test C_3_20190923_20190925.

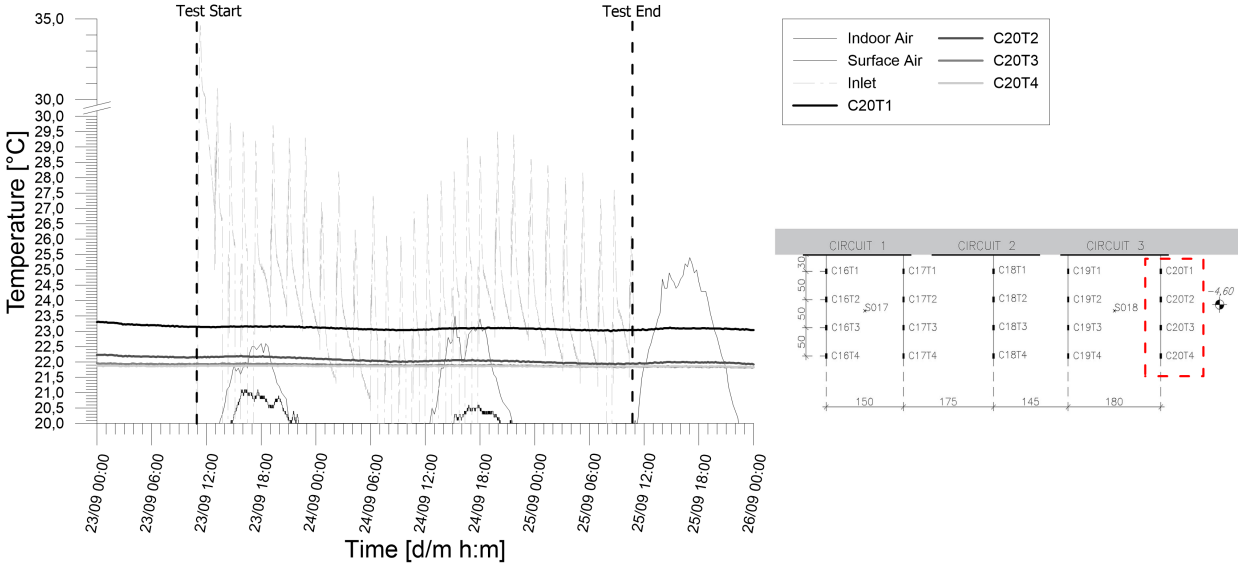

Figure A.46: Temperatures records from chain 20 of experimental test C_3_20190923_20190925.

A.3 Test H_1-2-3_20191024_20191119

Table A.3: Main features of the test.

Test start time	24/10/19 11.20
Test end time	20/11/19 14.20
Duration [h]	651.0
Operative mode	Heating
Active circuit(s)	1;2;3
Circuit link	Sequential
Target temperature user [°C]	45
Flow rate at the ground side [l/h]	670

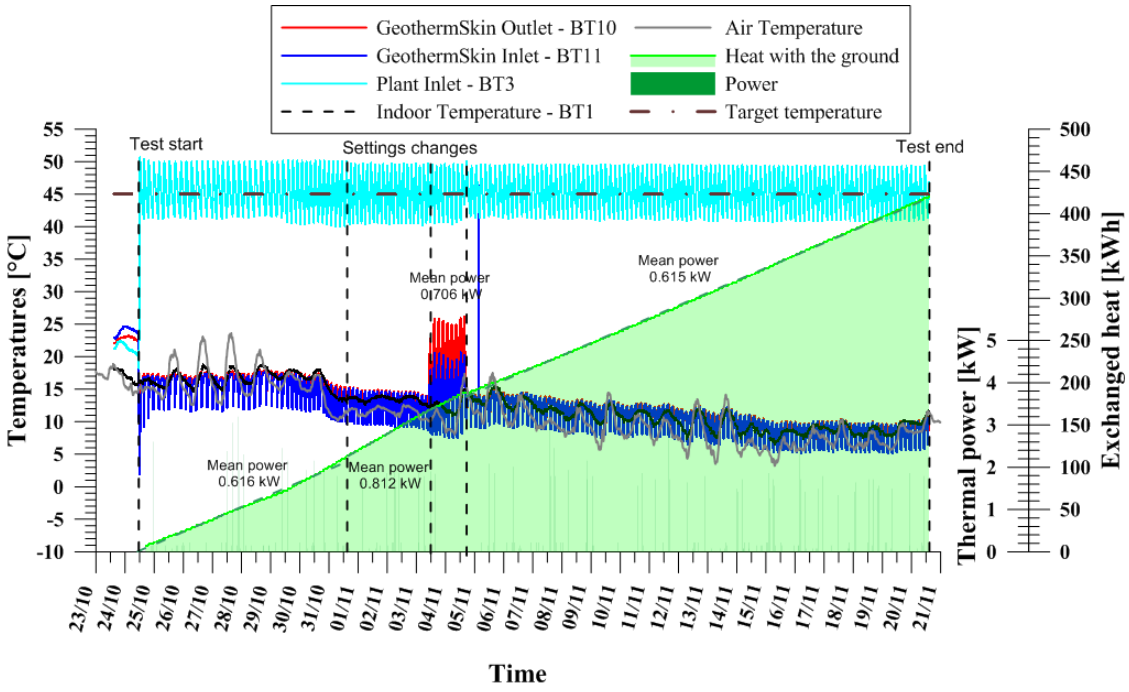

Figure A.47: Thermal performance interpretation of experimental test *H_1-2-3_20191024_20191119* with sequential link of circuit 1,2 and 3 in heating mode.

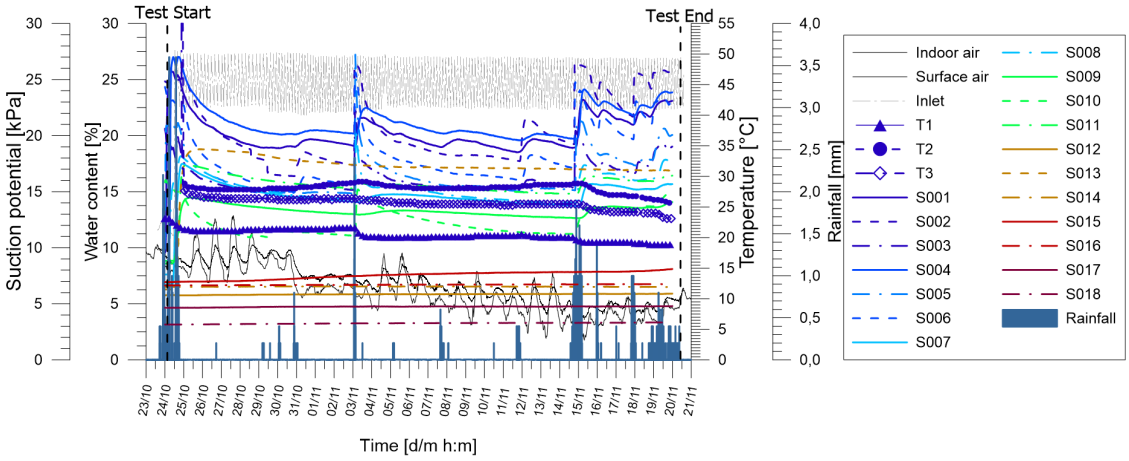

Figure A.48: Tensiometer and hygrometers records of experimental test H_1-2-3_20191024_20191119 together with monitored rainfall from Politecnico weather station.

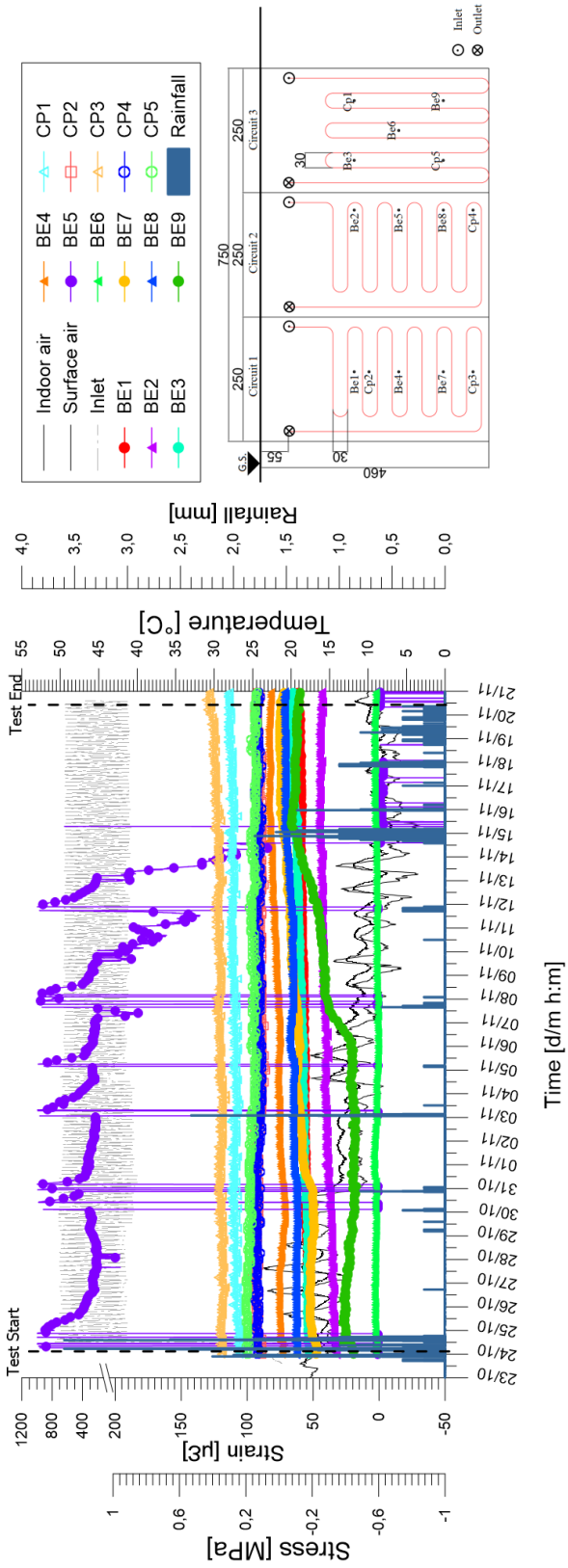

Figure A.49: Stresses and strains monitored at the wall external facade during experimental test H_1-2-3_20191024_20191119.

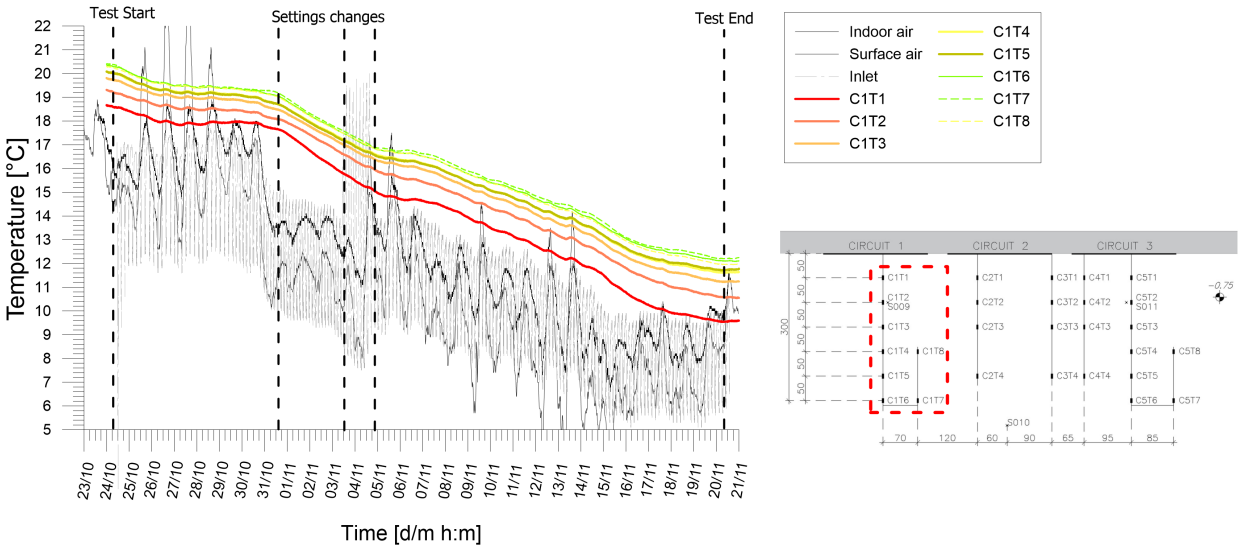

Figure A.50: *
Temperatures records from chain 1 of experimental test H_1-2-3_20191024_20191119.

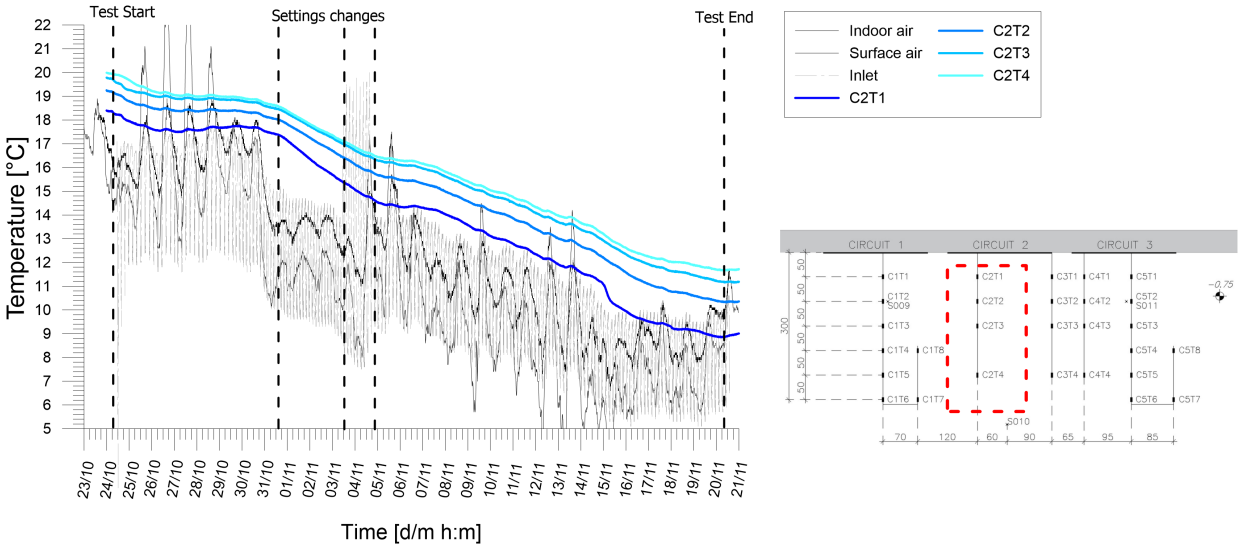

Figure A.51: Temperatures records from chain 2 of experimental test H_1-2-3_20191024_20191119.

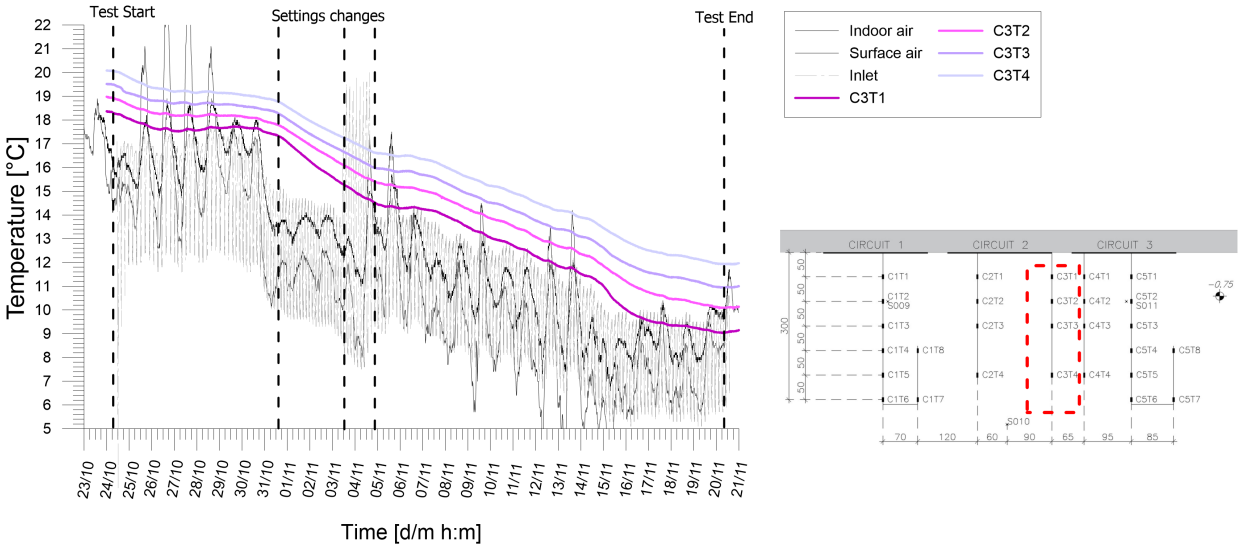

Figure A.52: Temperatures records from chain 3 of experimental test H_1-2-3_20191024_20191119.

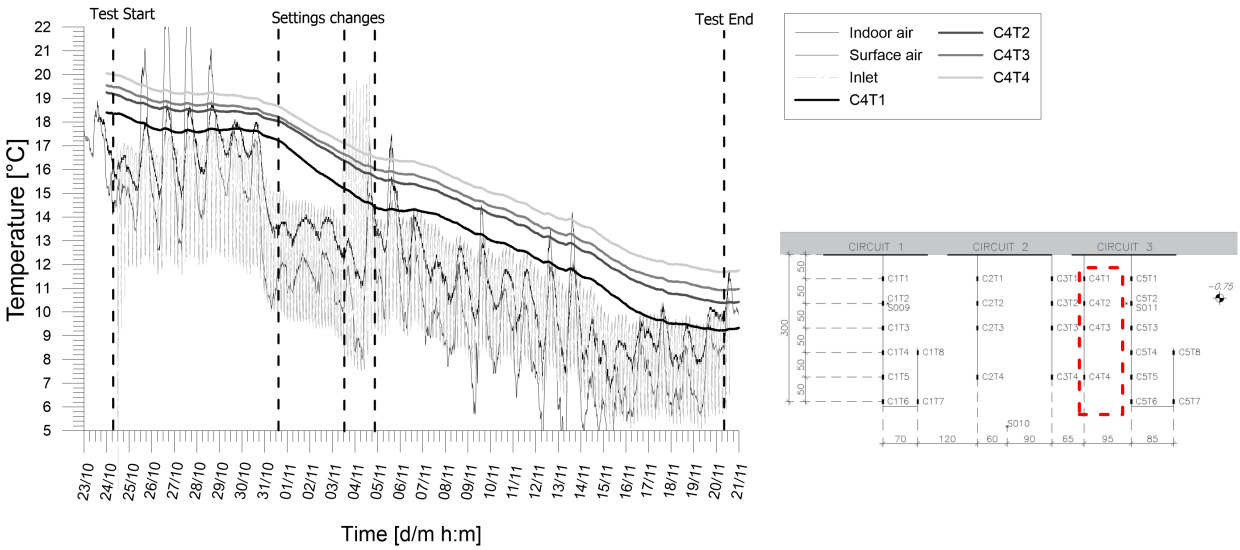

Figure A.53: Temperatures records from chain 4 of experimental test H_1-2-3_20191024_20191119.

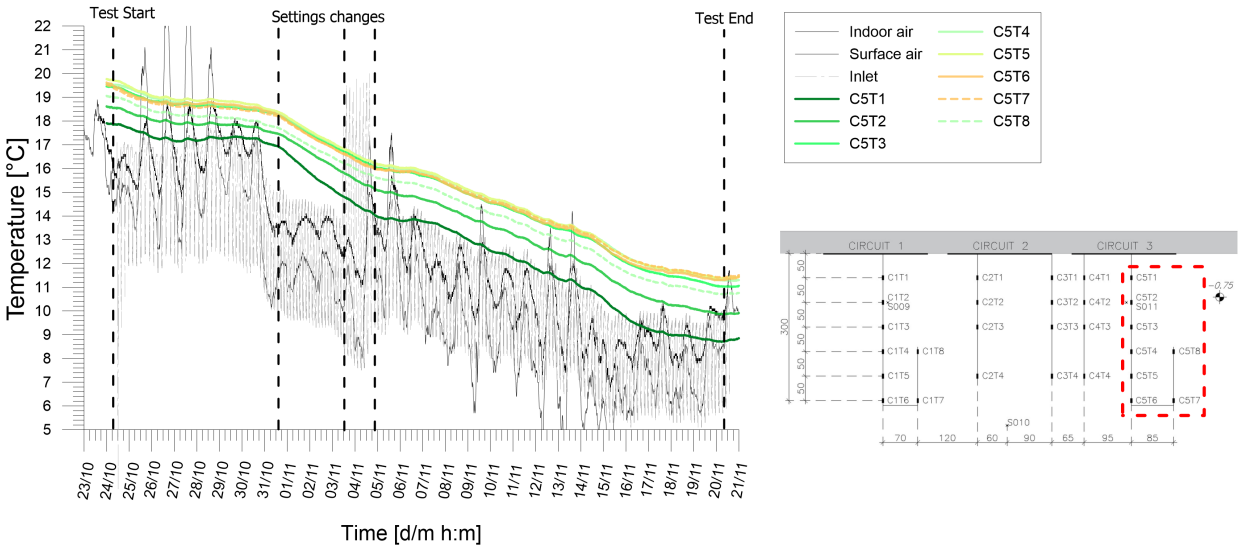

Figure A.54: Temperatures records from chain 5 of experimental test H_1-2-3_20191024_20191119.

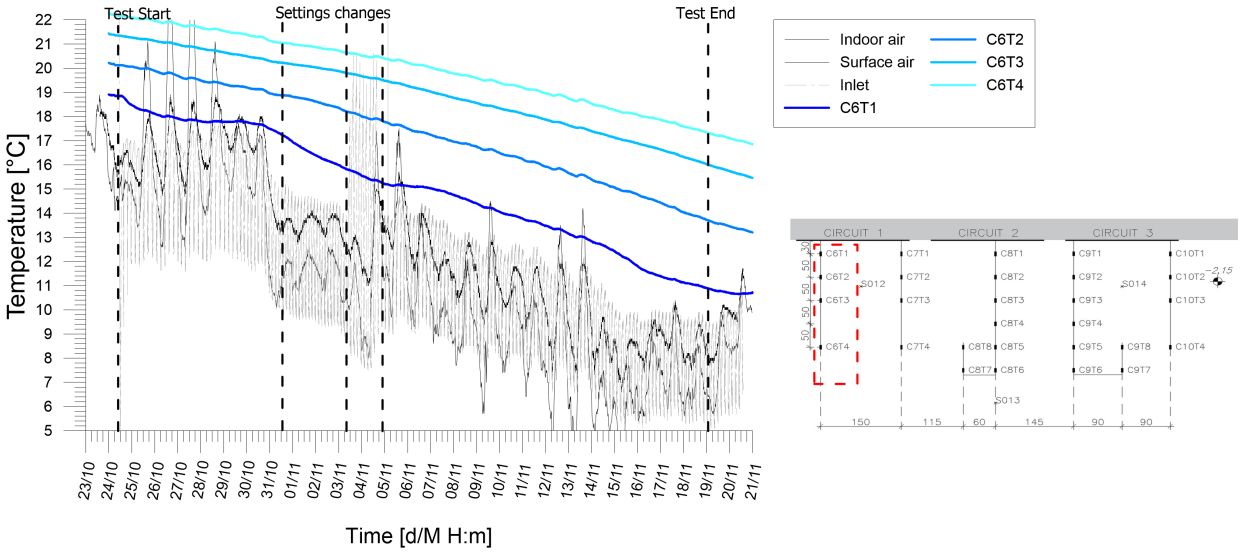

Figure A.55: Temperatures records from chain 6 of experimental test H_1-2-3_20191024_20191119.

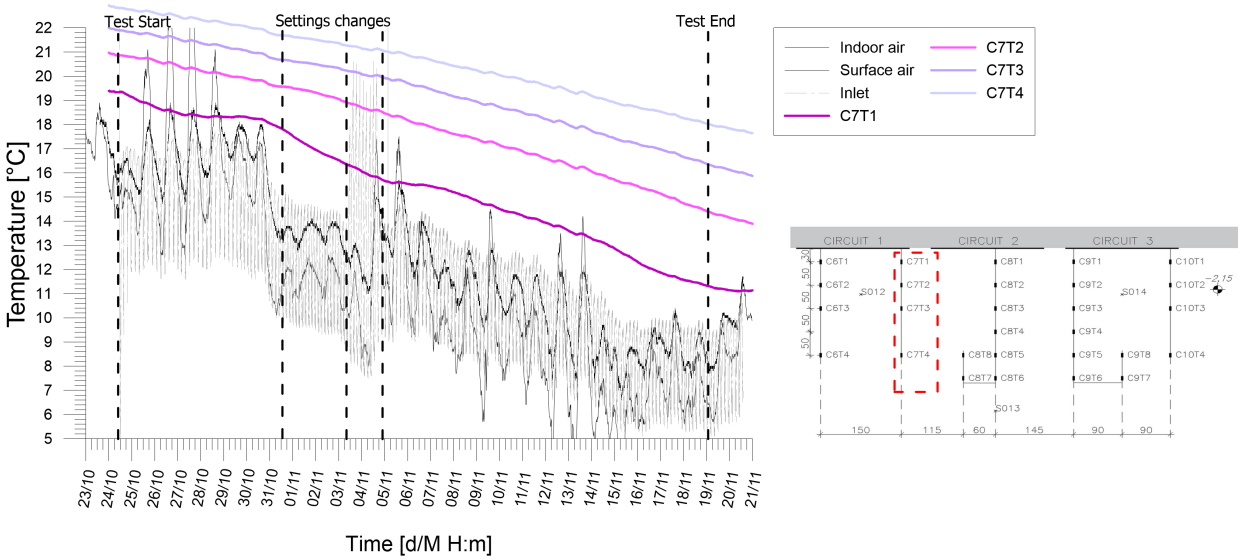

Figure A.56: Temperatures records from chain 7 of experimental test H_1-2-3_20191024_20191119.

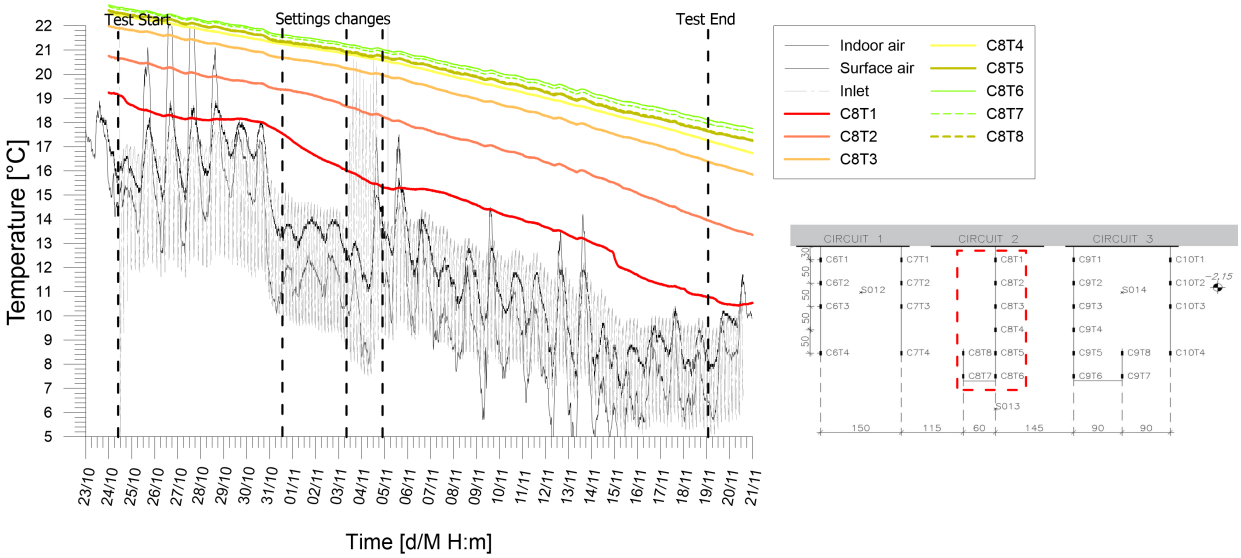

Figure A.57: Temperatures records from chain 8 of experimental test H_1-2-3_20191024_20191119.

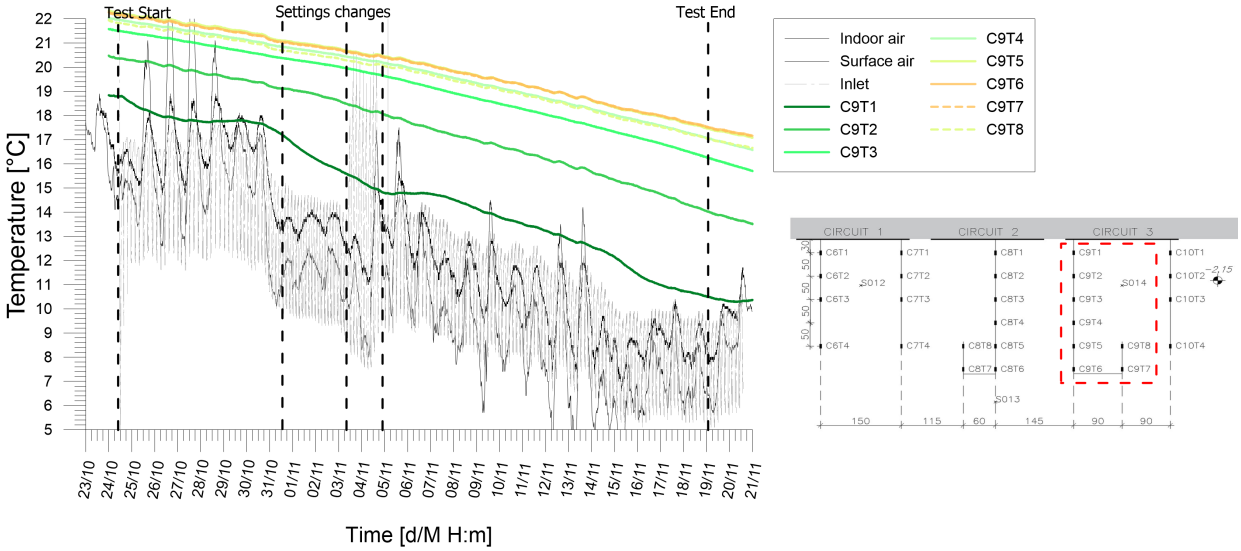

Figure A.58: Temperatures records from chain 9 of experimental test H_1-2-3_20191024_20191119.

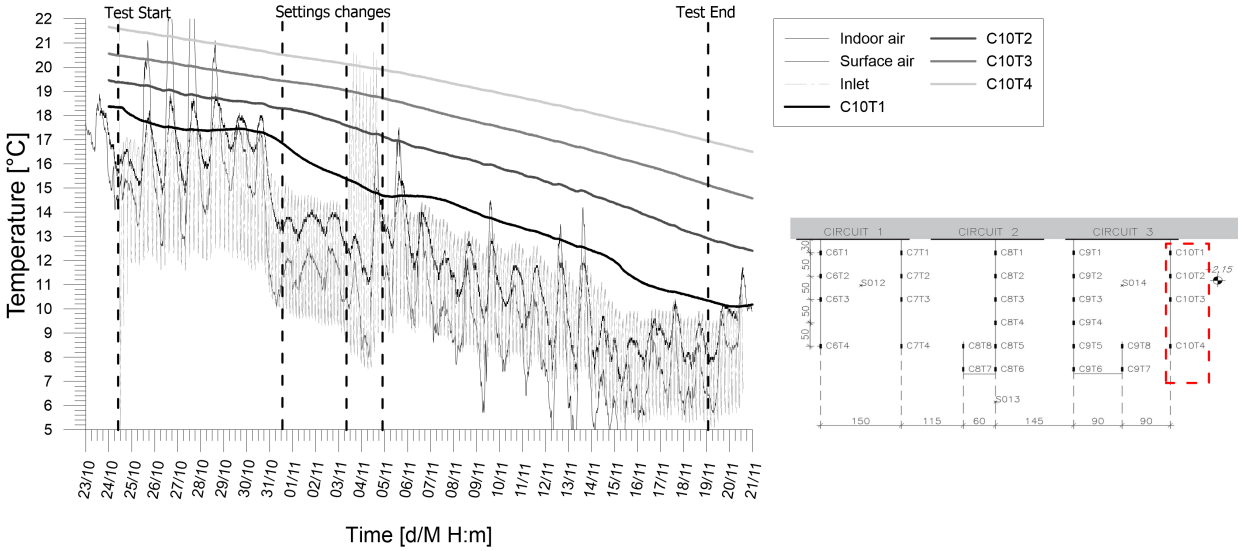

Figure A.59: Temperatures records from chain 10 of experimental test H_1-2-3_20191024_20191119.

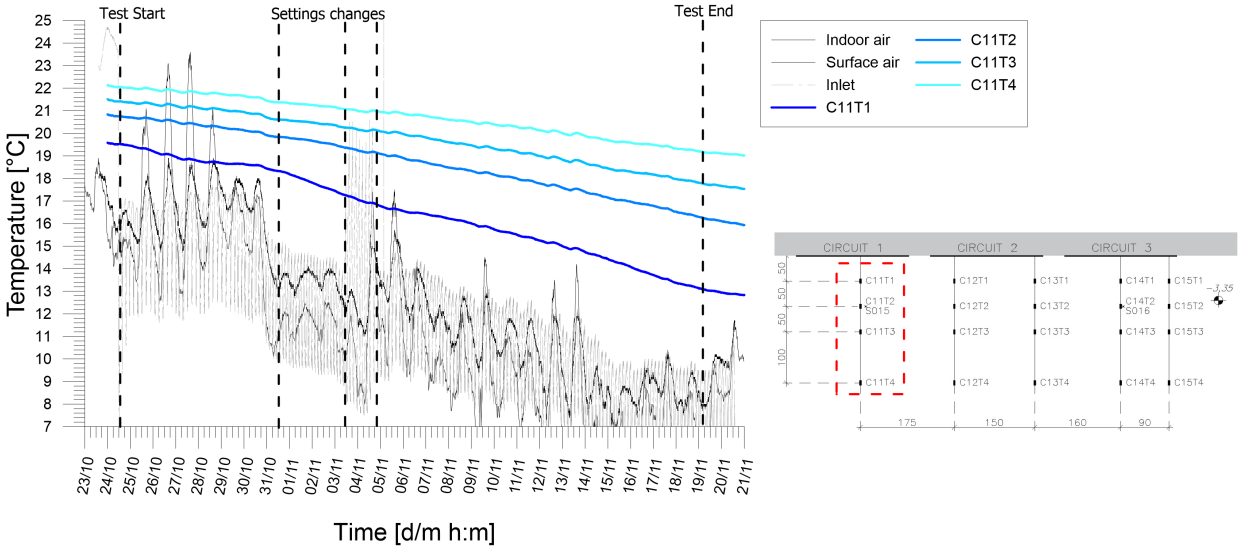

Figure A.60: Temperatures records from chain 11 of experimental test H_1-2-3_20191024_20191119.

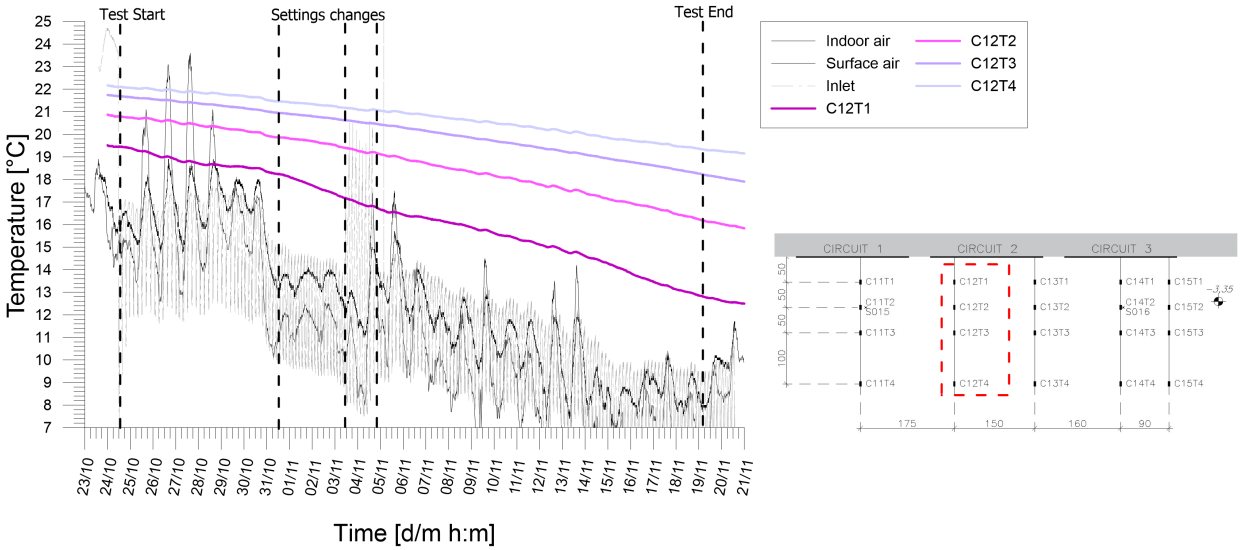

Figure A.61: Temperatures records from chain 12 of experimental test H_1-2-3_20191024_20191119.

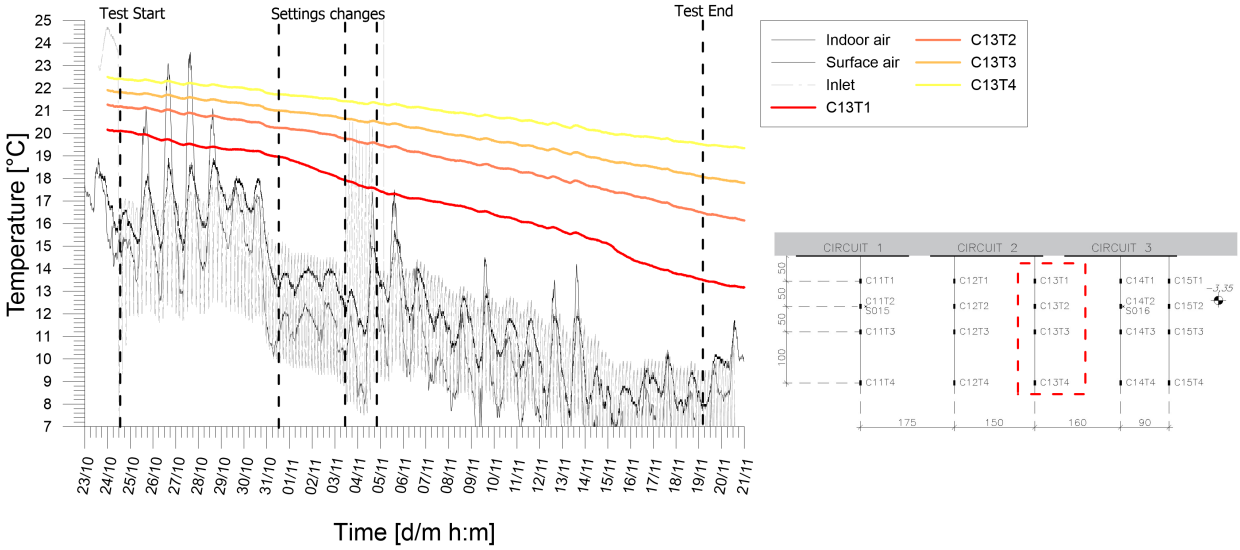

Figure A.62: Temperatures records from chain 13 of experimental test H_1-2-3_20191024_20191119.

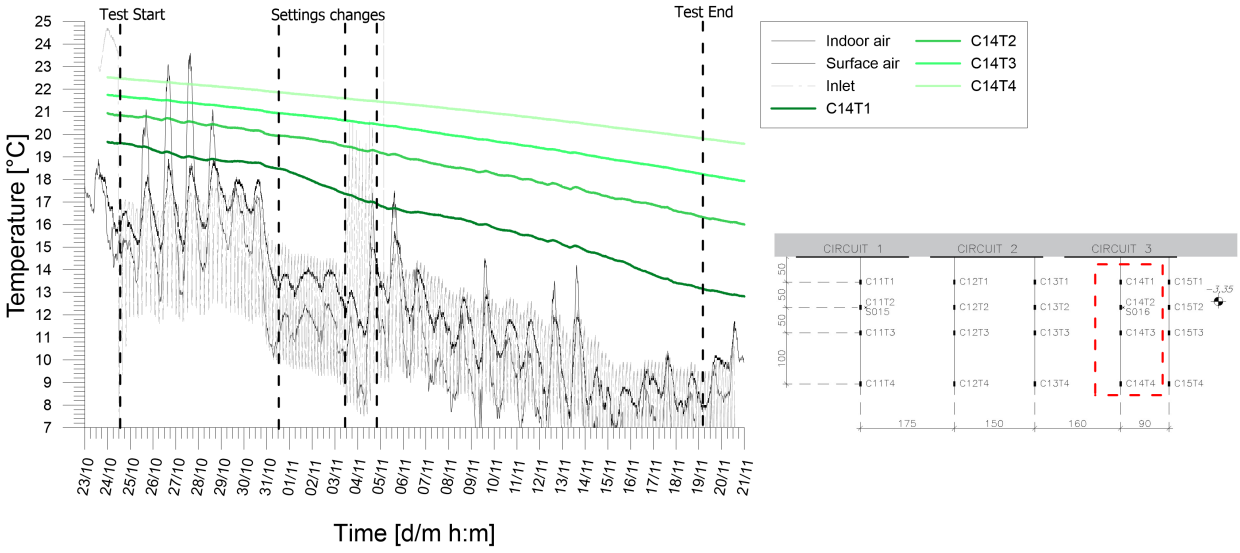

Figure A.63: Temperatures records from chain 14 of experimental test H_1-2-3_20191024_20191119.

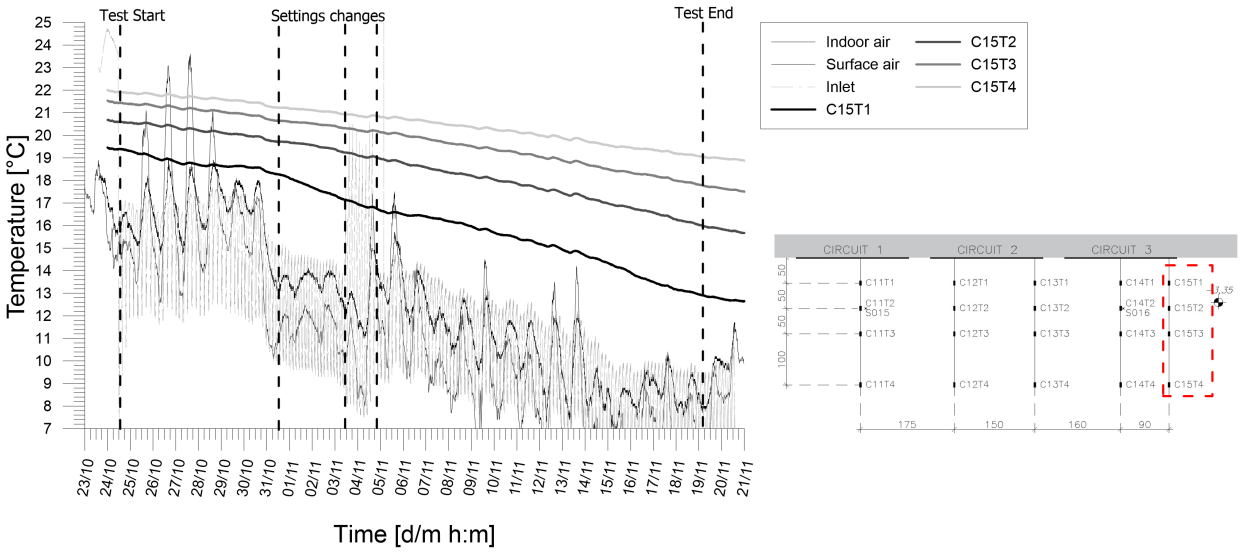

Figure A.64: Temperatures records from chain 15 of experimental test H_1-2-3_20191024_20191119.

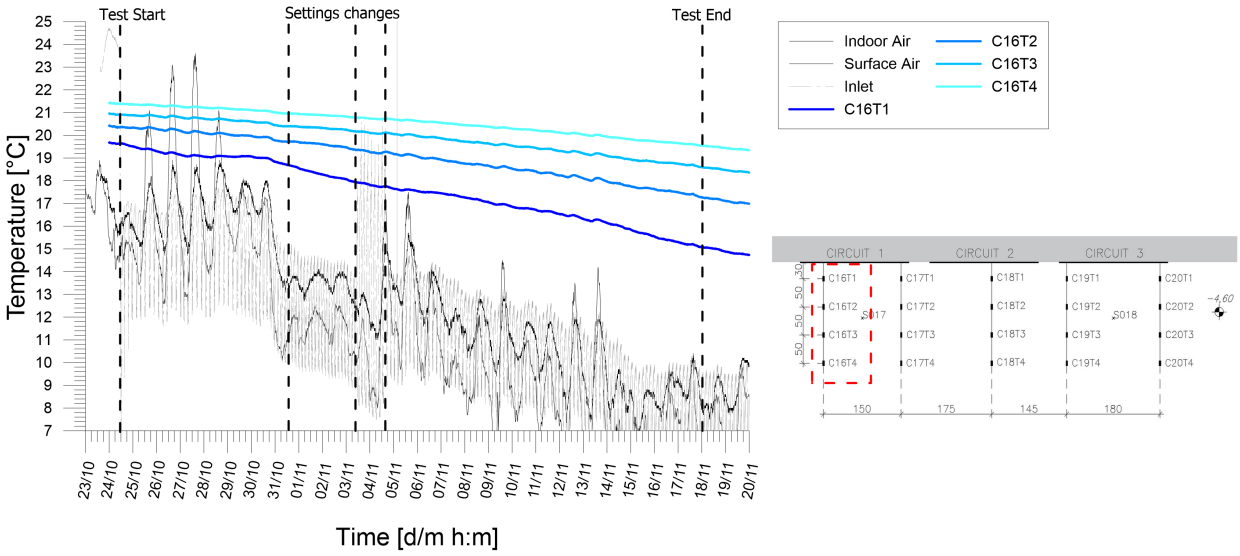

Figure A.65: Temperatures records from chain 16 of experimental test H_1-2-3_20191024_20191119.

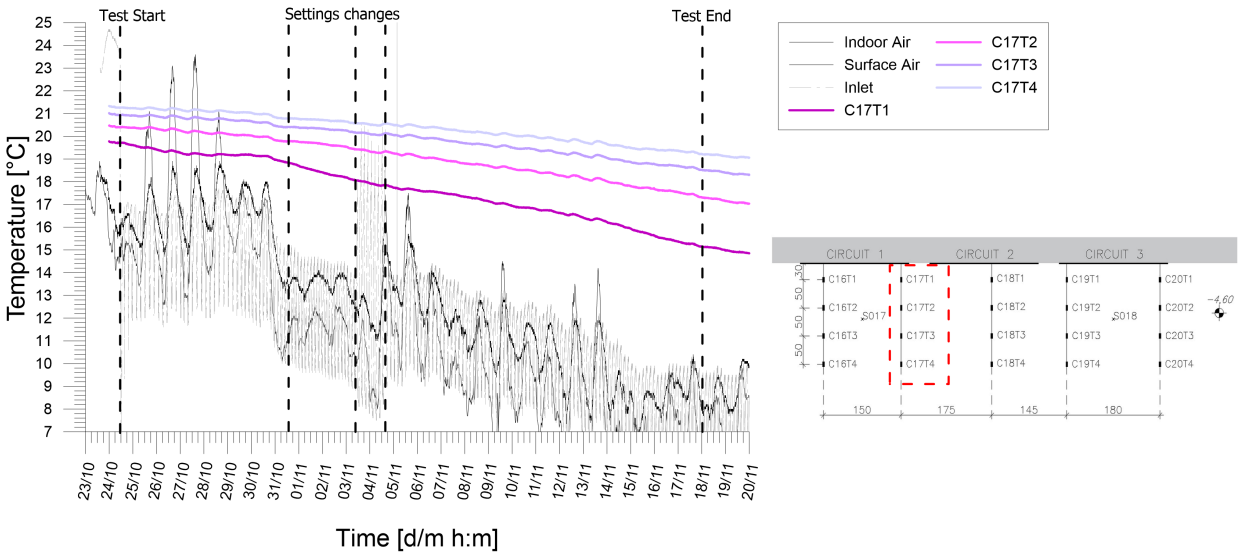

Figure A.66: Temperatures records from chain 17 of experimental test H_1-2-3_20191024_20191119.

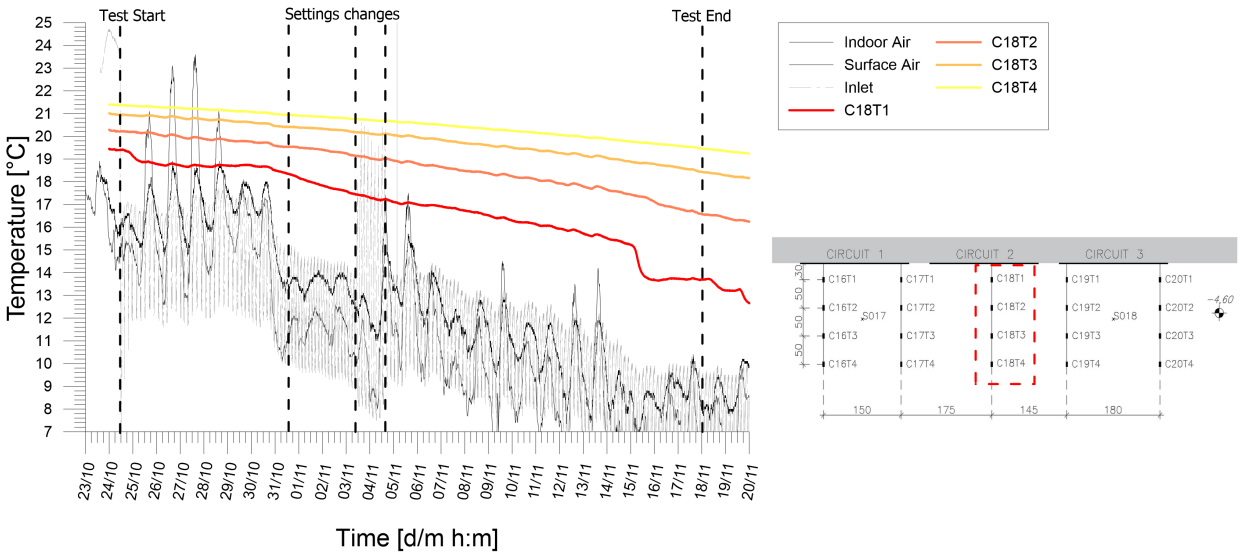

Figure A.67: Temperatures records from chain 18 of experimental test H_1-2-3_20191024_20191119.

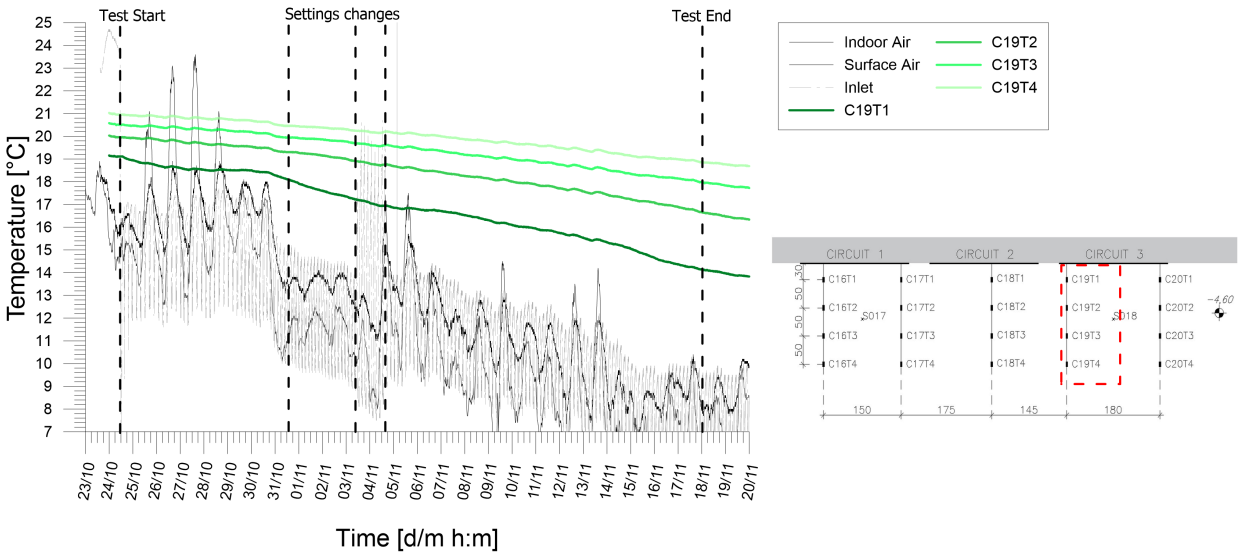

Figure A.68: Temperatures records from chain 19 of experimental test H_1-2-3_20191024_20191119.

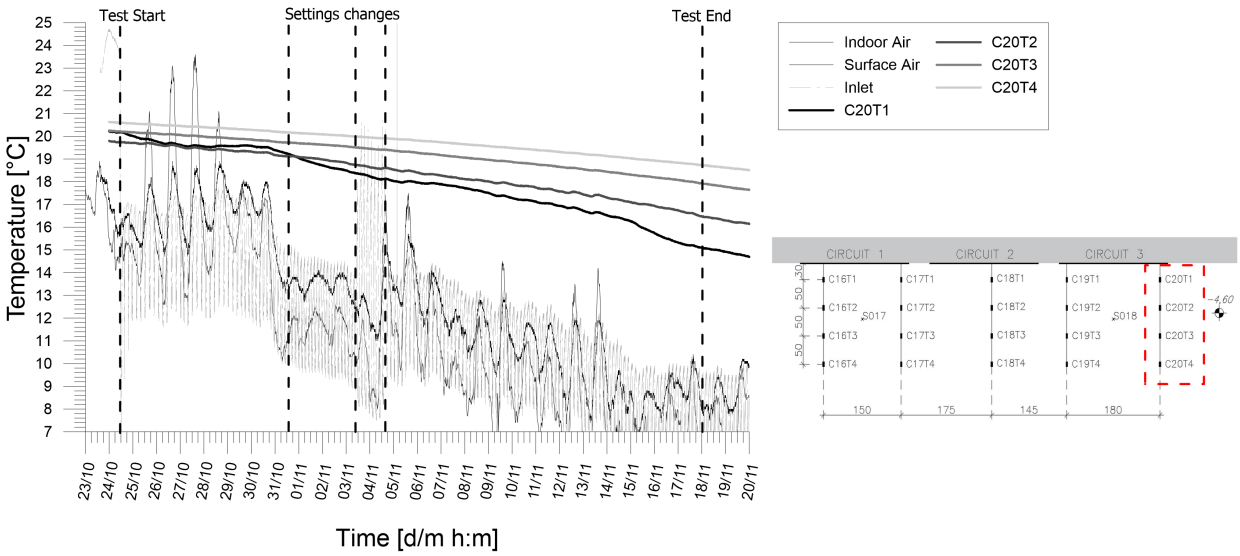

Figure A.69: Temperatures records from chain 20 of experimental test H_1-2-3_20191024_20191119.

A.4 Test H_1-2_20191128_20191202

Table A.4: Main features of the test.

Test start time	28/11/19 12.25
Test end time	02/12/19 16.00
Duration [h]	99.6
Operative mode	Heating
Active circuit(s)	1;2
Circuit link	Sequential
Target temperature user [°C]	45
Flow rate at the ground side [l/h]	546.1

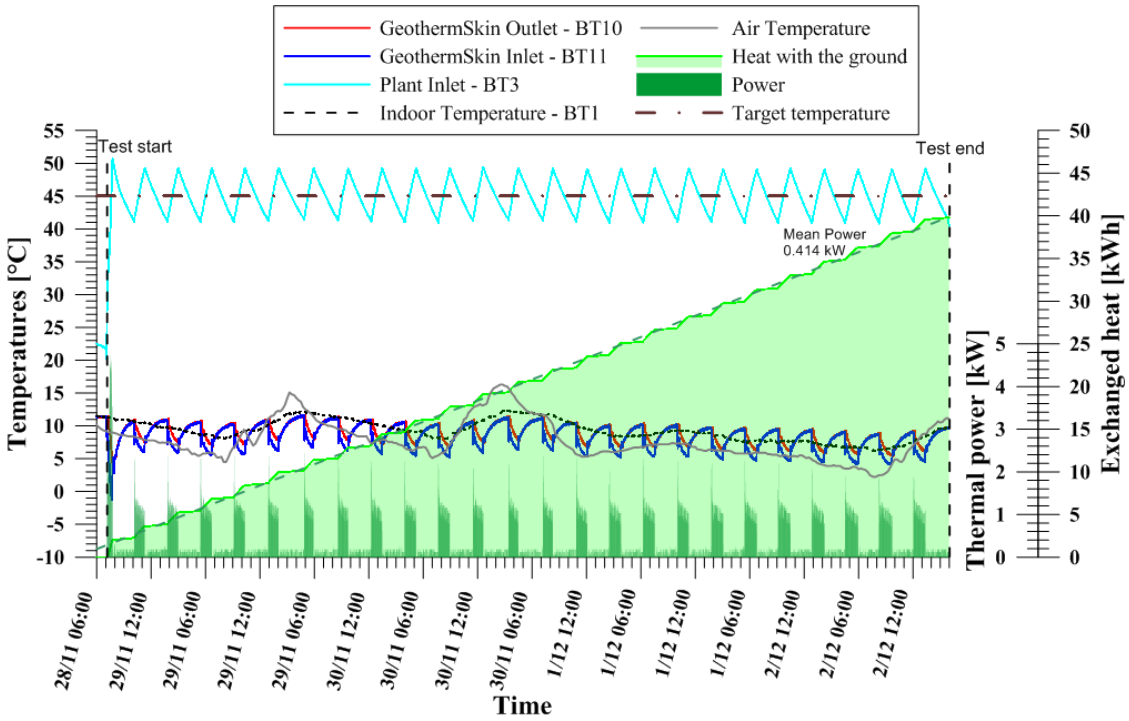

Figure A.70: Thermal performance interpretation of experimental test *H_1-2_20191128_20191202* with sequential link of circuit 1 and 2 in heating mode.

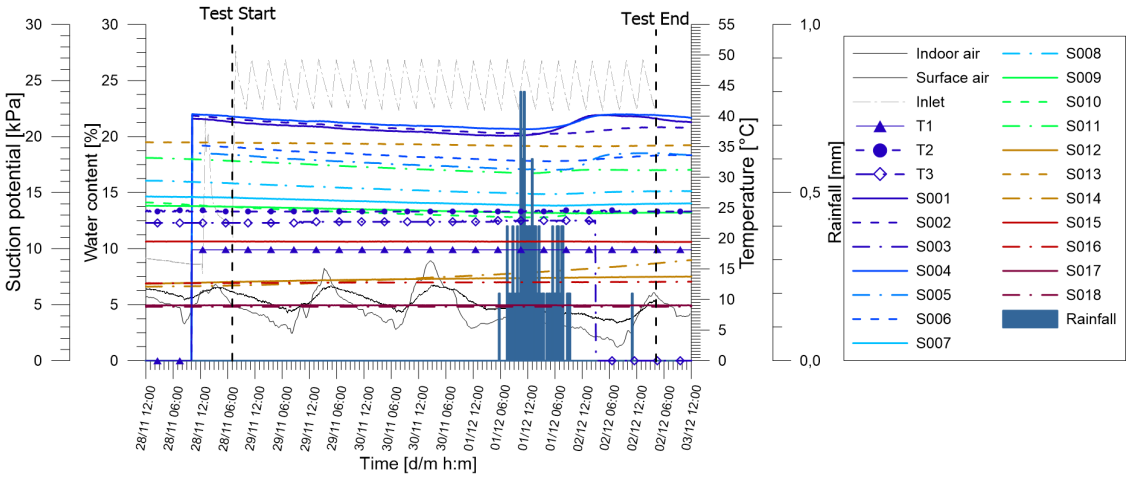

Figure A.71: Tensiometer and hygrometers records of experimental test H_1-2_20191128_20191202 together with monitored rainfall from Politecnico weather station.

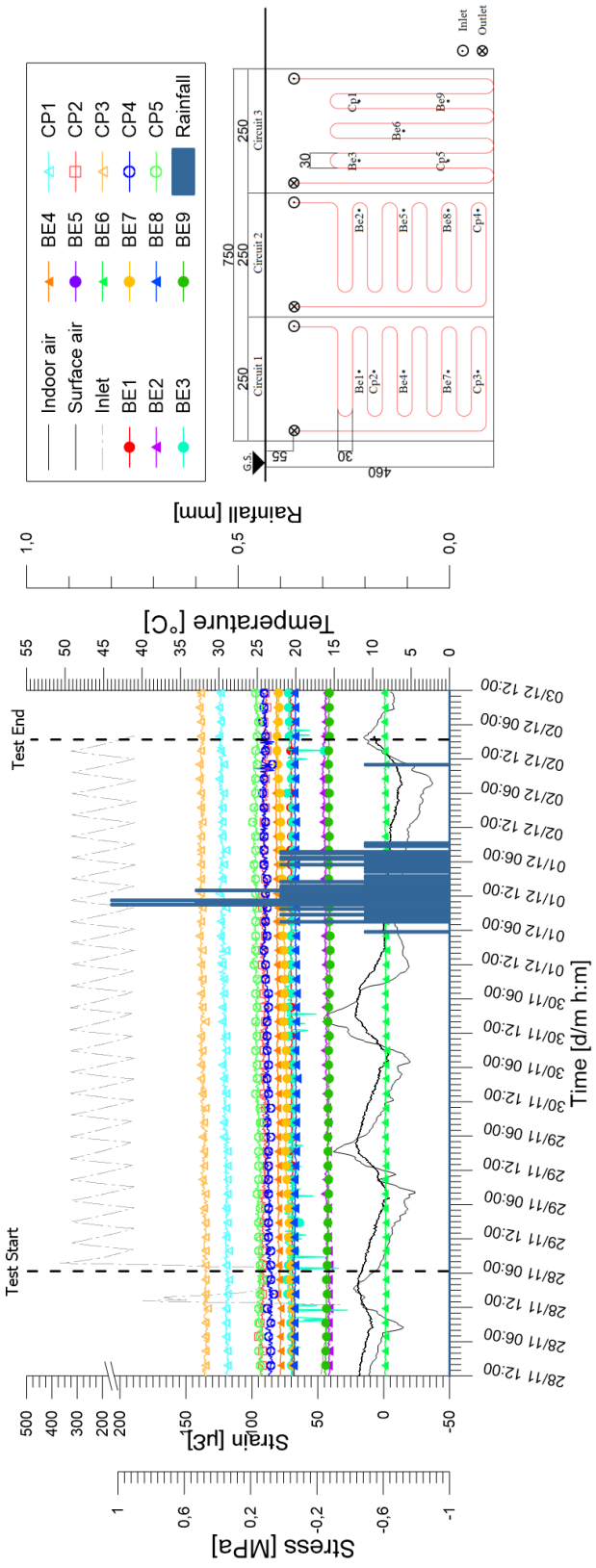

Figure A.72: Stresses and strains monitored at the wall external facade during experimental test H_1-2_20191128_20191202.

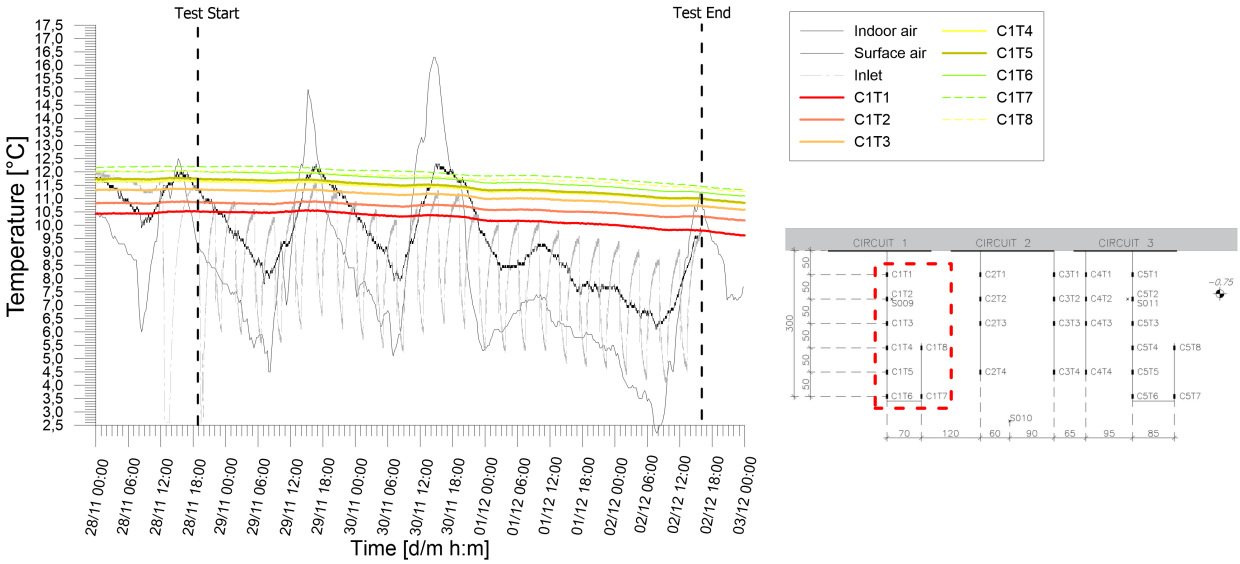

Figure A.73: Temperatures records from chain 1 of experimental test H_1-2_20191128_20191202.

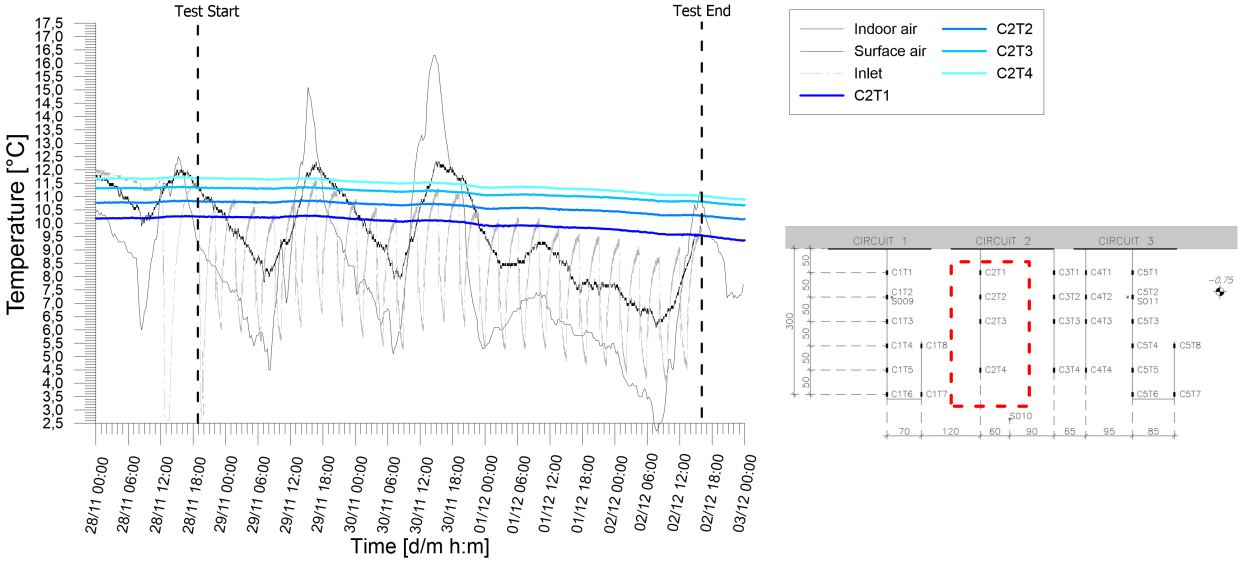

Figure A.74: Temperatures records from chain 2 of experimental test H_1-2_20191128_20191202.

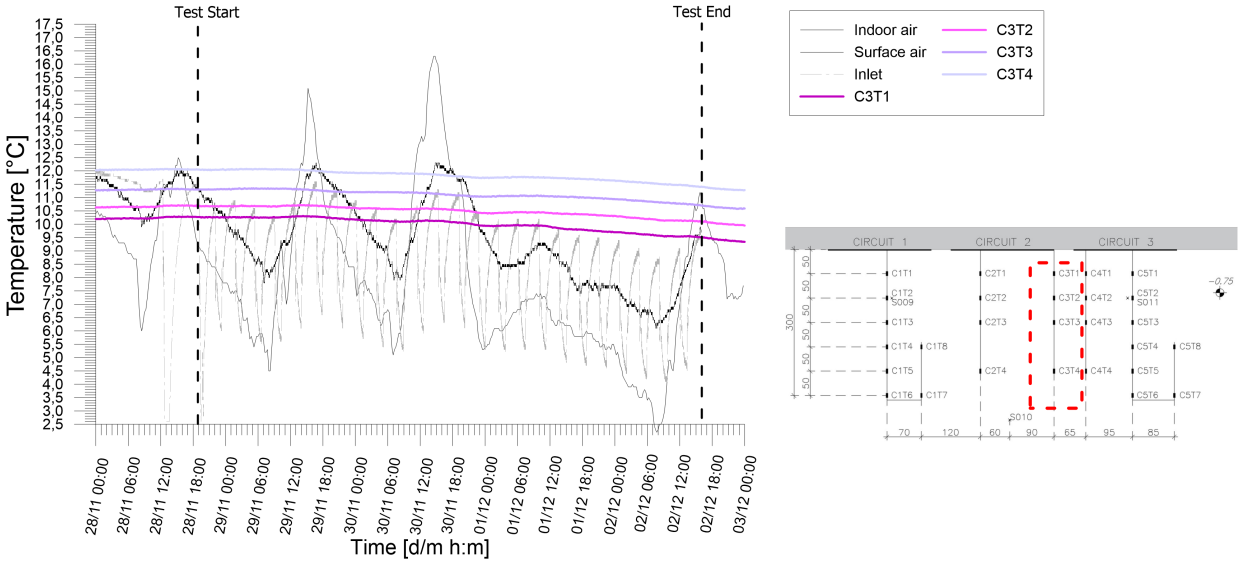

Figure A.75: Temperatures records from chain 3 of experimental test H_1-2_20191128_20191202.

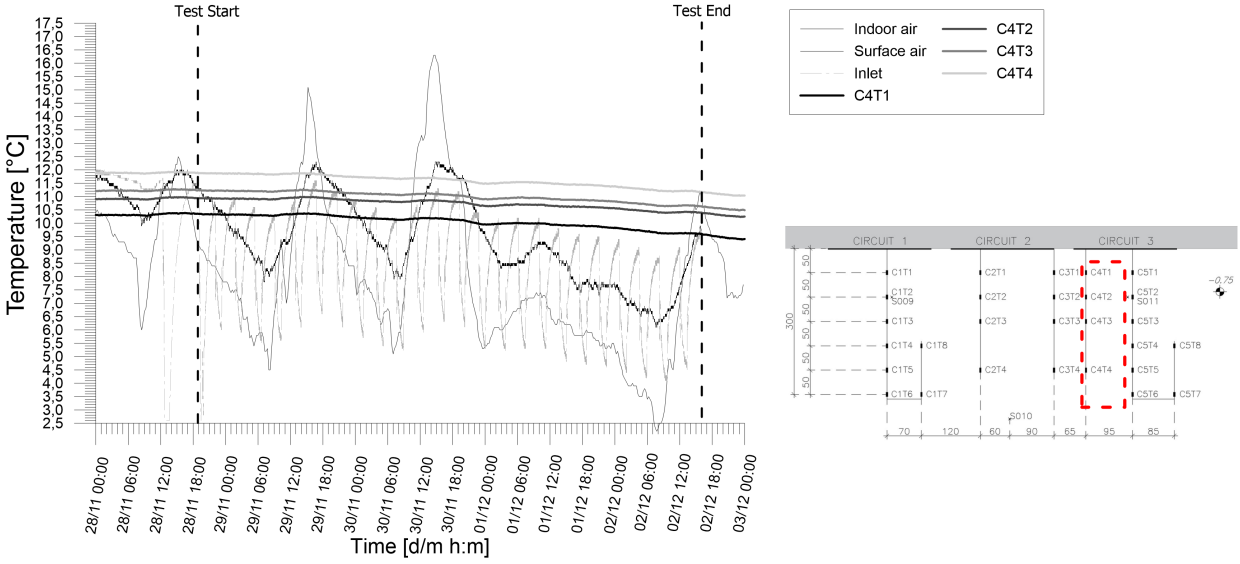

Figure A.76: Temperatures records from chain 4 of experimental test H_1-2_20191128_20191202.

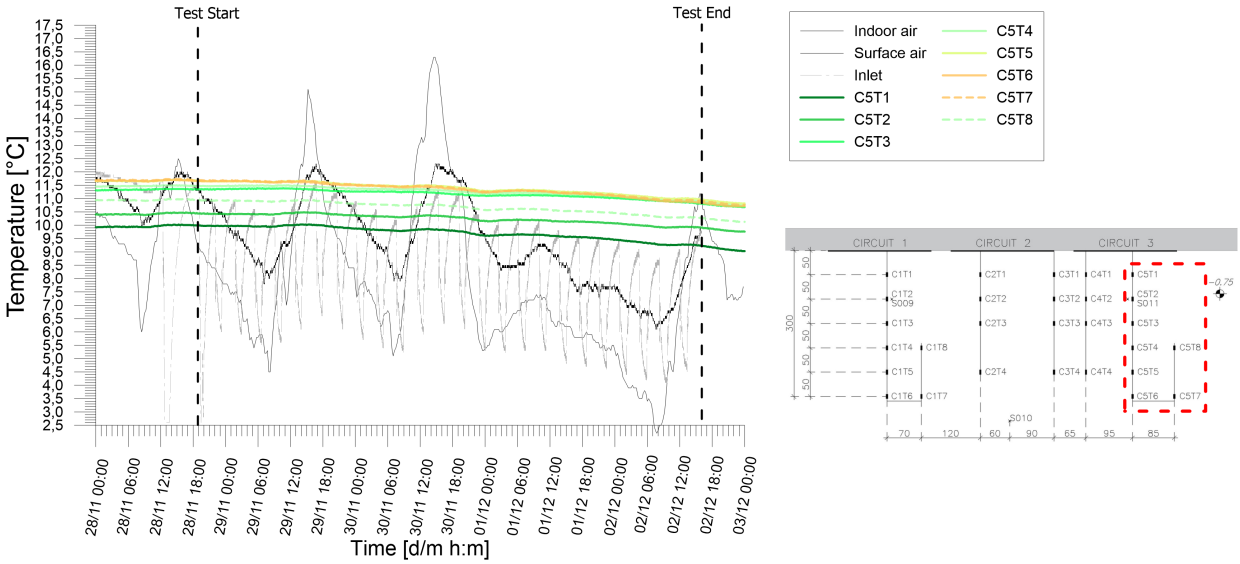

Figure A.77: Temperatures records from chain 5 of experimental test H_1-2_20191128_20191202.

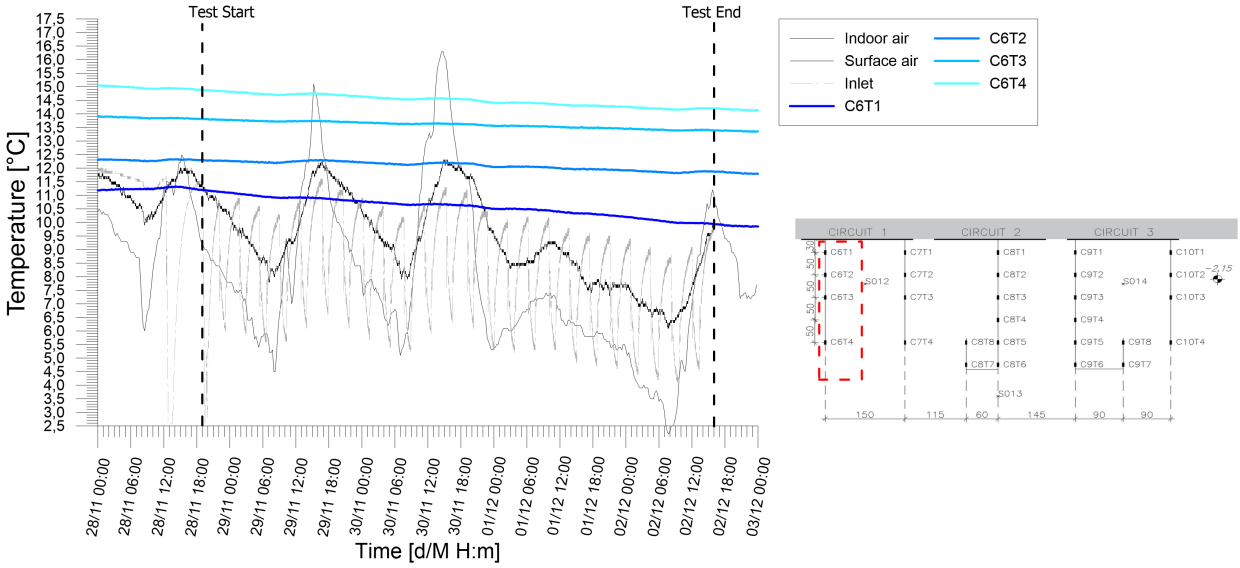

Figure A.78: Temperatures records from chain 6 of experimental test H_1-2_20191128_20191202.

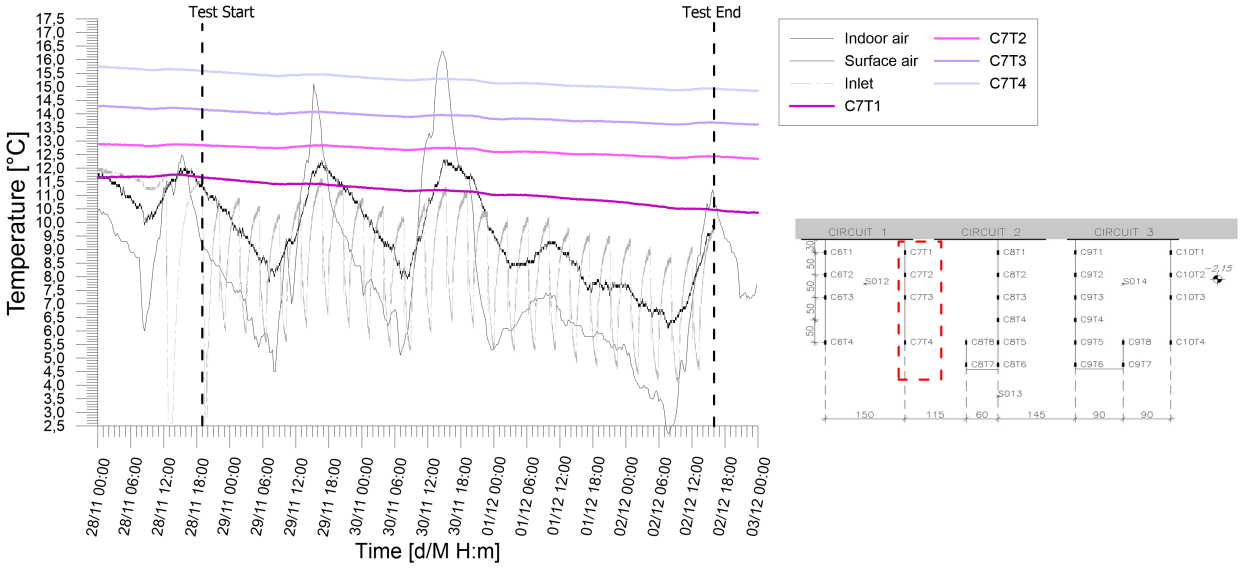

Figure A.79: Temperatures records from chain 7 of experimental test H_1-2_20191128_20191202.

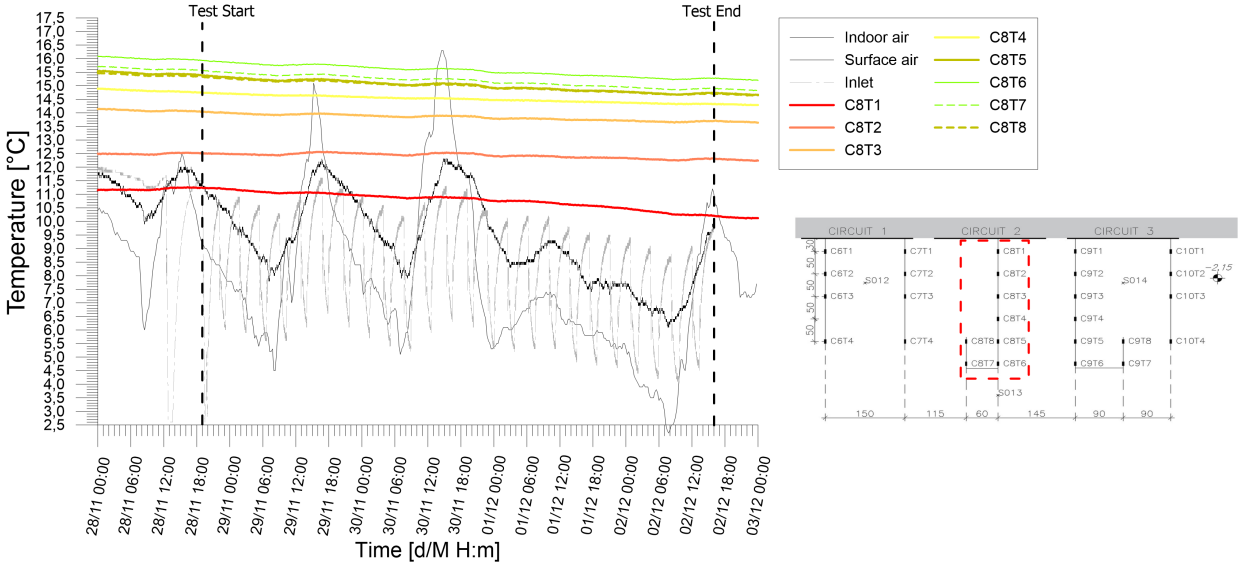

Figure A.80: Temperatures records from chain 8 of experimental test H_1-2_20191128_20191202.

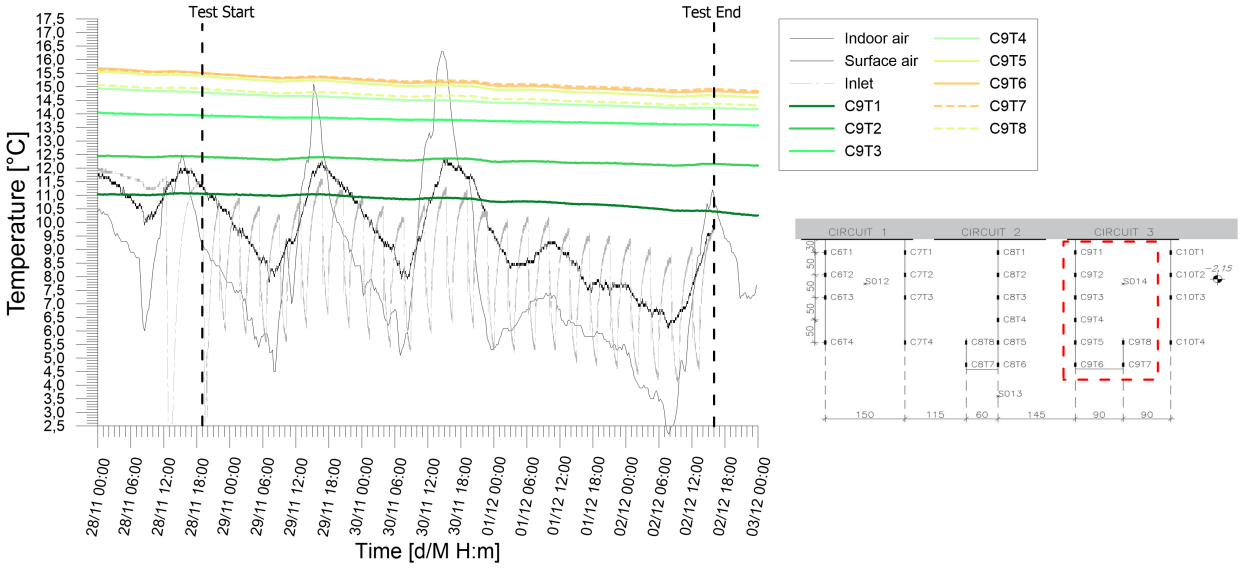

Figure A.81: Temperatures records from chain 9 of experimental test H_1-2_20191128_20191202.

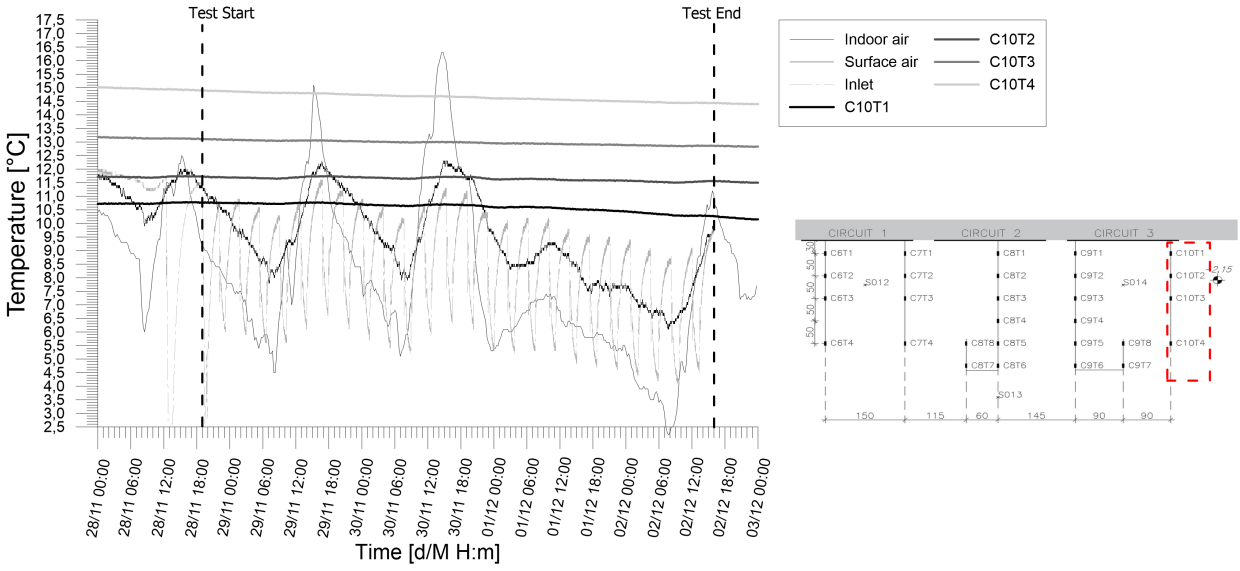

Figure A.82: Temperatures records from chain 10 of experimental test H_1-2_20191128_20191202.

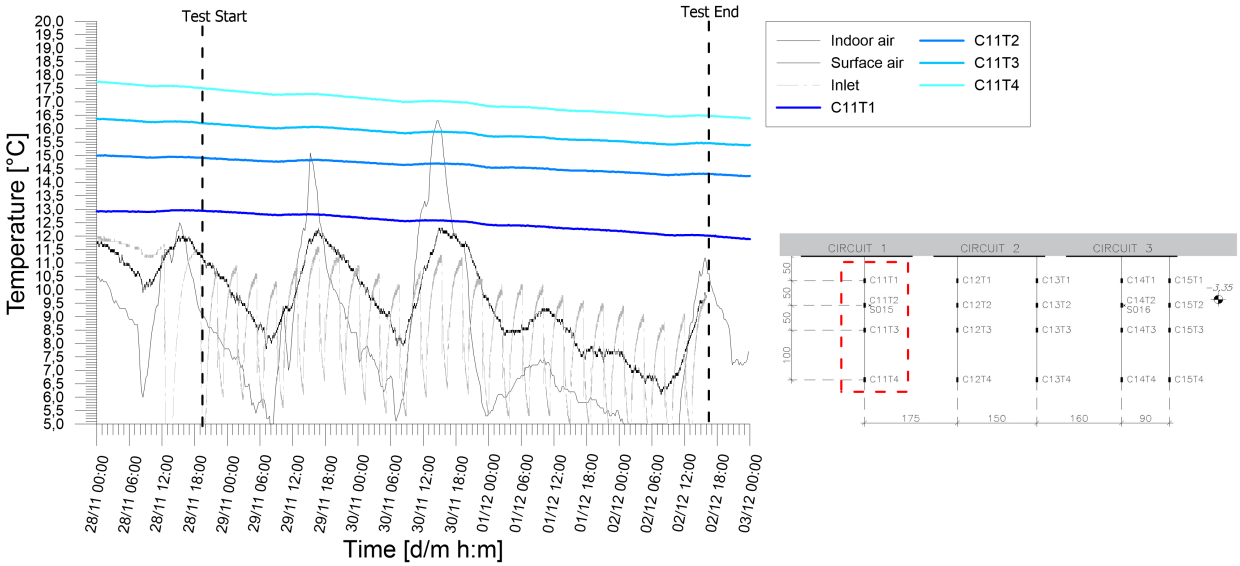

Figure A.83: Temperatures records from chain 11 of experimental test H_1-2_20191128_20191202.

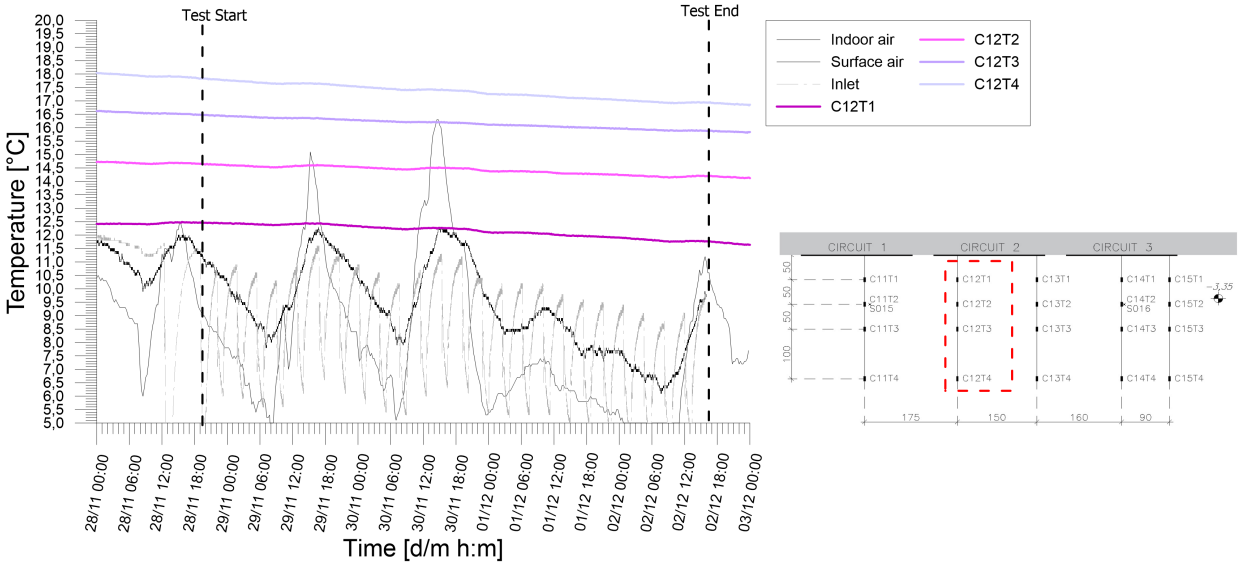

Figure A.84: Temperatures records from chain 12 of experimental test H_1-2_20191128_20191202.

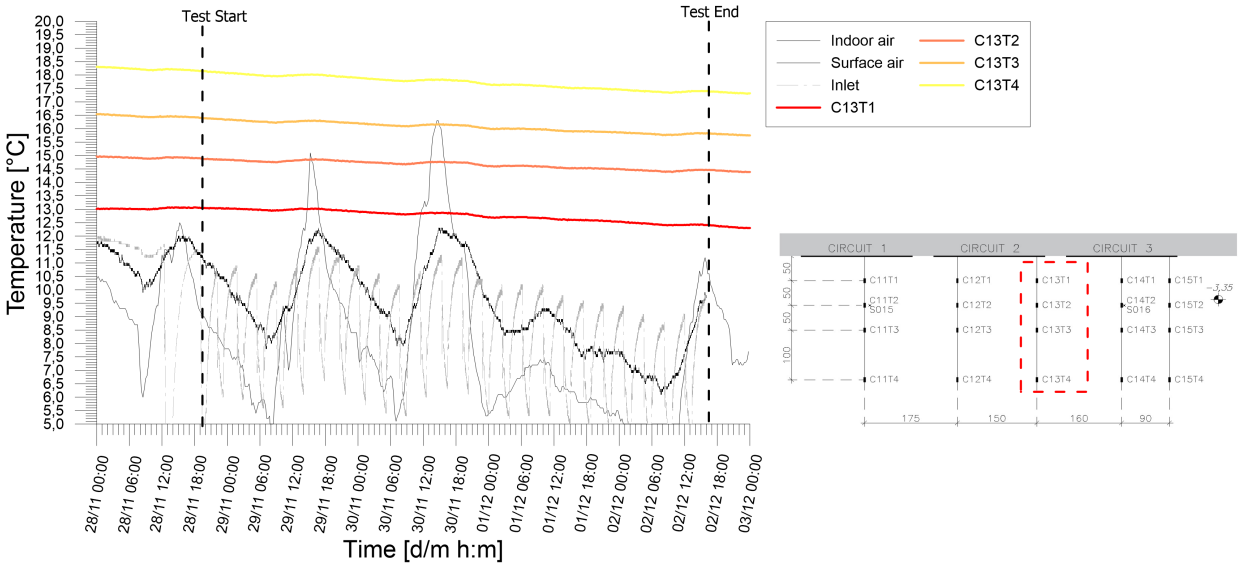

Figure A.85: Temperatures records from chain 13 of experimental test H_1-2_20191128_20191202.

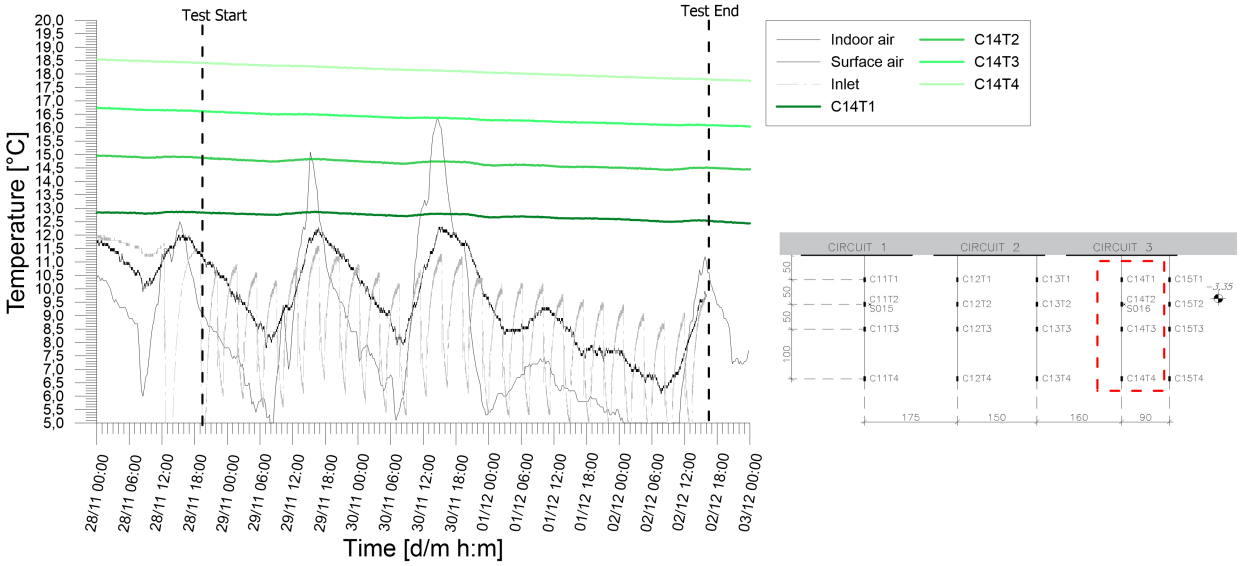

Figure A.86: Temperatures records from chain 14 of experimental test H_1-2_20191128_20191202.

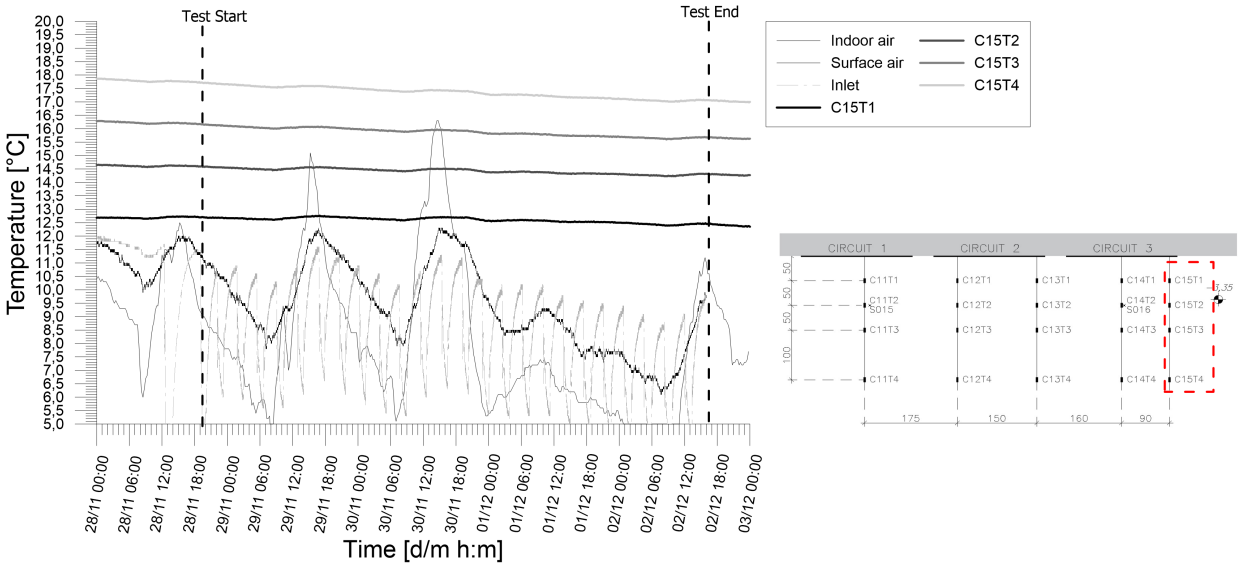

Figure A.87: Temperatures records from chain 15 of experimental test H_1-2_20191128_20191202.

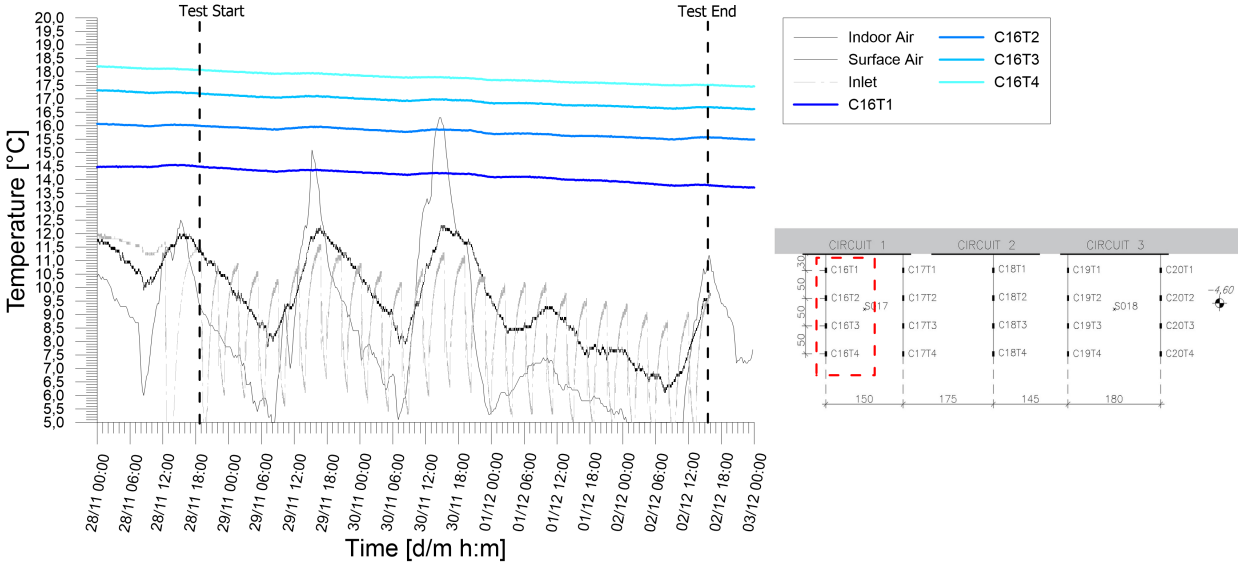

Figure A.88: Temperatures records from chain 16 of experimental test H_1-2_20191128_20191202.

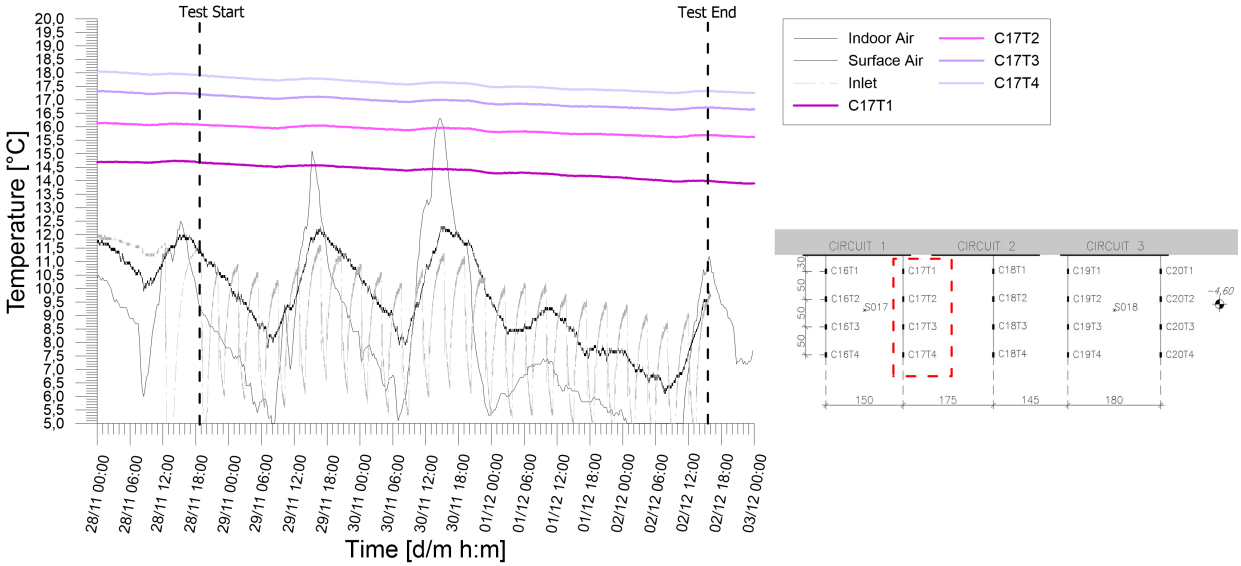

Figure A.89: Temperatures records from chain 17 of experimental test H_1-2_20191128_20191202.

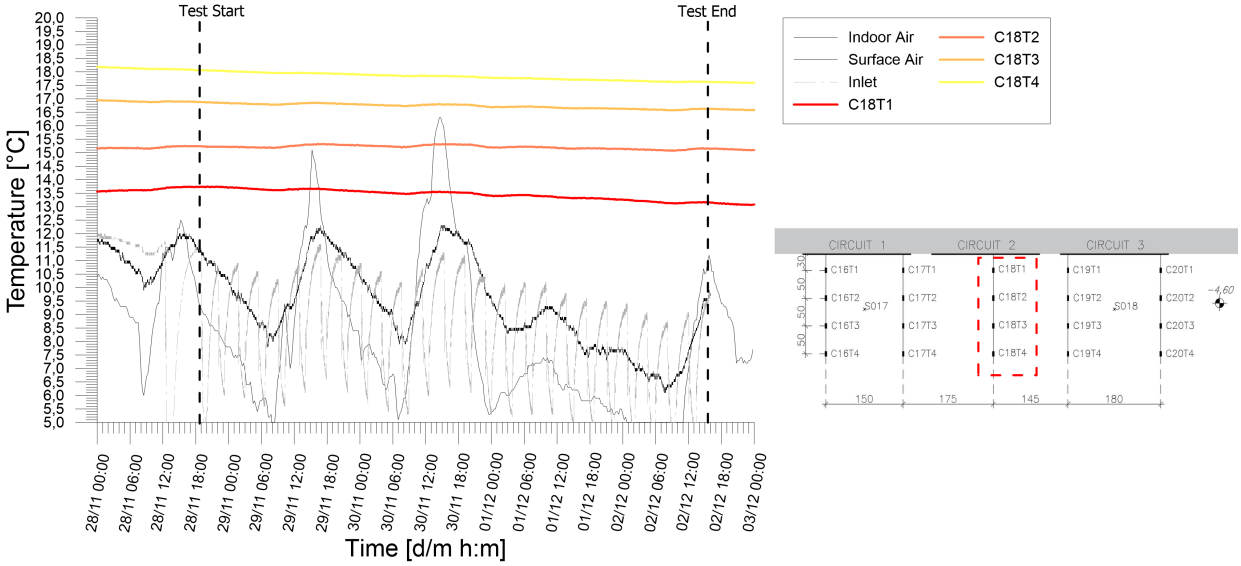

Figure A.90: Temperatures records from chain 18 of experimental test H_1-2_20191128_20191202.

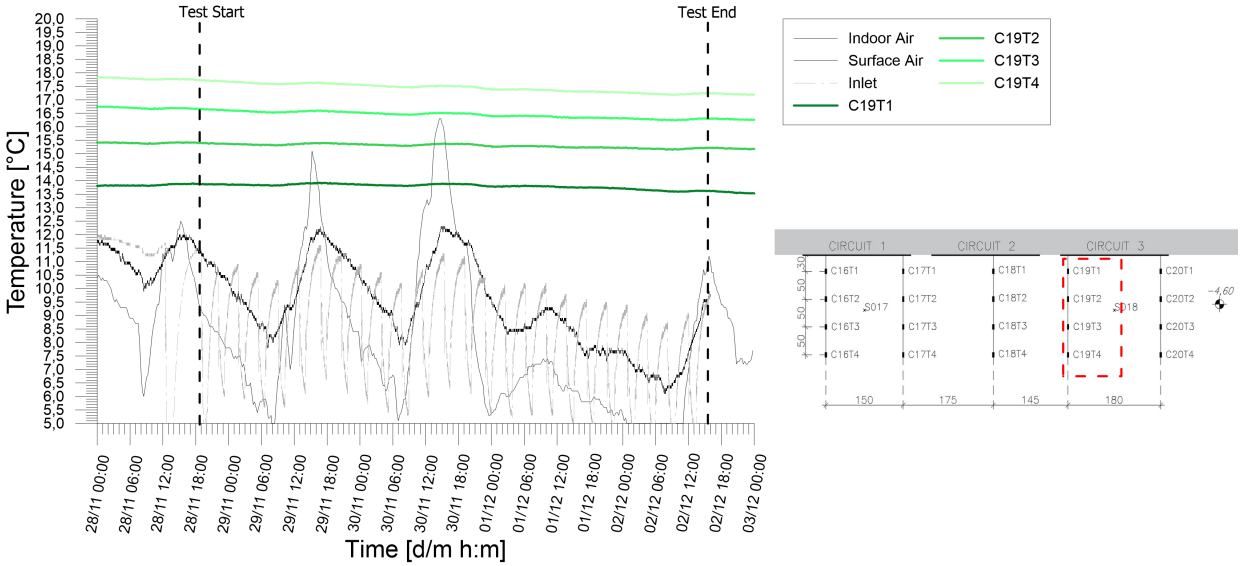

Figure A.91: Temperatures records from chain 19 of experimental test H_1-2_20191128_20191202.

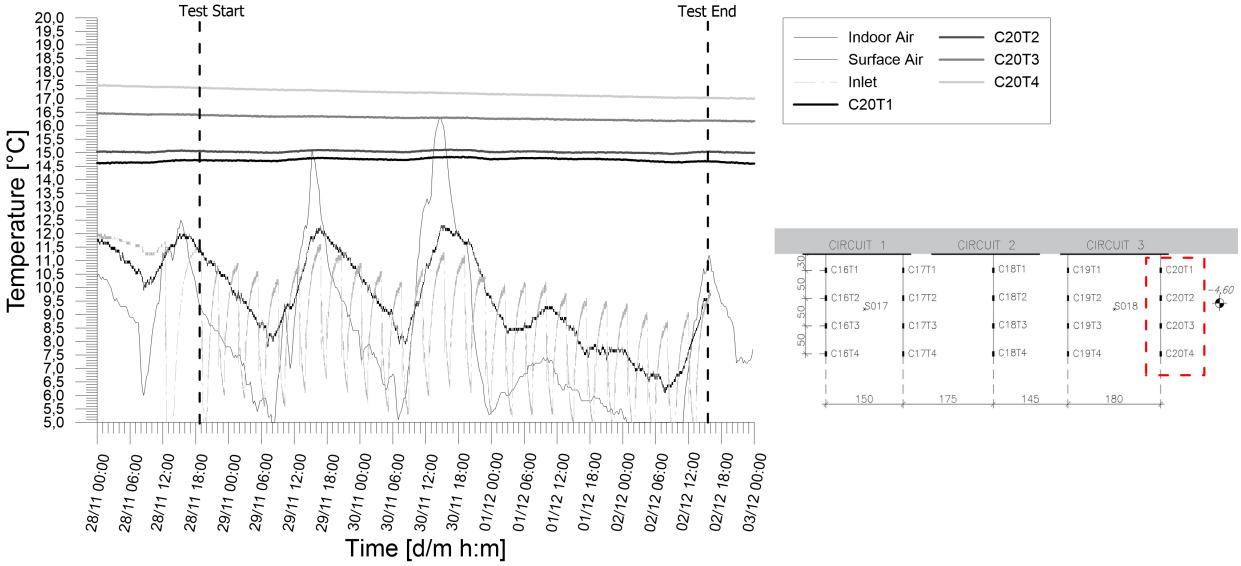

Figure A.92: Temperatures records from chain 20 of experimental test H_1-2_20191128_20191202.

A.5 Test H_2-3_20191207_20191210

Table A.5: Main features of the test.

Test start time	7/12/19 10.00
Test end time	10/12/19 9.25
Duration [h]	87.3
Operative mode	Heating
Active circuit(s)	2;3
Circuit link	Sequential
Target temperature user [°C]	45
Flow rate at the ground side [l/h]	530.0

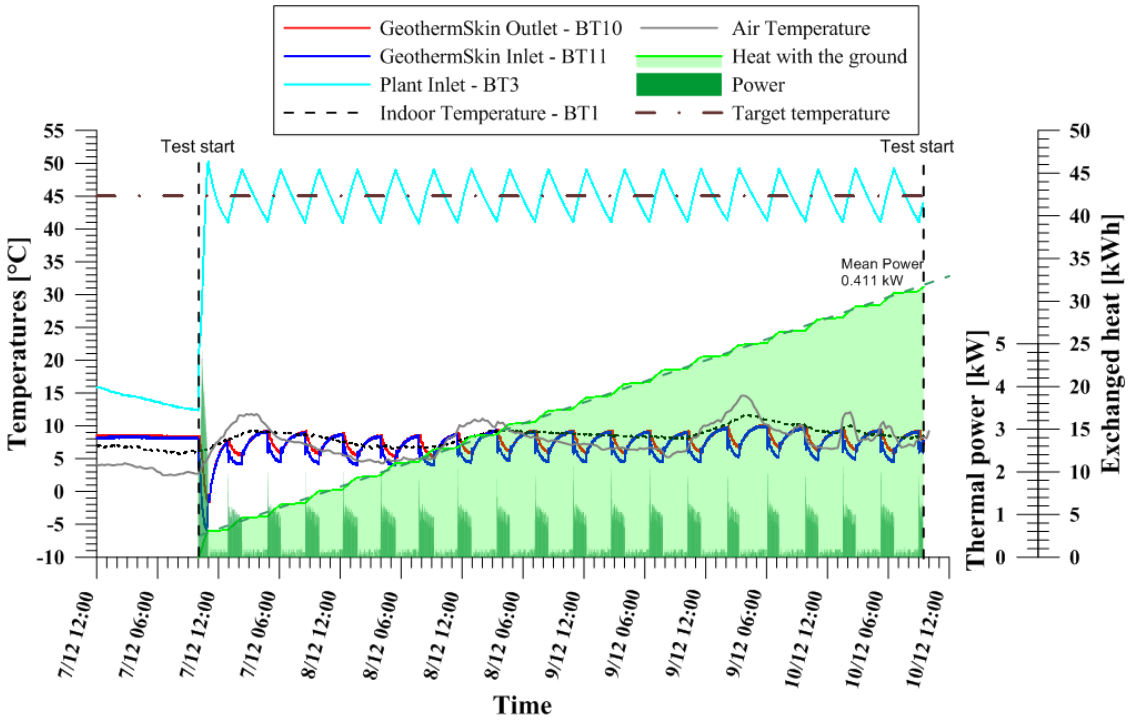

Figure A.93: Thermal performance interpretation of experimental test *H_2-3_20191206_20191210* with sequential link of circuit 2 and 3 in heating mode.

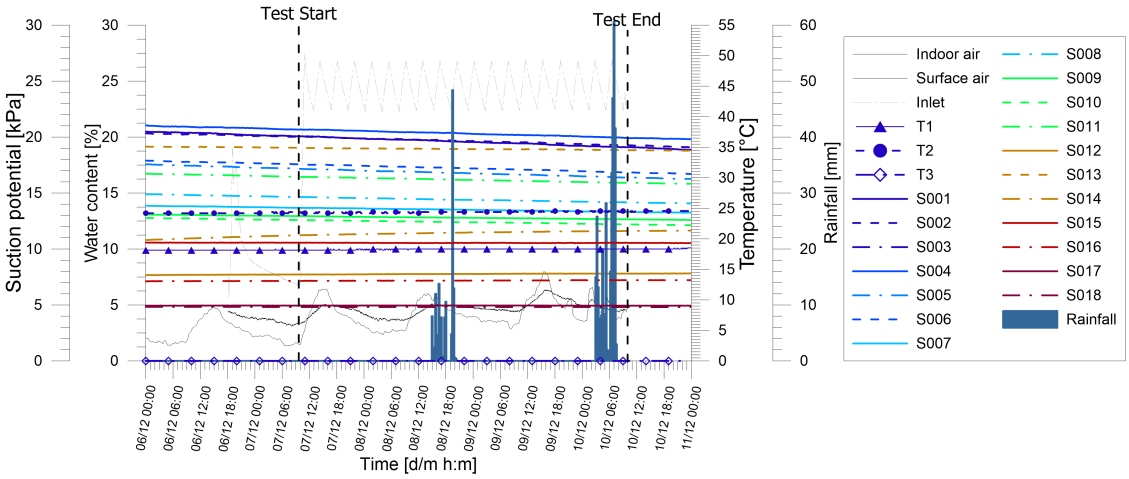

Figure A.94: Tensiometer and hygrometers records of experimental test H_2-3_20191206_20191210 together with monitored rainfall from Politecnico weather station.

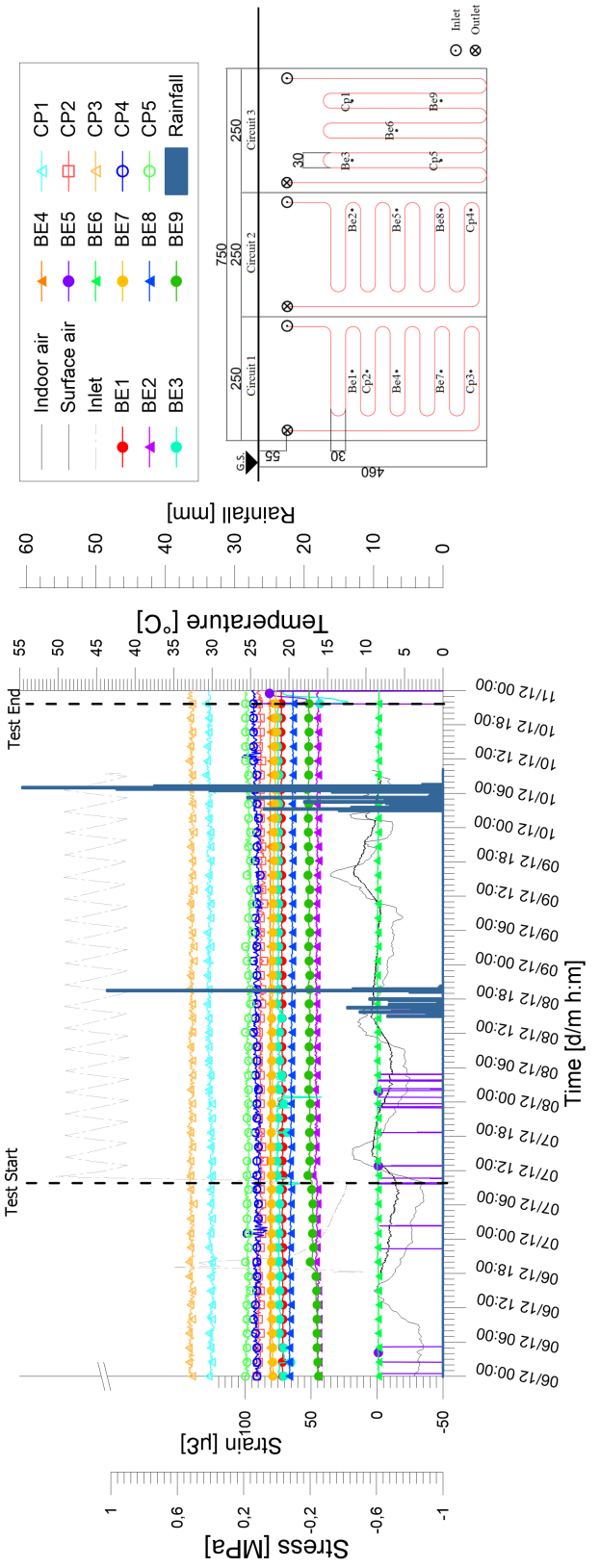

Figure A.95: Stresses and strains monitored at the wall external facade during experimental test H_2-3_20191206_20191210.

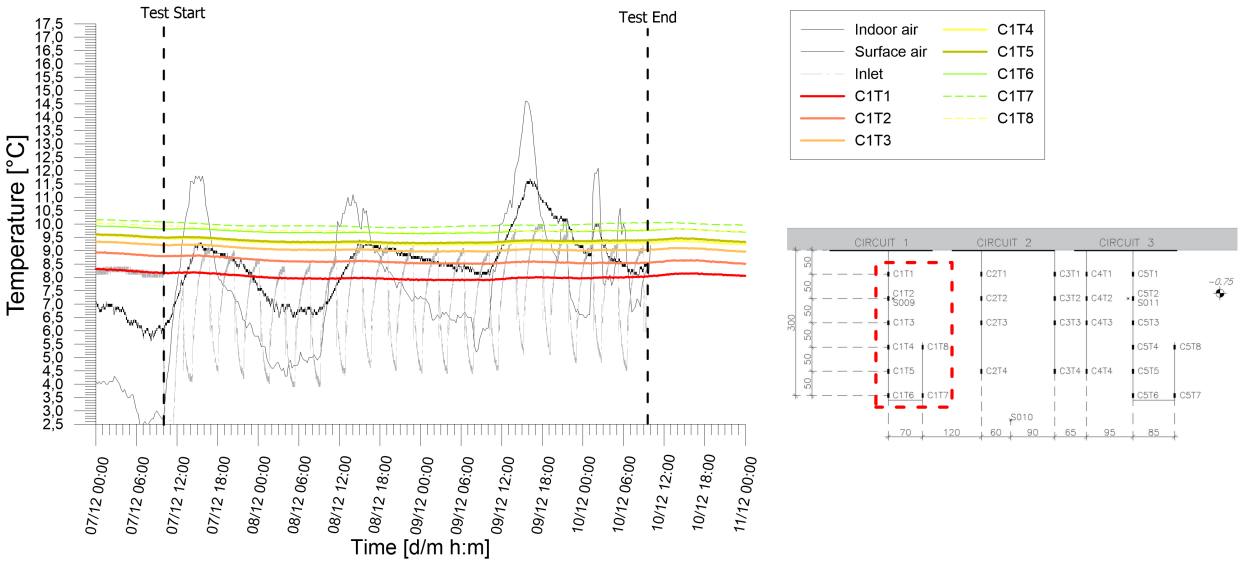

Figure A.96: Temperatures records from chain 1 of experimental test H_2-3_20191206_20191210.

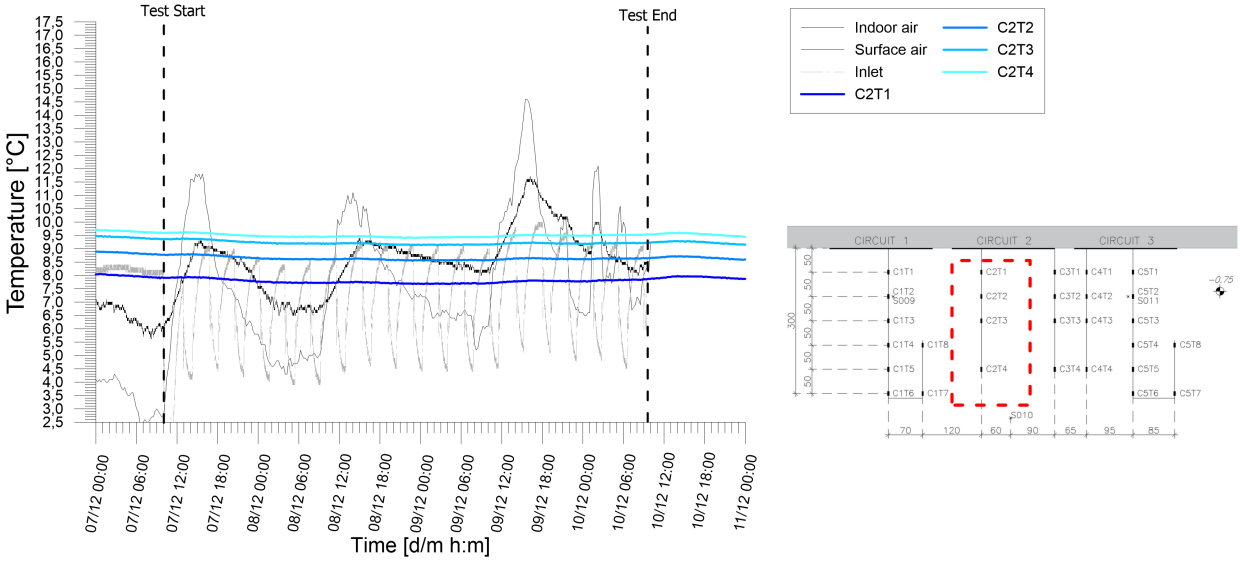

Figure A.97: Temperatures records from chain 2 of experimental test H_2-3_20191206_20191210.

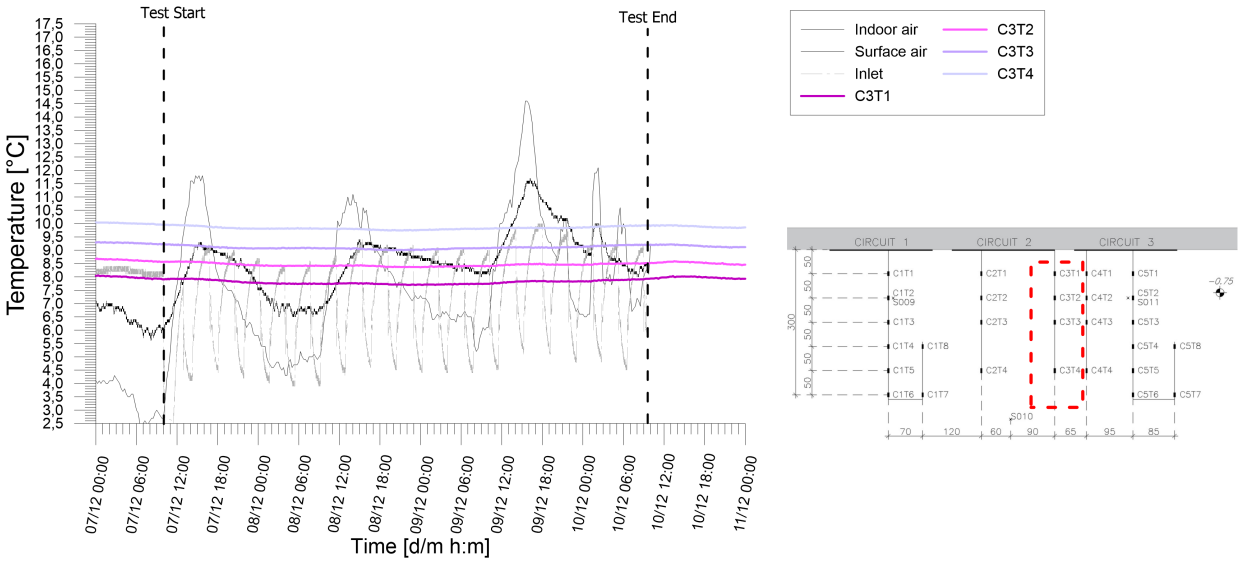

Figure A.98: Temperatures records from chain 3 of experimental test H_2-3_20191206_20191210.

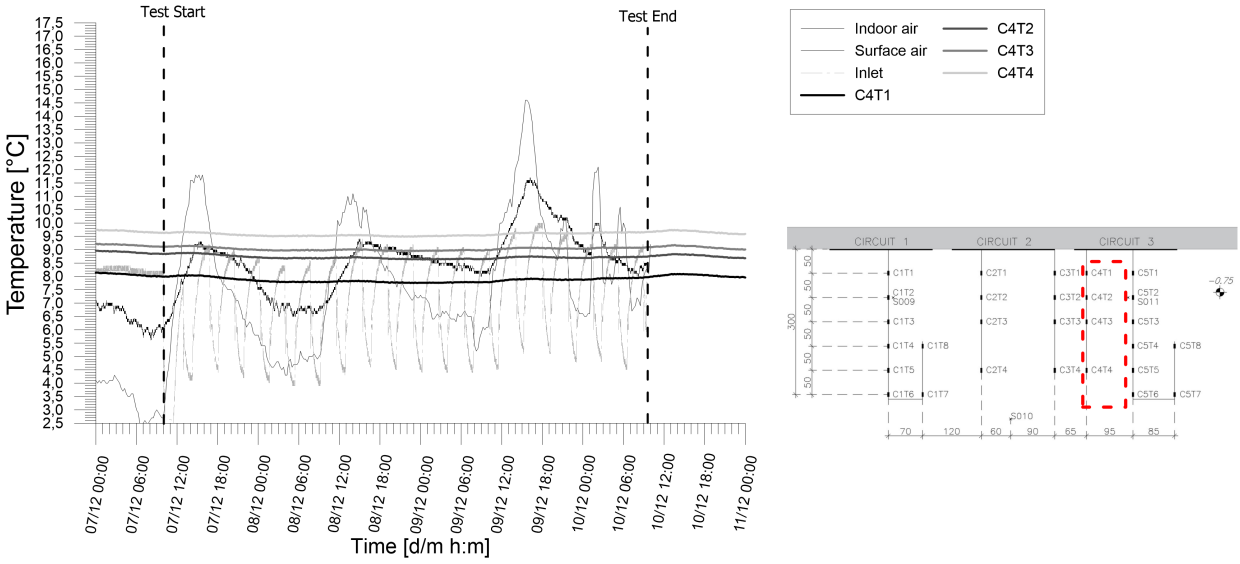

Figure A.99: Temperatures records from chain 4 of experimental test H_2-3_20191206_20191210.

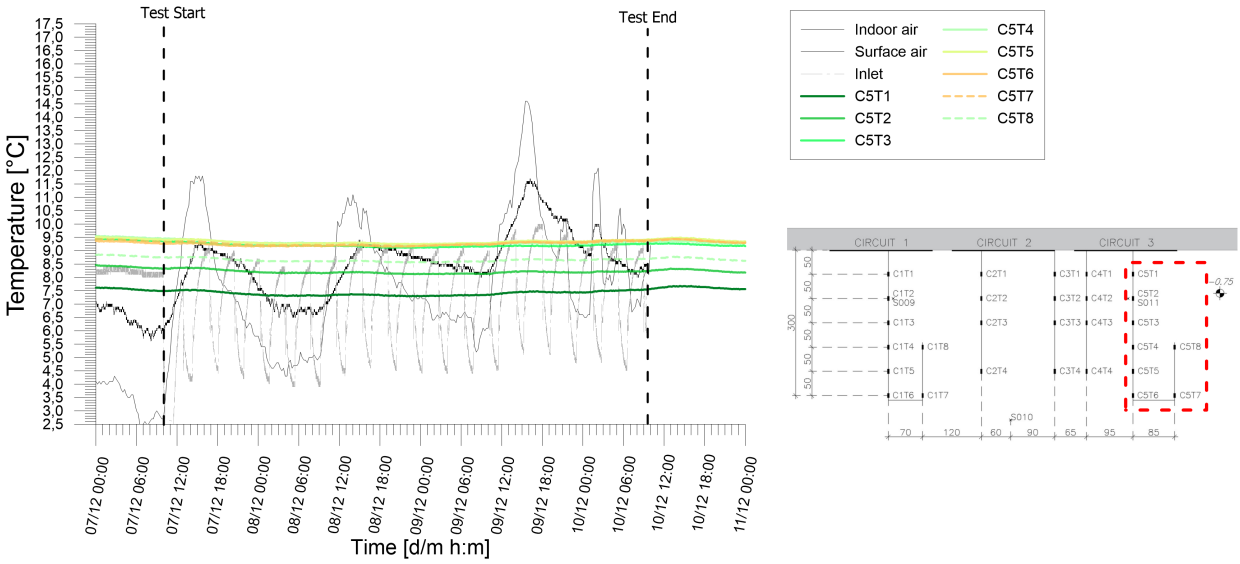

Figure A.100: Temperatures records from chain 5 of experimental test H_2-3_20191206_20191210.

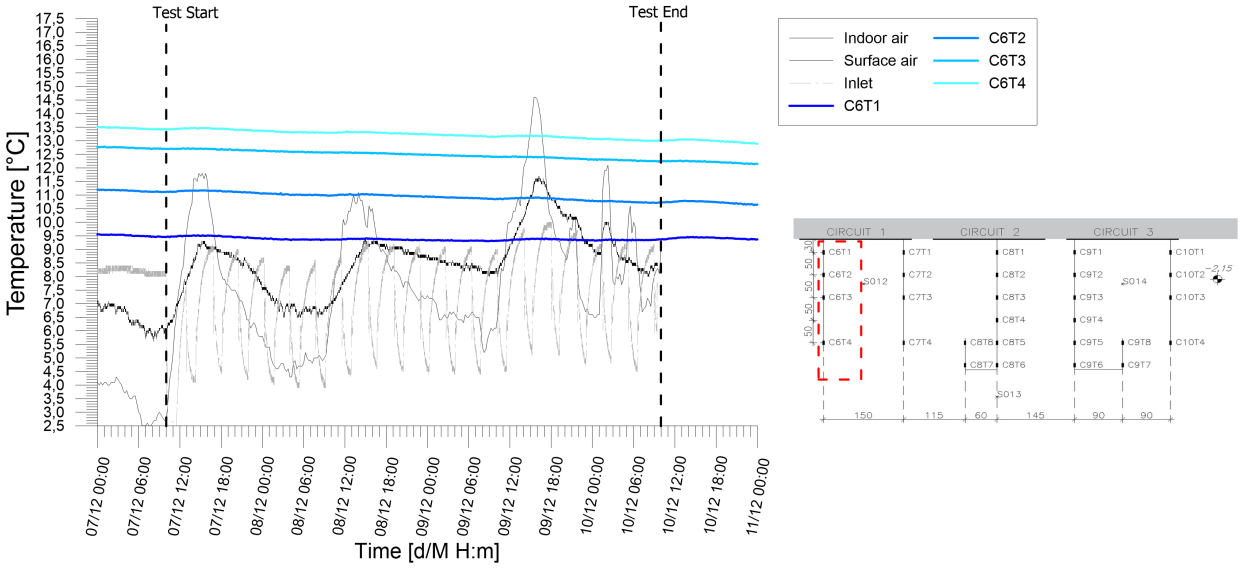

Figure A.101: Temperatures records from chain 6 of experimental test H_2-3_20191206_20191210.

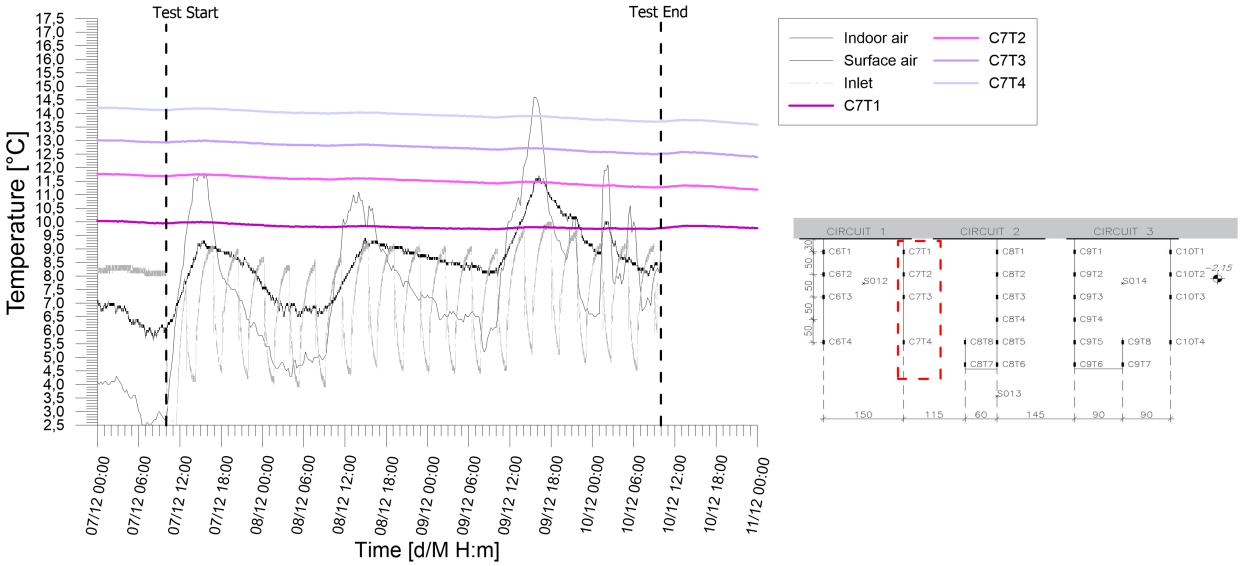

Figure A.102: Temperatures records from chain 7 of experimental test H_2-3_20191206_20191210.

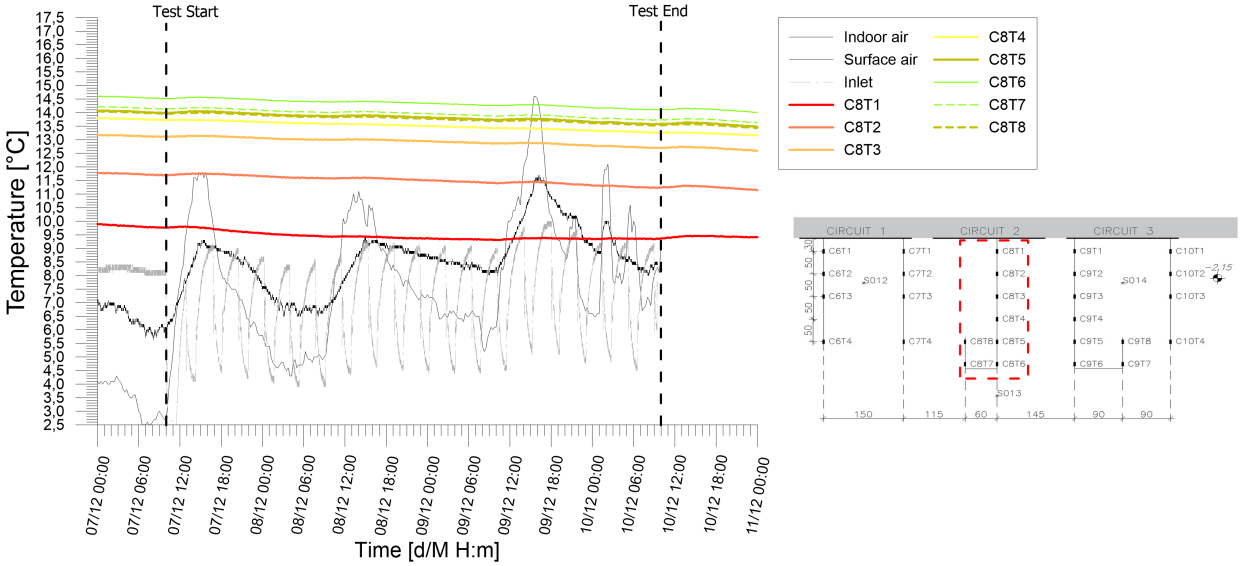

Figure A.103: Temperatures records from chain 8 of experimental test H_2-3_20191206_20191210.

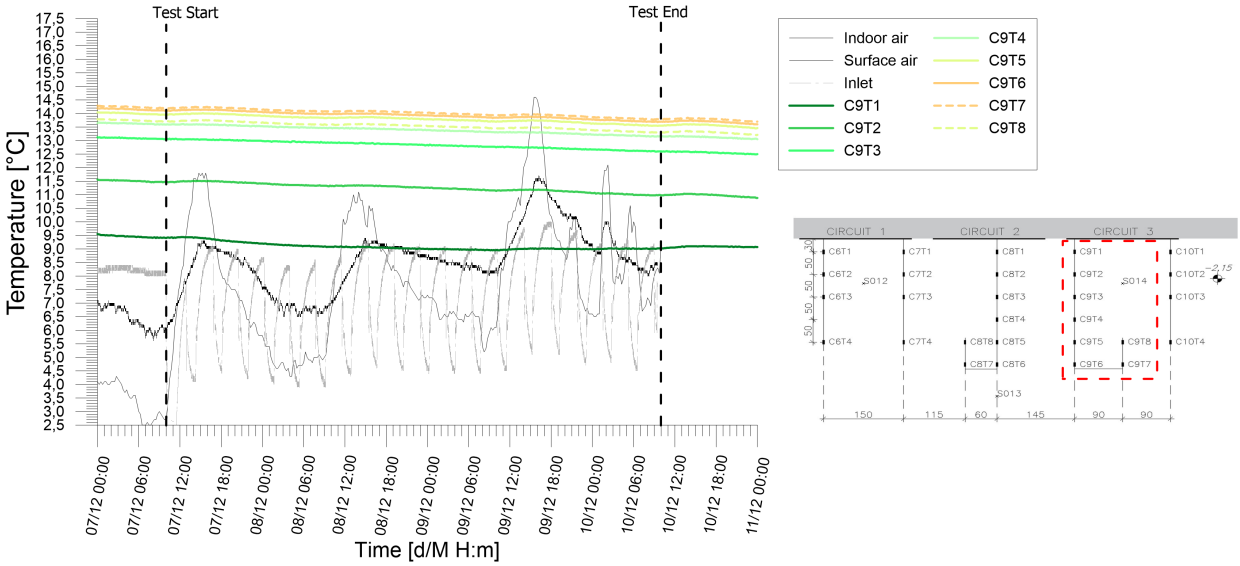

Figure A.104: Temperatures records from chain 9 of experimental test H_2-3_20191206_20191210.

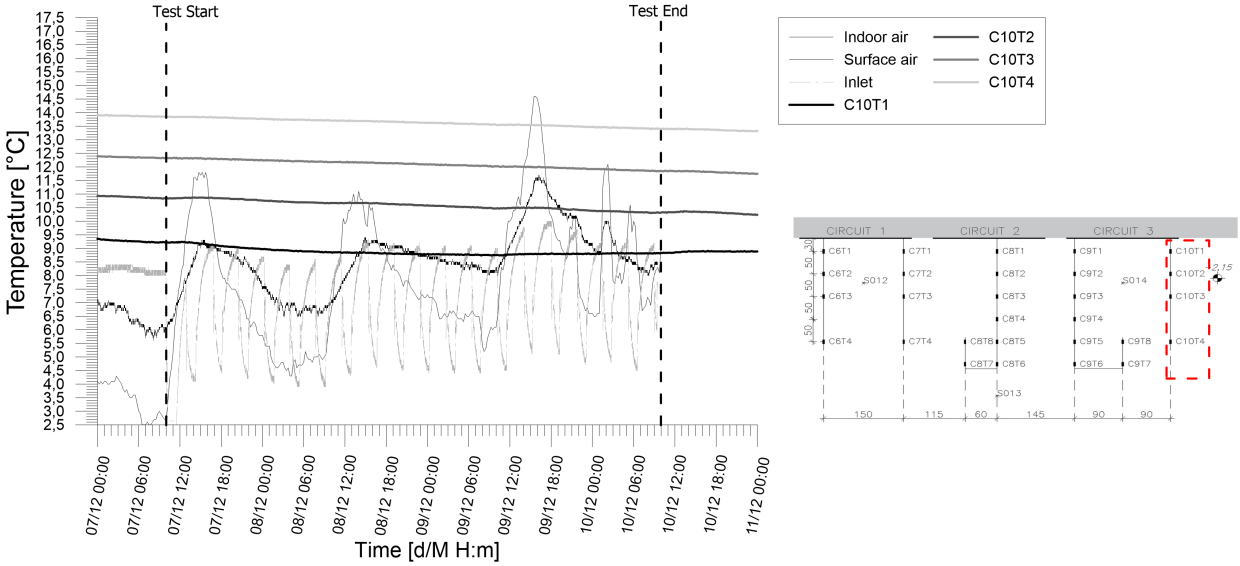

Figure A.105: Temperatures records from chain 10 of experimental test H_2-3_20191206_20191210.

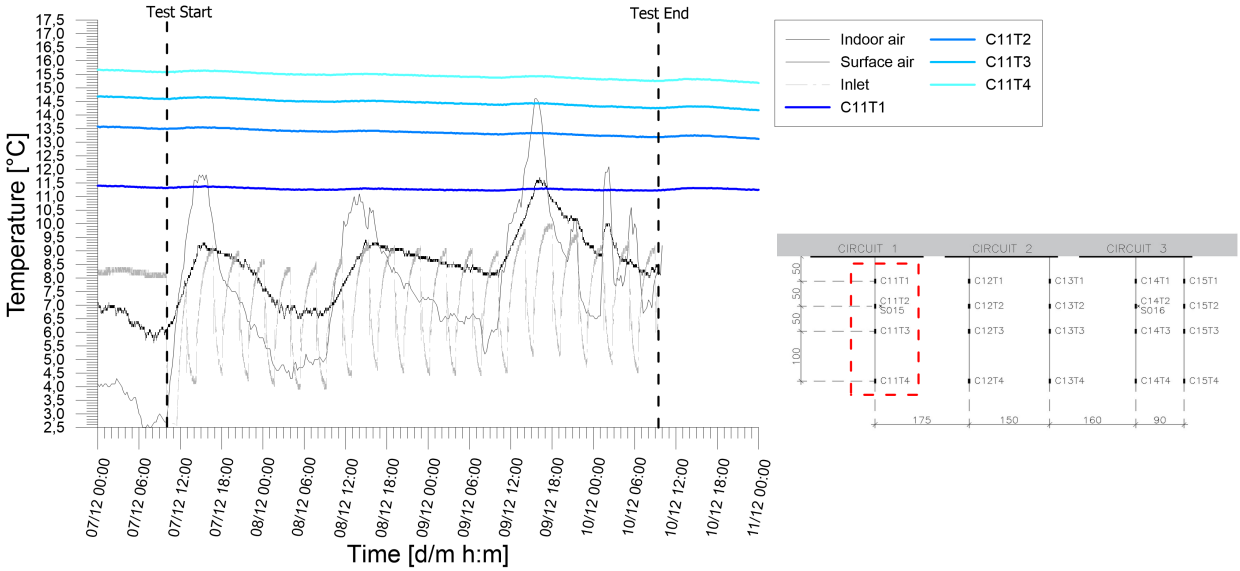

Figure A.106: Temperatures records from chain 11 of experimental test H_2-3_20191206_20191210.

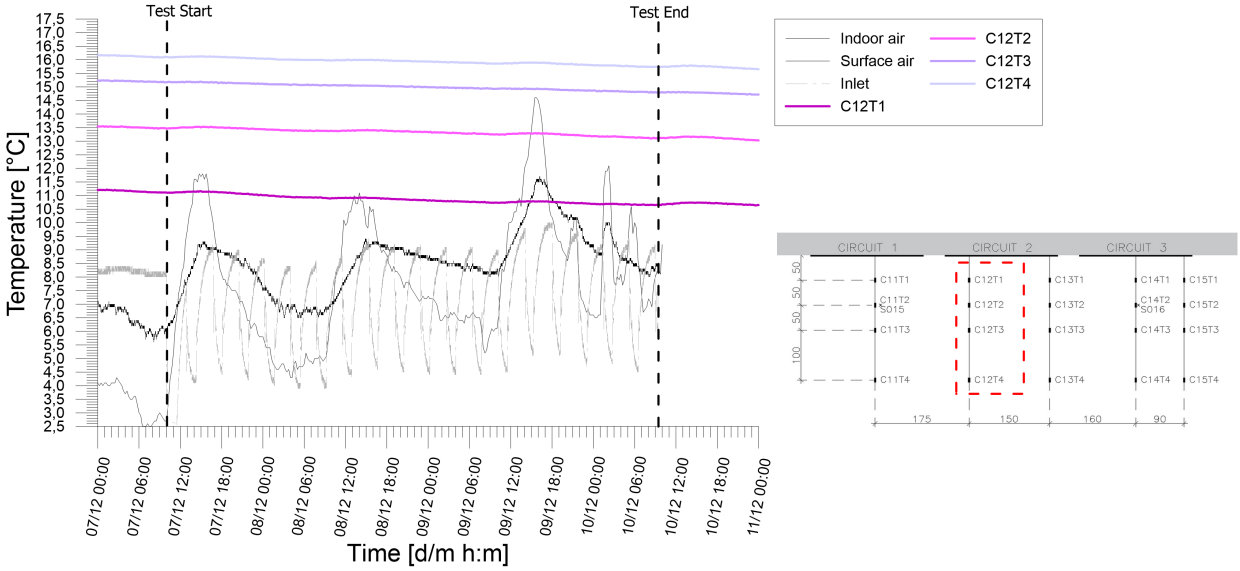

Figure A.107: Temperatures records from chain 12 of experimental test H_2-3_20191206_20191210.

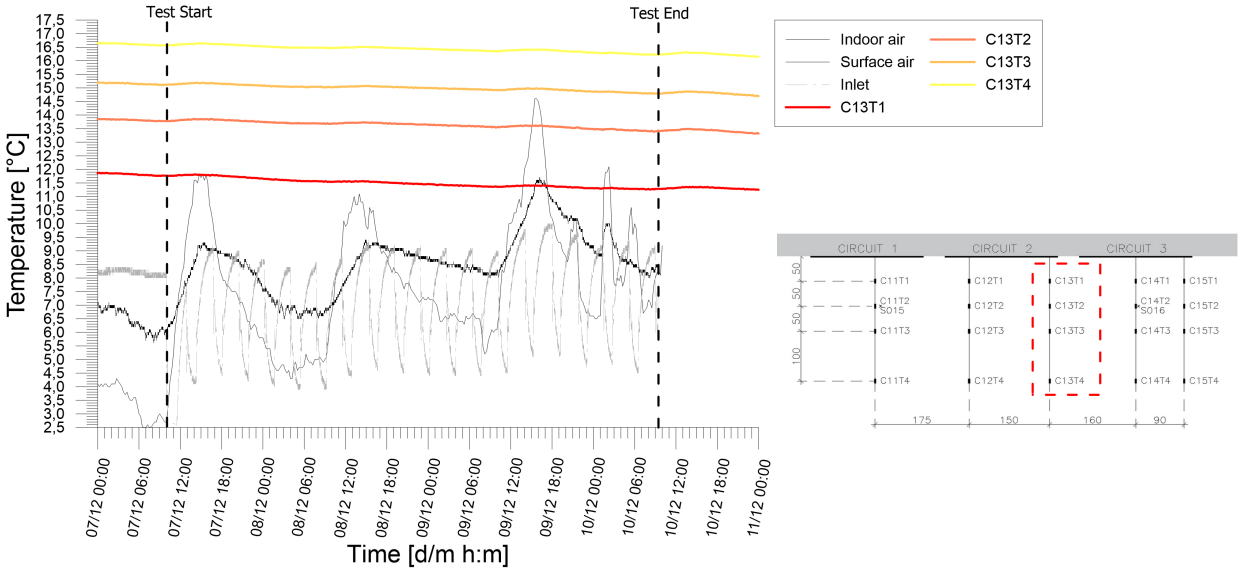

Figure A.108: Temperatures records from chain 13 of experimental test H_2-3_20191206_20191210.

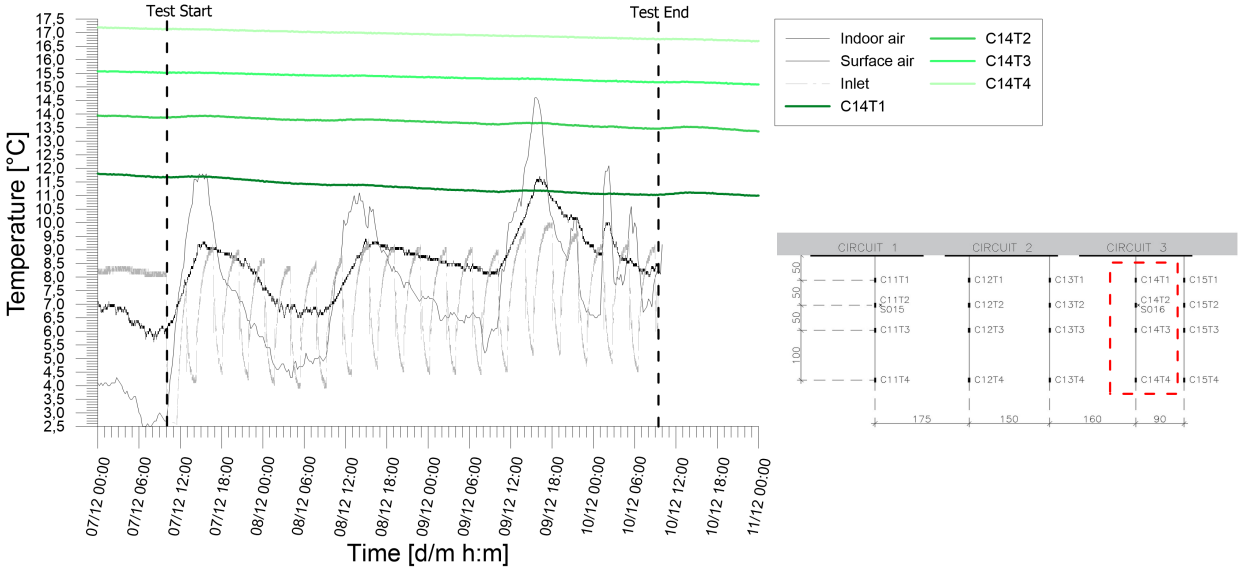

Figure A.109: Temperatures records from chain 14 of experimental test H_2-3_20191206_20191210.

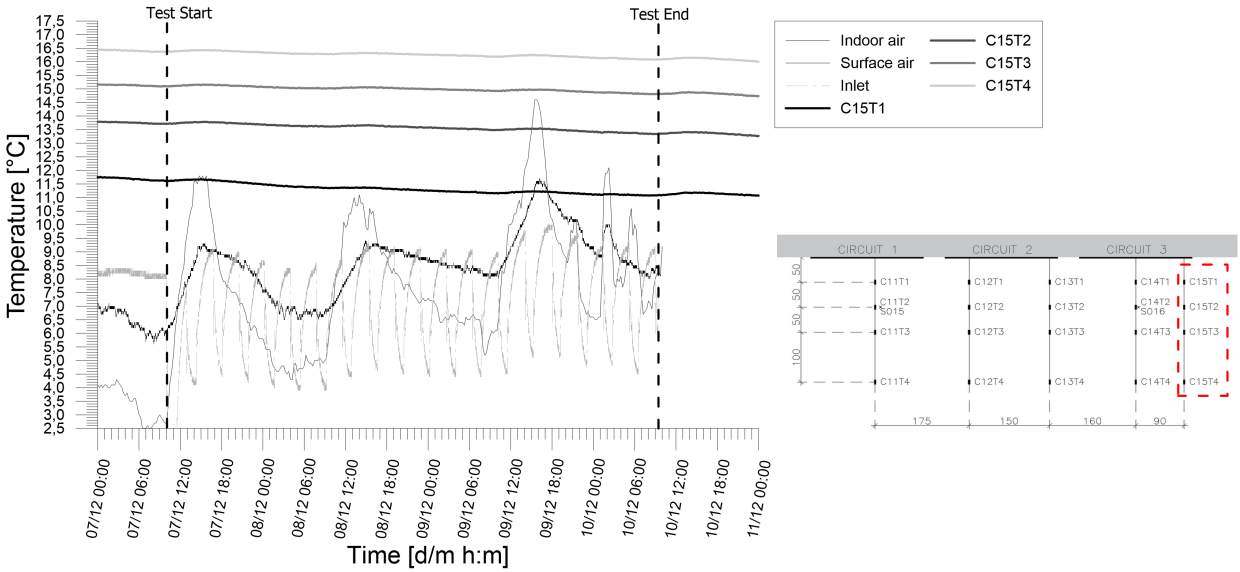

Figure A.110: Temperatures records from chain 15 of experimental test H_2-3_20191206_20191210.

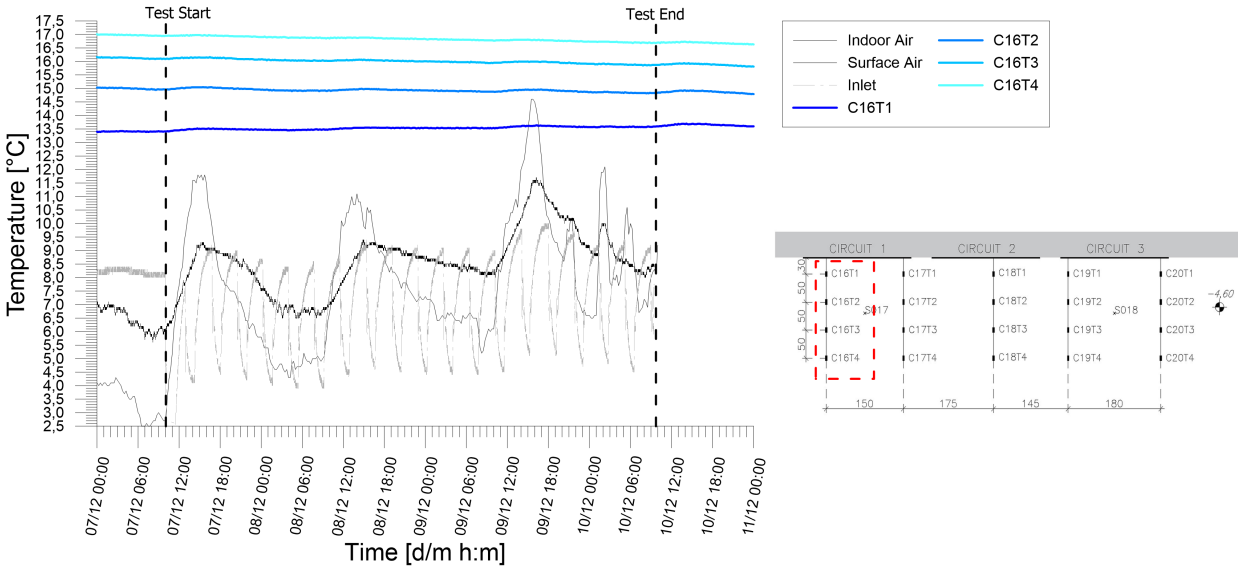

Figure A.111: Temperatures records from chain 16 of experimental test H_2-3_20191206_20191210.

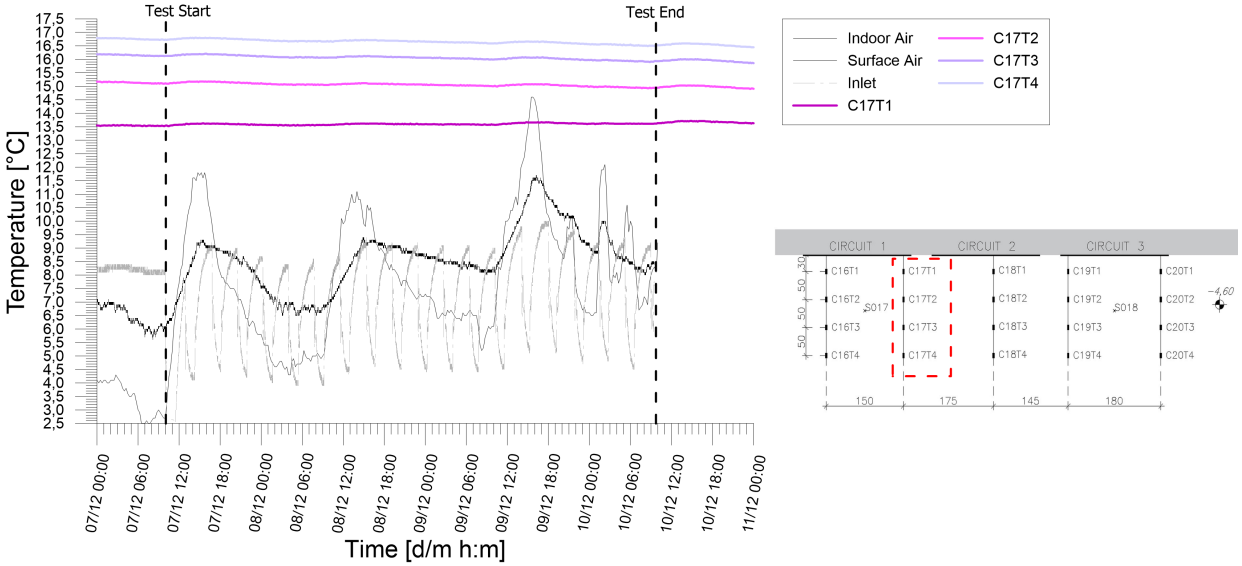

Figure A.112: Temperatures records from chain 17 of experimental test H_2-3_20191206_20191210.

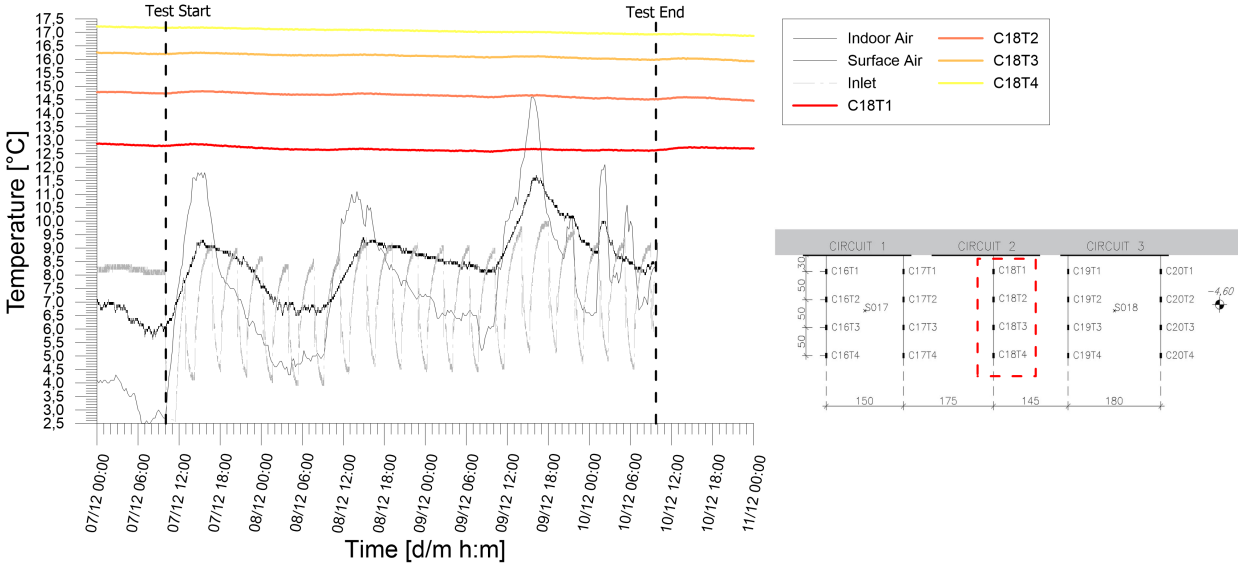

Figure A.113: Temperatures records from chain 18 of experimental test H_2-3_20191206_20191210.

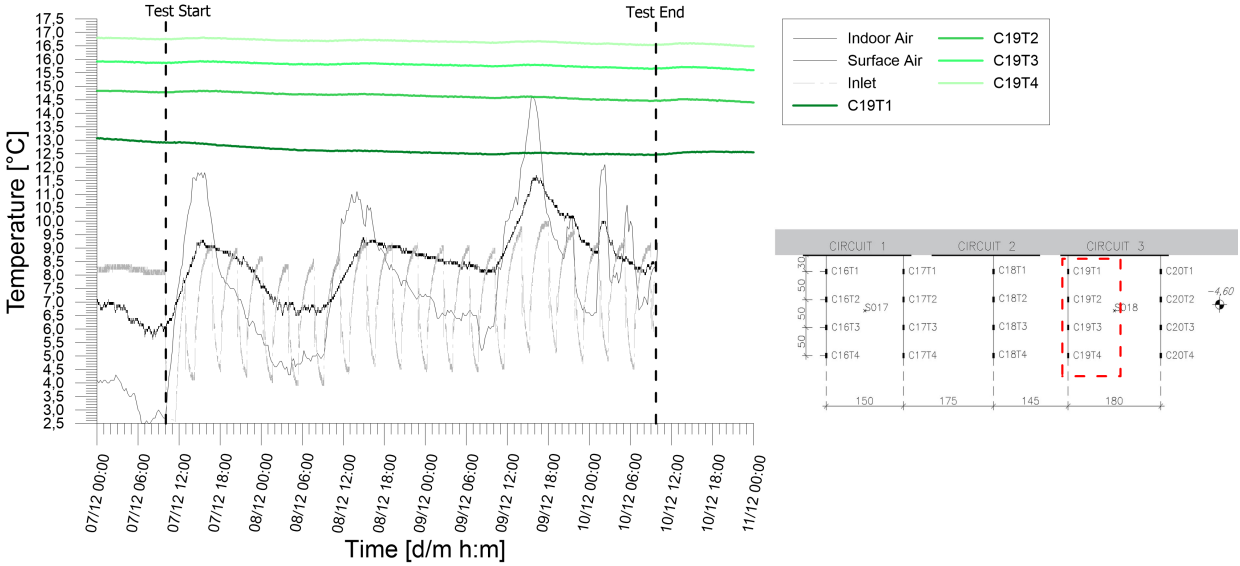

Figure A.114: Temperatures records from chain 19 of experimental test H_2-3_20191206_20191210.

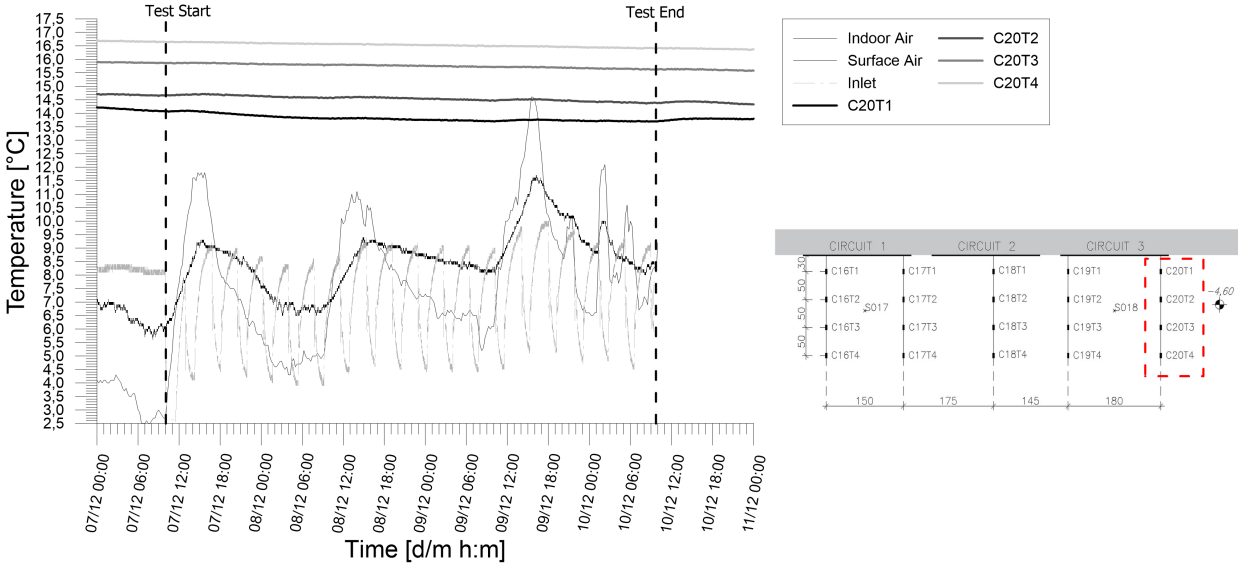

Figure A.115: Temperatures records from chain 20 of experimental test H_2-3_20191206_20191210.

A.6 Test H_1+2_20191220_20200113

Table A.6: Main features of the test.

Test start time	20/12/19 19.00
Test end time	13/1/20 10.50
Duration [h]	567.4
Operative mode	Heating
Active circuit(s)	1;2
Circuit link	Parallel
Target temperature user [°C]	45
Flow rate at the ground side [l/h]	Main: 930 Circuit 1: 442
Pressure at the user side [psi]	1.4
Pressure at the ground side [psi]	1.9

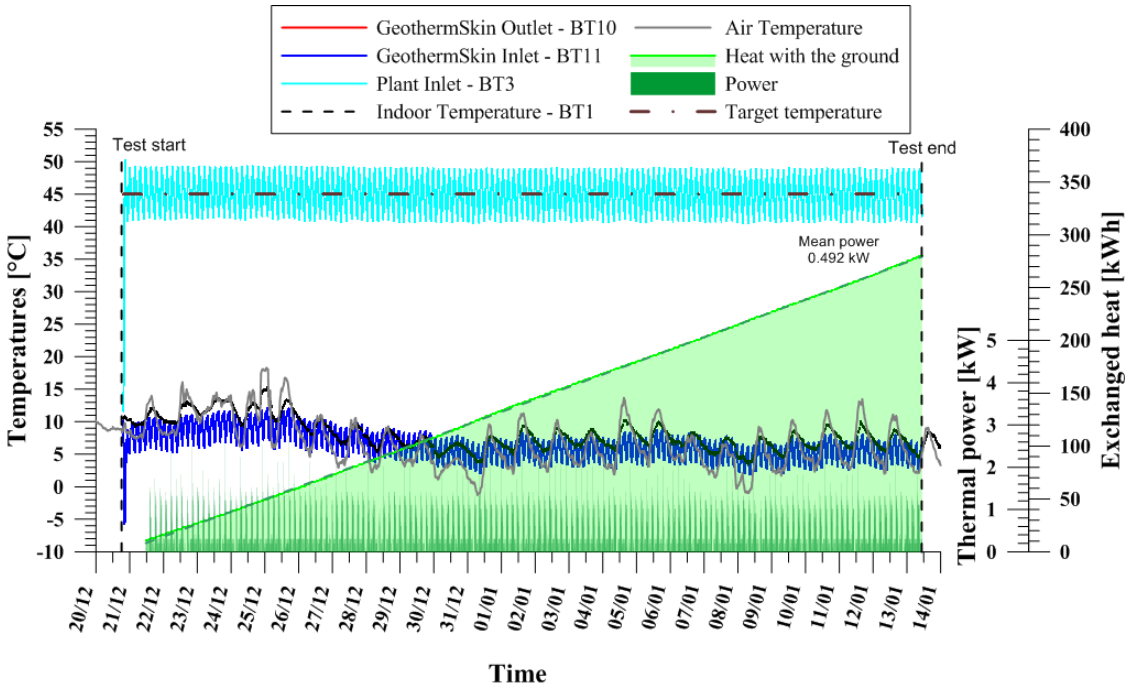

Figure A.116: Thermal performance interpretation of experimental test *H_1+2_20191220_20200113* with parallel link of circuit 1 and 2 in heating mode.

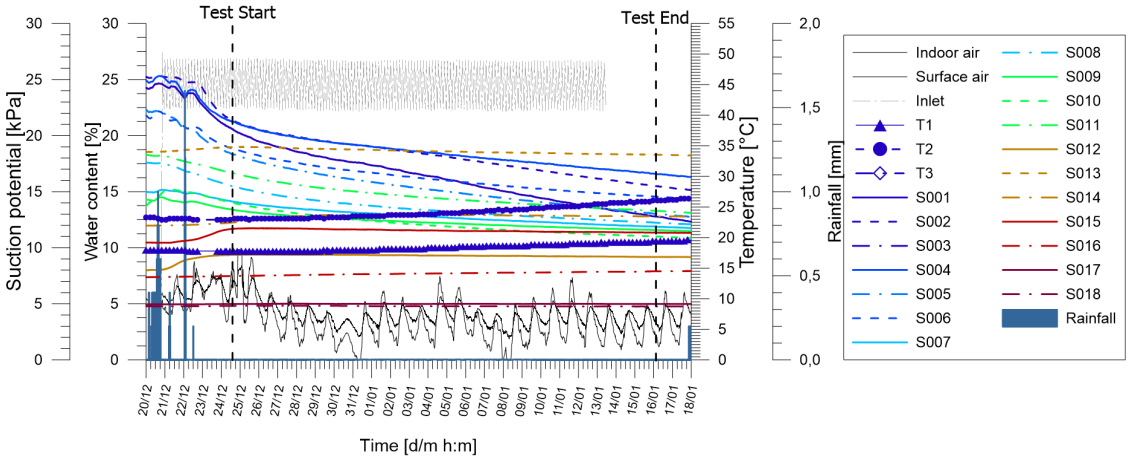

Figure A.117: Tensiometer and hygrometers records of experimental test H_1+2_20191220_20200113 together with monitored rainfall from Politecnico weather station.

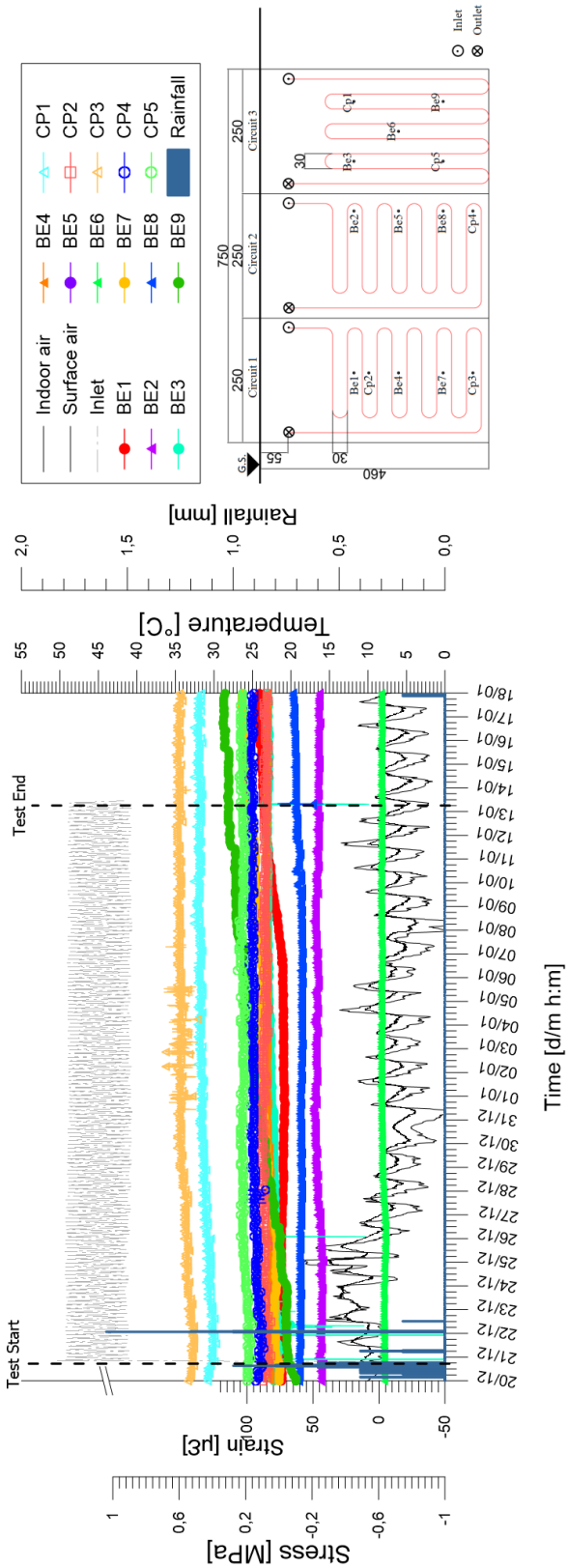

Figure A.118: Stresses and strains monitored at the wall external facade during experimental test H_1+2_20191220_20200113.

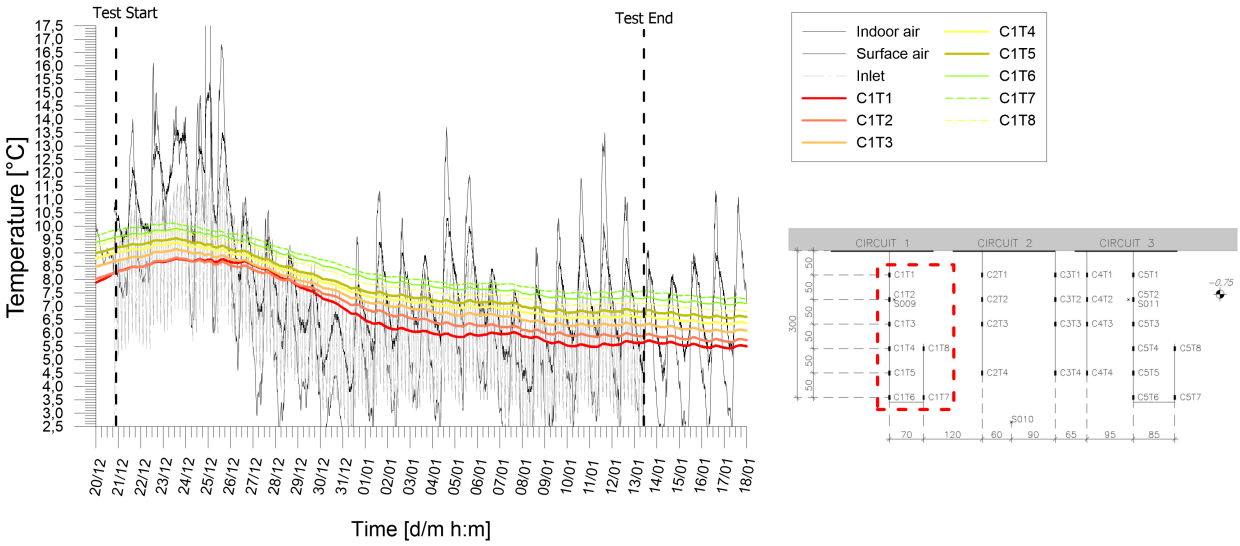

Figure A.119: Temperatures records from chain 1 of experimental test H_1+2_20191220_20200113.

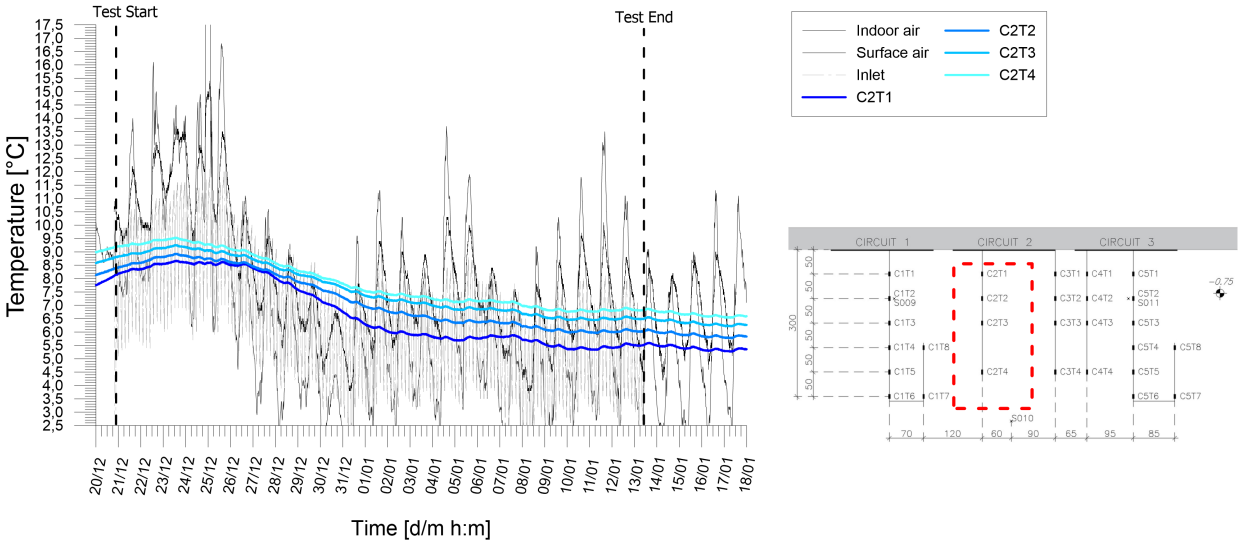

Figure A.120: Temperatures records from chain 2 of experimental test H_1+2_20191220_20200113.

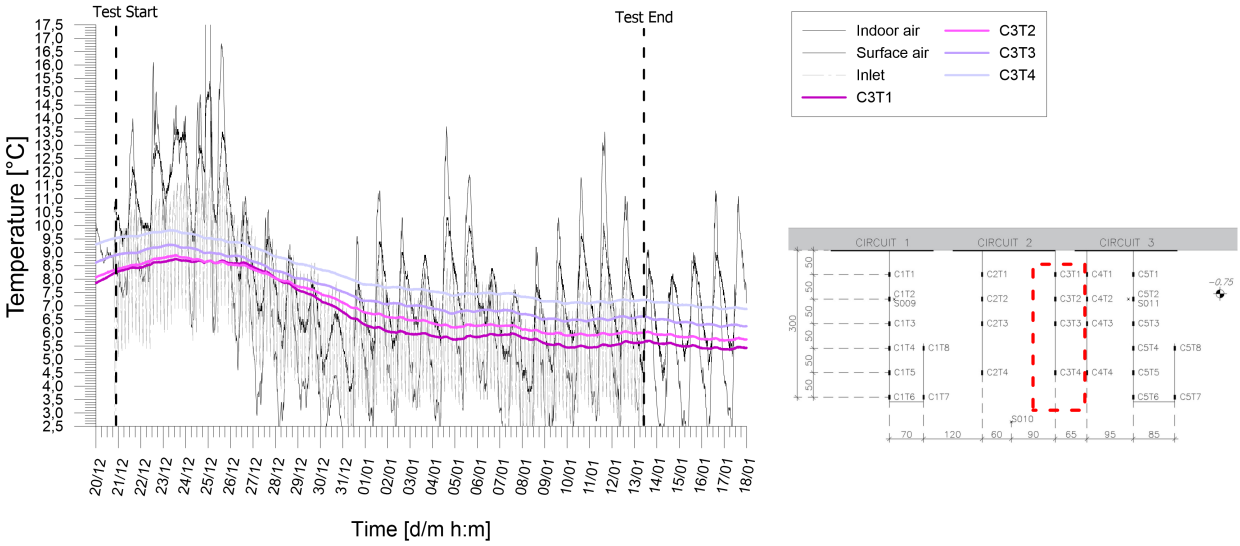

Figure A.121: Temperatures records from chain 3 of experimental test H_1+2_20191220_20200113.

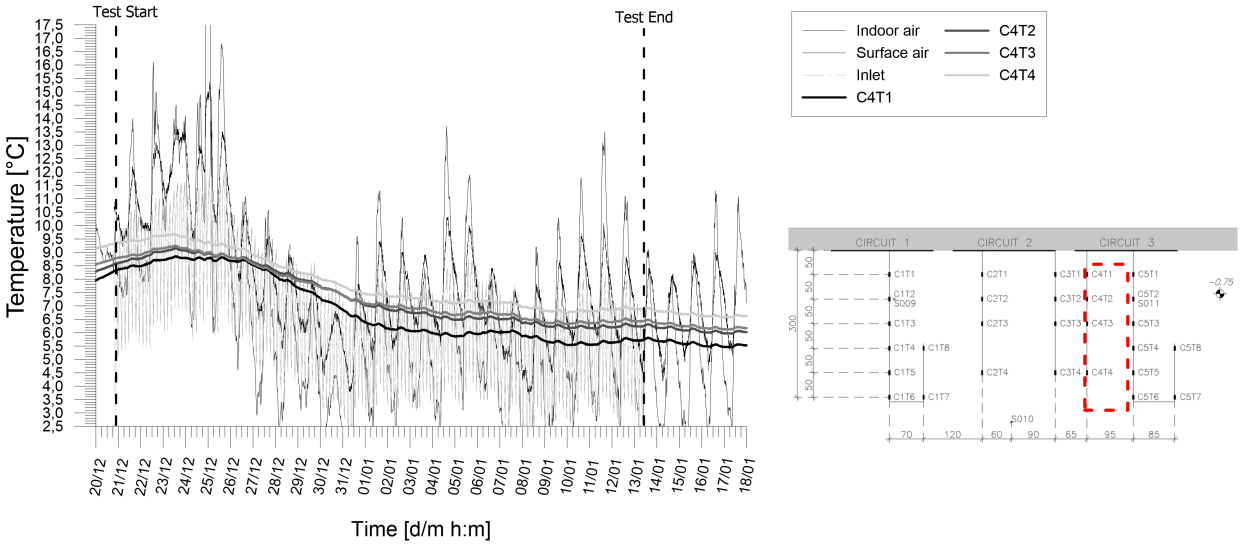

Figure A.122: *
Temperatures records from chain 4 of experimental test H_1+2_20191220_20200113.

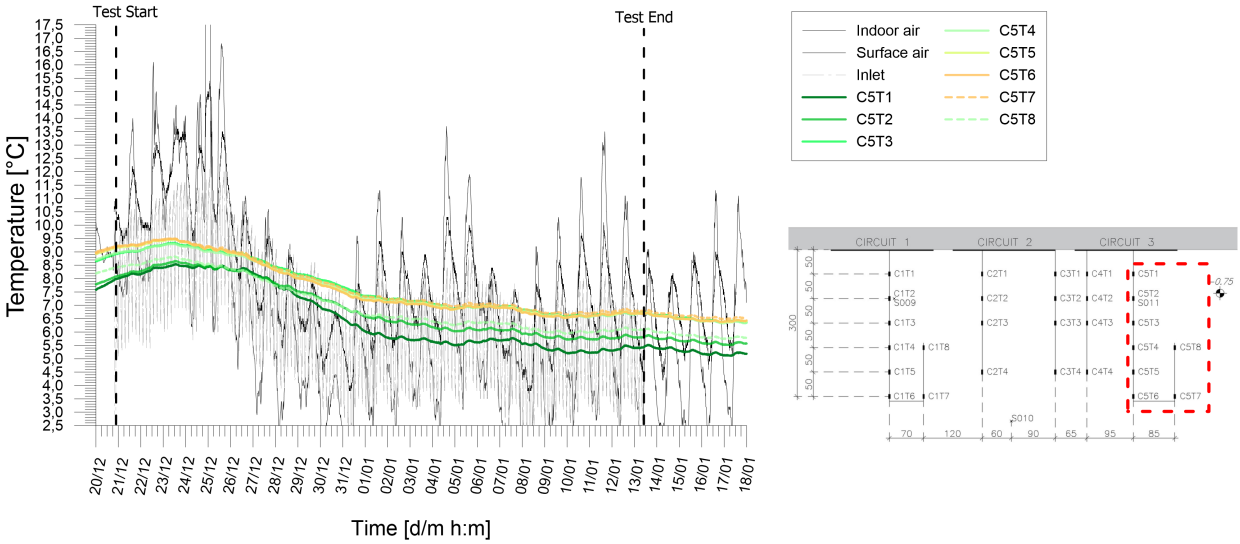

Figure A.123: Temperatures records from chain 5 of experimental test H_1+2_20191220_20200113.

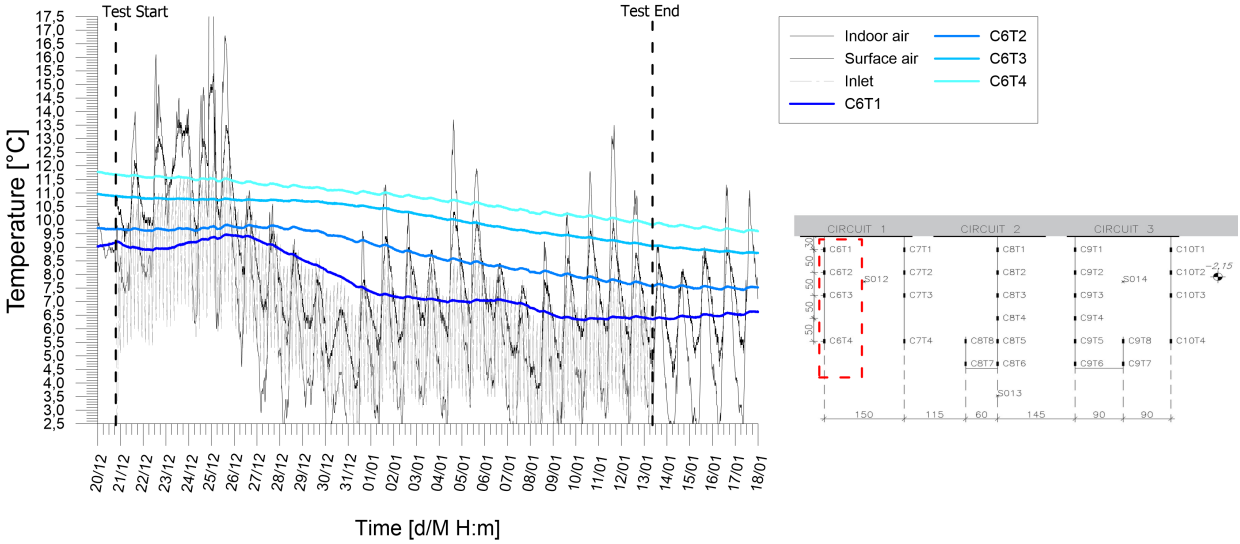

Figure A.124: Temperatures records from chain 6 of experimental test H_1+2_20191220_20200113.

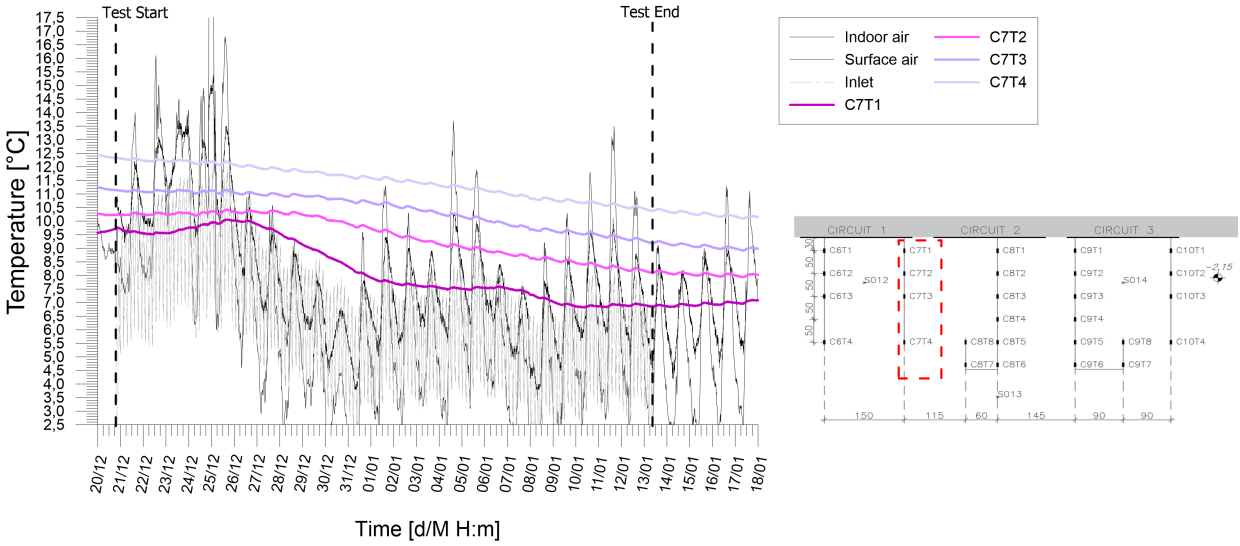

Figure A.125: Temperatures records from chain 7 of experimental test H_1+2_20191220_20200113.

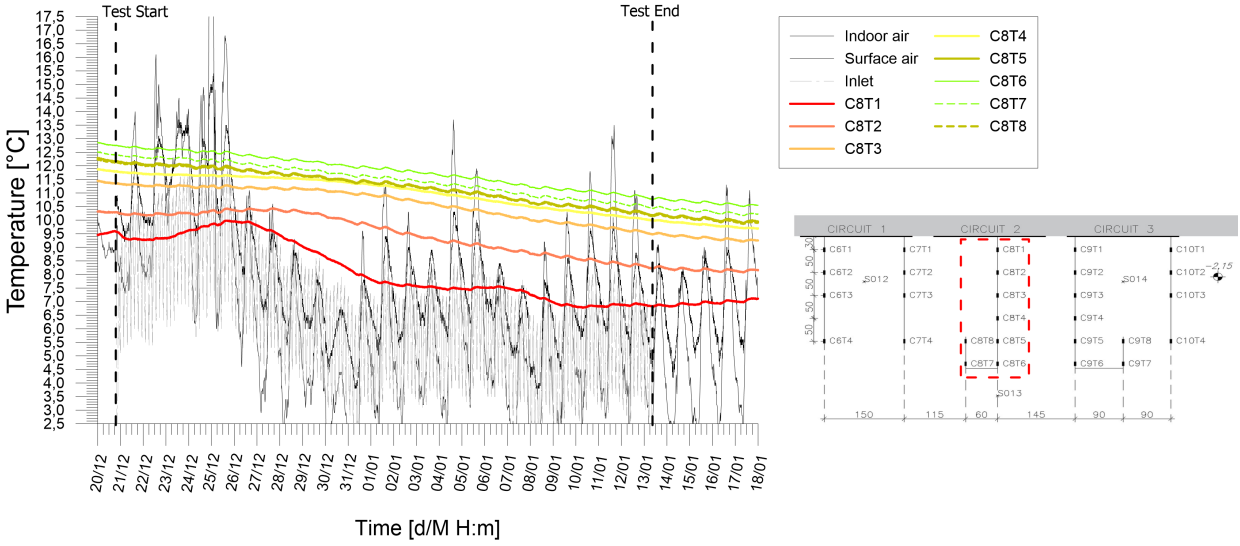

Figure A.126: Temperatures records from chain 8 of experimental test H_1+2_20191220_20200113.

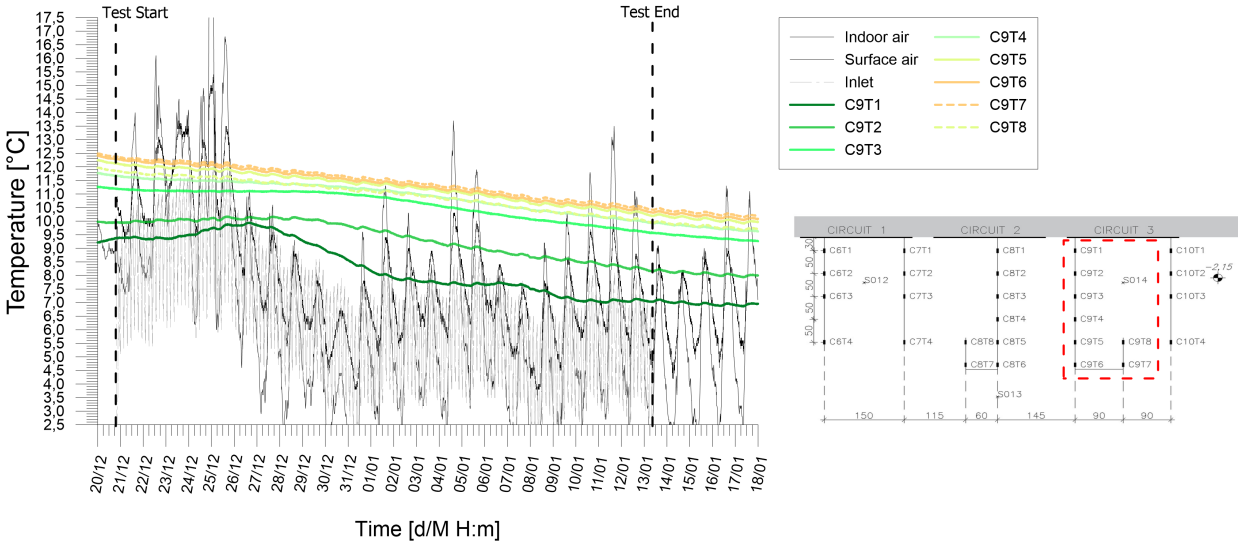

Figure A.127: Temperatures records from chain 9 of experimental test H_1+2_20191220_20200113.

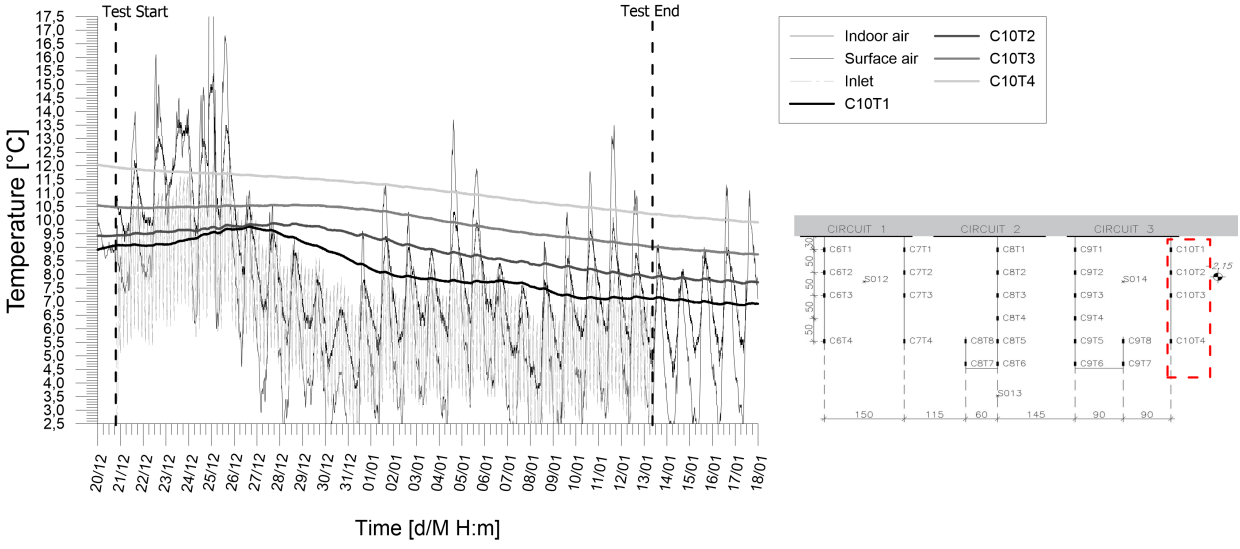

Figure A.128: Temperatures records from chain 10 of experimental test H_1+2_20191220_20200113.

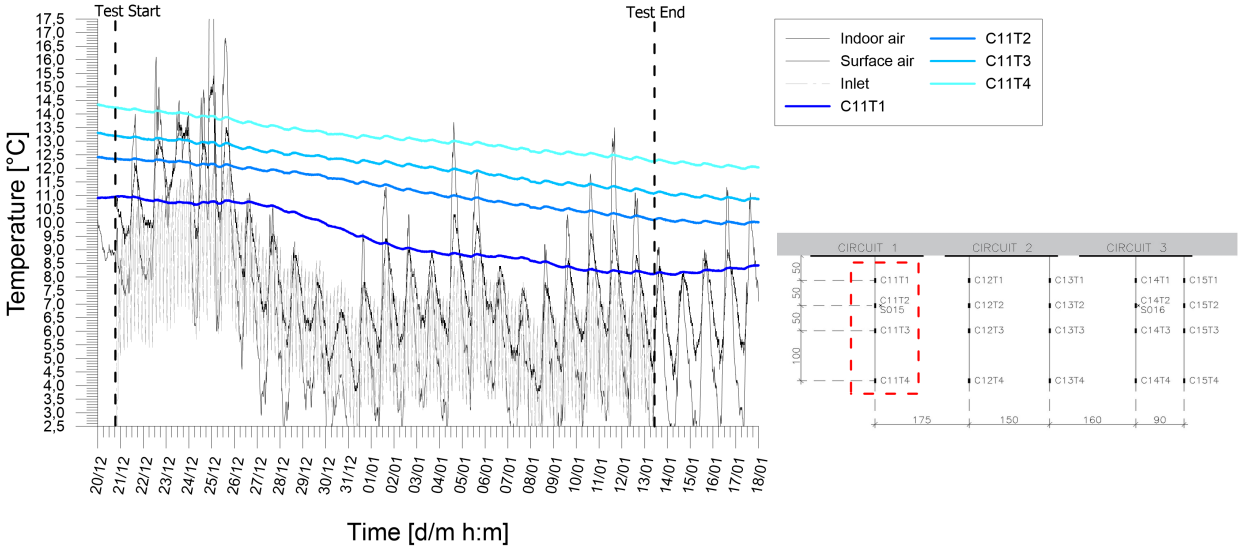

Figure A.129: *
Temperatures records from chain 11 of experimental test H_1+2_20191220_20200113.

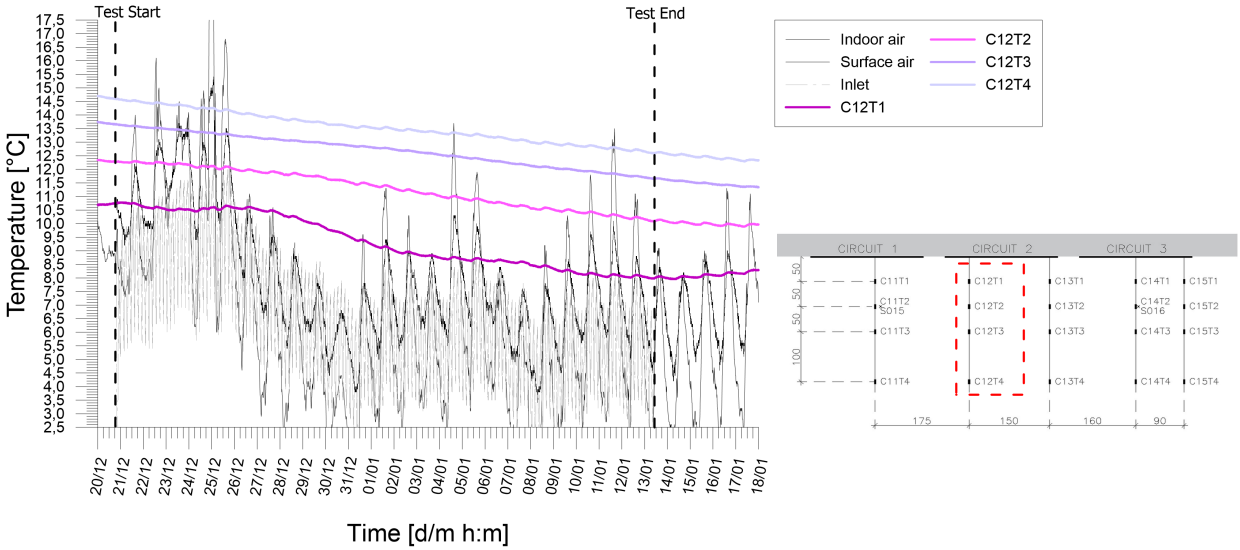

Figure A.130: Temperatures records from chain 12 of experimental test H_1+2_20191220_20200113.

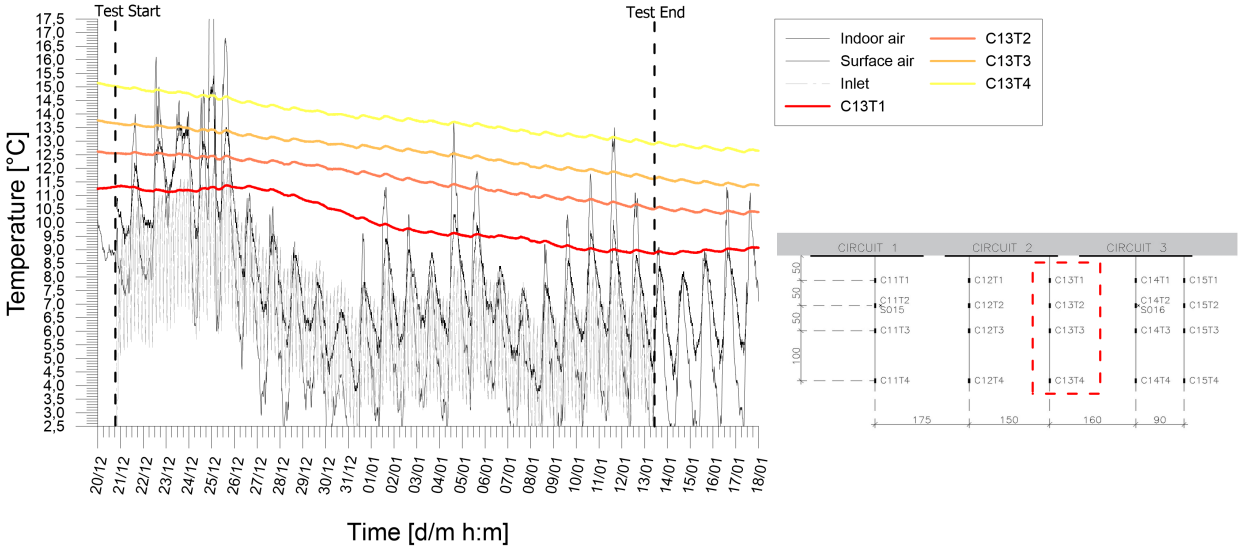

Figure A.131: Temperatures records from chain 13 of experimental test H_1+2_20191220_20200113.

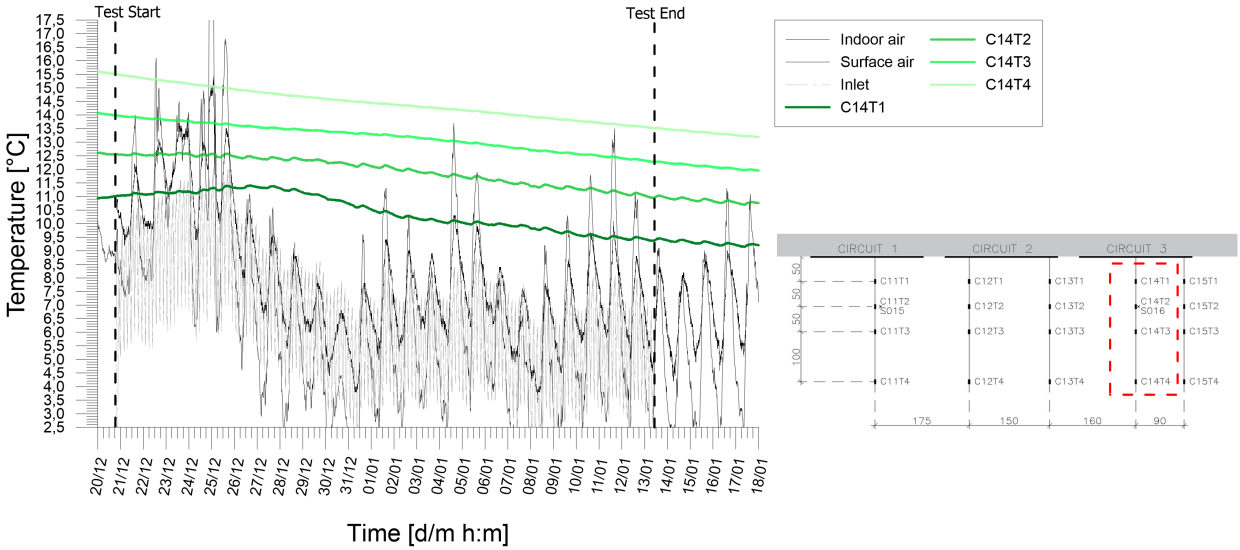

Figure A.132: Temperatures records from chain 14 of experimental test H_1+2_20191220_20200113.

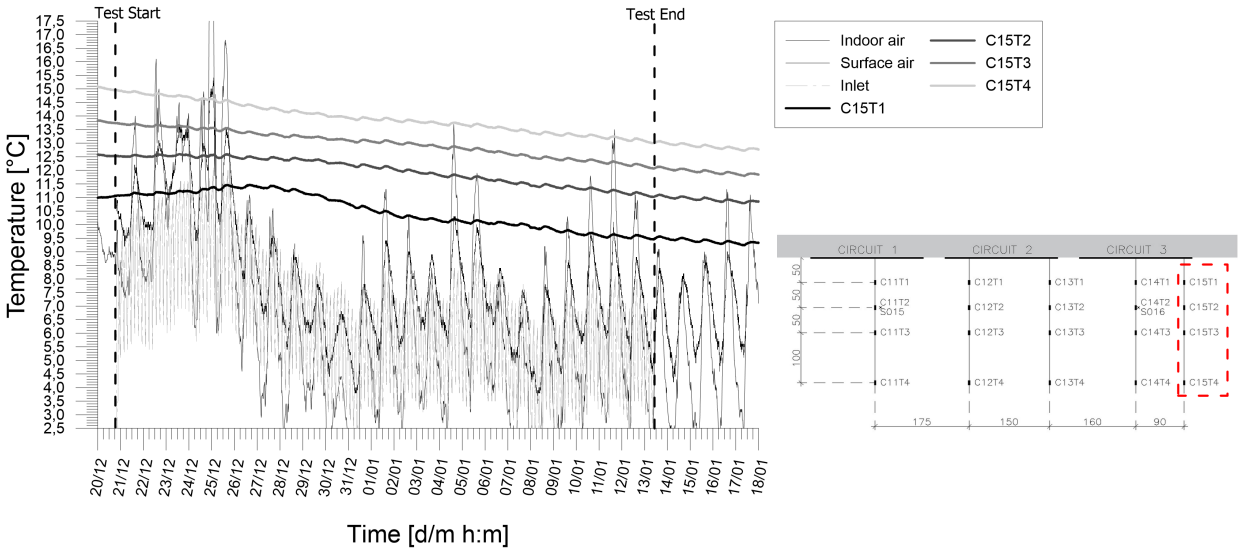

Figure A.133: Temperatures records from chain 15 of experimental test H_1+2_20191220_20200113.

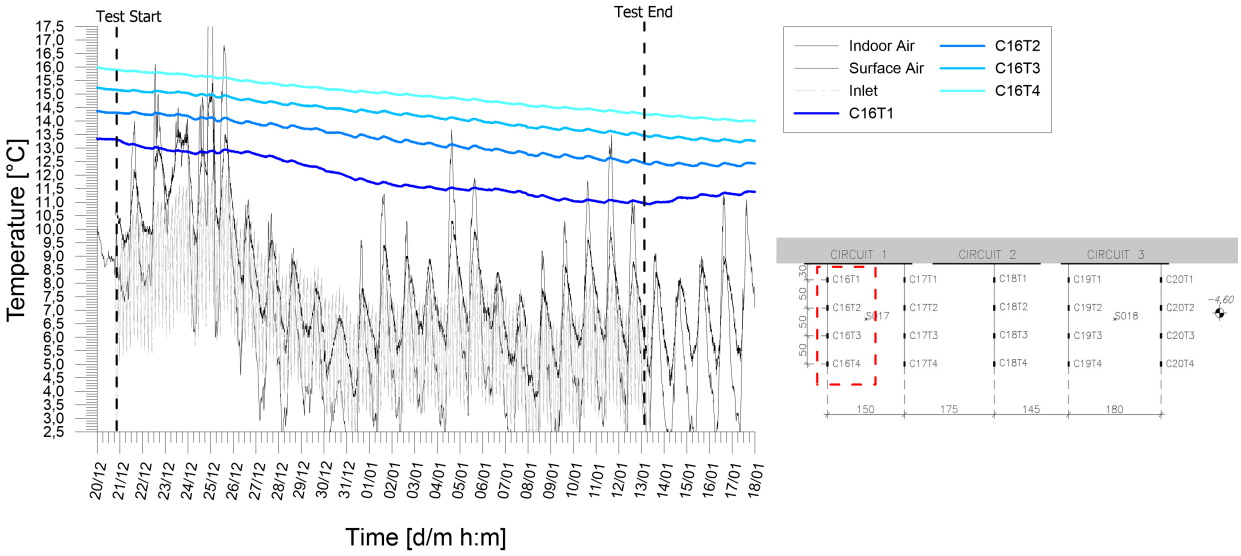

Figure A.134: Temperatures records from chain 16 of experimental test H_1+2_20191220_20200113.

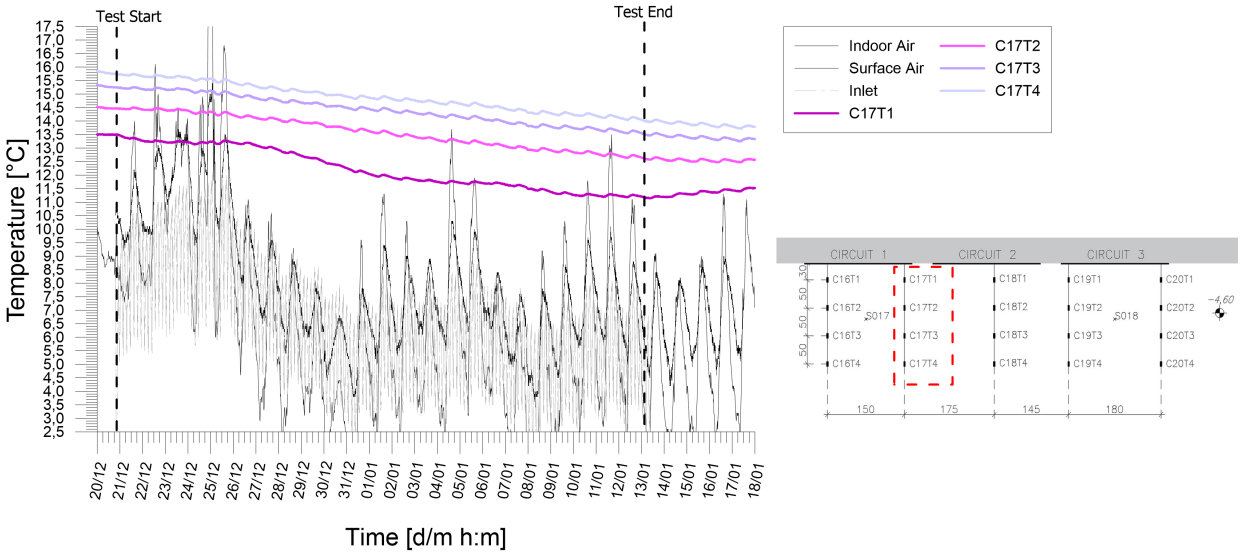

Figure A.135: Temperatures records from chain 17 of experimental test H_1+2_20191220_20200113.

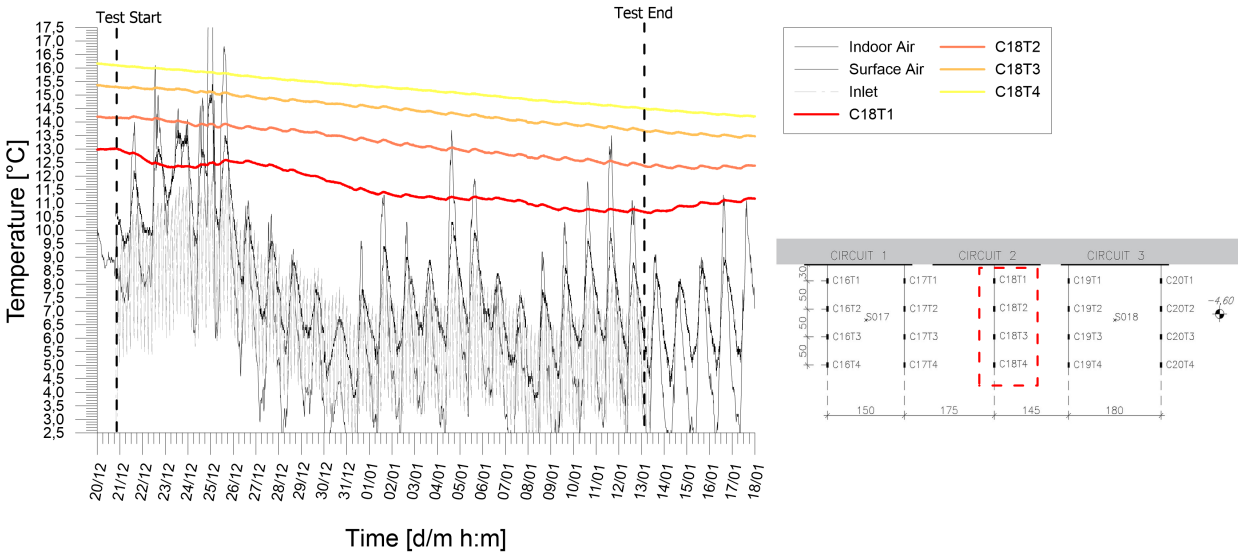

Figure A.136: Temperatures records from chain 18 of experimental test H_1+2_20191220_20200113.

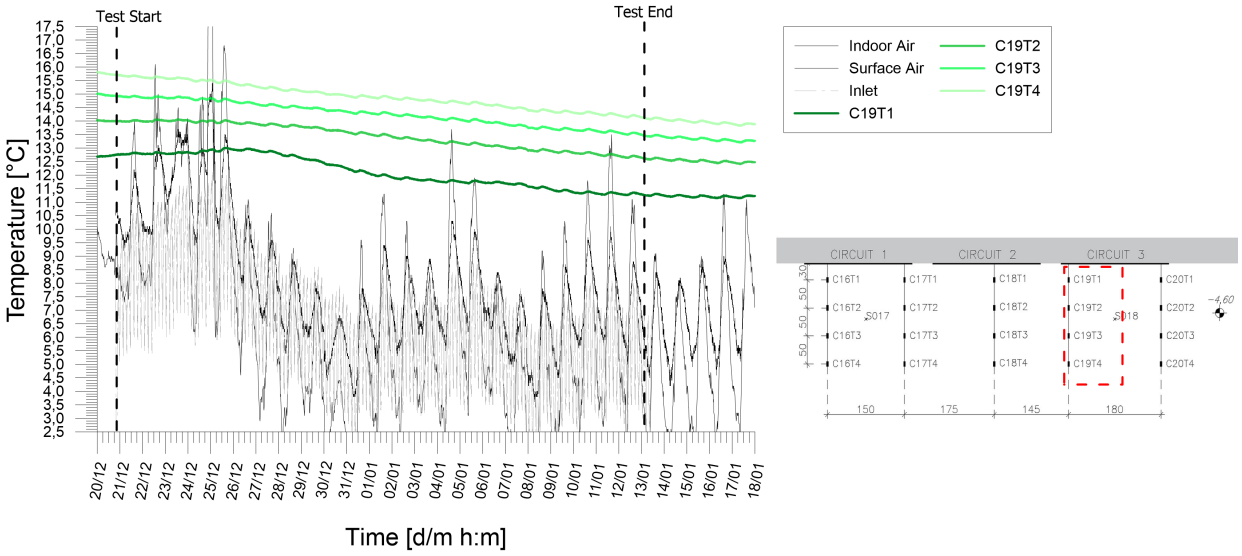

Figure A.137: Temperatures records from chain 19 of experimental test H_1+2_20191220_20200113.

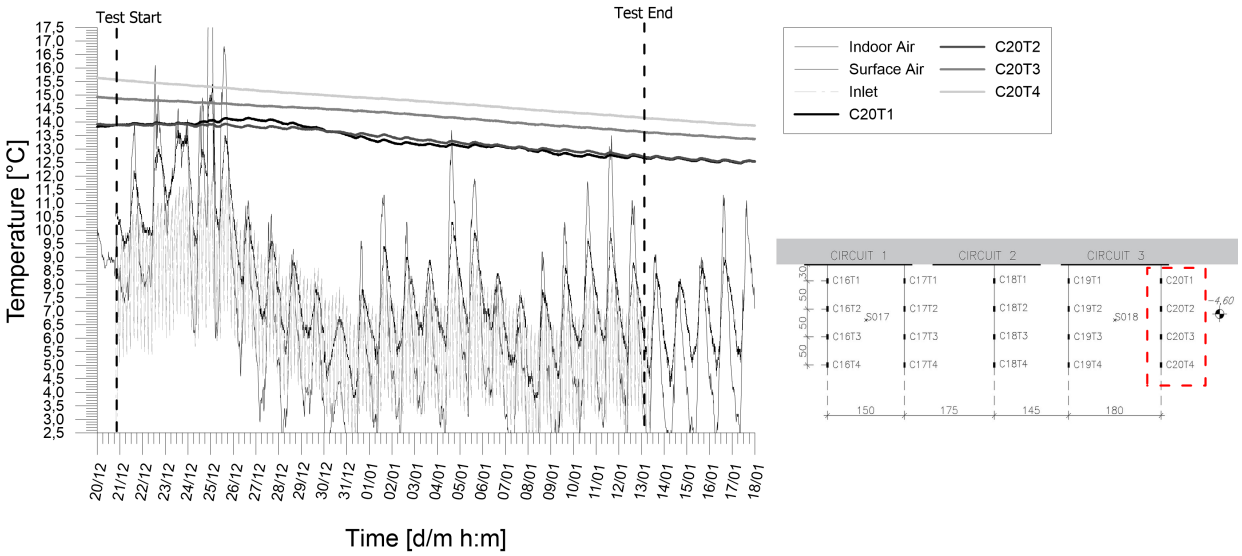

Figure A.138: Temperatures records from chain 20 of experimental test H_1+2_20191220_20200113.

A.7 Test H_1+2_20200124_20200128

Table A.7: Main features of the test.

Test start time	24/1/20 17.30
Test end time	28/1/20 9.20
Duration [h]	87.9
Operative mode	Heating
Active circuit(s)	1;2
Circuit link	Parallel
Target temperature user [°C]	55
Flow rate at the ground side [l/h]	Main: 910 Circuit 1: 430
Pressure at the user side [psi]	2.2
Pressure at the ground side [psi]	1.9
Total fluid volume [l]	Main: 78775 Circuit 1: 37483
Initial fluid temperature [°C]	9.5

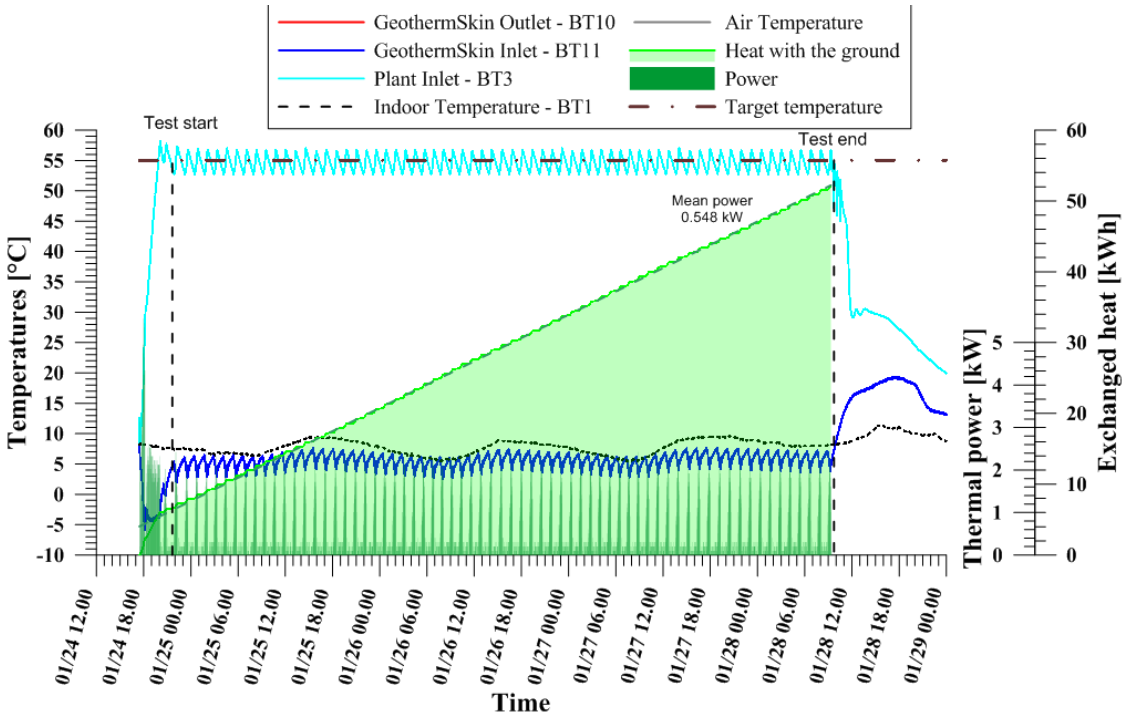

Figure A.139: Thermal performance interpretation of experimental test *H_1+2_20200124_20200128* with parallel link of circuit 1 and 2 in heating mode.

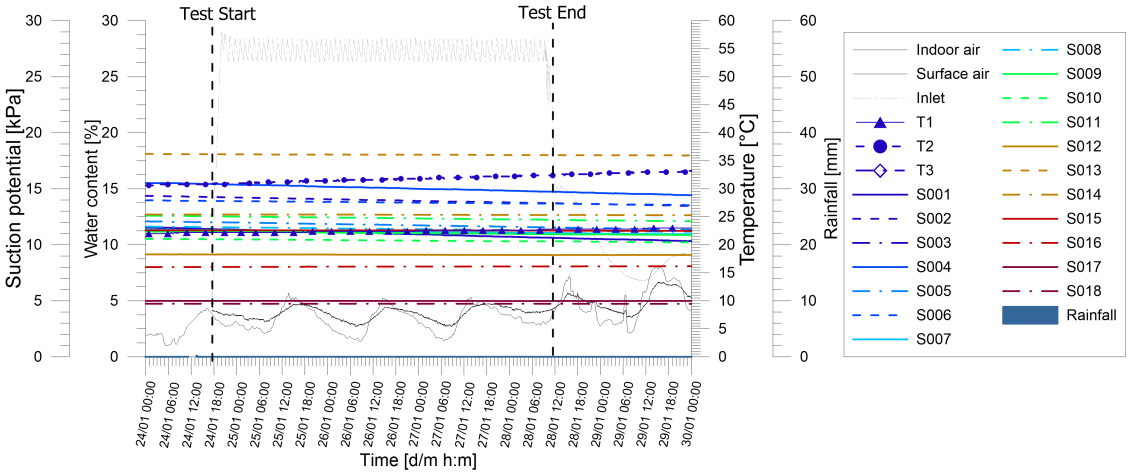

Figure A.140: Tensiometer and hygrometers records of experimental test H_1+2_20200124_20200128 together with monitored rainfall from Politecnico weather station.

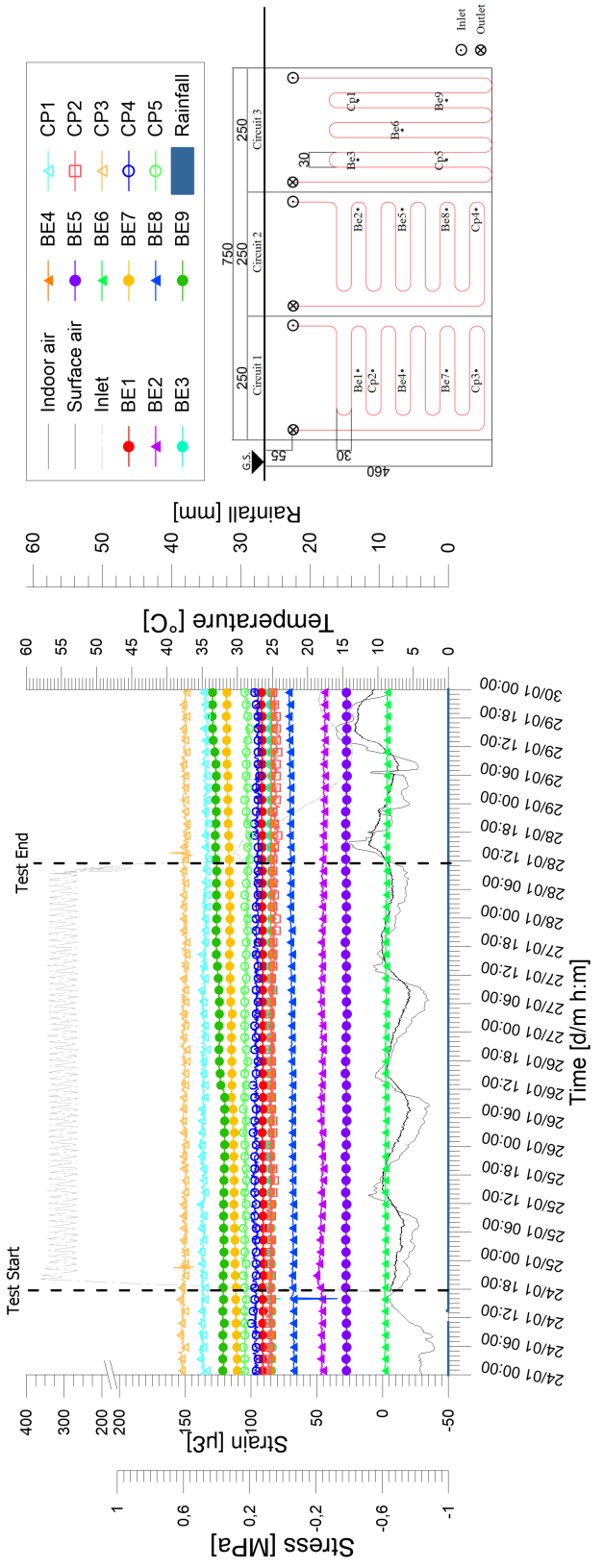

Figure A.141: Stresses and strains monitored at the wall external facade during experimental test H_1+2_20200124_20200128.

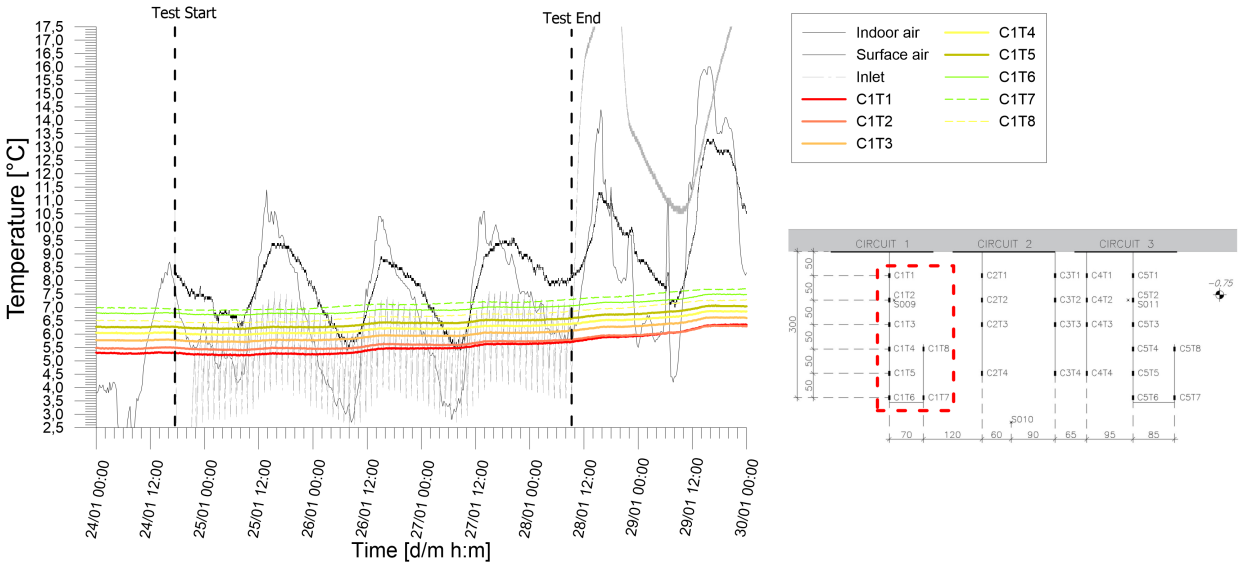

Figure A.142: Temperatures records from chain 1 of experimental test H_1+2_20200124_20200128.

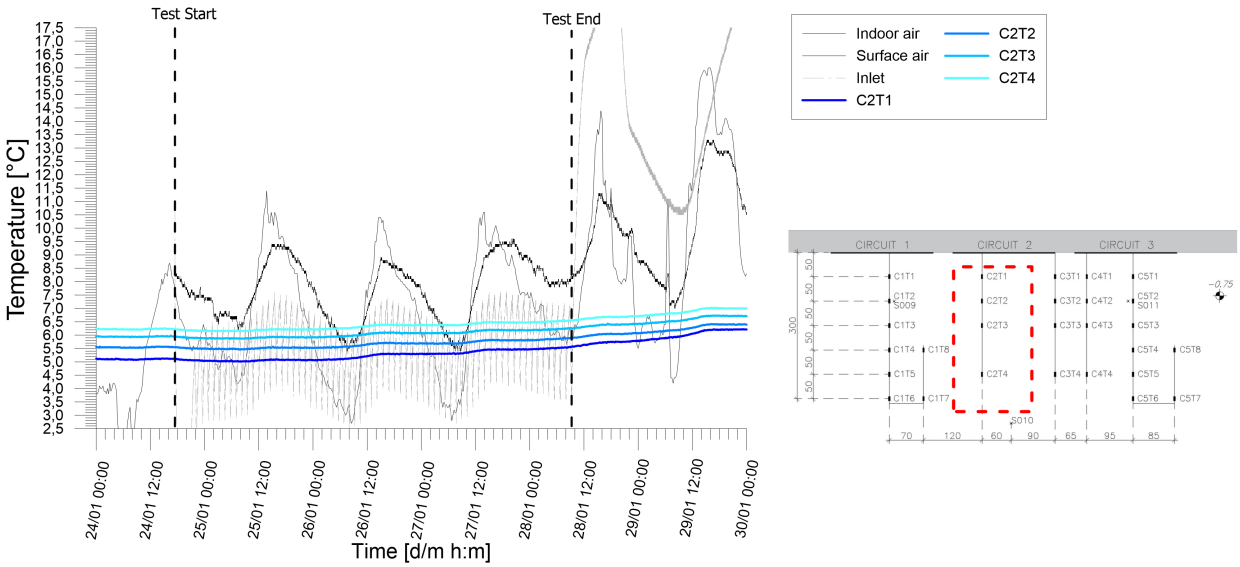

Figure A.143: Temperatures records from chain 2 of experimental test H_1+2_20200124_20200128.

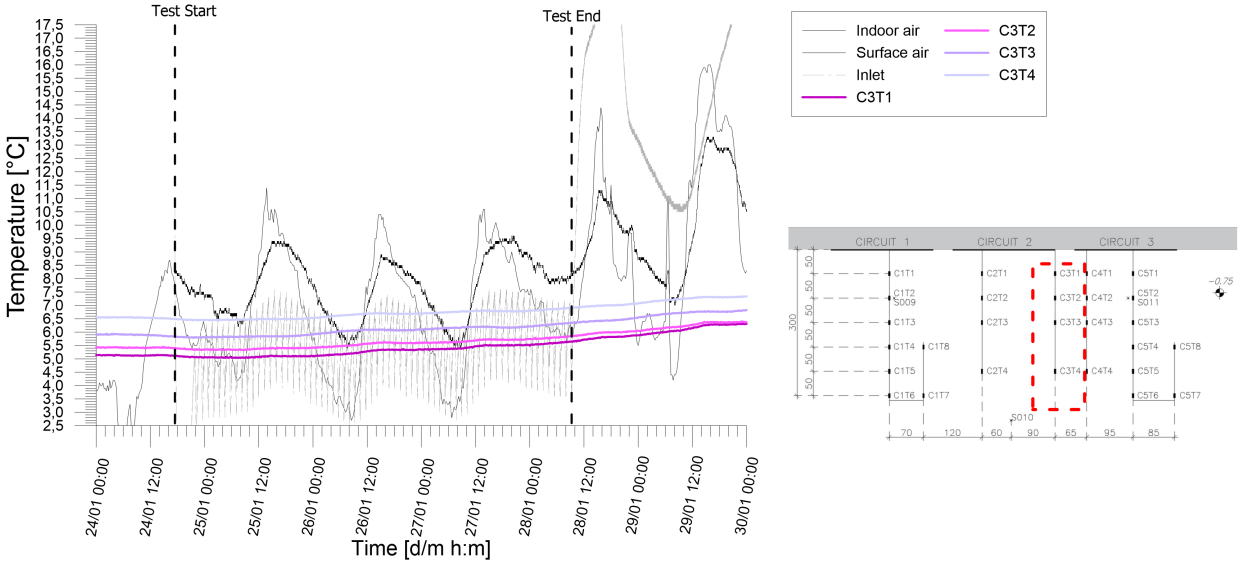

Figure A.144: Temperatures records from chain 3 of experimental test H_1+2_20200124_20200128.

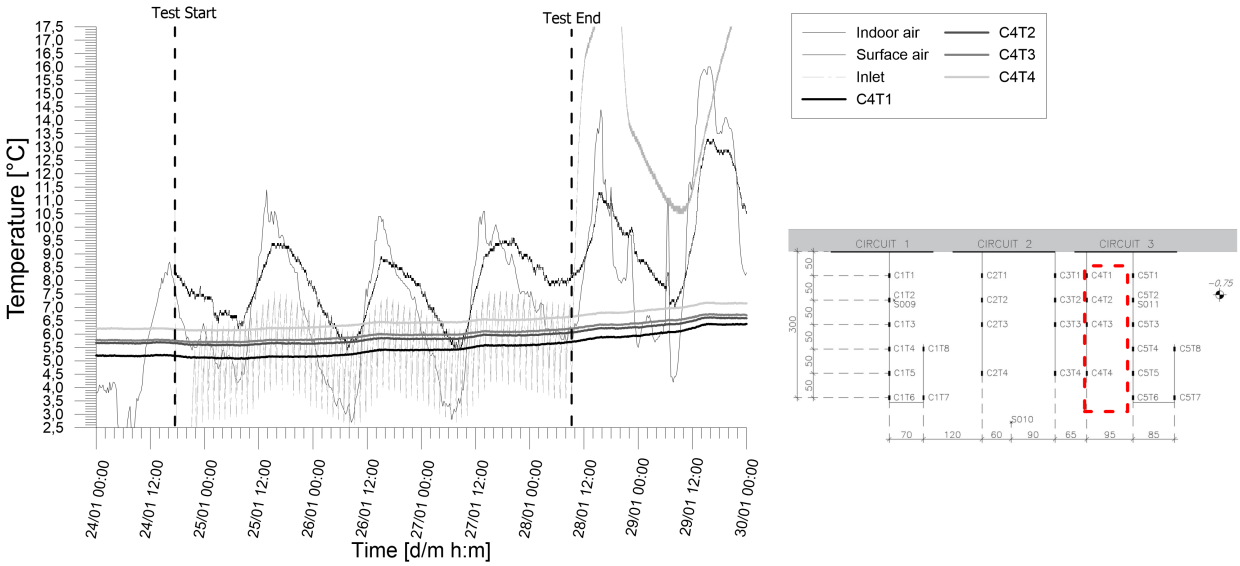

Figure A.145: *
Temperatures records from chain 4 of experimental test H_1+2_20200124_20200128.

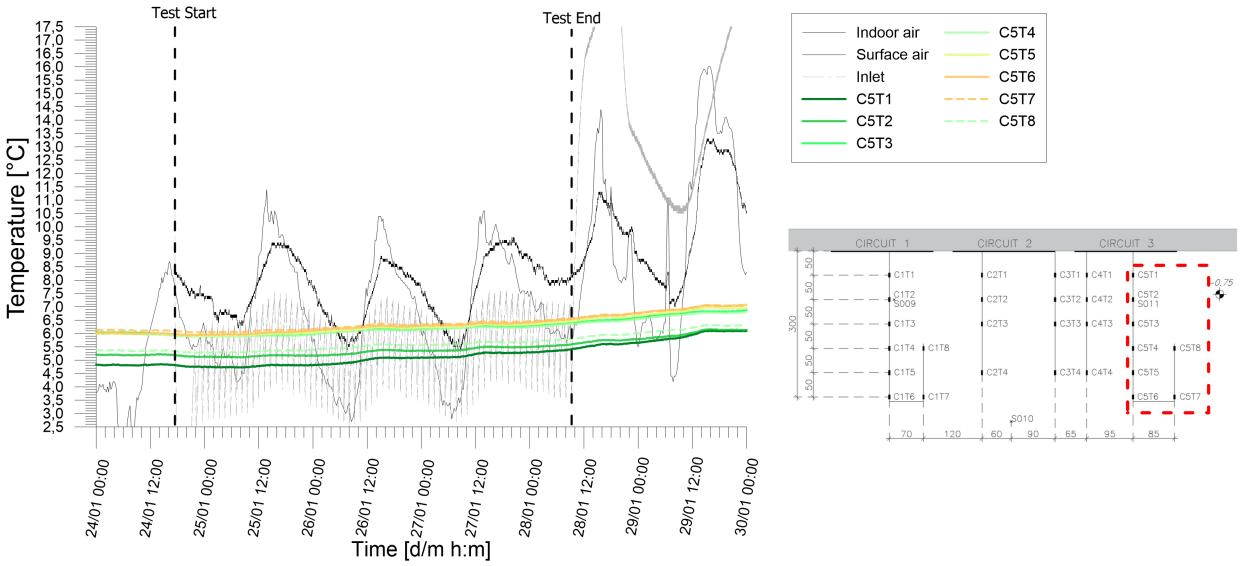

Figure A.146: Temperatures records from chain 5 of experimental test H_1+2_20200124_20200128.

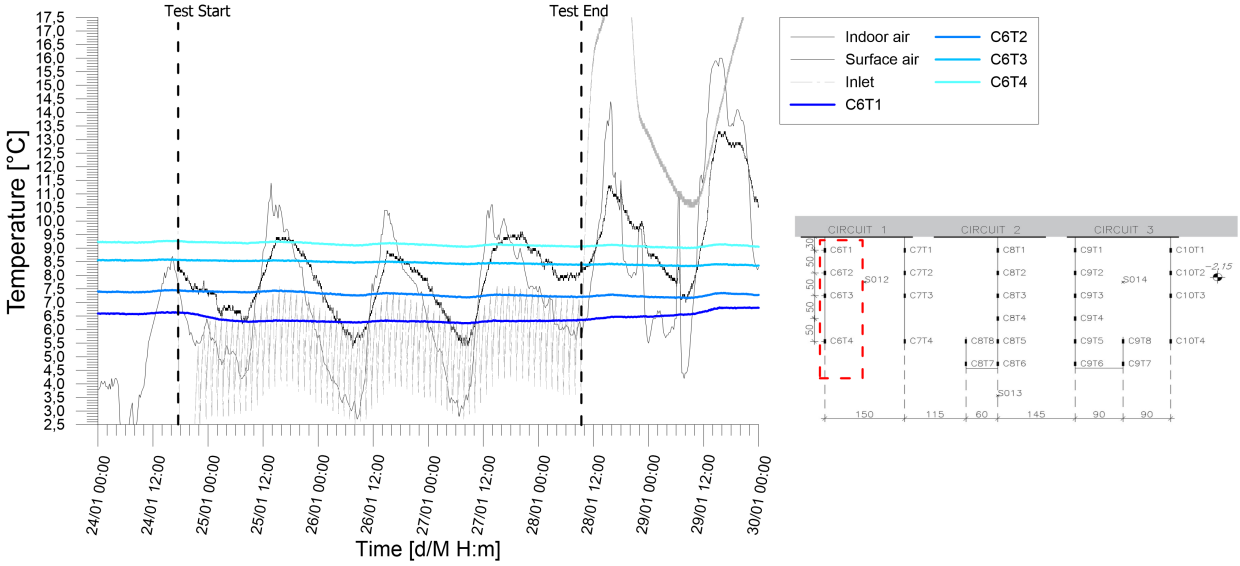

Figure A.147: Temperatures records from chain 6 of experimental test H_1+2_20200124_20200128.

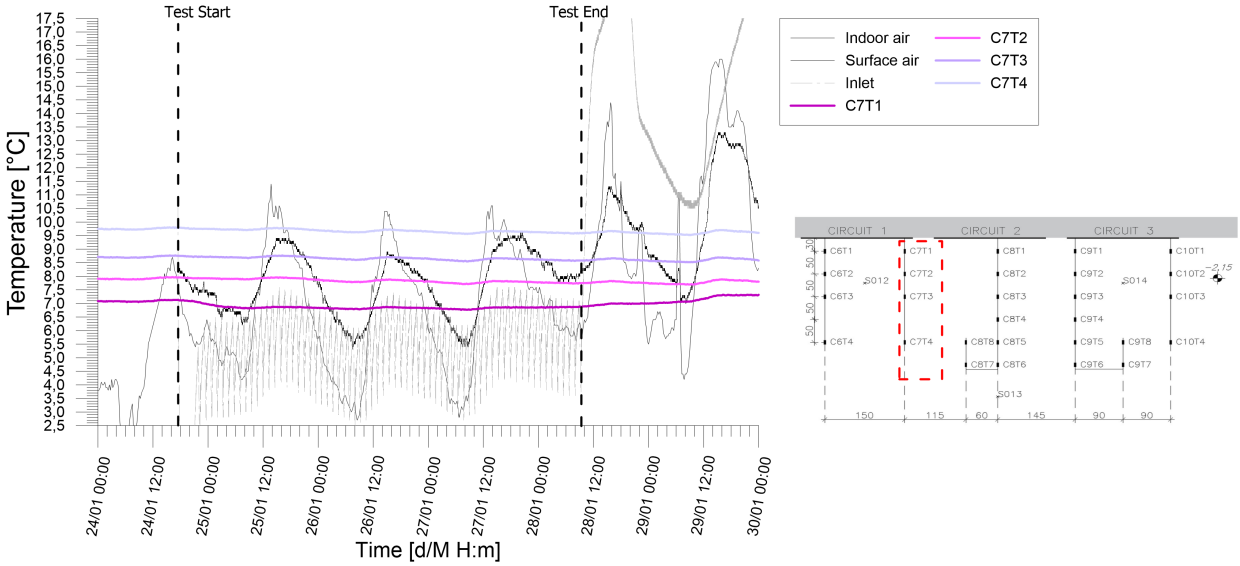

Figure A.148: Temperatures records from chain 7 of experimental test H_1+2_20200124_20200128.

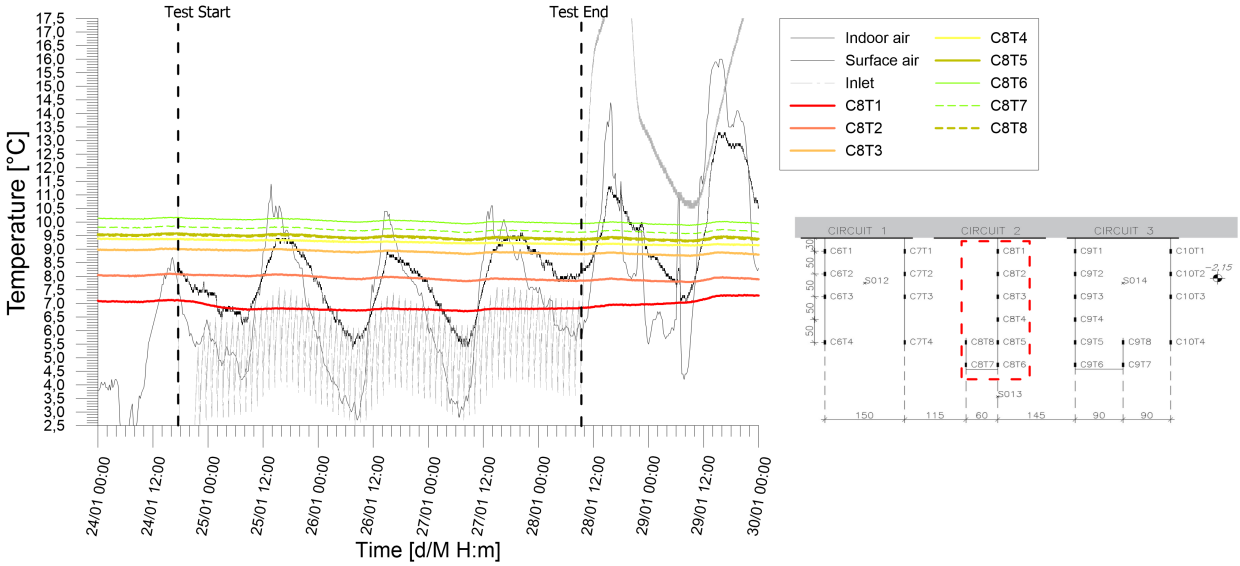

Figure A.149: Temperatures records from chain 8 of experimental test H_1+2_20200124_20200128.

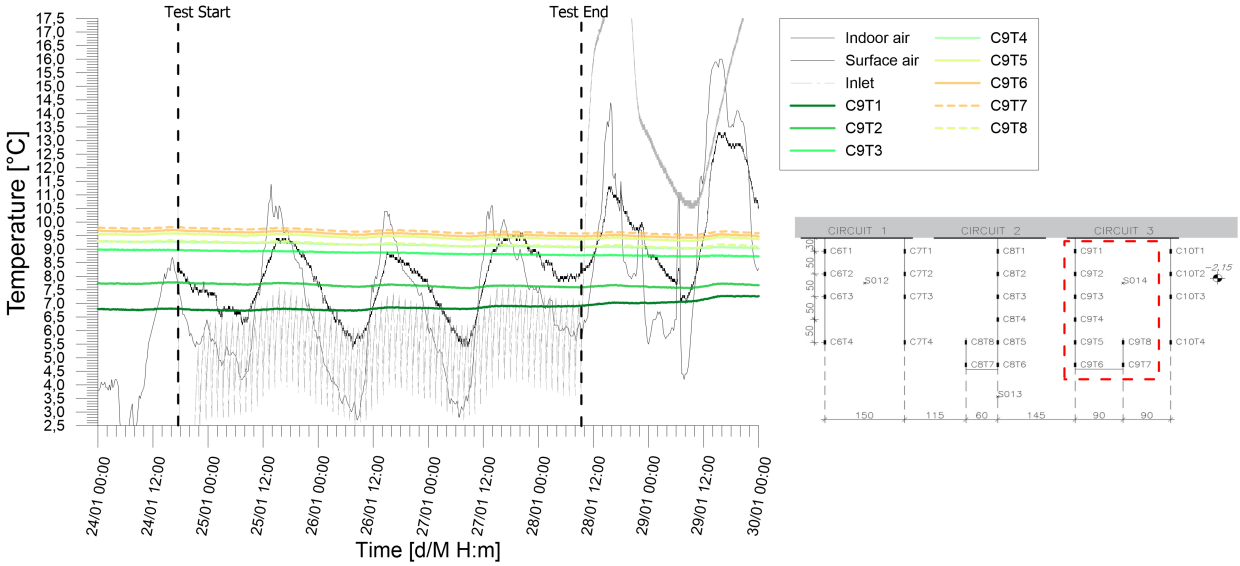

Figure A.150: Temperatures records from chain 9 of experimental test H_1+2_20200124_20200128.

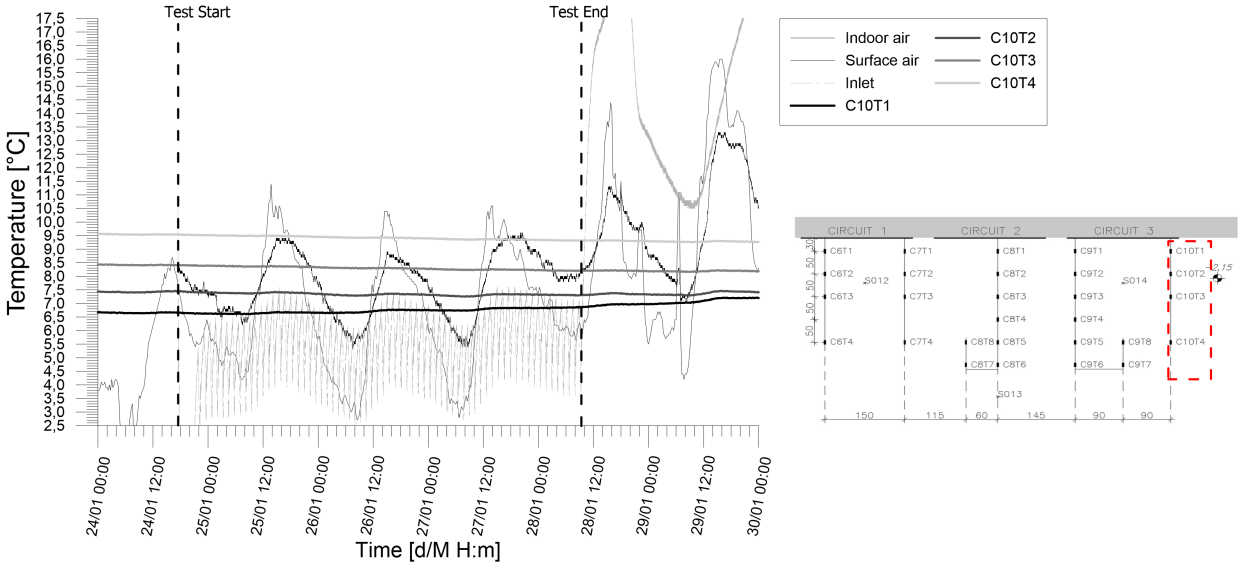

Figure A.151: Temperatures records from chain 10 of experimental test H_1+2_20200124_20200128.

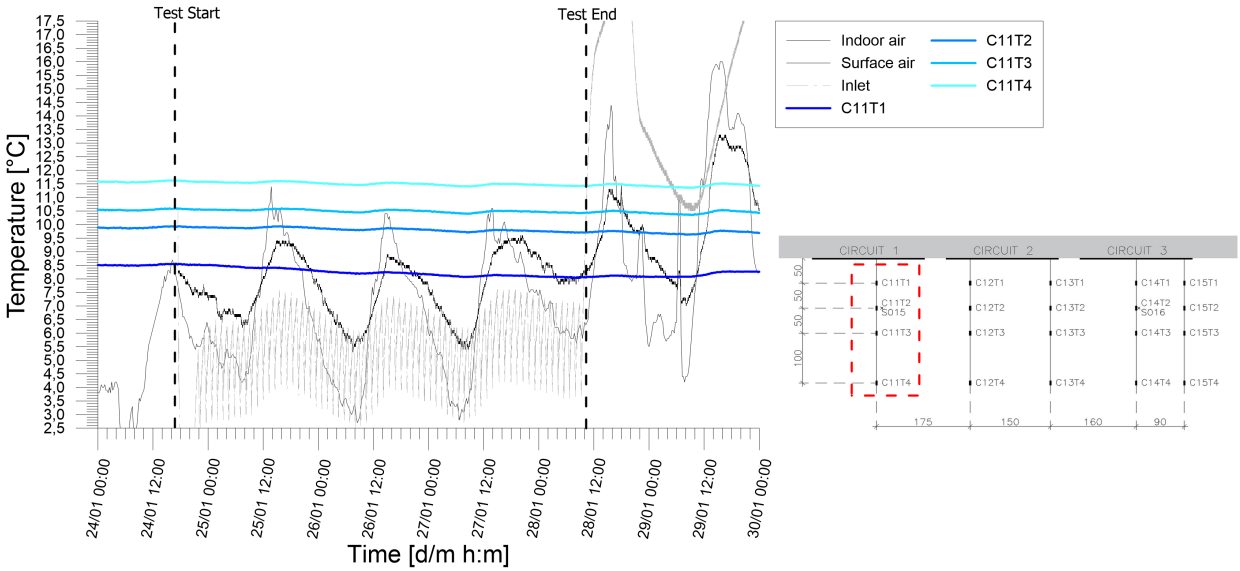

Figure A.152: *
Temperatures records from chain 11 of experimental test H_1+2_20200124_20200128.

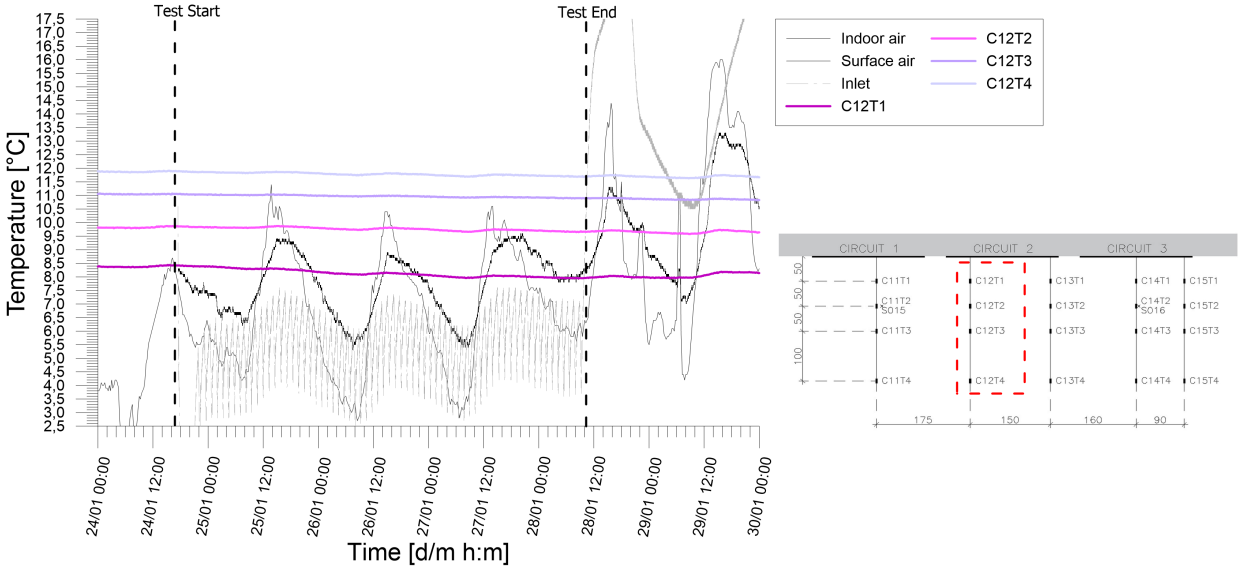

Figure A.153: Temperatures records from chain 12 of experimental test H_1+2_20200124_20200128.

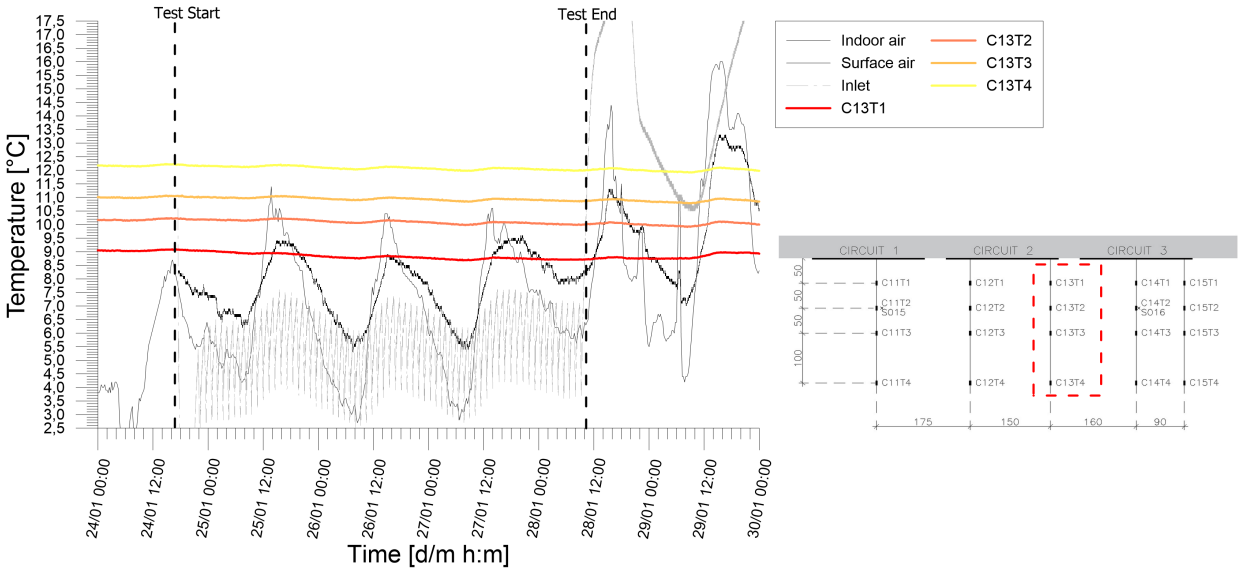

Figure A.154: Temperatures records from chain 13 of experimental test H_1+2_20200124_20200128.

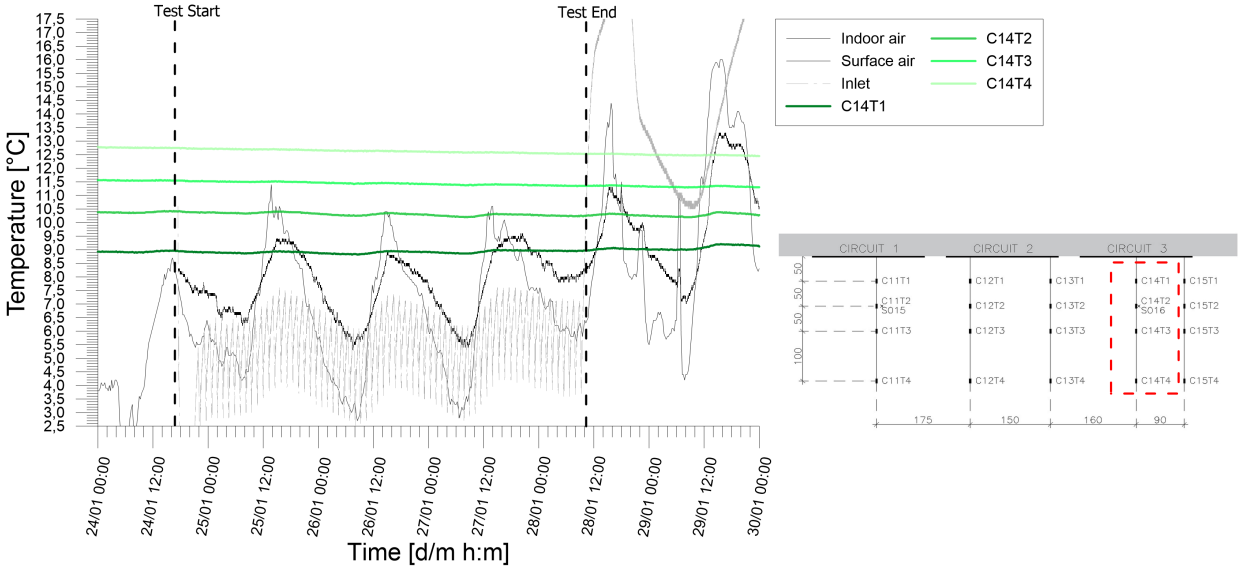

Figure A.155: Temperatures records from chain 14 of experimental test H_1+2_20200124_20200128.

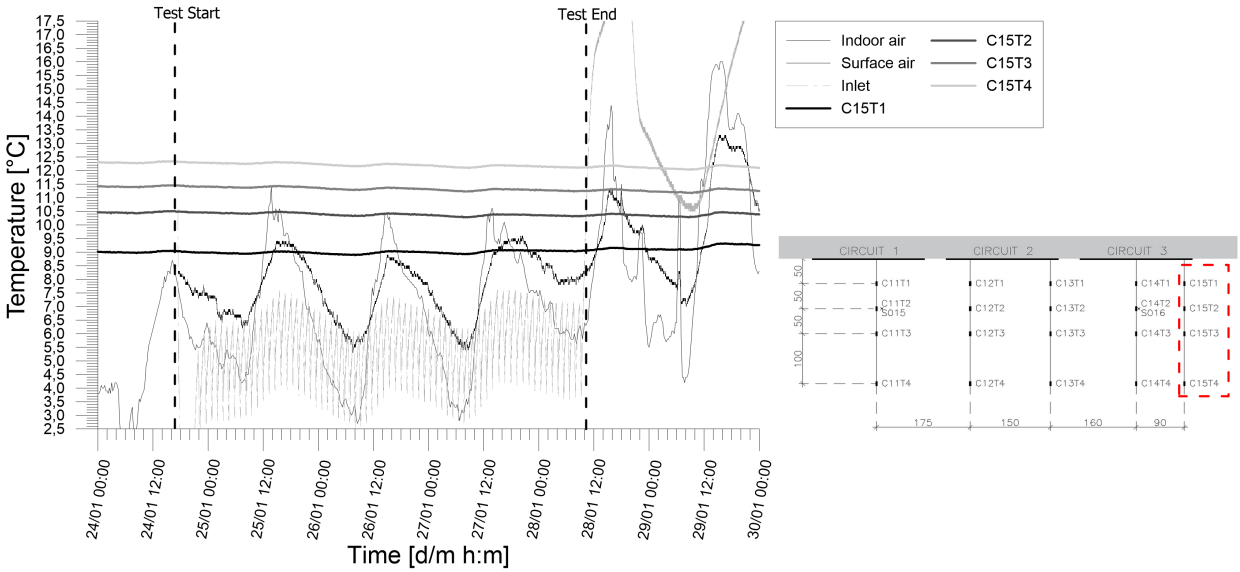

Figure A.156: Temperatures records from chain 15 of experimental test H_1+2_20200124_20200128.

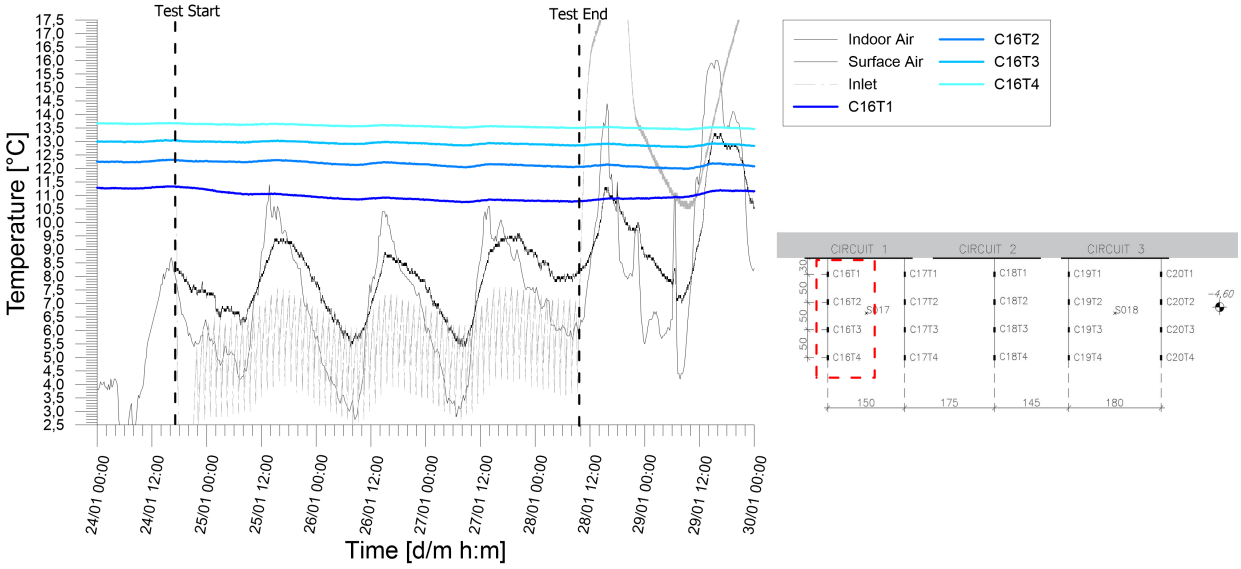

Figure A.157: Temperatures records from chain 16 of experimental test H_1+2_20200124_20200128.

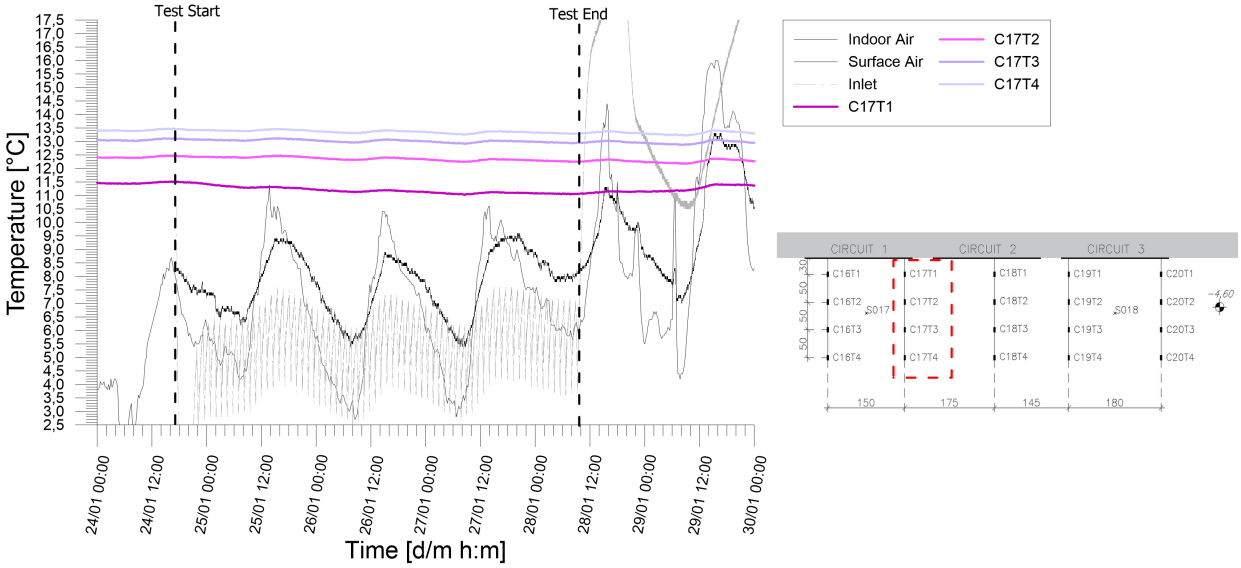

Figure A.158: Temperatures records from chain 17 of experimental test H_1+2_20200124_20200128.

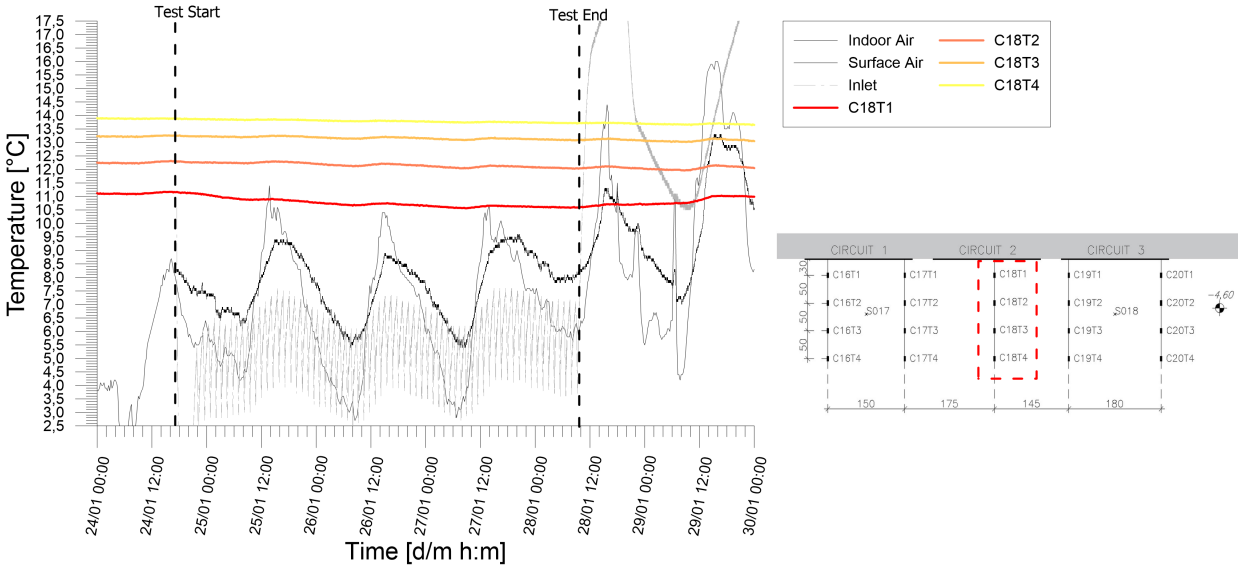

Figure A.159: Temperatures records from chain 18 of experimental test H_1+2_20200124_20200128.

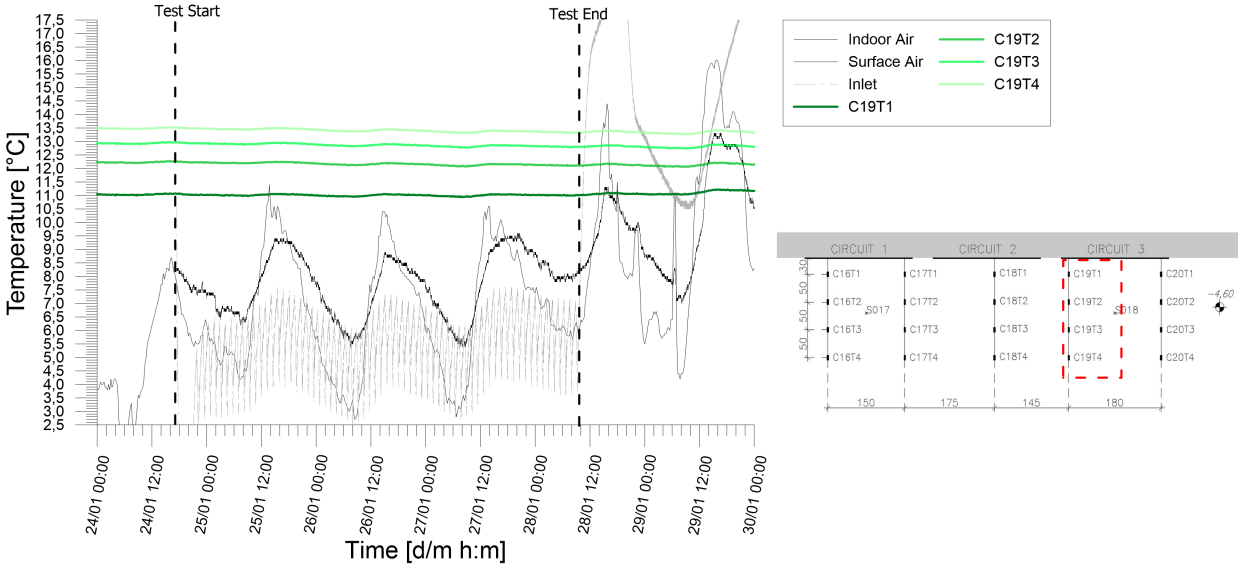

Figure A.160: Temperatures records from chain 19 of experimental test H_1+2_20200124_20200128.

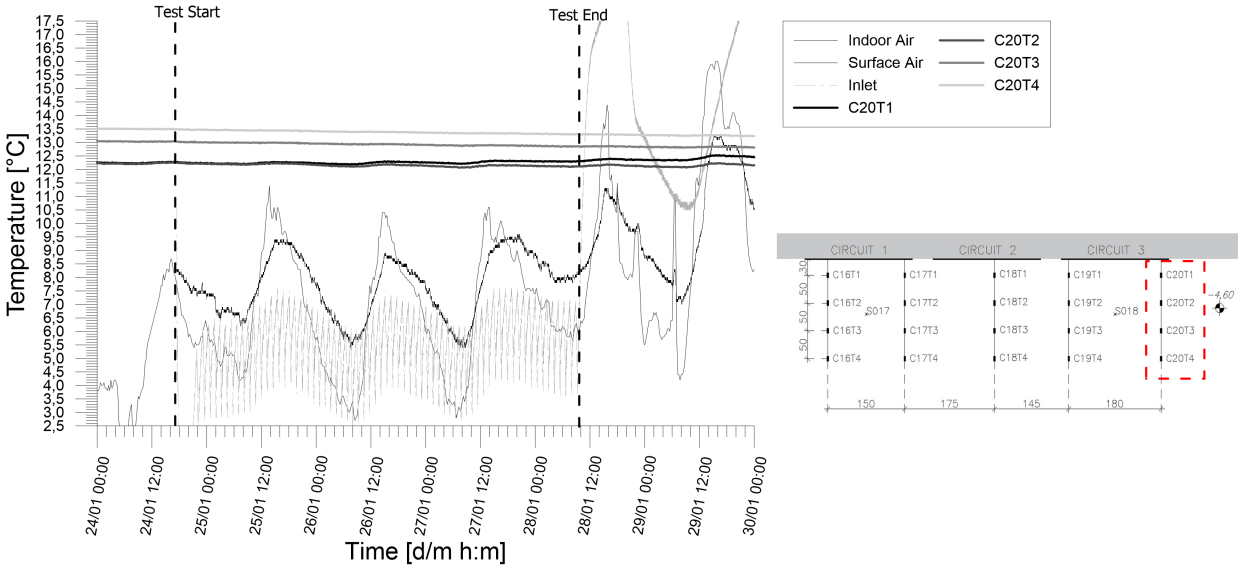

Figure A.161: Temperatures records from chain 20 of experimental test H_1+2_20200124_20200128.

A.8 Test H_1+2_20200131_20200203

Table A.8: Main features of the test.

Test start time	31/1/20 18.00
Test end time	3/2/20 9.20
Duration [h]	63.5
Operative mode	Heating
Active circuit(s)	1;2
Circuit link	Parallel
Target temperature user [°C]	35
Flow rate at the ground side [l/h]	Main: 923 Circuit 1: 430
Pressure at the user side [psi]	2.0
Pressure at the ground side [psi]	1.6
Total fluid volume [l]	Main: 58463 Circuit 1: 27801
Initial fluid temperature [°C]	9.7

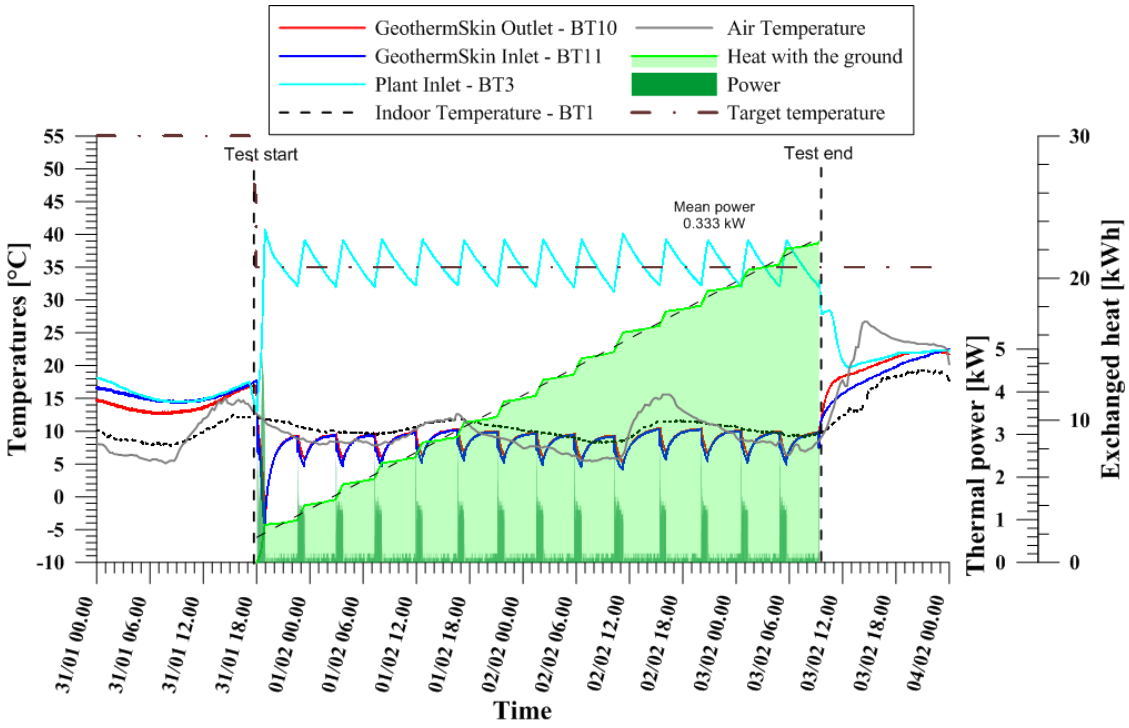

Figure A.162: Thermal performance interpretation of experimental test *H_1+2_20200131_20200203* with parallel link of circuit 1 and 2 in heating mode.

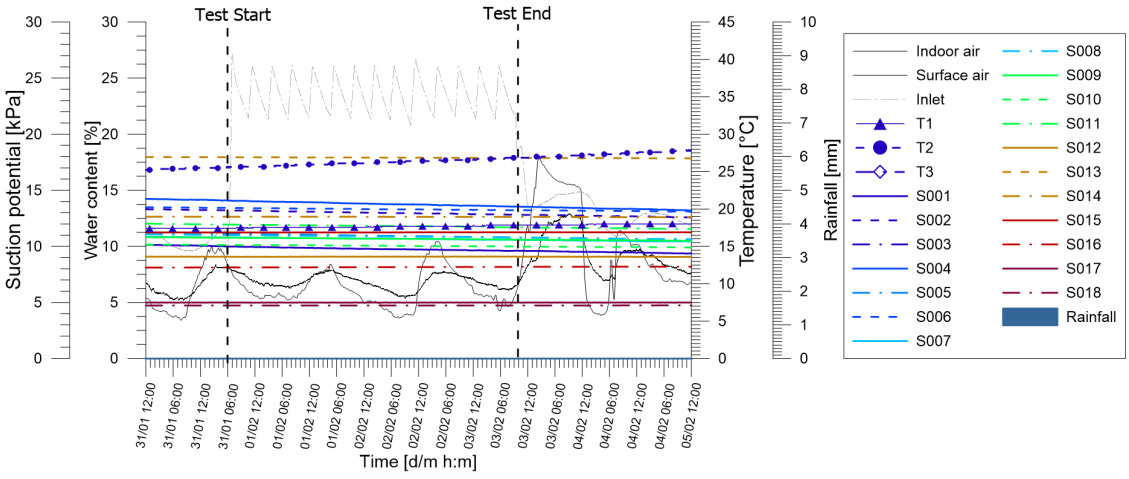

Figure A.163: Tensiometer and hygrometers records of experimental test H_1+2_20200131_20200203 together with monitored rainfall from Politecnico weather station.

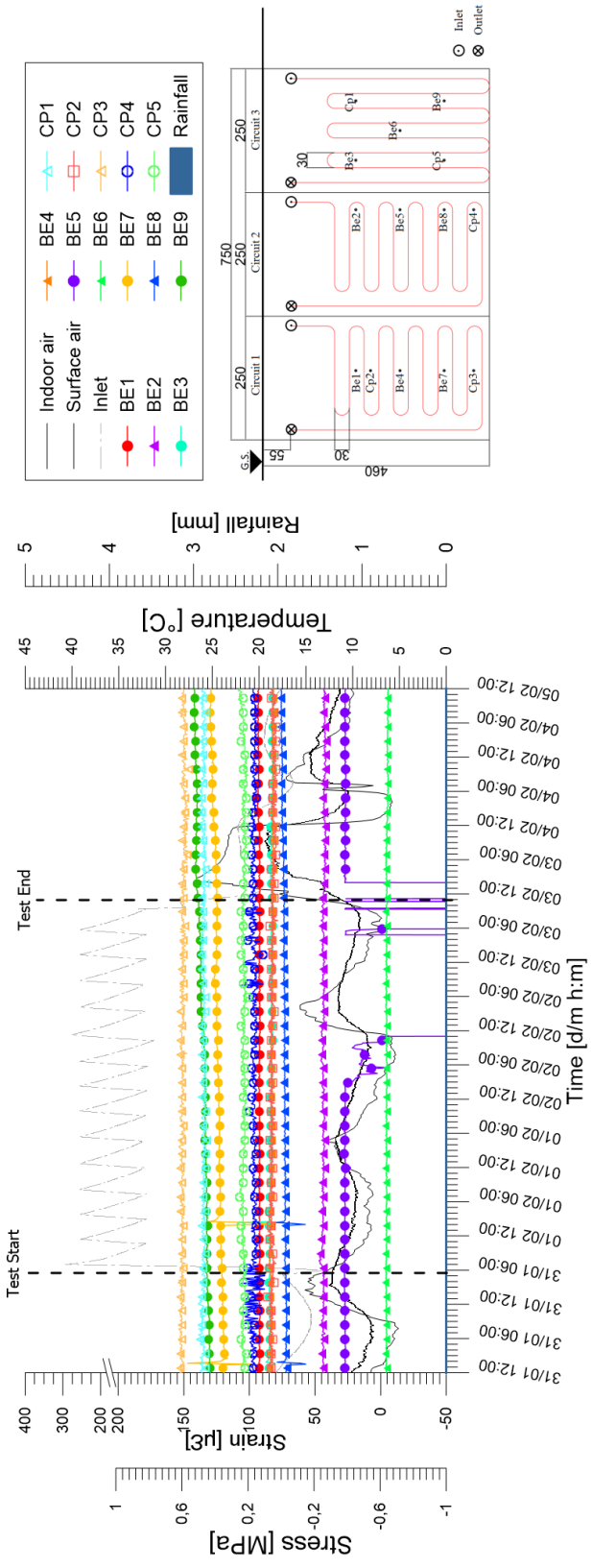

Figure A.164: Stresses and strains monitored at the wall external facade during experimental test H_1+2_20200131_20200203.

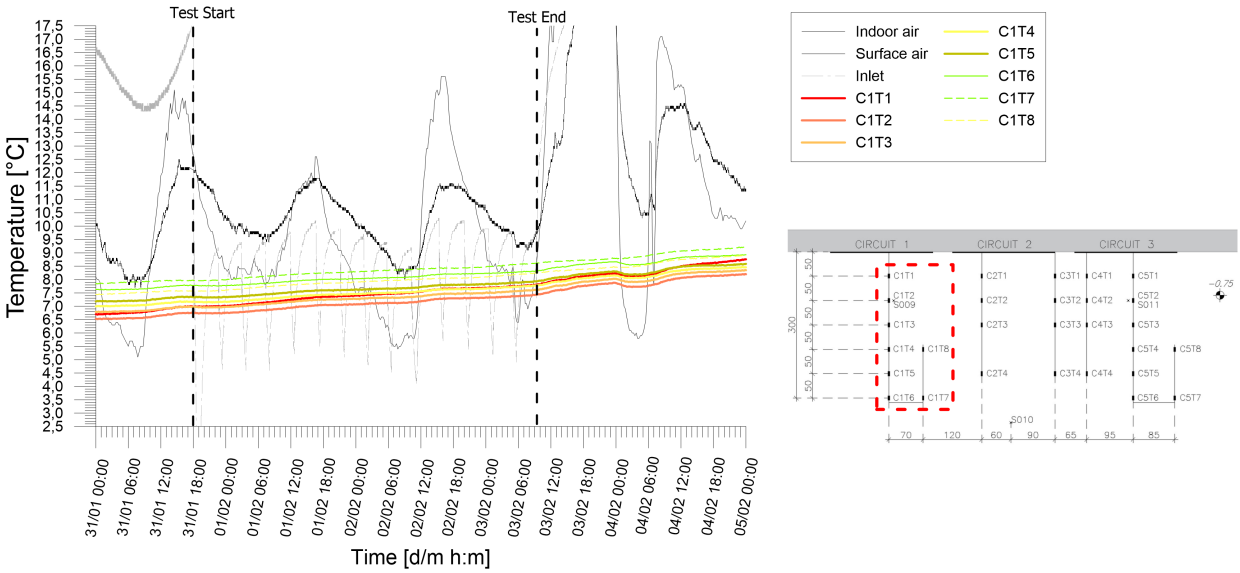

Figure A.165: Temperatures records from chain 1 of experimental test H_1+2_20200131_20200203.

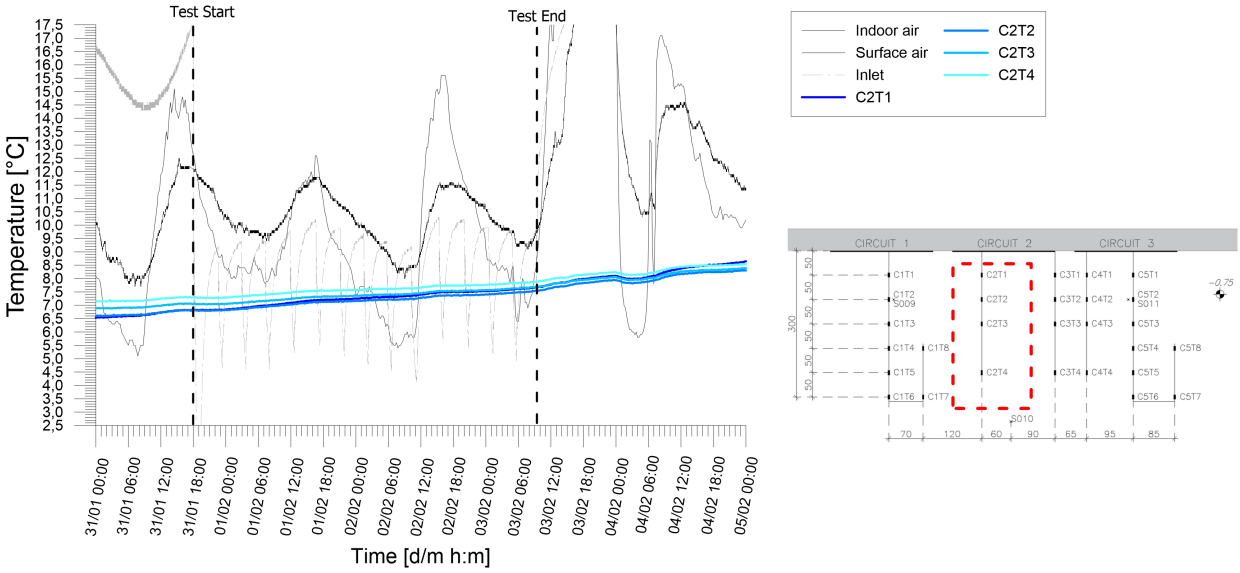

Figure A.166: Temperatures records from chain 2 of experimental test H_1+2_20200131_20200203.

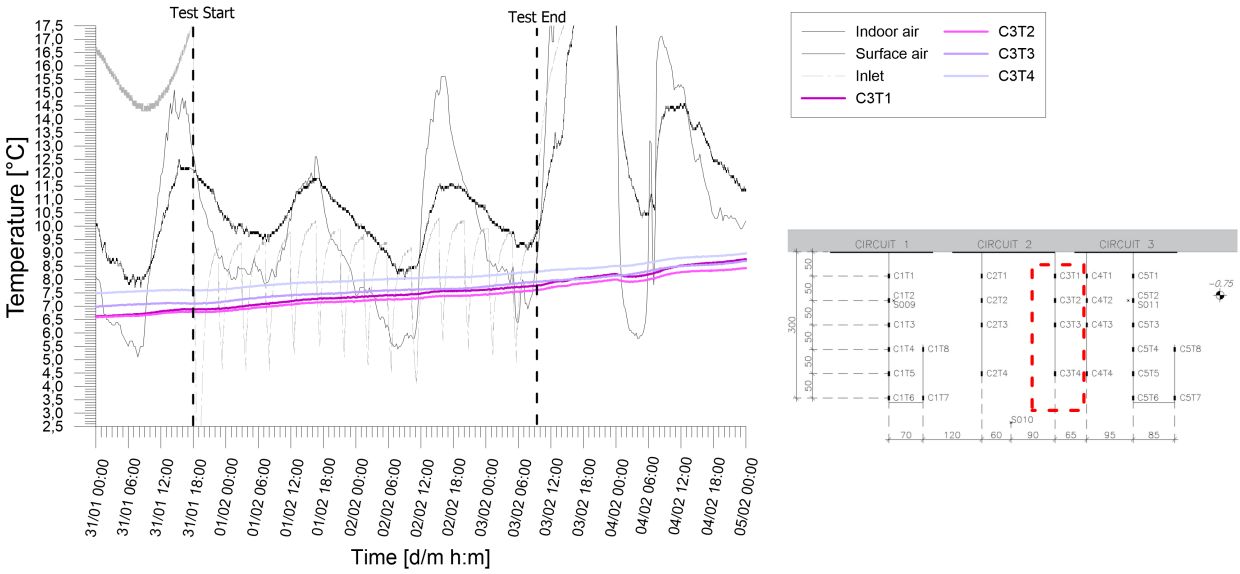

Figure A.167: Temperatures records from chain 3 of experimental test H_1+2_20200131_20200203.

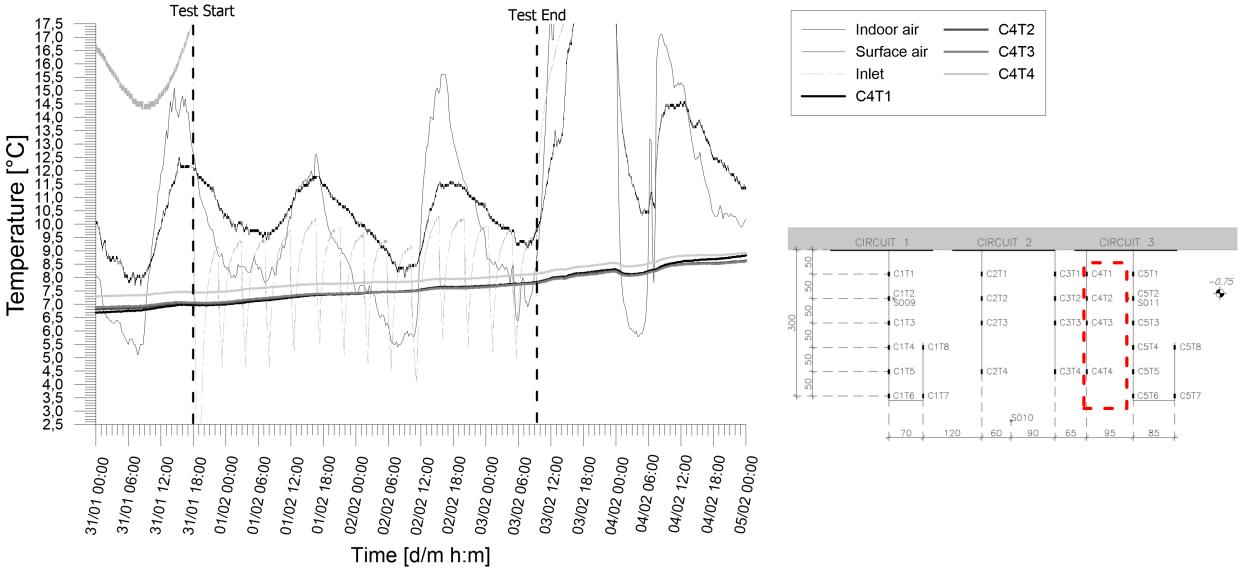

Figure A.168: *
Temperatures records from chain 4 of experimental test H_1+2_20200131_20200203.

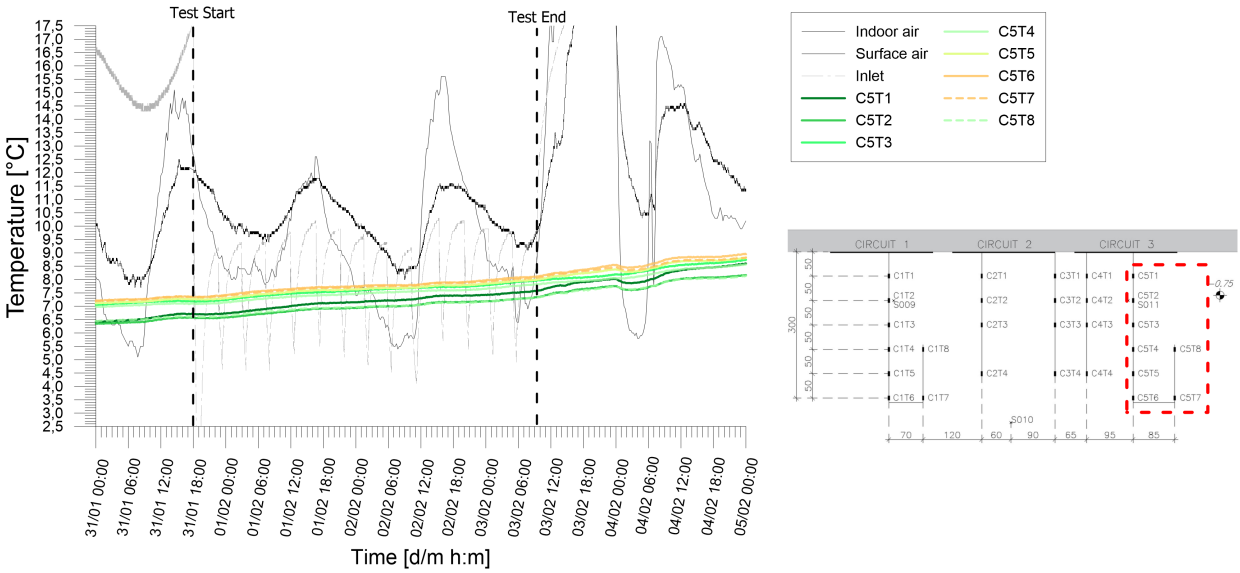

Figure A.169: Temperatures records from chain 5 of experimental test H_1+2_20200131_20200203.

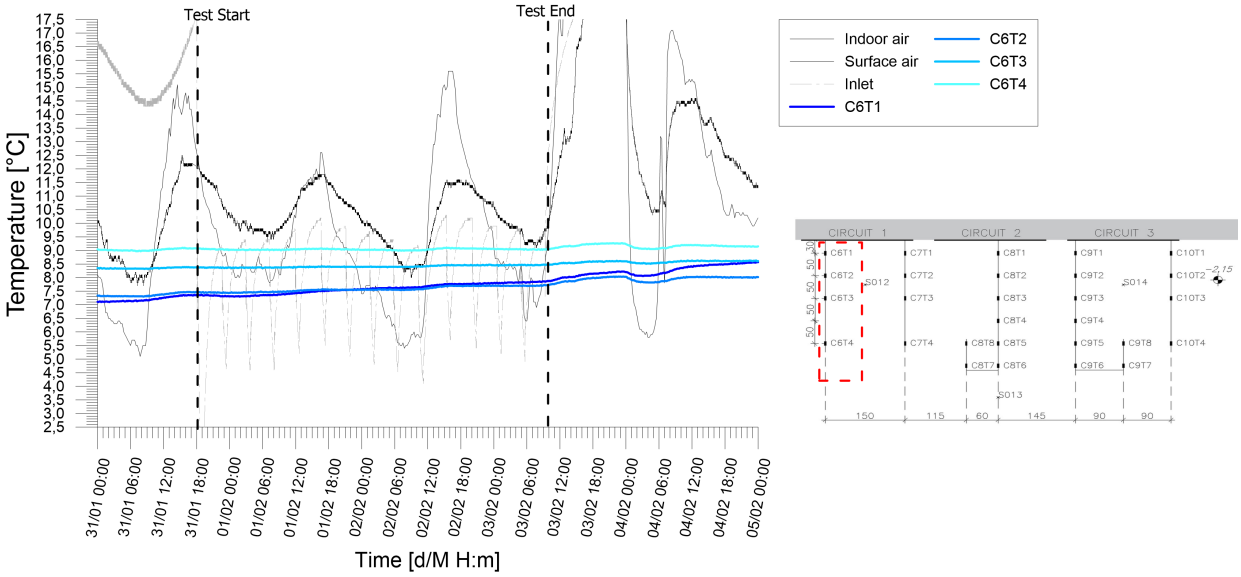

Figure A.170: Temperatures records from chain 6 of experimental test H_1+2_20200131_20200203.

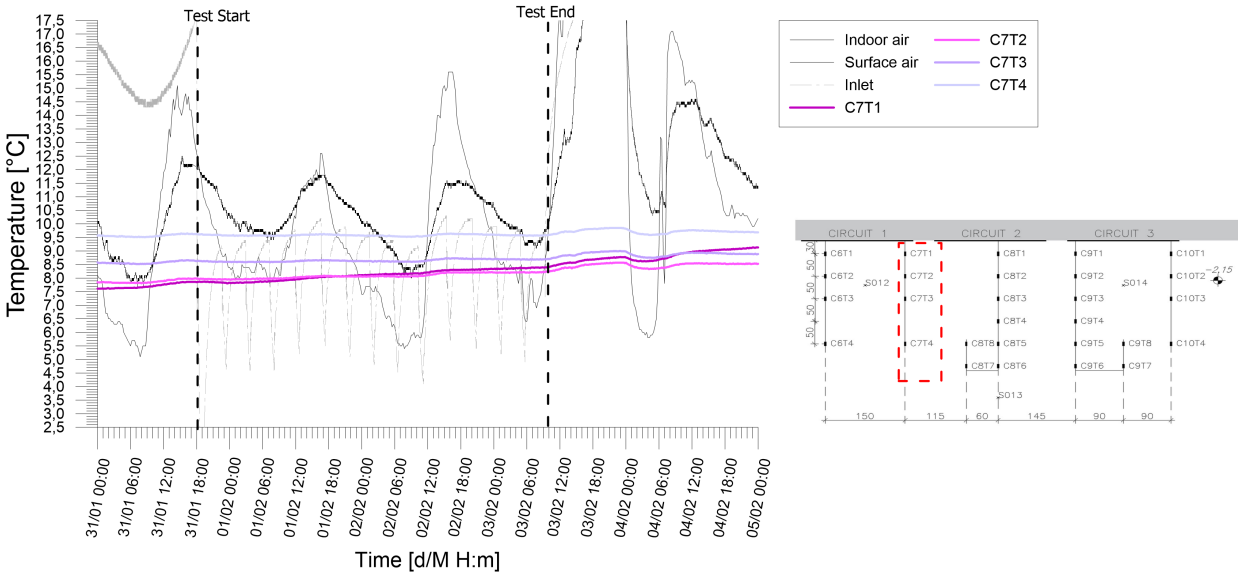

Figure A.171: Temperatures records from chain 7 of experimental test H_1+2_20200131_20200203.

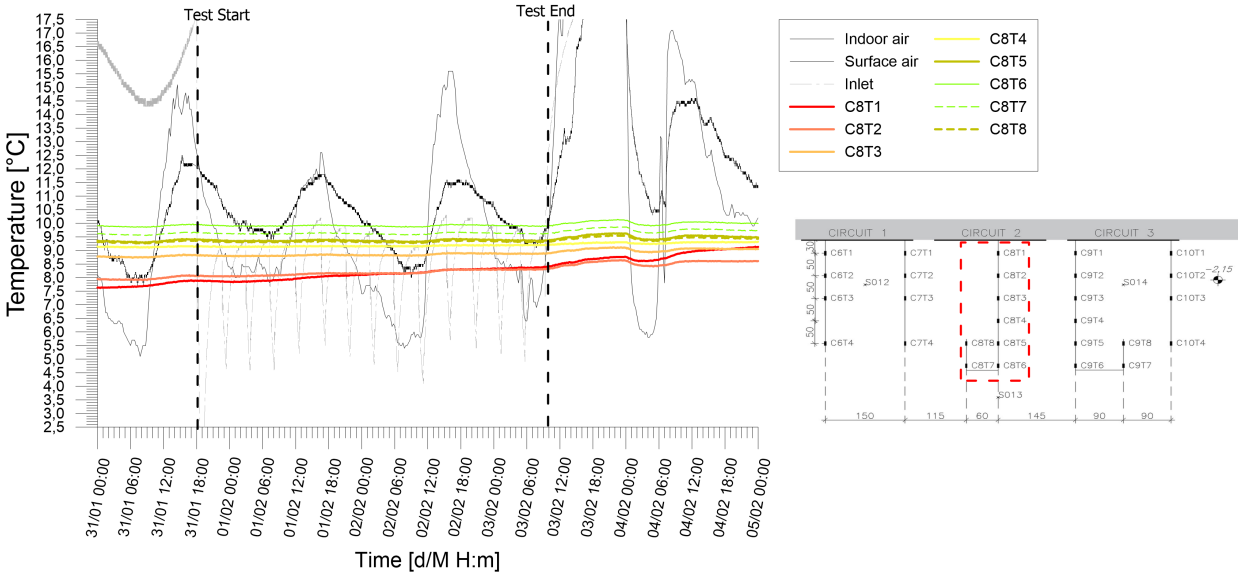

Figure A.172: Temperatures records from chain 8 of experimental test H_1+2_20200131_20200203.

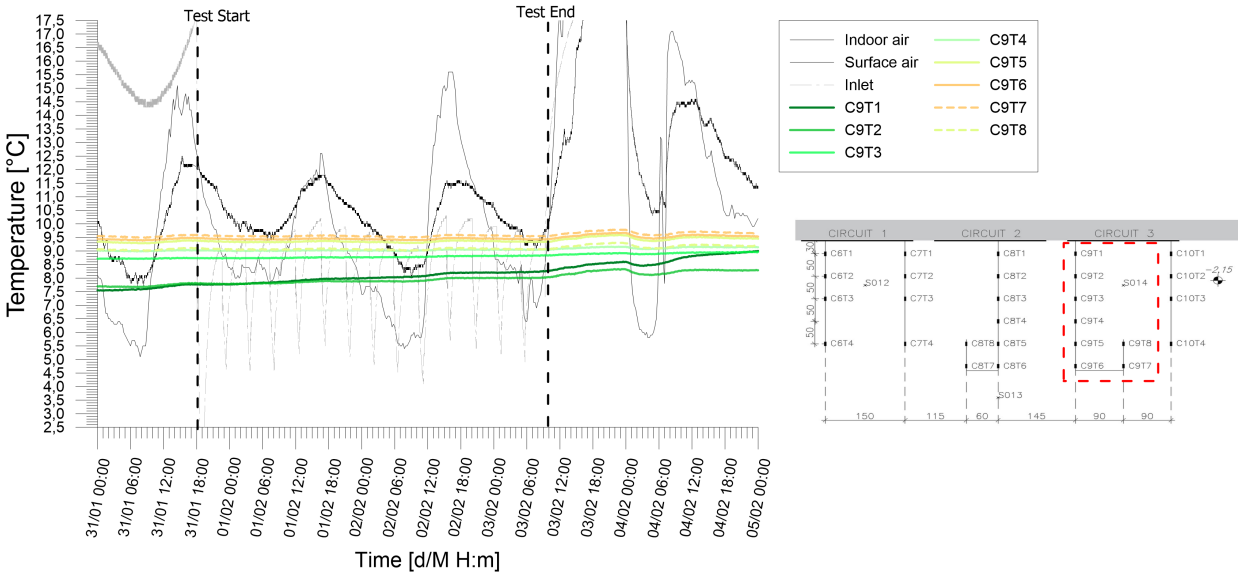

Figure A.173: Temperatures records from chain 9 of experimental test H_1+2_20200131_20200203.

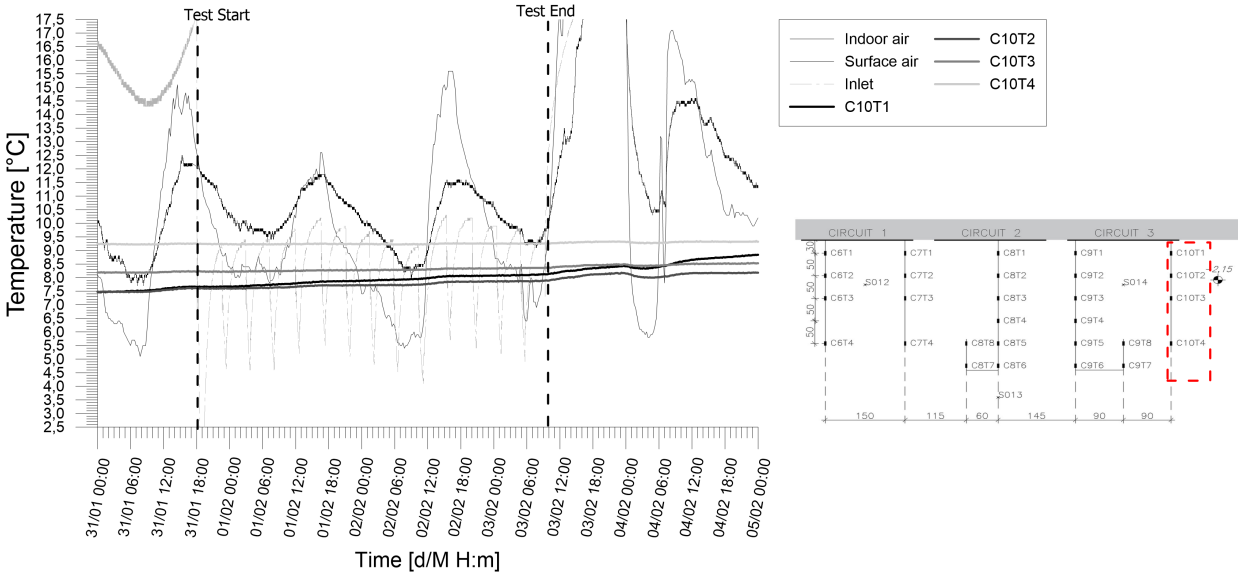

Figure A.174: Temperatures records from chain 10 of experimental test H_1+2_20200131_20200203.

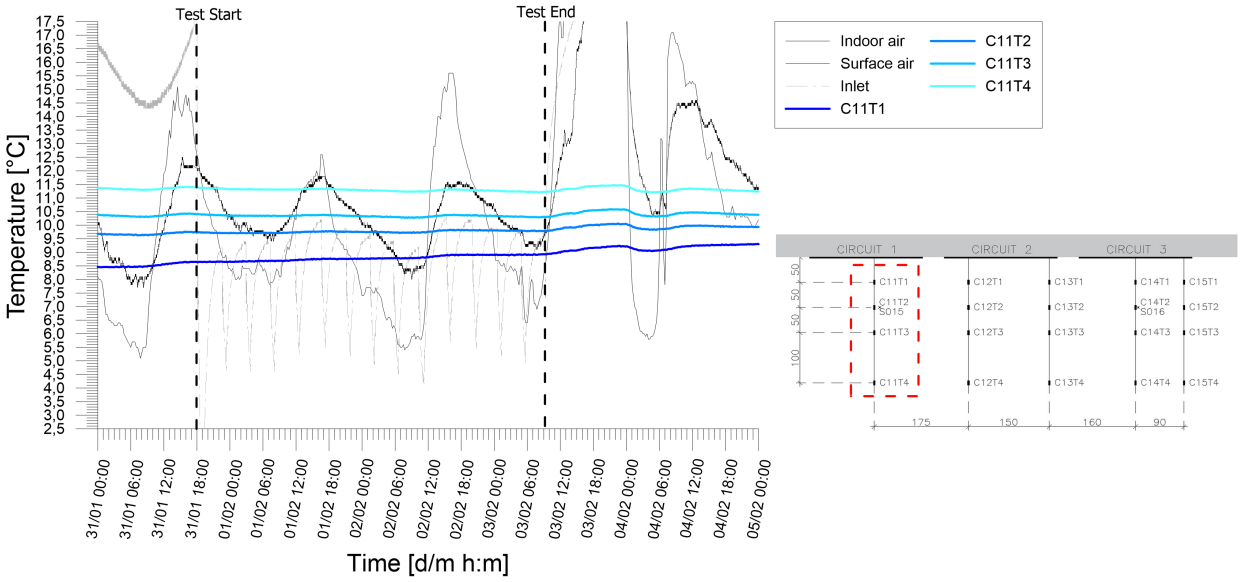

Figure A.175: *
Temperatures records from chain 11 of experimental test H_1+2_20200131_20200203.

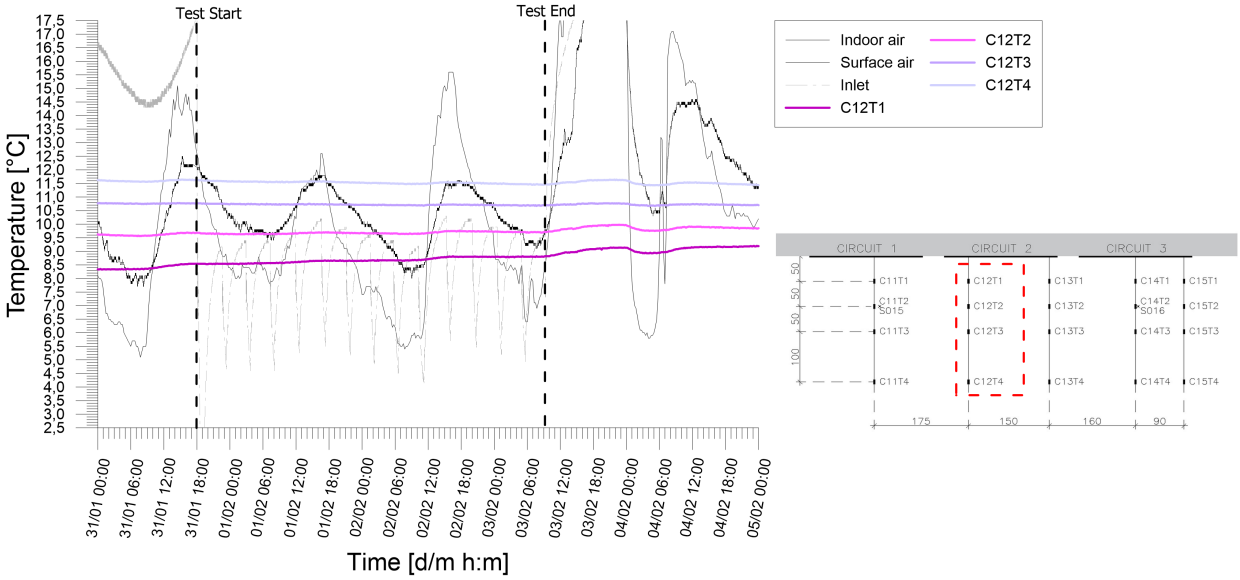

Figure A.176: Temperatures records from chain 12 of experimental test H_1+2_20200131_20200203.

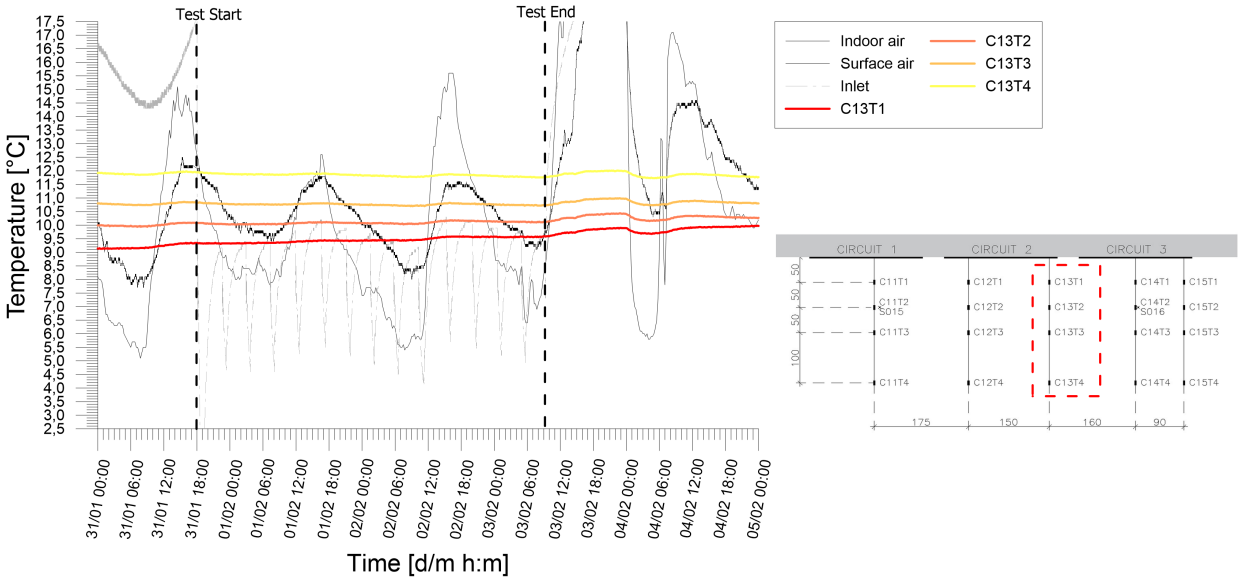

Figure A.177: Temperatures records from chain 13 of experimental test H_1+2_20200131_20200203.

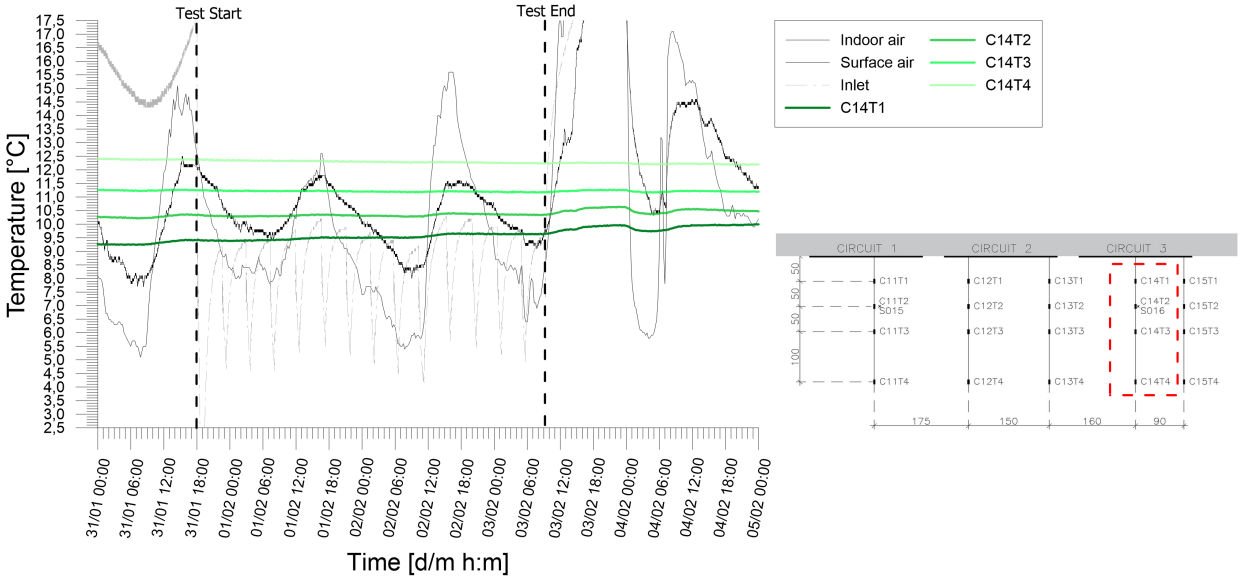

Figure A.178: Temperatures records from chain 14 of experimental test H_1+2_20200131_20200203.

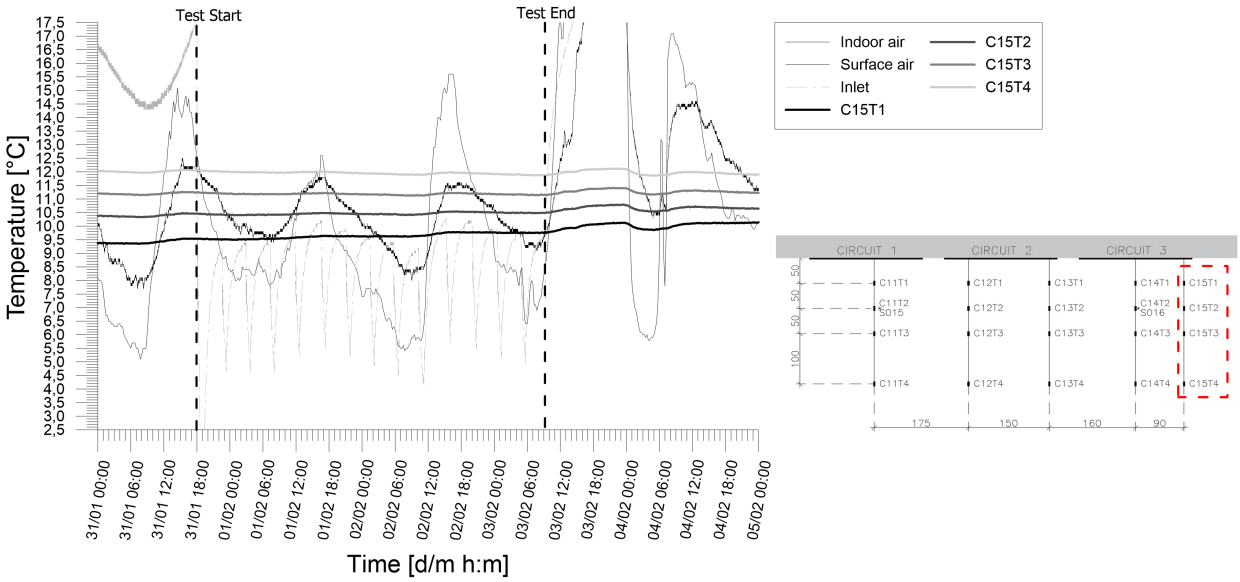

Figure A.179: Temperatures records from chain 15 of experimental test H_1+2_20200131_20200203.

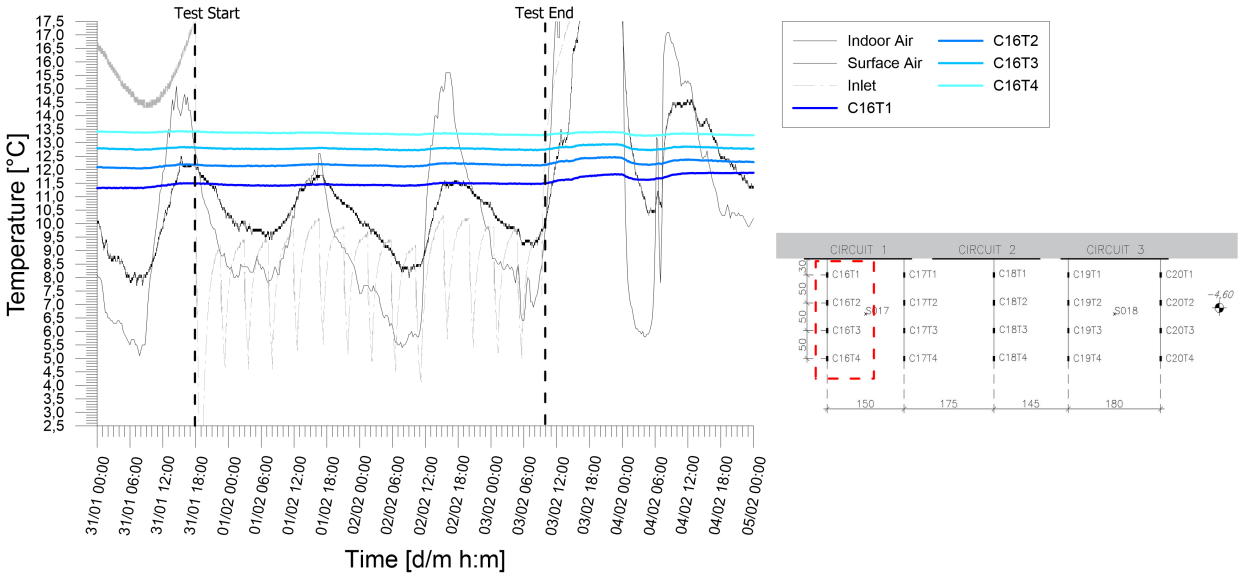

Figure A.180: Temperatures records from chain 16 of experimental test H_1+2_20200131_20200203.

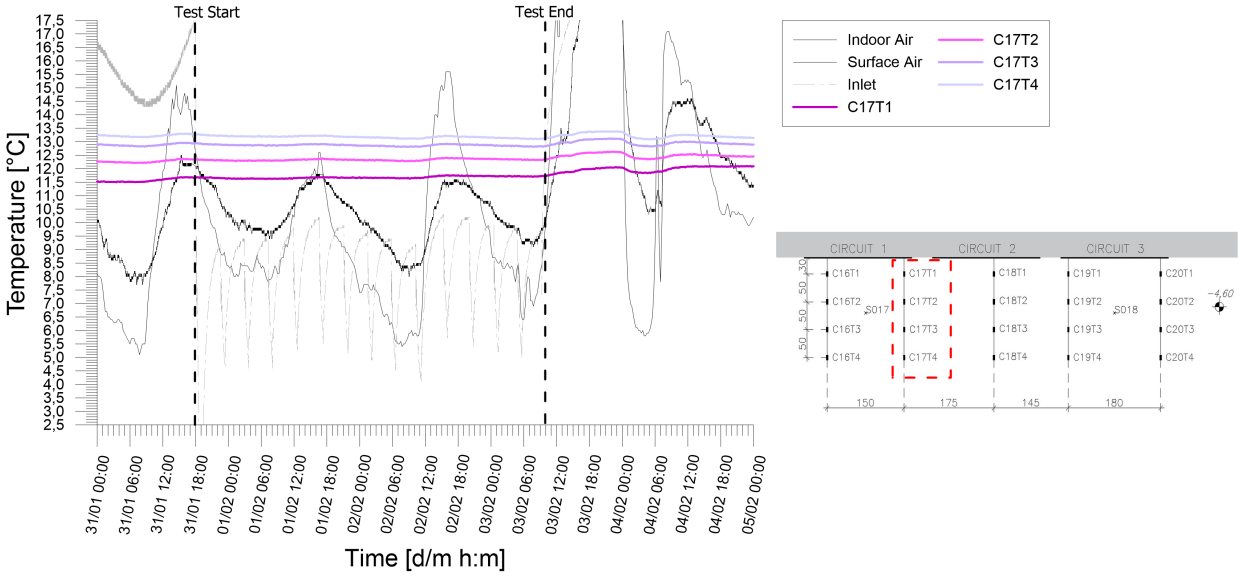

Figure A.181: Temperatures records from chain 17 of experimental test H_1+2_20200131_20200203.

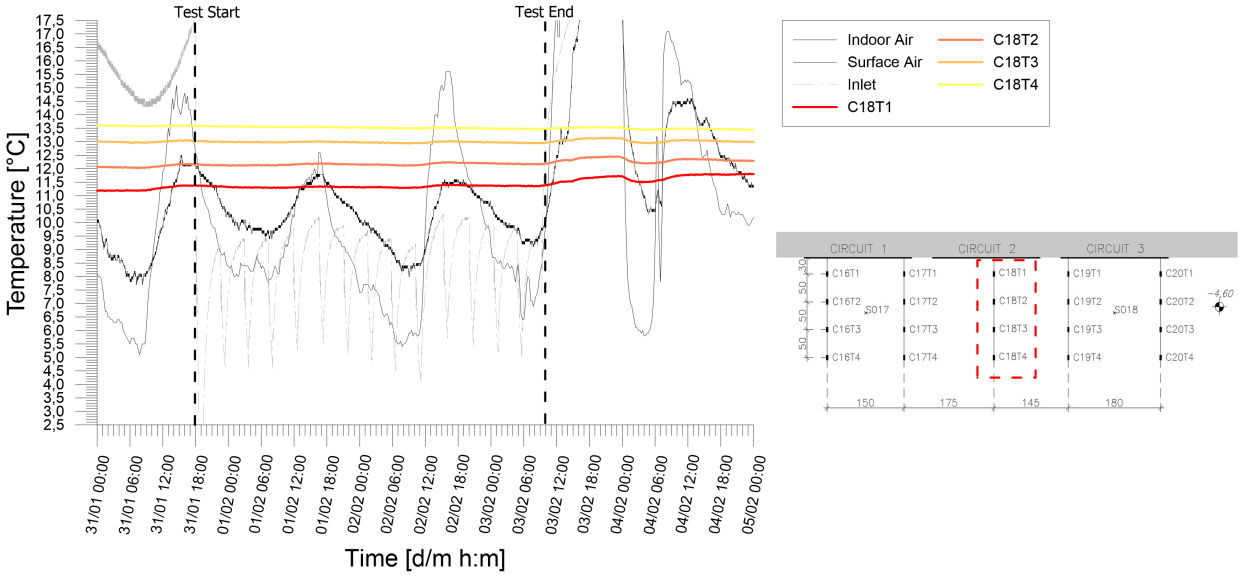

Figure A.182: Temperatures records from chain 18 of experimental test H_1+2_20200131_20200203.

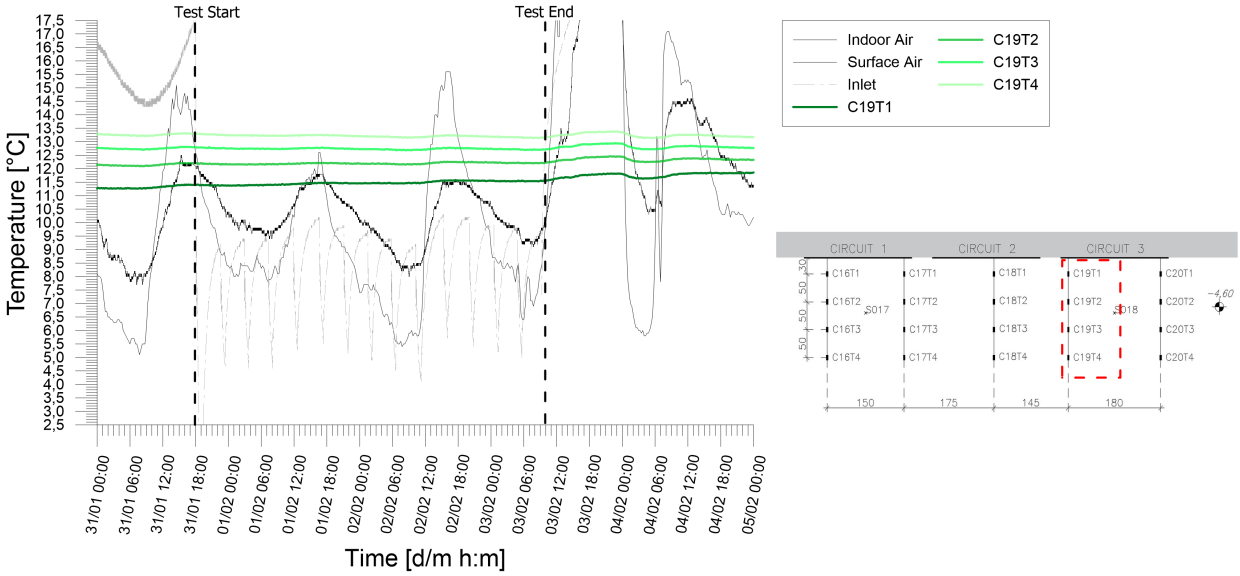

Figure A.183: Temperatures records from chain 19 of experimental test H_1+2_20200131_20200203.

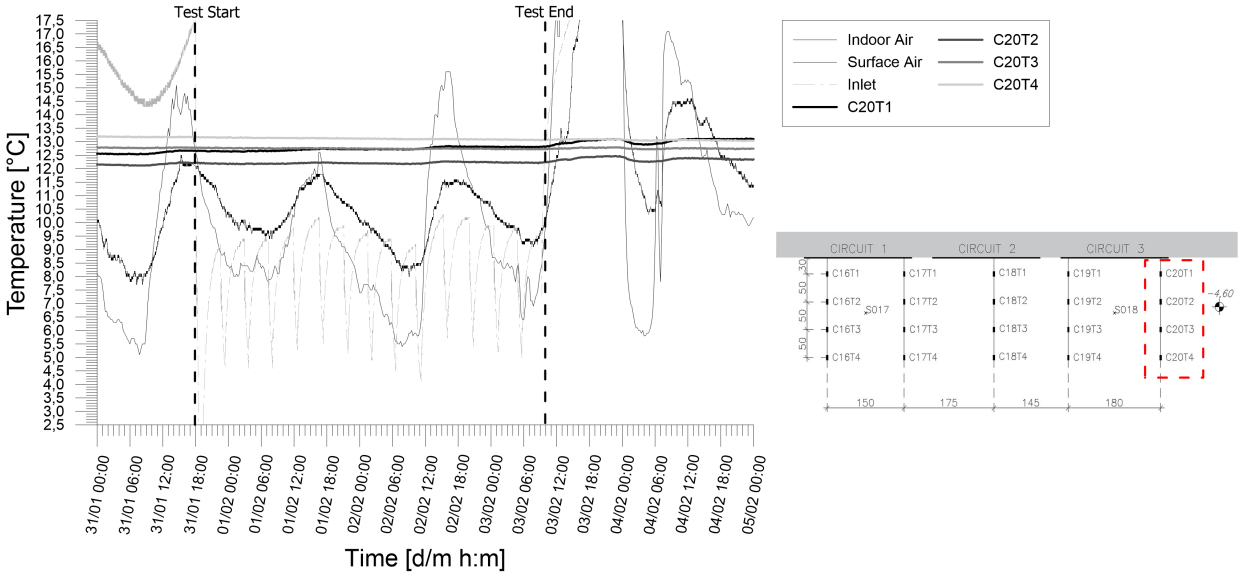

Figure A.184: Temperatures records from chain 20 of experimental test H_1+2_20200131_20200203.

Appendix B

Piezometer measurement campaign

A measurement campaign was carried out in December 2019 at the points of the metropolitan piezometric network. In this expeditious campaign the depth to the water table was measured by means of a level sensor with centimetric precision. The level sensor was also equipped with a temperature sensor. Hence the temperature at different depths along the column was observed up to the bottom. In a part of the piezometers the absolute elevation was measured by means of a GNSS receiver with n-RTK correction together with a reference measure on the nearest reference point of the municipal network.
In the following a sheet for each of the piezometers analysed is reported, sorted by its unique identifiers.

POLITECNICO
DI TORINO

SCHEDA RILEVAMENTO LIVELLO FALDA E TEMPERATURA POZZI/PIEZOMETRI

DATA	ID PIEZOMETRO/POZZO	LOCALITA'
18/12/2019	2972	Via Fagnano, 18 - Torino
TIPOLOGIA/DIAMETRO	**Quota bocca foro**	**Quota p.c.**
4"	237.825	237.915
SOGGIACENZA FALDA [m]	**Da bocca foro [m]**	**Da p.c. [m]**
8.61	☑ 8.61	☐ 8.70

NOTE: GPS fix point at g.s. (RTK correction fixed)
GPS fix point at altimetric reference point (RTK correction not completed)
Tube top at -0.09 m b.g.s.

PROFONDITA' [m]	TEMPERATURA [°C]	NOTE
8.61	14.6	Air temperature = 14.0°C
9.10	15.0	
9.60	14.9	
10.60	14.4	
11.60	13.9	
12.60	13.6	
13.60	13.3	
14.60	13.1	
16.60	13.0	
17.50	13.0	Piezometer bottom

OPERATORE: Matteo Baralis

Dipartimento di Ingegneria Strutturale, Edile e Geotecnica
Politecnico di Torino Corso Duca degli Abruzzi, 24 – 10129 Torino – Italia
www.diseg.polito.it www.polito.it

POLITECNICO
DI TORINO

SCHEDA RILEVAMENTO LIVELLO FALDA E TEMPERATURA POZZI/PIEZOMETRI

DATA	ID PIEZOMETRO/POZZO	LOCALITA'
18/12/2019	2976	Viale Ottavio Mario Mai, 43
TIPOLOGIA/DIAMETRO	**Quota bocca foro**	**Quota p.c.**
4"	222.379	222.459
SOGGIACENZA FALDA [m]	**Da bocca foro [m]**	**Da p.c. [m]**
8.75	☑ 8.75	☐ 8.83

NOTE: GPS point fix at g.s. (RTK correction)
GPS point fix at altimetric reference point (RTK correction not complete)
Piezometer top at -0.08 m b.g.s
Near active well field for hydraulic barrier

PROFONDITA' [m]	TEMPERATURA [°C]	NOTE
8.75	16.1	Air temperature 16.1°C
9.25	16.0	
9.75	16.2	
10.75	16.2	
11.75	16.2	
12.75	16.2	
13.75	16.2	
15.75	16.2	Piezometer bottom

OPERATORE: Matteo Baralis

Dipartimento di Ingegneria Strutturale, Edile e Geotecnica
Politecnico di Torino Corso Duca degli Abruzzi, 24 – 10129 Torino – Italia
www.diseg.polito.it www.polito.it

POLITECNICO
DI TORINO

SCHEDA RILEVAMENTO LIVELLO FALDA E TEMPERATURA POZZI/PIEZOMETRI

DATA	ID PIEZOMETRO/POZZO	LOCALITA'
18/12/2019	3011	Via Bioglio, 33/A - Torino
TIPOLOGIA/DIAMETRO	**Quota bocca foro**	**Quota p.c.**
4"	227.971	228.061
SOGGIACENZA FALDA [m]	**Da bocca foro [m]**	**Da p.c. [m]**
11.77	☑ 11.77	☐ 11.86

NOTE: GPS fix point at g.s. (RTK correction)
Tube top at -0.09 m b.g.s.

PROFONDITA' [m]	TEMPERATURA [°C]	NOTE
11.77	17.0	Air temperature= 16.8°C
12.27	17.1	
12.77	16.9	
13.77	16.8	
14.77	16.7	
15.77	16.5	
16.77	16.3	
18.77	16.2	
19.20	16.1	Piezometer bottom

OPERATORE: Matteo Baralis

Dipartimento di Ingegneria Strutturale, Edile e Geotecnica
Politecnico di Torino Corso Duca degli Abruzzi, 24 – 10129 Torino – Italia
www.diseg.polito.it www.polito.it

POLITECNICO
DI TORINO

SCHEDA RILEVAMENTO LIVELLO FALDA E TEMPERATURA POZZI/PIEZOMETRI

DATA	ID PIEZOMETRO/POZZO	LOCALITA'
18/12/2019	3018	Piazza Carducci 134 - Torino
TIPOLOGIA/DIAMETRO	**Quota bocca foro**	**Quota p.c.**
3"	234.218	234.498
SOGGIACENZA FALDA [m]	**Da bocca foro [m]**	**Da p.c. [m]**
	☑ 12.31	☐ 12.59
NOTE: GPS fix point at ground surface		

PROFONDITA' [m]	TEMPERATURA [°C]	NOTE
12.45	17.4	
12.95	17.6	
14.45	17.4	
15.45	17.4	
16.45	17.3	Piezometer bottom

OPERATORE: Matteo Baralis

Dipartimento di Ingegneria Strutturale, Edile e Geotecnica
Politecnico di Torino Corso Duca degli Abruzzi, 24 – 10129 Torino – Italia
www.diseg.polito.it www.polito.it

POLITECNICO
DI TORINO

SCHEDA RILEVAMENTO LIVELLO FALDA E TEMPERATURA POZZI/PIEZOMETRI

DATA	ID PIEZOMETRO/POZZO	LOCALITA'
18/12/2019	3021	Largo Marconi - Torino
TIPOLOGIA/DIAMETRO	**Quota bocca foro**	**Quota p.c.**
3"	236.636	236.826
SOGGIACENZA FALDA [m]	**Da bocca foro [m]**	**Da p.c. [m]**
14.82	☑ 14.82	☐ 15.01

NOTE: GPS fix at g.s. (RTK correction)
GPS fix at altimetric reference point (RTK partial connection)
Tube top at -0.19 m b.g.s.

PROFONDITA' [m]	TEMPERATURA [°C]	NOTE
14.82	16.8	Air temperature 16.4°C
15.30	16.9	
15.80	16.6	
16.80	16.4	
17.80	16.2	
18.80	16.1	
19.80	15.9	
20.80	15.9	Piezometer bottom

OPERATORE: Matteo Baralis

Dipartimento di Ingegneria Strutturale, Edile e Geotecnica
Politecnico di Torino Corso Duca degli Abruzzi, 24 – 10129 Torino – Italia
www.diseg.polito.it www.polito.it

POLITECNICO
DI TORINO

SCHEDA RILEVAMENTO LIVELLO FALDA E TEMPERATURA POZZI/PIEZOMETRI

DATA	ID PIEZOMETRO/POZZO	LOCALITA'
18/12/2019	3024	Corso Ferrucci - Torino
TIPOLOGIA/DIAMETRO	**Quota bocca foro**	**Quota p.c.**
4"	250.894	250.994
SOGGIACENZA FALDA [m]	**Da bocca foro [m]**	**Da p.c. [m]**
22.15	☑	☐

NOTE: GPS fix at ground surface (RTK correction)
GPS fix at altimetric reference point (RTK correction)
Tube top at -0.10 m b.g.s.

PROFONDITA' [m]	TEMPERATURA [°C]	NOTE
22.15	15.7	
22.65	16.1	
23.15	16.1	
24.15	16.1	
25.15	16.1	
26.15	16.1	
27.15	16.1	
28.15	16.1	
29.15	16.1	
30.15	16.1	

OPERATORE: Matteo Baralis

Dipartimento di Ingegneria Strutturale, Edile e Geotecnica
Politecnico di Torino Corso Duca degli Abruzzi, 24 – 10129 Torino – Italia
www.diseg.polito.it www.polito.it

POLITECNICO
DI TORINO

SCHEDA RILEVAMENTO LIVELLO FALDA E TEMPERATURA POZZI/PIEZOMETRI

DATA	ID PIEZOMETRO/POZZO	LOCALITA'
18/12/2019	3045	Via Alfieri - Grugliasco
TIPOLOGIA/DIAMETRO	**Quota bocca foro**	**Quota p.c.**
3"	268.501	268.601
SOGGIACENZA FALDA [m]	**Da bocca foro [m]**	**Da p.c. [m]**
	☑ 22.15	☐ 22.25
NOTE: GPS positioning ground surface. Top of the tube: -0.10 m b.g.s.		

PROFONDITA' [m]	TEMPERATURA [°C]	NOTE

OPERATORE: Matteo Baralis

Dipartimento di Ingegneria Strutturale, Edile e Geotecnica
Politecnico di Torino Corso Duca degli Abruzzi, 24 – 10129 Torino – Italia
www.diseg.polito.it www.polito.it

Appendix C

Numerical models and results

The present Appendix is intended to show the numerical results for the evaluation of the thermal and hydrodynamic regime of the subsoil beneath the central district of the city of Torino. In Chapter 6 numerical results were reported just partially due to conciseness reasons. Thus in this Appendix, further time histories at significant points are reported together with the pertaining measured expected values. Furthermore some integrative data about post processing are reported referring also to operative seasons different from the one deeply analysed in Chapter 6.

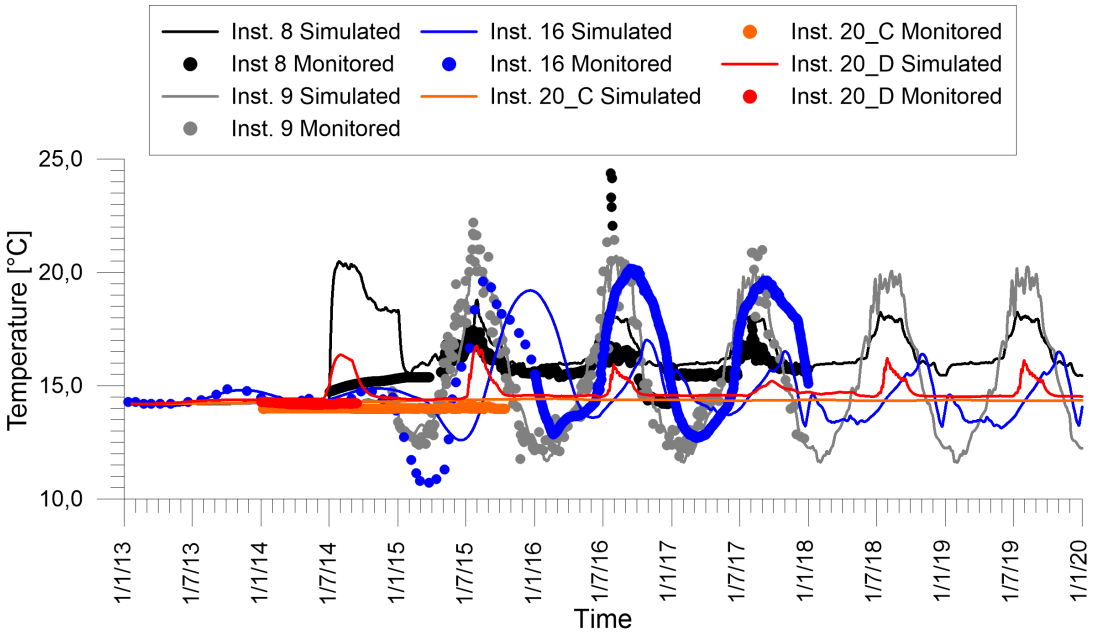

(a)

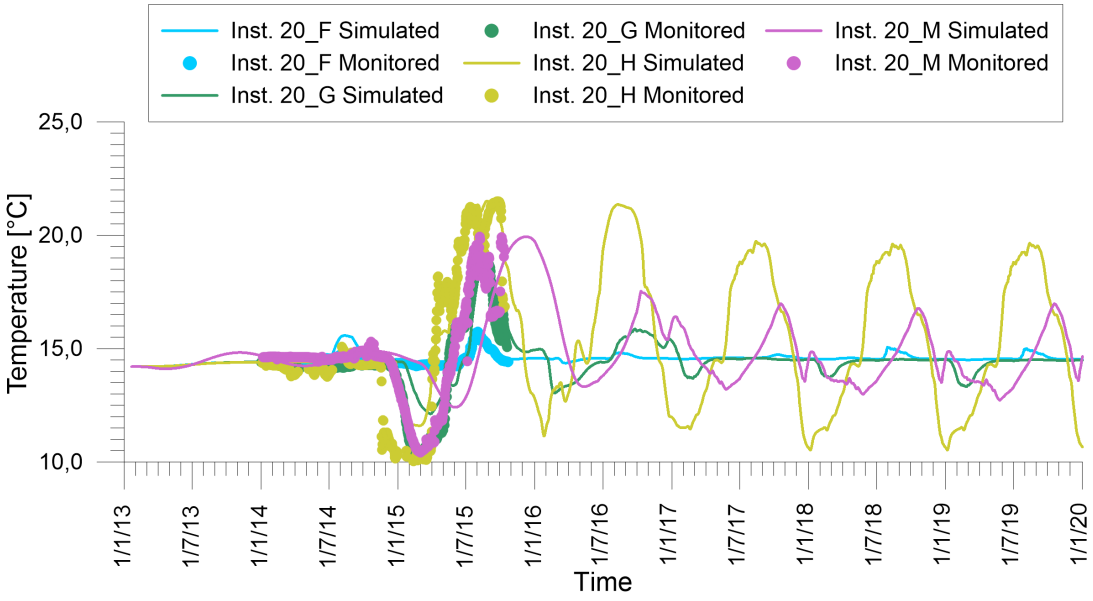

(b)

Figure C.1: Temperatures at geothermal installations piezometers, part I. The continuous lines represent the numerical analysis results while dots the measured values for comparison. The numerical trends obtained for last year are identically duplicated with cyclic behaviour until the end of the simulation.

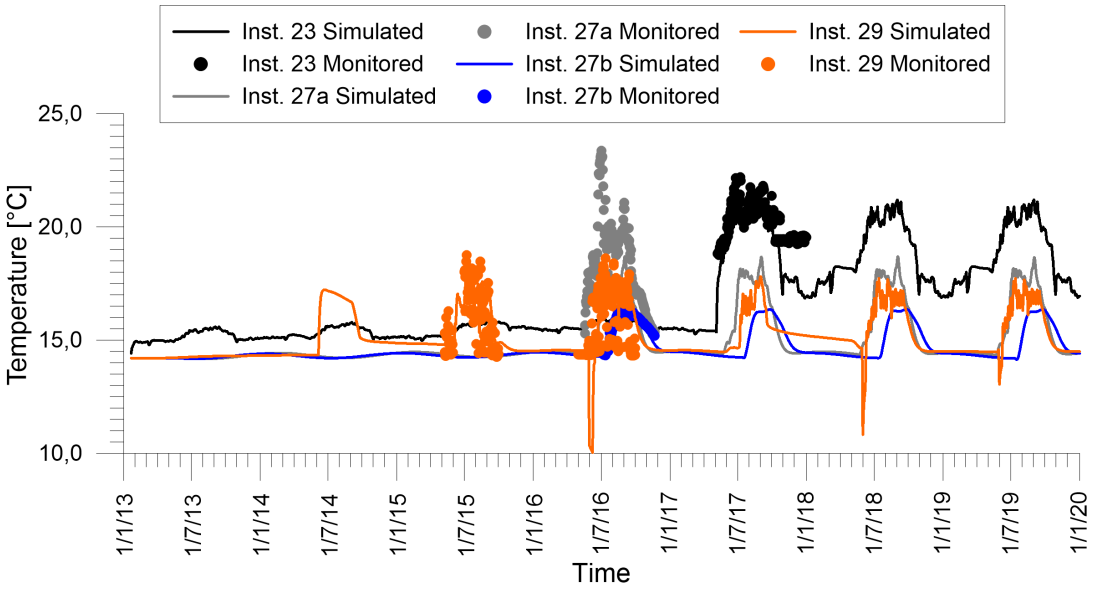

(a)

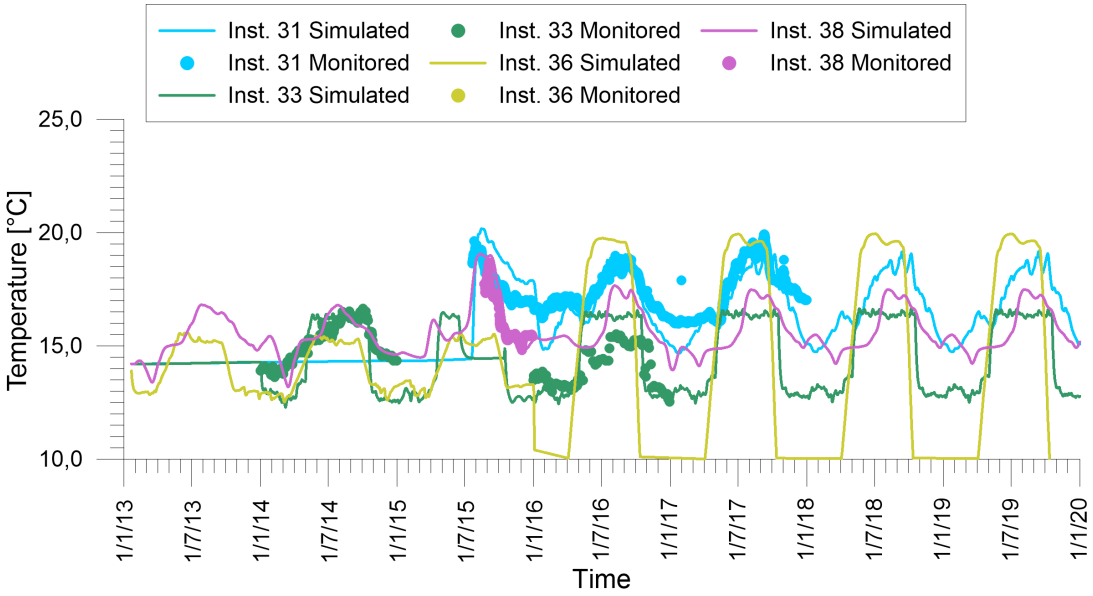

(b)

Figure C.2: Temperatures at geothermal installations piezometers, part II. The continuous lines represent the numerical analysis results while dots the measured values for comparison. The numerical trends obtained for last year are identically duplicated with cyclic behaviour until the end of the simulation.

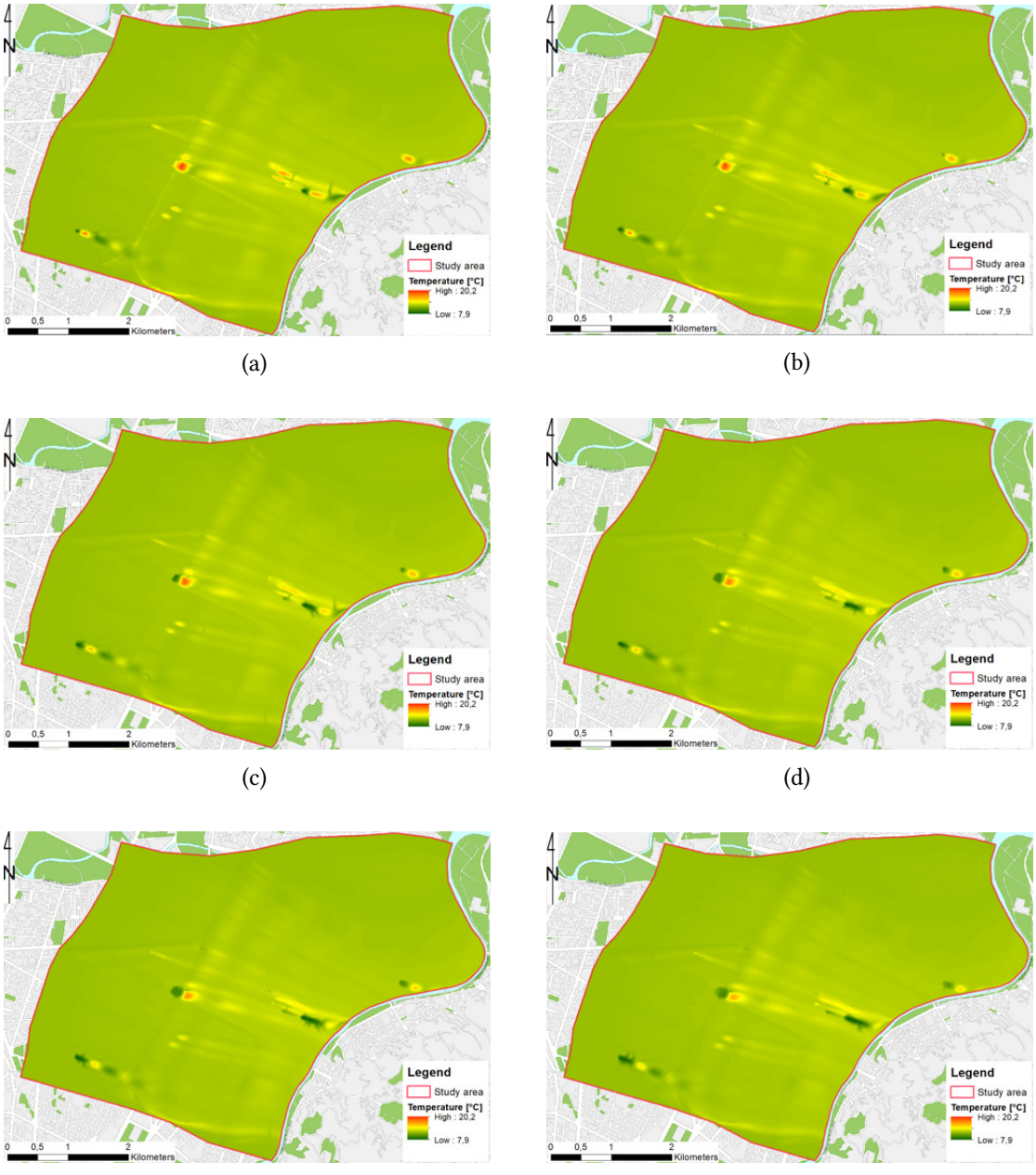

(a) (b)

(c) (d)

(e) (f)

Figure C.3: Temperatures expected in the model area during heating season 2024/2025 at (a) November, 1 (b) December, 1 (c) January, 1 (d) February, 1 (e) March, 1 and (f) April, 1.

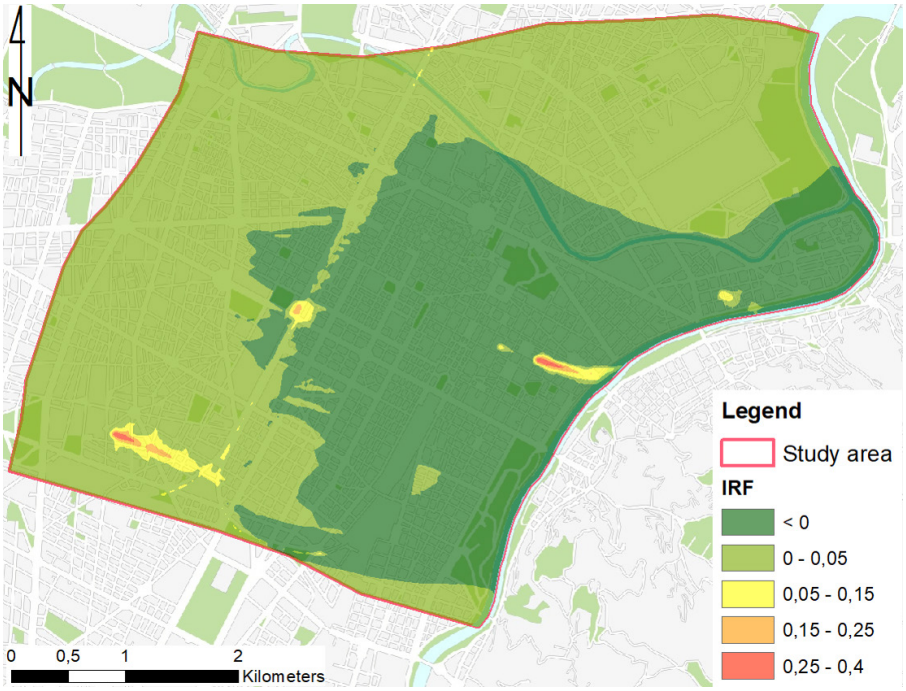

Figure C.4: Integrated Relaxation Factor for the City of Torino for heating season.

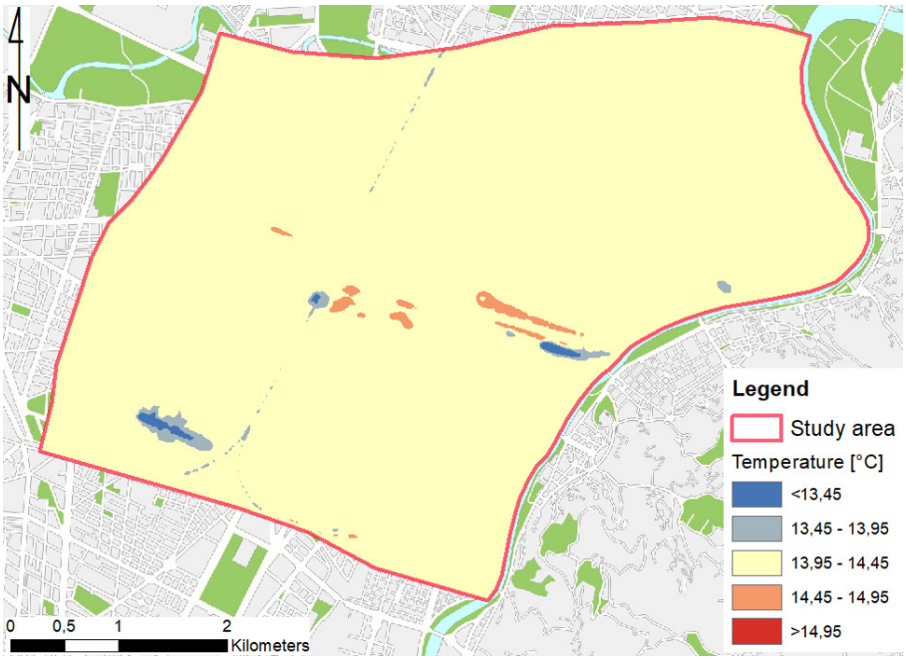

Figure C.5: Background temperature T_0^* for heating season in Torino central districts referred to year 2016/2017.

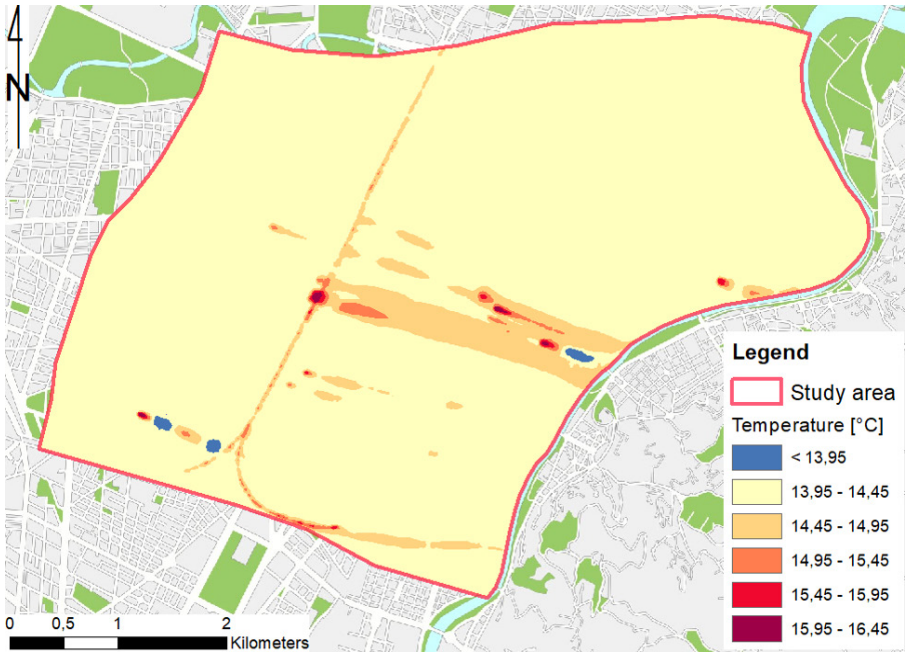

Figure C.6: Background temperature T_0^* for cooling season in Torino central districts referred to year 2025.

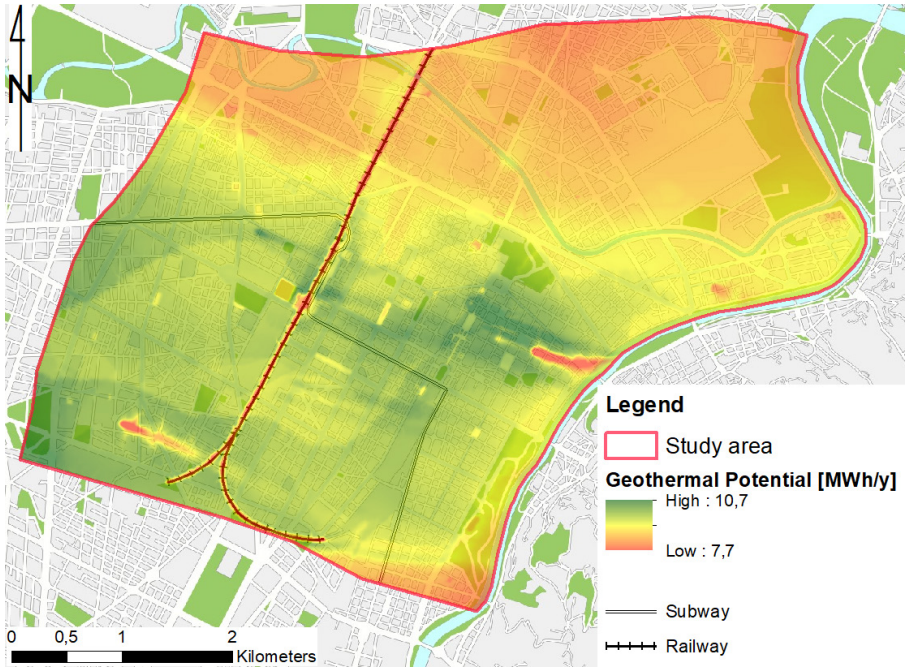

Figure C.7: Site specific shallow geothermal heating potential in Torino central district without accounting for groundwater fluxes. The reference season is winter 2025.

List of Symbols

Greek Symbols

α	Soil thermal diffusivity
α^*	Thermal idrodispersive diffusivity
α_L	Longitudinal thermal dispersivity
α_T	Transverse thermal dispersivity
$\tilde{\beta}$	Thermal expansion coefficient of the fluid
γ	Euler's constant
$\tilde{\gamma}$	Compressibility of the fluid
Λ	Temperature fluctuation wavelength
Λ_1	Spherical part of the thermal conductivity tensor
$[\lambda]$	Thermal conductivity 2nd order tensor
λ_f	Fluid phase thermal conductivity
λ_g	Ground thermal conductivity
λ_l	Thermal conductivity longitudinal component
λ_s	Solid phase thermal conductivity
λ_t	Thermal conductivity transverse component
λ_{ij}	Component of the thermal conductivity tensor
λ_{ij}^{cond}	Component of the conductive thermal conductivity tensor
λ_{ij}^{disp}	Component of the thermo-dispersive thermal conductivity tensor

μ_f Dynamic viscosity of the fluid

ρ Mass density

ρ_f Fluid phase mass density

$\rho_{f,ref}$ Fluid mass density at standard reference conditions

ρ_s Solid matrix mass density

ρ_w Water mass density

τ Aquifer transmissivity

ϕ_{air} Heat transfer coefficient of air layer

ϕ_{th} Thermal transfer coefficient

ϕ_{tunnel} Heat transfer coefficient pertaining urban tunnel

Operators

Δ Variation

δ_{ij} Kronecker's delta

∂ Partial derivative

∇ Gradient

$\nabla\cdot$ Divergence

$Ei(\cdot)$ Exponential integral function

exp Natural exponent

$K_0(\cdot)$ Modified Bessel function of second kind order zero

ln Natural Logarithm

tr Trace of a tensor

$\sum$ Sum

Roman Symbols

$A_{plume,i}$ Thermal plume areal extension

B Aquifer thickness

b Thickness of aquifer

C_{gw} Correction factor for groundwater flow

COP Coefficient Of Performance

COP_{th} COP of Carnot ideal cycle

c specific heat capacity

c_f Fluid phase specific heat capacity

c_s Solid matrix specific heat capacity

c_w Specific heat capacity of water

d_w Distance between wells in a doublet

E_{th} Theoretical geothermal potential

EER Energy Efficiency Ratio

F_{sc} Short circuit heat loss factor

H Building height

H_{roof} Height of the roof space in buildings

h Hydraulic head

$\boldsymbol{I}$ Identity matrix

IRF Integrated Relaxation Factor

$[K]$ Hydraulic conductivity tensor

k Hydraulic conductivity

L Borehole length

L_0 Latent heat of phase transformation

L_c Borehole length needed for building cooling purposes

L_h Borehole length needed for building heating purposes

$\dot{m}$ Mass flow rate

$\dot{m}_w$ Water mass flow rate

n Porosity

n_e Effective porosity

n_{fl} Number of storeys of a building

PLF_m Part-load factor during month

Pe Peclet number

p Pressure

p_{ref} Reference pressure

Q Heat source/sink

Q_{BHE} Borehole geothermal potential

Q_{OL} Heat potential of an open loop system

Q_b Building seasonal thermal load

Q_i Local geothermal potential

Q_p Pump rate

$\bar{q}$ Total heat flux

$\bar{q}_{cond}$ Conductive heat flux vector

$\bar{q}_{conv}$ Convective heat flux vector

$\bar{q}_{lat}$ Latent heat flux vector

$q(t)$ Thermal load

q_{BHE} Borehole geothermal potential per unit area

q_a Net annual average heat transfer to the ground

q_l Borehole heating rate per unit length

q_D Hydraulic flux

q_{lc} Building design cooling load

q_{lh} Building design heating load

R Radius of influence of well

R_b Borehole thermal resistance

R_{ga} Effective thermal resistance of the ground in annual pulse

R_{gd} Effective thermal resistance of the ground in daily pulse

R_{gm} Effective thermal resistance of the ground in monthly pulse

r Distance from well

SPF Seasonal Performance Factor

r_b Borehole radius

SR Satisfaction ratio

$\bar{T}$ Annual average of tunnel air temperature

s Drawdown

$T_{\bar{g}}$ Vertical mean ground temperature

T Temperature

T_0 Undisturbed ground temperature

T_0^* Corrected background temperature

T_C Temperature at the cold side of the Carnot cycle

T_H Temperature at the hot side of the Carnot cycle

T_Δ Calculated temperature drop

T_{calc} Heat pump target temperature

T_{in} Inlet temperature

T_{lim} Heat carrier fluid limit temperature

T_m Air annual mean temperature

T_{max} Tunnel internal air maximum temperature

T_{min} Tunnel internal air minimum temperature

T_{out} Outlet temperature

T_p Temperature penalty for adjacent borehole interference

T_{real} Heat pump outlet temperature at the user side

T_{ref} Reference temperature

T_{res} Residual temperature drop

T_{tunnel} Tunnel internal air temperature

t Time

t_0 Time period

t_c Load cycle time

t_s Installation lifetime

t_s^* Starting operation time

t_y Period between two identical operative seasons

th Homogeneous layer thickness

V_e Interconnected pore volume

V_r Reservoir volume

$\bar{v}$ Velocity

v_d Darcy velocity

v_i Velocity component in the i-th direction

$\bar{W}_c$ Power input at design cooling load

$\bar{W}_h$ Power input at design heating load

x Space coordinate x

y Space coordinate y

z Depth

Bibliography

Adam, D. and Markiewicz, R. (2009), Energy from earth-coupled structures, foundations, tunnels and sewers, *Géotechnique*, 59(3), 229–236, ISSN 0016-8505, doi: 10.1680/geot.2009.59.3.229.

Aiassa, S. and Antolini, F. (2019), Relazione tecnica sulle indagini "Digital revolution House", Technical report, Torino.

Al-Khoury, R., Kölbel, T. and Schramedei, R. (2010), Efficient numerical modeling of borehole heat exchangers, *Computers and Geosciences*, 36(10), 1301–1315, ISSN 00983004, doi:10.1016/j.cageo.2009.12.010.

Alcaraz, M., García-Gil, A., Vázquez-Suñé, E. and Velasco, V. (2016), Use rights markets for shallow geothermal energy management, *Applied Energy*, 172, 34–46, ISSN 03062619, doi:10.1016/j.apenergy.2016.03.071.

Amis, T., A. W. Robinson, C. and Wong, S. (2011), Integrating geothermal loops into the diaphragm walls of the bulgari hotel knightsbridge london.

Anstett, M., Hubbuch, M., Laloui, L., Matthey, B., Morath, M. et al. (2005), Utilisation de la chaleur du sol par des ouvrages de fondation etde soutènement en béton. Guide pour la conception, la realization et la maintenance, Technical report, Société Suisse des ingénieurs et des architects, Zurich, Swtizerland.

Arola, T., Eskola, L., Hellen, J. and Korkka-Niemi, K. (2014), Mapping the low enthalpy geothermal potential of shallow Quaternary aquifers in Finland, *Geothermal Energy*, 2(1), 9, ISSN 2195-9706, doi:10.1186/s40517-014-0009-x.

ARPA Piemonte (2015), Rete piezometrica metropolitana, Città di Torino.

Baehr, H. and Stephan, K. (1998), *Heat and mass transfer*, Springer-Verlag.

Baek, S.H., Yeo, M.S. and Kim, K.W. (2017), Effects of the geothermal load on the ground temperature recovery in a ground heat exchanger, *Energy and Buildings*, 136, 63–72, ISSN 03787788, doi:10.1016/j.enbuild.2016.11.056.

Banks, D. (2009), Thermogeological assessment of open-loop well-doublet schemes: A review and synthesis of analytical approaches, *Hydrogeology Journal*, 17(5), 1149–1155, ISSN 14312174, doi:10.1007/s10040-008-0427-6.

Baralis, M., Barla, M., Bogusz, W., Di Donna, A., Ryzynski, G. et al. (2018), Geothermal Potential of the NE Extension Warsaw Metro Tunnels, *Environmental Geotechnics*, doi:https://doi.org/10.1680/jenge.18.00042.

Barbero, D., De Luca, D.A., Forno, M.G. and Lasagna, M. (2016), Preliminary results on temperature distribution in the Quaternary fluvial and outwash deposits of the Piedmont Po Plain (NW Italy): A statistical approach, *Rendiconti Online Societa Geologica Italiana*, 41, 272–275, ISSN 20358008, doi:10.3301/ROL.2016.146.

Barla, G., Antolini, F., Barla, M., Bonini, M., Debernardi, D. et al. (2013b), Analisi e Verifica delle Condizioni di Esercizio in Sicurezza del Palazzo Uffici Provinciali di Corso Inghilterra 7 tenuto conto del Centro Direzionale di Intesa Sanpaolo - Modellazione numerica, analisi di interazione e piano di monitoraggio, Technical report, Politecnico di Torino, Torino.

Barla, G. and Barla, M. (2005), Assessing design parameters for tunnelling in a cemented granular soil by continuum and discontinuum modelling, in: *Proc. 11th Iacmag Conference*, pp. 475–484, Torino.

Barla, G., Barla, M., Bonini, D., Debernardi, D., Perino, A. et al. (2015), 3D thermo-hydro modeling and real-time monitoring for a geothermal system in Torino, Italy, in: *proceedings of XVI ECSMGE*, pp. 2481–2486, ICE Publishing, Edinburgh, ISBN 9780727760678, doi:10.1680/ecsmge.60678.

Barla, G. and Vai, L. (1999), Indagini geotecniche per la caratterizzazione del sottosulo di Torino lungo il tracciato del passante ferroviario, in: Associazione Geotecnica Italiana (ed.), *20th, Convegno nazionale di geotecnica;*, pp. 335–342, Patron Editore, Parma.

Barla, M., Baralis, M., Insana, A., Zacco, F., Aiassa, S. et al. (2019b), Feasibility study for the thermal activation of Turin Metro Line 2, in: *Tunnels and Underground Cities: Engineering and Innovation meet Archaeology, Architecture and Art- Proceedings of the WTC 2019 ITA-AITES World Tunnel Congress*, doi:10.1201/9780429424441-24.

Barla, M. and Barla, G. (2012), Torino subsoil characterization by combining site investigations and numerical modelling / Charakterisierung des Turiner Untergrunds mithilfe von Feldstudien und numerischer Modellierungen, *Geomechanics and Tunnelling*, 5(3), 214–232, ISSN 18657362, doi:10.1002/geot.201200008.

Barla, M. and Camusso, M. (2013), A method to design microtunnelling installations in randomly cemented Torino alluvial soil, *Tunnelling and Underground Space Technology*, 33, 73–81, ISSN 08867798, doi:10.1016/j.tust.2012.09.002.

Barla, M., Di Donna, A. and Insana, A. (2017), Energy tunnel experimental site in turin metro, in: *Proceedings of the 15th International Conference of the International Association for Computer Methods and Advances in Geomechanics*.

Barla, M., Di Donna, A. and Insana, A. (2019), A novel real-scale experimental prototype of energy tunnel, *Tunnelling and Underground Space Technology*, 87(February), 1–14, ISSN 08867798, doi:10.1016/j.tust.2019.01.024.

Barla, M., Di Donna, A. and Perino, A. (2016), Application of energy tunnels to an urban environment, *Geothermics*, 61, 104–113, ISSN 03756505, doi:10.1016/j.geothermics.2016.01.014.

Barla, M., Donna, A.D. and Baralis, M. (2018), City-scale analysis of subsoil thermal conditions due to geothermal exploitation, *Environmental Geotechnics*, pp. 1–11, ISSN 2051-803X, doi:10.1680/jenge.17.00087.

Barla, M. and Insana, A. (2018), Energy Tunnel Segmental Lining: an Experimental Site in Turin Metro, in: *World Tunnel Congress 2018.*, p. 12, -, Dubai, United Arab Emirates.

Barla, M. and Perino, A. (2015), Energy from geo-structures: a topic of growing interest, *Environmental Geotechnics*, 2(1), 3–7, ISSN 2051-803X, doi:10.1680/envgeo.13.00106.

Bayer, P., Attard, G., Blum, P. and Menberg, K. (2019), The geothermal potential of cities, *Renewable and Sustainable Energy Reviews*, 106(February), 17–30, ISSN 13640321, doi:10.1016/j.rser.2019.02.019.

Bayer, P., de Paly, M. and Beck, M. (2014), Strategic optimization of borehole heat exchanger field for seasonal geothermal heating and cooling, *Applied Energy*, 136, 445–453, ISSN 03062619, doi:10.1016/j.apenergy.2014.09.029.

Bear, J. (1988), *Dynamics of fluids in porous media / Jacob Bear*, Dover books on physics and chemistry, Dover, New York, ISBN 0-486-65675-6.

Benz, S.A., Bayer, P., Menberg, K., Jung, S. and Blum, P. (2015), Spatial resolution of anthropogenic heat fluxes into urban aquifers, *Science of the Total Environment*, 524-525, 427–439, ISSN 18791026, doi:10.1016/j.scitotenv.2015.04.003.

Bernier, M.A., Pinel, P., Labib, R. and Paillot, R. (2004), A multiple load aggregation algorithm for annual hourly simulations of GCHP systems, *HVAC and R Research*, 10(4), 471–487, ISSN 10789669, doi:10.1080/10789669.2004.10391115.

Bonsor, H.C., Dahlqvist, P., Moosmann, L., Classen, N., Epting, J. et al. (2015), Groundwater, Geothermal Modelling and Monitoring at City-Scale - identifying good practice and effective knowledge exchange, Technical report, British Geological Survey Open Report.

Böttcher, F., Casasso, A., Götzl, G. and Zosseder, K. (2019), TAP - Thermal aquifer Potential: A quantitative method to assess the spatial potential for the thermal use of groundwater, *Renewable Energy*, 142, 85–95, ISSN 18790682, doi:10.1016/j.renene.2019.04.086.

Bottino, G. and Civita, M.V. (1986), Engineering geological features and mapping of subsurface in the metropolitan area of Turin, North Italy, in: *5th International IAEG Congress*, pp. 1741–1753, Buenos Aires.

Bourne-Webb, P., Bodas Freitas, T. and da Costa Gonçalves, R. (2016), Thermal and mechanical aspects of the response of embedded retaining walls used as shallow geothermal heat exchangers, *Energy and Buildings*, 125, 130–141, ISSN 03787788, doi:10.1016/j.enbuild.2016.04.075.

Bove, A., Casaccio, D., Destefanis, E., De Luca, D.A., Lasagna, M. et al. (2005), Piezometria della falda superficiale nel territorio di pianura della Regione Piemonte, in: Regione Piemonte (ed.), *Idrogeologia della pianura piemontese*, chapter 2, p. 10, Mariogros Industrie grafiche S.p.A.

Brandl, H. (2006), Energy foundations and other thermo-active ground structures, *Géotechnique*, 56(2), 81–122, ISSN 0016-8505, doi:10.1680/geot.2006.56.2.81.

Brandl, H. (2016), Geothermal Geotechnics for Urban Undergrounds, *Procedia Engineering*, 165, 747–764, ISSN 18777058, doi:10.1016/j.proeng.2016.11.773.

Bucci, A., Barbero, D., Lasagna, M., Forno, M.G. and De Luca, D.A. (2017), Shallow groundwater temperature in the Turin area (NW Italy): vertical distribution and anthropogenic effects, *Environmental Earth Sciences*, 76(5), 1–14, ISSN 18666299, doi:10.1007/s12665-017-6546-4.

Buhmann, P., Moormann, C., Westrich, B., Pralle, N. and Friedemann, W. (2016), Tunnel geothermics—A German experience with renewable energy concepts in tunnel projects, *Geomechanics for Energy and the Environment*, 8, 1–7, ISSN 23523808, doi:10.1016/j.gete.2016.10.006.

Camusso, M. (2008), *Particle element modelling of the Torino subsoil to improve microtunnelling installations*, Doctorate thesis, Politecnico di Torino.

Carotenuto, A., Ciccolella, M., Massarotti, N. and Mauro, A. (2016), Models for thermo-fluid dynamic phenomena in low enthalpy geothermal energy systems: A review, doi:10.1016/j.rser.2016.01.096.

Carslaw, H.S. and Jaeger, J.C. (1959), Conduction of heat in solids, *Oxford: Clarendon Press, 1959, 2nd ed.*

Casasso, A., Della Valentina, S., Di Feo, A.F., Capodaglio, P., Cavorsin, R. et al. (2018), Ground Source Heat Pumps in Aosta Valley (NW Italy): assessment of existing systems and planning tools for future installations, *Rendiconti Online della Società Geologica Italiana*, 46, 59–66, ISSN 20358008, doi:10.3301/ROL.2018.53.

Casasso, A., Pestotnik, S., Rajver, D., Jež, J., Prestor, J. et al. (2017), Assessment and mapping of the closed-loop shallow geothermal potential in Cerkno (Slovenia), *Energy Procedia*, 125, 335–344, ISSN 18766102, doi:10.1016/j.egypro.2017.08.210.

Casasso, A. and Sethi, R. (2014), Efficiency of closed loop geothermal heat pumps: A sensitivity analysis, *Renewable Energy*, 62, 737–746, ISSN 09601481, doi:10.1016/j.renene.2013.08.019.

Casasso, A. and Sethi, R. (2015), Modelling thermal recycling occurring in groundwater heat pumps (GWHPs), *Renewable Energy*, 77, 86–93, ISSN 18790682, doi:10.1016/j.renene.2014.12.003.

Casasso, A. and Sethi, R. (2016), G.POT: A quantitative method for the assessment and mapping of the shallow geothermal potential, *Energy*, 106, 765–773, ISSN 03605442, doi:10.1016/j.energy.2016.03.091.

Casasso, A. and Sethi, R. (2017), Assessment and mapping of the shallow geothermal potential in the province of Cuneo (Piedmont, NW Italy), *Renewable Energy*, 102, 306–315, ISSN 18790682, doi:10.1016/j.renene.2016.10.045.

CENSIS (2008), *42° rapporto sulla situazione del paese : 2008 / CENSIS ; con il patrocinio del CNEL*, Angeli, Milano, ISBN 978-88-568-0530-7.

Civil Code of Italy, Art 889 (1942), Distances of wells, tanks, ditches and pipes.

Civita, M. and Pizzo, S. (2001), L'evoluzione spazio temporale del livello piezometrico dell'acquifero libero nel sottosuolo di torino, 38/4, 271–287.

Consiglio Nazionale delle Ricerche, 2014 (), Geothopica project cnr/eni web site.

Corrado, V., Ballarini, I. and Corgnati, S.P. (2012), National scientific report on the TABULA activities in Italy, Technical report, Politecncico di Torino, Torino.

de Rienzo, F. and Oreste, P. (2011), Analyses of the Distribution and Nature of the Natural Cementation of Quaternary Sediments: The Case of the Turin Subsoil (Italy), *Geotechnical and Geological Engineering*, 29(3), 319–328, ISSN 09603182, doi:10.1007/s10706-010-9378-5.

Delerablee, Y., Eric, A., Reiffsteck, P., Bernard, J.B., Berthelot, P. et al. (2017), Recommandations pour la conception, le dimensionnement et la mise en oeuvre des geostructures thermiques, 149, 120, doi:10.1051/geotech/2017012.

Di Donna, A., Barla, M. and Amis, T. (2017), Energy Geostructures : Analysis from research and systems installed around the World, *DFI 42th Annual Conference on Deep Foundations, New Orleans, USA*, pp. 1–11.

Di Donna, A., Cecinato, F., Loveridge, F. and Barla, M. (2016), Energy performance of diaphragm walls used as heat exchangers, *Proceedings of the Institution of Civil Engineers - Geotechnical Engineering*, 170, 1–14, ISSN 17518563, doi:10.1680/jgeen.

Diersch, H.J. (2009), *FEFLOW Reference manual.*

Director of the environment and territory protection of Piemonte region (21/04/2016), Determina dirigenziale n. 66 del 3 marzo 2016: Approvazione delle linee guida regionali per l'installazione e la gestione delle sonde geotermiche (Italian) (Regional guidelines for installation and management of BHE's), *Bollettino ufficiale della Regione Piemonte*, 2016(16).

Doherty, J. and Hunt, R.J. (2010), Approaches to highly parameterized inversion: a guide to using PEST for groundwater-model calibration, Technical report, U. S. Geological Survey, doi:2010-5211.

Dong, Y., McCartney, J.S. and Lu, N. (2015), Critical Review of Thermal Conductivity Models for Unsaturated Soils, *Geotechnical and Geological Engineering*, 33(2), 207–221, ISSN 15731529, doi:10.1007/s10706-015-9843-2.

Dorfner, J. (2011), GIS-based mapping tool of urban energy demand for room heating and hot water, in: *17th Building Services, Mechanical and Building Industry Days*, October, pp. 31–35, Debrecen, Hungary.

Environment bureau of the Piemonte region (21/04/2016), Aggiornamento della cartografia della base dell'acquifero superficiale nelle aree di pianura alla scala 1:50.000 e revisione dei parametri numerici relativi ai criteri tecnici orientativi - Legge regionale 30 aprile 1996 n. 22, articolo 2, comma 7. (Update of the cartography of the base of the shallow aquifer in the plain area at the scale 1:50.000 and revision of the numerical parameters pertaining the qualitative technical criteria of Regional Law 30 April 1996 n. 22, article 2, paragraph 7, *Bollettino ufficiale della Regione Piemonte*, 2012(3).

Epting, J., García-Gil, A., Huggenberger, P., Vázquez-Suñe, E. and Mueller, M.H. (2017a), Development of concepts for the management of thermal resources in urban areas – Assessment of transferability from the Basel (Switzerland) and Zaragoza (Spain) case studies, *Journal of Hydrology*, 548, 697–715, ISSN 00221694, doi:10.1016/j.jhydrol.2017.03.057.

Epting, J., Händel, F. and Huggenberger, P. (2013), Thermal management of an unconsolidated shallow urban groundwater body, *Hydrology and Earth System Sciences*, 17(5), 1851–1869, ISSN 1607-7938, doi:10.5194/hess-17-1851-2013.

Epting, J. and Huggenberger, P. (2013), Unraveling the heat island effect observed in urban groundwater bodies – Definition of a potential natural state, *Journal of Hydrology*, 501, 193–204, ISSN 00221694, doi:10.1016/j.jhydrol.2013.08.002.

Epting, J., Müller, M.H., Genske, D. and Huggenberger, P. (2018), Relating groundwater heat-potential to city-scale heat-demand: A theoretical consideration for urban groundwater resource management, *Applied Energy*, 228(March), 1499–1505, ISSN 03062619, doi:10.1016/j.apenergy.2018.06.154.

Epting, J., Scheidler, S., Affolter, A., Borer, P., Mueller, M.H. et al. (2017b), The thermal impact of subsurface building structures on urban groundwater resources – A paradigmatic example, *Science of the Total Environment*, 596-597, 87–96, ISSN 18791026, doi:10.1016/j.scitotenv.2017.03.296.

Erol, S. and François, B. (2018), Multilayer analytical model for vertical ground heat exchanger with groundwater flow, *Geothermics*, 71(April 2017), 294–305, ISSN 03756505, doi:10.1016/j.geothermics.2017.09.008.

Eskilson, P. and Claesson, J. (1988), SIMULATION MODEL FOR THERMALLY INTERACTING HEAT EXTRACTION BOREHOLES, *Numerical Heat Transfer*, 13(2), 149–165, ISSN 0149-5720, doi:10.1080/10407788808913609.

European Commission (2016), *Overview of support activities and projects of the European Commission on energy efficiency and renewable energy in the heating and cooling sector*, Publication office of the European Union, Luxembourg, ISBN 9789292022075, doi: 10.2826/607102.

European Commission (2019), Directive (EU) 2019/1024 of the European Parliament and of the Council of 20 June 2019 on open data and the re-use of public sector information.

European Environment Agency (2019), Air quality in Europe — 2019 report — EEA Report No 10/2019, Technical Report 5, European Environment Agency, Copenhagen, doi:10.2800/822355.

European Parliament and European Council (2002), DIRECTIVE 2002/91/EC OF THE EUROPEAN PARLIAMENT AND OF THE COUNCIL of 16 December 2002 on the energy performance of buildings, *Official Journal of the European Communities*, (1), 65–71.

European Parliament and European Council (2010), Directive 2010/31/EU of the European Parliament and of the Council of 19 May 2010 on the energy performance of buildings, *Official Journal of the European Union*, L(153), 13 – 35, ISSN 00327867.

European Parliament; European Council (2009), Directive 2009/28/EC on the promotion of the use of energy from renewable sources.

Ferguson, G. and Woodbury, A.D. (2007), Urban heat island in the subsurface, *Geophysical Research Letters*, 34(23), 2–5, ISSN 00948276, doi:10.1029/2007GL032324.

Franzius, J.N. and Pralle, N. (2011), Turning segmental tunnels into sources of renewable energy, *Proceedings of the Institution of Civil Engineers - Civil Engineering*, 164(1), 35–40, ISSN 0965-089X, doi:10.1680/cien.2011.164.1.35.

Fry, V. (2009), Lessons from London: regulation of open-loop ground source heat pumps in central London, *Quarterly Journal of Engineering Geology and Hydrogeology*, 42(3), 325–334, ISSN 1470-9236, doi:10.1144/1470-9236/08-087.

Galgaro, A., Di Sipio, E., Destro, E., Chiesa, S., Uricchio, V. et al. (2012), Methodological approach for evaluating the geo-exchange potential: VIGOR Project, *Acque Sotterranee - Italian Journal of Groundwater*, 1(3), 43–53, ISSN 2280-6458, doi:10.7343/as-014-12-0029.

Galgaro, A., Di Sipio, E., Teza, G., Destro, E., De Carli, M. et al. (2015), Empirical modeling of maps of geo-exchange potential for shallow geothermal energy at regional scale, *Geothermics*, 57, 173–184, ISSN 03756505, doi:10.1016/j.geothermics.2015.06.017.

García-Gil, A., Epting, J., Garrido, E., Vázquez-Suñé, E., Lázaro, J.M. et al. (2016), A city scale study on the effects of intensive groundwater heat pump systems on heavy metal contents in groundwater, *Science of The Total Environment*, 572, 1047–1058, ISSN 00489697, doi:10.1016/j.scitotenv.2016.08.010.

García-Gil, A., Goetzl, G., Kłonowski, M.R., Borovic, S., Boon, D.P. et al. (2020), Governance of shallow geothermal energy resources, *Energy Policy*, 138(January), ISSN 03014215, doi:10.1016/j.enpol.2020.111283.

García-Gil, A., Vázquez-Suñe, E., Alcaraz, M.M., Juan, A.S., Sánchez-Navarro, J.Á. et al. (2015a), GIS-supported mapping of low-temperature geothermal potential taking groundwater flow into account, *Renewable Energy*, 77, 268–278, ISSN 09601481, doi:10.1016/j.renene.2014.11.096.

García-Gil, A., Vázquez-Suñe, E., Schneider, E.G., Sánchez-Navarro, J.Á. and Mateo-Lázaro, J. (2015b), Relaxation factor for geothermal use development – Criteria for a more fair and sustainable geothermal use of shallow energy resources, *Geothermics*, 56, 128–137, ISSN 03756505, doi:10.1016/j.geothermics.2015.04.003.

Gemelli, A., Mancini, A. and Longhi, S. (2011), GIS-based energy-economic model of low temperature geothermal resources: A case study in the Italian Marche region, *Renewable Energy*, 36(9), 2474–2483, ISSN 09601481, doi:10.1016/j.renene.2011.02.014.

Hamada, Y., Marutani, K., Nakamura, M., Nagasaka, S., Ochifuji, K. et al. (2002), Study on underground thermal characteristics by using digital national land information, and its application for energy utilization, *Applied Energy*, 72(3), 659–675, ISSN 03062619, doi:10.1016/S0306-2619(02)00055-7.

Han, C. and Yu, X.B. (2016), Sensitivity analysis of a vertical geothermal heat pump system, *Applied Energy*, 170, 148–160, ISSN 03062619, doi:10.1016/j.apenergy.2016.02.085.

Hein, P., Kolditz, O., Görke, U.J., Bucher, A. and Shao, H. (2016a), A numerical study on the sustainability and efficiency of borehole heat exchanger coupled ground source heat pump systems, *Applied Thermal Engineering*, 100, 421–433, ISSN 13594311, doi:10.1016/j.applthermaleng.2016.02.039.

Hein, P., Zhu, K., Bucher, A. and Kolditz, O. (2016b), Quantification of exploitable shallow geothermal energy by using Borehole Heat Exchanger coupled Ground Source Heat Pump systems, *Energy Conversion and Management*, 127(March 2016), 1–12, ISSN 0196-8904, doi:10.1016/j.enconman.2016.08.097.

Herbert, A., Arthur, S. and Chillingworth, G. (2013), Thermal modelling of large scale exploitation of ground source energy in urban aquifers as a resource management tool, *Applied Energy*, 109, 94–103, doi:10.1016/j.apenergy.2013.03.005.

HGC Hydro-Geo-Consult GmbH (), Karte 02.18.5 spezif. entzugsleistung bis 40 m, für 1.800 h/a.

Hu, J. (2017), An improved analytical model for vertical borehole ground heat exchanger with multiple-layer substrates and groundwater flow, *Applied Energy*, 202, 537–549, ISSN 03062619, doi:10.1016/j.apenergy.2017.05.152.

Huber, M.L., Perkins, R.A., Laesecke, A., Friend, D.G., Sengers, J.V. et al. (2009), New International Formulation for the Viscosity of H2O, *Journal of Physical and Chemical Reference Data*, 38(2), 101–125, ISSN 0047-2689, doi:10.1063/1.3088050.

Ilievski, N. (), Attivazione termica di muri controterra.

INSPIRE Thematic working group Geographical Names (2014), Data Specification on Geographical Names - Technical Guidelines, Technical report, European Commission Joint Research Centre, Bruxelles.

Italian ministry of Economic Development (25/06/2015), Decreto interministeriale del 25 giugno 2015: Applicazione delle metodologie di calcolo delle prestazioni energetiche e definizione delle prescrizioni e dei requisiti minimi degli edifici (Italian), *Gazzetta Ufficiale della Repubblica Italiana*, Serie Generale(162).

Italian ministry of Economic Development (26/06/2015), Decreto interministeriale 26 giugno 2015 - adeguamento linee guida nazionali per la certificazione energetica degli edifici (Italian), *Gazzetta Ufficiale della Repubblica Italiana*, Serie Generale(162).

Javadi, H., Mousavi Ajarostaghi, S.S., Pourfallah, M. and Zaboli, M. (2019), Performance analysis of helical ground heat exchangers with different configurations, *Applied Thermal Engineering*, 154(March), 24–36, ISSN 13594311, doi:10.1016/j.applthermaleng.2019.03.021.

Kalogirou, S.A., Florides, G.A., Pouloupatis, P.D., Christodoulides, P. and Joseph-Stylianou, J. (2015), Artificial neural networks for the generation of a conductivity map of the ground, *Renewable Energy*, 77, 400–407, ISSN 09601481, doi:10.1016/j.renene.2014.12.033.

Kavanaugh, S.P. and Rafferty, K. (1997), Ground-Source Heat Pumps: Design of Geothermal Systems for Commercial and Institutional Buildings, Technical report.

Köhler, M., Händel, F., Epting, J., Binder, M., Mueller, M.H. et al. (2015), Numerical Evaluation and Optimization of Depth-oriented Temperature Measurement for the Investigation of Thermal Influences on Groundwater Resources, *Energy Procedia*, 76, 371–380, ISSN 18766102, doi:10.1016/j.egypro.2015.07.844.

Kupfersberger, H., Rock, G. and Draxler, J.C. (2017), Inferring near surface soil temperature time series from different land uses to quantify the variation of heat fluxes into a shallow aquifer in Austria, *Journal of Hydrology*, 552, 564–577, ISSN 00221694, doi:10.1016/j.jhydrol.2017.07.030.

Laloui, L. and Di Donna, A. (2013), *Energy Geostructures*, John Wiley & Sons, Inc., Hoboken, NJ USA, ISBN 9781118761809, doi:10.1002/9781118761809.

Lavezzo, M. and Monti, S. (2012), Progettazione della residenza universitaria "Cesare Codegone" nell'area delimitata dalle vie borsellino - Relazione geologica e geotecnica, Technical report, Torino.

Le-van, L. (2015), Etude de la faisabilité des cycle sous-critiques et supercritiques de rankine pour la valorisation de rejets thermiques, doi:10.13140/RG.2.1.1481.1688.

Lee, K.C. (2001), Classification of geothermal resources by exergy, *Geothermics*, 30(4), 431–442, ISSN 03756505, doi:10.1016/S0375-6505(00)00056-0.

Legislative Decree 11st February 2010, n. 22 (2010), Reorganisation of regulations on search and management of geothermal resources.

Lekshmi, K.R.A. and Arnepalli, D.N. (2017), A Review on Coupled Heat and Water Vapour Transport in Unsaturated Soils, in: *Geotechnical Frontiers 2017*, GSP 280, pp.

746–755, American Society of Civil Engineers, Reston, VA, ISBN 9780784480472, ISSN 08950563, doi:10.1061/9780784480472.079.

Li, C., Cleall, P.J., Mao, J. and Muñoz-Criollo, J.J. (2018), Numerical simulation of ground source heat pump systems considering unsaturated soil properties and groundwater flow, *Applied Thermal Engineering*, 139(May), 307–316, ISSN 13594311, doi:10.1016/j.applthermaleng.2018.04.142.

Link, K., Rybach, L., Imhasly, S. and Wyss, R. (2015), Geothermal Energy in Switzerland – Country Update, in: *Proceedings World Geothermal Congress 2015*, April, p. 10, Melbourne, Australia.

Liu, C., Shi, B., Tang, C. and Gao, L. (2011), A numerical and field investigation of underground temperatures under Urban Heat Island, *Building and Environment*, 46(5), 1205–1210, ISSN 03601323, doi:10.1016/j.buildenv.2010.12.015.

Lo Russo, S. and Civita, M.V. (2009), Open-loop groundwater heat pumps development for large buildings: A case study, *Geothermics*, 38(3), 335–345, ISSN 03756505, doi:10.1016/j.geothermics.2008.12.009.

Lo Russo, S., Gnavi, L., Roccia, E., Taddia, G. and Verda, V. (2014), Groundwater Heat Pump (GWHP) system modeling and Thermal Affected Zone (TAZ) prediction reliability: Influence of temporal variations in flow discharge and injection temperature, *Geothermics*, 51, 103–112, ISSN 03756505, doi:10.1016/j.geothermics.2013.10.008.

Lo Russo, S., Taddia, G., Baccino, G. and Verda, V. (2011), Different design scenarios related to an open loop groundwater heat pump in a large building: Impact on subsurface and primary energy consumption, *Energy and Buildings*, 43(2-3), 347–357, ISSN 03787788, doi:10.1016/j.enbuild.2010.09.026.

Lokoshchenko, M.A. and Korneva, I.A. (2015), Underground urban heat island below Moscow city, *Urban Climate*, 13, 1–13, ISSN 22120955, doi:10.1016/j.uclim.2015.04.002.

Lund, J.W. and Boyd, T.L. (2016), Direct utilization of geothermal energy 2015 worldwide review, *Geothermics*, 60, 66–93, ISSN 03756505, doi:10.1016/j.geothermics.2015.11.004.

Luo, J., Luo, Z., Xie, J., Xia, D., Huang, W. et al. (2018), Investigation of shallow geothermal potentials for different types of ground source heat pump systems (GSHP) of Wuhan city in China, *Renewable Energy*, 118, 230–244, ISSN 09601481, doi:10.1016/j.renene.2017.11.017.

Man, Y., Yang, H. and Wang, J. (2010), Study on hybrid ground-coupled heat pump system for air-conditioning in hot-weather areas like Hong Kong, *Applied Energy*, 87(9), 2826–2833, ISSN 03062619, doi:10.1016/j.apenergy.2009.04.044.

Marcotte, D. and Pasquier, P. (2008), Fast fluid and ground temperature computation for geothermal ground-loop heat exchanger systems, *Geothermics*, 37(6), 651–665, ISSN 03756505, doi:10.1016/j.geothermics.2008.08.003.

Menberg, K., Blum, P., Schaffitel, A. and Bayer, P. (2013), Long-Term Evolution of Anthropogenic Heat Fluxes into a Subsurface Urban Heat Island, *Environmental Science & Technology*, 47(17), 9747–9755, ISSN 0013-936X, doi:10.1021/es401546u.

Mielby, S., Eriksson, I., Diarmad, S., Campbell, G. and Lawrence, D. (2017), Opening up the subsurface for the cities of tomorrow The subsurface in the planning process, *Procedia Engineering*, 209, 12–25, ISSN 1877-7058, doi:10.1016/j.proeng.2017.11.125.

Miglani, S., Orehounig, K. and Carmeliet, J. (2018), A methodology to calculate long-term shallow geothermal energy potential for an urban neighbourhood, *Energy and Buildings*, 159, 462–473, ISSN 03787788, doi:10.1016/j.enbuild.2017.10.100.

Milenić, D., Vasiljević, P. and Vranješ, A. (2010), Criteria for use of groundwater as renewable energy source in geothermal heat pump systems for building heating/cooling purposes, *Energy and Buildings*, 42(5), 649–657, ISSN 03787788, doi:10.1016/j.enbuild.2009.11.002.

Milnes, E. and Perrochet, P. (2013), Assessing the impact of thermal feedback and recycling in open-loop groundwater heat pump (GWHP) systems: a complementary design tool, *Hydrogeology Journal*, 21(2), 505–514, ISSN 1431-2174, doi:10.1007/s10040-012-0902-y.

Molina-Giraldo, N., Bayer, P. and Blum, P. (2011), Evaluating the influence of thermal dispersion on temperature plumes from geothermal systems using analytical solutions, *International Journal of Thermal Sciences*, 50(7), 1223–1231, ISSN 12900729, doi:10.1016/j.ijthermalsci.2011.02.004.

Muffler, P. and Cataldi, R. (1978), Methods for regional assessment of geothermal resources, *Geothermics*, 7(2-4), 53–89, ISSN 03756505, doi:10.1016/0375-6505(78)90002-0.

Muñoz, M., Garat, P., Flores-Aqueveque, V., Vargas, G., Rebolledo, S. et al. (2015), Estimating low-enthalpy geothermal energy potential for district heating in Santiago basin-Chile (33.5°S), *Renewable Energy*, 76, 186–195, ISSN 18790682, doi:10.1016/j.renene.2014.11.019.

Nam, Y. and Ooka, R. (2011), Development of potential map for ground and groundwater heat pump systems and the application to Tokyo, *Energy and Buildings*, 43(2-3), 677–685, ISSN 03787788, doi:10.1016/j.enbuild.2010.11.011.

Ondreka, J., Rüsgen, M.I., Stober, I. and Czurda, K. (2007), GIS-supported mapping of shallow geothermal potential of representative areas in south-western Germany—Possibilities and limitations, *Renewable Energy*, 32(13), 2186–2200, ISSN 09601481, doi:10.1016/j.renene.2006.11.009.

Parriaux, A., Tacher, L. and Joliquin, P. (2004), The hidden side of cities — towards three-dimensional land planning, 36, 335–341, doi:10.1016/j.enbuild.2004.01.026.

Piemonte regional authority (2007), Water protection plan - regional council decree 117-10731.

Piga, B., Casasso, A., Pace, F., Godio, A. and Sethi, R. (2017), Thermal Impact Assessment of Groundwater Heat Pumps (GWHPs): Rigorous vs. Simplified Models, *Energies*, 10(9), 1385, ISSN 1996-1073, doi:10.3390/en10091385.

Raymond, J., Malo, M., Tanguay, D., Grasby, S. and Bakhteyar, F. (2015), Direct Utilization of Geothermal Energy from Coast to Coast: a Review of Current Applications and Research in Canada, in: *Proceedings World Geothermal Congress 2015*, April, pp. 19–25.

Regione Piemonte and CSI Piemonte (2016), Catalogo dei dati territoriali (Italian), Technical report, Regione Piemonte, Torino, Italia.

Reuss, M., Konstantinidou, E. and Sanner, B. (2006), 10 Years VDI 4640—German Guidelines for Ground Coupled Heat Pumps, UTES and Direct Thermal use of the Underground, in: *proceedings of ECOSTOCK, Stockton College, New Jersey, USA*, p. 8.

Rivera, J.A. (2016), *Analytical framework for simulating borehole heat exchangers in urban environments*, Doctoral thesis, ETH Zurich, doi:10.3929/ethz-a-010866579.

Rivera, J.A., Blum, P. and Bayer, P. (2015), Analytical simulation of groundwater flow and land surface effects on thermal plumes of borehole heat exchangers, *Applied Energy*, 146, 421–433, ISSN 03062619, doi:10.1016/j.apenergy.2015.02.035.

Rivera, J.A., Blum, P. and Bayer, P. (2017), Increased ground temperatures in urban areas: Estimation of the technical geothermal potential, *Renewable Energy*, 103, 388–400, ISSN 09601481, doi:10.1016/j.renene.2016.11.005.

Rivoire, M., Casasso, A., Piga, B. and Sethi, R. (2018), Assessment of Energetic, Economic and Environmental Performance of Ground-Coupled Heat Pumps, *Energies*, 11(8), 1941, ISSN 1996-1073, doi:10.3390/en11081941.

Rybach, L. (2015), Classification of geothermal resources by potential, *Geothermal Energy Science*, 3(1), 13–17, doi:10.5194/gtes-3-13-2015.

Ryżyński, G. and Bogusz, W. (2016), City-scale perspective for thermoactive structures in Warsaw, *Environmental Geotechnics*, 3(EG4), 280–290, ISSN 2051-803X, doi: 10.1680/jenge.15.00031.

Sanner, B. (2016), Shallow geothermal energy – history , development , current status , and future prospects, in: *European Geothermal Congress 2016*, pp. 19–24, Strasbourg, France.

Sanner, B., Systems, O., Systems, C. and Pumps, G.s.H. (2001), Shallow geothermal energy, *Geo-Heat Center Bulletin*, (June), 19–26.

Santilano, A., Donato, A., Galgaro, A., Montanari, D., Menghini, A. et al. (2016), An integrated 3D approach to assess the geothermal heat-exchange potential: The case study of western Sicily (southern Italy), *Renewable Energy*, 97, 611–624, ISSN 18790682, doi: 10.1016/j.renene.2016.05.072.

Schiel, K., Baume, O., Caruso, G. and Leopold, U. (2016), GIS-based modelling of shallow geothermal energy potential for CO2 emission mitigation in urban areas, *Renewable Energy*, 86, 1023–1036, ISSN 18790682, doi:10.1016/j.renene.2015.09.017.

Sethi, R. and Di Molfetta, A. (2007), Heat transport modeling in an aquifer downgradient a municipal solid waste landfill in Italy, *American Journal of Environmental Sciences*, 3(3), 106–110, ISSN 1553345X, doi:10.3844/ajessp.2007.106.110.

Shewchuk, J.R. (1996), Applied Computational Geometry Towards Geometric Engineering, in: M.C. Lin and D. Manocha (eds.), *WACG 1996: Applied Computational Geometry Towards Geometric Engineering*, volume 1148 of *Lecture Notes in Computer Science*, pp. 203–222, Springer Berlin Heidelberg, Berlin, Heidelberg, ISBN 978-3-540-61785-3, ISSN 00983004, doi:10.1007/BFb0014474.

Si, H. (2015), Tetgen, a delaunay-based quality tetrahedral mesh generator, *ACM Trans. Math. Softw.*, 41(2), ISSN 0098-3500, doi:10.1145/2629697.

Signorelli, S. (2004), *Geoscientific investigations for the use of shallow low-enthalpy systems*, Doctoral thesis, ETH Zurich, doi:10.3929/ethz-a-004818477.

Somogyi, V., Sebestyén, V., Domokos, E., Zseni, A. and Papp, Z. (2015), Thermal impact assessment with hydrodynamics and transport modeling, *Energy Conversion and Management*, 104, 127–134, ISSN 01968904, doi:10.1016/j.enconman.2015.04.045.

Somogyi, V., Sebestyén, V. and Nagy, G. (2017), Scientific achievements and regulation of shallow geothermal systems in six European countries – A review, *Renewable and Sustainable Energy Reviews*, 68, 934–952, ISSN 13640321, doi:10.1016/j.rser.2016.02.014.

Sterpi, D., Angelotti, A., Corti, D. and Ramus, M. (2014), Numerical analysis of heat transfer in thermo-active diaphragm walls, in: B.&.R. Hicks (ed.), *Proc. 8th Europ. Conf. Numerical Methods in Geotechnical Engineering, NUMGE 2014*, pp. 1043–1048, Taylor & Francis Group, London, ISBN 9781138001466.

Sterpi, D., Angelotti, A., Habibzadeh Bigdarvish, O. and Jalili, D. (2017), On the modelling of thermo-active diaphragm walls based on monitoring data, in: *15th IACMAG proceedings*, October, Wuhan, China.

Sterpi, D., Angelotti, A., Habibzadeh-Bigdarvish, O. and Jalili, D. (2018b), Assessment of thermal behaviour of thermo-active diaphragm walls based on monitoring data, *Journal of Rock Mechanics and Geotechnical Engineering*, 10(6), 1145–1153, ISSN 16747755, doi:10.1016/j.jrmge.2018.08.002.

Sterpi, D., Coletto, A. and Mauri, L. (2017b), Investigation on the behaviour of a thermo-active diaphragm wall by thermo-mechanical analyses, *Geomechanics for Energy and the Environment*, 9, 1–20, ISSN 23523808, doi:10.1016/j.gete.2016.10.001.

Sterpi, D., Tomaselli, G. and Angelotti, A. (2020), Energy performance of ground heat exchangers embedded in diaphragm walls: Field observations and optimization by numerical modelling, *Renewable Energy*, 147, 2748–2760, ISSN 09601481, doi:10.1016/j.renene.2018.11.102.

Tang, F. and Nowamooz, H. (2019), Factors influencing the performance of shallow Borehole Heat Exchanger, *Energy Conversion and Management*, 181(September 2018), 571–583, ISSN 01968904, doi:10.1016/j.enconman.2018.12.044.

Taylor, C.A. and Stefan, H.G. (2009), Shallow groundwater temperature response to climate change and urbanization, *Journal of Hydrology*, 375(3-4), 601–612, ISSN 00221694, doi:10.1016/j.jhydrol.2009.07.009.

Thum, P. (2009), One for all - the new SAMG solver control within FEFLOW, Postdam, Germany.

Tinti, F., Barbaresi, A., Ferrari, M., Elkarmoty, M., Torreggiani, D. et al. (2017), Experimental calibration of underground heat transfer models under a winery building in a rural area, *Rudarsko-geološko-naftni zbornik*, 32(3), 35–43, ISSN 03534529, doi:10.17794/rgn.2017.3.4.

Tinti, F., Boldini, D., Ferrari, M., Lanconelli, M., Kasmaee, S. et al. (2017b), Exploitation of geothermal energy using tunnel lining technology in a mountain environment. A feasibility study for the Brenner Base tunnel – BBT, *Tunnelling and Underground Space Technology*, 70(June), 182–203, ISSN 08867798, doi:10.1016/j.tust.2017.07.011.

Tinti, F., Kasmaee, S., Elkarmoty, M., Bonduà, S. and Bortolotti, V. (2018), Suitability evaluation of specific shallow geothermal technologies using a GIS-Based multi criteria decision analysis implementing the analytic hierarchic process, *Energies*, 11(2), ISSN 19961073, doi:10.3390/en11020457.

Tinti, F., Pangallo, A., Berneschi, M., Tosoni, D., Rajver, D. et al. (2016), How to boost shallow geothermal energy exploitation in the adriatic area: The LEGEND project experience, *Energy Policy*, 92, 190–204, ISSN 03014215, doi:10.1016/j.enpol.2016.01.041.

Tsagarakis, K.P., Efthymiou, L., Michopoulos, A., Mavragani, A., Anđelković, A.S. et al. (2018), A review of the legal framework in shallow geothermal energy in selected European countries: Need for guidelines, *Renewable Energy*, ISSN 09601481, doi:10.1016/j.renene.2018.10.007.

United Nations (2018), The speed of urbanization around the world, *Population Facts*, p. 2.

United Nations (2019), World Urbanization Prospects: The 2018 revision, Technical report, Department of Economic and Social Affairs, Population Division, New York, NY.

van Rooyen, M. and Winterkorn, H.F. (1957), Theoretical and Practical Aspects of the Thermal Conductivity of Soils and Similar Granular Systems, *Highway Research Board Bulletin 168 - Fundamental and Practical Concepts of Soil Freezing*, (168), 143–205.

Vanzetti, C. (2015), Attività ARPA nella gestione della rete di monitoraggio delle acque sotterranee, Technical report, Agenzia Regionale per la Protezione Ambientale del Piemonte, Torino, Italy.

VDI (2010), VDI 4640 Thermal use of the underground. Part 1: Fundamentals, approvals, environmenal aspects., Technical report.

Wang, Z., Wang, F., Ma, Z., Wang, X. and Wu, X. (2016), Research of heat and moisture transfer influence on the characteristics of the ground heat pump exchangers in unsaturated soil, *Energy and Buildings*, 130, 140–149, ISSN 03787788, doi:10.1016/j.enbuild.2016.08.043.

Zhang, Y., Soga, K., Choudhary, R. and Bains, S. (2015), GSHP Application for Heating and Cooling at 'City Scale' for the City of Westminster, in: *Proceedings World Geothermal Congress*, Melbourne.

Zhu, K., Blum, P., Ferguson, G., Balke, K.D. and Bayer, P. (2010), The geothermal potential of urban heat islands, *Environmental Research Letters*, 5(4), ISSN 17489326, doi:10.1088/1748-9326/5/4/044002.

Candidate publication list

Journals

- Baralis, M., Barla, M., Bogusz, W., Di Donna, A., Ryzynski, G. and Zerun, M. (2020), Geothermal potential of the NE Extension Warsaw (Poland) metro tunnels, *Environmental Geotechnics*, 7 (4), 282-294, DOI: 10.1680/jenge.18.00042.

- Barla, M., Di Donna, A., and Baralis, M. (2020), City-scale analysis of subsoil thermal conditions due to geothermal exploitation, *Environmental Geotechnics*, 7 (4), 306-316, DOI: 10.1680/jenge.17.00087.

- Epting, J., Baralis, M., Künze, R., Mueller, M. H., Insana, A., Barla, M., and Huggenberger, P. (2020), Geothermal potential of tunnel infrastructures – development of tools at the city-scale of Basel, Switzerland, *Geothermics*, 83, pp. 12, DOI: 10.1016/j.geothermics.2019.101734.

- Tsagarakis, K.P., Efthymiou, L., Michoupolos, A., Mavragani, A., Andelkovic, A.S., Antolini, F., Bacic, M., Bajare, D., Baralis, M., Bogusz, W., Burlon, S., Figueira, J., Genc, M.S., Javed, S., Jurelionis, A., Koca, K., Ryzynski, G., Urchueguia, J.F., and Zlender, B. (2018) A review of the legal framework in shallow geothermal energy in selected European countries: Need for guidelines, *Renewable Energy*, 147 (2), 2556-2571, DOI: 10.1016/j.renene.2018.10.007.

Conference papers

- Baralis, M., and Barla, M. (2018) Ottimizzazione nell'uso della risorsa geotermica superficiale nei centri urbani (Optimisation in shallow geothermal energy resources use in urban areas). Incontro Annuale Giovani Ricercatori di Geotecnica 2018, 4-6 July, Genova, Italy.

- Baralis, M., and Barla, M. (2019) Evaluating borehole heat exchanger long term potential including the influence of advection and dispersion, *Geophysical Research Abstracts*, 21. EGU General Assembly 2019, 7–12 April, Wien, Austria.

- Barla, M., Baralis, M., Insana, A., Zacco, F., Aissa, S., Antolini, F., Azzarone, F., and Marchetti, P. (2019) Feasability study for the thermal activation of Turin Metro Line 2. *Tunnels and Underground Cities. Engineering and Innovation Meet Archaeology, Architecture and Art.*. Proceedings of the WTC 2019 ITA-AITES World Tunnel Congress, 3-9 May, Napoli, Italy. DOI: 10.1201/9780429424441-24.

This Ph.D. thesis has been typeset by means of the TEX-system facilities. The typesetting engine was LuaLATEX. The document class was `toptesi`, by Claudio Beccari, with option `tipotesi=scudo`. This class is available in every up-to-date and complete TEX-system installation.